



National Centre for Petroleum Geology and Geophysics

**Controls on Reservoir Development
and Quality in a Glacial Sequence ;
A Study of the Late Palaeozoic, Cooper Basin
South Australia and Queensland, Australia**

Thesis submitted to the University of Adelaide
in fulfillment of the requirement for the
Degree of Doctor of Philosophy

July 2000

Volume 1

Chris Cubitt

*B App Sci (Geology)
Royal Melbourne Institute of Technology
B Sci (Hons) (Geology and Geophysics)
University of Adelaide*

STATEMENT OF AUTHENTICITY

This work contains no material that has been previously accepted for the award of any degree or diploma in any university or other tertiary institution and, to the best of my knowledge and belief, contains no material previously published or written by another person, except where due reference has been made in the text.

I give my consent to reproduce any part of this thesis, when deposited at the University of Adelaide library, being available for loan and photocopying.

Chris Cubitt

July 2000

**I DEDICATE THIS THESIS TO
DR DAVE GRAVESTOCK**

ACKNOWLEDGEMENTS

The main participants in this project were Mines and Energy South Australia (now Dept. of Primary Industry and Resources - PIRSA), The National Centre for Petroleum Geology and Geophysics (NCPGG) and the South Australian Business Unit (SABU) of Santos Ltd. The Australian Petroleum Collective Research Centre (APCRC) also provided project funding. I thank all of these institutions for financially supporting this research.

Further technical assistance was provided by the Department of Geology and Geophysics, CEMMSA (Adelaide University) and AMDEL laboratories. Boral Energy (now Origin Energy) kindly allowed access to a large number of unpublished reports. Lastly Mines and Energy Victoria (Petroleum Division) and the Dept. of Geological and Environmental Engineering (RMIT) gave access to petrological microscopes whilst in Melbourne.

To the NCPGG family, of which I have been a part of since 1992, the completion of this work marks the end of our long formal association. I thank all who have helped over the many years. The list is long, however I particularly want to mention, Maureen Sutton, Barbara Wallis, Andy Mitchell, Cedrick Griffiths, Nick Man, John Kaldi, and Ted Moorcroft. To my fellow PhD students Alex Kaiko, Stu Smith, Simon Polomoka and Johnny Hull the long chats over "a few cups of tea" out the back will always be remember and sorely missed.

Special mention must be made of Drs Bill Stuart and Dave Gravestock. Bill gave me the chance to carry out this research and Dave through what was then MESA provided the majority of the funds for this project. I sincerely thank you both wherever you both are.

Dr Nick Lemon, has also been a constant help and guide through the various PhD "traps". Thanks Nick for your help through out my time at the NCPGG. Sorry for giving you all my manuscripts in late October-early November. My timing with respect to honours corrections was never that flash and never improved!

I would like to thank Dr Peter Tingate for providing specialist commentary on the diagenesis and the thermal history aspects of this project. I also extend many thanks to Dr Paul Tarabbia for proof reading the final manuscript.

Other people without whom this project would not have been possible include Jay Mathews, Mohamed Rezaee, John Stanely (the XRD master), Eleanor Alexander, Wayne Musared (for his running repairs on faulty thin sections), Alan Web of AMDEL and Keith Turnbull of Adelaide University. The help and banter of John Terlet (CEMMSA) made the endless microprobe and SEM hours tolerable. Brian Logan of the PIRSA core library became a vital project participant constantly doing the impossible with core layouts. Thanks mate for the humble pie!

Gerry Carne, Chris Porter, Steve Mackie and particularly Stuart Jones of Santos Ltd. have showed an overwhelming enthusiasm for this research supporting it's digitisation. I also want to thank Darren Evans who at the end of my PhD journey guided me through tricky statistical corrections. Cheers mate. Ralph Panait, also of Santos Ltd., needs to be recognised and thanked as the creator of the "art work" seen throughout this thesis. His ability to turn a set of petrographic images into a coherent form is acknowledged here.

The following body of work was done in parallel with Dr Alistair Chaney and Aberdeen University. I thank Al for his friendship, and his technical data. I also thank Brian Williams and Aberdeen University for supporting this research.

I want to thank my family, Kay, Len, Danielle, Mark and Dylan who have supported me through all the years, putting up with my infrequent and brief visits and my inability to use a telephone. I especially want to say thanks to my parents for giving the occasional, and very much needed, "study grants", and for allowing me unlimited access to a car ("the Kingswood"). The "Kingswood" was invaluable being the only form of motorised transport for NCPGG PhD "study trips" to the Barossa Valley and Mc Laren Vale wine regions. Thanks.

Sharon Tiainen, who initially held a healthy scepticism towards PhD study, has over the years, warmed to the notion and value of post graduate research, showing, amazing patience and generosity throughout this time. Without her I would have found the road a lot lonelier. She has been throughout this time my inspiration, teaching me that out of adversity can come something beautiful if you wait a while. Thanks mate.

To my friends, scattered all over the world, thank you for filling my numerous photo albums with mirth, merriment and mayhem. In particular, I want to single out the following antagonists who have done me the most damage: Tobes, Teresa, Marcus

Plugga, Stu, Shag, Christine, Jensy, Johnny Duka, BJ, Andy, Mandy, Jazz, Ed, Stods and Brincat. I would also like to incriminate: Ange, Toni, Dight, Josephine, Sarah, Tomasz, Ando, Pete, and Fi who have in the last few years also helped to distract me from this body of work.

I have a special thank you to the members of the Gifford Hotel and Dew St. Firstly I acknowledge the magic that was the Gifford Hotel and heartily thank DJ Meags, Bridge, Johnny and Alistair for their enduring friendship. Those days were the most memorable of my PhD candidature. Secondly I want to say a special thanks to Bridge and Johnny, house mates, dearest friends and fellow post grads. The endless encouragement and support will always be remembered. To Alistair I never knew Buffy Beaumont existed! Thanks for showing me he does!!!. Meags, thanks for rekindling that ABBA and Diamond fire.

The last institution I want to thank is Hamish "Chunga" Young. Hamish, I thank you for making this whole period filled with laughter, frivolity and farce, but above all for instilling a burning hatred of all things Essendon. You truly have a gift that makes people feel happy and very much alive. Thanks for the experience mate!

Cover Page Photo Credits

Volume One:

Goodley River entering Lake Tekapo, New Zealand Alps, New Zealand (S. Tiainen, 1999).

Volume Two:

Tasman Glacier, New Zealand Alps, New Zealand (C. Cubitt, 1999).

ABSTRACT

The Merrimelia Formation is a complex mosaic of glacial facies in which the Tirrawarra Sandstone and Merrimelia Formation exhibit an interfingering relationship. This study, has defined this relationship further, indicating that the Tirrawarra Sandstone should be included in the Merrimelia Formation as a "facies type" as both Merrimelia and Tirrawarra sediments form an integrated suite of sediments. Within this context, all glacio-fluvial braided outwash sandstones are called "Tirrawarra type" sandstones.

The kaleidoscope of facies which forms the Merrimelia-Tirrawarra glacial complex (MTGC) have been deposited directly from the action of glacial meltwater and sediment output; a consequence of the Permo-Carboniferous Gondwanan glaciation which covered the early Cooper Basin. Merrimelia (and Tirrawarra) sediments were deposited in both terminoglacial or proglacial depositional realms depending on the relative position of Gondwanan glaciers and ice sheet.

Merrimelia Formation sediments contain up to 76 different rock fragment species. Rock fragments in Merrimelia (and Tirrawarra) sediments are either intrabasinal or extrabasinal. Intrabasinal rock fragments are mainly derived from the underlying Warburton Basin units, whereas extrabasinal rock fragments have been sourced from outside the Cooper Basin and transported via the action of glaciers and glacial meltwaters. Three rock fragment domains were defined. The northern rock fragment domain area was possibly sourced from the north (Arunta Block) while the western and southern rock fragment domains were possibly sourced from the west (Officer Basin), southwest (Mt. Painter region), and the south (Benagerie Ridge, Willyama Supergroup) respectively.

The composition of authigenic illite (poly type 1Md) in argillaceous Merrimelia sediments, was found to be consistent with a mixed layered I/S clay. This mixed layered clay exhibited an I/S ratio of 0.95. Preliminary illite dating data combined with geohistory analysis suggests that illite has formed between 75°C and 95°C. This formation range matches petrographic observations.

Controls on illite growth in MTGC sediments include, temperature, cation supply, pore water acidity, water/rock ratio and the size of pore spaces. Initially illite formed in a closed system where reactant supply was sourced locally (closed system) and, in the later stages of diagenesis, illite is neoformed by interaction with circulating pore fluids (open system).

A new petrographic technique was developed for the study of illite in the Merrimelia Formation; illite fluorescence. Illite fluorescence microscopy was found to be an effective tool in observing relationships between diagenetic illite and other authigenic phases. Illite fluorescence microscopy in combination with image analysis, was also used to quickly and accurately assess illite proportions from normally prepared, unpolished thin sections. This study has shown that by utilising the fluorescent properties of illite, a more accurate assessment of reservoir quality of illitic glacial sediments is possible.

A pilot illite dating study was undertaken. The results showed good agreement with diagenetic observation indicating that standard illite dating techniques can be successfully applied to the Cooper Basin.

Using diagenetic observations to better defined geohistory parametres, led to a greater understanding of the thermal history of the southern Cooper Basin region,

where aquifer effects on the thermal regime were found to be more extensive than previously considered.

Standard and fluorescent thin section petrography, SEM, TEM and microprobe analyses of Merrimelia sediments delineated a paragenetic sequence similar to that previously published for the Tirrawarra Sandstone. A generalised paragenetic sequence for the whole MTGC was subsequently constructed. Variations in the Merrimelia and Tirrawarra paragenetic sequences are localised and attributable to lithology variations.

Provenance of sediment source regions can exert a strong control on reservoir quality, as rock fragment litho-type and proportion are crucial to compactional effects and clay authigenesis. These latter processes are linked to diagenetic adjustments, and the thermal regime operating in the basin. The principle diagenetic events which effect reservoir performance in the MTGC are compaction, quartz precipitation (Tirrawarra sediments) and the formation of authigenic clays (kaolin - Tirrawarra Sandstone and illite - Merrimelia Formation).

Hydrocarbon bearing Merrimelia sandstone packages at Malgoona and Merrimelia fields have permeabilities that vary enormously. This variability has been attributed to facies as matrix-rich facies in terminoglacial environments form poorly permeable intervals and proglacial quartzose facies exhibit better reservoir attributes. Thus differing facies types govern the textural and mineralogical maturity of sediments controlling any reservoir potential a sediment may possess. Deltaic, braidplain and glacio-aeolian sandstones have the greatest reservoir potential of all MTGC facies types.

The presence of illite does not necessarily negate a potential reservoir interval as distribution is as important as mere presence. The longitudinal bar sandstones at Malgoona Field show boxwork illite morphologies isolated as clumps formed from the breakdown of rock fragments and feldspars. This mode of illite occurrence has little effect on reservoir quality as the clay does not block pore throats. Conversely only a small proportion of illite in the porous glacio-aeolian sandstones of the Merrimelia Field drastically diminishes the quality of these reservoirs.

In general, illite was found to dictate reservoir quality in all Merrimelia facies. Consequently, understanding the morphology, formation, timing and distribution of illite is critical for risking the likelihood of favourable reservoir attributes in the Merrimelia Formation.

Development of potential reservoir sediments in the MTGC is controlled by:

- Climatic changes.
- Basin topography.
- Sediment distribution.
- Sediment composition.

Reservoir quality in the MTGC is primarily controlled by:

- Facies type (terminoglacial or proglacial).
- Diagenetic overprint (illite and quartz cement authigenesis).
- Geothermal gradient (acceleration of illite and quartz cement formation).
- Rock fragment composition (competent or incompetent).
- Mechanical compaction.
- Rock fragment proportion.

TABLE OF CONTENTS

VOLUME ONE

Statement Of Authenticity	<i>ii</i>
Dedication	<i>iii</i>
Acknowledgments	<i>iv</i>
Abstract	<i>vii</i>
Table Of Contents	<i>ix</i>
List Of Figures	<i>xix</i>
List Of Plates	<i>xxiii</i>
List Of Tables	<i>xxiv</i>
Objectives Of Study.	<i>xxvi</i>
Terminology	<i>xxvii</i>
CHAPTER ONE: INTRODUCTION	1
1.0 PREAMB	1
2.0 LE	
1.1 LOCATION	2
1.2 STUDY AREA	3
1.3 PREVIOUS STUDIES	3
1.4 COOPER BASIN STRATIGRAPHY	8
1.4.1 DISCUSSION	10
1.5 LITHOSTRATIGRAPHIC DEFINITIONS	11
1.5.1 DEFINITIONS: TIRRAWARRA SANDSTONE AND MERRIMELIA FORMATION	12
1.5.1.1 Tirrawarra Sandstone	12
1.5.1.2 Merrimelia Formation	14
1.6 DISTRIBUTION OF THE TIRRAWARRA SANDSTONE AND MERRIMELIA FORMATION	16
1.6.1 MERRIMELIA FORMATION	18
1.6.2 TIRRAWARRA SANDSTONE	18
1.7 STRUCTURE OF THE COOPER BASIN	19
1.8 STRATIGRAPHIC UNITS WITHIN THE COOPER, EROMANGA AND WARBURTON BASINS.	21
1.8.1 CRYSTALLINE BASEMENT	21
1.8.2 WARBURTON BASIN	21
1.8.2.1 Mooracoochie Volcanics	23
1.8.2.2 Vuggy Dolomite	23
1.8.2.3 Kalladeina Formation	23
1.8.2.4 "Innamincka Red Beds" Or Innamincka Formation	24
1.8.2.5 Mudrangie Sandstone	24
1.8.2.6 Dullingari Group	24
1.8.2.7 Pando Formation	25
1.8.3 BIG LAKE SUITE GRANODIORITE	25
1.8.4 COOPER BASIN	27
1.8.4.1 Merrimelia Formation	27
1.8.4.2 Tirrawarra Sandstone	27

1.8.4.3 Patchawarra Formation	28
1.8.4.4 Murteree Shale	28
1.8.4.5 Epsilon Formation	29
1.8.4.6 Roseneath Shale	29
1.8.4.7 Daralingie Formation	29
1.8.4.8 Toolachee Formation	30
1.8.4.9 Nappamerri Group	30
1.8.4.9.1 Arrabury Formation	31
1.8.4.9.2 Tinchoo Formation	31
1.8.4.10 Cuddapan Formation	31
1.8.5 EROMANGA BASIN	32
1.9 PETROLEUM GEOLOGY OF THE COOPER BASIN	35
CHAPTER TWO METHODOLOGY	39
2.0 INTRODUCTION	39
2.1 LITERATURE REVIEW.	39
2.2 IDENTIFICATION OF MERRIMELIA FORMATION AND TIRRAWARRA SANDSTONE LITHOLOGIES	39
2.3 IDENTIFICATION OF WARBURTON BASIN LITHOLOGIES	42
2.4 LITHOLOGICAL LOGGING.	42
2.5 THIN SECTION SAMPLING.	43
2.5.1 MERRIMELIA FORMATION.	43
2.5.2 TIRRAWARRA SANDSTONE.	43
2.6 PETROLOGY TECHNIQUES.	44
2.6.1 POINT COUNTING AND PETROGRAPHY	44
2.6.2 THIN SECTION DESCRIPTIONS	45
2.7 X RAY DIFFRACTION (XRD) TECHNIQUES	46
2.8 MICROSCOPY TECHNIQUES.	46
2.8.1 CATHODOLUMINECENCE MICROSCOPY (CL)	46
2.8.2 FLUORESCENCE MICROSCOPY (FM)	46
2.8.2.1 Illite Fluorescence – An Introduction	47
2.8.3 REFLECTED LIGHT MICROSCOPY	47
2.8.4 SCANNING ELECTRON MICROSCOPY (SEM)	50
2.8.5 TRANSITION ELECTRON MICROSCOPY (TEM)	50
2.9 MICROPROBE TECHNIQUES.	50
2.10 K-AR DATING TECHNIQUES.	50
2.11 STATISTICAL TECHNIQUES	53
2.11.1 CLUSTER ANALYSIS	54
2.11.2 VARIOGRAM ANALYSIS	57
2.12 THERMAL MODELLING	59
CHAPTER THREE: GONDWANAN GLACIAL SETTING	60
3.0 PREAMBLE	60
3.1 INTRODUCTION	60
3.2 GONDWANAN GLACIATION IN AUSTRALIA	63
3.2.1. ALPINE STYLE GLACIATION	64
3.2.2 CONTINENTAL ICE SHEET GLACIATION	64
3.2.2.1 Western Australia	64
3.2.2.2 South Australia	65
3.2.2.3 Victoria and Tasmania	66
3.2.2.4 New South Wales	66
3.2.2.5 Queensland	66

3.3 CONTROLS ON GONDWANAN GLACIATION	67
3.4 CONCLUSIONS	67
CHAPTER FOUR: SEDIMENTOLOGY	69
4.0 INTRODUCTION	69
4.1 SEDIMENTOLOGY OF THE MERRIMELIA-TIRRAWARRA GLACIAL COMPLEX	71
4.2 SEDIMENTOLOGY OF THE MERRIMELIA FORMATION	72
4.2.1 TERMINOGLACIAL ENVIRONMENTS	72
4.2.1.1 TERMINOGLACIAL FACIES ASSOCIATIONS	76
4.2.1.1.1 Terminoglacial Tunnel Mouth Deposits (TTMD)	76
4.2.1.1.2 Rain-Out Diamictites (RD)	79
4.2.1.1.3 Terminoglacial Outwash Fan (TOF)	80
4.2.1.1.4 Terminoglacial Lucustrine Sand Flow (LSF)	81
4.2.1.1.5 Subaqueous Channel Gravel (SACG)	85
4.2.2 PROGLACIAL ENVIRONMENTS	86
4.2.2.1 PROGLACIAL FACIES ASSOCIATIONS	88
4.2.2.1.1 Proglacial Fluvial Outwash Plain Facies	88
A) Longitudinal Bar (LB)	89
B) Linguoid Bars (LIB)	92
C) Fluvial (FL)	93
D) Fluvial Bar Top (FBT)	94
E) Back Swamp (BS)	95
F) Discussion	95
4.2.2.1.2 Proglacial Aeolian Facies	96
A) Glacial Aeolian Dune (DU)	96
B) Glacial Aeolian Interdune (ID)	100
C) Discussion	100
4.2.2.1.3 Proglacial Deltaic And Lacustrine Facies	102
A) Lacustrine Shore Zone (LSZ)	102
B) Frozen Shore Zone (FSZ)	103
C) Delta Topsets (DTS)	104
D) Delta Foresets (DFS)	105
E) Delta Bottom sets (DBS)	109
F) Delta Flows (DF)	110
G) Deep Glacio-lacustrine (DGL)	111
4.3 FACIES TYPE, SORTING AND GRAIN SIZE	113
4.4 THE EVOLUTION OF THE MERRIMELIA-TIRRAWARRA GLACIAL COMPLEX	114
4.5 CONCLUSIONS	117
CHAPTER FIVE: FRAMEWORK COMPONENTS & PROVENANCE	119
5.0 INTRODUCTION	119
5.1 COMPOSITION	120
5.2 MERRIMELIA FORMATION: PETROGRAPHY AND PROVENANCE	122
5.2.1 FRAMEWORK COMPONENTS	122
5.2.1.1 Quartz Grain Component: Petrography And Provenance	124
5.2.1.1.1 Petrography and Provenance	124
5.2.1.2 Rock Fragment Component: Composition And Provenance	126
5.2.1.3 Rock Fragment Component: Petrography	131
5.2.1.3.1 Sedimentary Rock Fragments: Petrography	131
5.2.1.3.2 Volcanic Rock Fragments: Petrography	134

A) Rhyodacite Rock Fragments	135
i) Spherulite Rhyodacite Rock Fragments	138
ii) Devitrified Acid Volcanic Rock Fragments	138
iii) Hyaloclastite And Granoblastic Rhyolite Rock Fragments	141
B) Pyroclastic Rock Fragments	141
C) Basic Volcanic Rock Fragments	142
i) Trachytic Basalt Rock Fragments	142
ii) Amygdaloidal Rock Fragments	142
iii) Ultrabasic Rock Fragments	142
5.2.1.3.3 Micro-Pegmatite And Granite Rock Fragments: Petrography	142
A) Micro-Pegmatite Rock Fragments	142
B) Granitic Rock Fragments	145
i) Graphic Textured Granite Rock Fragments	145
ii) Granular Granite Rock Fragments	145
5.2.1.3.4 Metamorphic Rock Fragments: Petrography	148
A) Low Grade Metamorphic Rock Fragments	149
B) Phyllite Rock Fragments	149
C) Schist And Gneissic Rock Fragments	149
D) Psammite And Pelite Rock Fragments	152
E) Quartzite Rock Fragments	152
F) Meta-Acid Volcanic Rock Fragments	152
G) Meta-Poly-Crystalline Quartz Grains Rock Fragments	153
5.2.1.3.5 Feldspar And Accessory Component: Petrography	153
A) Feldspar	153
B) Micas	156
C) Accessory Minerals	156
5.2.1.2.6 Organic Matter And Soil Development	156
5.2.2 FACIES CONTROL ON SEDIMENT COMPOSITION	159
5.2.3 COMPETENT AND INCOMPETENT ROCK FRAGMENTS	159
5.3 TIRRAWARRA SANDSTONE: PETROGRAPHY AND PROVENANCE	161
5.4 RELATIONSHIP BETWEEN THE TIRRAWARRA SANDSTONE AND MERRIMELIA FORMATION	166
5.5 ROCK FRAGMENT PROVENANCE: RESULTS AND DISCUSSION	168
5.5.1 STATISTICS INTRODUCTION	168
5.5.1.1 Pearson Correlation Coefficients	168
5.5.1.2 Principle Components Analysis (PCA)	170
5.5.1.3 Cluster Analysis	171
5.5.2 ROCK FRAGMENT MOVEMENTS IN THE COOPER BASIN: DISCUSSION	176
5.5.2.1 Metamorphic Rock Fragments	176
5.5.2.1.1 Rock Fragment Domains: A Discussion	176
A) Rock Fragment Mixing Zone: A Discussion	180
5.5.2.2 Volcanic Rock Fragments	180
5.5.3 CHANGES IN SEDIMENT INPUT DIRECTIONS THROUGH TIME	182
5.6 CONCLUSIONS	184
CHAPTER SIX AUTHIGENIC COMPONENT & DIAGENESIS	187
6.0 INTRODUCTION	187
6.1 STATISTICS	188
6.2 PETROGRAPHY	190

6.2.1 QUARTZ CEMENT	190
6.2.2 AUTHIGENIC CLAYS	193
6.2.2.1 Illite	195
6.2.2.1.1 Illite Literature Review	195
6.2.2.1.2 Distribution Of Illite In The Merrimelia Formation	198
6.2.2.1.3 Illite In The Merrimelia Formation: Nature And Composition	200
6.2.2.1.4 Illite In The Merrimelia Formation: Optical Petrography	202
A) <i>Air Drying Effects On Illite</i>	202
B) <i>Illite Morphologies</i>	205
C) <i>Illite Textures</i>	208
6.2.2.2 Glauconitic Illite	208
6.2.2.3 Kaolin	211
6.2.2.4 Dickite	211
6.2.2.5 Chlorite	211
6.2.3.6 Pyrophyllite	213
6.2.3. CARBONATE CEMENT	213
6.2.3.1 Siderite	213
6.2.3.1.1 S1 – Early Siderite cement Phase	220
6.2.3.1.2 S2 – Mid Siderite cement Phase	222
A) <i>S2a – Siderite Cement Zone</i>	222
B) <i>S2b - Siderite Cement Zone</i>	222
6.2.3.1.3 – S3 Late Siderite Cement Phase	222
A) <i>S3a – Siderite Cement Zone</i>	225
B) <i>S3b – Siderite Cement Zone</i>	225
6.2.3.2 Ferroan Dolomite/Ankerite	225
6.2.3.3 Calcite	225
6.2.4 OPAQUE CEMENTS: PYRITE, GOETHITE AND LEUCOXENE	227
6.2.5 MATRIX COMPONENT	227
6.2.5.1 Argillaceous Matrix	227
6.2.5.2 Pseudo-Matrix	230
6.3 DIAGENESIS OF MERRIMELIA SEDIMENTS	230
6.3.1 THE EFFECT OF ELEVATED BASIN TEMPERATURES ON DIAGENESIS	230
6.3.2 SUMMARY OF PARAGENESIS	231
6.3.3 SUMMARY OF DIAGENESIS	233
6.3.4 DIAGENETIC EVENTS IN THE MERRIMELIA FORMATION	235
6.3.4.1 Mechanical Compaction	235
6.3.4.1.1 Key Observations	235
6.3.4.1.2 Discussion	237
6.3.4.1.3 Key Findings	237
6.3.4.2 Quartz Authigeneis	240
6.3.4.2.1 Early Quartz Cementation and Co-Genetic Illite and Kaolin	240
A) <i>Key Observations</i>	240
B) <i>Discussion</i>	240
C) <i>Key Findings</i>	244
6.3.4.2.2 Chemical Compaction/Late Quartz Cementation	244
A) <i>Chemical Compaction</i>	244
i) <i>Key Observations</i>	245
ii) <i>Discussion</i>	245
iii) <i>Key Findings</i>	249

B) Late Quartz Cementation	249
i) Key Observations	249
ii) Discussion	250
iii) Key Findings	253
6.3.4.3 Clay Diagenesis	253
6.3.4.3.1 Illite Authigenesis	253
A) Key Observations	253
B) Discussion: Illite Diagenesis, A Review	257
i) Controls On Illite Formation	257
ii) Smectite To Illite Transformation	259
a) The Interlayer Model	259
b) The Interparticle Model	259
c) Interparticle And Interlayer Models: A Discussion	259
d) Cation Sources For Smectite/Illite Transformation Models	260
iii) Neoformation Of Illite	261
C) Illite Formation Mechanisms In The Merrimelia Fm.	
i) Illite Growth In The Merrimelia Fm.	261
ii) Smectite/Illite Transformation Merrimelia Sediments	262
iii) Sources Of Detrital Clay In Merrimelia Sediments	265
iv) Formation Of Illite Textures Observed In The Merrimelia Formation	267
a) Illitisation Of Labile Components	267
b) Grain Coating Clay	267
c) Formation Of Illite Coatings In Glacio-Aeolian Sandstones	273
d) Formation Of Flame/Filamentous Illite Textures	275
e) Formation Of Honeycomb/ Filamentous Textures	275
v) Neoformation Of Illite In Merrimelia Sediments	275
vi) Illitisation Of Kaolin	279
vii) Illite Authigenesis In Merrimelia Sediments: Open Or Closed Diagenesis?	282
D) Key Findings	283
6.3.4.3.2 Segregation Of Illite And Kaolin	283
A) Key Observation	283
B) Discussion	283
C) Key Findings	284
6.3.4.3.3 Feldspar Dissolution	285
A) Key Observations	285
B) Discussion	285
C) Key Findings	287
6.3.4.3.4 Kaolin Authigenesis	287
A) Key Observations	287
B) Discussion	288
C) Key Finding	289
6.3.4.3.5 Kaolin Formation And S2 Siderite Dissolution	289
A) Key Observation	289
B) Discussion	289

C) Key Finding	290
6.3.4.3.6 Dickite Authigenesis	290
A) Key Observations	290
B) Discussion	290
C) Key Finding	290
6.3.4.3.7 Chlorite Formation	291
A) Key Observations	291
B) Discussion	291
C) Key Findings	292
6.3.4.4 Carbonate Authigenesis	292
6.3.4.4.1 S1 Siderite Formation	292
A) <i>Key Observations</i>	292
B) <i>Discussion</i>	293
C) <i>Key Finding</i>	293
6.3.4.4.2 D1 Early Siderite Dissolution	293
A) <i>Key Observations</i>	293
B) <i>Discussion</i>	293
C) <i>Key Findings</i>	294
6.3.4.4.3 S2 Siderite Formation	294
A) <i>Key Observations</i>	294
B) <i>Discussion</i>	294
C) <i>Key Findings</i>	299
6.3.4.4.4 D2 Late Siderite Dissolution	301
A) <i>Key Observations</i>	301
B) <i>Discussion</i>	301
C) <i>Key Findings</i>	302
6.3.4.4.5 S3 Siderite Formation	302
A) <i>Key Observations</i>	302
B) <i>Discussion</i>	302
C) <i>Key Findings</i>	303
6.3.4.4.6 Calcite (Twinned, Cowpat) Formation	303
A) <i>Key Observations</i>	303
B) <i>Discussion</i>	303
i) <i>Cowpat Calcite</i>	306
C) <i>Key Findings</i>	308
6.3.4.4.7 Ferroan Dolomite Authigenesis	308
A) <i>Key Observation</i>	308
B) <i>Discussion</i>	309
C) <i>Key Findings</i>	308
6.3.4.5 Secondary Porosity Formation	309
6.3.4.5.1 Key Observation	309
6.3.4.5.2 Discussion	310
6.3.4.5.3 Key Findings	311
6.3.4.6 Feldspar Overgrowths	312
6.3.4.6.1 Key Observations	311
6.3.4.6.2 Discussion	311
6.3.4.6.3 Key Finding	312
6.3.4.7 Pyrite Authigenesis	312
6.3.4.7.1 Key Observations	312
6.3.4.7.2 Discussion	312
6.3.4.7.3 Key Finding	312
6.3.4.8 Pyrophyllite Authigenesis	313

6.3.4.8.1 Key Observation	313
6.3.4.8.2 Discussion	313
6.3.4.8.3 Key Finding	313
6.3.4.9 Zeolite(?)	313
6.3.4.9.1 Key Observation	313
6.3.4.9.2 Discussion	313
6.3.4.9.3 Key Finding	315
6.4 PARAGENETIC SEQUENCE: REGIONAL VARIATIONS	315
6.5 FACIES CONTROLS ON DIAGENESIS	316
6.6 DISTRIBUTION OF AUTHIGENIC MINERALS	318
6.7 CONCLUSIONS	323

VOLUME TWO

TABLE OF CONTENTS: VOLUME TWO	<i>i-iv</i>
--------------------------------------	-------------

CHAPTER SEVEN: ILLITE FLUORESCENCE	329
7.0 INTRODUCTION	329
7.1 A REVIEW OF LUMINESCENCE IN GEOLOGY	329
7.2 INITIAL OBSERVATIONS	332
7.3 POSSIBLE CAUSES OF ILLITE FLUORESCENCE	335
7.3.1 ILLITE FLUORESCENCE: EXPERIMENT DESIGN AND RESULTS	335
7.3.2 OTHER POSSIBLE CAUSES OF ILLITE FLUORESCENCE	338
7.4 UTILISING THE FLUORESCENCE OF ILLITE	341
7.4.1 ILLITE FLUORESCENCE AND ILLITE DIAGENESIS	341
7.4.2 ESTIMATING ILLITE PROPORTIONS: ILLITE FLUORESCENCE TECHNIQUE	344
7.4.3 ILLITE FLUORESCENCE AND RESERVOIR QUALITY	345
7.4.4 SUMMARY	347
7.5 CONCLUSIONS	347
CHAPTER EIGHT PARAGENETIC MODEL	349
8.0 INTRODUCTION	349
8.1 THERMAL HISTORY MODEL	350
8.1.1 MODEL CONSTRUCTION	350
8.2 ILLITE DATING PILOT STUDY	358
8.2.1 ILLITE DATING PILOT STUDY: DESCRIPTION AND LIMITATIONS	358
8.2.2 ILLITE DATING: THE EFFECT OF OPEN AND CLOSED DIAGENETIC SYSTEMS	360
8.2.3 ILLITE DATING: PRELIMINARY RESULTS	361
8.2.4 ILLITE DATING: DIAGENETIC OBSERVATIONS	361
8.2.5 ILLITE DATING: PRELIMINARY INTERPRETATIONS	362
8.2.5.1 Illite Dates And The Thermal Regime In The Cooper Basin	362
8.2.5.2 Illite Formation And The Applicability Of K-Ar Illite Dating To Cooper Basin Sediments	363
8.3 MERRIMELIA-TIRRAWARRA DIAGENESIS MODEL INTERGRATION	364
8.3.1 THERMAL MODEL INTEGRATION	364
8.3.2 DIAGENETIC MODEL INTEGRATION	365
8.3.2.1 Diagenetic And Thermal Model: Implications For Siderite Cementation	368
8.4 CONCLUSIONS	370

CHAPTER NINE: RESERVOIR DEVELOPMENT & QUALITY	372
9.0 INTRODUCTION	372
9.1 CONTROLS ON RESERVOIR DEVELOPMENT	372
9.1.1 GONDWANAN GLACIATION: A REVIEW	372
9.1.2 DEVELOPMENT OF RESERVOIR UNITS IN THE MERRIMELIA-TIRRAWARRA GLACIAL COMPLEX	373
9.1.3 PROVENANCE ANALYSIS AND FACIES CORRELATIONS	379
9.1.4 TERMINOGLACIAL AND PROGLACIAL SEDIMENTS: RESERVOIR QUALITY	379
9.2 CONTROLS ON RESERVOIR QUALITY	380
9.2.1 PROVENANCE	381
9.2.2 FACIES TYPE	385
9.2.2.1 Merrimelia Formation; Cooper Basin, Australia	385
9.2.2.2 Lower Haushi Group; Dohfar Province, Oman	389
9.2.2.3 Discussion	390
9.2.3 RESERVOIR QUALITY CONTROLS: FACIES TYPE VERSUS PROVENANCE	394
9.2.4 CONTROLS ON POROSITY IN MERRIMELIA SEDIMENTS	395
9.2.4.1 Thermal Regime And Illite/Quartz Cement	395
9.2.4.2 Controls On Porosity	399
9.2.4.2.1 Preservation Of Primary Pore Space	401
A) <i>Primary Pore Space Preservation In Terminoglacial and Proglacial Sediments</i>	401
B) <i>Compaction Model For The Merrimelia Formation</i>	403
9.2.4.2.2 Controls On Secondary Pore Space Evolution	417
A) <i>Intragranular Secondary Porosity</i>	418
B) <i>Carbonate Dissolution</i>	421
9.2.5 CONTROLS ON PERMEABILITY IN MERRIMELIA SEDIMENTS	423
9.2.5.1 Controls On Permeability: Kaolin And Illite	423
9.2.5.2 Controls On Permeability: Ductile Rock Fragments	425
9.2.5.3 Controls on Permeability: Formation Damage	427
9.2.5.4 Controls On Permeability: Illite Morphology	430
9.2.5.5. Controls On Permeability: Glacial Sedimentation	430
9.2.5.6 Permeability Controls: Summary	433
9.3 CASE STUDIES: MALGOONA AND MERRIMELIA FIELDS	433
9.3.1 MALGOONA FIELD	433
9.3.2 MERRIMELIA FIELD	439
9.3.2.1 Introduction	439
9.3.1.2 High Porosity And Low Porosity Zones	441
9.3.2.3 Sedimentation And Diagenesis Controls On Reservoir Quality	448
9.4 CONCLUSIONS	453
CHAPTER TEN: CONCLUSIONS & RECOMENDATIONS	457
10.1 CONCLUSIONS	457
10.1.1 RESERVOIR DEVELOPMENT IN A GLACIAL SEQUENCE	457
10.1.2 RESERVOIR QUALITY CONTROLS IN A GLACIAL SEQUENCE	460
10.2 RECOMMENDATIONS	469
10.2.1 K-AR ILLITE DATING STUDY	469
10.2.2 PROVENANCE ANALYSIS STUDY	469
10.2.3 CAUSE OF ILLITE FLUORESCENCE STUDY	469
CHAPTER ELEVEN: BIBLIOGRAPHY	471

APPENDICES (Appendices 1-10 on CD ROM)**Appendix One: Palynology Results****Appendix Two: Lithological Tops****Appendix Three: Thin Section Lists**

- A) *Merrimelia Formation*
- B) *Tirrawarra Sandstone*
- C) *Warburton Basin*

Appendix Four: Rock Fragment Data

- A) *Rock Fragment Lithology Definitions*
- B) *Rock Fragment Provenance Discussion*
- C) *Rock Fragment Percentages*

Appendix Five: Compositional Data

- A) *Whole Rock Compositions*
- B) *Framework Component Compositions*
- C) *Authigenic Component Compositions*

Appendix Six: K-Ar Analytical Procedures

- A) *Argon Determination*
- B) *Potassium Determination*

Appendix Seven Quantitative XRD Table**Appendix Eight Statistics**

- A) *Pearson Correlation Tables*
 - I) *Merrimelia*
 - II) *Tirrawarra*
- B) *Cluster Dendrograms*
 - I) *Merrimelia*
 - II) *Tirrawarra*
- C) *Variograms*

Appendix Nine: Lithology Logs and Thin Section Descriptions

- A) *Lithology Logs*
- B) *Thin Section Descriptions*
 - I) *Merrimelia*
 - II) *Tirrawarra*
 - III) *Warburton*

Appendix Ten: Exploration History of the Cooper Basin**Appendix Eleven Publications (Paper Copy)**

Chaney A.J., Cubitt C.J. and Williams B.P.J. (1997) Reservoir Potential of Glacio-Fluvial Sandstones: Merrimelia Formation, Cooper Basin, South Australia.

Cubitt C.J., Chaney A. and Gravestock D.I. (1998) Merrimelia Formation.

Cubitt C.J. and Kaiko A. (2000) Illite, The Key to Understanding Reservoir Quality in the Merrimelia Formation; Cooper Basin, South Australia.

LIST OF FIGURES

CHAPTER ONE: INTRODUCTION		
Figure 1.1	Late Palaeozoic Sedimentary Basins On The Australian Portion Of Gondwana.	2
Figure 1.2	Cooper Basin Location Map With Major Fields Marked.	4
Figure 1.3	Stratigraphy of The Warburton, Cooper And Eromanga Basins.	6
Figure 1.4	Stratigraphic Column Of The Cooper Basin.	7
Figure 1.5	Lower Gidgealpa Group Stratigraphic Table.	8
Figure 1.6	Stratigraphy Of Late Carboniferous-Early Permian Basins Adjacent To The Cooper Basin.	11
Figure 1.7	Schematic Model Of The Merrimelia-Tirrawarra Depositional System.	13
Figure 1.8	Isopach Map Of The Tirrawarra Sandstone And Merrimelia Formation.	17
Figure 1.9	Structural Elements Of The Cooper Basin, South Australia And Queensland.	20
Figure 1.10	Eastern Warburton Basin Sub-Cropping Lithologies.	22
Figure 1.11	Magnetic Intensity Map Of The Cooper Basin.	26
Figure 1.12	Cooper Basin Infrastructure Map.	36
CHAPTER TWO: METHODOLOGY		
Figure 2.1	Thin Section Naming Convention.	43
Figure 2.2	K-Ar Dating Sample Selection And Clay Fraction Separation Procedures.	52
Figure 2.3	Illite Sample Purity Assessment Procedures.	53
Figure 2.4	Cluster Analysis Procedure.	55
Figure 2.5	An Example Of A Cluster Dendrogram Displaying Two Data Groupings.	56
Figure 2.6	Theoretical Semivariogram.	58
CHAPTER THREE: GONDWANAN GLACIAL SETTING		
Figure 3.1	Inferred Gondwanan Ice Volumes.	61
Figure 3.2	Icesheet Development Across Gondwana From Late Devonian To Late Westphalian.	62
Figure 3.3	Ice Cap Wander Path Across The Gondwana Super Continent .	63
Figure 3.4	Location Of Ice Cap On The Australian And Antarctic Continents.	63
Figure 3.5	Ice Sheet Location On The Australian Continent.	65
CHAPTER FOUR: SEDIMENTOLOGY		
Figure 4.1	Model Of The Merrimelia-Tirrawarra Glacial Complex (MTGC).	70
Figure 4.2	A Model Of The Terminoglacial Depositional Realm.	73
Figure 4.3	Typical Diurnal And Monthly Run Off Hydrographs In A Glacial System.	74
Figure 4.4	Meltwater Hydrographs.	75
Figure 4.5	Proglacial Depositional Realm.	87
Figure 4.6	Basin Topography And Proglacial Environments.	88
Figure 4.7	Delta Sediments.	104
Figure 4.8	Sediment Flow Regimes In A Lacustrine Setting.	109
Figure 4.9	Evolution Of The Merrimelia-Tirrawarra Glacial Complex (MTGC) (M1, M2, M3 & T1).	115
Figure 4.10	Merrimelia Formation: Rock Fragments Versus Depth (Merrimelia Datums, M1, M2 And M3 Are Indicated).	116

CHAPTER FIVE: FRAMEWORK COMPONENTS & PROVENANCE

Figure 5.1 Petrographic Composition Of The Merrimelia Formation.	120
Figure 5.2 Composition Of The Merrimelia Formation.	121
Figure 5.3 Geological Provinces Surrounding The Cooper Basin.	122
Figure 5.4 Distributions Of Straight, Undulose And Poly-Crystalline Quartz Framework Grains.	123
Figure 5.5 Trend Maps Of Undulose And Straight Extinction Quartz Grains: Merrimelia Formation.	125
Figure 5.6 Statistically Significant Rock Fragment Types: Merrimelia Formation.	127
Figure 5.7 Rock Fragment Lithologies In The Merrimelia Formation.	127
Figure 5.8 Frequency Histogram Of Volcanic Rock Fragment In Merrimelia Sediments.	134
Figure 5.9 Composition Of Volcanics In The Warburton Basin.	135
Figure 5.10 Mooracoochie Volcanics Facies Associations.	138
Figure 5.11 Rock Fragment Domains Overlain By The Distribution Of Graphic Textured Granite In The Merrimelia Formation And Tirrawarra Sandstone.	148
Figure 5.12 Histogram Of Metamorphic Rock Fragments In Merrimelia Sediments.	149
Figure 5.13 Principle Components Analysis (PCA) Of Rock Fragments From The Tirrawarra Sandstone.	162
Figure 5.14 Merrimelia Formation And Tirrawarra Sandstone Rock Fragment Comparison.	163
Figure 5.15 Rock Fragment Proportions In The Tirrawarra Sandstone.	164
Figure 5.16 Quartz Vs Rock Fragment Scattergrams: Merrimelia Formation And Tirrawarra Sandstone	165
Figure 5.17 Rock Fragment Movements In The South Australian Portion Of The Cooper Basin.	167
Figure 5.18 Positive And Negative Pearson Correlation Coefficients Plots.	169
Figure 5.19 Cluster Dendrogram Of Competent Rock Fragment Types: Merrimelia Formation.	173
Figure 5.20 Cluster Dendrogram Of Competent Rock Fragment Types: Tirrawarra Sandstone.	175
Figure 5.21 Inferred Movement Of Competent Rock Fragments In The Merrimelia Formation.	177
Figure 5.22 Comparison Of Basement Highs Of The Present Day Antarctic Margin And The Permo-Carboniferous Cooper Basin (SA Sector).	179
Figure 5.23 Eastern Warburton Basin Sub-Cropping Lithology Map.	181
Figure 5.24 Variation Of Sediment Input Directions Into The South Australian Sector Of The Cooper Basin During Merrimelia Formation And Tirrawarra Sandstone Deposition.	183

CHAPTER SIX: AUTHIGENIC COMPONENT & DIAGENESIS

Figure 6.1 Authigenic Mineral Statistics: Merrimelia Formation.	189
Figure 6.2 Clay Proportions In Merrimelia Sediments.	194
Figure 6.3 The Basic Structure Of The Most Common Clays Observed In Merrimelia Sediments.	197
Figure 6.4 Illite And Ductile Rock Fragment Trend Maps.	199
Figure 6.5 Illite Identification.	201
Figure 6.6 Kaolin And Chlorite Clay Identification.	212
Figure 6.7 Carbonate Cements; Composition And Sample Frequency.	214
Figure 6.8 Pore Fill, "Seed" And Patch Siderite Cement Morphologies.	219
Figure 6.9 Siderite Cement Identification.	221
Figure 6.10 Ferroan Dolomite/Ankerite Identification.	224
Figure 6.11 Calcite Cement Identification.	226

Figure 6.12	Rates Of Quartz Precipitation Versus Mean Precipitation Temperature.	231
Figure 6.13	Mechanical Compaction Of Ductile-Rich Merrimelia Sediments.	236
Figure 6.14	Stylolite Quartz Cementation Model.	248
Figure 6.15	Quartz Cement Volume Percentages Versus Depth.	249
Figure 6.16	Quartz Cementation In A Arenaceous/Argillaceous System.	250
Figure 6.17	Ranked Cumulative Histogram Of Illite Proportion Versus Facies Type.	256
Figure 6.18	Illite Growth Stages.	262
Figure 6.19	Water Expulsion Volumes Arising From The Transformation Of S/I.	264
Figure 6.20	Palaeolatitude Positions Of The Cooper Basin During Patchawarra Formation, Merrimelia Formation And Tirrawarra Sandstone Deposition.	266
Figure 6.21	Identification Of Inherited Clay Rims.	273
Figure 6.22	Cartoon Of "Open And Closed" Diagenetic Systems Operating In Merrimelia Sediments.	276
Figure 6.23	Illite Growth Rates.	278
Figure 6.24	Feldspar Proportion In Merrimelia Formation Sediments.	287
Figure 6.25	Scattergram Of Kaolin Proportion Versus Depth.	288
Figure 6.26	Ranked Cumulative Histogram Of Kaolin Proportions In Merrimelia Facies.	289
Figure 6.27	Mg ²⁺ Proportions In S1, S2, And S3 Siderite Phases.	298
Figure 6.28	Organic Maturation And The Main Diagenetic Adjustments Observed In The Merrimelia Formation.	300
Figure 6.29	Scattergram Of Rigid Grain Content Versus The Maximum Amount Of Secondary Porosity.	311
Figure 6.30	Pyrophyllite, Zeolite And Feldspar Overgrowths.	314
Figure 6.31	Paragenetic Sequences In Argillaceous And Arenaceous Merrimelia Sediments.	315
Figure 6.32	Regional Paragenetic Sequences.	317
Figure 6.33	Quartz Cement And Clay Proportions Along With Rock Fragment Percentages Of Merrimelia Facies.	319
Figure 6.34	Scattegrams Of Illite Versus Quartz Cement Proportions And Quartz cement Versus Kaolin Proportions In Merrimelia Sediments.	320
Figure 6.35	Cluster Dendrogram Of Illite, Kaolin And Quartz In Merrimelia Sediments.	321
Figure 6.36	Rock Fragment And Illite Trend Maps.	322
CHAPTER SEVEN: ILLITE FLUORESCENCE		
Figure 7.1	The Nature Of Luminescence, Illustrating CL And UV Emissions.	330
Figure 7.2	Quantum Principle Of Fluorescence.	331
Figure 7.3	Illite Proportions Estimated Using Illite Fluorescence.	346
CHAPTER EIGHT: PARAGENETIC MODEL		
Figure 8.1	Cartoon Of Heat Transfer Mechanism Involving Cooper Basin Sediments And Upper Eromanga Basin Aquifers.	351
Figure 8.2	Cooper/Eromanga Basins Heat Flow Evolution Diagram.	351
Figure 8.3	Eromanga And Lake Eyre Basin Aquifers.	352
Figure 8.4	Gidgeapla #7 Maturity Profile.	353
Figure 8.5	Heatflow (mw/m ²) Versus Time In Study Wells Merrimelia #18 And Malgoona #4.	354
Figure 8.6	Heatflow Map In °C/100m For The Cooper Basin.	355
Figure 8.7	Vitrinite Reflectance And Maturity Profiles Of Merrimelia #18 And Malgoona #4.	356
Figure 8.8	Geohistory Diagrams Constructed Of Merrimelia #18 And Malgoona #4.	357
Figure 8.9	Illite Fraction Size And Effect On Illite Dating.	359

Figure 8.10 Geothermal Gradients Relative To Basin Fill Sediments And Crystalline Basement In The Cooper Basin.	362
Figure 8.11 Combined Merrimelia-Tirrawarra Paragenetic Sequence.	366
Figure 8.12 Geohistory Analysis And S2 Siderite Composition.	369
Figure 8.13 Scattergrams Of Mg ²⁺ Proportions In S1, S2 And S3 Siderite Phases With Depth.	370
CHAPTER NINE: RESERVOIR DEVELOPMENT & QUALITY	
Figure 9.1 Evolution Of Gondwanan Ice Cover And Resulting Sedimentation.	374
Figure 9.2 A) Porosity Versus Facies Type Cumulative Histogram. B) A Comparison Of The Facies Nomenclature Used By Chaney, (1998) And The Facies Nomenclature Used In This Study.	382
Figure 9.3 Flow Chart Illustrating The Main Parameters Controlling Reservoir Quality In Merrimelia-Tirrawarra Glacial Sediments.	383
Figure 9.4 Ranked Rock Fragment Compressibility Index And Rock Fragment Statistics For The Merrimelia Formation And Tirrawarra Sandstone.	384
Figure 9.5 Quartz Percentage, Rock Fragment Percentage And Sorting Coefficients Of Merrimelia And Tirrawarra Sediments.	387
Figure 9.6 Schematic Illustrating The Location Of Facies Types Within The Merrimelia-Tirrawarra Glacial Complex.	389
Figure 9.7 Merrimelia-Tirrawarra Sedimentation Model For The Big Lake Field.	391
Figure 9.8 Reservoir Potential Map Of The Merrimelia And Tirrawarra Sandstone.	393
Figure 9.9 A Comparison Of Porosity In Merrimelia And Tirrawarra Sediments.	397
Figure 9.10 Compaction Indices Versus Quartz Cement Proportion.	402
Figure 9.11 Reduction Of Primary Porosity By Ductile Grain Squeezing.	407
Figure 9.12 Ductile Rock Fragment And Compaction Index (CI) Trend Maps.	409
Figure 9.13 Ductile Grain Compaction Scenarios.	410
Figure 9.14 Ductile Grain Composition And Compaction.	411
Figure 9.15 Cartoon And Image Of A Ductile Rock Fragment Squeezing Into Pore Space.	412
Figure 9.16 Cumulative Histogram Showing Porosity Loss By Ductile Grain Squeezing.	413
Figure 9.17 Sorting And Grain Size Criteria: Merrimelia Formation.	415
Figure 9.18 Cartoon Illustrating The Compaction Effects Of Compressible Clasts.	416
Figure 9.19 Porosity Occlusion Ratio (OR) For The Merrimelia Formation.	417
Figure 9.20 Carbonate (Siderite) Dissolution.	422
Figure 9.21 Illite Micro-Pore Space.	424
Figure 9.22 Permeability Effects Of Kaolin And Illite Clay.	426
Figure 9.23 The Effects Of Clay Morphology On Permeability.	427
Figure 9.24 Permeability And Porosity Effects Of The Main Authigenic Minerals Observed In Merrimelia Sediments.	428
Figure 9.25 Clay Filled And Clay Free Porosity.	429
Figure 9.26 Compaction Index (CI) Vs Rock Fragment Proportions In Merrimelia Sediments.	432
Figure 9.27 Malgoona Field: Location, Play Concept And Core Images.	434
Figure 9.28 Malgoona #4: Dip Meter Log (7125'-7155').	436
Figure 9.29 Malgoona #4: Fluorescent Core Image (7125'-7155').	438
Figure 9.30 Merrimelia Field: Location, Play Concept And Core Images.	440
Figure 9.31 Merrimelia Field: Glacio-Aeolian Sandstone Evolution.	442
Figure 9.32 Cartoon Of Low And High Porosity Zones (LPZs And HPZs) Diagenetic Adjustments And Resulting Permeability Barriers.	451
Figure 9.33 Permeability Barriers And Flow Units Within The Rotliegend Reservoir, North Sea.	452

LIST OF PLATES

PLATE 1	Warburton Basin/Merrimelia Formation Lithologies.	15
PLATE 2	Tirrawarra, Merrimelia & Warburton Basin Lithologies.	41
PLATE 3	Fluorescence Illite: An Introduction.	49
PLATE 4	TEM Sample Purity.	51
PLATE 5	Terminoglacial Lithologies: 1.	78
PLATE 6	Terminoglacial Lithologies: 2.	84
PLATE 7	Proglacial Lithologies :1.	91
PLATE 8	Proglacial Lithologies: 2.	98
PLATE 9	Proglacial Lithologies: 3.	107
PLATE 10	Quartz Grain Types.	124
PLATE 11	Sedimentary Rock Fragments: 1.	133
PLATE 12	Acid Volcanic Rock Fragments (Rhyodacite): 1.	137
PLATE 13	Acid Volcanic Rock Fragments (Rhyodacite & Pyroclastic): 2.	140
PLATE 14	Basic Volcanic & Pegmatitic Rock Fragments: 1.	144
PLATE 15	Granitic & Metamorphic Rock Fragments.	147
PLATE 16	Metamorphic Rock Fragments.	151
PLATE 17	Accessory Detrital Minerals: 1.	155
PLATE 18	Accessory Detrital Minerals: 2.	158
PLATE 19	Authigenic Minerals: Quartz Cement.	192
PLATE 20	Authigenic Minerals: Pyrophyllite & Illite.	204
PLATE 21	Authigenic Minerals: Illite: Illite Morphologies.	207
PLATE 22	Authigenic Minerals: Illite: Illite textures and Glauconitic Illite.	210
PLATE 23	Authigenic Minerals: Siderite Cement.	217
PLATE 24	Authigenic Minerals: Matrix, Psuedo-Matrix & Accessory Minerals.	229
PLATE 25	Compactional Effects.	239
PLATE 26	Paragenetic Relationships: Quartz Cement, Siderite, Kaolin & Illite.	243
PLATE 27	Diagenetic Reactions: Chemical Compaction.	247
PLATE 28	Authigenic Minerals: Drusy Quartz Cement.	252
PLATE 29	Authigenic Mineral: Illite.	255
PLATE 30	Authigenic Minerals: Illitisation Of Rock Fragments.	269
PLATE 31	Authigenic Minerals: Relationship Between Illite Clay Rims And Syntaxial Quartz Cement.	272
PLATE 32	Diagenetic Reactions: Illitisation Of Kaolin And Co-Genetic Siderite/Kaolin.	281
PLATE 33	Siderite Precipitation And Dissolution.	296
PLATE 34	Authigenic Mineral: Calcite.	305
PLATE 35	Illite Fluorescence: Initial Observations.	334
PLATE 36	Illite Fluorescence: Experimental Results.	337
PLATE 37	Illite Fluorescence: Fluorescence Intensity.	340
PLATE 38	Illite Fluorescence: Illite, Kaolin And Siderite.	343
PLATE 39	Porosity Development: 1.	405
PLATE 40	Porosity Development: 2.	420
PLATE 41	Glacio-Aeolian Sandstone: Reservoir Characteristics.	445
PLATE 42	Poikilotopic Calcite Cement In Glacio-Aeolian Sandstones.	447
PLATE 43	Grain Coating Illite In Glacio-Aeolian Sandstones.	449

LIST OF TABLES

CHAPTER TWO: METHODOLOGY	
Table 2.1 Accuracy Of Petrographical Estimations.	45
CHAPTER FOUR: SEDIMENTOLOGY	
Table 4.1 Sorting Coefficient Ranges.	71
Table 4.2 Terminoglacial Tunnel Mouth Deposits (TTMD).	76
Table 4.3 Rain Out Diamictite (RD).	79
Table 4.4 Terminoglacial Outwash Fan (TOF).	81
Table 4.5 Terminoglacial Lacustrine Sand Flow (LSF).	82
Table 4.6 Subaqueous Channel Gravel (SACG).	85
Table 4.7 Longitudinal Bars (LB).	92
Table 4.8 Linguoid Bars (LIB).	93
Table 4.9 Fluvial Sandstone Facies (FL).	94
Table 4.10 Fluvial Bar Top Facies (FBT).	94
Table 4.11 Dune (DU) And Interdune (ID) Facies.	101
Table 4.12 Lacustrine Shore Zone (LSZ) And Frozen Shore Zone (FSZ) Facies.	103
Table 4.13 Delta Topsets (DTS).	105
Table 4.14 Delta Foresets (DFS).	108
Table 4.15 Delta Bottom Set Facies.	110
Table 4.16 Delta Flow Facies (DF).	111
Table 4.17 Deep Glacio-Lacustrine Rhythmites (DGL).	113
Table 4.18 Facies Type Vs Grain Size, Sorting, Quartz And Rock Fragment Proportions.	113
CHAPTER FIVE: FRAMEWORK COMPONENTS & PROVENANCE	
Table 5.1 Average Percentages Of Quartz Framework Component.	124
Table 5.2 Rock Fragment Percentages: Merrimelia Formation And Tirrawarra Sandstone.	128
Table 5.3 Rock Fragment Type And Relevant Thin Section Description.	129
Table 5.4 Summary Of Sediment Provenance: Merrimelia Formation.	130
Table 5.5 Rutile Microprobe Composition.	156
Table 5.6 Facies Vs Rock Fragment And Quartz Percentages.	160
Table 5.7 Competent And Incompetent Rock Fragment Types.	161
Table 5.8 Pearson Correlation Coefficients For Selected Tirrawarra And Merrimelia Rock Fragments.	169
Table 5.9 Results Of Kolmogorov-Smirnov And Shapiro-Wilks Tests Of Normality (Merrimelia Formation).	171
Table 5.10 Results Of Kolmogorov-Smirnov And Shapiro-Wilks Tests Of Normality (Tirrawarra Sandstone).	174
CHAPTER SIX: AUTHIGENIC COMPONENT & DIAGENESIS	
Table 6.1 Microprobe Analysis Of Selected Quartz Overgrowths.	193
Table 6.2 Microprobe Composition Of Glaucony, "Glauconitic Illite", Kaolin And Illite.	195
Table 6.3 XRD Responses Of Major Clay Minerals.	196
Table 6.4 Composition Of Mica-Like Clays.	198
Table 6.5 Transmission Electron Microscopy (TEM)/EDAX Illite Lath And Flake Compositions.	202
Table 6.6 Illite Morphology Compositions.	205

Table 6.7	Illite Textures And Corresponding Illite Morphology Type.	208
Table 6.8	Carbonate Cement Composition.	214
Table 6.9	Composition Of S1, S2 And S3 Siderite Cement Phases.	215
Table 6.10	Microprobe Composition Of Patch, "Seed" And Pore-Filling Siderite Cement.	218
Table 6.11	Siderite Dissolution Events: A Comparison Of Results.	223
Table 6.12	General Paragenetic Sequence For The Merrimelia Formation.	232
Table 6.13	Summary Of Diagenetic Events In The Merrimelia Formation.	234
Table 6.14	S2 and S3 Siderite Compositions [In Plate 33].	296
Table 6.15	Composition Of "Cowpat Calcite" And "Cowpat Illite" [In Plate 34].	305
Table 6.16	Proportion Of Porosity Types In The Merrimelia Formation.	310
CHAPTER SEVEN: ILLITE FLUORESCENCE		
Table 7.1	Elemental Composition Of Platy Illite.	335
CHAPTER EIGHT: PARAGENETIC MODEL		
Table 8.1	Preliminary K-Ar Illite Dating Results For Both <2 And <4 Micron Fractions.	360
CHAPTER NINE: RESERVOIR DEVELOPMENT & QUALITY		
Table 9.1	Reservoir Quality Potential Of The Main Facies Types In The Merrimelia-Tirrawarra Glacial Complex.	388
Table 9.2	Pearson Correlation Coefficients Of Compaction Indices (CI), Sorting Coefficients And Grain Size.	410
Table 9.3	Initial Porosity Loss In Proglacial And Terminoglacial Sediments.	413

PROJECT OBJECTIVES

- Identify and distinguish Merrimelia Formation and Tirrawarra Sandstone lithologies.
- Confirm relationships between the Merrimelia Formation and Tirrawarra Sandstone by petrographic means.
- Delineate the provenance of Merrimelia Formation and Tirrawarra Sandstone sediments by petrographic and statistical means.
- Assess the role of authigenic minerals, particularly illite, with regards to reservoir quality and potential in the Merrimelia Formation.
- Identify controls on reservoir development and quality in a glacial sequence.

TERMINOLOGY

- **Allometamorphism:** Pertaining to the end of diagenetic conditions and start of metamorphic processes.
- **Amygdales:** A gas cavity or vesicle within a volcanic rock filled with secondary minerals such as chlorite and zeolites.
- **Ar:** Argon.
- **Authigenic mineral/phase:** A mineral that has formed *insitu* within the sedimentary pile.
- **BSE:** Back scattered emission.
- **Cement:** One phase of precipitated mineral (i.e. quartz cement).
- **Cementation:** The diagenetic process by which authigenic minerals/phases form filling pore space and replacing detrital minerals.
- **Clast(s):** Country rock that is incorporated into a sediment. This term is used for the macroscopic and microscopic scales.
- **Cluster Analysis:** A statistical technique which classifies data into homogeneous groups.
- **Competent Rock Fragment:** A rigid rock fragment that does not deform due to overburden pressure.
- **Detrital:** Pertaining to rock matter and minerals that have not formed *insitu*.
- **Detritus:** Minerals and rock matter that have been incorporated into a sediment sourced from surface sedimentation processes.
- **Diagenesis:** Geochemical and mineralogical reactions that occur in sedimentary rocks at temperatures and pressures below metamorphism.
- **Eskers:** Elongate ridges that accumulate in glacial meltwater tunnels, that are composed of sand, gravel and mud.
- **Fiamme:** Elongated and contorted acid volcanic glass fragments
- **Formation:** A formally defined sequence of sediments. (i.e. Merrimelia Formation).
- **Framework Component:** The component of a sedimentary rock which forms the hard skeleton of a sediment.
- **Gondwana:** Palaeozoic super continent predominantly in the southern hemisphere which included, Australia, Arabia, Antartica, India, South America and Africa.

- **Granophyric Texture:** Fine grained intergrowths of quartz and alkali feldspar.
- **Incompetent Rock Fragment:** A rock fragment that plastically deforms with overburden pressure.
- **K:** Potassium.
- **Labile/Ductile Rock Fragment:** Same as incompetent rock fragment.
- **Matrix:** Fine grained component of a sedimentary rock.
- **Neof ormation:** The formation of an authigenic mineral from circulating pore fluids.
- **Paragenesis:** The relative timing of diagenetic events.
- **Poikilotopic:** Carbonate cement where very large cement crystals form enveloping framework grains.
- **Porosity Occlusion:** The obliteration of pore spaces by either mechanical or mineral precipitation processes.
- **Primary Porosity:** Porosity that formed via depositional processes.
- **Principle Components Analysis (PCA):** Statistical technique which assesses data normality.
- **Proglacial:** Pertaining to the depositional region or processes that are distal to the glacier.
- **Provenance:** The region(s) where sediments have been derived.
- **Rock Fragment(s):** Country rock that is incorporated into a sediment.
- **Sandur (Plural-Sandar):** Outwash fans produced by the action of glacial meltwater.
- **Scattergram:** Statistical plot that illustrates the relationship between two variables.
- **Secondary Porosity:** Porosity that has formed via diagenetic processes.
- **SEM:** Scanning electron microscopy.
- **TEM:** Transmission electron microscopy.
- **Terminoglacial:** Pertaining to the depositional region or processes proximal to the glacier.
- **Variogram:** Statistical plot that assess the variability of a chosen variable with respect to the geographic spread of data.
- **XRD:** X-ray diffraction.



INTRODUCTION

1.0 PREAMBLE

The Cooper Basin is Australia's largest onshore gas basin, being one of a number of remnant Late Carboniferous to Early Permian depocentres which lay in the Australian interior of the Gondwana Supercontinent (Gravestock and Jensen-Schmidt, 1998) (Fig. 1.1). The basin is situated in central Australia and extends from the north-east corner of South Australia into south-west Queensland (Fig. 1.2), extending over an area of approximately 130 000 km². The basin preserves up to 1,200m of non-marine clastic sediments of Late Carboniferous to Middle Triassic age. The basal Gidgealpa Group is composed of sediments that are Late Carboniferous to Late Permian in age while the overlying Nappamerri Group comprises sediments that are Late Permian to mid-Triassic in age. The Cooper Basin sediments are overlain by Jurassic to mid-Cretaceous sediments of the Eromanga Basin (Fig. 1.3a), and unconformably overlies clastics, acid volcanics\pyroclastics and carbonates of the Cambrian to Ordovician Warburton Basin (Fig. 1.3b).

The Merrimelia Formation is the basal unit within the Gidgealpa Group (Williams and Wild, 1984b), and represents a package of Gondwanan intracratonic glacial and proglacial sediments. The oldest unit in the Cooper Basin, the Merrimelia Formation was deposited unconformably on the tectonically deformed Warburton Basin (Fig. 1.4). Directly associated with the Merrimelia Formation is the Tirrawarra Sandstone, one of the main hydrocarbon producing reservoirs in the basin (Fig. 1.4). The Merrimelia Formation has been traditionally regarded as non-economic basement and the contact with the Tirrawarra Sandstone was perceived as an unconformity.

The first chapter of this thesis outlines the general geology of the Cooper Basin concentrating on the geology of the Warburton Basin from which the majority of Merrimelia and Tirrawarra sediments have been derived. Chapter two outlines the methods used throughout this study. Chapter three gives a brief overview on the development of the Gondwanan ice sheet over southern Australia putting into context

the development of glacial sediments of the Cooper Basin. Chapter four describes in detail the glacial sedimentology of these sediments while chapter five describes the movement of glacial material within the Cooper Basin during Merrimelia-Tirrawarra deposition. Chapter six discusses the diagenesis of Gondwanan glacial detritus with emphasis on illite diagenesis. Chapter seven describes the fluorescence nature of illite when exposed to UV radiation, detailing how this characteristic can be used as a new petrological tool for the optical characterisation of illite. Chapter eight combines diagenetic observations to form a regional paragenetic sequence of the Merrimelia-Tirrawarra Glacial Complex (MTGC). The results of a pilot illite dating/geohistory study are also given in chapter eight. Chapter nine synthesises all results delineating the controls on reservoir development and quality in the glacial sediments of the Cooper Basin. Chapter ten summarises conclusions and recommendations that have resulted from this study.

1.1 LOCATION

The location of the Cooper Basin is shown relative to other mid-Palaeozoic and Cainozoic basins within Australia (Fig. 1.2).

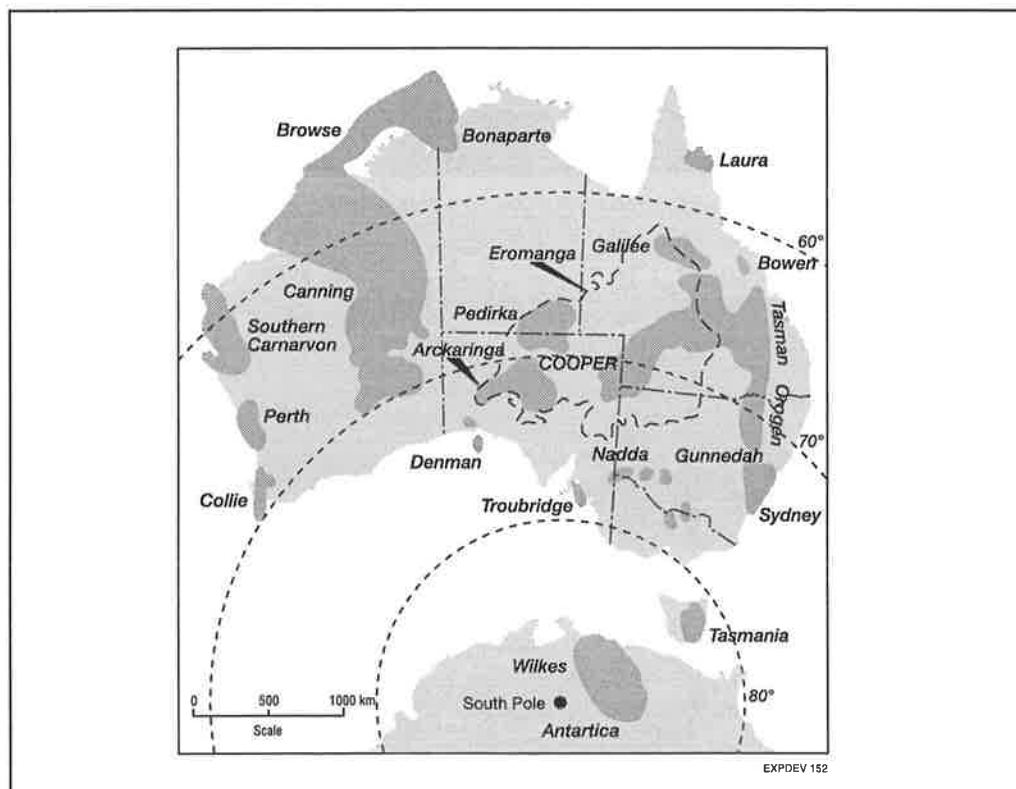


Figure 1.1 Late Palaeozoic sedimentary basins on the Australian portion of Gondwana. (After Gravestock and Jensen-Schmidt, 1998).

The Cooper Basin is entirely buried, having been defined by approximately 1500 well bores and 19,000 seismic lines. The south western, and most intensively explored portion of the basin, lies within South Australia while the least explored portion of the basin, lies in Queensland (Fig. 1.2).

1.2 STUDY AREA

This study collected information from both the Queensland and South Australian sectors of the Cooper Basin (Fig. 1.2). The amount of information collected in the South Australian sector however, substantially outweighs the data collected in the Queensland portion.

1.3 PREVIOUS STUDIES

There have been no regional investigations of the Merrimelia Formation where the diagenesis and provenance of this unit is the main focus. The first study of the Merrimelia Formation was carried out by Grund (1966) as part of an honours project. He described in detail the sedimentology of the glaciogenic sediments on a regional basis with emphasis on describing clast attributes from core. He indicated that the majority of clasts have been sourced from the basement (Warburton Basin). Until the mid-eighties, the Merrimelia Formation was regarded as economic basement for hydrocarbon exploration and accordingly, few if any investigations concentrated on this unit.

Renewed interest in the Merrimelia Formation was provided by a series of unpublished reports and published papers by Williams (1982 and 1984), Wild (1987), Williams and Wild (1984a and 1984b) and Williams *et al.* (1985 and 1987). These authors primarily concentrated on the sedimentology, not only of the Merrimelia Formation, but also of the Tirrawarra Sandstone, (on a regional basis) with a view to understanding the evolution of this glacial system. Williams and Wild (1984) were the first to argue that the Tirrawarra Sandstone and Merrimelia Formation represented an evolving glacial system. Williams *et al.* (1985 and 1987) first described and detailed the development of cold climate aeolian sandstones within the Merrimelia Formation at the Merrimelia Field.

Reservoir quality aspects of the glacio-aeolian sandstones in the Merrimelia Field were touched upon by Williams *et al.* (1985) where they describe the diagenetic phases in relation to reservoir quality and seismic facies.

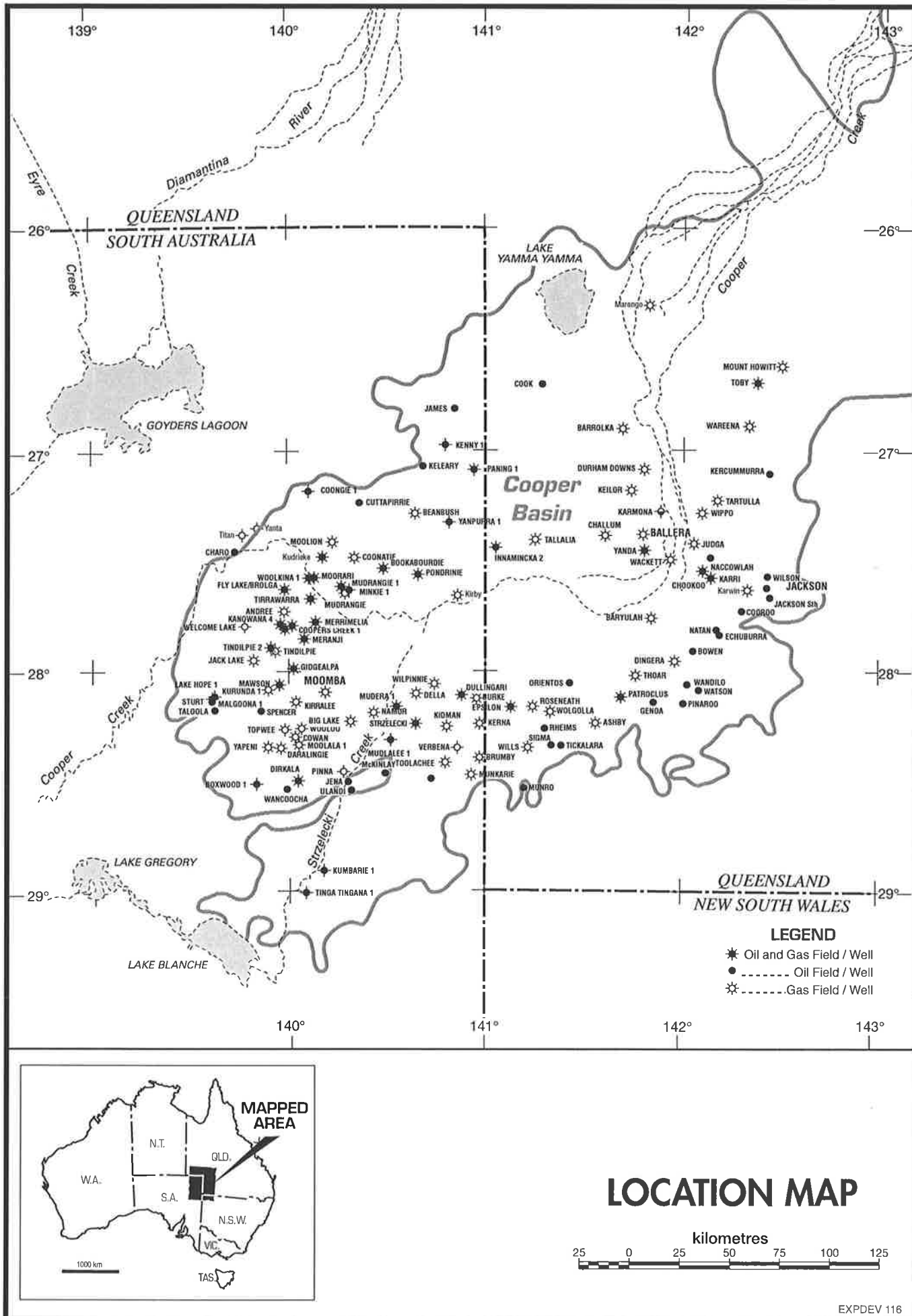


Figure 1.2 Location map of the Cooper Basin with major fields and wells shown.

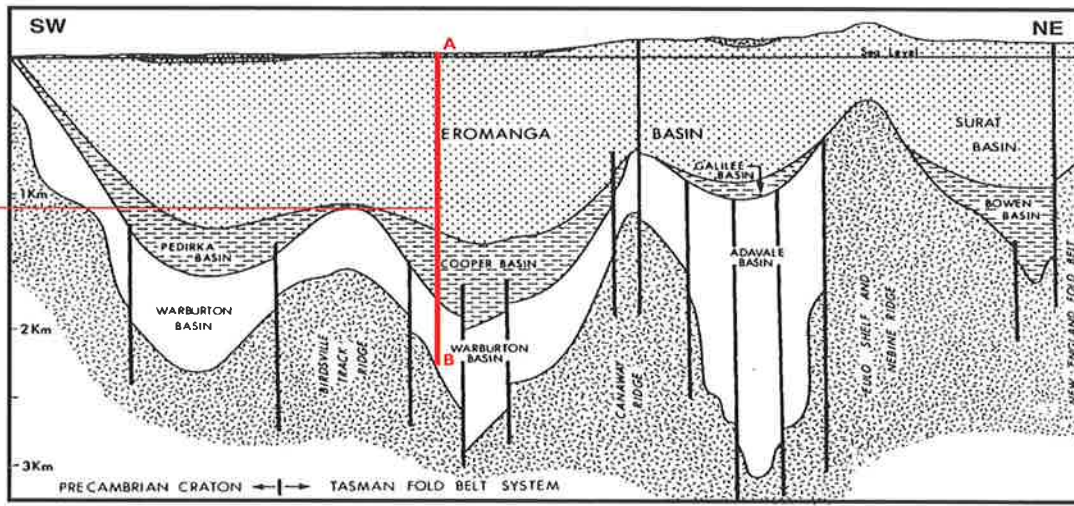
Other diagenetic/reservoir quality investigations have been done by Lemon (1990) in the Malgoona and Lake Hope Fields with a more recent reservoir quality investigation of the glacio-aeolian sandstones at Merrimelia #37 completed by the same author (Lemon and Mathews, 1997). He concluded that compaction of labile fragments and extensive illitisation had a major impact on porosity and permeability reduction.

As the Tirrawarra Sandstone and Merrimelia Formation are interlinked, investigations within the Tirrawarra Sandstone are relevant to this present study. A number of workers have investigated the reservoir quality of this unit. Schulz-Rojhan (1991), in describing the diagenesis of all Permian formations in the Cooper Basin, on a regional basis, included the Tirrawarra Sandstone. Rezaee (1996), on the other hand, published numerous papers on differing aspects of diagenesis, reservoir quality and log response of the Tirrawarra Sandstone at the Tirrawarra, Moorari, and Fly Lake-Brolga fields. He suggested that quartz cementation and mechanical compaction are the main processes reducing porosity within the Tirrawarra Sandstone. Seggie *et al.* (1994), in an attempt to better understand the nature of the Tirrawarra Sandstone, divided this unit in the Tirrawarra Field, into several flow units and described each in terms of their depositional environment and reservoir quality.

This study is the first to assess the diagenesis, provenance and reservoir quality of the Merrimelia Formation on a regional basis and combine the findings with the conclusions of other workers in related areas. The published results from the present study are given in Appendix Eleven.

This study also includes a hitherto unattempted analysis of rock fragments within the Tirrawarra Sandstone on a regional basis. To the best of my knowledge, this has not been done before.

A number of key studies have been used to assist in the identification of the provenance of lithic components in the Merrimelia Formation. Gatehouse (1986) first reviewed the geology of the eastern Warburton Basin. More recently a very comprehensive Warburton Basin study has been done by Sun (1996). This author described most aspects of the geology of the Warburton Basin, concentrating on the sequence stratigraphy and sedimentology of the basin. Boucher (1996) reviewed the tectonic and structural development of the Warburton Basin with emphasis on the volcanics at Jena #1 and Murteree wells.



A

B

Basin	Age	Palynological Zone	Stratigraphy	Depositional environment	Major seismic horizon	Tectonic events		
Lake Eyre	Tertiary / Recent	Ma	Namba Fm.	Fluvial and aeolian		Tertiary folding		
			Eyre Fm.					
Eromanga	Cretaceous	91.0	Winton Fm.	Non-marine to marginal marine	A	Phase 3 mild folding		
		L	PK7	Mackunda Formation	Marginal marine			
				Oodnadatta Fm.	Marine			
				Allaru Mudstone	Marine			
				Toolibuc Fm.	Marine			
				Coorikiana Sst.	Marine shoreface			
		M	PK4	Bulldog Shale	Open marine transgression		Local uplift	
				Wallumbilla Fm.				
				Wyandra sst. Mbr.				
				Cadna-Owie Fm.	Non-marine to marginal marine	C		
				Murta Fm.	Lacustrine turbidites, deltas			
		E	PK1.2	Hooray Sst.				
				Namur Sst.				
				Westbourne Fm.				
				Adon Sst.				
Birkhead Fm.	Braided fluvial with aeolian influence							
Jurassic	L	PK1.1	Hutton Sst.	Meandering fluvial	L			
			Poolowanna Fm. or basal Jurassic					
			M	PJ5	Birkhead Fm.			
					Hutton Sst.			
					Westbourne Fm.			
Adon Sst.								
Cooper	Triassic	205.0	NAPPAMERRI GROUP	Fluvial		Phase 2 Uplift		
		L	PT5	Tinchoo Fm.	Meandering fluvio-lacustrine	N		
				Callamurra Mbr.				
		M	PT2	Daralinge Fm.	Meandering fluvial / deltaic	P	Uplift (Daralinge Movement)	
				Callamurra Mbr.				
		Permian	E	PP4	Footaches Fm.	Lacustrine	V	Base level changes
					Rosemeath Shale	Fluvio-deltaic		
					Epsilon Fm.			
					Murreea Shale			
					Patchawarra Formation	Fluvio-deltaic, lacustrine		Uplift
Tirrawarra Sst.					W	Rejuvenation of pre-existing faults		
Merrimelia Fm.	Terrestrial / subaqueous glaciogene				Z			
PP1.1								
Warburton	Cambrian	M	Dullingari Group	Deep-water turbidite		Phase 1 Alice Springs Orogeny with granite intrusion		
			Innaminka Fm.	Shallow subtidal Shelf to red bed transition		Dullingari Movement		
			Kalladeina Formation	Shallow shelf		Backarc-rifting		
				Slope and basin		Mootwingee Movement		
				Shallow shelf		Kangarooian Movement		
				Volcanic eruption				

Figure 1.3 A) Schematic cross section through the Eromanga, Cooper and Warburton Basins (After Carne, 1986). B) Stratigraphic table of the Eromanga, Cooper and Warburton Basins (After Sun, 1996).

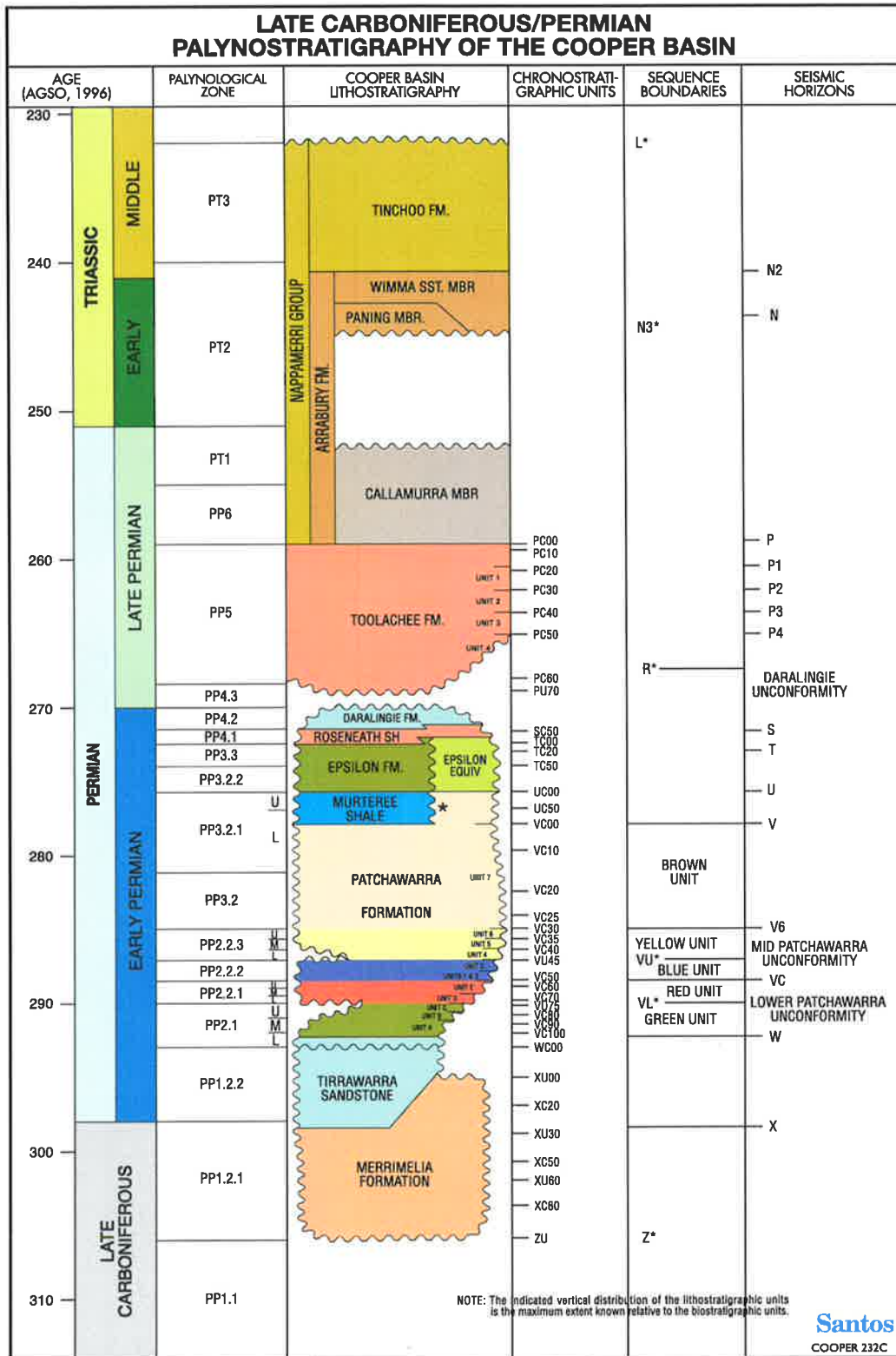


Figure 1.4 Stratigraphic column of the Cooper Basin (After Santos, 1999).

Geological provinces such as the Arunta Block (N.T.), Curnamona Province (N.S.W), Broken Hill Block (N.S.W), Olary Block (S.A.), Benagerie Ridge (S.A.) as well as the Mt Painter (S.A.), Mt Babbage (S.A.) and Peak and Denison Inliers (S.A.), were also

investigated in this study as possible sources of Cooper Basin sediments (Chapter Five - Fig. 5.3). This involved the collection of published and unpublished reports from the respective state government bodies and the University of Adelaide.

1.4 COOPER BASIN STRATIGRAPHY

Sediments of the Cooper Basin were first intersected by an exploratory well (Innamincka #1) in 1959. In 1961-62, Delhi Petroleum Ltd, using aeromagnetic surveys, further delineated this basin (Wopfner, 1970). This newly-delineated Permian basin was named the, Coopers Creek Basin, by the then Bureau of Mineral Resources (BMR), now AGSO, in 1963 and was found to contain sediments that were Late Carboniferous to Late Triassic in age.

Initially, the entire basin fill was considered as the Gidgealpa Formation, composed of upper, middle and lower members (Kapel, 1966). Kapel (1972) elevated the Gidgealpa Formation to group status and the members to formation status. Gatehouse (1972) modified the stratigraphic nomenclature of Kapel (1972) into a form recognisable today.

Age	Palyn Zone <small>(mod from Price et. al., 1985)</small>	Stratigraphy of the Lower Gidgealpa Group
Early Permian	PP2.1	Patchawarra Formation
	PPI.2.2	Tirrawarra Sandstone
Late Carboniferous	PPI.2.1	Merrimelia Formation
Cambrian - Devonian		Warburton Basin

EXPDEV 072 B

Figure 1.5 Lower Gidgealpa Group stratigraphic table. (Adapted from Chaney et al., 1997).

Gostin (1973) defined the Tirrawarra Sandstone and recognised three subdivisions, which were revised and modified into four subdivisions by Williams (1982).

The first study on the Carboniferous conglomerates and tillites in the Cooper Basin was conducted by Grund (1966). He noted that the first well to penetrate glacial sediments in the basin was Dullingari #1 in 1962. These glacial sediments were encountered in later wells with the first accurate palynological dating gained from the Merrimelia #1 well in 1964. Grund (1966) suggested naming the lower Permian glacial sediments of the Cooper Basin, the Strzelecki Formation but later in the same year Martin (1967) proposed the name Merrimelia Formation, after the Merrimelia #1 well. Williams and Wild (1984a) formally incorporated the Merrimelia Formation into the Gidgealpa Group. Following this, Price *et al.* (1985) fixed the palynological zone of the Tirrawarra Sandstone as *PP1.2.1*, correlating this unit with the Treachery Shale, a Permian glacio-marine unit in the Upper Kuriyippi Formation of the Bonaparte Basin in Western Australia (Fig. 1.1) (Wood pers. comm., 1998). In addition Redfern (1990) and Redfern and Millward (1994) describe equivalent aged strata (Hoya Formation) in the Canning Basin of Western Australia. This formation is regarded as part of the Grant Group and is considered by these authors to have been deposited in the Late Carboniferous at the same time as Merrimelia and Tirrawarra sediments.

The stratigraphic subdivisions within the Cooper Basin have been mainly based on palynology (Paten, 1969). The broad stratigraphic and palynological divisions in the basin are based on work done by Thornton (1979) and Price *et al.* (1985) respectively. Further refinement of these subdivisions has been carried out by Santos Ltd and PIRSA, with the most recent stratigraphic column used at present, illustrated in Figure 1.4.

The Cooper Basin unconformably overlies the Cambrian-Devonian Warburton Basin sequence, and is in turn overlain, unconformably, by the Mesozoic-Tertiary Eromanga Basin (Fig. 1.3b). The spatial relationships of these three basins is illustrated in Figure (1.3a).

Uncertainty of the relationship between the Tirrawarra Sandstone and Merrimelia Formation and associated nomenclature has traditionally lead to confusion. These issues are addressed in full in section 1.5. However recently, workers such as Williams and Wild (1984a) and Chaney *et al.* (1997) have, as a result of comprehensive studies on the lower Gidgealpa Group (Fig. 1.4), revised and simplified the stratigraphic

relationships (Fig. 1.5). The resulting definitions of the Tirrawarra Sandstone and Merrimelia Formation are given in the following section.

1.4.1 DISCUSSION

Grund (1966) concluded that glacial sedimentation was effectively continuous from the base of the Patchawarra Formation to the base of the Merrimelia Formation. However, Kapel (1972) and Battersby (1976) considered the Tirrawarra Sandstone and Merrimelia Formation as two units, separated by an unconformity. Kapel (1972) did, however, state that the Tirrawarra Sandstone is in part derived from the Merrimelia Formation. This concept was expanded upon by Williams and Wild (1984a), stating that the Tirrawarra Sandstone and Merrimelia Formation are intimately related and illustrate the evolution of a predominantly glacial system into one in which fluvial processes dominate. These authors contradicted the popular thinking of the day and concluded that these two units interdigitated where typical "Tirrawarra Type" fluvial deposits were present in typical glacial "Merrimelia Type" deposits. Chaney *et al.* (1997) more recently reiterated these conclusions and expanded by suggesting that not only do the sedimentological relationships between the two units point to their interwoven relationship, but petrology of both formations indicates that they share the same rock fragment suites. This indicates that the Tirrawarra Sandstone is derived from the same source regions as the Merrimelia Formation as suggested earlier by Kapel (1972). Consequently, Tirrawarra detritus has been deposited via reworking of the Merrimelia sedimentary pile or sourced directly from surrounding basement outcrop.

The glacial sediments of the Cooper Basin can be correlated with Gondwanan aged glacial sediments in adjoining basins (Fig. 1.6). Consequently, the Crown Point Formation in the neighbouring Pedirka Basin equates with the Merrimelia Formation and the Purni Formation, according to Giuliano (1988), is a lateral equivalent of the Tirrawarra Sandstone (Fig. 1.6). In the Bowen and Galilee Basins of Queensland equivalent units to the Merrimelia Formation/Tirrawarra Sandstone include the Jericho and Jochmus Formations (Galilee Basin) and the Comet Volcanic Beds in the Denison Trough (Bowen Basin) (Fig. 1.6).

Brief descriptions of the other Cooper Basin units are detailed in this chapter in order to place the Merrimelia Formation and Tirrawarra Sandstone within a basin context. Warburton Basin units are also described as they have provided the majority of rock fragments contained within the Merrimelia Formation and Tirrawarra Sandstone, and

are vital to an understanding of the provenance (Chapter Five) and reservoir quality discussions (Chapter Nine).

1.5 LITHOSTRATIGRAPHIC DEFINITIONS

Ongoing terminology and conceptual conventions in the Lower Gidgealpa Group necessitates the following sections which define both the Tirrawarra Sandstone and the Merrimelia Formation. These definitions and terms will then be used throughout this entire document.

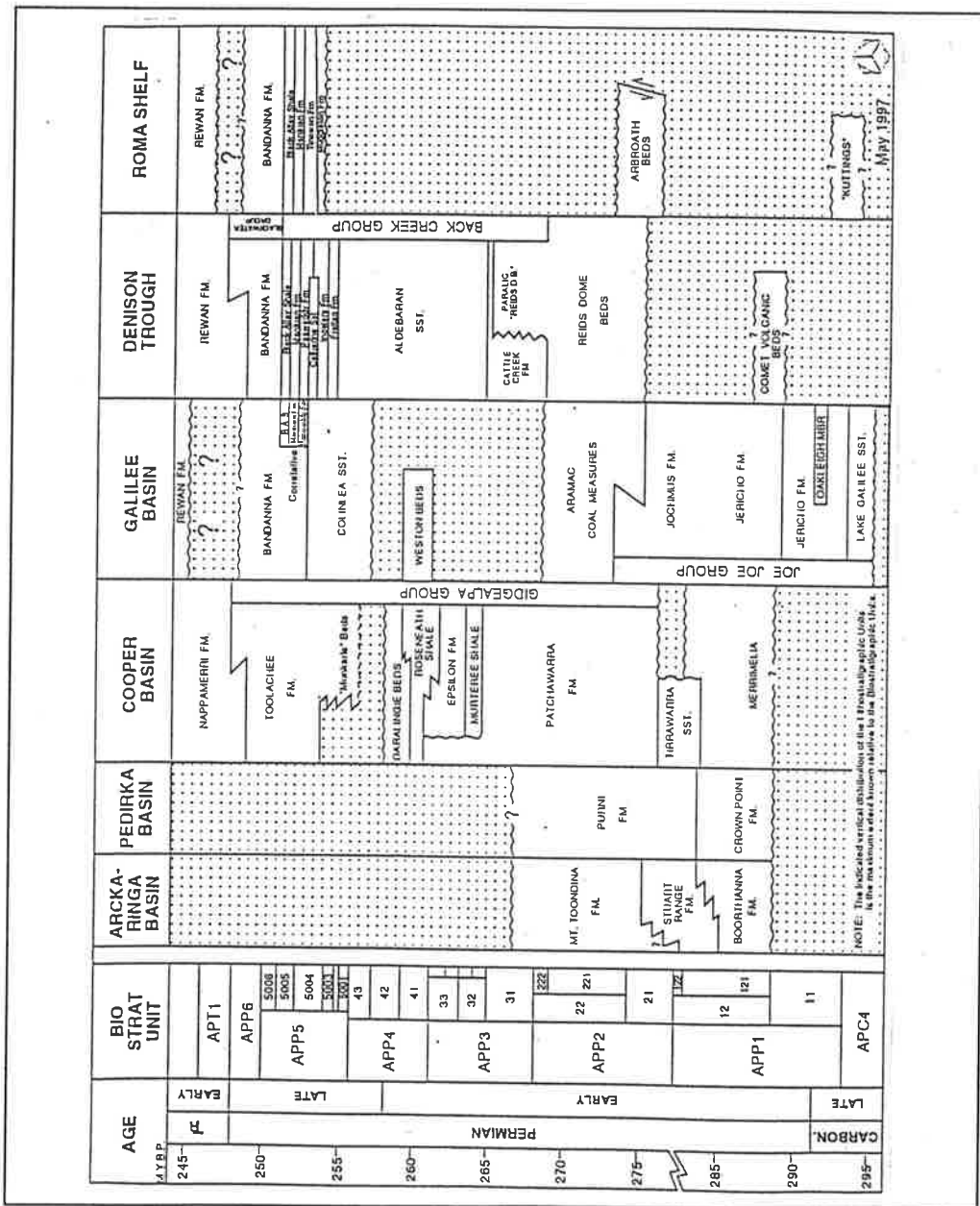


Figure 1.6 Stratigraphy of Late Carboniferous-Early Permian basins adjacent to the Cooper Basin (After Price, 1997).

1.5.1 DEFINITIONS: TIRRAWARRA SANDSTONE AND MERRIMELIA FORMATION

The definition of the Tirrawarra Sandstone and Merrimelia Formation has changed several times. Listed are the various definitions that have been proposed in the literature over the past thirty years:

- Merrimelia Formation constitutes all glacial detritus from the basement to the Patchawarra Formation (Grund, 1966).
- The Merrimelia Formation is a distinct sequence of rocks unrelated to the Tirrawarra Sandstone, where a regional unconformity separates both units (Gostin, 1973).
- The Merrimelia Formation and Tirrawarra Sandstone forms a sedimentological continuum with no regional unconformity separating the units (Williams and Wild, 1984a).
- The Merrimelia Formation and Tirrawarra Sandstone forms a depositional continuum where the Tirrawarra Sandstone represents only one of numerous facies types within the Merrimelia-Tirrawarra Glacial Complex (Chaney *et al.*, 1997). The phrase “Merrimelia-Tirrawarra Glacial Complex” can get cumbersome and is consequently shortened to MTGC throughout this document.

The last two definitions have been adopted in this study. Hence, the Tirrawarra Sandstone is regarded as one facies type in a glacial sequence, which contains in excess of twenty major facies types (see Chapter Four). Consequently, all braid plain sandstones in this model are regarded as the Tirrawarra Sandstone. In addition, facies types, other than braid plain sandstones within the Merrimelia-Tirrawarra Glacial Complex, are called the Merrimelia Formation (i.e. conglomerates and mudstones). Collectively both Merrimelia and Tirrawarra facies are termed the Merrimelia-Tirrawarra Glacial Complex. The following sections detail the nomenclature used throughout this document.

1.5.1.1 Tirrawarra Sandstone

The Tirrawarra Sandstone is a collection of stacked bar facies, which form part of the Merrimelia-Tirrawarra glacio-fluvial outwash braid plain complex (Fig. 1.7). Thus when specifically speaking of braid plain sandstones the following terms are used:

- 1) *Tirrawarra type facies* (refers to - the braid plain sandstones facies in the Merrimelia-Tirrawarra Glacial Complex).
- 2) *Tirrawarra type sandstone* (refers to - a braid plain sandstone within predominantly Merrimelia facies types).

- 3) Tirrawarra sediments (refers to - all braid plain sandstones facies in the Merrimelia-Tirrawarra Glacial Complex).
- 4) Tirrawarra Sandstone (refers to - all braid plain sandstones within the Merrimelia-Tirrawarra glacial complex).
- 5) Tirrawarra.(pertaining to braid plain sandstones).

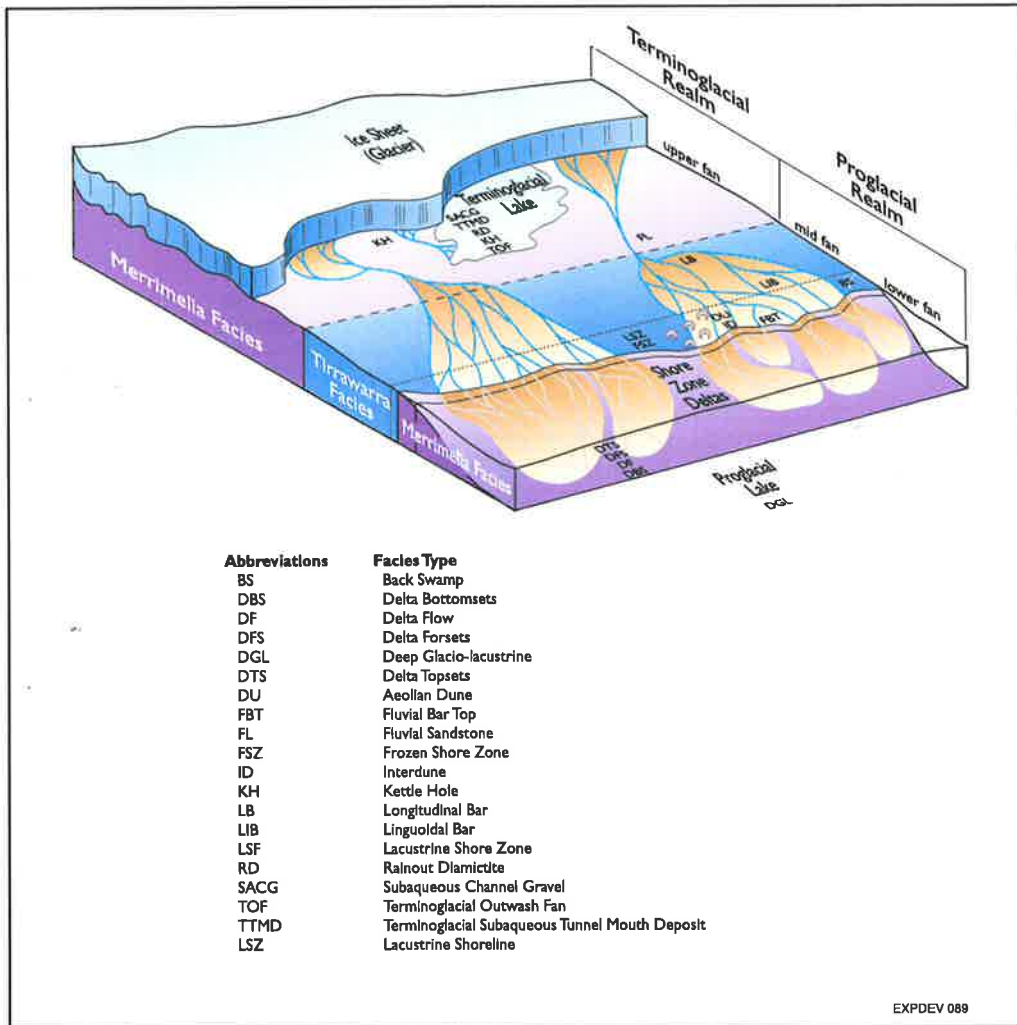


Figure 1.7 Schematic model of the Merrimelia-Tirrawarra Glacial Complex (MTGC).

Considering the definitions above along with the findings of Williams and Wild (1984a) and Chaney *et al.* (1997) the Tirrawarra Sandstone only exists where it has been derived from Merrimelia facies. Thus sediments that appear similar to the Tirrawarra Sandstone but have no Merrimelia sediment source, such as those in the Moomba region (Fig. 1.2), are then by definition not Tirrawarra sediments.

An example of this situation is seen in the Moomba region. The Merrimelia Formation was never deposited at the Moomba Field as this area was, according to Carne (1986) and Chaney (1998), a topographic high. Thus, if there were no Merrimelia Formation

sediments deposited; then there were no sediments from which the Tirrawarra Sandstone could form. This is of course contingent on no sediment supply sweeping in and around the highs. Boucher (1996) concluded similarly, stating that the unit commonly interpreted as the Tirrawarra Sandstone at the Moomba field is in fact not the Tirrawarra Sandstone but an altered granodiorite of the Big Lake Granodiorite Suite.

1.5.1.2 Merrimelia Formation

The Merrimelia Formation is a collection of twenty facies types (see Chapter Four), which form part of the Merrimelia-Tirrawarra Glacial Complex (Fig. 1.7). Thus when specifically speaking of Merrimelia facies types, that is to say all facies types except braid plane sandstones, the following terms are used:

- 1) *Merrimelia type facies* (refers to - all Merrimelia facies in the Merrimelia-Tirrawarra Glacial Complex apart from braid plain sandstones).
- 2) *Merrimelia facies* (refers to - all Merrimelia facies in the Merrimelia-Tirrawarra Glacial Complex apart from braid plain sandstones).
- 3) *Merrimelia Formation* (refers to - all Merrimelia facies in the Merrimelia-Tirrawarra Glacial Complex apart from braid plain sandstones).
- 4) *Merrimelia sandstones* (refers to - all non-braid plain sandstones in the Merrimelia-Tirrawarra Glacial Complex).
- 5) *Merrimelia sediments* (refers to - all Merrimelia facies in the Merrimelia-Tirrawarra Glacial Complex apart from braid plain sandstones).
- 6) *Merrimelia* (pertaining to all facies within the Merrimelia-Tirrawarra Glacial Complex apart from braid plain sandstones).

In most parts of the Cooper Basin the identification of Merrimelia facies in open boreholes is generally straight forward, however on occasion Merrimelia sediments can be difficult to distinguish from Warburton Basin lithologies. An example of this can be seen in the Spencer region (Plates 1a & 1b).

It can be seen in Plate 1a that this rock is a volcanoclastic conglomerate dominated by porphyritic, flow-banded and devitrified rhyodacitic lavas as well as ignimbrites, crystal tuffs and sedimentary quartzite clasts. Higher up the sequence, matrix supported, muddy diamictites and conglomerates are observed (Plate 1b). These units exhibit rounded to rectangular clasts with the composition of the majority of clasts mirroring the lower volcanoclastic breccias (Plate 1). Sun (1996) interpreted the lower volcanoclastic breccias as lava and pumice rich breccias, which have been proximally reworked from nearby Mooracochie Volcanics within the Warburton Basin.

Plate I

A



CORE DESCRIPTION						
DATE: 09/01/1998						
WELL NAME: SPENCER 1 PAGE: 1 OF 1						
FORMATION: MERRIMELIA						
DEPTH (ft)	DEPTH (m)	STRUCTURES GRAINSIZE				COMMENTS
		MUD	SAND	GRAVEL	CONGL.	
-6598	2011.0					Diamitite Shale matrix. Clasts are rectangular (faceted) to round in shape. Clast size does not exceed 3cm. Clast types include: Rhyodacite (Dom), Quartzite (Black), Ignimbrite and Volcanic Conglomerate.
-6599	2011.2					
-6600	2011.4					
-6601	2011.6					
-6602	2011.8					
-6603	2012.0					
-6604	2012.2					
-6605	2012.4					
-6606	2012.6					
-6607	2012.8					
-6608	2013.0					Higher proportion of basement clasts than diamitites above.
-6609	2013.2					Basement clasts of clasts noted (Fluvial units of basements)
-6610	2013.45					Diamitite unit as above
-6611	2013.7					
-6612	2013.9					
-6613	2014.1					Basement Facies: Congl. Clast types include :- Red volc. (Dom.) - Green Qz. Porphyry - Red Qz.
-6614	2014.3					
-6615	2014.42					
-6734	2052.52					
-6735	2052.7					Very coarse to coarse grained rock with clasts of varying conditions.
-6736	2052.9					[Fluvial reworking of pyroclastic deposits]
-6737	2052.1					
-6738	2052.3					Horiz. orientation of clasts in places [Fluvial] Clasts are uniform in size and are angular to sub rounded these units are red/purple in colour
-6739	2052.5					
-6740	2052.7					
-6741	2052.9					

B



EXPDEV 077 F

Plate 1 A) Spencer 1 (2012.59m). Merrimelia Formation; volcaniclastic conglomerate sample. B) Spencer 1 (2092.77m - 2093.02m). Mooracochie Volcanics; ignimbrites, volcaniclastic conglomerates, sandstone clasts.

Visual inspection suggests that the upper units in this section are consistent with typical terminoglacial¹ Merrimelia sedimentation styles. They are interpreted to be basal Merrimelia conglomerates, having formed as a result of terminoglacial deltaic sedimentation reworking Warburton Basin volcanoclastic conglomerates and acid volcanic rocks.

In the Spencer area a small proportion of clasts within Merrimelia Formation conglomerates are composed of Warburton Basin volcanoclastic breccias (illustrated in Plate 1b). However, petrographic observations indicate, that the majority of rock fragments in Merrimelia conglomerates at Spencer 1 are composed of individual rock types (mainly acid volcanics - rhyodacite) and not volcanoclastic breccias which are amalgamation of individual rock types (clasts). It is likely that the clasts within the Warburton breccias were subsequently "liberated" by erosion. The resulting re-sedimentation of these clasts into Merrimelia conglomerates destroyed the original matrix, effectively breaking down Warburton breccias into their component parts. These "liberated clasts", along with subordinate amounts of still-lithified Warburton Basin breccias, were incorporated into the Merrimelia sedimentary pile forming the conglomerates illustrated in Plate 1. There are thus more clasts composed of one lithology, than clasts composed of a number of lithologies in Merrimelia Formation conglomerates at Spencer 1.

In addition the lithologies of clasts, both individual and conglomeratic, within Merrimelia conglomerates at Spencer are the same, indicating a common provenance. The similarity between Merrimelia and Warburton sediments at Spencer negates using logs or cuttings as a way to discriminate between the Warburton Basin and Merrimelia conglomerates. Core analysis however reveals, that they belong to two differing basins separated by approximately 150 Ma.

1.6 DISTRIBUTION OF THE TIRRAWARRA SANDSTONE AND MERRIMELIA FORMATION

The distribution of Merrimelia Formation and Tirrawarra Sandstone sediments tend to mirror each other both in vertical thickness and in areal extent. This distribution is a further reflection of the interlinked depositional nature of these two units. A combined isopach map of the Tirrawarra Sandstone and Merrimelia Formation within the South Australian sector of the Cooper Basin is shown in Figure (1.8).

¹ For terminoglacial and proglacial glacial sedimentation styles see Chapter Four.

According to Hill and Gravestock (1995), the southern Cooper Basin (SA sector) contains the thickest (1600m) and most complete Permian succession, whereas in the northern and Queensland sectors of the basin, beyond the Curnamona Trend (Fig. 1.9), only a thin Permian package (300m) is intersected.

1.6.1 MERRIMELIA FORMATION

The thickness and distribution of the Merrimelia Formation is irregular within both the South Australian and Queensland sectors of the Cooper Basin (Fig. 1.8). Apak (1994) stated that the largest accumulations are noted along the GMI trend, with the thickest being at Merrimelia #1 (363m). In general, the thickest deposits of Merrimelia sediments are noted within palaeo-depressions and grabens (Apak, 1994) (Fig. 1.8). In the Patchawarra Trough, Merrimelia sediments are on average only 33 metres thick (Carne, 1986; Apak, 1994). It appears from these observations that structural inversion has taken place, where what are now highs were once troughs into which Merrimelia sediments were actively deposited. Apak (1994) concluded that the lack of Merrimelia Formation development in the Patchawarra Syncline is attributed to this feature being a smoothly undulating basement surface with low relief at the Tirrawarra and Fly Lake Fields. The Merrimelia Formation has been observed as far south as Tinga Tingana #1 (Hill and Gravestock, 1995) and as far north as Paning #1 (Fig. 1.2).

1.6.2 TIRRAWARRA SANDSTONE

Distribution of Tirrawarra Sandstone sediments occurs irregularly throughout the Patchawarra, Nappamerri and Tenappera Troughs (Thornton 1979) (Fig. 1.9). Tirrawarra sediments have been observed as far south as Cherri #1 and as far east as Mount Howitt #1 (Qld) (Fig. 1.2). Apak (1994) concluded that the thickness of this unit is highly variable with the greatest accumulations, like the Merrimelia Formation, occurring on the flanks of the GMI Trend (Fig. 1.9). The thickest intersections noted by Apak (1994), were observed at Kurunda #1 (99m) and Tindilpie #1 (85m) wells (Fig. 1.2). Rezaee (1996) concluded that the Tirrawarra Sandstone in the Moorari and Fly Lake fields has an average thickness of approximately 62 metres. On a regional basis the average thickness of the Tirrawarra Sandstone is approximately 70m (Hill and Gravestock, 1995). Like the Merrimelia Formation, the Tirrawarra Sandstone is absent from palaeo-highs, both structural and stratigraphic (Fig. 1.8).

The subsurface distribution of the Tirrawarra Sandstone is related to the present structural trend of the basin suggesting that the structural features were imposed on the basin after the deposition of the Tirrawarra Sandstone. The proposed

palaeodispersal direction for the Tirrawarra Sandstone was towards the east and east-north-east (Thornton, 1979).

1.7 STRUCTURE OF THE COOPER BASIN

The structural prehistory of the Cooper Basin was dominated by granite emplacement (10 million years prior to Cooper Basin initiation), followed by uplift and glaciation (Gravestock and Jensen-Schmidt, 1998). The exposure of these granites on the basin floor of the Cooper Basin indicates that there was considerable, and very rapid, uplift and erosion. Both the emplacement of granite and unroofing were events that were associated with a high thermal regime in the upper crust. The cooling granite along with rapid sediment stripping saw an exponential decay of heat flows and subsequent crustal contractions (Gravestock and Jensen-Schmidt, 1998). The same authors conclude that the resulting cessation of elevated thermal conditions caused subsidence, forming the Cooper Basin.

The structure of the Cooper Basin comprises a series of NE/SW trending anticlinal ridges and synclinal basins, with smaller structural elements possessing NW/SE orientation (Chaney *et al.* 1997). In the southern Cooper Basin the synclines are termed Patchawarra, Nappamerri and Tenappera while the anticlinal ridges are termed the Gidgealpa-Merrimelia-Innamincka (GMI) and the Murteree-Nappacoongee (MN) Highs (Fig. 1.9). The major structural features within the Queensland sector of the Cooper Basin include the Arrabury Trough, Karmona Trend Nappamerri Trough, Strathmore Embayment and Tickalara Trend (Fig. 1.9).

There is some conjecture still as to whether the Cooper Basin is a compressional or extensional basin. The latest published discussion on this topic suggests that the Cooper Basin has formed by mild compression with localised extension tectonics, which resulted from sideways steps between adjacent fault blocks (Apak *et al.*, 1997). These authors believe that the earliest part of the Cooper Basin sequence may have been influenced by extensional forces, but inversion features formed during Patchawarra sedimentation is indicative, they argue, of a change to a compressional regime.

The rejuvenation of northwest and northeast orientated pre-Permian features, in the Sakmarian (Early Permian), resulted in the subsequent formation of the Gidgealpa-Merrimelia-Innamincka (GMI) Trend which separates the Patchawarra and Nappamerri Troughs (Apak *et al.*, 1993 and 1997) (Fig. 1.9). Apak *et al.* (1997) stated that the GMI trend did not exist during the early stages of basin development and

thus did not act as a sediment barrier, unlike the Jackson-Naccowlah structural zone which restricted sediment movement from the southern portion (SA sector) of the Cooper Basin to the northern (Queensland) region. The GMI Trend became a more positive feature in the Permian, as indicated by the Patchawarra Formation onlapping the GMI Trend. Further evidence of structural rejuvenation was described by (Thornton, 1979) who indicated that the Gidgealpa Group attains its thickest development on structural 'high's'.

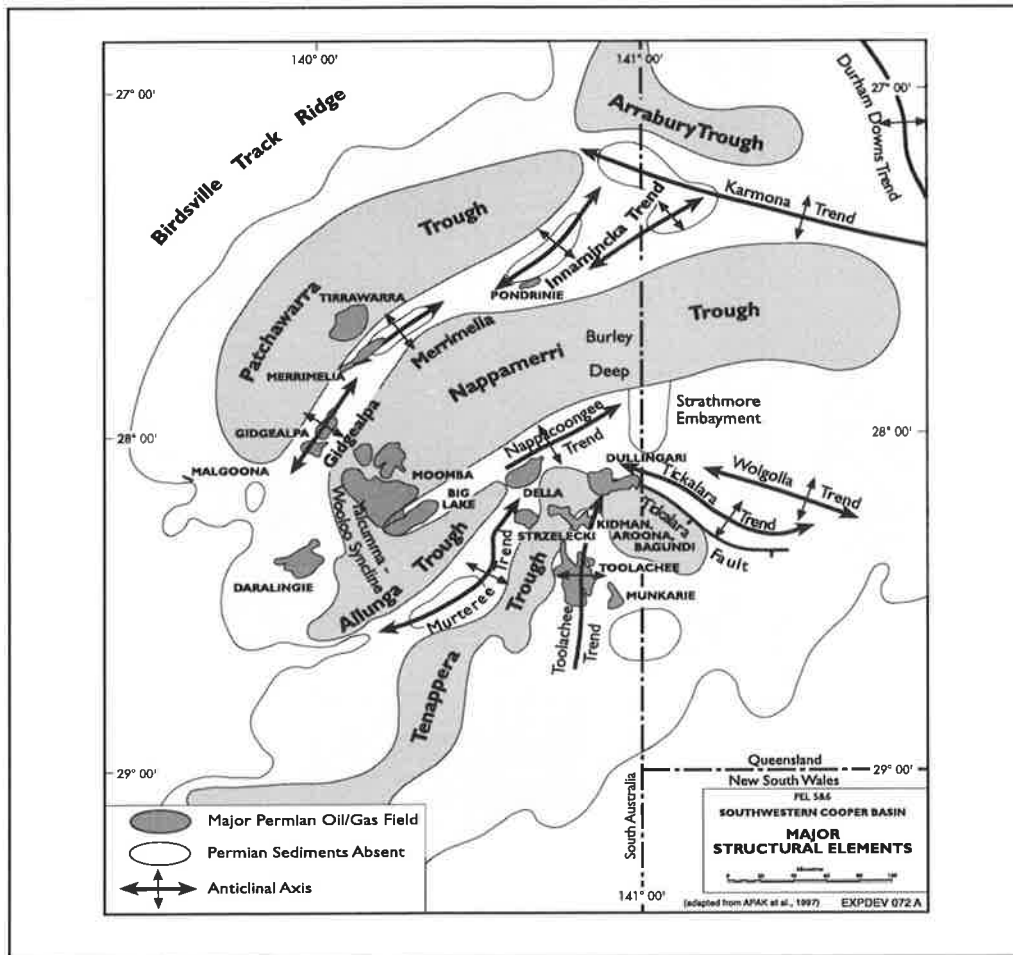


Figure 1.9. Structural elements of the Cooper Basin, South Australia and Queensland (Modified from Apak *et al.*, 1997).

Apak *et al.* (1997) concluded likewise, stating that some of the thicker parts of the Merrimelia Formation are to be found on the flanks of the GMI Trend implying that the Cooper Basin had an inverted topography during the deposition of Merrimelia glacial sediments. Apak *et al.* (1997) also observed that the GMI Trend, along with the Patchawarra Trough, behaved as a flank to the Nappamerri Trough. The Patchawarra Trough did not act as a major depocentre until after the Daralingie unconformity (Fig. 1.4). It was postulated by Apak (1994), that the Patchawarra Trough only became a

major depocentre as the Cooper Basin tilted northwards during the deposition of the Nappamerri Group (Fig. 1.4).

1.8 STRATIGRAPHIC UNITS WITHIN THE COOPER, EROMANGA AND WARBURTON BASINS.

The following section gives a brief description of units within both the Warburton and Cooper Basins. A brief discourse on the Eromanga Basin is also given.

1.8.1 CRYSTALLINE BASEMENT

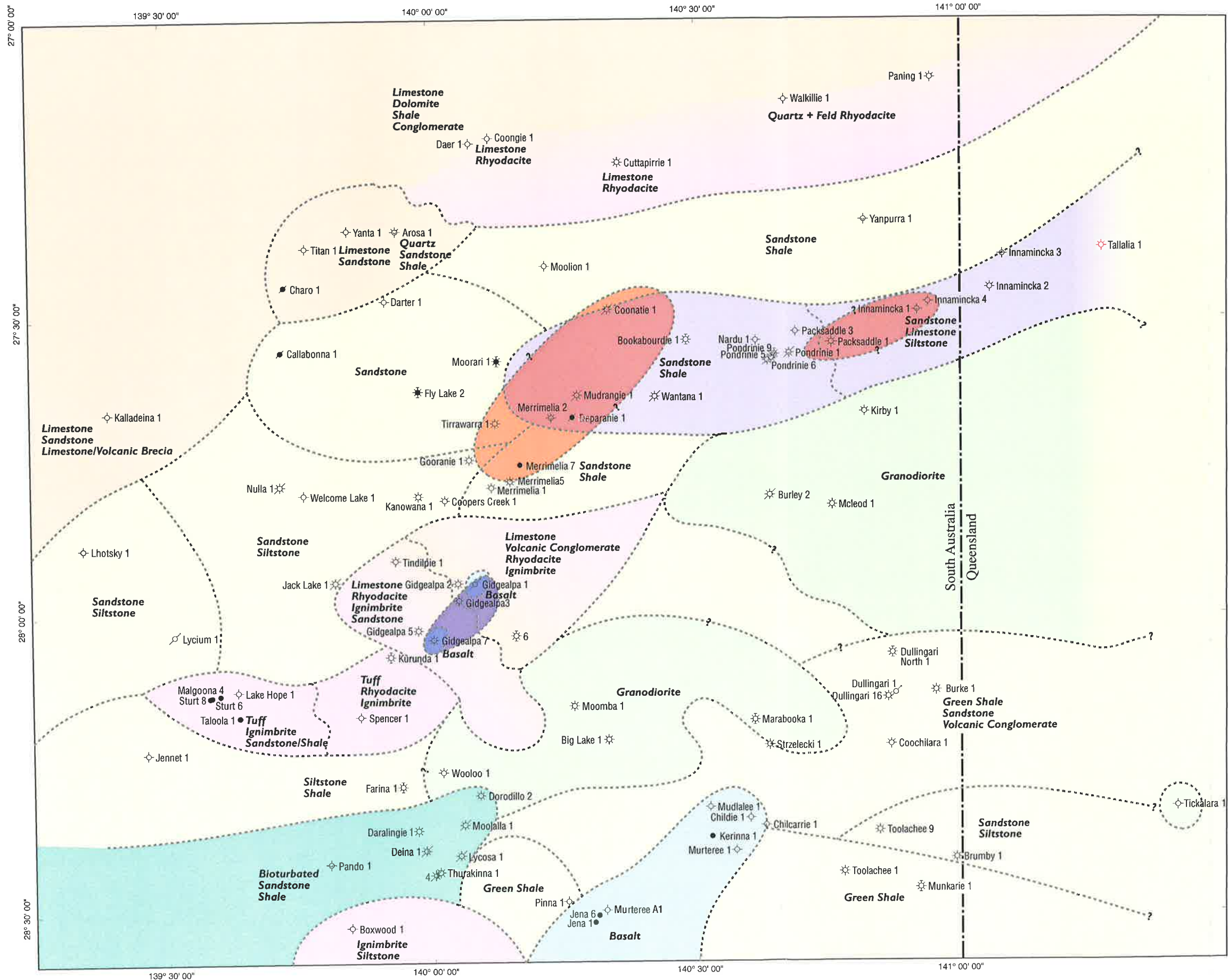
The Warburton Basin is a Cambrian-Devonian intracratonic basin. The underlying crystalline basement is only known from a handful of drillholes. Rankin and Gatehouse (1990) describe a crystalline lithology in Haddon Downs #1 as containing a proto-mylonitic pegmatitic gneiss and interpreted this intersection to be basement to the Warburton Basin and belonging to a southerly extension of the Arunta Block. The rock displayed moderate intensity, sub-vertical foliation defined by elongate "quartz ribbons" surrounding sub-euhedral to euhedral megacrysts of K-feldspar and plagioclase which is not comparable to the Carboniferous granites (Big Lake Suite Gneiss) intersected at Moomba (Fig. 1.10).

Low grade metamorphic rock were intersected at Naryilco #1, Mulga #1 and Fortville #3. These rocks are considered to be part of the Gnalta Shelf a northern extension of the Willyama Supergroup (Wopfner and Cornish, 1967; In Rankin and Gatehouse, 1990; Gatehouse, 1986).

1.8.2 WARBURTON BASIN

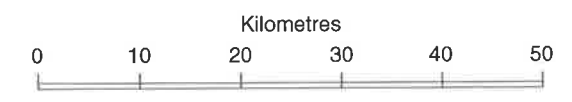
The Warburton Basin is an entirely concealed Early Palaeozoic basin that underlies the Pedirka, Cooper and Eromanga Basins (Fig. 1.3a). The basin is bounded to the north by the Arunta Block and to the south and west by the Muloorina Ridge and Musgrave Block.

The basin is divided into western and eastern regions by the Birdsville Track Ridge (Fig. 1.3a). The unit descriptions below are concerned only with the Eastern Warburton Basin, as the Cooper Basin overlies this portion. The Pedirka Basin overlies the western portion of the Warburton Basin (Fig. 1.3a). The stratigraphy of the Eastern Warburton Basin is shown in Figure 1.3b (Sun, 1996).



- Mudrangie Sandstone
- Vuggy Dolomite
- Kalladeina Formation
- Big Lake Suite Granodiorite
- Dullingari Group
- Mooracoochie Volcanics
- Innamincka Red Beds
- Pando Formation
- Basalt
- Schist / Phyllite - Willyama Supergroup

Eastern Warburton Basin Sub Cropping Lithologies Domains



① (Subcropping data derived from Big Lake Suite Granodiorite Distribution interpreted from mag intensity map Santos (1998))
(Contributions from Sun, (1996); Baines, (1996); Tiainen pers comm, 1998)

Figure 1.10 Eastern Warburton Basin Sub Cropping Lithology Domains ①

Cherri 1
 Gurra 1
 Mulga 1
These three well locations shown for illustration purposes only.

Lithostratigraphic relationships of the major units in this basin, according to Sun (1996), still remain elusive. A comprehensive study conducted by that author, however, has clarified the inter-relationships of Warburton Basin units and suggested a number of new units. Sun (1996) suggested that the chronological order of Warburton Basin units is as follows: Mooracoochie Volcanics, Vuggy Dolomite, Kalladeina Formation, "Innamincka Red Beds", Mudrangie Sandstone and then the Dullingari Group. The age and sedimentary origin of the Pando Formation still remains a point of conjecture. In the following section the Pando Formation has been described last and in no way reflects any chronostratigraphic position within the basin. Figure 1.10 is a subcrop map illustrating the distribution of lithostratigraphic units of the eastern Warburton Basin.

1.8.2.1 Mooracoochie Volcanics

This unit is composed of mainly acidic to intermediate lavas including rhyodacite, dacite, and minor alkali basalts (Sun, 1996) (Chapter Five - Fig. 5.11). In addition to these main lithologies, Sun (1996) also describes ignimbrites (Plate 1b) and associated volcanoclastics as well as epiclastics and sandstones. The same author divides this unit into six facies assemblages that range from effusive, explosive, reseedimented and epiclastic facies types. Both Boucher (1996) and Sun (1996) argue that the Mooracoochie Volcanics have formed in a continental rift, and not an island arc setting as proposed by Gatehouse (1986). Commercial flows of oil of Permian origin have been recorded from up-dip traps within the Mooracoochie Volcanics in Sturt #6 (Gravestock and Gatehouse, 1995).

1.8.2.2 Vuggy Dolomite

This unit has been suggested by Sun (1996) to be a separate unit from the Kalladeina Formation. Gravestock and Gatehouse (1995) however include this vuggy dolomite within the basal reaches of the Kalladeina Formation. Sun (1996) believes that, as this unit was not noted in the type section at Kalladeina #1 and in only five wells in the Gidgealpa Field, that it may represent an as yet undefined rock unit. This unit has undergone complete dolomitisation and karstification creating secondary vuggy and inter-crystalline porosity (Sun, 1996). The same author suggested that the precursor of this dolomite unit may have been an oncoid-intraclastic wackestone/packstone, deposited in a peritidal environment.

1.8.2.3 Kalladeina Formation

According to Sun (1996), the Kalladeina Formation is composed of two main types of lithologies, representing two stages of deposition. Gravestock and Gatehouse (1995),

however, described the Kalledeina Formation in sequence stratigraphic terms, highstand and transgressive deposits. The transgressive deposits are composed mainly of chert and grey micaceous shales, bioturbated siltstones and limestones (Gravestock and Gatehouse, 1995). The highstand deposits represent a return to shallow marine conditions with grey shale, siltstone and recrystallised limestone predominant (Gravestock and Gatehouse, 1995; Sun, 1996).

1.8.2.4 "Innamincka Red Beds" or Innamincka Formation

According to Gravestock and Gatehouse (1995), the Innamincka Red Beds is equivalent to the lower Dullingari Formation and the upper section of the Kalladeina Formation (Sun, 1996). Sun (1996) described the "Innamincka Red Beds" in terms of two members: the lower member and upper member. The lower member is red, composed of cross-laminated and bioturbated mudstone, shale and siltstone. The upper member is green and primarily composed of horizontally laminated glauconitic shale that is sandier than the lower member. The distribution of these sediments is extensive throughout the northeastern edge of the eastern Warburton Basin (Fig. 1.10) and extends southwards to the Moomba area.

1.8.2.5 Mudrangie Sandstone

This unit, proposed by Sun (1996), consists of a white to light grey sandstone which exhibits frequent cross beds and cross-laminations along with rounded greenish mudstone/shale pebbles within bedding planes. Zang (1993b) and Sun (1996) envisage that this unit was formed in a shallow marine setting dominated by fluvial input, where tidal and storm surges produce scour surfaces, rip up clasts and over sized pebbles within the sandstone. This sandstone is widespread and distinctive in appearance and can possibly be used as a marker bed to correlate between isolated wells (Sun, 1996).

1.8.2.6 Dullingari Group

The Dullingari Group is composed of two different units: a lower dark grey to black pyritic shale and an upper greenish siltstone and shale separated by a thin bed of pebbly sandstone or breccia (Gravestock and Gatehouse, 1995; Sun, 1996). The lower unit comprises dark grey to black, horizontally laminated siltstone and shale with abundant pyrite nodules, and is common in the south eastern part of the Warburton Basin (Fig. 1.10). The upper member consists of green laminated siltstones and shales (Sun, 1996). A sandy layer occurs between these units and most likely represents a grain flow or a slump deposit as suggested by its brecciated nature (Sun, 1996). All

evidence suggests that these sediments have been deposited on a delta slope within deep water.

1.8.2.7 Pando Formation

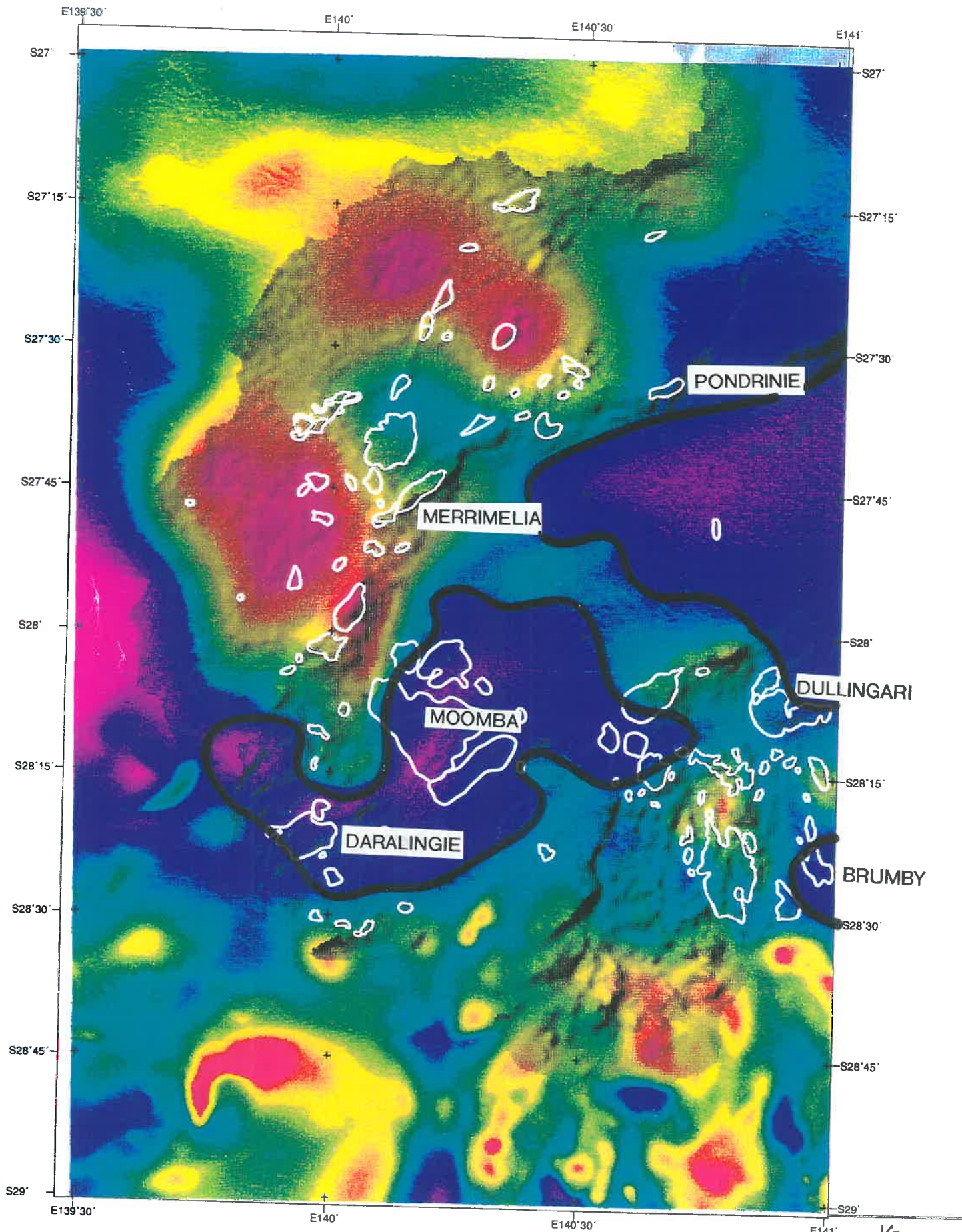
Siliclastics of the Pando Formation, first described by Gravestock *et al.* (1995), occur beneath and interfinger with the Mooracoochie Volcanics (Fig. 1.3) (Gatehouse 1983: In Gravestock and Gatehouse, 1995). Sun (1996) argues however, that the Pando Formation may be equivalent to the "Innamincka Red Beds", while Zang (1993a) has revised the Pando Formation name to Pando Sandstone.

The Pando Formation (or Pando Sandstone) consists of pale green-grey, irregularly laminated, bioturbated silty sandstone with abundant glaucony and detrital zircons (Gravestock and Gatehouse, 1995). Sun (1996) and Gravestock and Gatehouse (1995) conclude that the Pando Formation was deposited in a marginal to shallow marine setting of unknown extent. Gravestock and Gatehouse (1995) stated that this unit acts as a reservoir for Permian gas in Moolalla #1.

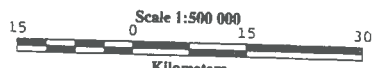
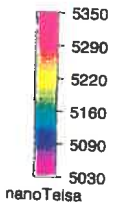
1.8.3 BIG LAKE SUITE GRANODIORITE

The Big Lake Suite Granodiorite (Plate 2g) (Gatehouse *et al.*, 1995) or Moomba Granite has been intersected by 23 drill holes. In Moomba #2 these granodiorites have intruded into Warburton Basin sediments with contact metamorphic effects evident in Kalladeina Formation sediments (Gatehouse *et al.*, 1995). The granodiorite body lies primarily beneath the Moomba and Big Lake Fields but was also intersected in the McLeod #1 drill hole to the north east (Fig. 1.10). This suggests that the Big Lake Suite underlies most of the Nappamerri Trough. A magnetic intensity map of the Cooper Basin (Fig. 1.11) indicates that the sub-cropping distribution of this granodiorite² is more complicated than the distribution inferred by drill hole intersections. A dividing ridge of higher response magnetic material appears to separate the granodiorite into southern and northern batholiths. The southern batholith is centered beneath the Moomba/Big Lake field and extends down towards the Daralingie Field in the south (Fig. 1.11). The northern batholith appears to be centered in Queensland extending south west beneath the South Australian portion of the Nappamerri Trough. Big Lake Suite granodiorite was also intersected at Tickalara #1 in Queensland (Plate 2g). This well is located east of the Dullingari field and may indicate that the northern Big Lake Suite granodiorite batholith extends southwards into Queensland.

² The Big Lake Suite Granodiorite is represented by the deep purple/pink in Figure 1.11.



Key
 ——— OUTLINE
 OF SUB-CROPPING
 GRANODIORITE



Universal Transverse Mercator Projection
 Zone 54 South (CM 141E)
 Spheroid: WGS84

SANTOS NTAG		
TMI (colour)		
P Depth (shaded relief)		
Illumination Direction: 310		
Illumination Elevation: 45		
Gas fields outlined in white		
DATE: 23/05/88	BY: DJG/DSW	PLANNING
SCALE: 1:500 000	PIB	

FIGURE 1.11 DISTRIBUTION OF THE BIG LAKE SUITE GRANODIORITE BENEATH THE COOPER BASIN S.A

The western edge of this southern extension can be observed on the edge of the map sheet between S28°15" and S28°30" (Fig. 1.11).

The granodiorite at Big Lake #1 is coarse grained and moderately weathered, consisting of abundant quartz (~40%), microcline, orthoclase and sericite (Gatehouse *et al.*, 1995). At Moomba, the granite is also very coarse grained but contains predominantly orthoclase (~60%), quartz (~30%), plagioclase (5%-10%) and chloritised biotite (5%) (Gatehouse *et al.*, 1995). These authors dated Big Lake Suite Granodiorite samples from McLeod #1 and Moomba #1 using U-Pb isotopic analyses and established ages of emplacement at between 298±4Ma and 323±Ma (Early-Middle Carboniferous). These dates correspond with the Devonian-Early Carboniferous Alice Springs Orogeny along with the formation of the Radium Ridge Beds and Mt Gee Sinter (Gatehouse *et al.*, 1995; Priess, 1995).

1.8.4 COOPER BASIN

1.8.4.1 Merrimelia Formation

The Merrimelia Formation is the basal unit of the Cooper Basin and was deposited unconformably on the deformed Warburton Basin (Fig. 1.3). According to Williams and Wild (1984a) and Chaney *et al.* (1997) the Merrimelia Formation is composed of glacial and peri-glacial sediments which form a depositional continuum with the overlying Tirrawarra Sandstone. Glacio-fluvial, glacio-lacustrine, deltaic and aeolian facies form the bulk of the Merrimelia Formation. No glacio-marine sediments were observed. A detailed description of the various facies types observed in the Merrimelia Formation is given in chapter four.

The Merrimelia Formation has been traditionally regarded as economic basement until the drilling of Pondrinie 5 in 1989 and Malgoona 1A in 1990. Both wells penetrated commercial hydrocarbons columns, with the Pondrinie 8 well intersecting 56m of net pay in a sandstone sequence that exhibited an average porosity of 18% (Gravestock *et al.* 1998). On test Pondrinie 8 flowed at 8.71mmcf/d while Malgoona 1A flowed oil at 640bbl/d.

1.8.4.2 Tirrawarra Sandstone

The Tirrawarra Sandstone has long been accepted as a sequence of fluvial sediments deposited on a broad outwash braidplain (Gostin, 1973). The sandstone is of variable thickness (average 70m) and generally interfingers with the Merrimelia Formation (Williams and Wild, 1984a). Locally, near basement highs, Tirrawarra sediments may however unconformably overlie Merrimelia sediments (i.e. Big Lake Field – see

Chapter Nine). The depositional geometry has been likened to that of a braid delta (Hamblin *et al.*, 1996) in part reworked by a transgressive and regressive lacustrine shorezone which prograded and retrograded across the area in response to frequent changes in lake level (Seggie *et al.*, 1994).

The Tirrawarra Sandstone is subdivided into four facies associations (Williams and Wild, 1984a & 1984b). Association 2 comprises the main net pay horizon for hydrocarbon production (Chaney *et al.*, 1997). Association 2 consists of a medium-coarse grained sublitharenite with trace conglomerate, mudrock and coal intervals. The sandstone architecture reveals multiple stacking patterns with rarely defined upward-fining or coarsening facies transitions (Chaney *et al.*, 1997). The sandstone packages locally preserve vegetated (and coalified) bar tops and the whole of Association 2 was deposited in a proglacial braidplain in which bed accretion of low amplitude medial bars led to the stacking patterns observed within the sandstones (Chaney *et al.*, 1997).

1.8.4.3 Patchawarra Formation

The Patchawarra Formation in general unconformably overlies the Tirrawarra Sandstone in the deeper parts of the Cooper Basin. This unit also unconformably overlies the Merrimelia Formation and Warburton Basin sediments at basin margins or near structural highs (see Tallalia #1 lithology log Appendix 9a).

The Patchawarra Formation is a coal measure sequence up to 680m thick composed of interbedded, fluvial, fluvio-lacustrine, flood plain and deltaic sediments.

Thick sandsheet deposition occurred where early fault movement produced areas of positive relief (Stuart, 1976). These sandsheets also contain siltstones and minor coals and represent the lowermost Patchawarra Formation. The middle section exhibits extensive point bar and channel sediments within a system that is dominated by coal seams (some up to 30m thick). The uppermost Patchawarra Formation is characterised by widespread flood-plain sediments consisting of lacustrine shales and delta sandstones (Hill and Gravestock, 1995). According to Carne (1986), the middle part of the formation contains the most important commercial reservoir rocks.

1.8.4.4 Murteree Shale

The Early Permian Murteree Shale comprises a uniform suite of dark grey to black carbonaceous shales (micaceous in places), with minor interbedded siltstone and sandstone (Carne, 1986). These sediments formed in an extensive fresh water lake that

possibly transgressed from the southeast to the northwest across the Cooper Basin (Carne, 1986). This unit is generally uniform in thickness varying from 30m-60m and forms a regional seal above the Patchawarra Formation. This unit attains its greatest thickness in the Nappamerri Trough (Hill and Gravestock, 1995). The Murteree Shale is considered a source rock and has been attributed with providing both gas and condensate in Patchawarra and Epsilon reservoirs (Carne, 1986).

1.8.4.5 Epsilon Formation

The retreat of the Murteree lake is marked by shoreline and delta plain sediments in the lower Epsilon Formation (Carne, 1986). This unit, Early Permian (Artinskian to Kungurian) in age (Price *et al.*, 1985), is composed of 156m of fluviodeltaic sediments, lacustrine shales, siltstones, sandstones and minor coals. The Epsilon Formation is mainly developed in the Nappamerri Trough with the unit absent along the northern flank of the Patchawarra Trough and on the western flank of the Cooper Basin (Hill and Gravestock, 1995). According to Carne (1986), the sandstones within the Epsilon Formation are thin and commonly fine to very fine grained, exhibiting abundant quartz overgrowths and clay matrix within the pore space which can destroy reservoir quality. Commercial quantities of hydrocarbons have been found in this formation at the Toolachee, Daralingie and Cuttapirrie fields (Carne, 1986).

1.8.4.6 Roseneath Shale

The Roseneath Shale, according Price *et al.* (1985), is Kungurian (Early Permian) in age. This unit, in the Nappamerri Trough, attains a maximum thickness of 100m (Alexander, 1998) overlying the Epsilon Formation. The Roseneath Shale has similar characteristics to the Murteree Shale, in that it is generally restricted to the Nappamerri and Tenappera Troughs and comprises shales and siltstones that were formed in an extensive lake system (Hill and Gravestock, 1995). The present day distribution of this unit does not reflect its original extent with erosion at the end of the early Permian stripping these sediments from off the flanks of the GMI Trend and basin margins (Carne, 1986). This unit is considered a source rock unit and has possibly acted as a source for hydrocarbons within the Epsilon and Toolachee Formations (Carne, 1986). This unit also acts as a seal for the upper Epsilon Formation.

1.8.4.7 Daralingie Formation

The retreat of the "Roseneath lake" led to the deposition of regressive sediments such as fluviodeltaic sandstones, siltstones and minor coal sequences (Thornton, 1979), the lower Daralingie Formation. According to the same author, this formation is absent on structural ridges and is thickest in the Nappamerri Trough (100 metres thick). The

sandstones in this formation are thought to be deltaic in nature, representing distributary mouth bars (Stuart, 1976). Price *et al.* (1985) assign this formation to the PP4 (Kungurian to Ufimian) palynozone.

The upper parts of the Daralingie Formation were truncated by a regional erosional event. This erosional event exposed basement on structural highs, with subsequent uplift resulting in the gradual removal of older Permian strata in the Patchawarra Trough (Hill and Gravestock, 1995). The same authors suggested that any connection with the Arckaringa and Pedirka Basins (Fig. 1.1) would have been severed at this time. The sands within the Daralingie Formation are tight, commonly exhibiting very low porosities. These sandstones are accordingly are only productive along the southwest flank of the Moomba structure (Carne, 1986).

1.8.4.8 Toolachee Formation

The Daralingie erosional event effectively peneplained the entire Cooper Basin (Carne, 1986). The deposition of the Late Permian Toolachee Formation was very widespread across the basin, with only a few emergent palaeo-highs not covered by this unit. This unit is the most extensive Permian unit observed in the Cooper Basin.

The Toolachee Formation (Kazanian to Tatarian) commonly attains a thickness of 100 metres (up to 175 metres in the Nappamerri Trough) and is composed of sandstones that have been deposited in mixed-load fluvial channels, and mudstones which have formed in overbank and lacustrine settings. Alongside these deposits peat swamps developed, forming coals (Stuart *et al.*, 1988). These sediments are observed in equal proportions within this unit (Carne, 1986), but are not necessarily evenly distributed throughout the unit. The formation, in general, comprises an upper and lower section. The lower unit is composed predominantly of coarse grained sandstones, the main hydrocarbon-bearing reservoirs in this unit. The upper unit is dominated by interbedded coals and sandstones which dominantly exhibit poor reservoir quality. Gas has, however, been found in this upper section at the Della Field (Carne, 1986). During Toolachee deposition, the Cooper Basin was covered by extensive flood plains across which meandered large rivers, with peat swamps over large areas of the basin (Carne, 1986). Thornton (1979) envisaged that Toolachee sediments were brought into the basin from the west.

1.8.4.9 Nappamerri Group

The Nappamerri Group consists of the Late Permian to Middle Triassic Arrabury Formation, which comprises the Callamurra, Paning and Wimma Sandstone Members

and the Middle Triassic Tinchoo Formation (Hill and Gravestock, 1995). According to Alexander (1998) the Nappamerri Group can attain thicknesses, in the South Australian portion of the Cooper Basin, of up to and in excess of 500 metres.

1.8.4.9.1 Arrabury Formation

The sediments of the Tatarian to Anisian aged Arrabury Formation were deposited in a broad floodplain setting that frequently supported lakes and was crossed by extensive river systems (Hill and Gravestock, 1995). These sediments are red, representing an oxidising environment compared with the coal-forming environments below. Hill and Gravestock (1995) interpret this shift in depositional style to be related to continental scale climate change in the Triassic, which, when compared to the Permian, is temperate (the climate of the Permian was polar to cool temperate). The Callamurra Member is composed of carbonaceous reddish to purple mudstones and siltstones containing thin interbeds of sandstone (Youngs and Boothby, 1985). The Paning Member consists of upward-fining sandstones with minor mudstone deposition in a fluvio-lacustrine environment along the flanks of the GMI Trend (Youngs and Boothby, 1985). The Wimma Sandstone Member is a clean interbedded sandstone with minor mudstone having formed in a braided stream system (Hill and Gravestock, 1995).

1.8.4.9.2 Tinchoo Formation

The Middle to early Late Triassic (Anisian to Ladinian) Tinchoo Formation conformably overlies the Wimma Sandstone Member and is confined to the Patchawarra and Nappamerri Troughs (Hill and Gravestock, 1995). This unit, composed primarily of interbedded sandstones, siltstones and mudstones, reaches a maximum thickness of 100 metres.

Youngs and Boothby (1985) interpreted a high-sinuosity fluvial environment to be the dominant Tinchoo Formation sedimentation style. In describing the basal part of the Tinchoo Formation Hill and Gravestock (1995) concurred with the previous authors but also noted that the lower part of the unit was dominated by upward-fining sandstone beds, which graded into laterally extensive lacustrine mudstones and siltstones, forming a regional seal.

1.8.4.10 Cuddapan Formation

This is an areally-restricted sandstone, siltstone and coal unit observed in the Patchawarra Trough (Krieg, 1995). This unit is recognised as the last deposited within the Cooper Basin (Late Triassic – Carnian to Narian) obtaining a thickness of 67

metres in Beanbush #1. The Cuddapan Formation unconformably overlies the Nappamerri Group and is in turn unconformably overlain by the Poolowanna Formation of the Eromanga Basin.

1.8.5 EROMANGA BASIN

The Eromanga Basin is the largest of three epicontinental basins that form the Jurassic to Cretaceous Great Artesian Basin (Krieg *et al.*, 1995). Only the southwestern portion of the Eromanga Basin occurs in South Australia. The sedimentary record of the Eromanga Basin extends without a major break from the Early Jurassic to Mid-Cretaceous (Fig. 1.3) and consists of cyclical sandstone and mudstone units (Krieg *et al.*, 1995). The lower portion of the basin is composed of cross-bedded sandstone sequences that formed in braided river environments (Hutton Sandstone) and contain significant hydrocarbon reserves, particularly in Queensland. These sediments were sourced, in a large part, from underlying Cooper Basin sediments (Krieg *et al.*, 1995). The upper portion of the basin is composed of low energy, fine-grained lacustrine siltstones and mudstones, which formed predominantly in floodplain environments. A marine incursion is recorded by a grey, fossiliferous mudstone-siltstone sequence and regressive sandstone-siltstone unit in the upper part of the Eromanga Basin.

Deposition of the Eromanga sedimentary sequence commenced in the Early Jurassic with the Poolowanna Formation (a maximum thickness of 206 metres is described in the Windorah Trough). This unit consists of fluvial quartzose sandstones, interbedded with carbonaceous siltstone/shale and coal (Carne, 1986). It grades into the overlying Hutton Sandstone exhibiting both good reservoir quality and oil prone source rocks. Commercial quantities of oil have been found within this unit at the Bodalla South and Kenmore Fields (Carne, 1986).

The Hutton Sandstone consists of a sequence of anastomosing and aggrading braided stream deposits. Sediment influx, according to Carne (1986), outpaced subsidence such that braided fluvial deposition was superseded by meandering stream deposition in the upper sections. The formation is composed of up to 200 metres of very fine to conglomeratic, moderately to well sorted sandstones. Minor siltstone and shale interbeds do occur. Although the sandstone pore space is dominated by quartz overgrowths and kaolin clay, this unit displays excellent reservoir quality and represents the major hydrocarbon bearing zone in the Eromanga sequence. The majority of oil accumulations reseroired in the Hutton Sandstone occur around the edges of the Nappamerri Trough in both South Australia and Queensland (Carne, 1986).

In places the Birkhead Formation lies conformably on the Hutton Sandstone. This unit consists of shallow lacustrine, swamp, interfluvial and overbank deposits and attaining a maximum thickness, in the Windorah Trough, of 100 metres. The Birkhead Formation formed via coalescing fluvial systems where relief was low and extensive lakes formed. Extensive floodplain and backswamp environments have also been interpreted, with coal formation common in a moist and temperate climate capable of supporting conifer forests (Carne, 1986). Oil generation from the shales and coals in the Birkhead Formation has only been moderate with accumulations noted at Moorari #3 and Big Lake #26. Importantly the Birkhead Formation acts as a seal for Hutton Sandstone reservoirs.

The contact between the Adori Sandstone and the underlying Birkhead Formation is generally abrupt (Carne, 1986). This formation is approximately 30 metres thick, composed of braided and meander sandstones where stacked point bar sequences predominant. The rocks in this unit appear to have been deposited in a high energy environment (as opposed to the low energy environment of the Birkhead Formation). The sandstones exhibit porosity ranging from poor to very well developed and grain sizes that vary from very fine to conglomeratic. Sorting accordingly is moderate where grains are angular to sub-angular in nature. Only minor accumulations of hydrocarbons (Koorra #1 and Koorapora #1) have been found in this unit (Carne, 1986).

The deposition of the Westbourne Formation (average thickness of 110 metres) represents deposition in a predominantly flood plain setting which eventually became dominated by lacustrine sedimentation. Accordingly the formation consists of a fining upwards sequence composed of thinly bedded, fine grain sandstones, and shales as well as rare coals. Quartz and calcite cements are common with kaolin the dominant pore filling diagenetic phase. Commercial accumulations of hydrocarbons are found in this unit at the Jackson Field (Carne, 1986). The Hooray Sandstone (114 metres thick in the type section) is interpreted to occur where the top Westbourne correlation is uncertain and where the lacustrine facies in this formation are not present. This occurs predominantly in the southern flanks of the basin where the Hooray Sandstone consists of braided sandstones.

Following lacustrine Westbourne sedimentation, extensive braided stream sedimentation occurred. These strata are assigned to the Namur Sandstone Member. The sandstones in this unit are consistently massive in nature, fine to coarse-grained, predominantly quartzose with minor feldspar. The Namur Sandstone generally attains a thickness of 200 metres (Moomba Field). Carne (1986) describes fining

upwards sequences with the top cycle grading into lacustrine conditions (Murta Shale Member). This unit represents a major reservoir for both hydrocarbons and artesian water. Gas has been found accumulated in Namur sands in the Namur and Marabooka Fields (Carne, 1986).

The Murta Shale Member (approximately 73 metres thick) is a lacustrine sequence consisting of shallow siltstones and shales with minor deep-water mudstones. Flood deposits, turbiditic grain flows and deltaic sediments also comprise this unit (Carne, 1986). The rock quality is regarded as fair to poor (Carne, 1986).

The Cadna-owie Formation ranges in thickness from 40 to 90 metres and represents the transition between the terrestrial sedimentation of the lower Eromanga sequence and the predominantly marine deposition which prevailed through much of the Cretaceous (Kreig and Rogers, 1995). This formation consists of fine to medium grained quartzose to sub-labile sandstones and basal siltstones with minor shales noted. Pebbly layers, conglomerates and diamictites occur locally (Kreig and Rogers, 1995). The whole unit is upward coarsening in nature. Hydrocarbons have been generally noted in the Wyandra Member (200 metre thick in Rolwegan Creek #1), which is representative of a transgressive beach sand.

Other Cretaceous units include the Wallumbilla Formation, Bulldog Shale, Corrikiana Sandstone, Toolebuc Formation, Allaru Mudstone, Oodnadatta Formation, Mackunda and Winton Formations.

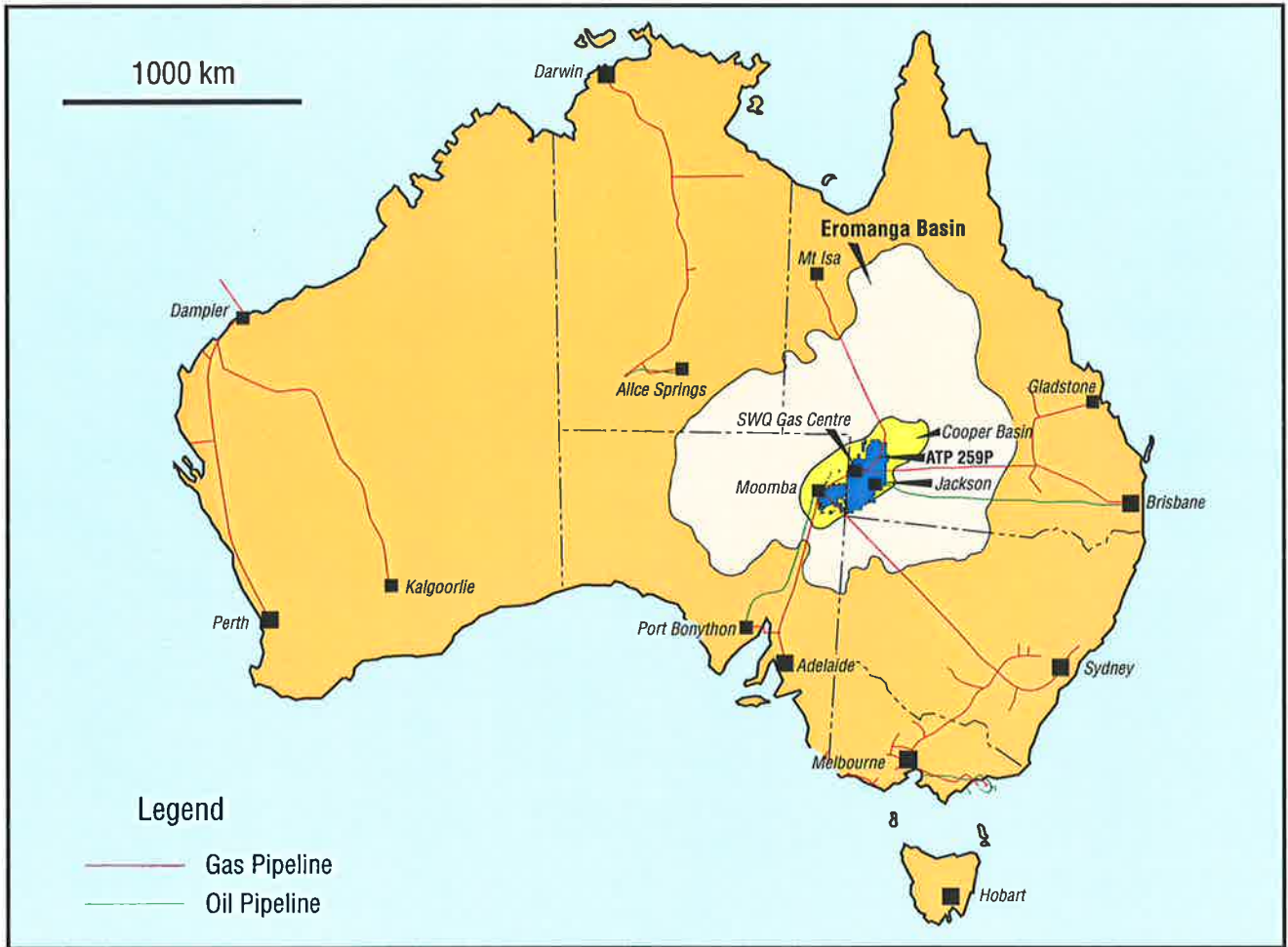
The Wallumbilla Formation (361 metres thick in Cuttahirrie #1) consists of grey siltstone with minor mudstone having formed in a shallow, epicontinental marine environment. The Bulldog Shale (up to 350 metres of section is observed in the Nappamerri Trough) is similar to the Wallumbilla Formation, consisting of dark grey carbonaceous shale with concretionary limestone (Carne, 1986). Fine interbeds of sandstone have been reported along with fossilised wood (Kreig and Rogers, 1995). The Corrikiana Sandstone is a thin unit (10 metres thick on average) consisting of bioturbated sandstone, having been formed in a shallow marine environment. The Toolebuc Formation has a variable thickness of 3 to 75 metres and consists of dark grey to black siltstone, mudstones and marl (Carne, 1986). This unit formed in shallow marine conditions. The Albian aged Allaru Mudstone (197 metres thick in Coopers Creek #1) rests conformably on the Toolebuc Formation. This unit contains thin interbeds of grey siltstone/mudstone and calcareous siltstone (Kreig and Rogers, 1995). Concretionary limestones have also been reported from this formation (Senior

et al., 1978). This unit is interpreted by these workers as having formed in quiet marine conditions. Consisting of mainly shale and siltstone, with minor calcareous sandstone and rare limestone the Oodnadatta Formation, like the Allaru Mudstone, is interpreted to have been deposited in quiet shallow marine conditions (Carne, 1986). The Oodnadatta Formation attains a maximum thickness of 300 metres in the Moomba region. The Mackunda Formation (generally 100 metres thick) represents a marginal marine sequence of siltstones, calcareous sandstones and shales that represent the transition between the marine Allaru Mudstone and the terrestrial Winton Formation (Senior *et al.*, 1978). The Winton Formation is a 900 metre thick sequence of interbedded grey shales and siltstones that formed in a low energy meander system (Kreig and Rogers 1995).

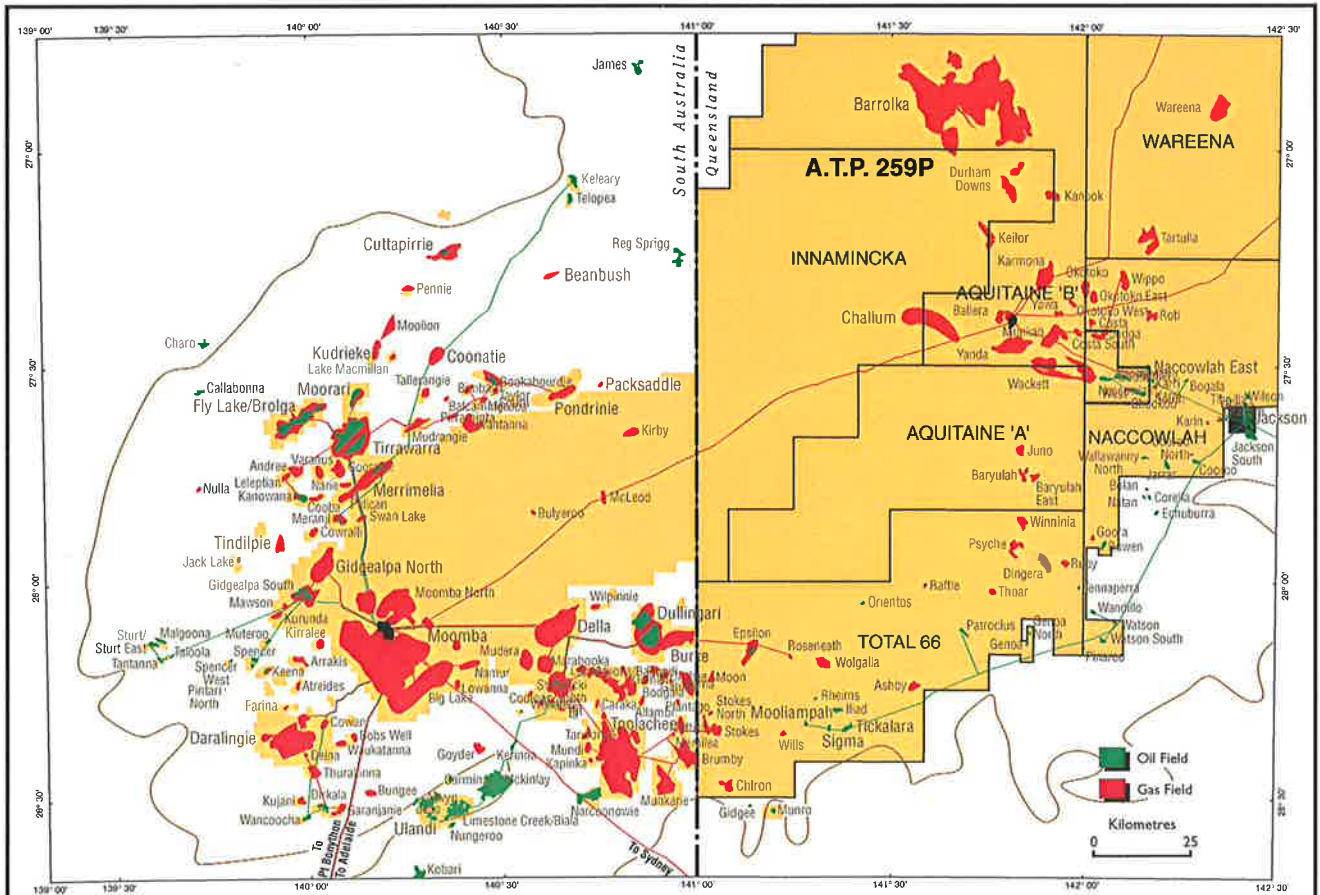
1.9 PETROLEUM GEOLOGY OF THE COOPER BASIN

The first commercial hydrocarbon discovery was made at the Gidgealpa #2 well in 1963. Subsequently 121 gas fields and 25 oil fields have been delineated (Hill and Gravestock, 1995) (Fig. 1.12). Morton (1998) estimates that the present discovered recoverable reserves within the Cooper Basin amount to 8.2 TCF ($229 \times 10^9 \text{m}^3$) of raw gas and 43.9 MMSTB ($6.9 \times 10^6 \text{kl}$) of oil. These reserves are mainly reservoirized within four way dip closures on the flanks of intrabasinal highs (such as the GMI Trend) (Schulz-Rojahn, 1993; Apak *et al.* 1997). To date, in excess of 1500 exploration and development wells have been drilled within the Cooper Basin with the greatest exploration successes coming from drilling large anticlines and drape structures (e.g. Moomba anticline in 1966). Only a limited number of stratigraphic targets have been drilled (Heath, 1989), with commercial hydrocarbon accumulations found at Pondrinie, Wackett and Naccowlah South (Stanmore, 1989). The discovery of stratigraphic hydrocarbon accumulations is becoming more commonplace (Hill and Gravestock, 1995).

The Patchawarra, Toolachee and Daralingie Formations (Fig. 1.4) are the most productive gas-bearing units whilst approximately 95% of Cooper Basin oil is reservoirized in the Tirrawarra Sandstone at the Tirrawarra Field (Heath, 1989).



A



B

PEL/56 546 I

Figure 1.12 A) Oil and gas pipelines of Australia. B) Cooper Basin infrastructure and the main producing oil and gas fields.

Additional gas reserves occur in the Epsilon Formation and the Triassic sediments of the Nappamerri Group (Kantsler *et al.*, 1983; Heath, 1989).

The bulk of hydrocarbons is reservoirised within fluvial channels and point bar deposits with subordinate quantities found in lacustrine shoreline sandstone reservoirs. According to Apak *et al.* (1997), fluvial channel and point bar sandstones are characterised by low porosities (average 11%) and permeabilities (average, 30md). Schulz-Rojahn and Stuart (1991) were more pessimistic stating that 75% of reservoir sandstones within the Cooper Basin exhibit permeabilities of 5md. Micro-porosity within kaolin booklets is important, especially for the storage of gas (Tingate and Luo, 1992). The Roseneath and Mutreree Shales provide good to excellent regional seals for the principle reservoir zones within the Cooper Basin (Kantsler *et al.*, 1983; Heath, 1989).

Cooper Basin oils and condensates are typically medium to light (43^o-56^o API), highly paraffinic, low in sulphur, with variable low to high wax contents (Kantsler *et al.* 1983). These hydrocarbons also exhibit high pristane/phytane ratios, indicative of a land plant origin. Hunt *et al.* (1989) stated that most Permian oils contain significant amounts of dissolved gas, with little evidence of water washing. McKirdy (1989) found this to be also true for hydrocarbons sourced from glaciogenic sediments of the Cooper Basin, concluding that coals within the Tirrawarra Sandstone have great hydrocarbon generating potential with the generated product likely to be light oil with gas. The same author also observed that the Merrimelia Formation was lean in organic carbon. The generation of Tirrawarra crudes, according to Hunt *et al.* (1989), was from inter-seam coal measures of the upper Patchawarra Formation rather than Tirrawarra coal seams.

Hydrocarbon gases within the Cooper Basin include methane (C₁), ethane (C₂), propane (C₃), butane (C₄) and pentane (C₅) (Hunt *et al.*, 1989). Other gases include N, H, He, H₂S and CO₂, with the CO₂ percentage varying from 10% to 40%. Kantsler *et al.* (1983) demonstrated that the origin of CO₂ was from both basement granites and the thermal breakdown of humic sediments. These authors went on to say that the primary source of wet gas and oil found within Permian reservoirs in the Patchawarra Trough and GMI Trend are the shales between coals. Smyth (1983) disagreed, citing that the vitrinite in dispersed organic matter within intraformational coals, represent the primary source of oils reservoirised in the Cooper Basin. Hunt *et al.* (1989) agreed with Smyth (1983), suggesting that the potential for both gaseous and liquid hydrocarbon generation within coals is high. Kantsler *et al.* (1983) however, cautions

that the dominance of Type III kerogen in source sediments will yield low volumes of liquid hydrocarbons. In summary no one specific oil prone source rock has been identified as the source of hydrocarbon accumulations in the basin.

Kanstler *et al.*, (1983) stated that the juxtaposition of sources, seals and reservoirs within Cooper Basin formations is extremely favourable for hydrocarbon migration and entrapment. Within these formations vertical and lateral migration of hydrocarbons is facilitated by communication of channel and point bar sandstones (Kanstler *et al.*, 1983). The timing of hydrocarbon expulsion from source rock varies as the maturity of these rocks vary (Tupper and Burckhardt, 1990). These authors consider that the expulsion of oil in the central Nappamerri Trough began in the early Triassic, while Patchawarra Trough generation occurred in the Early Late Cretaceous. These dates are certainly not universally agreed upon with Kanstler *et al.*, (1983) considering that oil generation occurred in the Patchawarra Trough after Cretaceous deposition. Conflicting views also exist regarding the onset of gas generation in the Cooper Basin. In the Nappamerri Trough, gas generation was thought to have occurred from the Jurassic onwards (Tupper and Burckhardt, 1990).

The lowest geothermal gradients according to Bone and Russell (1988) are observed in the Patchawarra Trough (lowest Innamincka #1, 32°C/km). Whilst the Nappamerri and Tenappera Troughs have the highest recorded geothermal gradients in the Cooper Basin (highest 50°C/km, Moomba #3). This difference in geothermal heat is related to the lithology of the underlying basement. For example, the Nappamerri Trough is underlain by a "hot" granite batholith (Big Lake Suite Granodiorite), rich in radioactive minerals. In contrast, the Patchawarra Trough is situated on top of sedimentary and volcanic rocks of the Warburton Basin where more typical heat production prevails.

Tingate *et al.* (1992) contend that thermal conditions in the Cooper Basin have recently been elevated, but hotter conditions have been experienced by some parts of the Cooper Basin in the past. These authors also stated that the Eromanga Basin and Nappamerri Trough (Cooper Basin) are currently in an elevated thermal phase, hotter than for any period in the past.

Kanstler *et al.* (1983) and Tingate *et al.* (1992) both agree that a late stage elevation of basin temperatures occurred in the last 10 million years. Tingate *et al.* (1992) believes that this recent rise in Cooper Basin temperatures is a response to the diminished cooling effects of aquifers within the Eromanga Basin (see Chapter Eight).

METHODOLOGY

2.0 INTRODUCTION

This chapter outlines the various analytical methods and equipment used in this study.

2.1 LITERATURE REVIEW.

All available literature from SANTOS Ltd., Boral Energy Ltd., Primary Industries and Resources (PIRSA) and the University of Adelaide library pertaining to the Cooper Basin and in particular Merrimelia Formation was summarised. Key papers on adjacent basins, concerning studies on Permian sediments, were also dealt with in the same manner. The summaries were bound in a single volume (Cubitt, 1994), with copies made available to the project sponsors.

2.2 IDENTIFICATION OF MERRIMELIA FORMATION AND TIRRAWARRA SANDSTONE LITHOLOGIES

The identification of Tirrawarra Sandstone lithologies was achieved via visual inspection. Palynological confirmation was used where uncertainty existed. Plates 1a and 1b are typical of the bulk of Tirrawarra sandstones being moderately sorted, medium to course grained sub-litharenites arranged in cross bedded sets up to a meter thick. Tirrawarra sandstones exhibit a consistent appearance across the basin (Plates 2a & 2b). These two samples are separated by approximately 25 kilometres.

Rezaee (1996) divided the Tirrawarra Sandstone into seven different facies types, several of these facies are thin, and/or have limited geographical extent. It has been found, however, that in the majority of cases the Tirrawarra Sandstone, at the Merrimelia interface, has an appearance that is consistent enough to make confident identification possible.

PLATE 2

Tirrawarra, Merrimelia & Warburton Basin Lithologies

UP SECTION IS TOWARDS THE CORE IDENTIFICATION STICKER IN VERTICAL PLATES AND
TO THE LEFT IN HORIZONTAL PLATES

A) *Core photograph - Tirrawarra #3 (2988.86m). A typical Tirrawarra braid plain sandstone exhibiting low angle sinusoidal bedding.*

B) *Core photograph - Merrimelia #1 (2614.44m). A typical Tirrawarra sandstone illustrating a rock that is quartzose in nature with horizontal bedding.*

C) *Core photograph - Tirrawarra #2 (3107.20m - 3107.43m). Arenaceous Merrimelia lithology exhibiting flaser and trough cross bedding typical of a Deltaic sandstone.*

D) *Core photograph - Merrimelia #5 (2718.4m - 2718.56m). Arenaceous Merrimelia lithology illustrating pinstripe lamination and high angle cross bedding typical of a glacio-aeolian sandstone.*

E) *Core photograph - Moorari #2 (3174.31m - 3174.46m). Argillaceous Merrimelia lithology with abundant syn-depositional and post-depositional micro-faulting and soft-sediment-deformation (varvite mudstone).*

F) *Core photograph - Jack Lake #1 (3240.49m - 3240.55m). Argillaceous Merrimelia lithology with abundant faceted pebbles of exotic composition (petromict diamictite). NB: A petromict diamictite is a bimodal sediment that contains clasts which have not been sourced locally.*

G) *Core photograph - Tickalara #1 (1785.69m - 1785.84m). Typical Big Lake Suite granodiorite showing large feldspar, mica and hornblende crystals.*

H) *Core photograph - Innamincka #2 (3621.93m - 3622.06m). Warburton Basin, Kalladeina Formation lithology (limestone breccia).*

Plate 2

Tirrawarra Lithologies

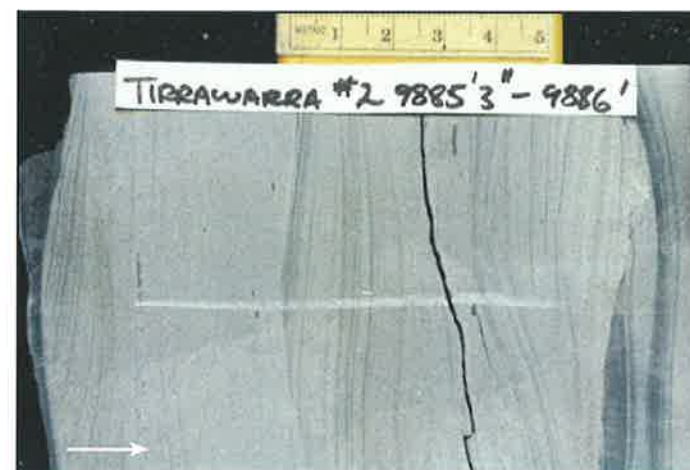
Merrimelia Lithologies Merrimelia Fm



A - Braid Plain Sst



B - Braid Plain Sst



C - Deltaic Sst



D - Aeolian Sst

Merrimelia Lithologies Merrimelia Fm

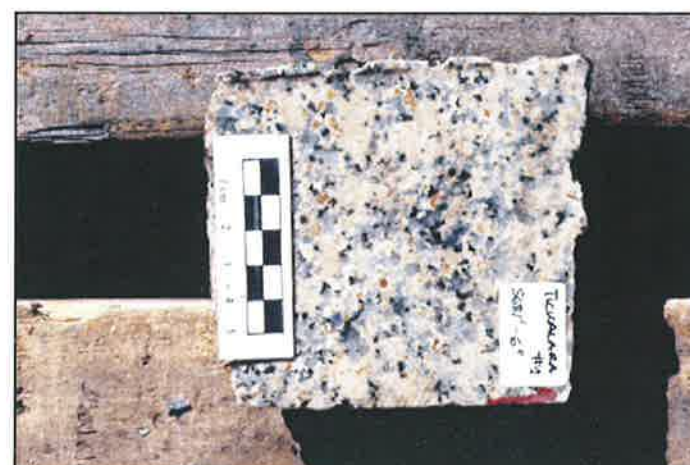
Basement Lithologies



E - Deep Lacustrine Varvite Mudstone



F - Petromict Diamictite



G - Weathered Granodiorite
Big Lake Suite



H - Recrystallised Limestone
Warburton Basin - Kalladeina Fm

In the majority of cases the Tirrawarra Sandstone, at the Merrimelia interface, has an appearance that is consistent enough to make confident identification possible.

The Merrimelia Formation, while mainly composed of argillaceous glacial rocks, also contains sandstones (Plates 2c & 2d). These sandstones are generally deltaic (Plate 2c), aeolian (Plate 2d) and shoreline in nature. These environments are regarded as typical Merrimelia facies while the sandstones illustrated in Plates (2a & 2b) are formed in a braided river environment. These sandstones are therefore not a Merrimelia facies type but are representative of Tirrawarra style sedimentation. It is therefore possible to differentiate between Merrimelia and Tirrawarra sandstones by observing sedimentological character.

Most Merrimelia facies are however not arenaceous, but argillaceous. These argillaceous lithologies are varied (Plates 2e & 2f) and are easily distinguished from Tirrawarra braid plain sandstones (Plates 2a & 2b).

The identification of Merrimelia and Tirrawarra lithologies involved the inspection of approximately 110 wells in the South Australian and Queensland sectors of the Cooper Basin, utilising the above identification criteria. Merrimelia and Tirrawarra facies were positively identified in cored intervals in 70 wells (Appendix 9a). The Merrimelia facies in these cored intervals became the primary resource for thin section sampling (Appendix 3a). A smaller number of thin sections were sampled from Tirrawarra facies (Appendix 3b).

2.3 IDENTIFICATION OF BASEMENT LITHOLOGIES

Identification of Warburton Basin facies and Big Lake Suite granodiorites, were based purely on core inspection.

2.4 LITHOLOGICAL LOGGING.

Extending from the work of Williams and Wild (1984a) and Williams *et al.* (1985 & 1987), identification of Merrimelia glacial facies was completed on 70 wells in both the South Australian and Queensland sectors of the Cooper Basin. All cores were logged with a view to reservoir quality and clast lithology. Detailed sedimentological interpretations were not recorded.

Detailed sedimentological analysis was, however, performed on exactly the same core intervals by A. Chaney (Aberdeen University) as the basis of his PhD study (see

Chaney, 1998). His facies interpretations are used (and acknowledged) throughout this thesis, particularly in Chapter Four.

Photographs of all thin section core samples were taken. In most cases, this was done prior to the core being cut. The subsequent images made it possible to relate the thin section samples with the core.

2.5 THIN SECTION SAMPLING.

2.5.1 MERRIMELIA FORMATION.

In total 160 core samples were collected from throughout the Cooper Basin, encompassing maximum stratigraphic and facies variations within the Merrimelia Formation. Thin sections were then cut from each core sample taken. The nomenclature used in naming thin section samples, (referred to throughout the text and in diagrams), is shown in Figure 2.1.

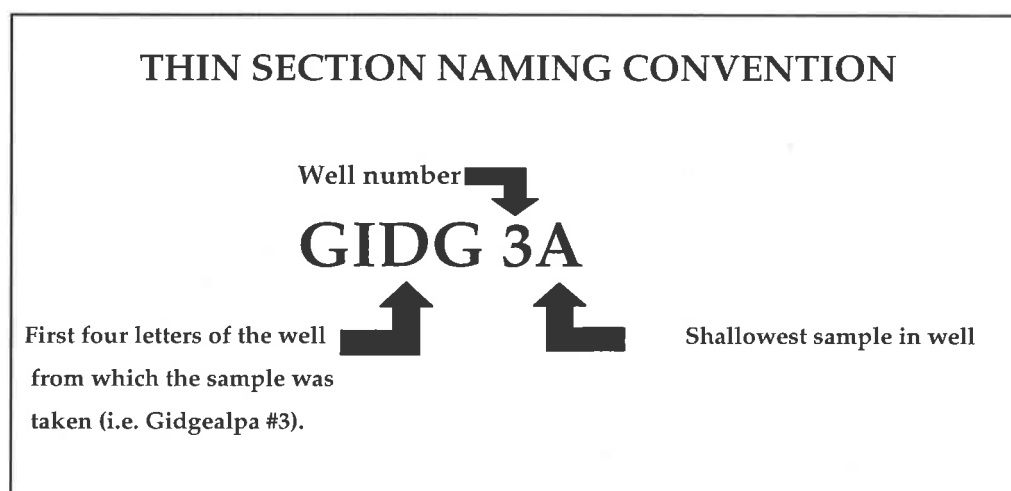


Figure 2.1 *Thin section naming convention.*

GIDG 3B is the next deepest sample from the Gidgealpa #3 well followed by GIDG 3C etc. Clay fraction samples are labelled such that the fraction size of the sample is used as a prefix i.e. 2MAL 4H (<2 micron clay fraction from Malgoona #4 well).

A full list of thin section samples in both the Merrimelia Formation and Tirrawarra Sandstone and their respective depths (in meters) is given in Appendix Three.

2.5.2 TIRRAWARRA SANDSTONE.

Forty three thin sections were prepared from Tirrawarra facies with the view to obtaining maximum stratigraphic and geographic coverage. The Tirrawarra thin section database used in this study is not evenly distributed across the basin with half

of the samples concentrated around the Fly Lake - Brolga, Moorari, Tirrawarra and Merrimelia Fields.

2.6 PETROLOGY TECHNIQUES.

2.6.1 POINT COUNTING AND PETROGRAPHY

A total of 144 thin sections were impregnated with blue epoxy resin to facilitate porosity identification. Rock fragment lithology identification and authigenic mineral recognition was performed on an *Olympus BHT* petrological microscope. Photomicrographs were taken of every rock fragment type identified and of all the main diagenetic features.

Quantification of thin section sample mineralogy was achieved with a combination of visual percentage estimation charts (Terry and Chilingar, 1955), traditional microscope point counting (200 counts per slide) and a video image analysis system linked to an *Olympus* petrological microscope. All 144 thin sections were initially analysed using the visual estimation charts developed by Terry and Chilingar (1955), as the oversized dimensions of rock fragment clasts in the majority of thin sections precluded the use of traditional point counting methods. To check the accuracy of visual estimation, 80 thin sections with grain size ranging from very coarse to very fine were randomly selected and point counted utilising the image analysis technique. A comparison of results gained by both techniques (visual estimation and image analysis) reveals that there is little variation between estimated and counted data (Table 2.1).

The image analysis system utilises *VIDEO PRO 32™* image processing and statistical analysis software. Sandstone compositions were calculated using *TRIPLLOT 3.0™* ternary diagram software and classified according to Dott (1964).

All rock fragments observed were defined. Thus consistent identification of rock fragments was possible between all thin sections analysed. The clast definitions used are presented in Appendix 4a.

Specialised petrographic techniques such as cathodoluminescence (CL), reflected light and fluorescence microscopy (FM) were also used to better ascertain diagenetic relationships.

	COLUMN A	COLUMN B	COLUMN C
COMPONENT OF ROCK	POINT COUNTING	VISUAL ESTIMATION	DIFFERENCE BETWEEN
	(Image Analysis) Ave. Percentage	Terry & Chilinger (1955) Ave. Percentage	COLUMN A) & COLUMN B)
Rock Components			
Rock Fragments	22.8	22	0.8
Quartz & Feldspar Total	38	38	0
Authigenic Phases Total	24	29.8	-5.8
Porosity Total	6.2	6.1	0.1
TOTALS	101	100.2	0.8
Framework Component			
Quartz Total	36.6	38.3	-1.7
Feldspar Total	1.2	0.8	0.4
Accessory Minerals Total	0.5	0.4	0.1
Sedimentary Total	10.7	10.2	0.5
Igneous Total	11.2	6.1	5.1
Pyroclastic Total	1.3	1.2	0.1
Metamorphic Total	9.5	4.1	5.4
Authigenic Component			
Quartz Cement	1.8	34.4	-2.6
Carbonate Cement	6.3	11.2	-4.9
Clay Cement	16.5	12.4	4.1
Opaque Minerals Total	1	1.5	-0.5
Porosity Component			
Primary Porosity	1.2	1.9	-0.7
Secondary Porosity	5	3.1	1.9
Plucked Porosity	1.9	0.5	1.4
Total Porosity	6.2	6.0	0.2

Table 2.1 Comparison of image analysis point counting data and data derived from using visual estimation charts developed by Terry and Chilinger (1955), in an attempt to assess the accuracy of petrographical estimations of authigenic and framework components.

2.6.2 THIN SECTION DESCRIPTIONS

Framework, authigenic and matrix components, in each thin section, were described with particular emphasis on diagenetic relationships and rock fragment lithology (Appendix 9b). A paragenetic sequence was recorded for each thin section. This was then combined with adjacent thin section descriptions, to produce regional paragenetic sequences (Chapter Eight).

2.7 X RAY DIFFRACTION (XRD) TECHNIQUES

As part of routine mineralogical investigations, bulk air dried XRD smears were produced and analysed for each thin section core sample obtained. Clay separates (<4 and <2 micron) were prepared and run for selected illite-rich samples identified from bulk XRD analyses. The clay fractions were run air dried and glycolated, as oriented samples using the filter transfer method outlined in Moore and Reynold (1989). The amount of expandable layers in the illitic I/S mixed layered clay was estimated from broad XRD peaks using peak positions given in Moore and Reynold (1989) and by comparison with calculated XRD profiles generated using NEWMOD (Moore and Reynold, 1989). Mineral identification was performed using TRACES 3.0™ software.

All XRD samples were run on a *Philips PW1050* X-ray diffractometer at 50KV and 35mA, using Co-K α -radiation, at a scan speed of 2° per minute. XRD-derived mineral proportions for all of the bulk samples analysed (which correspond with thin section samples), are given in Appendix Seven.

2.8 MICROSCOPY TECHNIQUES.

2.8.1 CATHODOLUMINESCENCE MICROSCOPY (CL)

Twelve samples were studied by CL to identify quartz cement stratigraphy, carbonate cement zoning, kaolin/quartz relationships and authigenic illite response. The CL analyses were performed on a *Patco ELRM-RX Luminoscope* which was used in conjunction with a *Leitz Orthomat E automatic camera*. Acceleration voltages of 6kV were used for carbonate minerals and 12kV for quartz. The beam current was set at 200mA whilst the polished thin sections were held under vacuums of between 70 and 100 mTorr. Photomicrographs were taken of all relevant relationships observed using *Kodak Ektapress 1600 ASA* film in a *Leitz* camera with exposure times ranging from 2 to 15 minutes.

2.8.2 FLUORESCENCE MICROSCOPY (FM)

A total of 24 thin section samples from 23 wells were selected for standard fluorescence microscopy. The light source consisted of a 100W *Olympus (BH2-RFL-T3)* mercury vapour lamp which was connected to an *Olympus BHSP* binocular petrological microscope. Photomicrographs were taken of all relationships observed with an *Olympus* SLR camera utilising normal *Kodak 800 ASA* film.

2.8.2.1 Illite Fluorescence – An Introduction

Throughout this thesis the use of fluorescent photomicroscopy to characterise illite is common. To the best of my knowledge illite fluorescence has not been described in sandstones as any discussion appears to be absent in the published literature world wide. This technique has proved to be a valuable new tool for the optical characterisation of illite and as such a whole chapter (Chapter Seven) has been devoted to the phenomena. In an attempt to aid the reader in the interpretation of fluorescence photomicrographs, without going into a premature discourse of the phenomenon, a cursory explanation and identification of fluorescing species is given here.

Plate 3a illustrates abundant illite in an altered feldspar phenocryst within a rhyodacite rock fragment. The same field of view when exposed to UV radiation produces brightly luminescing patches (Plate 3c). The fluorescing patches correspond with the illite illustrated in Plate 3a. This relationship is clearly shown in the inset Plate 3b. The surrounding rhyodacite groundmass is also dominated by illite and also fluoresces (Plate 3c). Other fluorescing species observed in Merrimelia sediments include zoned carbonate crystals (orange fluorescence) (Plate 3d) and the mounting media (green fluorescence) (Plate 3e).

2.8.3 REFLECTED LIGHT MICROSCOPY

Reflected light microscopy was used to delineate accessory minerals as an adjunct to normal petrological investigations. This technique was also employed to discriminate rock fragments from pseudo-matrix and matrix. The light source and microscope set-up used was identical to that used in the Fluorescence microscopy techniques previously mentioned (100W Olympus (BH2-RFL-T3) mercury vapour lamp connected to an Olympus BHSP binocular petrological microscope). The images produced were saturated blue in colour, which were then scanned into Corel Photo Paint 7™ and enhanced by using lighting levels, hue slider and monochrome filters within PhotoLab™.

The resulting images were monochrome, with edge enhancement set at high levels to emphasise textural differences between the various objects within the image (Plate 17c & 17e).

PLATE 3

Fluorescence Illite: An Introduction

A) *Photomicrograph - Lake Hope #1 (2493.70m) (Cross nicols x 10). Close up view of an illitised feldspar phenocryst within a rhyodacite rock fragment.*

B) *Inset - Lake Hope #1 (2493.70m) (Fluoro). Magnified view of siderite patches and illite clay within an illitised feldspar phenocryst.*

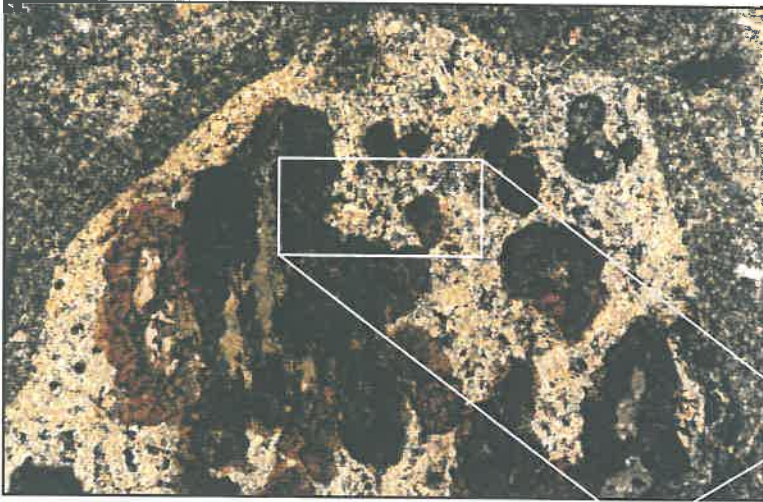
C) *Photomicrograph - Lake Hope #1 (2493.70m) (Fluoro x 10). Same view as Plate 2a, illustrating the association between the typical cross nicol appearance of illite (Plate 2a) and the appearance of fluorescing illite (Plates 2b & 2c).*

D) *Photomicrograph - Panning #1 (3129.90m) (Fluoro x 10). Broad view illustrating fluorescing matrix illite (green) and banded siderite seeds (orange).*

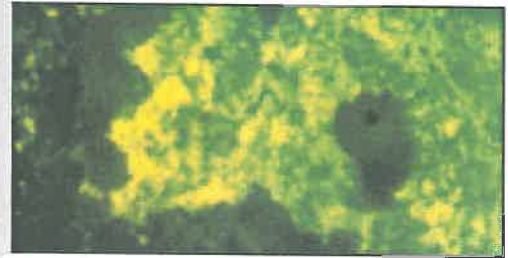
E) *Photomicrograph - Woolkina #1 (3038.8m) (Fluoro x 10). Broad view illustrating the distinct difference between the fluorescence response of thin section mounting media and illite.*

Plate 3

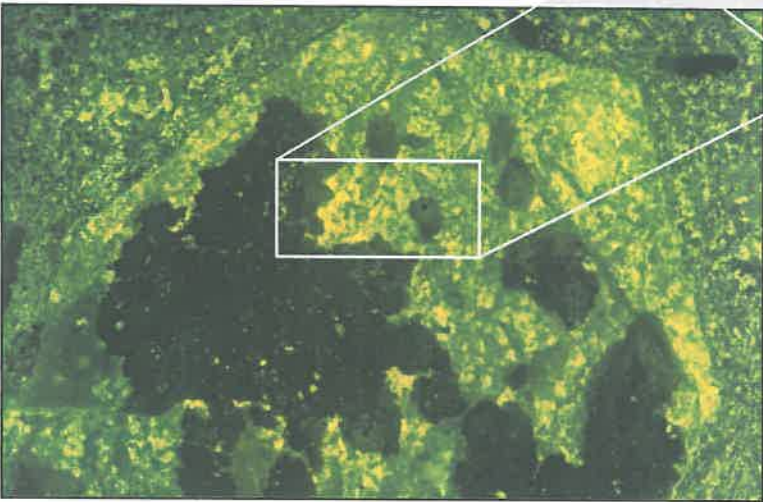
A



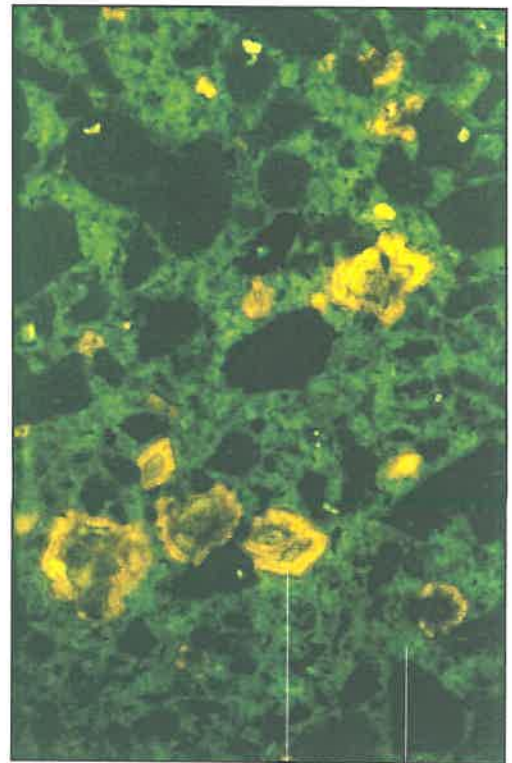
B



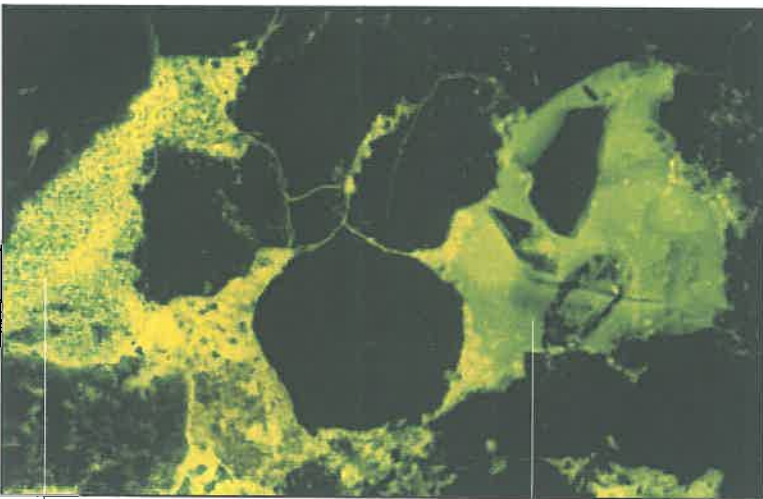
C



D



E



illite

mounting media

siderite

illite

2.8.4 SCANNING ELECTRON MICROSCOPY (SEM)

SEM studies were undertaken on freshly broken core samples as well as on the <2 and <4 micron clay separates sent for K-Ar dating. Both sample types were coated with carbon and gold/palladium. Scanning electron microscopy and semi-quantitative compositional analyses were performed on an *XL20 Philips* electron microscope with an energy dispersive X-ray (EDX) analysis system attached.

2.8.5 TRANSITION ELECTRON MICROSCOPY (TEM)

Identification of illite morphologies, composition of individual clay particles and a visual assessment of the purity of <2 micron K-Ar age dating samples were performed on a *Philips CM TEM-200*. The analyses were performed at an operating voltage of 200 kV with a spot size of 5⁰. An energy dispersive X-ray (EDX) analysis system connected to the TEM allowed compositions of individual clay particles to be obtained. Photomicrographs were taken of individual clay particles and at the sites where clay particle compositions were measured. Selected area diffraction (SAD) pattern images were recorded for representative clay particles from two <2 micron clay separate samples.

2.9 MICROPROBE TECHNIQUES.

Elemental compositions of all authigenic phases was performed on a *CAMECA SX 51* microprobe operating at 15kV to 20kV, using a 20nA beam current and a 0.2 μ beam diameter. A back scattered image analyser (BSE) was attached to the probe. BSE images were taken primarily of carbonate cement zonations (Chapter Six) and authigenic illite (Chapter Six).

2.10 K-AR DATING TECHNIQUES.

Through detailed XRD, petrographic and fluorescence analyses, samples that contained extensive authigenic illite were selected for K-Ar age dating. Two samples were chosen, from different and wide spaced wells (Merrimelia #18 and Malgoona #4). From these two samples both <4 and <2 micron clay separate samples were obtained via the processes outlined below in Figure 2.2. K-Ar dating was then performed on both clay separates from both samples according to the flow charts illustrated in Figures 2.2 and 2.3.

Sample purity was first assessed by XRD and SEM and then by TEM. Both the <4 and <2 micron size fractions were isolated, using Stoke's settling criteria (Tucker, 1988).

Sample collection was obtained by applying a simplified version of the illite separation procedure outlined in Hamilton *et al.* (1989) (Fig. 2.2).



Plate 4

TEM Sample Purity

TEM Photomicrograph Merrimelia #18 (2547.83m). K-Ar Illite dating clay separate sample (<2 micron size fraction). This view illustrates sample purity as only lath and flake illite particles can be observed.

Purity assessment by XRD and SEM observations of both size fractions indicated that there was some quartz contamination in the <4 fraction samples but no detectable contaminants in the <2 fraction separates. The purity of both <2 micron samples were further confirmed by TEM analysis where it was observed (Plate 4) that only euhedral illite laths and plates were present.

The potassium determination was performed at The University of Adelaide in the Department of Geology and Geophysics on a *VARIAN AA6D* Atomic Absorption Spectrometer (a detailed explanation of this process is given in Appendix Six).

The analysis of radiogenic ^{40}Ar was performed on a modified *MS-10 Mass-Spectrometer* at *Amdel Laboratories* in Adelaide (a detailed explanation of this process is given in Appendix Six).

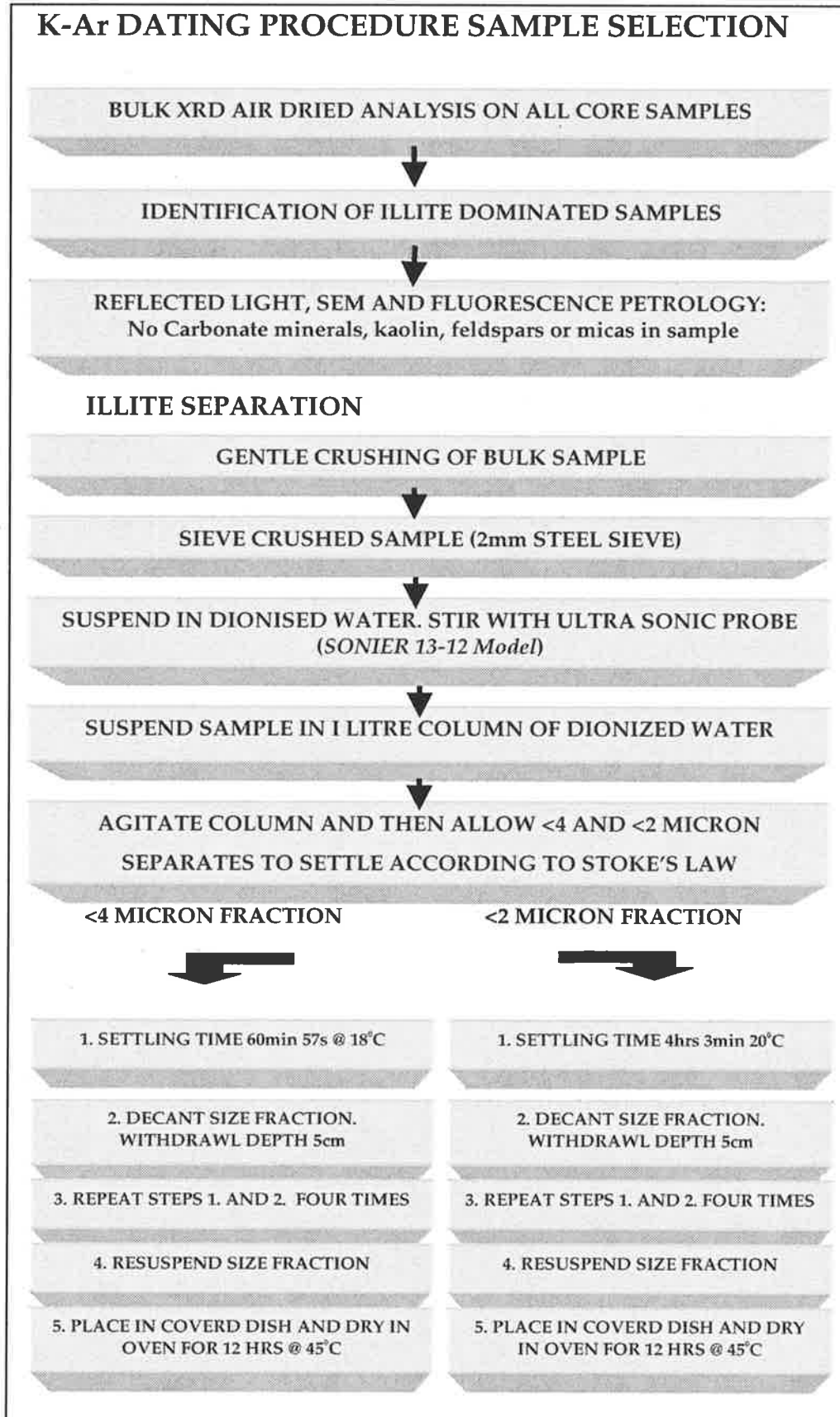


Figure 2.2 K-Ar dating sample selection and clay fraction separation procedures.

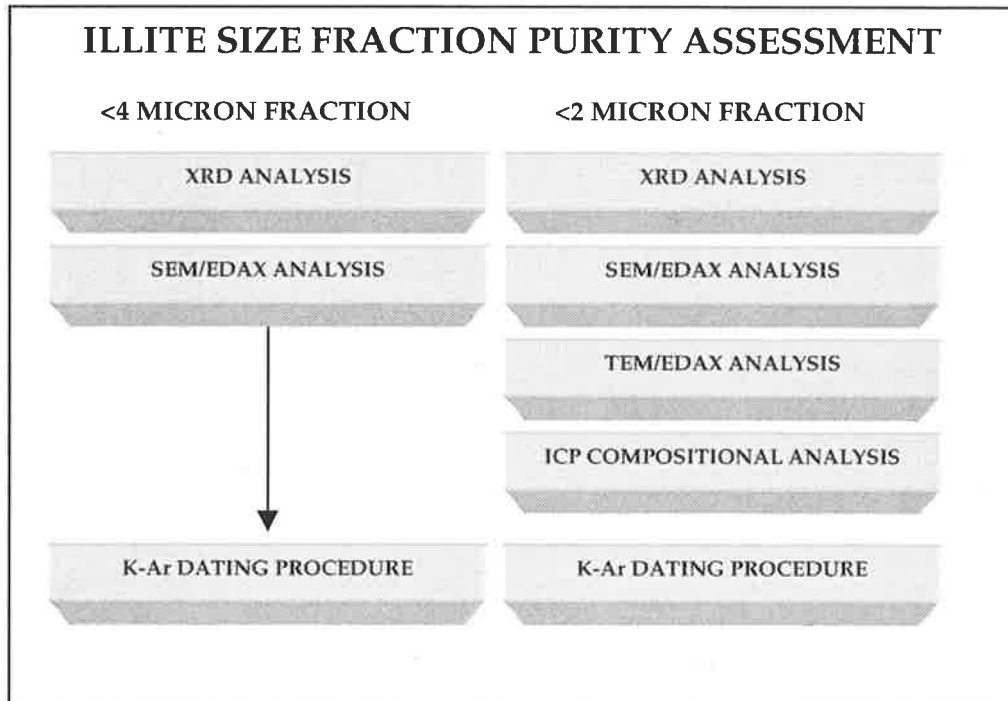


Figure 2.3 Sample purity assessment procedures.

The K-Ar ages were calculated using Equation 1:

$$T_c = \frac{1}{\lambda_\epsilon + \lambda_\beta} \text{Log}_e \left[\frac{{}^{40}\text{Ar}}{{}^{40}\text{K}} \left(\frac{\lambda_\epsilon + \lambda_\beta}{\lambda_\epsilon} \right) + 1 \right] \quad (\text{From Pethero and Schwab, 1996})$$

$T_c = \text{Age (Million Years)}$
 $\lambda_\beta = 4,962 \times 10^{-10} \text{ Ya}^{-1}$
 $\lambda_\epsilon = 0.581 \times 10^{-10} \text{ Yr}^{-1}$

Equation 1

2.11 STATISTICAL TECHNIQUES

Statistics has been used extensively throughout this study in order to:

- 1) Resolve rock fragment proportion trends in both Tirrawarra and Merrimelia petrographic data sets in order to highlight the movement of glacial sediments.
- 2) Resolve rock fragment populations in order to highlight provenance trends.
- 3) Resolve mineralogical trends in Tirrawarra and Merrimelia petrographic data sets with a view to highlighting diagenetic processes.

The following section describes the various statistical techniques used in this study.

Authigenic mineral and rock fragment datasets from both the Tirrawarra Sandstone and Merrimelia Formation were analysed using principle components analysis (PCA), Kolmogorov-Smirnov (KS) normality tests, Pearson correlation coefficients (using a “t” statistic 95% level of significance) and cluster analysis. In addition to this, compaction index, sorting and grain size data derived from Merrimelia sediments were also analysed statistically using the techniques outlined in Swan *et al.* (1995).

2.11.1 CLUSTER ANALYSIS

Cluster analysis is a widely employed technique that organises data into homogeneous groups so that the relationship between the data groups is revealed (Davis, 1986). It has been employed in this study to classify rock fragment types diagenetic minerals and reservoir characteristics in relation to geographical position.

A large number of cluster analysis techniques have been developed (Hair *et al.*, 1995). Davis (1986) describes cluster analyses as belonging to four groups: portioning, arbitrary, mutual singularity and hierarchal methods. Hierarchical techniques are the most commonly used clustering methods within the earth sciences (Davis, 1986) producing the most favourable results. Three hierarchical cluster techniques were used in this study:

- 1) Centroid linkage
- 2) Single linkage
- 3) Average linkage

Both raw and manipulated data (Z-scores)¹ were used in the three cluster techniques outlined above. The three differing cluster techniques were used in order to ascertain which cluster method produced the most consistent result. Kolmogorov-Smirnov tests of normality were performed on statistically significant rock fragment datasets to assess normality. If the data set was normally distributed then the data set was standardised (Z-Scores) and subsequently clustered. If no normality was found, the data set was left unstandardised and clustered (Fig. 2.4).

¹ Z scores are values gained by standardising normally distributed data (Swan *et al.*, 1995).

The selection of statistically significant variables in both the Tirrawarra Sandstone and Merrimelia Formation was performed by way of Pearson correlation coefficients and principle components analysis.

Pearson correlation matrices were constructed using a "t" statistic confidence level of 95% (Appendix 8a details the "t" statistic equation used). Variable pairings were then graded according to the value of their "t" statistic (both positive and negative associations). The most significant variable pairings (rock fragments and authigenic minerals) in both Tirrawarra and Merrimelia datasets were then able to be ascertained (Table 5.8).

In addition to Pearson correlation assessment, PCA was performed whereby raw Merrimelia and Tirrawarra data sets were transformed onto an arbitrary orthogonal axis (Davis, 1986). The assessment of correlation matrices produced via this transformation allowed identification of statistically significant rock fragments, authigenic minerals etc. in successive data sets (Appendix 8a). This technique also has the effect of removing sampling bias from a dataset while at the same time highlighting dependent variables (Smith, 1969; Davis, 1986).

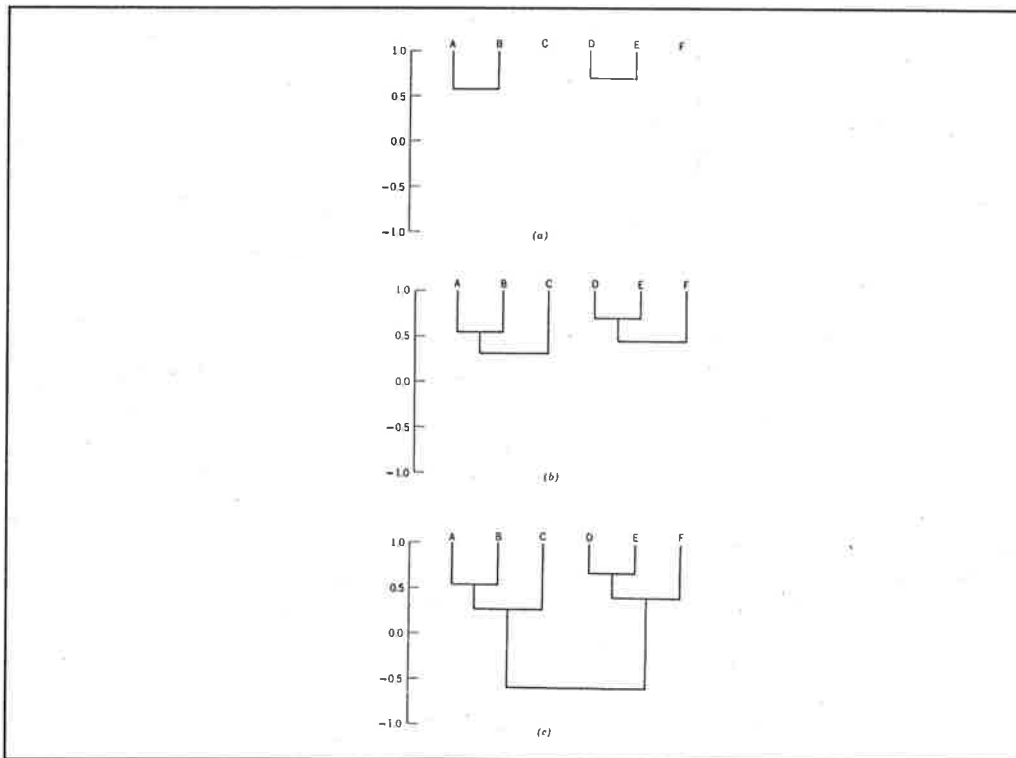


Figure 2.5 An example of a dendrogram which displays two data groupings (From Davis, 1986).

The dendrograms in this thesis were produced according to Figure 2.4 where the initial clusters form (Fig. 2.5a), followed by the connection of remaining data (Fig. 2.5b) and finally the two clusters are joined (Fig. 2.5c). The method by which the data is paired into clusters is what distinguishes differing cluster techniques.

The cluster analyses used in this study, group data according to the minimum distance between objects (single linkage), the average of distances between objects (average linkage) and the mode between objects (centroid linkage) (Hair *et al.*, 1995).

The centroid cluster analysis technique was employed in preference to the average and single linkage methods as the centroid method is less sensitive to outliers (Hair *et. al.*, 1995) and produced the most consistent results. This decision was made after comparing the dendrogram outputs of all three cluster methods alongside exotic rock fragment transport directions derived from petrographic analysis (see Chapter Five). The dendrogram in Figure (2.5c) is the standard visual output generated by hierarchical cluster analysis.

All multivariate analyses including cluster analysis, principle component analysis (PCA), Pearson correlation matrices and normal distribution graphs were computed using *SPSS 7.5.1™* software. Scattergrams and crossplots displayed throughout this document were all produced using *Microsoft Excel 7©* software. Pearson correlation coefficient 95% significance “*t*” statistic values were also produced using *Microsoft Excel 7©* software.

2.11.2 VARIOGRAM ANALYSIS

Diagenetic and rock fragment distribution maps were constructed using point counting and visual estimation techniques outlined in section 2.6. As the petrographic data sets are geographically skewed with most sampling (coring) concentrated in and around the major fields of the Cooper Basin, any map produced using petrographic data were deemed to have a high level of data “nuggeting” (bulls eye effect). To assess the amount of “nugget effect” semi-variogram analyses were performed on every map produced in this study. The resulting variogram gives a confidence rating for a map indicating over what distance (from a concentration of data) is contoured data accurate or a product of the contour algorithm.

The petrographic datasets were normally krigged using a spherical variogram model utilising *SURFER Version 5.01©* software. Medium contour smoothing and an overlay of sample wells was then applied to the final maps. To assess the nugget effect of each

map, semi-variograms were produced using *Variogran V2.2* and *Variowin V2.2* software, using a spherical variogram model with an anisotropy of one. Variograms for each map used in this study are illustrated in Appendix 8c.

The semi-variogram crossplots were constructed by plotting the semi-variance (2γ) along the Y-axis and distance between sample pairs ($|h|$) (in meters) on the X-axis according to the method outlined in Clark (1979) (Fig. 2.6).

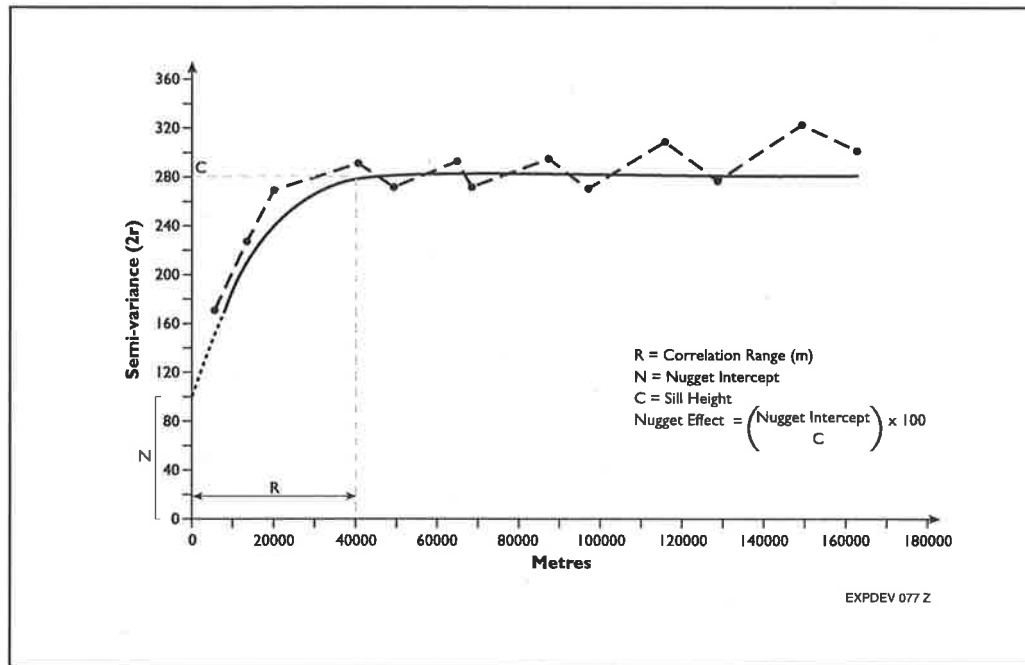


Figure 2.6 *Theoretical semivariogram (Modified from Prosser and Maskall, 1993).*

The correlation range (“R”) (Figure 2.6) provides a measure of the distance over which there is a reasonable correlation between sample values (Prosser and Maskall, 1993). In the case of Figure (2.6) data correlation is applicable up to 40km from the origin. When sample spacings are greater than “R” the variogram function becomes asymptotic forming a sill (Fig. 2.6). The level at which the data becomes asymptotic is then projected back to the Y-axis (C). Similarly the nugget (N) is calculated by projecting the data trend line to where it meets the Y-axis (Fig. 2.6). The nugget effect is then calculated using the following formulae:

$[\text{Nugget Intercept (N)} / \text{Sill Height (C)}] \times 100 = \text{Nugget Effect}$	Equation 2
--	-------------------

In the case of Figure 2.6 the nugget effect is 37%. The nugget effect represents a measure of the bias induced by repeated sampling at one location. Thus the semi-variogram in Figure 2.6 suggests that approximately 40% of the dataset is biased

towards sampling in one location exhibiting completely random behaviour (Clark, 1979). A flat semi-variogram, like those illustrated in Appendix Eight, where the nugget is equal to the sill, implies that there is no spatial correlation at all between the data (Prosser and Maskall, 1993).

2.12 THERMAL MODELLING (BASINMOD©)

A pilot illite dating/geohistory study was performed. The thermal modelling calculations for the geohistory plots in this study were performed by A. Kaiko using *BASINMOD* 4.2 on a Sun workstation utilising the Lawrence Livermore National Laboratories vitrinite calculation option. Open file vitrinite reflectance (%R_o) data were supplied by Santos Ltd. and Primary Industry and Resources (PIRSA). The thermal modelling was constrained by using a variable heat flow and heat sink model modified after Stuart *et al.* (1991) using a surface temperature of 20°C and corrected bottom hole temperatures for each of the wells.

No %R_o data was available for the individual wells studied, therefore data from adjacent wells within the same fields were used to help constrain the models. The lack of %R_o data necessitated, the generation of a regional thermal model. This model was determined by modelling data from Gidgealpa #7; a well that contained a set of measured %R_o data through Eromanga and Cooper Basin sediments.

GONDWANAN GLACIAL SETTING

3.0 PREAMBLE

The Merrimelia Formation and Tirrawarra Sandstone sediments were deposited during the waning stages of the glaciation on the Gondwanan supercontinent in the Late Carboniferous to Early Permian. One of the major controls on reservoir quality in these units is facies type (Chapter Nine), which was dictated by glacial/ice sheet movement (Chapter Four). Glacial movements in the Cooper Basin were, on a basinwide scale, controlled by the mechanisms which drove the Gondwana glaciation. Thus understanding the extent and controls on the Gondwanan glaciation provides a basis on which the sedimentology and reservoir quality of the Tirrawarra Sandstone and Merrimelia Formation can be discussed.

This chapter, describes the Gondwanan glaciation, first in terms of the supercontinent and then focuses on the Australian continent, with particular reference to the South Australian region. A brief discussion at the end of the chapter brings together the various arguments concerning the controls on the Gondwana glaciation with particular emphasis on the deposition of the Tirrawarra-Merrimelia glacial complex in the Cooper Basin.

3.1 INTRODUCTION

Veevers and Powell (1987) have described the Late Palaeozoic glaciation of Gondwana in terms of three distinct episodes. The first two episodes are confined to Africa and South America. The last glaciation episode (Episode III) extended across Gondwana (including south eastern Australia) and is considered the major glaciation to affect this supercontinent (Veevers and Powell, 1987) (Fig. 3.1). The Merrimelia

Formation and subsequently the Tirrawarra Sandstone were deposited in a shallow intra-cratonic depression under the control of this last episode of Gondwanan glaciation (Stephanian Fig. 3.1).

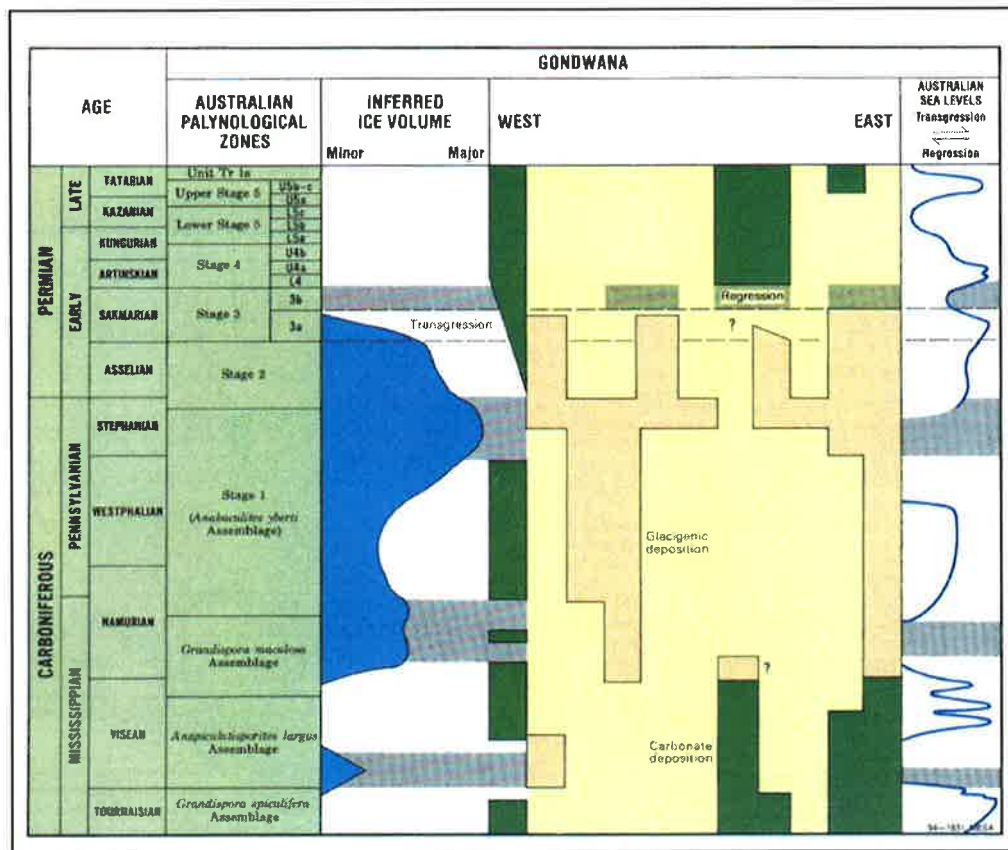


Figure 3.1 Inferred Gondwanan ice volumes (After Veevers and Powell, 1987).

The first Gondwanan glaciation affected the Australian continent in eastern Australia during the Namurian (Eyles and Young 1994) (Fig. 3.1). By the Westphalian and Stephanian, glaciation had spread to central Australia, Antarctica, southern Africa, India, the Arabian Peninsula (Oman) and Asia (Eyles and Young, 1994) (Fig. 3.2).

Although the Gondwana ice age lasted for 110 Ma, there was no enormous ice sheet covering the whole of Gondwana. Instead there was a series of small ice caps across Gondwana (Fig. 3.2) which advanced and retreated diachronously, moving from west to east (Caputo and Crowell, 1985) (Fig. 3.3). Glaciation is thus considered to have begun in western South America and moved to eastern Australia and Antarctica (Alley, 1995). Thus Australia and Antarctica, at the time of encroaching Gondwanan glaciation, were affected by polar latitudes and subsequently frozen. At the same time, according to Caputo and Crowell (1985), northern South America and Africa was beginning to warm (Fig. 3.2).

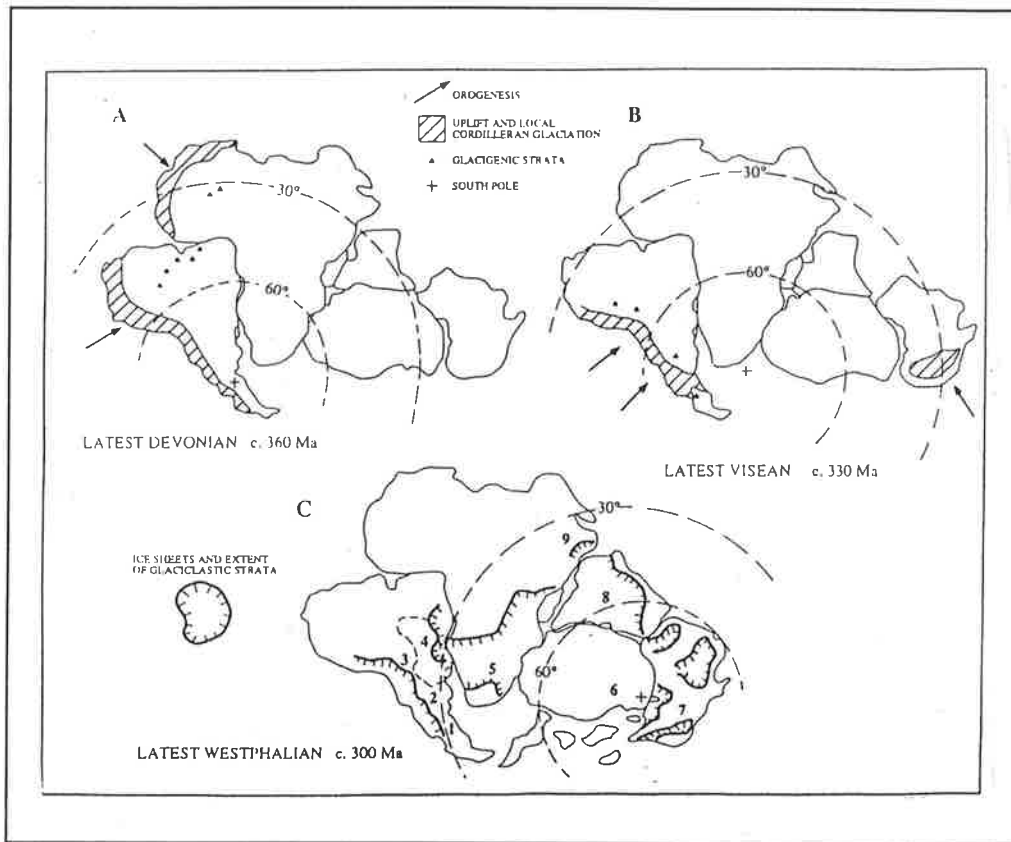


Figure 3.2 Icesheet development across Gondwana from Late Devonian to Late Westphalian (After Eyles and Young, 1994).

The scope of this section is to describe the affects of Gondwanan glaciation in the context of Australia and more specifically in the Cooper Basin. Detailed descriptions of Gondwanan glaciation in the surrounding regions of South America, Africa, India, Asia and the Arabian Peninsula are summarised by Eyles and Young (1994), Veevers and Powell (1987) and Caputo and Crowell (1985) and are not touched upon here. The proximity of Antarctica to Australia at this time (Fig. 3.4), however, warrants a brief description of Gondwanan glaciation in this region.

Veevers and Powell (1987) suggested that deposition from glaciers with fluid bases, or so called wet-based glaciers, occurred in the Stephanian and moved into rapidly subsiding basins on the seaward side of glaciated highlands on the eastern margin of Antarctica (Fig. 3.3). The same authors believe that glacial affects had ceased in Antarctica by the Late Permian (Kazanian). There is some conjecture as to whether ice caps covered all or differing parts of Antarctica. Veevers (1993) does, however, indicate that, although there is no depositional evidence of an extended ice cover across Antarctica (and indeed Gondwana), transport distances of some clasts have exceeded 2000 km.

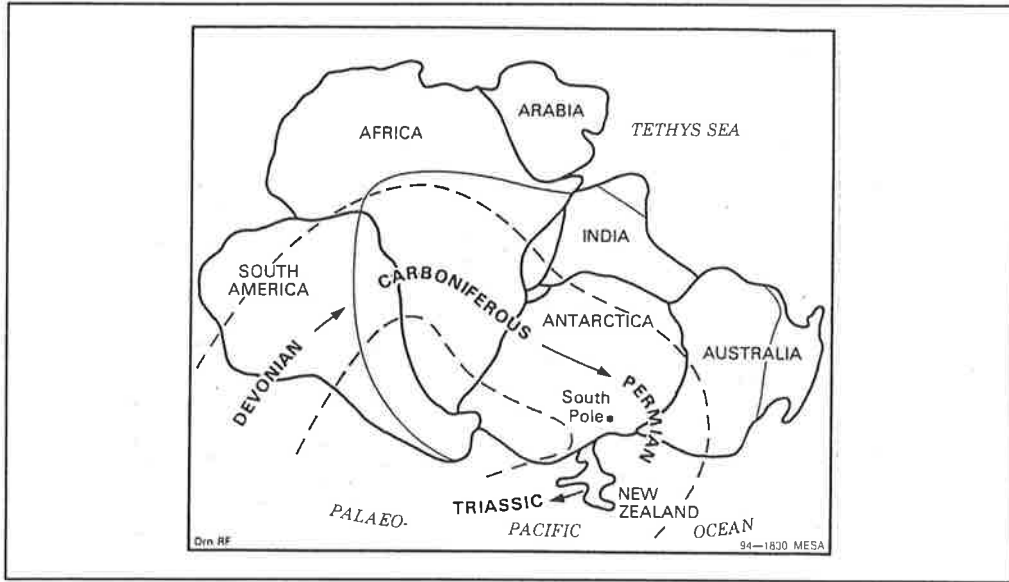


Figure 3.3 Ice cap wander path across the Gondwana super continent (After Caputo and Crowell, 1985; Veevers and Powell, 1987).

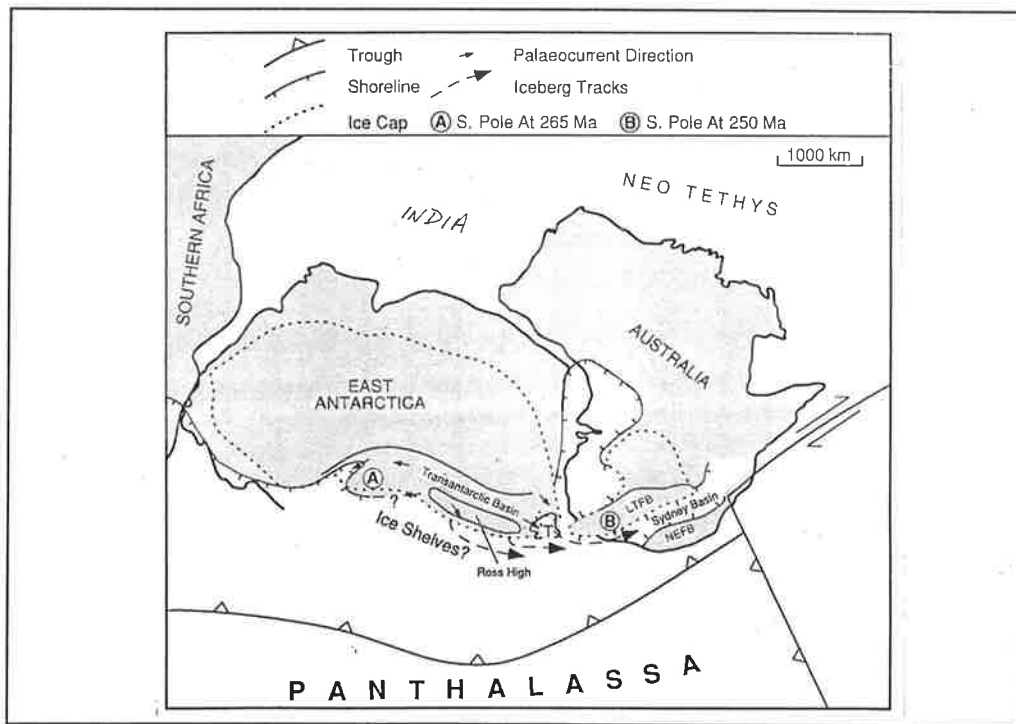


Figure 3.4 Location of ice cap on the Australian and Antarctic continents (After Eyles et al., 1998).

3.2 GONDWANAN GLACIATION IN AUSTRALIA

The precise dating of glacial events in Australia is complicated by a lack of agreement on the Permian-Carboniferous boundary (Alley, 1995). During this time period the

throughout the Australian continent allowing some degree of correlation (Chapter One). The Late Palaeozoic glaciation in Australia comprises two very distinct glaciation styles: alpine cordilleran in the east and intracratonic ice caps elsewhere (Eyles and Young, 1994; Veevers and Powell, 1987; and Caputo and Crowell, 1985). The montane glaciers were the first formed Palaeozoic glaciers in Australia and "grew" in the more eastern regions of the Australian continent (Crowell and Frakes, 1971; Veevers and Powell, 1987). As Gondwana drifted across the south rotational pole (Fig. 3.3), large continental-scale ice masses, initially formed in Antarctica, spread north through Tasmania and then filled depressions on continental Australia (including the Cooper Basin) (Alley, 1995). The discussions below describe in greater detail both alpine and continental ice mass glaciations that affected the Australian landmass.

3.2.1. ALPINE STYLE GLACIATION

Glaciation was initiated on the Australian continent on the eastern margin in the early Namurian (Crowell and Frakes, 1971). By the Stephanian most parts of the Australian continent were covered by glaciers (Fig. 3.5a), with the majority of glaciers having totally receded by the Sakmarian. The eastern margin of Australia at this time consisted of an active magmatic arc (similar to the present day Andes mountain range) with the Tamworth Trough and Sydney Basin representing forearc basins (Crowell and Frakes, 1971). Alpine glaciers covered the peaks of a series of volcanos with similar alpine-style glaciers capping a string of offshore island stratovolcanos further to the west (Chaney, 1998) (Fig. 3.5b). To the west in the Tamworth Trough, during the Namurian, alpine glaciers reached into the basin proper, providing ice-rafted detritus (Crowell and Frakes, 1971). Similarly, in the Sydney-Bowen Basin, alpine glaciers cut eastwards, draining into large palaeo-valleys and filling these features with a succession of diamictites and conglomerates (Eyles, 1993).

3.2.2 CONTINENTAL ICE SHEET GLACIATION

3.2.2.1 Western Australia

Continental ice sheets were initiated in the Stephanian much later than the alpine glaciation in the east. In Western Australia the Canning, Perth, Carnarvon, and Officer Basins contain the youngest Late Palaeozoic glacial deposits (Eyles, 1993). It is postulated by this author that ice centres may have been sited on the north slope of the Pilbara Block and on the southern Yilgarn Block to the east of the Perth Basin (Fig. 3.5a).

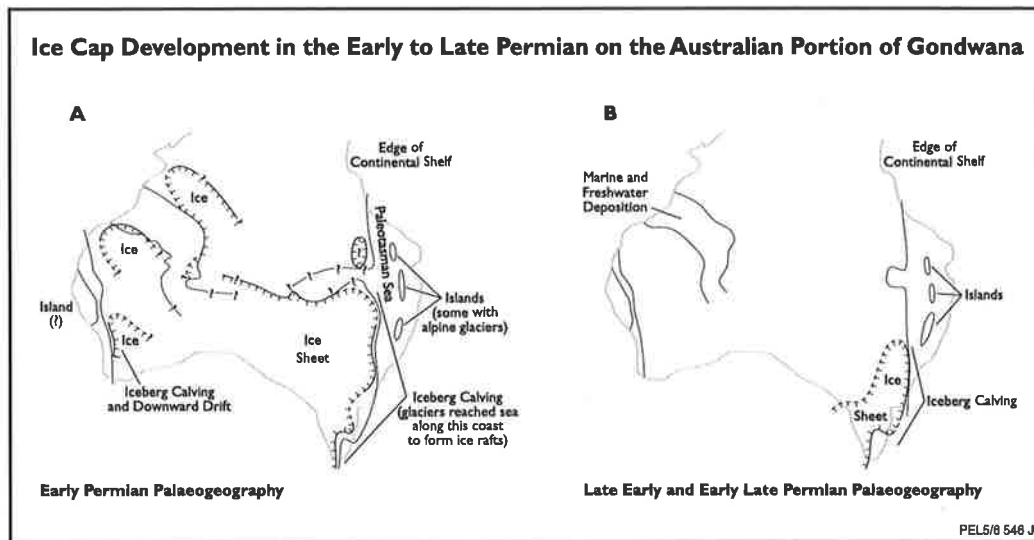


Figure 3.5 A) Early and B) late Permian Gondwanan Ice sheet location on the Australian continent (From Crowell and Frakes, 1971).

3.2.2.2 South Australia

Glaciation occurred in South Australia from the Stephanian to the Asselian. A broad ice cap covered the southern regions with northward-extending lobes (Alley, 1995). Glaciation extended across the whole of South Australia, but by the end of the Sakmarian glacial conditions had ceased (Crowell and Franks, 1971) (Fig. 3.5 a & b).

Glacial deposits accumulated in the Denman, Renmark, Arckaringa, Troubridge, Pedirka and Cooper Basins within South Australia (Fig. 1.1). The Permian glaciogene sediments in the aforementioned basins are individually described by Harris (1981).

Along with glacio-marine conditions, Alley and Bourman (1984) described scoured pavements (indicating a westward movement of ice), lodgement and flow till complexes within the Troubridge Basin. The inferred movement of ice within South Australia has been a point of prolonged discussion, with agreement having been reached on ice movement moving from the southeast towards the northwest (Alley, 1995). Local deviations of wet-based glaciers, like those mentioned above in the Troubridge Basin (Alley and Bourman, 1984), are a result of these glaciers flowing around palaeo-topography (Alley, 1995).

Apart from the Troubridge Basin, glacio-marine sediments have also been described in the Denman, Arckaringa and Renmark basins (Eyles and Young, 1994). The Cooper and Pedirka basins have, on the other hand, not been exposed to glacio-marine conditions. Harris (1981) indicates that the Crown Point Formation in the Pedirka

Basin has "a similar lithology to the Merrimelia Formation in the Cooper Basin..." inferring that similar glacial depositional processes prevailed in the separate basins.

3.2.2.3 Victoria and Tasmania

In Victoria, during the Early Permian continental glaciers moved north, forming scour pavements on which sandstones, shales and diamictites were deposited. These Permian glacial deposits outcrop in incised valleys shedding off the Ballan Horst block and in the Bacchus Marsh Sunland, with up to 51 individual tillite phases observed (Alley, 1995). These glacial deposits, along with diamictites located in Tasmania, represent the last vestiges of Gondwanan glaciation on the Australian landmass in the Kazanian. A large ice cap was centred on the Western Highlands of Tasmania in the Late Carboniferous (Fig. 3.5b) but had disappeared by the Sakmarian, after having deposited large volumes of diamictite. The last glacially-derived sediments in Tasmania were deposited by the action of icebergs that possibly originated from the nearby Antarctic highlands (Crowell and Frakes, 1971; Eyles *et al.*, 1998) (Fig. 3.4).

3.2.2.4 New South Wales

In New South Wales, glacial deposits from continental glaciation are not widespread with sediments having being derived from ice caps to the south in Victoria and South Australia.

3.2.2.5 Queensland

In the Bowen Basin of Queensland, fluviially-derived glacial sediments dominate the glacial successions, suggesting that there was little direct influence from the more southerly ice sheets (Chaney, 1998). Contrary to this, however, two thirds of the Cooper Basin is located in the far west of Queensland. The Merrimelia Formation occurs in Queensland and exhibits identical glacial features to those noted by Williams *et al.* (1985) and Chaney *et al.*, (1997) in the South Australian sector of the Cooper Basin with rhythmic varvites, fluviially-reworked conglomerates and diamictites the main glacial sediments observed.

The identification of rainout diamictites at Mount Howitt #1 (Chapter Four - Plate 5b) indicates that, at one stage, ice sheets covered a large proportion of both sectors (S.A. and QLD.) of the Cooper Basin. The development of rainout diamictites in Queensland suggests this, and indicates that icebergs shedding off nearby glaciers would have subsequently drifted on a large body of water, melted, and then formed rainout diamictites. The inferred direction of ice movement in the Queensland sector of the Cooper Basin is predominantly from the south east moving northwest

(Durham Downs #1, Mount Howitt #1) with the continental ice sheet lying to the south (Fig. 3.5a).

3.3 CONTROLS ON GONDWANAN GLACIATION

Several theories have been discussed in the literature as to controls and timing of glaciation on the Gondwana supercontinent. Alley (1995) pointed to worldwide climate changes that were related to plate tectonic events as having a considerable influence on climate in Gondwana. This author stated, that by the beginning of the Middle Carboniferous, the circum-global equatorial seaway had been closed by the connection of Laurentia and Gondwana. As a result of this continental arrangement, major cooling occurred in Australia and persisted until the Early Permian (Alley, 1995). Caputo and Crowell (1985) suggested that the movement of the palaeo-south pole traced the path of glaciation across Gondwana (Fig. 3.3). The location of the south pole migrated across Gondwana as the supercontinent moved by continental drift. It was also noted by the same authors that whenever the pole lay over oceanic areas, glaciation either didn't develop or disappeared but when, the pole was sited on the Gondwana landmass, glaciations developed. Veevers and Powell (1987), contrary to Caputo and Crowell (1985), argued that glaciation occurred at mid-latitudes (20° - 60°), having been initiated by the widespread development of highlands as Gondwana and Laurentia collided, with extensive ice developing as a response to low global temperatures related to low atmospheric CO_2 concentrations. Crowley and Baum (1992) go further by saying that the Late Palaeozoic exhibits the lowest CO_2 levels compared to other periods in the Earth's history.

3.4 CONCLUSIONS

- Glaciation on the Gondwana supercontinent was controlled by a number of factors, the main one being the movement of the Gondwana landmass into high latitude polar regions. Other factors include reduced global temperatures brought on by low CO_2 concentrations and a restriction in global equatorial currents which would have reduced the transfer of warm equatorial waters into Gondwana polar regions.
- Gondwana glaciation controls the style of sediment produced in the lower Gidgealpa Group of the Cooper Basin. The deposition of the Merrimelia-Tirrawarra Glacial Complex is a direct product of the Gondwanan glaciation.

- Merrimelia facies formed during the peak of glaciation in the late Stephanian to Asselian, in response to ice sheet and glacial melt.

- Towards the end of the Sakmarian, milder conditions started to prevail. The whole Cooper region still lay within polar latitudes but global temperatures started to rise (Alley, 1995). The grip of the Gondwanan glaciation on the Cooper Basin did not cease abruptly but fluctuated for a period of time until eventually glacial deposition was replaced by extensive cold climate coal deposition (Patchawarra Formation).

- As the influence of the Gondwanan glaciation fluctuated, interfingering Merrimelia facies and Tirrawarra facies Chaney *et al.* (1997) were deposited.

- Tirrawarra facies formed as the Gondwanan glacial ice cap retreated southwards.

- The start of Patchwarra Formation deposition is considered the end of direct Gondwanan glacial influence in the Cooper Basin.

SEDIMENTOLOGY

4.0 INTRODUCTION

The differing facies within a glacial depositional realm govern the textural and mineralogical maturity of sediments and thus influence any reservoir potential a given sediment may possess. This chapter documents twenty glacially-derived facies recognised in the Merrimelia Formation. Reservoir quality characteristics of each facies type will be dealt with in detail in Chapter Nine.

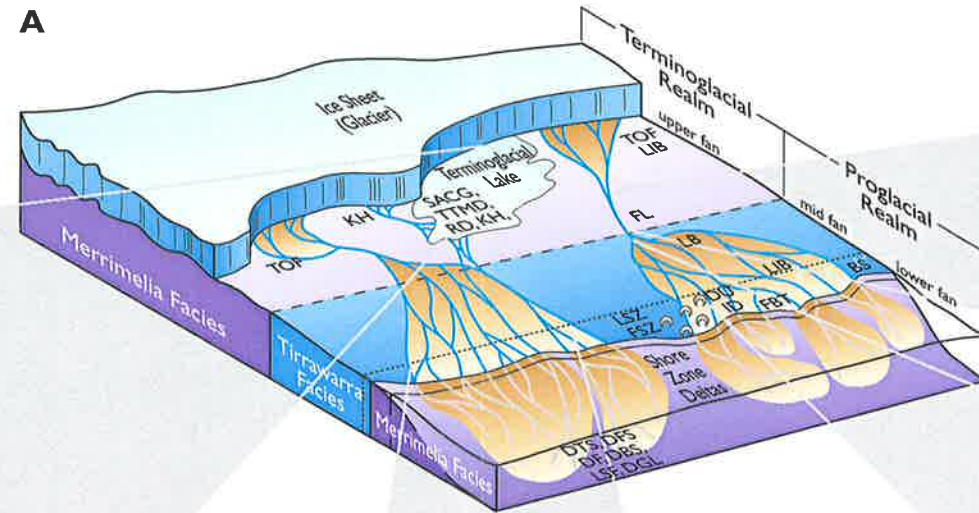
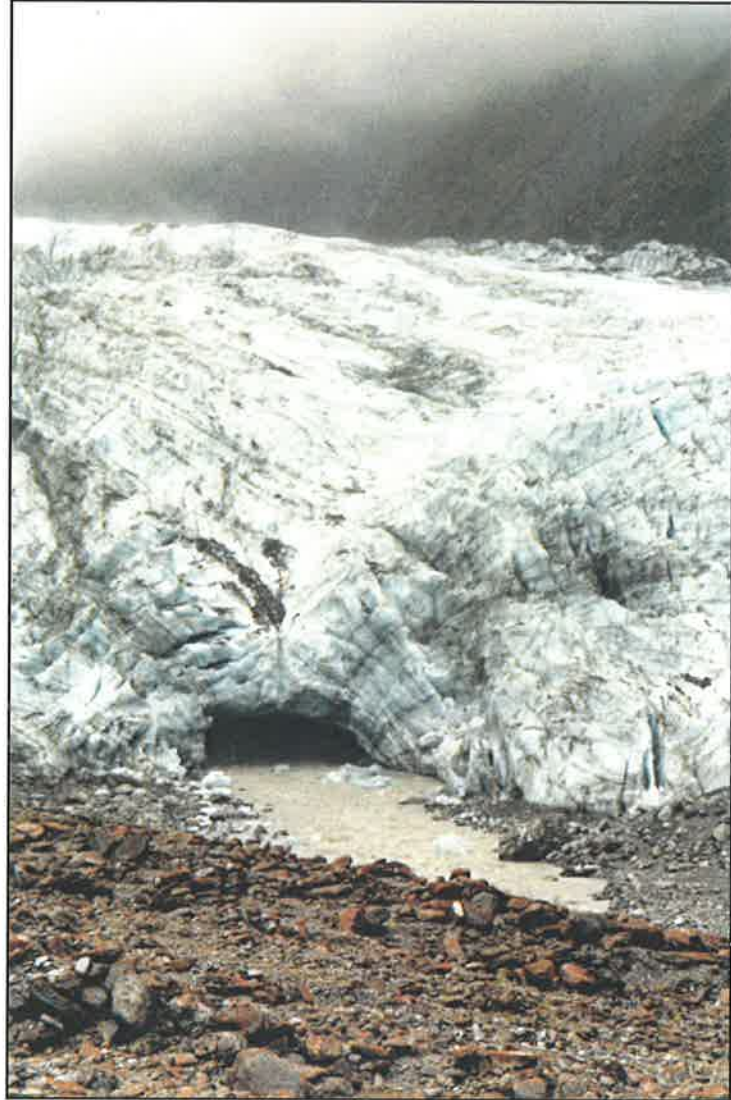
The evolution of the Merrimelia-Tirrawarra Glacial Complex (MTGC) in this study is described in terms of lower (M3), middle (M2), upper (M1) Merrimelia sections and a (T1) section which encompass Tirrawarra braid plain facies. The facies development of each level is briefly discussed in this chapter (section 4.4). The development of potential reservoir sandstones within each level is discussed in full in Chapter Nine.

To clearly and simply orientate the reader within the Merrimelia-Tirrawarra Glacial Complex, block diagrams are employed throughout the chapter (Fig. 4.1a). Chaney (1998) stated that such diagrams are by no means indicative of the facies architecture within the MTGC at a given location but are representative of overall glacial processes operating in the Cooper Basin. More specifically, Merrimelia facies have only been described from core in widely spaced wells and from depths over a two vertical kilometre range. Correlating between the "pin pricks" of core across the whole Cooper Basin is a risky venture at best. The terminoglacial and proglacial diagrams as well as the MTGC evolution diagrams are thus only representations of environments encountered within this glacial complex and are not paleogeographic reconstructions.

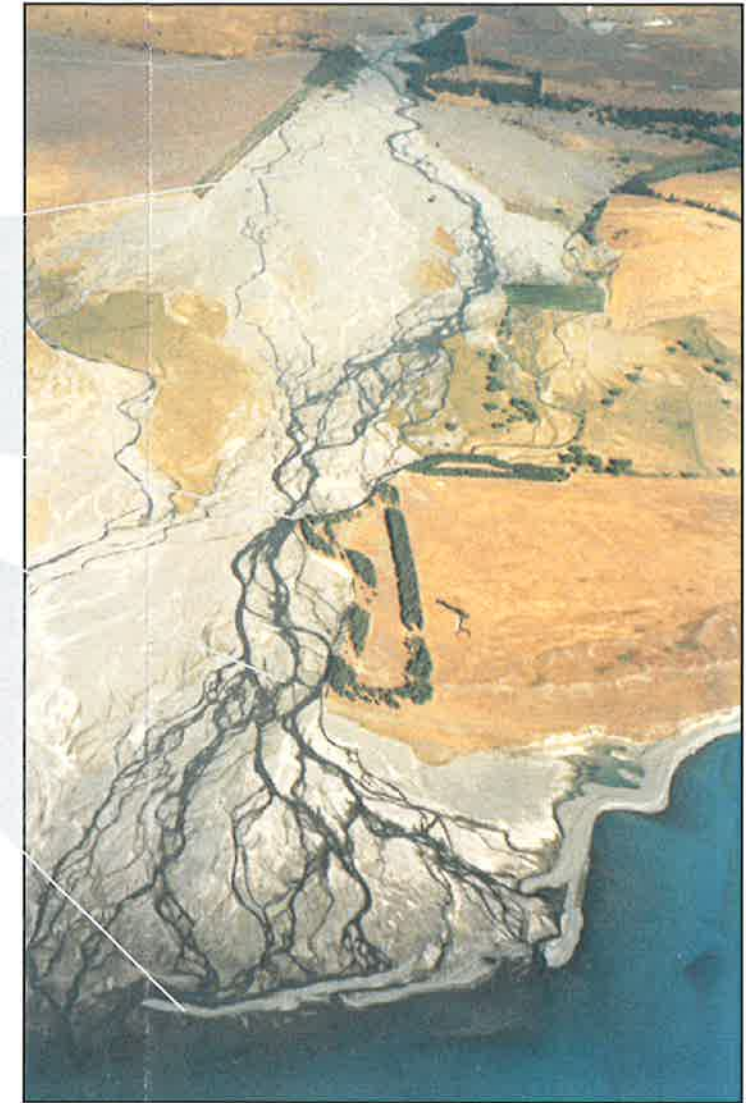
The detailed sedimentology outlined in this chapter was developed by A. Chaney, as part of his PhD project (Chaney, 1998). This author's sedimentology project was done in parallel with this reservoir quality/diagenesis study. The sedimentology core logging performed by Chaney (1998) was done in unison with the lithological core logging and core sampling of this project.

A model of the Merrimelia - Tirrawarra Glacial Complex (MTGC)

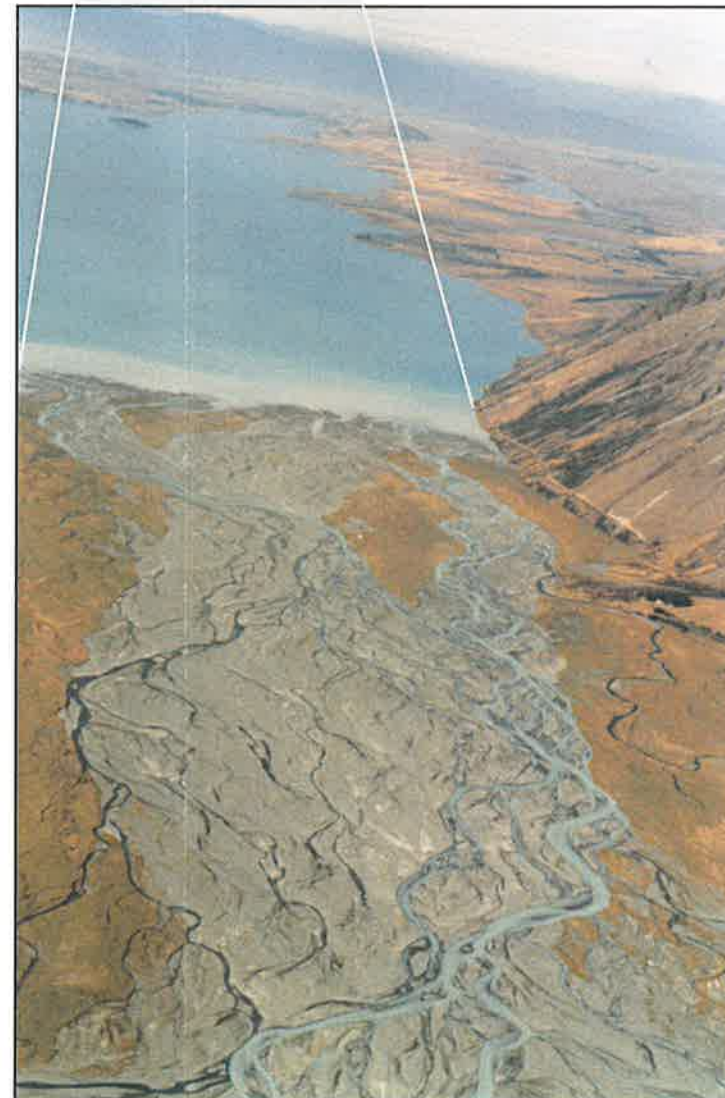
Inset A



Inset B



Inset C



B

Merrimelia Formation Facies Types

Abbreviations	Facies Type
BS	Back Swamp
DBS	Delta Bottomsets
DF	Delta Flow
DFS	Delta Forsets
DGL	Deep Glacio-lacustrine
DTS	Delta Topsets
DU	Aeolian Dune
FBT	Fluvial Bar Top
FL	Fluvial Sandstone
FSZ	Frozen Shore Zone
ID	Interdune
KH	Kettle Hole
LB	Longitudinal Bar
LIB	Linguoidal Bar
LSF	Terminoglacial Lacustrine Sand Flow
LSZ	Lacustrine Shore Zone
RD	Rainout Diamictite
SACG	Subaqueous Channel Gravel
TOF	Terminoglacial Outwash Fan
TTMD	Terminoglacial Subaqueous Tunnel Mouth Deposit

Figure 4.1 A) A model of the Merrimelia/Tirrawarra glacial complex. **Inset A)** Terminoglacial lake at the base of the Fox Glacier, N.Z. **Inset B)** Braid plain delta complex entering a proglacial lake (Cass River Delta-Lake Tekapo, N.Z.). **Inset C)** Braid plain outwash entering a proglacial lake (Godley River Delta-Lake Tekapo, N.Z.). **B)** Merrimelia Formation facies types.

Sediment sorting and grain size data was gathered on all facies types in the Merrimelia Formation (this data is presented in table form throughout this chapter). The raw point counting data was manipulated to express the grain size and sorting coefficients for each sample. The average grain size for each sample is given in millimetres, while the sorting coefficients are expressed in $\sigma\phi$ units. Sorting coefficient ranges used in this study are illustrated in table 4.1. The sorting values were derived using the Folk and Ward formulae (Folk and Ward, 1957) outlined below (Equation 3).

$$\sigma\phi = \frac{\phi_{84} - \phi_{16}}{4} + \frac{\phi_{95} - \phi_5}{6.6} \quad \text{Equation 3}$$

Sorting Coefficients (Phi Units)	Sorting Term
Less Than 0.35	Very Well
0.35 - 0.5	Well
0.5 - 0.71	Moderately Well
0.71 - 1.00	Moderate
1.0 - 2.0	Poor
Greater Than 2.0	Very Poor

Table 4.1 *Sorting coefficient ranges (phi units).*

4.1 SEDIMENTOLOGY OF THE MERRIMELIA-TIRRAWARRA GLACIAL COMPLEX

The Merrimelia Formation and Tirrawarra Sandstone comprise an integrated depositional continuum (Williams and Wild, 1984a; Chaney *et al.*, 1997). For the purposes of this study however, only the sedimentology of the Merrimelia Formation has been considered and is presented in this chapter. The sedimentology of the Tirrawarra Sandstone, on a regional basis, was initially documented by Gostin (1973), with further work done mainly by Mc Intyre (1982), Williams and Wild (1984a) and Williams *et al.* (1985, 1987). To comprehensively assess all the facies of the Merrimelia glacial complex on a regional basis, one must combine the sedimentology of the aforementioned authors with the sedimentology of the Merrimelia Formation. More recently, Rezaee (1996) has documented in detail the sedimentology of the Tirrawarra Sandstone in the Moorari, Fly Lake, Broilga and Tirrawarra Fields. Again, to assess the sedimentology of the entire Merrimelia-Tirrawarra Glacial Complex in these regions, one must integrate the sedimentology of the Tirrawarra Sandstone, as documented by Rezaee (1996), along with the sedimentology of the Merrimelia Formation.

4.2 SEDIMENTOLOGY OF THE MERRIMELIA FORMATION

Sedimentological analysis within the Merrimelia Formation has been undertaken by several workers (Grund, 1966; Williams and Wild, 1984a; Williams *et al.*, 1985 & 1987; Chaney *et al.*, 1997 and Chaney, 1998). Williams and Wild (1984a), Williams *et al.* (1985 and 1987) and Chaney *et al.* (1997) show that both the Tirrawarra Sandstone and Merrimelia Formation form a complex of inter related facies (MTGC). These facies were deposited within terminoglacial and proglacial environments, and interfinger constantly (laterally and vertically), exhibiting rapid environmental change related to the position of the Gondwana ice sheet (Chaney *et al.*, 1997). The terminoglacial environment forms from the frontal and marginal parts of the ice sheet (Fig. 4.1a), and the sediments generated are affected by ice melt, aeolian, fluvial, lacustrine, deltaic and mass flow depositional processes (Chaney, 1998). The proglacial depositional realm is distal to the ice sheet (Fig. 4.1a) with the size and character of this environment dependent on meltwater volumes.

All facies observed within the Merrimelia Formation are described in relation to the terminoglacial or proglacial depositional realms (Fig. 4.1a).

All facies types and abbreviations used in the diagrams and text throughout this chapter and subsequent chapters are also summarised in Figure 4.1b.

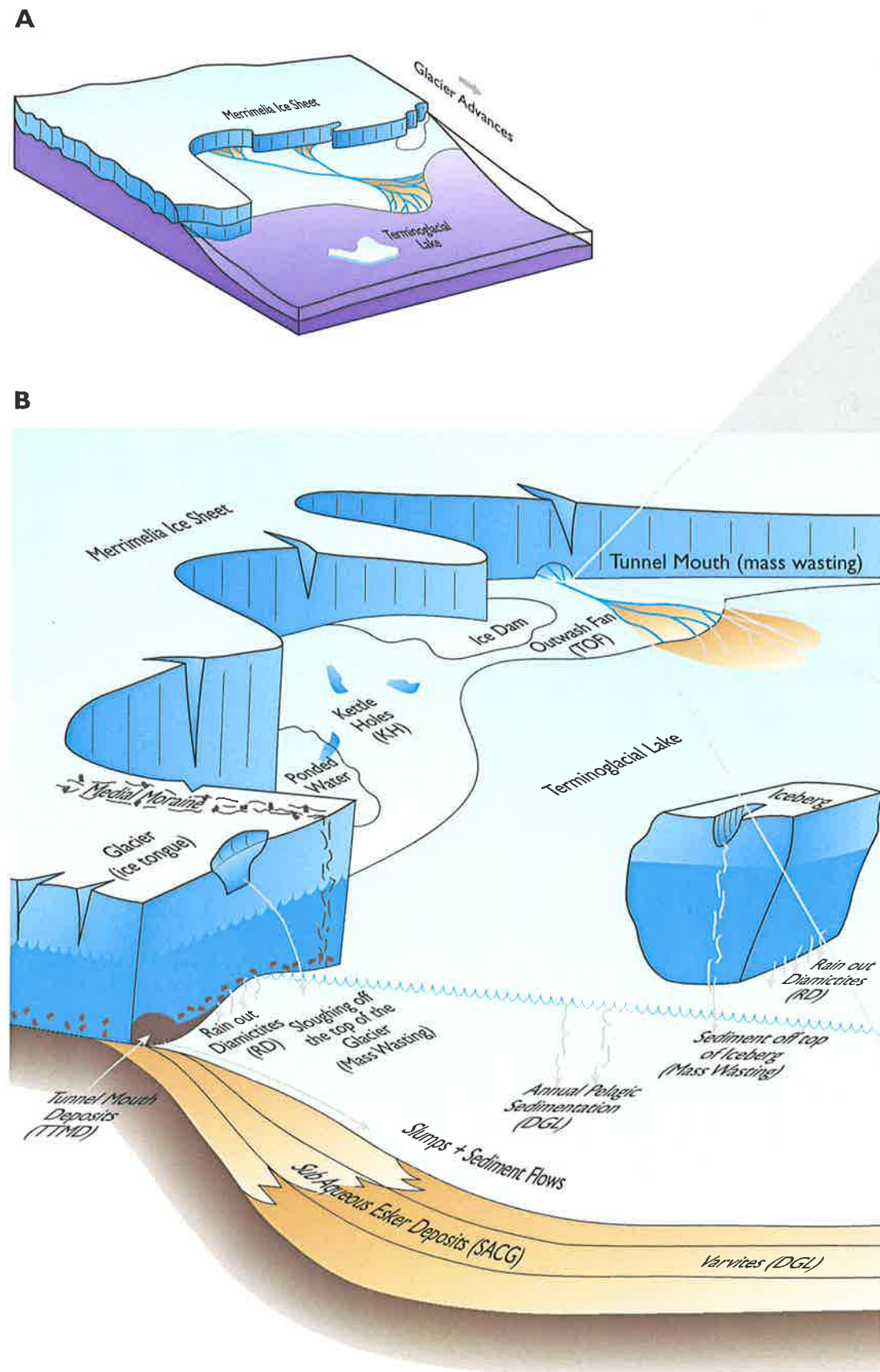
4.2.1 TERMINOGLACIAL ENVIRONMENTS

The terminoglacial zone forms a very narrow band relative to the ice sheet (Fig. 4.2a). This depositional realm shows a wide variety of morphological, and sedimentological structures and facies due primarily to the high energy of this zone (Fig. 4.2b[Inset A]). Most of the sediments found in the terminoglacial region are deposited in meltwater rivers and streams (Chaney, 1998) (Fig. 4.2a[Inset B]).

The terminoglacial realm is dominated by high energy conditions where sediment dispersal near the snout of the glacier is dictated by rapid changes in melt water volume and strength (Fig. 4.2b[Inset A]).

The coarse grained detritus is moved infrequently and only for short distances during high energy flows (Chaney, 1998). The fluvial regime in the terminoglacial environment is characterised by incised channels which are cut into the substrate by high energy meltwaters (Fig. 4.2b[Inset B]).

Terminoglacial Facies



Inset A



Inset B



Figure 4.2 A) A model of the terminoglacial depositional realm (modified from Cubitt et al., 1998). B) Facies observed in terminoglacial Merrimelia sediments (modified from Cubitt et al, 1998). **Inset A**) Terminoglacial tunnel mouth stream. Note : very high energy flow regime (Franz Josef Glacier, N.Z.). **Inset B**) View of a terminoglacial out wash fan (TOF) from the glacier snout (Franz Josef Glacier, N.Z.).

Fluvial sediments range from coarse grained, poorly sorted conglomerates to an array of variably sorted sandstones, siltstones and conglomerates. In most cases, the conglomerates are clast supported, with the interstitial matrix ranging from medium to very coarse sand although some do show a higher proportion of mud. These rather chaotic rocks are interpreted as high energy meltwater floods, perhaps because of a dam burst within the glacier, or in the terminoglacial environment itself (Chaney, 1998).

Slack water deposits are rarely preserved in such an environment due to the erosive capacity of subsequent major flood events. Kettle hole deposits however, represent a quiet water facies having formed by the action of melting dead ice, creating holes into the underlying topography where later ponded water was allowed quiet settling conditions (Bennett and Glasser, 1997). Kettle deposits were observed and described by Chaney (1998) within the Merrimelia Formation in Gidgealpa #3 and Malgoona #2 and #4.

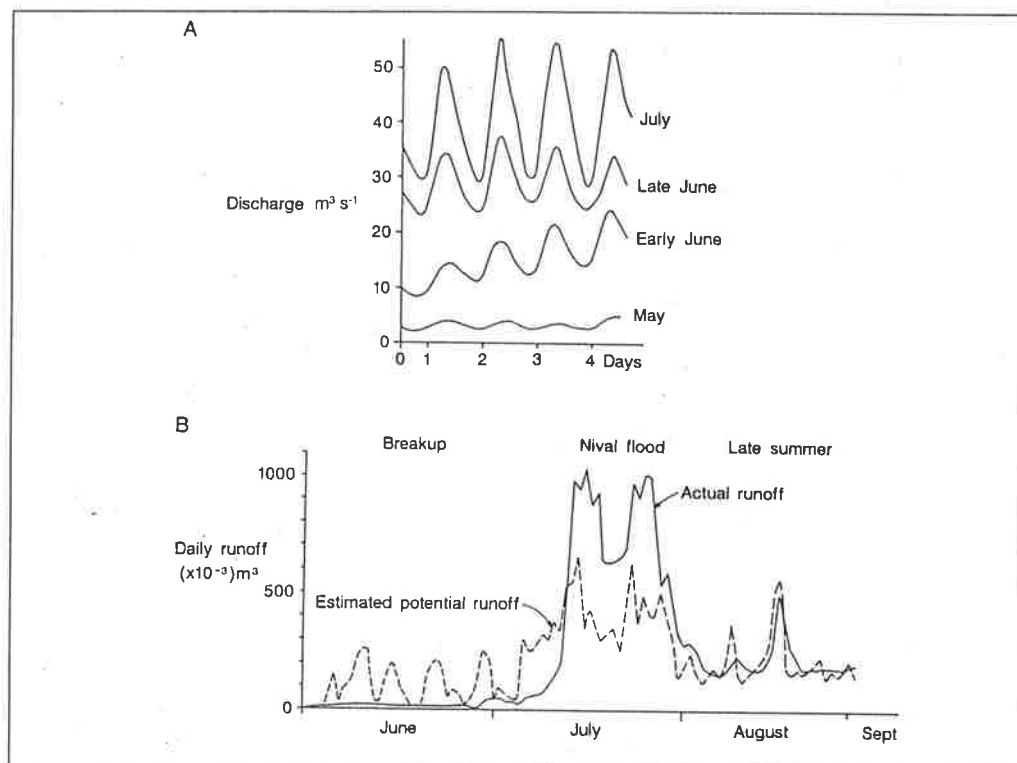


Figure 4.3 Typical diurnal and monthly run off hydrographs in a northern hemisphere glacial system (After Bennett and Glasser, 1997).

The water supply forming terminoglacial environments is not necessarily controlled by diurnal or seasonal variation (Fig. 4.3) but may be sourced from catastrophic floods due to ice dam collapse (Bennett and Glasser, 1997) (Fig. 4.4a). The net effect of such a

water supply is that fluvial sediments display extreme lateral and vertical variability and exhibit very high sediment loads (Fig. 4.4a).

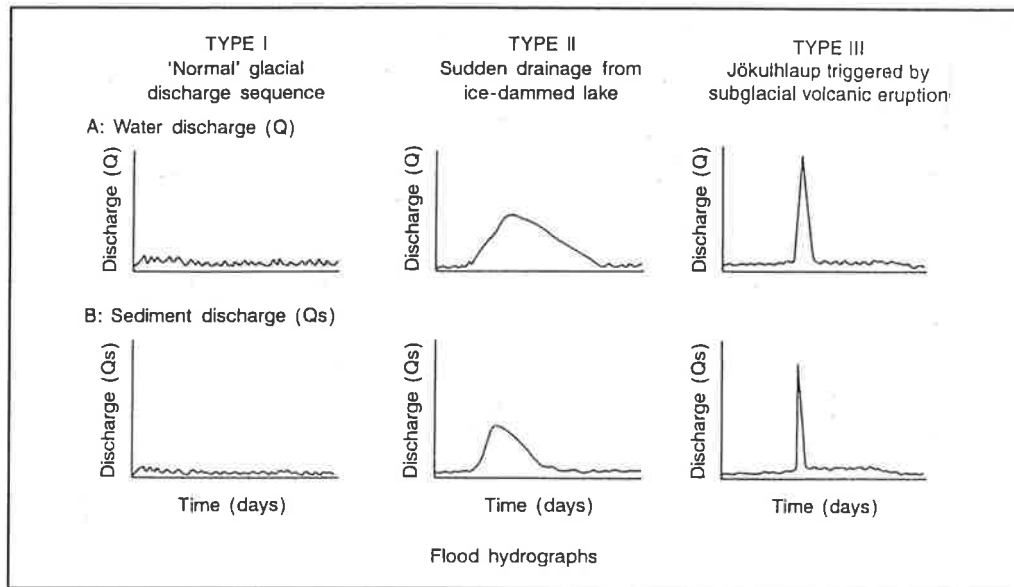


Figure 4.4. Meltwater hydrographs (After Bennett and Glasser, 1997).

Lakes are a common feature in terminoglacial environments resulting from high volumes of melt water discharge. The size of the lakes depends on bedrock and glacier topography, water volumes and the amount of detritus issuing from the glacier. Terminoglacial lakes, because they contact the glacier (Fig. 4.1a[Inset A]), and are therefore subject to very complex depositional conditions with melting ice having a strong influence on sedimentation (Chaney *et al.*, 1997). Sediments entering terminoglacial lakes do so via mass wasting, fluvial and subaqueous processes illustrated in Figure 4.2b.

Within the terminoglacial realm, lacustrine facies exhibit a wide variety of subaqueous deposits ranging from those released directly from the ice to those deposited from settling of surge flows (Chaney *et al.*, 1997). Rain-out diamictites are common, exhibiting a wide range of clast sizes (Table 4.2). The matrix in these sediments is mostly composed of homogenous silty mud within which dropstones appear to float. Chaney *et al.* (1997) stated that some of the diamictites are stratified. These diamictites show sandy layers which are usually not more than a few centimetres thick and abundant ripup clasts. Often they are disrupted by dropstones and occasionally exhibit isoclinal folding (Chaney, 1998). Such diamictites have been described by Evenson *et al.* (1977) as sub-aquatic flow tills, which have moved downslope as a coherent viscous block of sediment. Subaqueous tunnel mouth deposits, bottomsets and varvite mudstone were also observed and described by

Chaney *et al.* (1997) within the terminoglacial environment. The following section describes in detail all the various terminoglacial facies observed in the Merrimelia Formation and their modes of deposition.

4.2.1.1 TERMINOGLACIAL FACIES ASSOCIATIONS

4.2.1.1.1 Terminoglacial Tunnel Mouth Deposits (TTMD)

This facies is primarily composed of breccia with clast sizes up to 10cm common (Plate 5a). These breccia are matrix supported, with the matrix displaying no internal structure and ranging in size from fine sand to granule breccia (Table 4.2). The sorting of these sediments is accordingly very poor (Table 4.2).

Facies	Sample	Sorting Coefficient	Sorting	Grain Size (mm)	Grain Size
TTMD	PACK 3A	0.41	Well	0.13	Fine Sand
TTMD	PACK 3B	1.83	Poor	1.45	Fine Sand
TTMD	MOOR 2D	1.58	Poor	1.99	Granule
Ave.		1.3	Poor	1.2	Very Coarse Sand
Std.		0.8		1.0	

Table 4.2 *Terminoglacial tunnel mouth deposits (TTMD).*

Observations by Chaney (1998) suggested that reworking of these breccias was minimal. Minimal reworking, combined with the variation in grain size (indicated by poor sorting values), tends to suggest that these sediments have either been dumped as mass wasting tills or have been deposited directly from the glacier tunnel mouth (Fig. 4.2a[Inset A]).

Farther away from the glacier, within ice contacted terminoglacial lakes, sediments issuing from the glaciers will settle onto the floor of the lake, and may form a subaqueous esker composed of a complex interlayering of subaqueous flows (Fig. 4.2a). Chaney (1998) confirms that these stratified conglomerates are subaqueous sediments deposited directly from a glacial mouth.

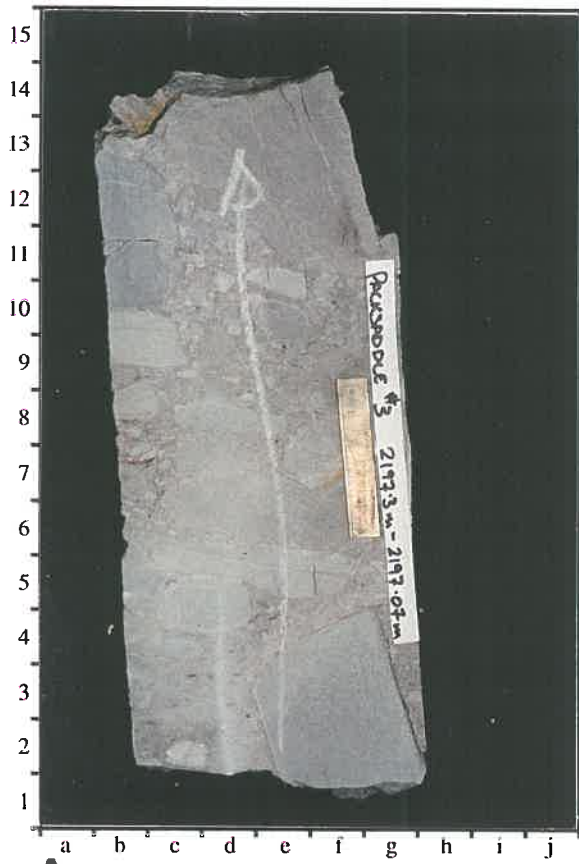
These subaqueous deposits have been observed in Moorari #2 and Packsaddle #3 wells (Chaney, 1998).

PLATE 5**Terminoglacial Lithologies: 1**

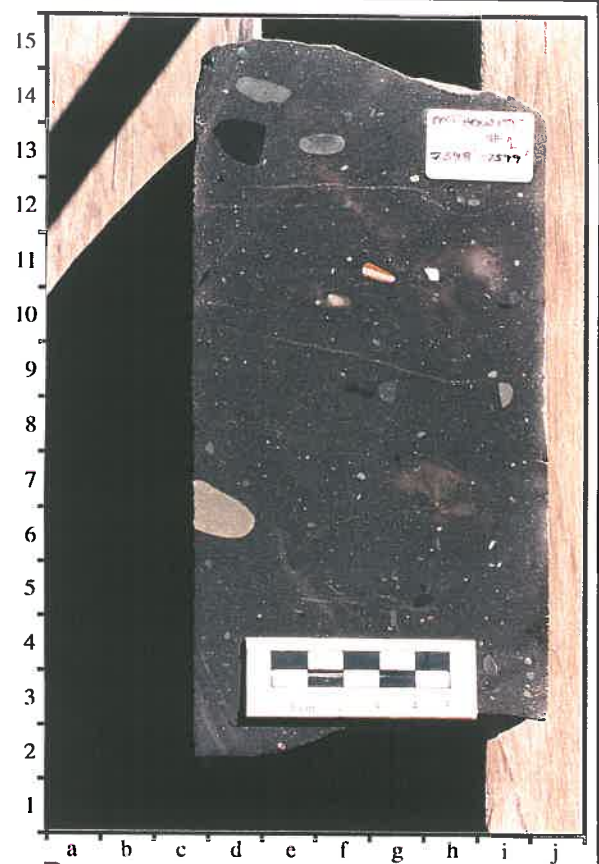
YOUNGING IS TOWARDS THE CORE IDENTIFICATION STICKER IN VERTICAL PLATES AND TO
THE LEFT IN HORIZONTAL PLATES

- A) Core photograph – Packsaddle #3 (2197.30m – 2197.07m). Sub-aqueous tunnel mouth breccia (TTMD).*
- B) Core photograph - Mount Howitt #1 (2325.39m – 2325.70m). Rain-out diamictite (RD) located in the eastern Cooper Basin (QLD).*
- C) Core photograph – Jack Lake #1 (3147.87m). Rain out diamictite (RD) located in the western Cooper Basin (S.A.).*
- D) Core photograph – Durham Downs #1 (2770.53m – 2770.79m). Stratified diamictite (RD) indicating strong current. Note loading of finer grained material into underlying diamictite [8f].*

Plate 5



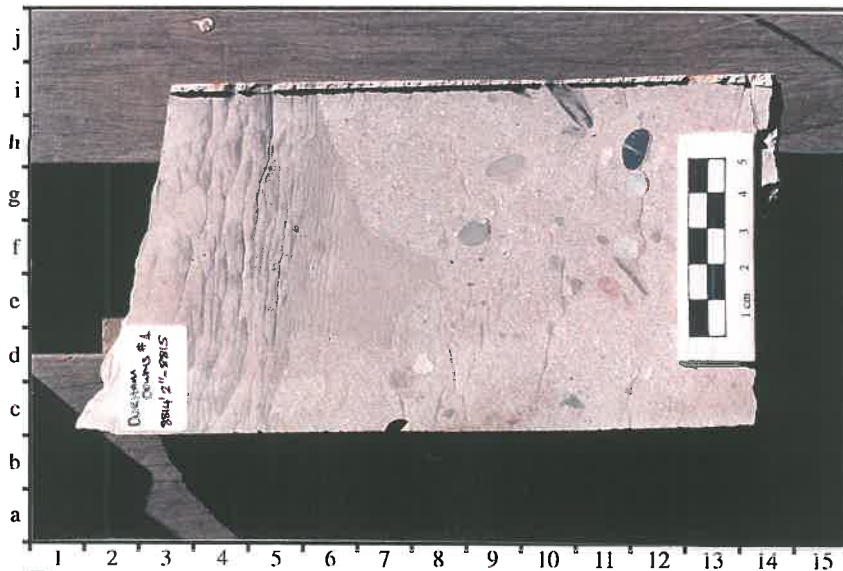
A



B



C



D

4.2.1.1.2 Rain-Out Diamictites (RD)

These sediments are mud or silt-supported sediments and are either massive or show some degree of stratification. Plates 5b & 5c illustrate typical examples of rain-out diamictites distinguishable as being of glacial origin by the presence of faceted clasts and the position of these conglomerates within a lacustrine dominated glacial sequence.

These two examples (Plates 5b & 5c) are separated by approximately 300 kms (Fig. 1.2), but display very similar features indicating that the same glacial processes were occurring in these widely spaced locations (but almost certainly not at the same time). Further analysis of the limited Merrimelia Formation core in the Queensland sector of the Cooper Basin, shows an apparent dominance of terminoglacial facies that include rainout diamictites (Plate 5b) and stratified diamictites (Plate 5d). The very limited amount of core coupled with the enormous distances between cored Merrimelia intervals in Queensland constrains any discussion of depositional environment to that of the individual wells. However, the evidence suggests that, at differing time intervals, large portions of the Cooper Basin, in both South Australia and Queensland, may have experienced direct glacial conditions.

Facies	Sample	Sorting Coefficient	Sorting	Grain Size (mm)	Grain Size
RD	MOOR 1B	0.81	Moderate	0.39	Medium Sand
RD	KENY 1B	0.83	Moderate	0.49	Medium Sand
RD	CONA 1B	0.72	Moderate	0.54	Coarse Sand
RD	MTHOW	1.20	Poor	0.60	Coarse Sand
RD	JAC 1A	1.92	Poor	0.76	Coarse Sand
RD	CONA 1A	1.30	Poor	0.77	Coarse Sand
RD	DULN 1A	2.15	Very Poor	0.92	Coarse Sand
RD	MERRI 3A	2.16	Very Poor	0.93	Coarse Sand
RD	WEL 1C	2.43	Very Poor	0.98	Coarse Sand
RD	MOOR 2C	1.06	Poor	0.98	Coarse Sand
RD	KENY 1A	2.44	Very Poor	1.09	Very Coarse Sand
RD	MOOR 1A	1.63	Poor	1.85	Very Coarse Sand
Ave.		1.6	Poor	0.9	Coarse Sand
Std.		0.65		0.4	

Table 4.3 Rain out diamictite (RD).

Rainout diamictites of varying clast sizes are found in seven wells in the South Australian sector of the basin: Jack Lake #1, Merrimelia #3 and #18, Welcome Lake #1, Tindilpie #2, Kenny #1 and Moorari #1. These sediments may represent some of the first glacial sediments preserved within the Cooper Basin (Chaney, 1998). Diamictites

were observed in Mount Howitt #1, Tallalia #1 and Durham Downs #1 in Queensland. Diamictites throughout the basin are generally similar in nature showing a massive substrate, are mud supported and exhibit angular to sub-angular clasts (Plate 5).

Massive rainout diamictites are formed from the direct action of melting icebergs, ice rafts and even ice sheets melting over time and shedding detritus onto a lake floor (Fig. 4.2b). Stratified diamictites form by the same depositional mechanism as massive diamictites, but stratified diamictites form by a combination of rainout sedimentation and downslope subaqueous traction currents (Fig. 4.2b). Some stratified diamictites include thin sand flows and ripup clasts of the underlying muds and silts (Chaney, 1998).

The sorting of rain-out and stratified diamictites observed in the Merrimelia Formation is very poor with grain sizes highly variable (Table 4.3).

4.2.1.1.3 Terminoglacial Outwash Fan (TOF)

Terminoglacial outwash fan sediments formed proximal to the glacier (Fig. 4.2b[Inset C]). These sediments represent fluvial deposition that initially issues from glaciers and shows extreme lateral and vertical variability (Chaney, 1998). These sediments are thus classed according to the subdivisions of Boothroyd and Ashley (1975) as being part of the upper fan within a glacial braid plain depositional complex (Figs. 4.2a & 4.2a[Inset B]). The proximity of these sediments to glaciers places them in the terminoglacial depositional realm (Chaney, 1998).

The narrow stream architecture observed in upper fan regions (Fig. 4.2b[Inset B]) is controlled by the occasional high water flow rates emanating from the glacier and the inclined nature of the upper fan slope. Chaney (1998) stated that, in many modern examples of glacial outwash braid plains, the grain size decreases as the slope of the outwash fan decreases. This is certainly true for the Merrimelia Formation where a predominance of coarse grained sediments in the upper fan grades into finer grained sandstones in the lower fan reaches. The dominant bar form in the upper fan tends to be gravel dominated longitudinal bar forms where sand development is rare and restricted to matrix (Chaney, 1998).

The coarse grained nature of these sediments is a reflection of the proximity of glaciers. Similar to other terminoglacial facies described, these sediments have formed in a high energy environment in which occasional catastrophic flood events may occur (Fig. 4.4). This would imply a certain degree of sediment reworking, which is

true for the most part, but only a narrow zone of the upper fan experiences high energy flood events where large volumes of detritus are moved. Such movement is infrequent and occurs only over short distances, leaving these sediments poorly sorted.

The terminoglacial outwash sediments noted in core range from coarse sandstone and poorly sorted conglomerates (Plate 6a) to a series of variably sorted sandstones (rare) and siltstones (Chaney, 1998). These sediments are observed in Gidgealpa #3 as well as Malgoona #2 and #4, Kudrieke #1 and Tinga Tingana #1.

The conglomerates and sandstones of the terminoglacial outwash fan display a crude bedding where the clasts are dominantly igneous. Although illitised and ductile, these rock fragments exhibit angular to sub-angular clast shapes which is suggestive of a very proximal transport distance involving strong currents dumping sediment (Chaney, 1998). The absence of extensive sediment reworking, in the terminoglacial outwash fan, and the dumping of coarse material produces sediments dominated by a large size fractions (Table 4.4).

Facies	Sample	Sorting Coefficient	Sorting	Grain Size (mm)	Grain Size
TOF	MAL 4C	1.24	Poor	0.16	Fine Sand
TOF	TINA 1E	0.39	Well	0.25	Medium Sand
TOF	GIDG 3C	1.41	Poor	0.92	Coarse Sand
TOF	MAL 4F	2.17	Very Poor	1.05	Very Coarse Sand
TOF	GIDG 3B	1.24	Poor	1.24	Very Coarse Sand
TOF	MAL 4E	1.28	Poor	1.34	Very Coarse Sand
TOF	GIDG 3A	1.58	Poor	1.49	Very Coarse Sand
TOF	MAL2D	0.98	Moderate	1.58	Very Coarse Sand
TOF	MAL 4D	0.92	Moderate	1.70	Very Coarse Sand
TOF	MAL 4H	1.60	Poor	2.13	Granule
TOF	MAL 4G	1.19	Poor	2.50	Granule
TOF	TINA 1G	1.67	Poor	2.55	Granule
TOF	TINA 1F	1.90	Poor	3.08	Pebble
TOF	MAL 2C	2.08	Very Poor	3.12	Pebble
TOF	KUD 1F	2.26	Very Poor	3.22	Pebble
Ave.		1.5	Poor	1.8	Very Coarse Sand
Std.		0.51		1.0	

Table 4.4 *Terminoglacial outwash fan (TOF).*

4.2.1.1.4 Terminoglacial Lacustrine Sand Flow (LSF)

Deposition within the terminoglacial lacustrine environment is very complex (Eyles and Miall, 1984), due mainly to the fact that detritus input into terminoglacial lakes

reaches of large terminoglacial lakes will contain detritus that is the same as sediments found in large proglacial lakes.

One obvious distinction between terminoglacial and proglacial lake sediments is that terminoglacial lacustrine sediments are composed of coarser grained material (Chaney, 1998). This coarser material, which represents individual grain flows, commonly interfingers with lacustrine mudstones. Both sediment types arrive in terminoglacial lakes via braid plain and deltaic deposition (Fig. 4.2b) where ice is not in direct contact with the lake.

The sandstone grain flows are generally well sorted (Table 4.5), with current ripples and loading features common. Flame structures and reactivation surfaces have also been noted (Chaney, 1998). The sand flows are of varying strength and duration and, when newly deposited, they load onto the deep water muds causing dewatering and flame structures to form (Plate 6b). These sand flows are termed bottomset flows (Chaney, 1998) and have been interpreted to flow along the lake floor (Fig. 4.2b). These sediments were described in Gidgealpa #5 only.

Facies	Sample	Sorting Coefficient	Sorting	Grain Size (mm)	Grain Size
LSF	JAC 1B	0.80	Moderate	0.02	Medium silt
LSF	TIRRA 8C	0.90	Moderate	0.03	Coarse Silt
LSF	TIRRA 7C	0.91	Moderate	0.04	Coarse Silt
LSF	BIMB 1A	0.57	Moderately Well	0.04	Coarse Silt
LSF	DARA 1A	0.75	Moderate	0.10	Very Fine Sand
LSF	DDOW 1B	0.66	Moderately Well	0.13	Fine Sand
LSF	DARA 1B	0.67	Moderately Well	0.14	Fine Sand
LSF	GIDG 5B	0.87	Moderate	0.20	Fine Sand
LSF	MOOR 2B	0.38	Well	0.26	Medium Sand
LSF	DARA 1C	0.96	Moderate	0.28	Medium Sand
LSF	DDOW 1A	1.35	Poor	0.75	Coarse Sand
Ave.		0.8	Moderate	0.2	Fine Sand
Std.		0.26		0.2	

Table 4.5 *Terminoglacial lacustrine sand flow (LSF).*

PLATE 6

Terminoglacial Lithologies: 2

YOUNGING IS TOWARDS THE CORE IDENTIFICATION STICKER IN VERTICAL PLATES AND TO THE LEFT IN HORIZONTAL PLATES

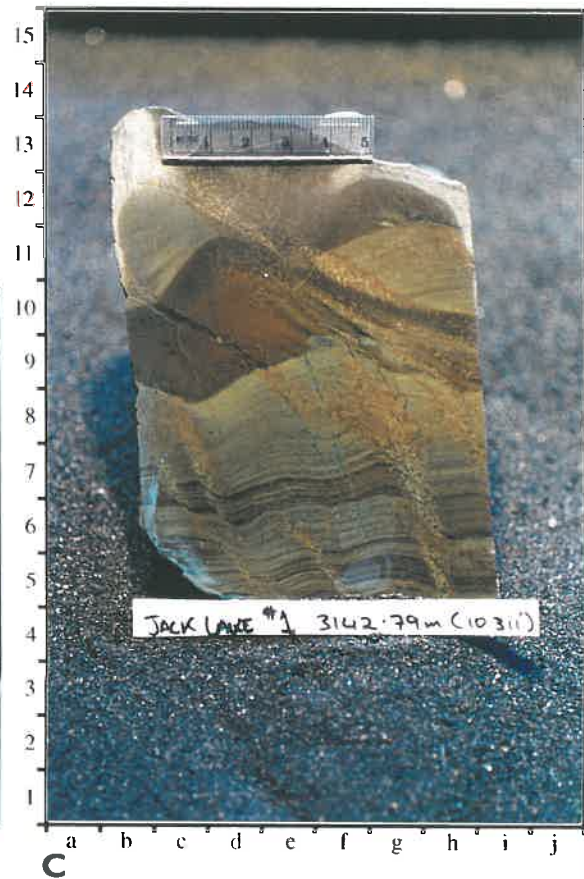
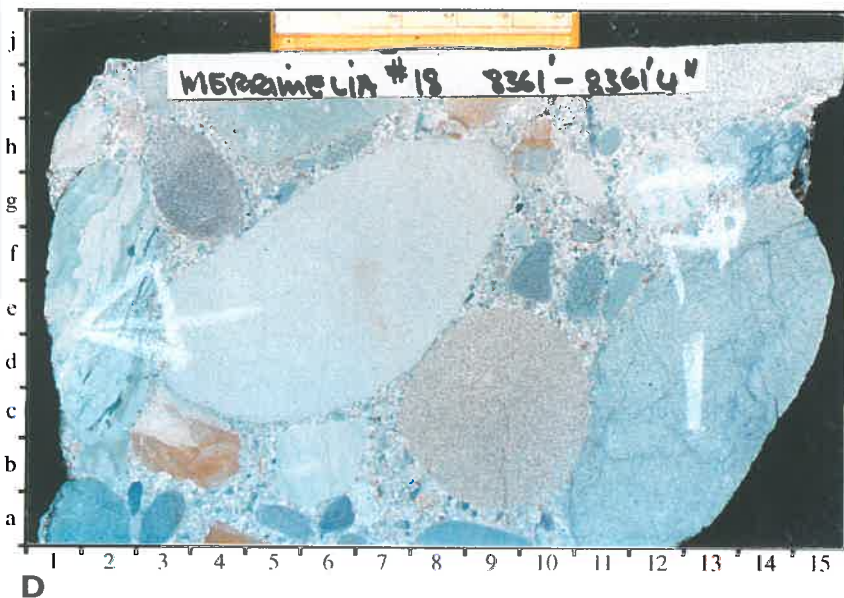
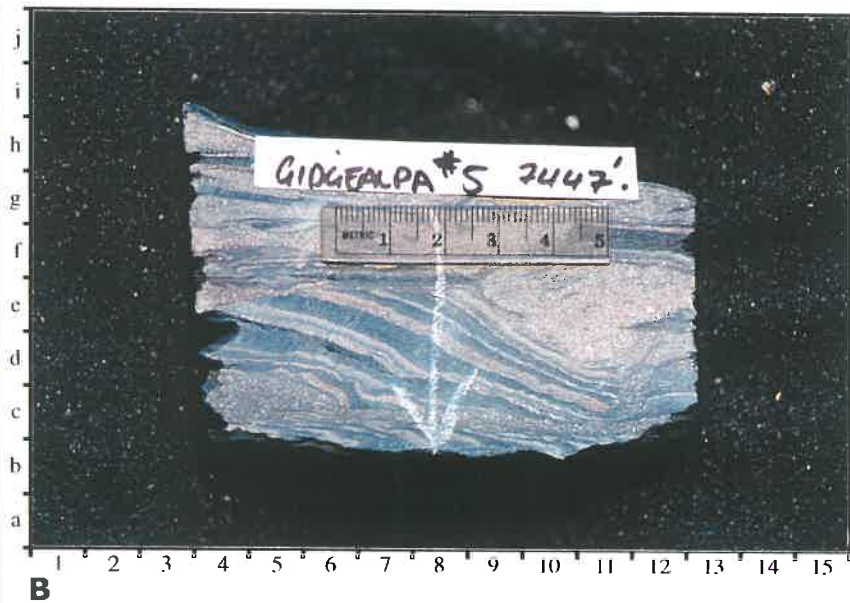
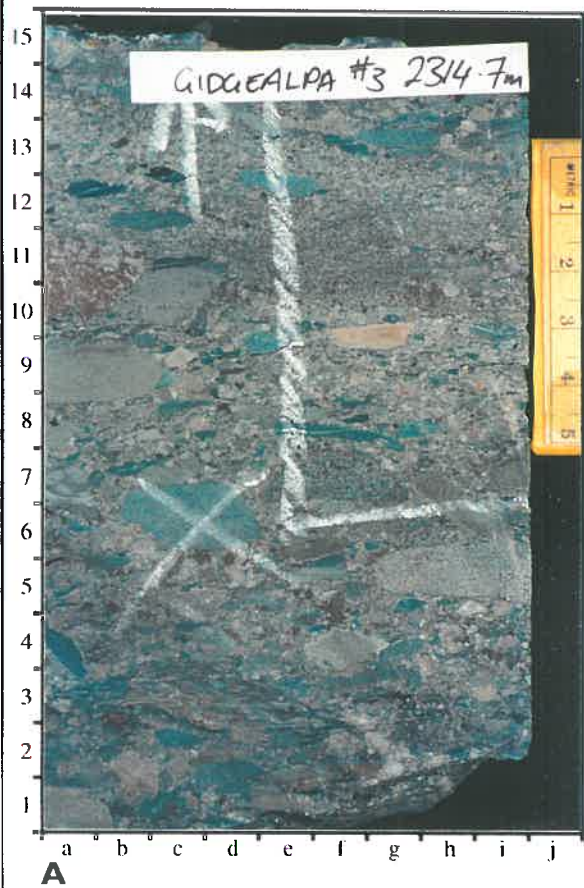
A) Core photograph – Gidgealpa #3 (2314.70m). Terminoglacial outwash conglomerate (TOF).

B) Core photograph – Gidgealpa #5 (2340.79m). Grain flow into terminoglacial lacustrine sediments (LSF). Note soft sediment deformation features such as post depositional folding and faulting are common [6c].

C) Core photograph – Jack Lake #1 (3142.79m). Unusual grain flow within a diamictite. Note climbing ripples/syn depositional micro-faults [7g] along which fluid has preferentially escaped (dewatering).

D) Core photograph – Merrimelia #18 (2628.08m – 2628.16m). Sub-aqueous channel gravel (SACG) (sub-aqueous esker) conglomerate. Note conglomerate is sand not mud supported indicating a degree of reworking [7b].

Plate 6



In Jack Lake #1, an unusual sand flow was observed (Plate 6c) not within a mudstone context but within a rainout diamictite. This sand flow exhibits climbing ripples along which unusual dewatering structures ("champagne bubbles") indicating that this flow was still plastic at the time of diamictite deposition (Chaney, 1998). Dewatering, rippling and loading features are all features that are indicative of subaqueous grain flow deposition. Other sand flows noted within diamictites were observed at Moorari #1 (Chaney, 1998).

The relatively strong currents with which these sand flows have been deposited suggests that sorting of these sediments should be good. The results shown in Table 4.5 indicate that this is indeed the case further suggesting that these sediments are distal to their sediment source. (Chaney, 1998) suggested that, under proglacial lake conditions, similar sediments would form varves. The coarse grained nature of these sediments however suggests that they have been deposited in a higher energy environment within an ice contact (terminoglacial) lake.

4.2.1.1.5 Subaqueous Channel Gravel (SACG)

These sediments were observed in only two wells Merrimelia #18 and Kenny #1 (Chaney, 1998). These sediments are dominantly conglomeratic with coarse sandy matrices (Plate 6d). Higher up the sequence, these conglomerates commonly grade into sandstones (Appendix 9a – Merrimelia #18). The sorting of the sandstone beds is good, but the sorting coefficients of the conglomerates are indicative of poor to very poorly sorted sediments (Table 4.6).

The clasts within the conglomerates display a well rounded nature with some faceting noted (Chaney, 1998) (Plate 6d). These conglomerates at first glance may be seen as indicative of a sub-aerial origin, possibly a longitudinal bar. However, the soft contact with the rainout diamictite below, as described by Chaney (1998), indicates that this conglomerate has been deposited in a subaqueous setting. Accordingly this author envisages these conglomerates to have formed within a terminoglacial lake setting.

Facies	Sample	Sorting Coefficient	Sorting	Grain Size (mm)	Grain Size
SACG	MRI 18A	0.47	Well	0.33	Medium Sand
SACG	MRI 18B	1.64	Poor	1.10	Very Coarse Sand
SACG	MRI 18C	1.28	Poor	1.31	Very Coarse Sand
Ave.		1.1	Poor	0.9	Coarse Sand
Std.		0.60		0.5	

Table 4.6 *Subaqueous channel gravel (SACG).*

Similar sediments have been noted in the literature. Chaney (1998) concluded that the gravels described by Banjeree and McDonald (1975) at the Peterborough esker (north of Lake Ontario, Canada) exhibit almost identical grading and parallel bedding properties to the conglomerates observed in Merrimelia #18 and Kenny #1.

These authors describe the Peterborough esker as forming part of a delta which formed at the ice front where meltwaters discharged into an ice contacted lake. Chaney (1998) interprets the conglomerates in Kenny #1 and Merrimelia #18 to have been deposited in a similar setting.

4.2.2 PROGLACIAL ENVIRONMENTS

Compared to the terminoglacial depositional realm, the proglacial realm is much greater in area. Accordingly, there are double the number of facies observed in the proglacial zone (14; 15 including braid plain Tirrawarra sandstones)¹ as compared to the terminoglacial zone (7).

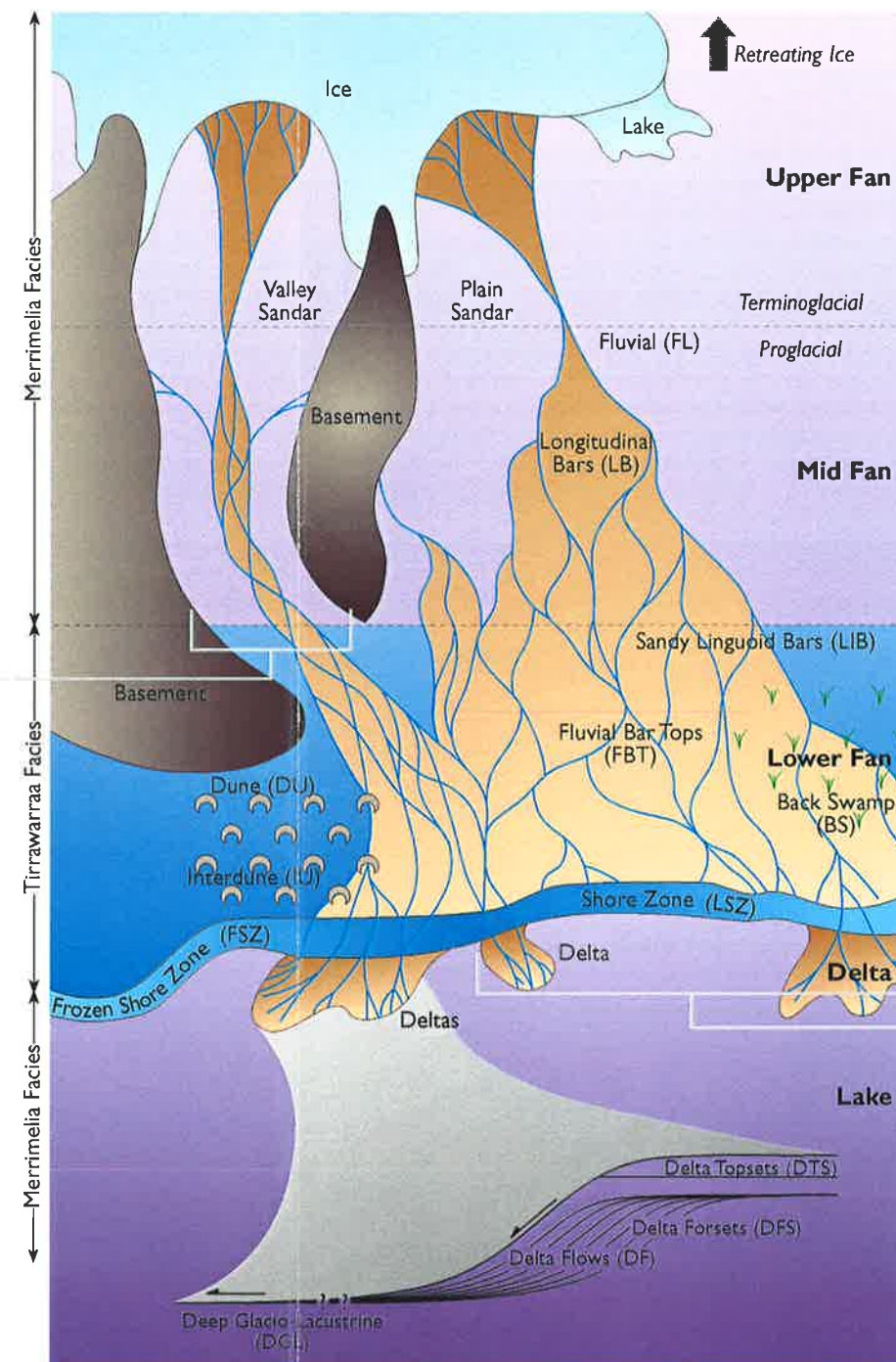
The proglacial depositional realm is beyond the terminoglacial realm and is dominated by fluvial processes (Fig. 4.1a[Insets B & C]). There is no ice cover within this region, but river ice and lake ice may prevail locally (Chaney, 1998). There is no direct glacial contact with these facies thus, the proglacial environments will have a similar appearance to sediments outside the glacial setting (Chaney *et al.*, 1997).

The size and character of the proglacial realm is controlled by both the topographical setting and the amount of meltwater provided (Fig. 4.5[Insets A & B]). The latter inset (Fig. 4.5[Inset B]) illustrates how meltwater volume can control the character of the proglacial realm. In this example only a small portion of the outwash braid plain is active, with the majority of the braid plain quiescent. In this instance, active sedimentation across the whole braid plain will occur at times of higher energy flow.

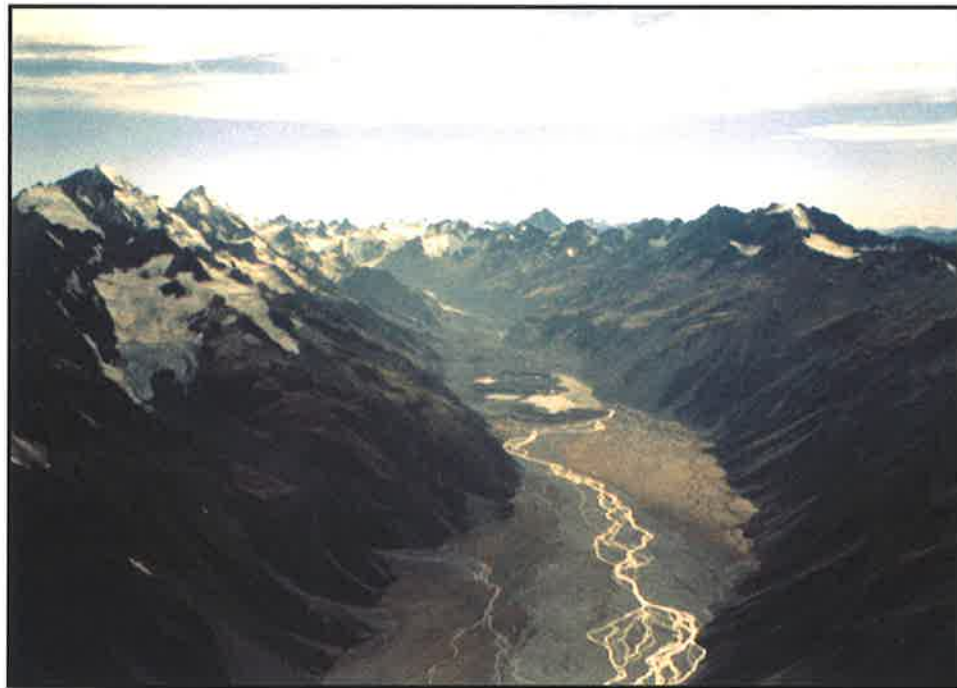
Figure 4.5[Inset A] illustrates how topography can influence the character of a proglacial facies within a glacial system. The braid plain in this case is elongated, restricted by the surrounding topography.

¹ The braid plain facies type (Tirrawarra Sandstone) forms exclusively in the proglacial depositional realm along with other proglacial facies types (Fig. 4.5). However, the sedimentology of braid plain sandstones is not within the scope of this PhD study. A detailed account of the sedimentology of the Tirrawarra Sandstone is given by Rezaee (1996).

Proglacial Facies



Inset A



Inset B

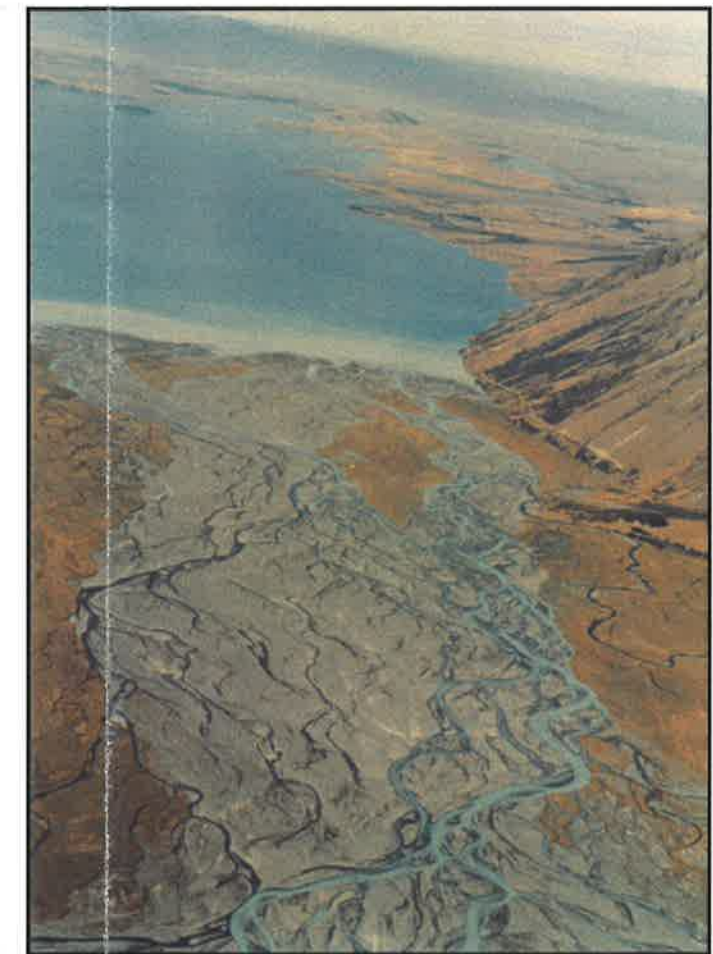


Figure 4.5 Proglacial depositional realm. **Inset A**) Valley sandur. Note : Alluvial fans bordering valley (Godley Valley, N.Z. Alps). **Inset B**) Plain sandur entering a proglacial lake (Godley River Delta/Lake Tekapo, N.Z. Alps).

Figure (4.6) further illustrates the differences original topography can have on the facies architecture of the proglacial zone. If the proglacial zone dips towards the ice, a small basin will form leading to a much smaller outwash braid plain and the preferential formation of lakes and swamps (Chaney, 1998) (Fig. 4.6a). If the dip of the proglacial zone is away from the ice, a much larger braid plain will develop with large anastomosing, braided streams dominating. Lake and marsh development will be limited in this setting as fluvial outwash fans and aeolian depositional environments dominate.

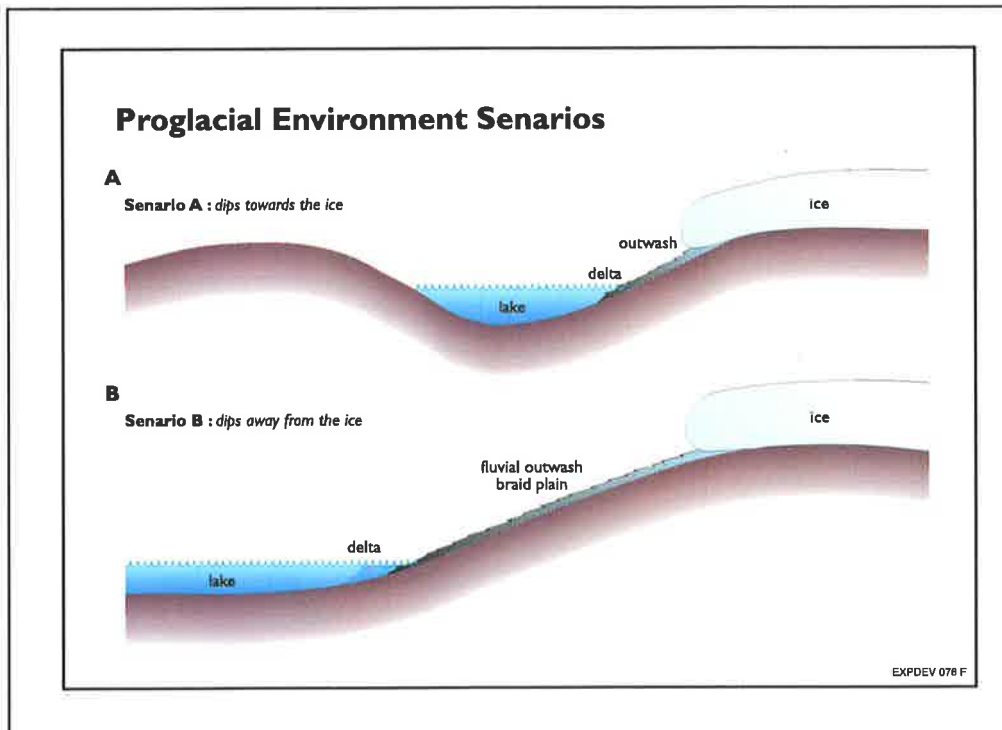


Figure 4.6 Basin topography and proglacial environments (After Chaney, 1998).

Brodsikowski and Van Loon (1991) envisaged that the latter scenario (scenario B) dominated the Australian Permo-Carboniferous glaciation. Chaney 1998, concurred with these earlier workers surmising that the proglacial realm in the Merrimelia-Tirrawarra Glacial Complex was most likely similar to scenario B (Figure 4.6b).

4.2.2.1 PROGLACIAL FACIES ASSOCIATIONS

4.2.2.1.1 Proglacial Fluvial Outwash Plain Facies

In a glacial setting, braided rivers form as a result of glacial meltwaters emanating from nearby glaciers (Figs. 4.2b[Inset B]). The braided rivers spread across enormous areas of the proglacial environment (Chaney, 1998) (Fig. 4.5[Inset B]). Such outwash alluvial plains are termed sandur (plural – sandar) of which there are two categories; valley (Fig. 4.5[Inset A]) and plain (Fig. 4.5[Inset B]) (Chaney, 1998). The difference

between the two sandar types is topographical, with valley walls restricting the lateral accretion of valley sandar while plain sandar have no such lateral topographic restrictions. The lateral spread of a valley sandur maybe confined by topography, but the horizontal extent of both valley and plain sandar maybe enormous (Fig. 4.5[Inset A]). According to Miall (1983), modern sandar can reach up to 100km in length from glacier snout to the terminus at a lake or the ocean.

Many parallels are seen between braided fluvial systems in and outside a glacial realm. There are differences, such as the freezing action of ice and the seasonal and occasional catastrophic discharge of glacial melt water. Chaney (1998) concluded, that the overall similarity of braided rivers whether they are in cold, temperate or even arid climates, means that what applies to braided rivers in non-glacial areas applies to proglacial sandar.

Fluvial sediments generated in a glacially affected braided outwash plain tend to be composed of well sorted, medium grained, sandstones. These sandstone types are observed often within the Merrimelia Formation (Chaney, 1998). Abundant planar and low angle bedforms can be found throughout all the of these sandstones, along with thin layers of medial bar top muds (Chaney *et al.*, 1997).

In addition to well sorted sandstone facies, longitudinal and linguoidal bars commonly developed in outwash braid plain settings (Fig. 4.5[Inset B]). These deposits are generally very coarse grained and reasonably well sorted. Frequently, these bar forms display crude low angle bedding which is often illustrated by changes in grain size (Chaney *et al.*, 1997). The conglomerates in these bar deposits are clast supported and are moderately well rounded, depending on composition. The interstitial matrix is generally of fine to medium grained sand.

Chaney *et al.* (1997) also stated that backswamp deposits are closely associated with glacio-fluvio/deltaic environments. These deposits are rarely preserved in the core (Chaney, 1998) and are represented by homogenous carbonaceous mud layers (up to half a metre thick) with varying degrees of sand influx.

A) Longitudinal Bar (LB)

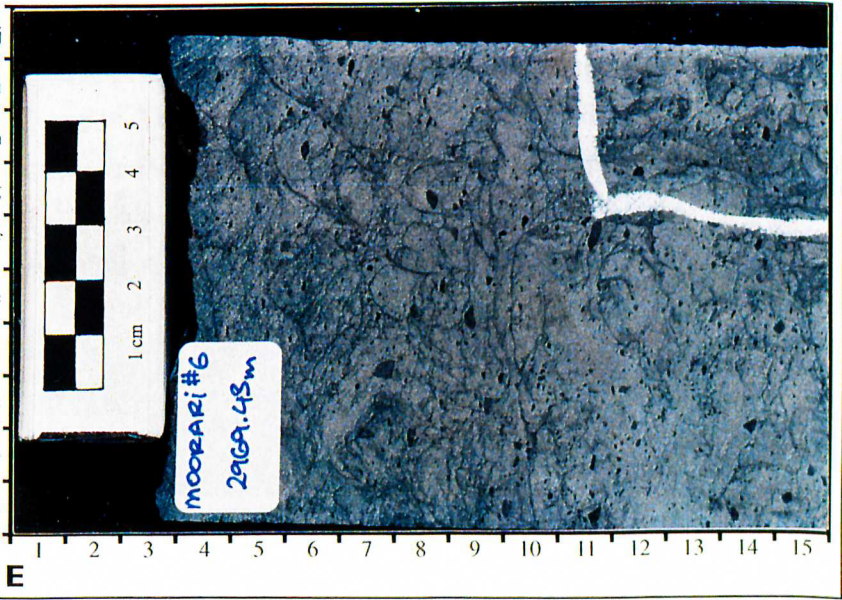
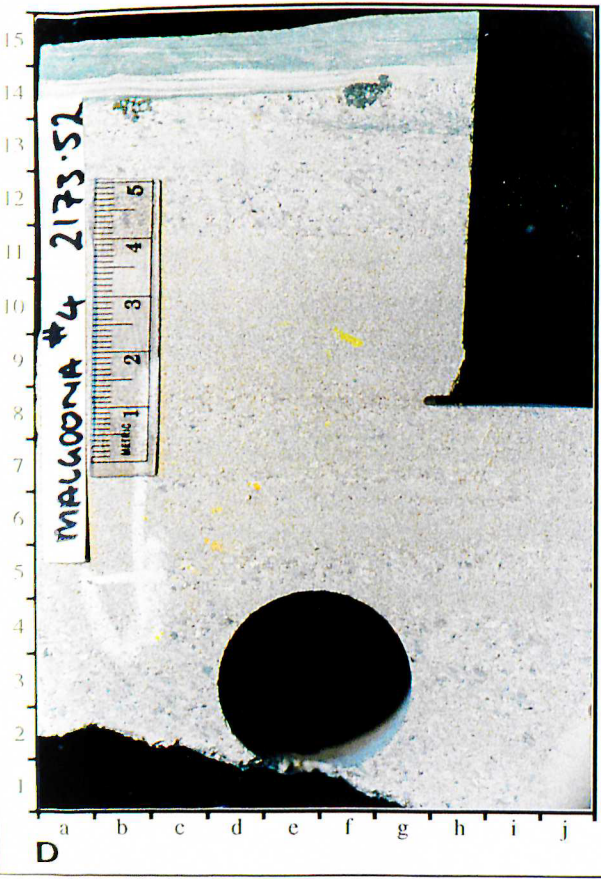
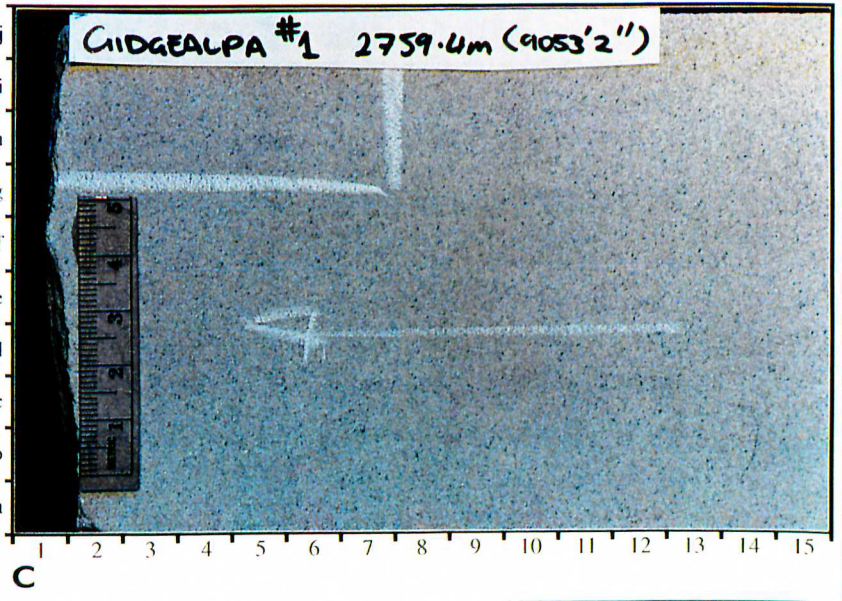
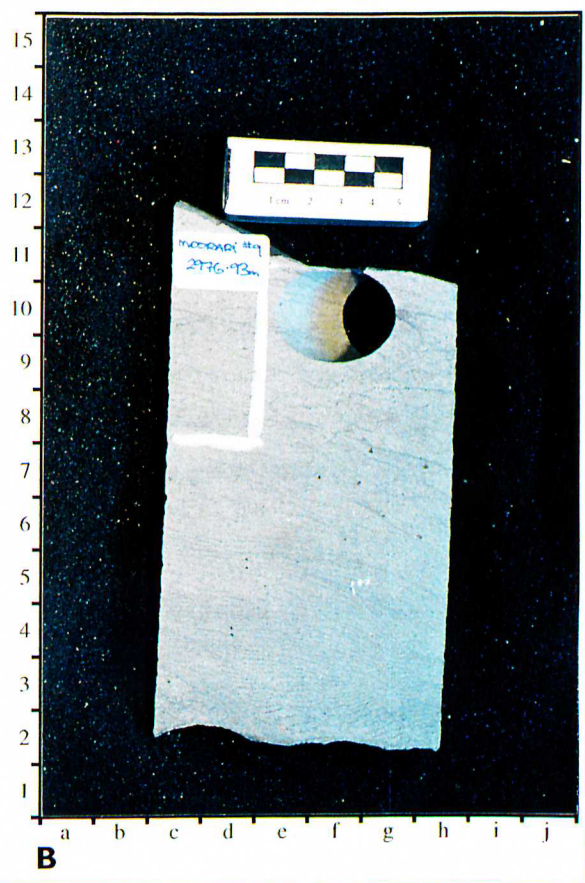
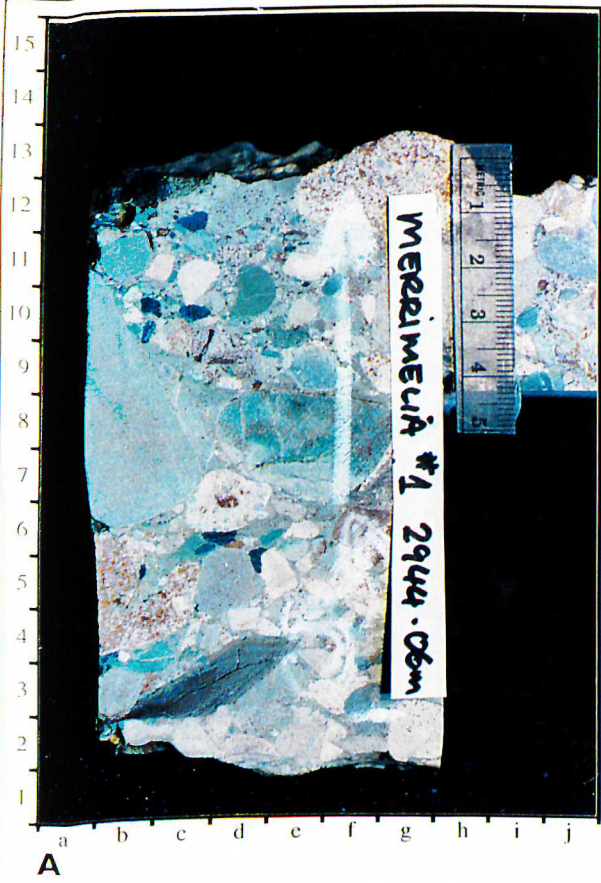
Longitudinal bar facies are often called "diamond bars", a reference to their distinctive shape (Fig. 4.2[Inset B]). They are elongate parallel to sub-parallel with the dominant flow direction and are commonly situated in the mid-channel, reaching sizes of several hundred metres long (Brodsikowski and Van Loon, 1991; Miall, 1983).

PLATE 7**Proglacial Lithologies :1**

YOUNGING IS TOWARDS THE CORE IDENTIFICATION STICKER IN VERTICAL PLATES AND TO THE LEFT IN HORIZONTAL PLATES

- A) *Core photograph – Merrimelia #1 (2944.06m). Crudely bedded conglomerate indicative of longitudinal bar deposition. (LB)*
- B) *Core photograph – Moorari #9 (2976.93m). Ripple drift laminated sandstone typical of slip-face development in linguoidal barforms (LIB).*
- C) *Core photograph - Gidgealpa #1 (2759.4m). Fluvial sandstone (FL). Quartzose, fine grained sandstone indicative of extended transport.*
- D) *Core photograph – Malgoona #4 (2173.52m). Quiescent argillaceous sedimentation on top of linguoidal bar form. Note pyrite associated with argillaceous beds (FL) [14f].*
- E) *Core photograph – Moorari #6 (2969.43m). Siltstone indicative of backwater swamp (BS) deposition. Note abundant organic matter interspersed throughout sediment.*

Plate 7



These bars consist of sand and gravel and exhibit crude horizontal bedding with rounded to angular clasts (Plate 7a). The same plate shows that longitudinal bar sediments are dominated by gravels with subordinate sand.

The size of clasts is highly variable (Table 4.7), with clasts greater than 15cm observed (Chaney, 1998). These bars are generally observed towards the apex of the braid plain (Fig. 4.5) and tend to migrate downstream with the formation of slip faces on the bar margins (Chaney, 1998). This bar form is considered to be a stable feature, even during floods (Chaney, 1998).

Facies	Sample	Sorting Coefficient	Sorting	Grain Size (mm)	Grain Size
LB	MERU 1C	0.64	Moderately Well	0.07	Very Fine
LB	HOP 1C	0.91	Moderate	0.49	Medium
LB	CONG 1B	0.63	Moderately Well	0.55	Medium
LB	CONG 1C	0.91	Moderate	0.73	Coarse Sand
LB	HOP 1A	1.08	Poor	1.17	Very Coarse
LB	HOP 1B	1.39	Poor	2.04	Granule
LB	MERRI 1F	1.83	Poor	2.11	Granule
LB	MERRI 1G	2.30	Very Poor	2.30	Granule
LB	MERRI 1I	2.26	Very Poor	2.37	Granule
LB	MERRI 1H	1.25	Poor	2.79	Granule
Ave.		1.3	Poor	1.5	Very Coarse
Std.		0.6		1.0	

Table 4.7 Longitudinal bars (LB).

Longitudinal bar sediments are widely observed having been described by Chaney (1998) in: Coonatie #1, Fly Lake #1, Lake Hope #1, Merrimelia #1, Coongie #1, Kenny #1 and Merupa #1.

B) Linguoid Bars (LIB)

Linguoid bar sediments, often called transverse or cross channel bars (Chaney, 1998) are dominantly sandy in nature as opposed to the gravel-dominated longitudinal bars discussed in the preceding sub-section. This bar form has a characteristic spoon shape with a downstream-facing sinuous slip face (Miall, 1977; Brodskowski and Van Loon, 1991). They can vary in length from a few metres to up to 150m and can reach lengths up to 300m (Chaney, 1998). According to Chaney (1998), linguoid bars tend to form en-echelon arrangements.

Like longitudinal barforms, slip-face development promotes the downstream migration of linguoid bars and the formation of planar cross-bedding and ripple drift cross-lamination. The development of these lamination types can be seen in Plate (7b), which also illustrates the sandy nature of this bar type. The sorting coefficients indicate that these sandstones are moderately well sorted (Table 4.8) but rare, poorly sorted gravels have been noted.

Facies	Sample	Sorting Coefficient	Sorting	Grain Size (mm)	Grain Size
LIB	MUDR 1A	0.43	Well	0.03	Coarse Silt
LIB	FLY 1A	0.60	Moderately Well	0.18	Fine Sand
LIB	MOOR 9A	0.65	Moderately Well	0.21	Fine Sand
LIB	WOOL 1A	0.42	Well	0.21	Fine Sand
LIB	MOOR 3B	0.34	Very well	0.32	Medium Sand
LIB	WOOL 1B	0.48	Well	0.38	Medium Sand
LIB	CONA 1C	1.50	Poorly	1.2	Very Coarse
Ave.		0.6	Moderately Well	0.4	Medium Sand
Std.		0.40		0.4	

Table 4.8 *Linguoid bars (LIB).*

These sediments have been observed by Chaney (1998) in the following wells: Woolkina #1, Coonatie #1, Fly Lake #1, Moorari #3 and #9 as well as Mudrangie #1.

C) Fluvial (FL)

Fluvial sediments of the Merrimelia Formation are dominated by sandstone but subordinate amounts of laminated mudstones, siltstones and conglomerates were also observed (Chaney, 1998). All of the fluvial facies described in this section are part of the fluvial braidplain. The fluvial facies described here is specifically the sandstone sediment formed within the lower or distal reaches of the braid plain. These sandstones are therefore grouped under the title "fluvial sandstones".

The sorting of facies (FL) is moderate (Table 4.9); a reflection on the large transportation distances and high degree of rinsing experienced by these sediments. Plate (7c) illustrates the well sorted nature of these sandstones. It can be seen in this plate that the framework still contains a reasonable percentage of rock fragments, unlike the more extensively reworked Tirrawarra Sandstone. These sandstones commonly display horizontal planar bedforms but well developed ripple lamination are observed (Chaney, 1998). Chaney (1998) further stated that these sediments can grade into fluvial bar top deposits as deposition of the fluvial barform slows because of waning water input.

Facies	Sample	Sorting Coefficient	Sorting	Grain Size (mm)	Grain Size
FL	MINK 1A	0.42	Well	0.12	Very Fine Sand
FL	MAL 4B	0.85	Moderate	0.17	Fine Sand
FL	MERU 1A	0.33	Very Well	0.22	Fine Sand
FL	MAL 2B	1.99	Poor	1.58	Very Coarse Sand
Ave.		0.90	Moderately Well	0.52	Coarse Sand
Std.		0.76		0.71	

Table 4.9 Fluvial sandstone facies (FL).

Fluvial sandstones were seen in a great number of wells, with the main deposits observed by Chaney (1998) in: Gidgealpa #1, Malgoona #2, Minkie #1, Lake Hope #1, Moorari #2, #3, #4, #6, #9 and Kenny #1.

D) Fluvial Bar Top (FBT)

Bar top deposits are thin layers of laminated siltstones and mudstones draped over pebbly conglomerates or poorly sorted sandstones (Plate 7d). Often isolated sand grains can be found within the siltstones and mudstones of the bar tops indicating that flow, over the top of the bar, had not completely ceased (Chaney, 1998). At Merrimelia #1 and Coongie #1, conglomeratic layers are seen within and on top of the laminated siltstones representing periods of high flow where the bars were drowned during flood events (Chaney, 1998).

Facies	Sample	Sorting Coefficient	Sorting	Grain Size (mm)	Grain Size
FBT	MOOR 4B	0.39	Well	0.11	Very Fine Sand
FBT	GIDG 1B	0.70	Moderately Well	0.28	Medium Sand
Ave.		0.5	Moderate	0.2	Fine Sand
Std.		0.22		0.1	

Table 4.10 Fluvial bar top facies (FBT).

Bar top deposits occur both on linguoid and longitudinal barforms and are formed as a result of quiescent sedimentation on top of fluvial bar forms. These mud accumulations are generally not thick (Plate 7d) with 10-15 centimetre deposits common (Chaney, 1998). The sorting of these sediments is moderate with the average grain size classed as very fine sand to clay (Table 4.10).

Fluvial bar top sediments were observed in: Coongie #1, Merrimelia #1, Gidgealpa #1 and Moorari#4 (Chaney, 1998).

E) Back Swamp (BS)

Back swamp sediments were only observed in Moorari #6 (Chaney, 1998). Other channel abandonment sediments were however noted by the same author in Moorari #3, #4 and #9. The channel abandonment units are 30-60cm thick and are dominated by black carbonaceous muds and siltstones, and maybe occasionally interbedded with braided outwash sandstones (Chaney, 1998). These abandonment units are commonly overlain or interbedded with matrix supported (sandy) conglomerates and coarse grained sandstones which exhibit well rounded clasts. These sandier sediments represent flood events where the quiet depositional conditions of the abandoned channels were interrupted by flood conditions.

The sediment illustrated in Plate (7e) from Moorari #6, has formed in a channel abandonment setting where the effects of flood waters were minimal and vegetation took hold, forming a swamp (Chaney, 1998). The position of possible swamp development within the proglacial realm is illustrated in Fig. (4.5).

It can be seen in Plate (7e) that any primary depositional features in this rock have been obliterated by dewatering processes. This author goes on to state that in the case of the swamp sediments in Moorari #6 that "the whole deposit has been distorted by dewatering and root development, with the fine grained sand in the unit having been trapped by vegetation".

The dominant lithology in these deposits are poorly sorted, very fine sandstones.

F) Discussion

According to Chaney (1998) the glacio-fluvial braidplains of the Cooper Basin can be likened to a combination of numerous modern analogues. He cites modern sandar in Iceland and Alaska as being the most similar to the sandar of the MTGC. Without doubt the enormous expanse of the Tirrawarra Sandstone, which covers two thirds of the Cooper Basin (60,000km²), indicates that the outwash plains from this hypothesised ice sheet covered enormous areas. This discounts the valley sandar (Fig. 4.5[Inset B]) as the dominant type of outwash plain. Similarly the presence of extensive longitudinal and linguoid bar deposits (Chaney, 1998) indicates that the mid and lower fan areas of the Cooper Basin glacial outwash plains were laterally

Merrimelia-Tirrawarra sediment thickness between basement highs (Fig. 1.8) suggests that valley sandar may have formed, particularly in the southern reaches of the basin where narrow restrictions between basement highs occurred. This style of sandar was most likely isolated with the development of dune fields and swamps on the lower reaches of outwash fans tending to suggest that the majority of sandar formation, in the Cooper Basin, occurred on an unconstrained, low relief, low angle plain.

In addition, Chaney (1998) concluded that the features observed in the Merrimelia-Tirrawarra Glacial Complex suggest that the outwash sediments formed in sandar plains that resemble present day plain sandar in Iceland. This author cites that the development of vegetation in the lower MTGC fan is similar to the vegetated nature of the Icelandic sandar as described by Boothroyd and Nummedal (1978).

4.2.2.1.2 Proglacial Aeolian Facies

One of the more unusual environments, from a preservation potential viewpoint, are the glacio-aeolian sandstones, first described by (Williams *et al.*, 1985 and 1987). These sandstones are well sorted, very well rounded, and exceptionally clean having first been observed in the Merrimelia Field and then at Pondrinie (Fig. 1.1).

These sediments are characterised by steep tabular cross bedding which contain distinctive stratification styles including abundant pinstripe lamination, grain flows and bounding surfaces (Plates 8a & 8b) (Chaney *et al.*, 1997). The dune areas are separated by interdune sequences which contain much finer sand "stuck" to abundant green mud laminae, which show some distortion, perhaps in response to the passage of an over-riding dune (Plate 8c). Chaney *et al.*, (1997) stated that, within some of the dune sands, well rounded pebble lags can be found. These lags are indicative of ephemeral floods and are suggestive of interdigitating aeolian and fluvial environments. The proximity of these two environments is illustrated in Figure (4.5).

A) Glacial Aeolian Dune (DU)

Glacio-aeolian sandstones in the Merrimelia Field were first recognised and described by Williams *et al.* (1985) with this initial interpretation further refined by the same authors, Williams *et al.* (1987). Cores penetrate the glacial aeolian facies in the Merrimelia Field at Merrimelia #1 (9661'-9684') and at Merrimelia #5 (8603'-8659') (Appendix 9a).

PLATE 8**Proglacial Lithologies: 2**

YOUNGING IS TOWARDS THE CORE IDENTIFICATION STICKER IN VERTICAL PLATES AND TO THE LEFT IN HORIZONTAL PLATES

A) Core photograph – Merrimelia #5 (2629.81m – 2629.96m). *Glacio-aeolian sandstone (DU) illustrating pin-stripe grain flow lamination and high angle cross bedding [8d]. Note annealed sub-vertical fracture bisecting bedding planes [13g].*

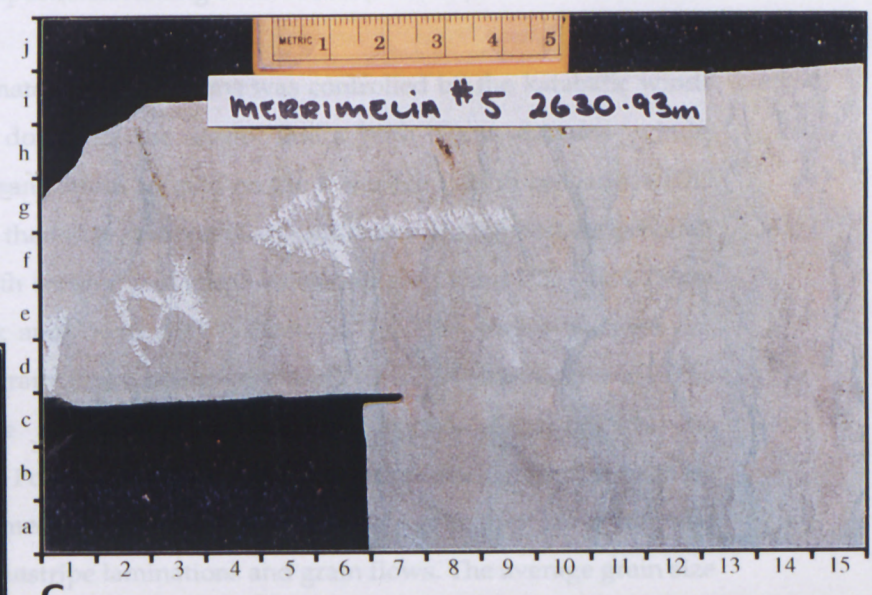
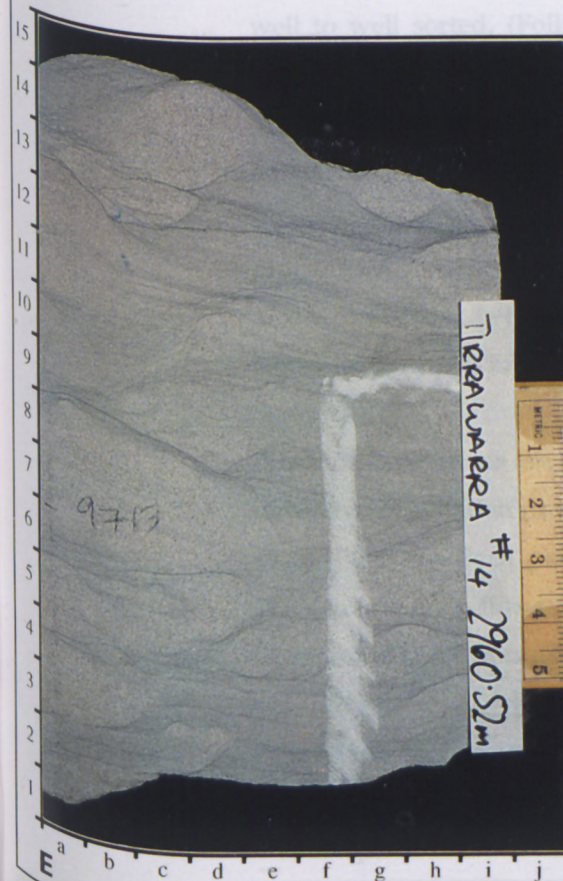
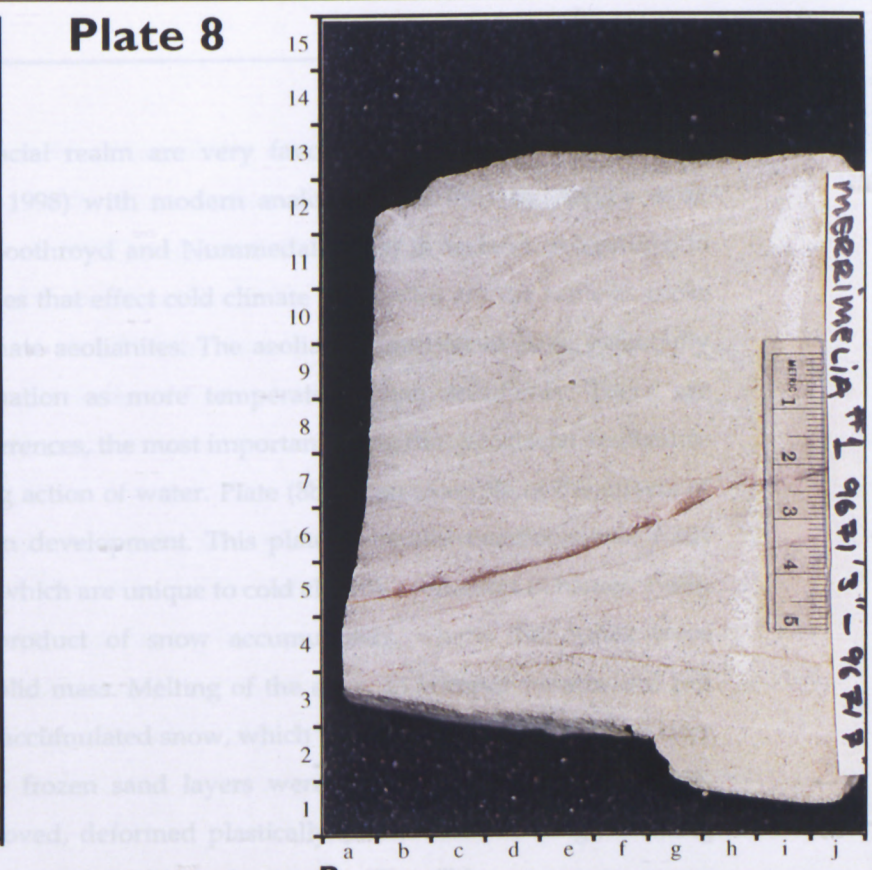
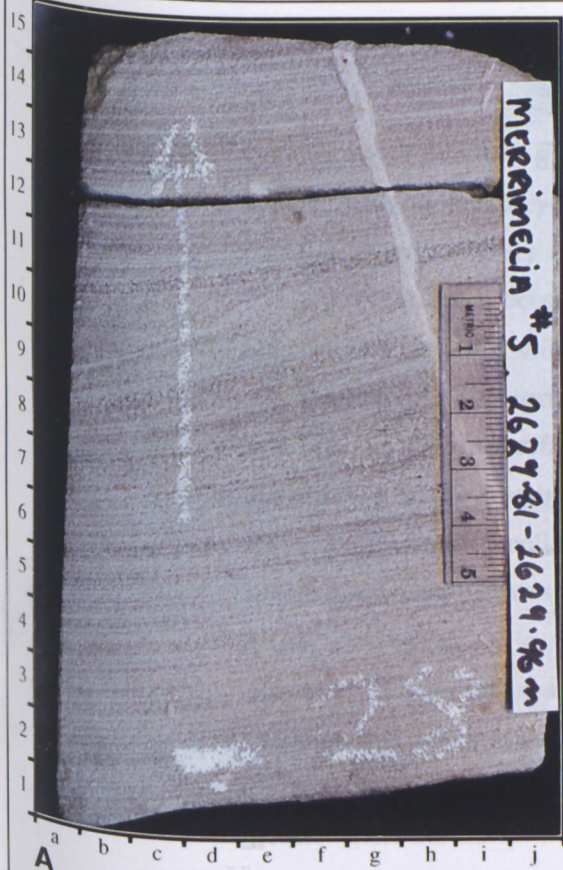
B) Core photograph – Merrimelia #1 (3039.96m – 3040.03m). *Glacio-aeolian sandstone (DU). Note the deformation of the pinstripe lamination [10f]. This deformation is attributed to, and is indicative of, cold climate aeolianite sandstones that are frozen and deformed by over-riding dune sandstones.*

C) Core photograph – Merrimelia #5 (2630.93m). *Glacio-aeolian interdune sandstone (ID) with abundant green muddy laminae (deformed).*

D) Core photograph – Tirrawarra #2 (3111.13m – 3111.18m). *Shoreline sandstone (LSZ) with indicative flaser bedding.*

E) Core photograph – Tirrawarra #14 (2960.52m). *Sandstone with augen-like structures, interpreted to be formed by the freezing action of ice (FSZ).*

Plate 8



Conditions within the glacial realm are very favourable for the development of aeolian systems (Chaney, 1998) with modern analogies described by Ashley *et al.* (1985) in Alaska and by Boothroyd and Nummedal (1978) in Iceland. According to Chaney (1998), the processes that effect cold climate aeolianites are the same as those affecting hot and arid climate aeolianites. The aeolianite sandstones have essentially the same modes of formation as more temperate aeolian sediments. There are however, a number of differences, the most important being that proglacial aeolianites are affected by the freezing action of water. Plate (8b), is an example of the effects of ice on cold climate aeolian development. This plate illustrates compressional folds and thrust faults; features which are unique to cold climate aeolianites (Chaney, 1998). These structures are a product of snow accumulation, where the dunes were effectively frozen into a solid mass. Melting of the snow in warmer months did not completely thaw all of the accumulated snow, which was subsequently buried by later aeolian development. The frozen sand layers were then buried within the dune, which when the dunes moved, deformed plastically (rather than flowing), creating the tension cracks and compactional folding observed in (Plate 8b).

The formation of cold climate aeolian systems was controlled by the katabatic winds descending off glaciers down to the basin floor. With these extreme winds, exceptionally well sorted sandstones formed on the lower fan (glacio-aeolianites [DU & ID]). It is not surprising then that glacio-aeolian sandstones are the best sorted of all Merrimelia sediments, with sorting coefficient values ranging from 0.25 – 0.51 (Very well to well sorted, (Folk and Ward, 1957)) (Table 4.11). The sorting is, however, bimodal in nature with grain flows being very well sorted (Table 4.11) while the pinstripe laminations are moderately well to well sorted. According to the nomenclature of Pettijohn, Potter and Siever (1987), the framework grain size of these sandstones ranges from medium to very fine grained. Again there is a bimodal distribution between the pinstripe laminations and grain flows. The average grain size of the sandstones between grain flows is 0.125mm (Table 4.11), while the pinstripe lamination samples are all fine grained (0.25mm) (Table 4.11).

Pinstripe laminations are representative of wind ripple sedimentation which is in turn indicative of saltation processes and grain flow forming by slip face failure (Chaney, 1998) (Plate 8a). Each pinstripe lamination is thin (1-2mm) and is inversely graded. The slip face grain flows on the other hand are coarser grained averaging 1-2cm thick. Slumps and bed truncations are also very common in these sandstones (Plate 8a).

Glacio-aeolian sandstones exhibit cross bedding with angles varying between 1° to 27° (Chaney, 1998). According to the same author, the steeper beds represent dune foresets while Williams *et al.* (1987) suggested that the more horizontally bedded sands may represent sandsheet deposition. Chaney (1998) disagreed with the interpretation of Williams *et al.* (1997) by stating that the low angle laminations interfinger with the high angle foresets, forming beds only 60cm-90 cm thick which is more indicative of dune sedimentation rather than sandsheet deposition.

Rock fragments within these sediments are rare (average 3% of the total grains counted) and are generally altered to kaolin and illite. Feldspars (microcline and plagioclase) are also very rare most having been partially or almost totally altered to illite (with minor kaolin). Very few squeezed ductile rock fragments were observed in these sandstones. The rounding of grains is high with some quartz grains exhibiting almost perfect sphericity.

Glacio-aeolianite sediments were only described from cores taken in Merrimelia #1 and #5. The glacio-aeolianite sequence has also been investigated in detail by Lemon and Matthews (1997) in the Merrimelia #37 well.

B) Glacial Aeolian Interdune (ID)

The interdunal areas are regions of relatively flat ground between migrating dunes (Fig. 4.5). Interdunal deposits were only sampled in Merrimelia #5 but were also observed by Chaney (1998) in Merrimelia #1. Plate (8c) illustrates that the interdune sediments are much finer grained than dune facies sandstones and have similar but constant sorting coefficients (Table 4.11). The interdune sediments attain a maximum thickness of 1.5m but are on average 0.5m thick (Chaney, 1998). The most distinctive feature of these sediments is the presence of abundant green mud laminations (Plate 8c), that are according to Ahlbrandt and Fryberger (1982), suggestive of wet interdunal regions. Chaney (1998), surmises that, ponded water collected in the interdune depressions allowing muds to accumulate. Being water saturated and thus less competent than dry dune sandstones, these mud laminations often deform as a result of sediment loading as adjacent dunes migrate over the top.

C) Discussion

Williams *et al.* (1985 & 1987) as well as Chaney (1998) have described aeolian sandstones in Merrimelia #1 overlain by a small gravel lag layer. Chaney (1998) stated that this lag indicates that the Merrimelia dune field is situated in close proximity to active braid plain channels. The lag conglomerate in this case represents a flood event



where the dune field was inundated by fluvial sedimentation. These flood deposits were reworked by the wind leaving only the coarsest grained sediments behind.

Continued dune migration then buried the coarse grained remnants of this flood event. Farther up the core, Chaney (1998) observed that the fluvial system eventually dominates. It seems probable then, that the aeolian field at Merrimelia formed between braided river channels on a plain sandur where occasional flooding events engulfed the low lying reaches of the aeolian field. The waterlogged nature of these low lying areas or interdune regions is indicated by the muddy and dewatered interdunal sandstones (Plate 8c).

Facies	Sample	Sorting Coefficient	Sorting	Grain Size (mm)	Grain Size
DU	MERRI 5F (LPZ)	0.44	Well	0.10	Very Fine
DU	MERRI 5G (LPZ)	0.51	Moderately Well	0.10	Very Fine
DU	MERRI 5C (LPZ)	0.46	Well	0.10	Very Fine
DU	MERRI 1K (LPZ)	0.41	Well	0.11	Very Fine
DU	MERRI 1L (LPZ)	0.50	Well	0.12	Very Fine
DU	MERRI 1J (HPZ)	0.47	Well	0.19	Fine Sand
DU	MERRI 5F (HPZ)	0.32	Very Well	0.21	Fine Sand
DU	MERRI 1L (HPZ)	0.35	Very Well	0.21	Fine Sand
DU	MERRI 5G (HPZ)	0.36	Very Well	0.22	Fine Sand
DU	MERRI 5D (HPZ)	0.42	Well	0.23	Fine Sand
DU	MERRI 5C (HPZ)	0.25	Very Well	0.26	Medium
DU	MERRI 1K (HPZ)	0.36	Very Well	0.26	Medium
Ave.		0.4	Very Well	0.2	Fine
Std.		0.08		0.1	
Facies	Sample	Sorting Coefficient	Sorting	Grain size mm	Grain size
ID	MERRI 5E	0.48	Well	0.10	Very Fine
ID	MERRI 5E	0.36	Very Well	0.19	Fine Sand
Ave.		0.4	Very Well	0.2	Fine
Std.		0.09		0.1	

Table 4.11 Dune (DU) and interdune (ID) facies.

Chaney (1998) also stated that the dune system at the Merrimelia Field was dominated by small dunes with bed thicknesses of only 30-60cm. These small dunes are consistent with other cold climate aeolianite deposits described by Koster and Dijkmans (1988) from the cold climate dune fields at Kobuk in Alaska. Authors in the past (Williams *et al.*, 1985; Seggie *et al.*, 1994) have also described the aeolian sandstones of the Merrimelia Field as similar to the cold climate dunes at Kobuk. Chaney (1998) concluded that this comparison is reasonable, stating, however, that

unlike the Kobuk dunes the Merrimelia Formation aeolianites did not form in a confined valley sandur but in a plain sandur of great lateral extent.

4.2.2.1.3 Proglacial Deltaic and Lacustrine Facies

A proglacial lake is not in contact with ice so detritus is brought into the proglacial lacustrine environment via terrestrial depositional processes (Chaney, 1998). The fluvial load of the meltwater-sourced outwash fans slows drastically as it enters the lacustrine realm, forming deltas. The size of the delta is dependent on the size of the lake and meltwater volume. Deltaic sediments tend to be sandstones of various grain sizes and sorting. The coarsest sand fractions are released first onto the proximal topsets whilst the finer sand fractions are deposited down slope to form delta foresets and bottom sets (Fig. 4.5). Farther down the delta slope, the bottom sets and mud-dominated varvite sequences grade into each other (Fig. 4.5). Turbiditic sand flows are also a feature of this environment. The proglacial lacustrine environment is dominated by deep water varvites and couplets. Varvites are seasonal. Other couplets are formed from turbiditic surge flows onto the lake floor (Ashley *et al.*, 1985). Chaney *et al.* (1997) stated that, occasionally, the quiet water sedimentation is interrupted by clean sand flows, or poorly sorted, re-sedimented sandy diamictites where the mud content has been washed out by the reworking process. Such subaqueous flows can be up to a metre thick (Chaney, 1998).

All of these deltaic and lacustrine facies were observed and described by Chaney *et al.* (1997) and Chaney (1998) within the Merrimelia complex. The following section briefly describes both the deltaic facies and lacustrine facies together as they are intrinsically interlinked. The following is a description of each facies type from the most proximal deltaic facies to the deep glacial lacustrine facies.

A) Lacustrine Shore Zone (LSZ)

Lacustrine shorezone sediments in the Merrimelia Formation are characterised by well developed flaser and lenticular bedding (Chaney *et al.*, 1997) (Plate 8d). The ripple cross-laminations are generally small to medium scale with an asymmetric morphology and do not conform to a single direction (Chaney, 1998). Shorezone sandstones have grain sizes that vary from coarse silt to very fine sand (Table 4.12). These sediments show variable sorting from moderate to well sorted (Table 4.12).

Mud laminae thicknesses vary, and the rippling within the sand layers often shows reactivation surfaces (Plate 8d). Other sedimentary structures such as loading and flame structures are also common (Chaney *et al.*, 1997).

The lacustrine shore zone is very thin (Fig. 4.5 Inset B) as the absence of tides means that wave action is limited to a very narrow zone. The preservation of these shorezone sediments occurs by stranding where changes in lake level leads to terracing in the lacustrine shore region (Chaney, 1998).

Lacustrine shorezone deposits are well preserved in the Merrimelia Formation with these sediments observed in 17 wells, the majority of which are in the Tirrawarra and Moorari Fields (Chaney, 1998).

Facies	Sample	Sorting Coefficient	Sorting	Grain Size (mm)	Grain Size
LSZ	BROL 1C	0.75	Moderate	0.02	Medium Silt
LSZ	FLY 2B	0.67	Moderately Well	0.04	Coarse Silt
LSZ	TIR 14C	0.57	Moderately Well	0.04	Coarse Silt
LSZ	FLY 2C	0.89	Moderate	0.05	Coarse Silt
LSZ	TIRRA 2C	0.59	Moderately Well	0.05	Coarse Silt
LSZ	MOOR 4A	0.49	Well	0.05	Coarse Silt
LSZ	TIRRA 9A	0.54	Moderately Well	0.05	Coarse Silt
LSZ	TIRW 1A	0.38	Well	0.06	Coarse Silt
LSZ	FLY 1C	0.77	Moderate	0.15	Fine Sand
LSZ	BROL 1B	0.44	Well	0.41	Medium Sand
Ave.		0.6	Moderately Well	0.09	Very Fine
Std.		0.17		0.11	
Facies	Sample	Sorting	Sorting	Grain size	Grain size
FSZ	MOOR 3A	0.39	Well	0.05	Coarse Silt
FSZ	TIR 14B	1.34	Poor	0.12	Fine Sand
Ave.		0.9	Moderate	0.1	Very Fine
Std.		0.67		0.9	

Table 4.12 Lacustrine shore zone (LSZ) and frozen shore zone (FSZ) facies.

B) Frozen Shore Zone (FSZ)

These sediments are very rare, having only been observed in Moorari #3 and Tirrawarra #14 (Chaney, 1998). These shorezone sediments are well sorted displaying a coarse silt grain size (Table 4.12). These sandstones contain fine mudstone laminae that have been distorted into augen-like structures (Plate 8e). Chaney (1998) explains that the augen structures are not formed by any depositional process but have formed from the freezing action of ice and subsequent partial thawing. He cites other examples of ice tectonics distorting shorezone sediments in Fly Lake #2, where fine grained sandstones that are distorted by thrusting and soft sediment faulting are more common place than the more usual slumping and overturned folds. Chaney (1998) proposes that these shorezone sediments have been deformed by the direct action of glaciers or grounded ice.

Technically, as there appears to be direct ice contact with the shorezone (and thus lake), these sediments could be classed as surrounding a terminoglacial lake rather than a proglacial lake. According to Chaney (1998) it is more than likely however, that these lakes are removed from the main glacial front and are therefore proglacial in nature.

Frozen shorezone development will be less in the proglacial zone than in the terminoglacial zone with the latter sediments being more readily effected by ice tectonics. Shorezone deposits in the proglacial realm on the other hand are more areally extensive and may experience ice-related deformation by way of seasonal freezing.

The inclusion here of frozen shorezone sediments in the proglacial section is done in attempt to present a logical progression of facies types. It is more likely that the development of sandy shorezone sediments will occur around proglacial lakes than around terminoglacial lakes and so these sediments are included here despite the direct influence of ice on these sediments.

C) Delta Topsets (DTS)

Delta topsets represent the deltaic extension of fluvial braid plains Chaney (1998). Delta topsets, according to Gustavson *et al.* (1975), can just as easily consist of meandering stream sediments as braided stream sediments. These deposits represent the most proximal of the deltaic facies described in the following sections (Fig. 4.7).

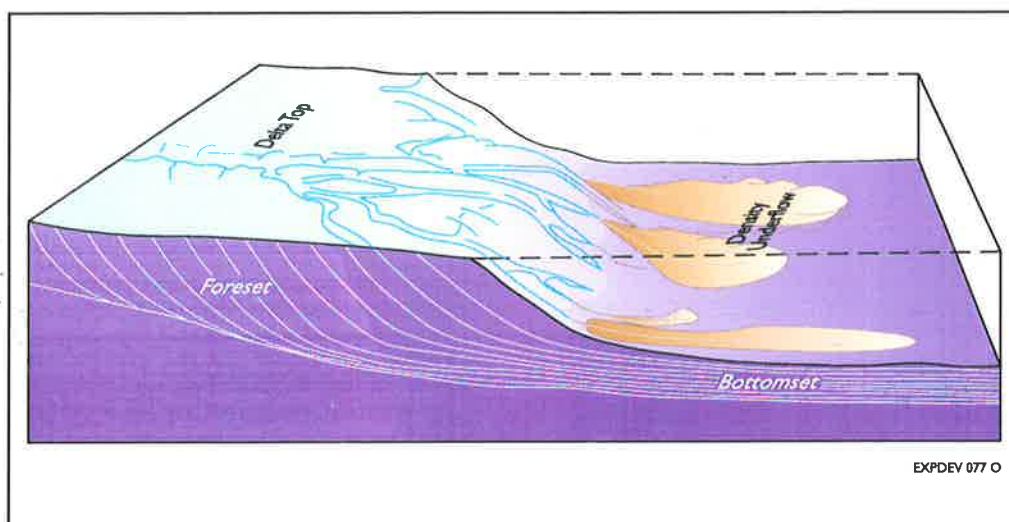


Figure 4.7. Delta sediments. (After Brodskowski and Van Loon, 1991).

Deltaic topset sediments are found in seven wells (Table 4.13) and are moderately well to poorly sorted (the majority being poorly sorted). The grain size in these sediments varies from medium silt to very coarse sand (Table 4.13).

Topset sediments can contain large amounts of woody material but more commonly contain rip up clasts. The rip up clasts noted in Coonatie #1 as an example, are angular and show internal structures that were formed in previous sedimentation.

Facies	Sample	Sorting Coefficient	Sorting	Grain Size	Grain Size
DTS	TIRRA 8A	1.93	Poor	0.02	Medium Silt
DTS	TIRRA 6A	0.96	Moderate	0.05	Coarse Silt
DTS	TIRRA 2D	1.04	Poor	0.05	Coarse Silt
DTS	TIRRA 2B	0.53	Moderately Well	0.09	Very Fine
DTS	TIRRA 2E	0.82	Moderate	0.10	Very Fine
DTS	TIRRA 2A	0.46	Well	0.09	Very Fine
DTS	BOX 1A	1.32	Poor	0.39	Medium
DTS	MOOR 6B	1.69	Poor	1.44	Very Coarse
DTS	GIDG 7A	1.02	Poor	1.44	Very Coarse
Ave.		1.1	Poor	0.5	Medium Sand
Std.		0.46		0.7	

Table 4.13 Delta topsets (DTS).

In Moorari #2 and #6, high fluid flow rates are also in evidence where rounded clasts form channel lag conglomerates within well sorted sandstones (Plate 9a). Along with these high flow rate sediments, quiet water sediments were observed in this facies. These fine grain sediments form on the delta plain and consist of fine sands and muds and may exhibit current ripples as well as horizontal lamination (Chaney, 1998). These muds show some of the characteristics of glaciolacustrine muds but are interpreted by Chaney (1998) to be mudflat deposits with the intervening sandstones representing regular flood events.

D) Delta Foresets (DFS)

This facies contains a wide variety of sediments, with coarser sediments found at the top of the foresets and finer sediments at the foreset toe (Fig. 4.7).

Deposits on the upper slope, not surprisingly, look similar to the sediments observed in the delta topsets with grainsize and sorting similar.

PLATE 9**Proglacial Lithologies: 3**

YOUNGING IS TOWARDS THE CORE IDENTIFICATION STICKER IN VERTICAL PLATES AND TO THE LEFT IN HORIZONTAL PLATES

A) Core photograph – Tirrawarra #8 (2937.70m). Fining up sandstone with high flow regime channel lag prominent [10c]. This core is a typical example of deltaic top sets (DTS).

B) Core photograph – Tirrawarra #2 (3098.95m – 3098.45m). Fine grained sandstone with abundant ripple drift laminae typical of deltaic foreset (DFS) sedimentation.

C) Core photograph – Kanowana #1 (3093.1m). Rhythmic siltstone typical of deltaic bottomset sediments (DBS).

D) Core photograph – Bimbaya #1 (2875.72m - 2874.99m). An example of a fluidised slump into muddy sandstone lacustrine sediments (DBS).

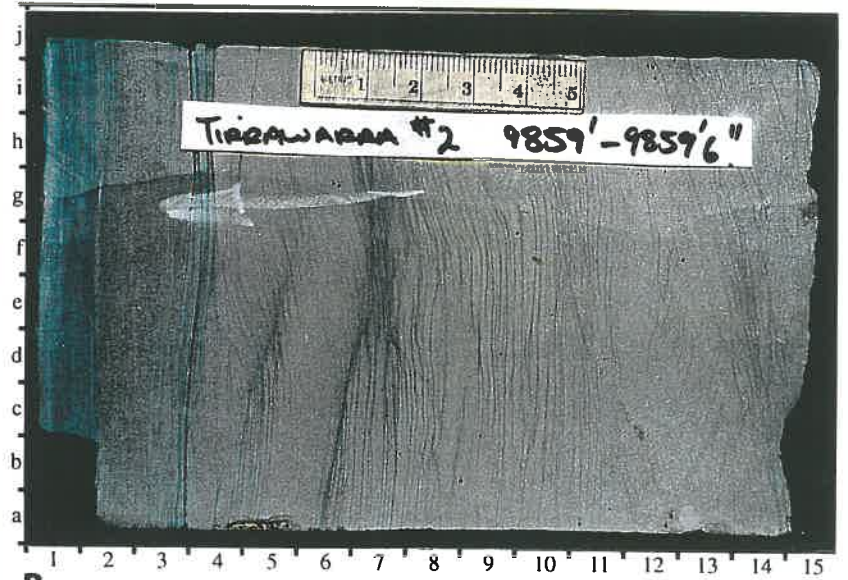
E) Core photograph – Gidgealpa #5 (2337.49m - 2337.54m). Thaw/freeze varvite mudstone and siltstone, typical of glacially influenced lacustrine sedimentation (DGS).

F) Core photograph – Merrimelia #1 (2644.67m). Sand supported diamictite, suggestive of turbiditic flow within the deltaic/lacustrine depositional realm (Deltaic Flow-DF).

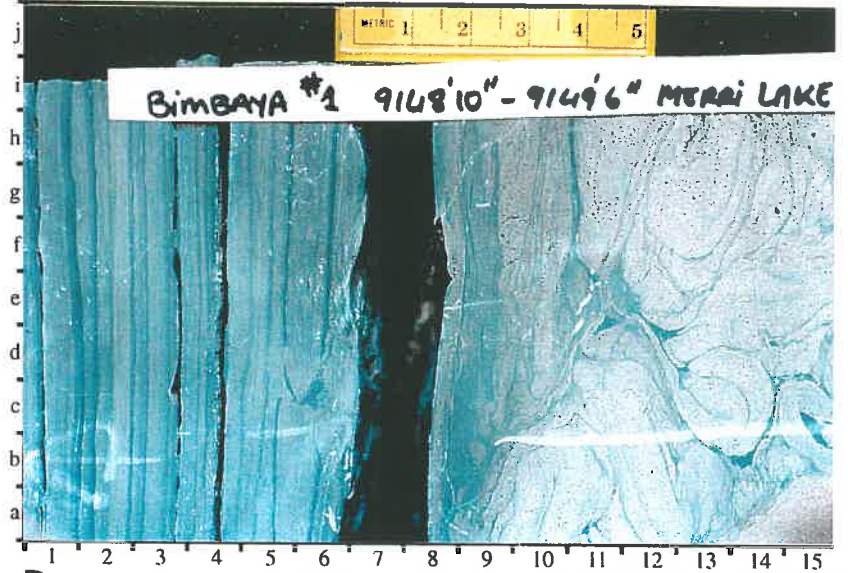
Plate 9



A



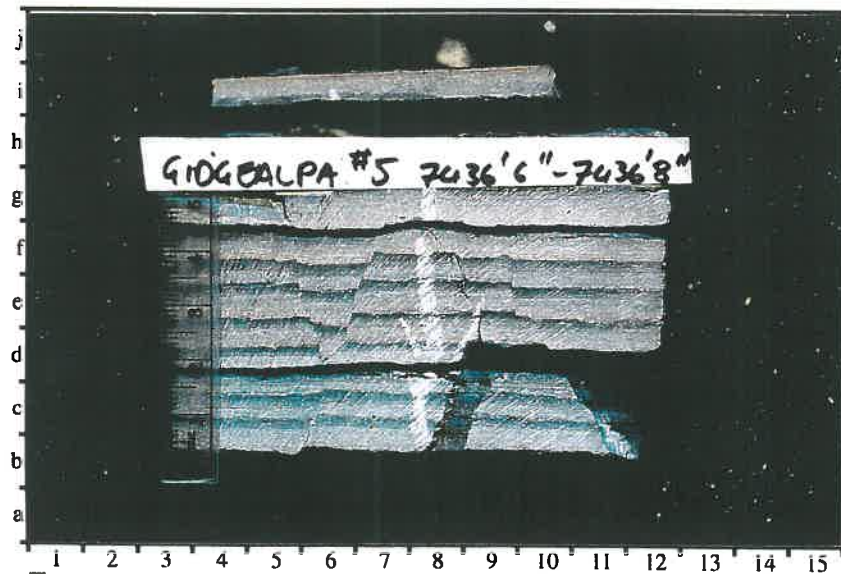
B



D



C



E



F

Chaney (1998) stated that such similarity between delta topsets and upper delta foreset makes distinguishing between these environments impossible. Mid to lower delta foreset deposits are thus described below.

The mid-delta slope sediments tend to be fine grained and composed mostly of sand. Deposition is primarily controlled by turbid underflows (Fig. 4.7), with ripple drift cross lamination characteristic of this depositional style. Chaney (1998) has identified mid delta slope sediments in 13 wells across the basin. According to this author, these sediments are composed of fine to medium grained sandstones that are moderately sorted and contain well rounded grains. It can be seen in Plate (9b) that black, hair line mud laminae trace out the depositional structures such as ripple drift cross laminations. Chaney (1998) explains that there are two types of ripple drift cross lamination in Merrimelia sediments representing the two end members of fluid flow. Both ripple laminations types, according to Smith and Ashley (1985), occur in response to slumping on the upper delta slope.

Facies	Sample	Sorting Coefficient	Sorting	Grain Size (mm)	Grain Size
DFS	GIDG 5A	0.39	Well	0.02	Medium silt
DFS	FLY 2A	0.55	Moderately Well	0.03	Medium silt
DFS	TIRRA 7B	1.12	Poor	0.03	Coarse silt
DFS	MOOR 7A	0.47	Well	0.05	Coarse Silt
DFS	TIRRA 8B	0.51	Moderately Well	0.07	Coarse Silt
DFS	TIR 14A	0.48	Well	0.09	Very Fine
DFS	WEL 1B	0.53	Moderately Well	0.10	Very Fine
DFS	MERU 1B	0.42	Well	0.11	Very Fine
DFS	GIDG 5F	0.53	Moderately Well	0.14	Fine Sand
DFS	WEL 1A	0.59	Moderately Well	0.16	Fine Sand
DFS	TIRRA 7A	0.41	Well	0.17	Fine Sand
DFS	FLY 1D	0.72	Moderate	0.33	Coarse Sand
DFS	TIND 2A	2.10	Very Poor	0.66	Coarse Sand
Ave.		0.7	Moderate	0.2	Fine Sand
Std.		0.47		0.2	

Table 4.14 *Delta foresets (DFS).*

Further refining the sorting and grain size observations of Chaney (1998), it was calculated that the sorting of the delta foreset sediments, is highly variable with sorting coefficients ranging from very poor to well sorted (Table 4.14). The size of framework grains is again variable with grain sizes ranging from coarse sand to medium silt (Table 4.14). Chaney (1998) notes that foreset sediments which contain a high concentration of mud laminae, tend to exhibit a small framework grain size (Plate 9b).

Deltaic foreset sediments were described by Chaney (1998), in the following wells: Gidgealpa #5, Fly Lake #1, #2, Merupa #1, Merrimelia #1, Welcome Lake #1, Moorari #6, #7, Tindilpie #2, Tirrawarra #9, #2, #7, #8, #14, Tirrawarra West #1 and Packsaddle #1. Samples were taken from a representative selection of these wells (Table 4.14).

E) Delta Bottom sets (DBS)

Brodzikowski and Van Loon (1991) stated that glaciolacustrine bottomsets are formed by annual sedimentation or turbidite flows where these sediments grade into delta toe sediments. Figure (4.5) indicates such a relationship where the delta bottomsets are lateral equivalents of deep glaciolacustrine sediments. The delta bottomsets, like the more distal lacustrine sediments, owe their formation more towards interflows and overflow deposition than to more turbiditic underflows (Fig. 4.8). According to Chaney 1998, however, some underflow (turbiditic) deposition does occur in Merrimelia lakes (Fig. 4.8).

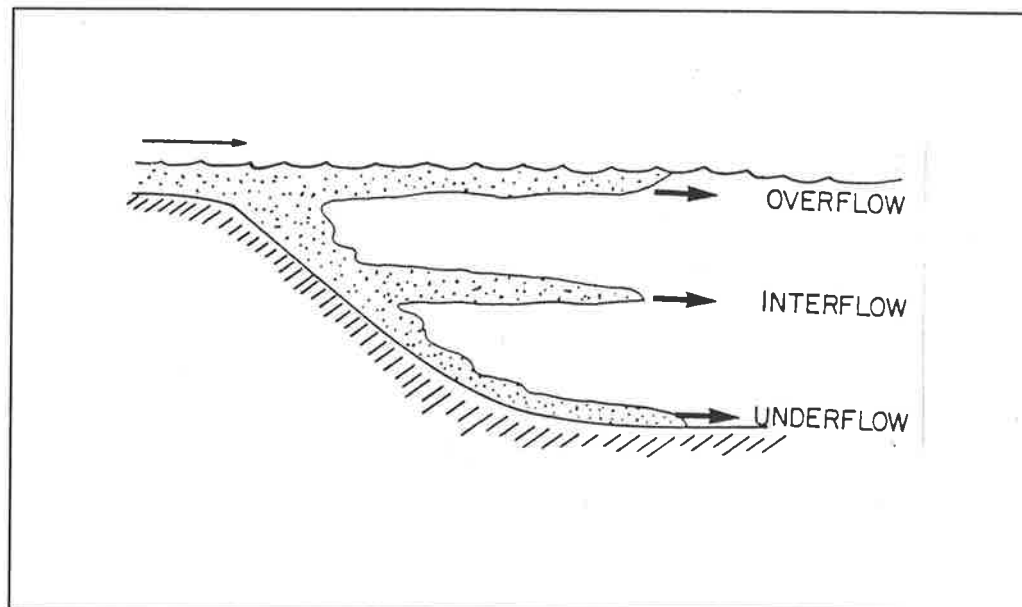


Figure 4.8 *Lacustrine sediment flow regimes (After Chaney, 1998).*

Delta bottomset deposits because of their distal setting, commonly exhibit a rhythmic appearance much like lacustrine rhythmites but are generally coarser grained, containing ripple laminations and exhibit normally graded beds of fine sand to medium sandstone (Table 4.15) (Chaney, 1998).

The overall sorting of these sediments indicates that they represent extremes, with sediment deposition by both gentle settling and turbiditic mechanisms. The majority

of these sediments have sorting coefficients that indicate that they are moderately well sorted (Table 4.15).

Plate (9c) illustrates the rhythmic and fine grained nature of deltaic bottomset sediments. Bottom set sediments, observed at Kanowana #1 by Chaney (1998), exhibit couplets that fine upwards and appear to be turbiditic in origin, suggesting that this particular rock is proximal to the delta toe and has formed via underflow deposition (Fig. 4.8).

As the deltaic bottomsets become more distal, they become more proximal to lacustrine mudstones and it is common to observe couplets of sandy sediments slumped into unsorted and mixed muddy slurries (Chaney, 1998). In Gidgealpa #5 for instance, the slumps are so fluidised that the sandstones and mudstones have been mixed up into a muddy sandstone (Chaney, 1998). Plate (9d) illustrates a fluidised sandstone slump that exhibits characteristic slump rolls which have firstly interrupted and secondly incorporated the muddy lake sediments into the turbidite flow.

Facies	Sample	Sorting Coefficient	Sorting	Grain Size	Grain Size
DBS	KANO 1A	1.10	Poor	0.17	Fine Sand
DBS	KUD 1B	0.55	Moderately Well	0.18	Fine Sand
DBS	KUD 1A	0.54	Moderately Well	0.19	Fine Sand
DBS	GIDG 5C	0.76	Moderately Well	0.21	Fine Sand
DBS	GIDG 5E	0.96	Moderately Well	0.30	Medium Sand
DBS	GIDG 5D	2.03	Very Poor	0.33	Medium Sand
Ave.		1.0	Poor	0.2	Fine Sand
Std.		0.6		0.1	

Table 4.15 Delta bottom set facies (DBS).

Deltaic bottomset sediments were observed in: Gidgealpa #5, Kanowana #1, Packsaddle #1, Tirrawarra #2, Moorari #7 and Kudrieke #1 (Chaney, 1998).

F) Delta Flows (DF)

Chaney (1998) observed this facies type in Gidgealpa #5, Merrimelia #1, Yanpurra #1 and Paning #1. In addition delta flows were observed in Kudrieke #1, Paning #1, Gidgealpa #7, Tallalia #1 (Qld), Spencer #1 and Mudlalee #1. These sediments are sand supported diamictites that contain rare rounded to sub-rounded clasts of a non-ductile nature. Plate (9f) also illustrates that these sediments are structureless, displaying little or no flow laminations. Chaney (1998) interprets these sediments as

being high density turbidity flows (traction currents) that have flowed down deltaic foresets in response to catastrophic water flows issuing from very distal glaciers.

The sorting coefficients of these sediments also hint at a chaotic formation. Table (4.16) indicates that the majority of these sediments are poorly sorted with a variable grain size from very fine to granule.

Facies	Sample	Sorting Coefficient	Sorting	Grain Size (mm)	Grain Size
DF	MERRI	0.68	Moderately Well	0.23	Fine Sand
DF	YAN 1C	1.62	Poor	0.26	Fine Sand
DF	KUD 1E	0.67	Moderately Well	0.27	Medium Sand
DF	MERRI 1E	0.69	Moderately Well	0.30	Medium Sand
DF	YAN 1A	0.95	Moderate	0.31	Medium Sand
DF	GIDG 5G	1.19	Poor	0.31	Medium Sand
DF	MERRI 1C	0.56	Moderately Well	0.33	Medium Sand
DF	YAN 1B	1.31	Poor	0.37	Medium Sand
DF	PAN 1C	0.99	Moderate	0.43	Medium Sand
DF	PAN 1B	1.15	Poor	0.45	Medium Sand
DF	GIDG 7B	1.09	Poor	0.50	Coarse Sand
DF	TALA 1B	1.39	Poor	0.66	Coarse Sand
DF	TALA 1C	1.41	Poor	0.77	Coarse Sand
DF	KUD 1C	1.60	Poor	0.88	Coarse Sand
DF	MUDL 1B	1.31	Poor	1.09	Very Coarse
DF	SPEN 1C	1.88	Poor	1.27	Very Coarse
DF	SPEN 1A	1.62	Poor	1.50	Very Coarse
DF	SPEN 1B	1.89	Poor	1.56	Very Coarse
DF	TALA 1A	0.92	Moderate	1.82	Very Coarse
DF	MUDL 1A	1.83	Poor	2.13	Granule
DF	PAN 1A	2.36	Very Poor	2.82	Granule
Ave.		1.3	Poor	0.8	Coarse Sand
Std.		0.5		0.7	

Table 4.16 *Delta flow facies (DF).*

G) Deep Glacio-lacustrine (DGL)

The lake sediments described here are those that have formed in a proglacial lake where there is no direct ice contact.

The development of deep glacial lake sediment depends on the size and depth of the lake as well as the longevity of the lake. This is true for lakes in both the terminoglacial and proglacial realms. The cyclicity or rhythmic nature of proglacial lacustrine sediments is constant and maybe generated via many mechanisms. Chaney (1998) defines the term rhythmite as meaning a couplet of sand/silt and clay that

repeats itself cyclically with no time constraint, having formed via turbiditic flows. Varvites are couplets that form within a space of one year.

It can be seen in Figure (4.8) that the detritus source of deep lacustrine sediments is the various flows emanating from deltas. Turbiditic underflows dominate close to the delta toe. These sediments were discussed in the previous two sections. Away from the delta, onto the lake floor proper, overflows and interflows (Fig. 4.8) are the dominant deep lacustrine sedimentation mechanisms. There is no sharp break between delta bottomset sediments and lacustrine sediments.

Surge deposits, according to Chaney (1998), represent rapid but continuous deposition where the whole couplet is normally graded and thus exhibits gradual progression from sand to clay. According to the same author boundaries between couplets are also gradual (Plate 9c). The thickness of the summer deposited sand/siltstone layers varies according to the summer detritus input. The clay layer or winter deposition, is very thin as underflow activity is minimal in the winter months. As a whole, surge rhythmites are characteristically thin, because of the limited carrying potential of underflows (Chaney, 1998). Rhythmite deposits that are purely turbiditic in nature are found in Gidgealpa #5, Tirrawarra #6 and #7 (Chaney, 1998).

Varves are formed by annual sedimentation, with the lower summer silt/sand (Lower) layer fluctuating in size depending on detritus input into the lake from the summer melt (underflow). In contrast the winter clay layer (upper) which remains constant in size as little detritus comes into the lake via the settling of suspended sediment plumes (interflow and overflow) (Chaney, 1998). Plate 9e illustrates a varvite mudstone that has formed by these mechanisms and has undergone post-depositional faulting. Unlike the turbiditic deposits, varvite deposits have sharp boundaries between silt/sand and clay couplets (Plate 9e). Finer sediments will dominate farther out into the lake as overflow and interflow sediments move farther out onto the lake floor than underflow sediments (Chaney, 1998). Underflow-dominated varvites are found in: Gidgealpa #5, Mudrangie #1, Bimbaya #1, Brolga #1, Kudrieke #1, Beanbush #1, Moorari #2, #3, #4, #7, and Tirrawarra #2, #3, #4, #8 and #9 (Chaney, 1998).

In summary, true varvites are dominated by summer (sand/silt) underflows beneath subordinate interflow and overflow deposited clay layers. Surge rhythmite deposits are much rarer and are purely deposited via underflow processes. All of these rhythmites do have some similarities, in that they are all in some way affected by

dewatering fluid escape structures, slumping and micro-faulting (Plates 9c & 9e). The overall sorting of rhythmites in the Merrimelia Formation is poor (Table 4.17).

Facies	Sample	Sorting	Sorting	Grain Size (mm)	Grain Size
DGL	MOOR 2A	1.27	Poor	0.04	Coarse silt
DGL	KUD 1D	1.80	Poor	0.05	Coarse silt
DGL	BEAN 1A	1.47	Poor	0.26	Medium
DGL	BIMB 1B	0.65	Moderately Well	1.44	Very Coarse
Ave.		1.3	Poor	0.4	Medium
Std.		0.48		0.7	

Table 4.17 Deep glacio-lacustrine rhythmites (DGL).

4.3 FACIES TYPE, SORTING AND GRAIN SIZE

The grain size of sediments in the Merrimelia Formation varies markedly, and is related to facies type.

Facies Type	Environmental Realm	Grain Size (mm)	Sorting Coefficient	RF Average	Quartz Average
ID	Proglacial	0.15	0.42	3.1	70.0
DFS	Proglacial	0.15	0.68	3.8	51.7
DU	Proglacial	0.18	0.40	3.5	61.4
FBT	Proglacial	0.20	0.54	7.8	53.0
LSF	Proglacial	0.20	0.80	8.1	45.9
DBS	Proglacial	0.24	1.04	13.0	42.3
LSZ	Proglacial	0.24	0.59	5.8	45.5
LIB	Proglacial	0.40	0.63	14.1	32.1
DGL	Proglacial	0.45	1.30	9.1	40.5
DTS	Proglacial	0.50	1.00	19.3	40.0
FL	Proglacial	0.66	1.06	41.9	28.3
FSZ	Proglacial	0.68	0.86	3.0	45.0
DF	Proglacial	0.86	1.27	27.8	33.1
RD	Terminoglacial	0.89	1.55	31.0	26.3
SACG	Terminoglacial	0.90	1.13	48.3	16.7
TTMD	Terminoglacial	1.20	1.27	38.3	36.0
LB	Terminoglacial	1.50	1.32	57.0	15.8
TOF	Terminoglacial	1.80	1.46	53.2	10.7

Table 4.18 Facies type vs grain size (mm), sorting ($\sigma\phi$), quartz and rock fragment percentages.

Table (4.18) demonstrates that not only do proglacial sediments have a smaller grain size than terminoglacial sediments but they are also better sorted.

Proglacial facies such as interdune, delta foreset and dunal sediments exhibit the smallest grain size, while aeolian dune sediments are the most texturally mature having markedly lower sorting coefficient values than all other sediments (Table 4.18).

The next most texturally mature proglacial rocks were fluvial, shorezone sandstones and delta foresets sediments. Deep water lacustrine, delta bottom, delta top and longitudinal bar sediments are the most poorly sorted of all proglacial sediments.

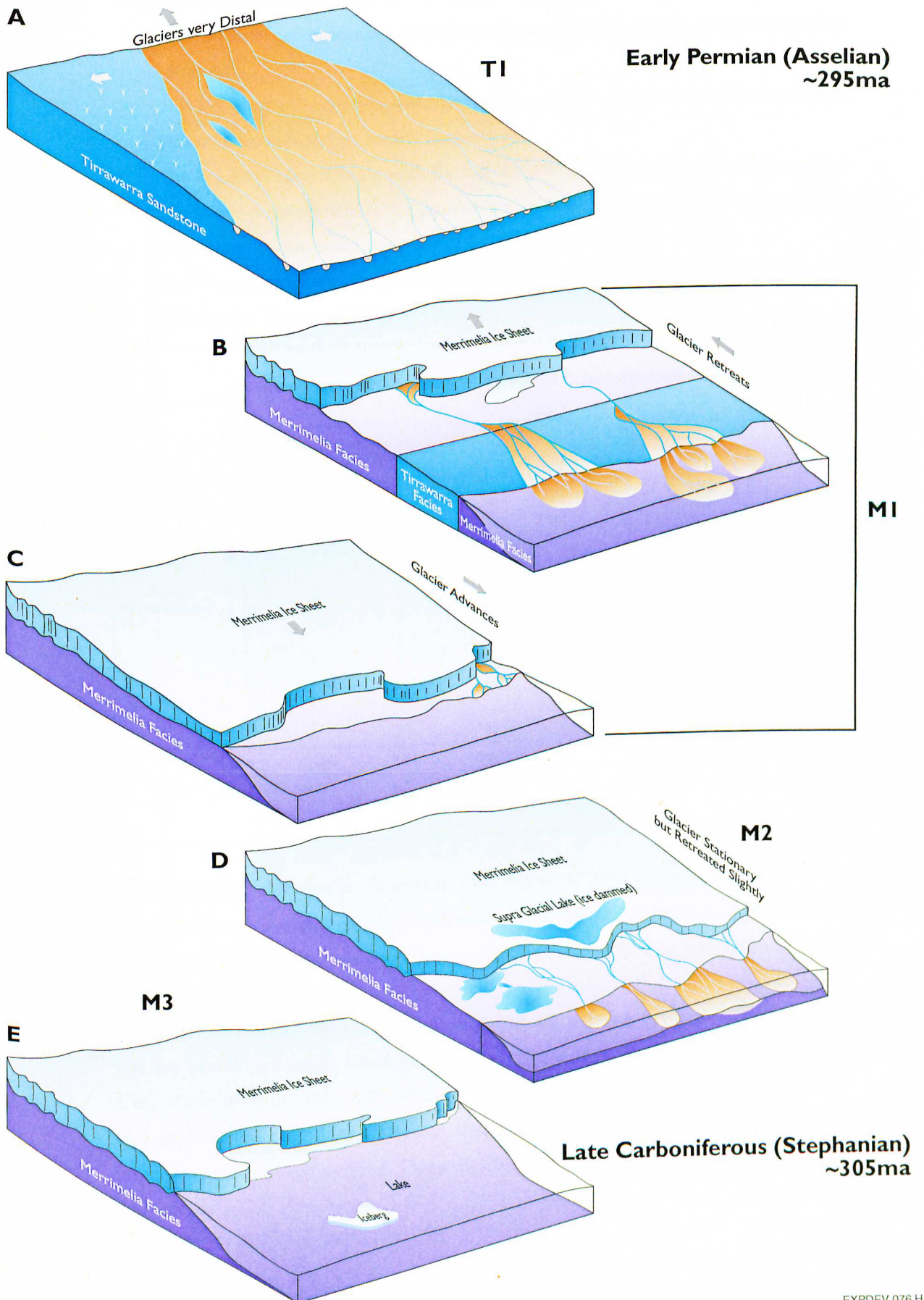
Terminoglacial facies such as subaqueous tunnel mouth deposits (TTMD), terminoglacial outwash fans (TOF), rain out diamictites (RD) and sub-aqueous channel (SACG) deposits consistently contained the largest framework grains and were also the most poorly sorted sediments of all Merrimelia sediments.

4.4 THE EVOLUTION OF THE MERRIMELIA-TIRRAWARRA GLACIAL COMPLEX

Both the proglacial and terminoglacial environments interfinger laterally and through time. As a result, rapid facies changes occur throughout the Merrimelia Formation. The diagrams in Figure 4.9 therefore are not palaeogeographic reconstructions, but simplified cartoons depicting the action of glaciers on sediment formation and facies distribution at representative time intervals.

The mechanisms which controlled the Gondwanan glaciation (see Chapter Three), influenced the position of glaciers in the southern part of the Australian continent, including the glaciers and ice cap which formed the Merrimelia Formation and Tirrawarra Sandstone. Initially Gondwanan glaciers were dominant, restricting sedimentation to "Merrimelia type facies" (Figures 4.9e). As glacial influence started to wane, Merrimelia sedimentation began to fluctuate (Figures 4.9d and 4.9c), to the point where both "Tirrawarra type" and "Merrimelia type" sediments were deposited in an interfingering manner (Figures 4.9c & 4.9b). The Gondwana glaciers retreated farther until only Tirrawarra Sandstone (braid plain) sedimentation dominated (Figure 4.9a). This evolving deposition is controlled by the action and position of Gondwanan glaciers, as they pass through cycles of ice advance and retreat (Cubitt *et al.* 1998).

Evolution of the Merrimelia - Tirrawarra Complex (MTGC)



EXPDEV 076 H

Figure 4.9 Evolution of the Merrimelia - Tirrawarra glacial complex (MTGC) (After Cubitt et al., 1998).

The Merrimelia Formation can be viewed as being composed of three separate sediment packages (M1, M2 & M3); a legacy of varying glacial influence (Fig. 4.9):

- The M3 level corresponds to the lower, most argillaceous third, of the Merrimelia Formation.
- The M2 level corresponds with the middle portion of the Merrimelia Formation where more arenaceous matrix is observed.
- The M1 level corresponds with the top third of the Merrimelia Formation where sandstone development is the greatest and interfingering with “Tirrawarra Type” sandstones is common (Figures 4.9c & 4.9b).
- The Tirrawarra Sandstone is regarded as the uppermost level (T1) within the Merrimelia-Tirrawarra Glacial Complex.

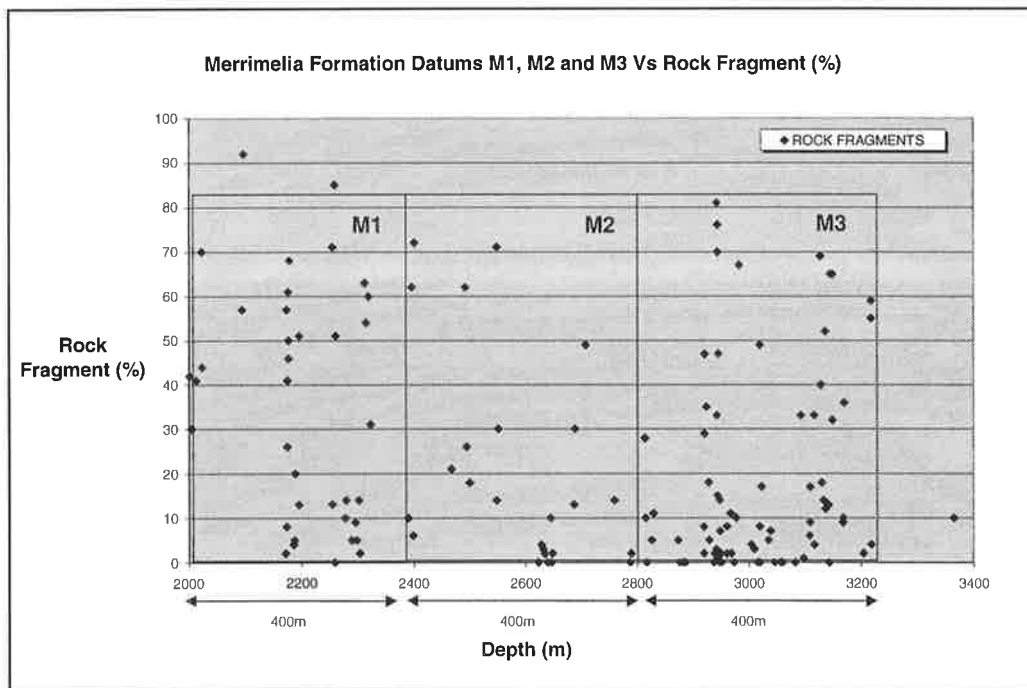


Figure 4.10 *Merrimelia Formation rock fragments versus depth (m) (Merrimelia Formation datums are shown). Merrimelia datums, M1, M2 and M3 were assigned to reflect the three dominant lithology packages that constitutes the Merrimelia Formation.*

The four divisions of the MTGC are broad and are not tied down to specific events but are based on overall lithological character and rock fragment percentage (Fig. 4.10). These divisions (M1, M2, M3 and T1) were assigned based on overall character and as such the boundaries between divisions (with the exception of the M1/T1 boundary) are not well defined. These divisions will be used extensively throughout this thesis.

4.5 CONCLUSIONS

- The Merrimelia Formation and Tirrawarra Formation formed by the action of glaciers issuing from a continental ice sheet. This continental ice sheet formed part of the Gondwanan glaciation which effected the south east portion of the Australian continent in the late Carboniferous and earliest Permian.
- The Merrimelia Formation is composed of a complex mosaic of glacial facies. These facies are observed throughout the Cooper Basin in South Australian and Queensland.
- The Tirrawarra Sandstone formed as a result of lower braid plain deposition, covering two thirds of the Cooper Basin. The Tirrawarra Sandstone forms part of the Merrimelia-Tirrawarra Glacial Complex.
- The Merrimelia Formation and the Tirrawarra Sandstone were formed on plain sandar with minimal lateral restrictions. Minor restricted or valley sandar are thought to have formed in the southern region, of the Cooper Basin.
- A model of the Merrimelia-Tirrawarra Glacial Complex (MTGC) was constrained using core and analogue observations.
- Merrimelia (and Tirrawarra) facies were deposited in terminoglacial and proglacial depositional realms depending on the relative position of Gondwanan glaciers and ice sheet.
- The proximity of terminoglacial environments to the glacier and/or ice sheet means that these facies types are dominated by high energy conditions. As a result, the sediments deposited are coarse grained and show exceptionally rapid lateral and vertical changes, a result of variation in melt water volume and strength.
- The terminoglacial zone forms a very narrow band relative to the ice sheet, where most of the sediments were deposited in melt water rivers and streams. Lacustrine, deltaic and mass flow depositional processes are subordinate.
- Proglacial environments are distal to the ice sheet/glaciers where the size and character of facies within this depositional realm are dependent on melt water volumes and topography.

- Compared to the terminoglacial depositional realm the proglacial environment is much greater in area. Accordingly there are a greater number of facies observed
- Proglacial environments form beyond terminoglacial facies and are dominated by fluvial and lacustrine processes. There is no ice cover within this region, but river ice and lake ice may prevail locally.
- Glacio-aeolianites were observed and described in the Merrimelia Field. These sediments represent the most well sorted of all Merrimelia facies. These sandstones formed on a plain sandur in very close proximity to active braidplain channels.
- A model that describes the evolution of the Merrimelia-Tirrawarra Glacial Complex (MTGC) both areally and through time was constrained.
- The entire Merrimelia-Tirrawarra Glacial Complex was subdivided into four packages (M1, M2, M3 & T1). These subdivisions correspond with the lower, middle and upper Merrimelia Formation along with the Tirrawarra Sandstone. These packages correspond to the lithological character of the glacial sequence, from glacial dominated sedimentation (M3), through to fluctuating glacial sedimentation (M2, M1) and dominant braid plain sedimentation (T1).

FRAMEWORK COMPONENTS & PROVENANCE

5.0 INTRODUCTION

Rock fragment lithology, in both the Merrimelia Formation and Tirrawarra Sandstone, profoundly effects reservoir quality (see Chapter Nine). With this in mind, the petrography of the framework component of Merrimelia sediments is presented and discussed in this chapter, with emphasis on describing rock fragment lithologies. Corresponding with these petrography descriptions, the likely provenance regions are discussed. The petrography and diagenesis of authigenic phases in Merrimelia lithologies is described in detail in the following chapter (Chapter Six).

The petrography of the Merrimelia Formation in part reflects mechanical weathering under glacial conditions. The rock fragment component, in coarse to conglomeratic sediments, for example, exhibits a kaleidoscopic range of up to seventy six different rock types. It is these conglomeratic sediments which contains the majority of rock fragments and are therefore the main focus of discussion in this chapter. However, all framework components (quartz, feldspar, rock fragments and accessory minerals), in all MTGC facies, regardless of grain size, were described in detail. The results of this analysis is presented in sections 5.2 and 5.3 of this chapter.

The petrography of the Tirrawarra Sandstone in the Fly Lake-Brolga and Tirrawarra regions (excluding rock fragment analysis) formed part of the study by Rezaee (1996), and readers wishing full descriptions of the Tirrawarra Sandstone in these regions should refer to that text. The rock fragment component of braid plain facies (Tirrawarra Sandstone) is presented in this chapter in order to better understand the relationships between Merrimelia and Tirrawarra facies types (see section 5.3).

The latter half of the chapter discusses rock fragment distribution within the basin and petrological and provenance relationships observed between Merrimelia Formation and Tirrawarra Sandstone facies.

A detailed discussion of primary and secondary porosity preservation is given in (Chapter Nine).

5.1 COMPOSITION

The composition of all Merrimelia facies is summarised in Fig. 5.1. The dominant component of Merrimelia sediments is quartz, with rock fragments, matrix and authigenic minerals equally subordinate. Feldspar and accessory minerals constitute a very small percentage of the total detritus in these rocks.

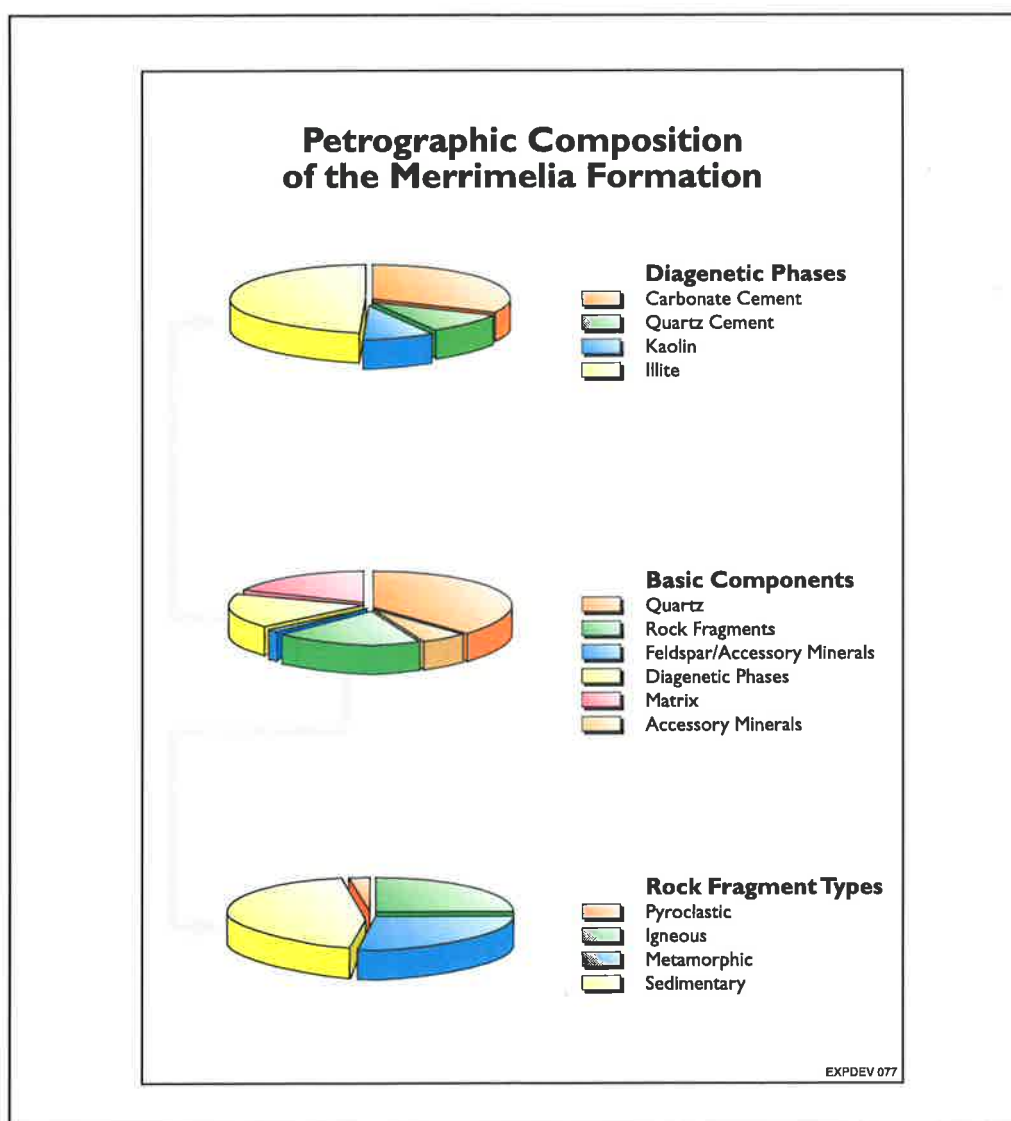
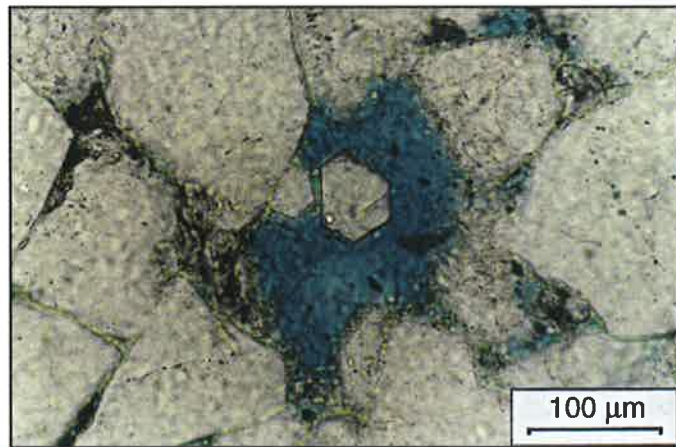
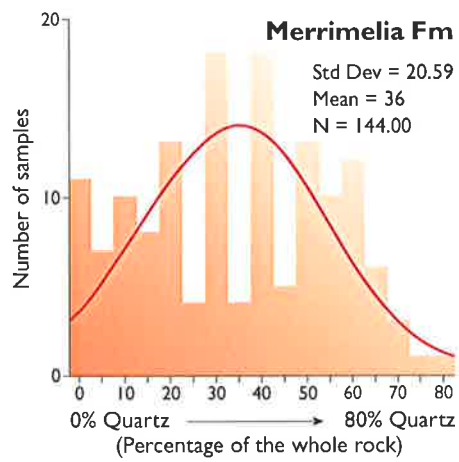


Figure 5.1 Composition of argillaceous and arenaceous facies: Merrimelia Formation.

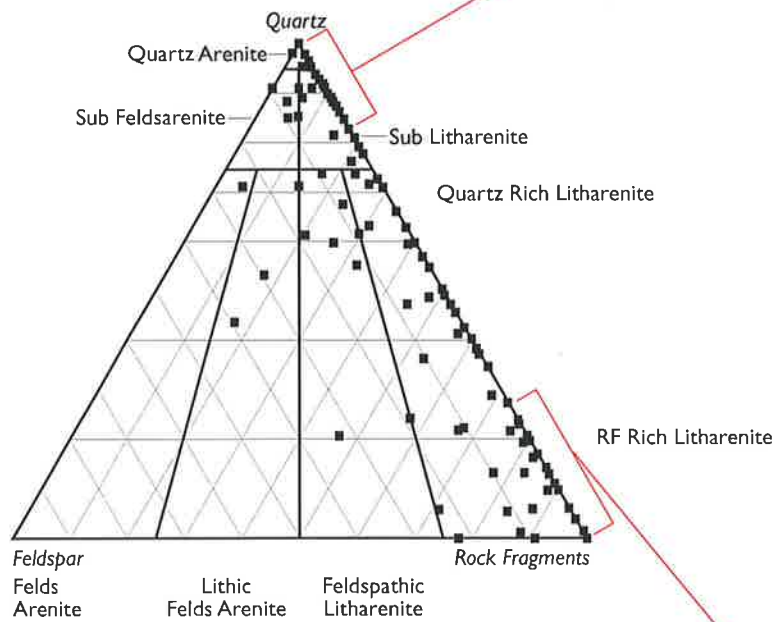
Composition of the Merrimelia Formation



A

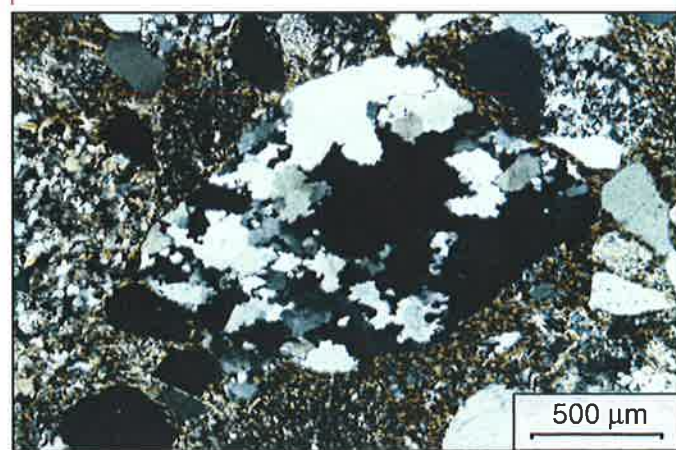
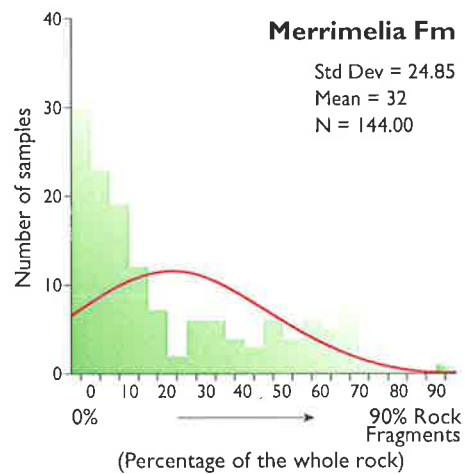
B

Arenaceous Merrimelia Sediment



C

Argillaceous Merrimelia Sediment



D

E

Figure 5.2 Composition of the Merrimelia Formation. A) Quartz percentage histogram. B) Merrimelia #1 (2946.8m) (Plane polarised x 20) Quartz arenite. C) Ternary diagram illustrating the compositions of Merrimelia sediments. D) Rock fragment percentage histogram. E) Moorari #2 (Cross nicols x 5) Litharenite.

Classification of Merrimelia sediments was undertaken using the nomenclature of Folk *et al.* (1970). According to this classification scheme, sublitharenites and litharenites are the most dominant Merrimelia litho-type with lesser amounts of quartz arenites and sub-feldsarenite lithologies (Fig. 5.2). Very rare feldspar-rich lithologies were observed, with only one feldsarenite rock type described (Fig. 5.2c).

5.2 MERRIMELIA FORMATION: PETROGRAPHY

5.2.1 Framework Components

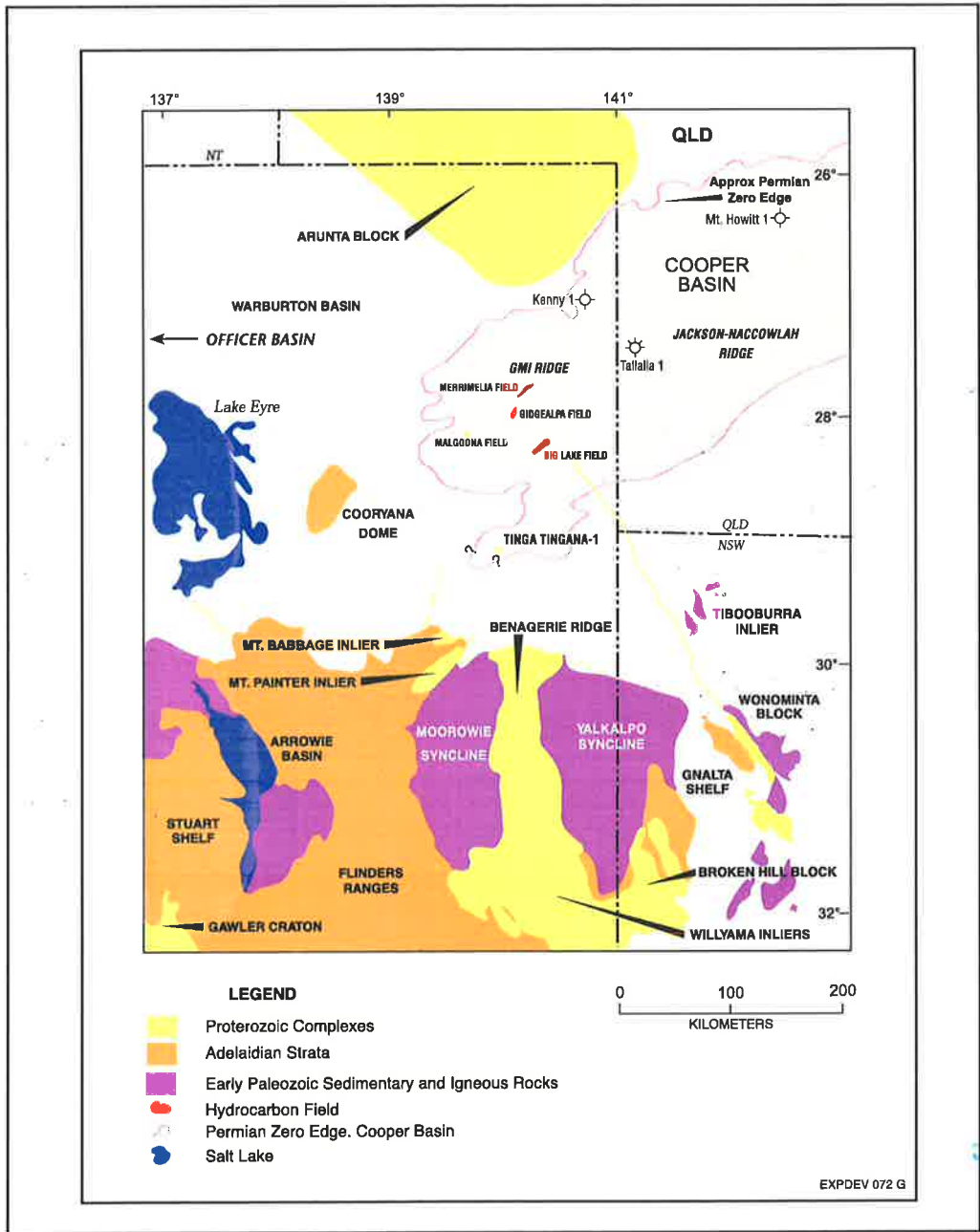


Figure 5.3 Geological provinces surrounding the Cooper Basin at the time of MTGC deposition.

Framework components within the Tirrawarra Sandstone and Merrimelia Formation have been sourced from an enormous area having possibly been transported hundreds of kilometres by the action of glaciers and meltwaters.

Throughout this chapter reference will be made to the surrounding the geological provinces as potential source regions for Merrimelia/Tirrawarra sediments. Figure 5.3 illustrates the relative position of surrounding geological provinces with respect to the Cooper Basin; provinces which at the time of the Permo-Carboniferous glaciation, were elevated.

The two main framework components (quartz and rock fragments) are not evenly distributed throughout Merrimelia sediments. Figure (5.2a) indicates that the distribution of quartz framework grains in Merrimelia sediments is normal, with the majority of samples containing between 20% and 50% quartz. In contrast the distribution of rock fragments shows a skewed distribution with a relatively high proportion of samples (~60%) containing less than 10% or no rock fragments (Fig. 5.2d). Similar skewed trends were observed in the distribution of straight extinction, undulose extinction and poly-crystalline quartz grains individually (Figs. 5.4a, 5.4b and 5.4c).

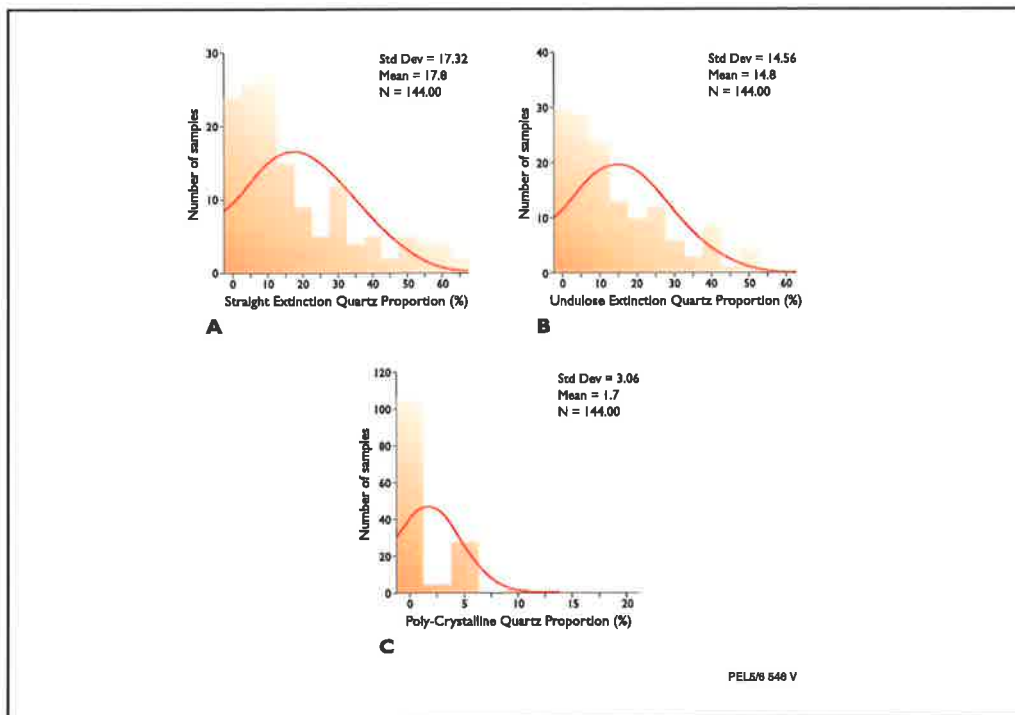


Figure 5.4 Distributions of straight extinction, undulose extinction and poly-crystalline quartz framework grains in the Merrimelia Formation (percentage of the framework component).

The photomicrographs in Figure (5.2) represent end member framework compositions of Merrimelia facies where Figure (5.2b) is a rock fragment-rich litharenite and Figure (5.2e) is a quartz arenite.

5.2.1.1 Quartz Grain Component: Petrography and Provenance

5.2.1.1.1 Petrography And Provenance

The majority of quartz grains exhibit straight extinction (Plate 10 [10d]). Undulose (Plate 10[9g]) and poly-crystalline quartz (Plate 10 [2h]) grains are less common (Table 5.1). Table (5.1) indicates the various proportions of quartz types observed in Merrimelia sediments.

QUARTZ TYPE	QUARTZ FRAMEWORK COMPONENT PERCENTAGE OF WHOLE ROCK
STRAIGHT EXTINCTION	20.8
UNDULOSE EXTINCTION	15.7
POLY-CRYSTALLINE	1.5

Table 5.1 Average percentages of quartz framework component.

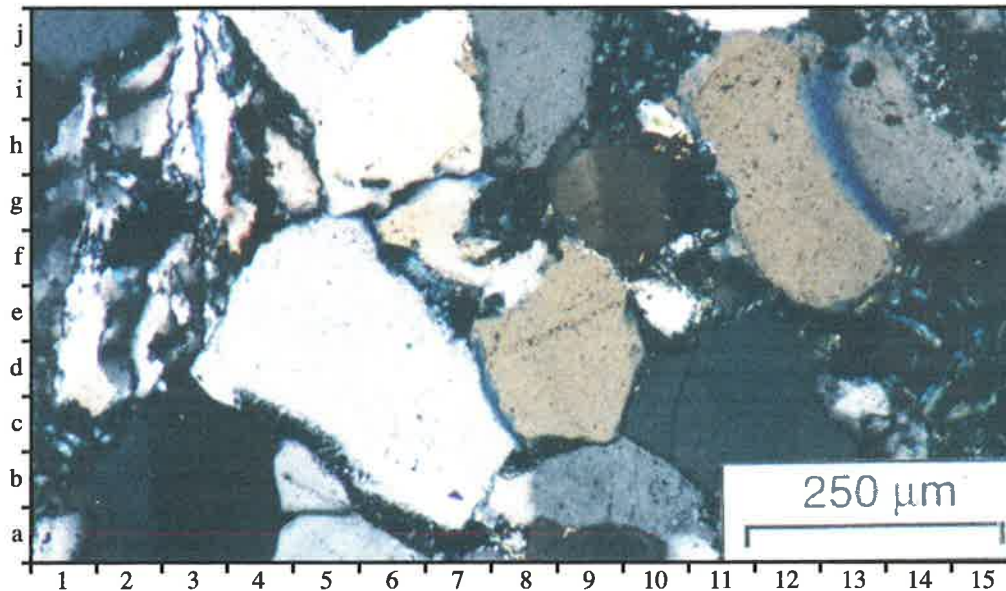


PLATE 10
Quartz Grain Types

Photomicrograph – Moorari #3 (2893.28m) (Cross nicols x 10). Broad view of a litharenite sandstone illustrating poly-crystalline quartz ([2g], straight extinction quartz [10d] and undulose extinction quartz [9g] framework grains.

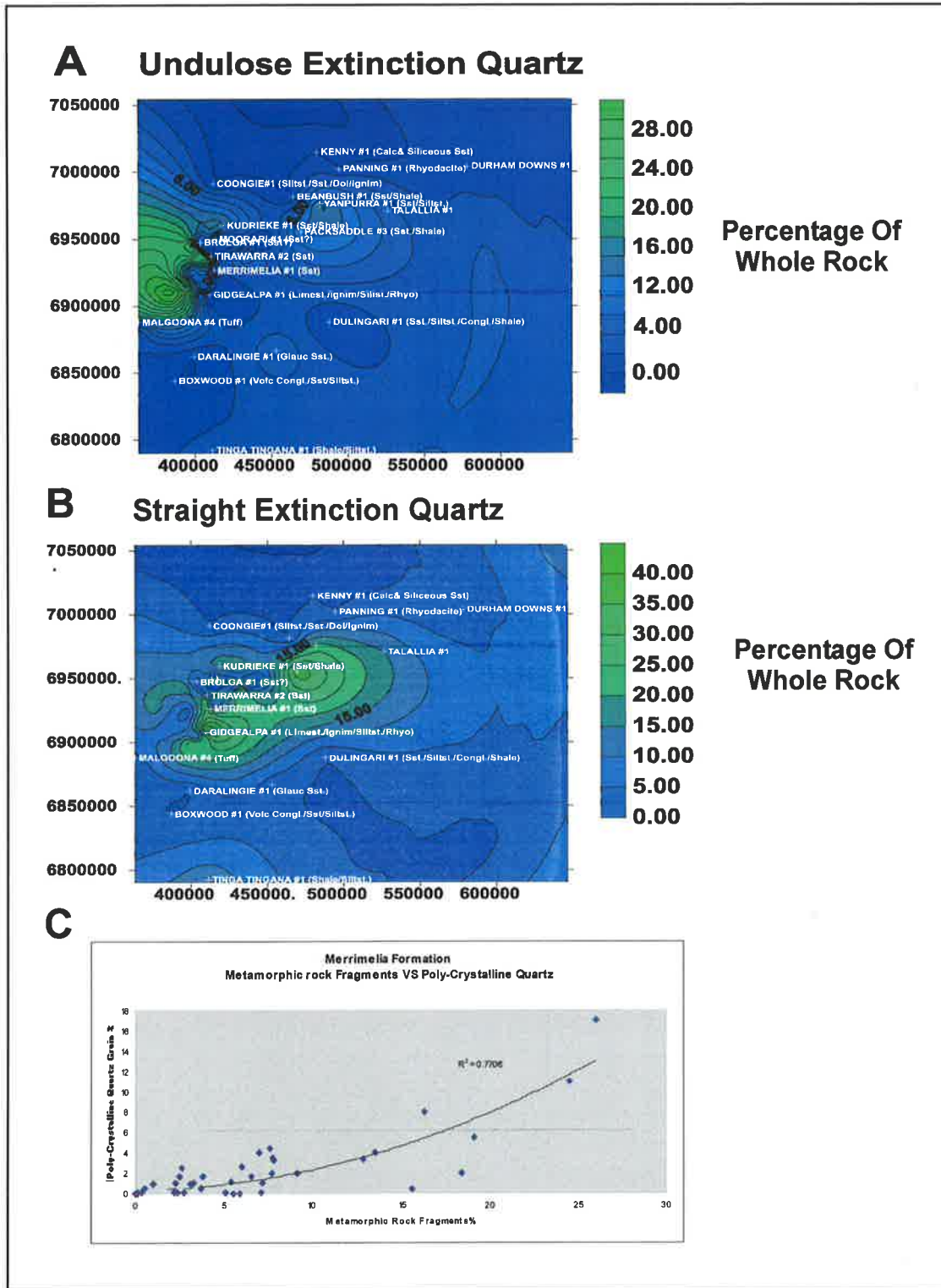


Figure 5.5 A) Trend map of undulose quartz grains of the Merrimelia Formation (M3). B) Trend map of straight extinction quartz grains of the Merrimelia Formation (M3). C) Scattergram of metamorphic rock fragments versus poly-crystalline quartz grains.

A clue to the possible source of undulose and straight extinction quartz grains can be seen in M3 trend maps illustrated in Figures 5.5a and 5.5b.

The undulose quartz distribution map (Fig. 5.5a), indicates that the majority of undulose quartz grains lie on the basin margin with a tentative suggestion that they have in fact been transported into the basin by the action of glaciers.

Conversely, figure 5.5b illustrates that the distribution of straight extinction quartz grains is restricted to an area corresponding with the GMI Trend, a palaeo low, suggesting an intrabasinal or Warburton Basin origin of these grains. In this scenario, the resulting sedimentation covers the Warburton source, effectively starving the sedimentary pile of straight extinction quartz grains. Hence in M1 and M2 sediments, a local source for straight extinction quartz grains maybe unlikely. It is plausible then that an extra-basinal source is contributing straight extinction quartz grains into upper Merrimelia or M1 sediments.

Poly-crystalline quartz grains are most likely derived from the breakdown of metamorphic lithologies like schist, gneiss and migmatites that were transported into the basin from surrounding metamorphic terranes. This relationship is supported by cross plotting poly-crystalline quartz grains and metamorphic rock fragments (Figure 5.5c); poly-crystalline quartz increases along with metamorphic rock fragments.

5.2.1.2 Rock Fragment Component: Composition and Provenance

Detailed petrological analyses of the rock fragment component in the Merrimelia Formation identified 76 differing rock fragment types (Appendix 4a). Pearson correlation coefficients followed by (PCA)¹ was performed on Merrimelia rock fragment data and quartz grain proportions revealing two distinct populations (Fig. 5.6).

These two groupings broadly correspond with intrabasinal and extrabasinal rock fragments and quartz grain types. From this and petrographic analyses, statistically and geologically significant rock fragment types were ascertained, described and likely provenance region discussed.

¹ See section 5.5.1.2 for an explanation of principle component analysis (PCA).

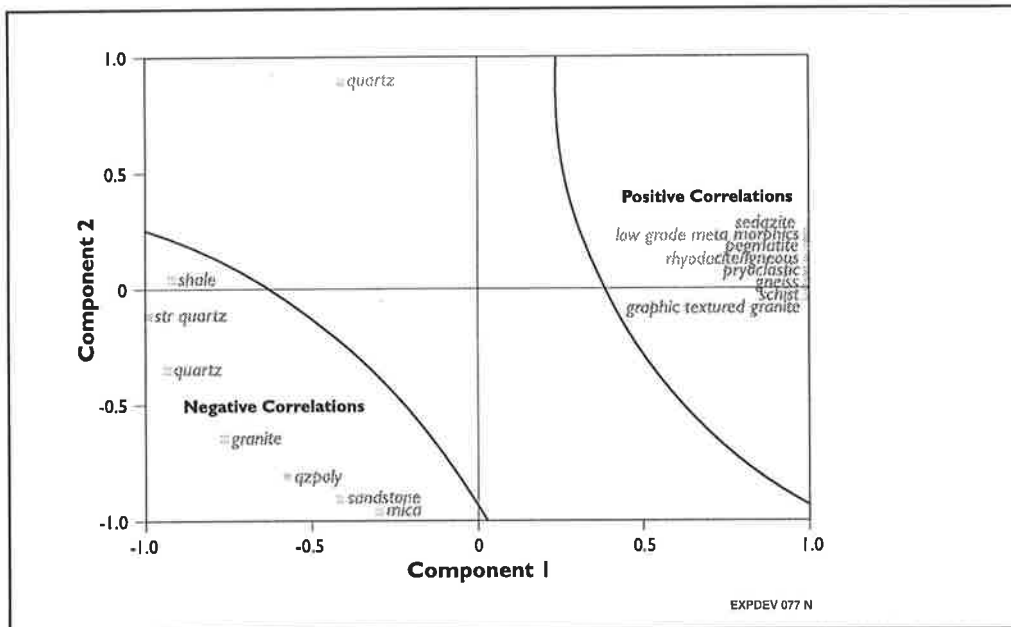


Figure 5.6 Statistically significant rock fragment types: Merrimelia Formation.

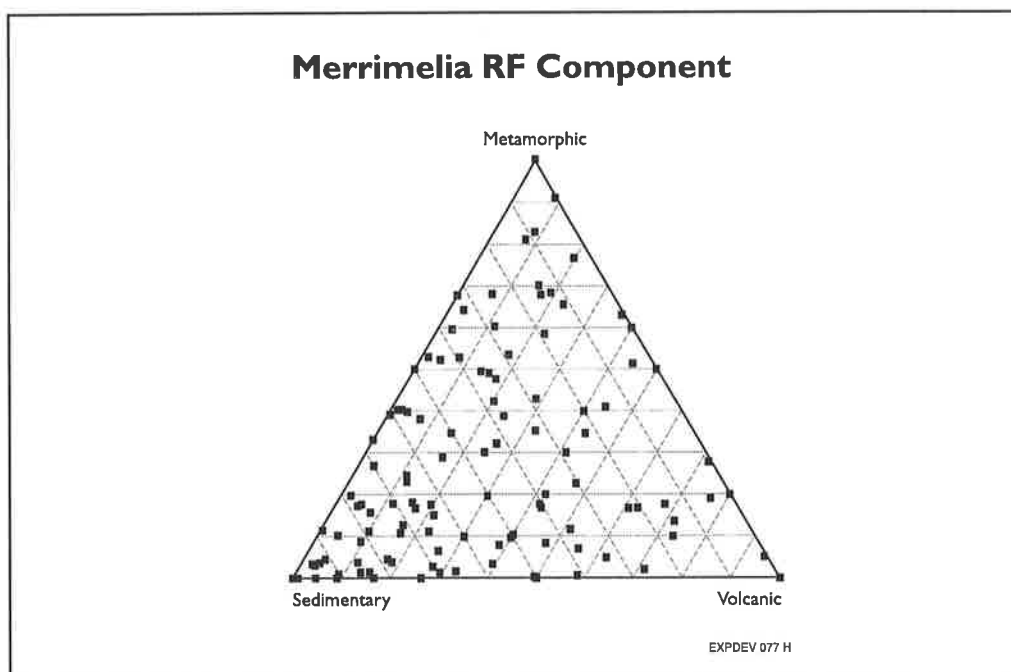


Figure 5.7 Rock Fragment Lithologies in the Merrimelia Formation

The most common rock fragment type observed in the Merrimelia Formation is shale (Table 5.2), with sedimentary rock fragments as a whole accounting for the majority of all rock fragments observed (Fig. 5.7).

Metamorphic and igneous rock fragments provide approximately equal, although subordinate, proportions of rock fragments (Table 5.2 – circled).

ROCK FRAGMENT LITHOLOGIES	MERRIMELIA FORMATION	MERRIMELIA FORMATION	TIRRAWARRA SANDSTONE.	TIRRAWARRA SANDSTONE.
	Percentage of Detrital Component	Percentage of Rock Fragment Component	Percentage of Detrital Component	Percentage of Rock Fragment Component
METAMORPHIC LITHOLOGIES (Totals)	6.2	25.5	9.1	37.2
Quartzite	1.0	4.1	2.5	10.2
Psammite	0.5	2.1	1.5	6.1
Phyllite	0.1	0.6	Tr	0.0
Schist	0.4	1.4	0.2	0.8
Gneiss	Tr	0.0	Tr	0.0
Schistose Poly-Crystalline Quartz	0.8	3.3	2.0	8.2
Poly-Crystalline Quartz	2.0	8.2	1.5	6.1
Recrystallized Poly-crystalline Quartz	0.5	2.1	1.2	4.9
Meta-Rhyodacite	0.9	3.7	0.2	0.8
IGNEOUS LITHOLOGIES (Totals)	6.5	26.8	3.3	13.5
Porphyritic Rhyolite	2.8	11.5	0.5	2.0
Flow Banded Rhyolite	0.2	0.8	Tr	0.0
Devitrified Acid Volcanics	1.6	6.6	2.0	8.2
Spherulite Rhyolite	Tr	0.0	Tr	0.0
Granite (Granular)	0.8	3.3	0.3	1.2
Granite (Graphic)	0.7	2.9	Tr	0.0
Pegmatite	0.4	1.6	0.5	2.0
Basalt	Tr	0.0	Tr	0.0
Trachytic Basalt	Tr	0.0	Not Observed	Not Observed
PYROCLASTIC LITHOLOGIES (Totals)	1.2	4.9	Not Observed	Not Observed
Crystal Tuff	Tr	0.0	Not Observed	Not Observed
Welded Ignimbrite	0.6	2.5	Not Observed	Not Observed
Ignimbrite	0.6	2.5	Not Observed	Not Observed
SEDIMENTARY LITHOLOGIES (Totals)	9.8	40.3	12.1	49.4
Quartz Arenite	0.1	0.4	Tr	0.0
Sub-litharenite	0.9	3.7	0.9	3.7
Litharenite	1.9	7.8	1.9	7.8
Greywacke	0.7	2.9	0.6	2.4
Mudstone	0.3	1.2	Not Observed	Not Observed
Shale	5.2	21.4	7.6	31.0
Siltstone	0.7	2.9	1.1	4.5
ACCESSORY MINERALS (Totals)	0.6	2.5	Tr	Tr
Glaucony	0.1	0.4	Tr	Tr
Zircon	0.3	1.2	Tr	Tr
Tourmaline	0.2	0.8	Tr	Tr
TOTAL ROCK FRAGMENT PERCENTAGE	24.3		24.5	

Table 5.2 Rock fragment percentages in the Merrimelia Formation and Tirrawarra Sandstone (percentage of the detrital component and percentage of the rock fragment component are shown).

Detailed thin section descriptions of all rock fragments listed in Table 5.2 are found in Appendix 4a. Table 5.3 lists in which thin section description(s) a particular rock fragment is described.

ROCK FRAGMENT LITHOLOGY	SAMPLE NAME
Shale	MERRI 1I
Litharenite	MERRI 1F, KUD 1D
Greywacke	KUD 1D, DARA 1D
Glauconitic Litharenite	MERRI 3A, MERRI 1F
Siltstone	PACK 3B
Arenite	MERRI 1F
Sub-litharenite	MERRI 1F
Feldspars	TIND 2A
Conglomerate	MERRI 3A, SPEN 1C
Rhyodacite (Facies A)	MAL 2D, MAL 2B, MAL 4D, MAL 4F, CONG 1C
Rhyodacite (Facies B)	MAL 4F
Feldspathic Litharenite	MAL 4E
Sphereulite Rhyodacite	MERR 1I
Devitrified Volcanics	MOOR 2D, MAL 4H
Vesicular/Amygdaloidal Basalt	TIND 2A
Trachytic Basalt	GIDG 5E, GIDG 3C
Crystal Tuff	MAL 2C, MAL 2B, MAL 2D
Welded Ignimbrite	MAL 2C, MAL 4C
Micro-pegmatite	MOOR 1A, BROL 1A
Graphic Granite	MERRI 1I, MERRI 1G, MAL 4F
Granular Granite	TALA 1B, MERRI 1G
Gneiss	DULN 1A
Schist	DULN 1A
Sedimentary Quartzite	KUD 1C
Hexagonal Quartzite	KUD 1C
Psammite/Pelite	MOOR 1A, PAN 1A, WEL 1C, SPEN 1A, TINA 1F
Meta-Rhyodacite	KUD 1F, MOOR 6B, MAL 4F
Meta-Poly-Crystalline Quartz	MERRI 1C, DULN 1A
Phyllite	MERRI 1D, MERRI 1G
Spotted Phyllite	MERRI 1G, MERRI 18B
Low Grade Metamorphics	MERRI 1D

Table 5.3 Rock fragment type and relevant thin section description (Appendix 9b).

ROCK FRAGMENT TYPE	FORMATION(S)/FACIES	BASIN(S)/REGION(S)	PLATE No.
Sedimentary Rock Fragments			
<i>Arenite/Litharenite/Sub-litharenite</i>	Dullingari Group/Mudrangie Sst/ Innamincka Red Beds	Warburton Basin	11d
<i>Arkose</i>	Extra-Cooper Basin	??	40a
<i>Glauconitic Sandstone</i>	Pando Formation/Dullingari Group	Warburton Basin	11e
<i>Shale/Siltstone/Greywacke/Mudstone</i>	Dullingari Group/Innamincka Red Beds	Warburton Basin	11
Acid Volcanic Rock Fragments			
<i>Porphyritic Rhyodacite</i>	Mooracoochie Volcanics: Facies Type A	Warburton Basin	12a
<i>Spherulite Rhyodacite</i>	Mooracoochie Volcanics	Warburton Basin	13a
<i>Devitrified Acid Volcanics</i>	Mooracoochie Volcanics: Facies Type A & B	Warburton Basin	13c & 13e
<i>Hyaloclastite/Granoblastic Rhyodacite</i>	Mooracoochie Volcanics: Facies Type D	Warburton Basin	12d
Pyroclastic Rock Fragments			
<i>Crystal Tuff</i>	Mooracoochie Volcanics: Facies Type C	Warburton Basin	13b
<i>Welded Ignimbrite</i>	Mooracoochie Volcanics: Facies Type C	Warburton Basin	13d
Basic Volcanic Rock Fragments			
<i>Trachytic Basalt</i>	Mooracoochie Volcanics: Facies Type G	Warburton Basin	14b
<i>Amygdaloidal Basalt</i>	Mooracoochie Volcanics: Facies Type H	Warburton Basin	14a
<i>Ultra Basic</i>	Mooracoochie Volcanics	Warburton Basin	No Illustration
Pegmatite & Granite Rock Fragments			
<i>Micro-Pegmatite</i>	Extra-Cooper Basin	??	14d & 14c
<i>Graphic/Myrmekitic Textured Granite</i>	Mount Neill Porphyry	Mount Painter/Mount Babbage Inliers/Arunta Block	15a & 15b
<i>Granular Granite</i>	Willyama Supergroup/Kingonya & Kokatha Granites Big Lake Suite Granodiorite/Tibooburra Granites	Broken Hill/Olary Blocks/Eastern Gawler Craton Warburton Basin/Curnomona Block	15c
Metamorphic Rock Fragments			
<i>Phyllite</i>	Willyama Supergroup/Yagdlin Phyllite	Broken Hill/Olary Blocks/Mount Painter Inlier/Arunta Block	No Illustration
<i>Schist/Gneiss</i>	Willyama Supergroup	Broken Hill/Olary Blocks/Mount Painter Inlier/Arunta Block	15d, 15e & 16a
<i>Psammitic/Pelite</i>	Parabaranna Hill Meta-sediments	Mount Painter Inlier/Broken Hill/Olary Blocks/Arunta Block	No Illustration
<i>Quartzite</i>	Dullingari Group/Willyama Supergroup/Baltucocanda Quartzite	Warburton Basin/Broken Hill Block/Peak and Denison Inliers Flinders Ranges (Adelaidian)	16b
<i>Meta-Acid Volcanic</i>	Mooracoochie Volcanics	Warburton Basin	16d
<i>Meta-Poly-Crystalline Quartz</i>	??	Warburton Basin ??	16e
Feldspar & Accessory Minerals			
<i>Plagioclase</i>	Big Lake Suite Granodiorite	Warburton Basin	17a
<i>Microcline</i>	Big Lake Suite Granodiorite	Warburton Basin	17b
<i>Micas</i>	Big Lake Suite Granodiorite	Warburton Basin	18a
<i>Zircons</i>	Big Lake Suite Granodiorite/Dullingari Gp	Warburton Basin	Fig. 5 14
<i>Rutile</i>	??	Warburton Basin	17e

Table 5.4 The provenance of Merrimelia Formation framework components and associated plate references. A detailed provenance discussion of all framework components is given in Appendix 4b.

The four principle source regions for Merrimelia Formation sediments are:

- 1) Warburton Basin
- 2) Mount Painter/Mount Babbage Inliers
- 3) Broken Hill/Olary Blocks
- 4) Arunta Block

Minor amounts of Merrimelia sediment are also thought to have been derived from:

- 1) Peak and Denison Inliers
- 2) Flinders Ranges (Adelaidean)
- 3) Eastern Gawler Ranges

The provenance of Merrimelia rock fragments and accessory minerals is given in Table 5.4. A detailed provenance discussion (with associated maps and diagrams) for each of the framework components outlined in Table 5.4 is given in Appendix 4b².

This table forms the basis of all provenance discussion throughout this thesis.

5.2.1.3 Rock Fragment Component: Petrography

5.2.1.3.1 Sedimentary Rock Fragments: Petrography

Sedimentary rock fragments are generally ductile although quartz-rich sandstone and a small proportion of silicified shale and mudstone clasts are relatively competent. The majority of shale clasts have been deformed by sediment overburden pressures (Plate 11a and 11d).

Despite shale clasts being the most abundant rock fragment type observed in Merrimelia sediments they are not present in all samples. Plate 11b, displays that shale fragments are not present in over half of the samples, with a third of samples containing <10% of shale clasts. Similar trends are noted for all other sedimentary rock fragments (Plate 11c). Considering the main sedimentary rocks on an individual basis, litharenite (Plate 11e) and greywacke (Plate 11d[14h]) clasts constitute 8.1% and 2.8% of the total rock fragments observed in the Merrimelia Fm. (Table 5.2). Rock fragments within litharenite rock fragments (Plate 11e[1j]), as well as the fine grained matrix of greywacke clasts, have generally been illitised. Litharenite rock fragments also exhibit abundant illite and kaolin between pores and with intergrown quartz cement.

² The length of the rock fragment provenance discussion necessitated inclusion into the Appendices (Appendix 4b) and not the main body of the text. Table 5.4 summarises the conclusions drawn in this discussion.

PLATE 11

Sedimentary Rock Fragments: 1

A) Photomicrograph - Merrimelia #1 (2942.11m) (Cross nicols x 4). Squeezed shale rock fragment [9e] (incompetent) between more competent poly crystalline-quartz [10a] and [15e] basic volcanic rock fragments.

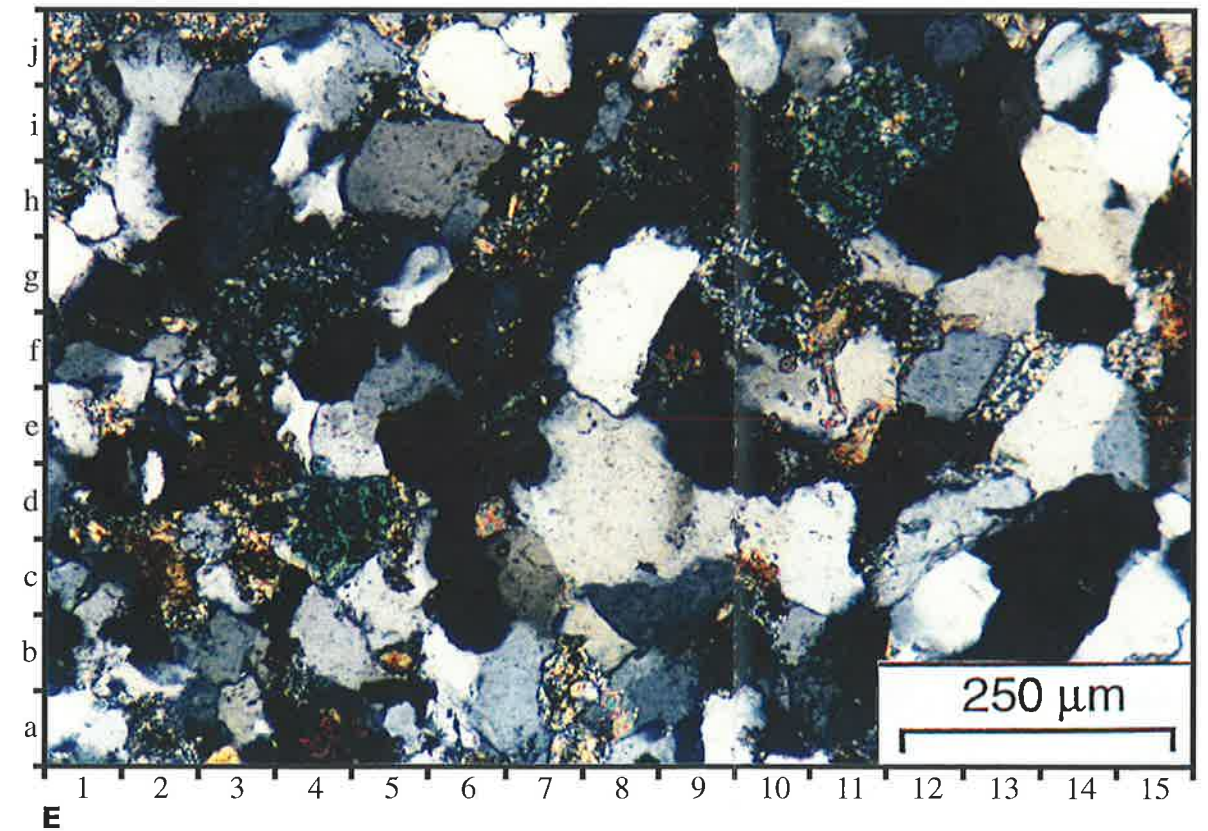
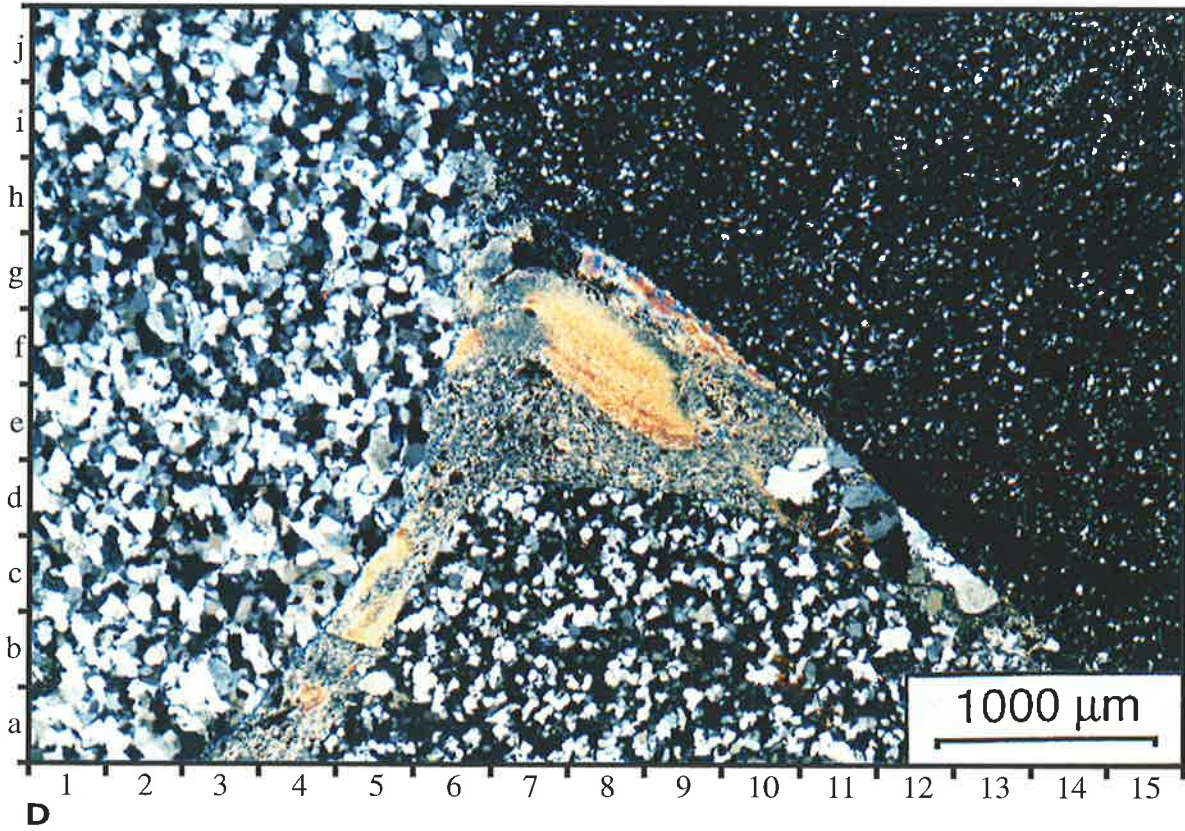
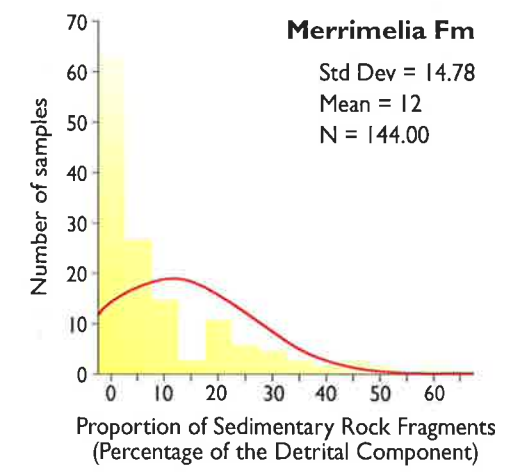
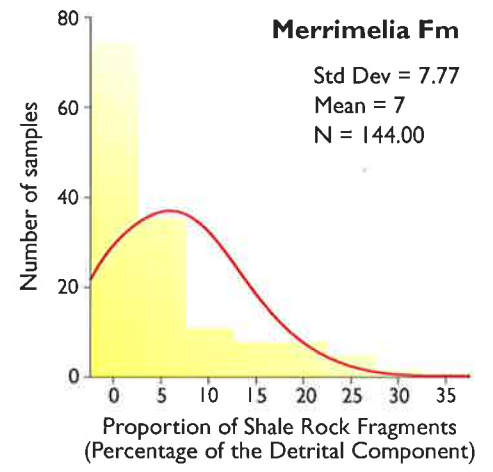
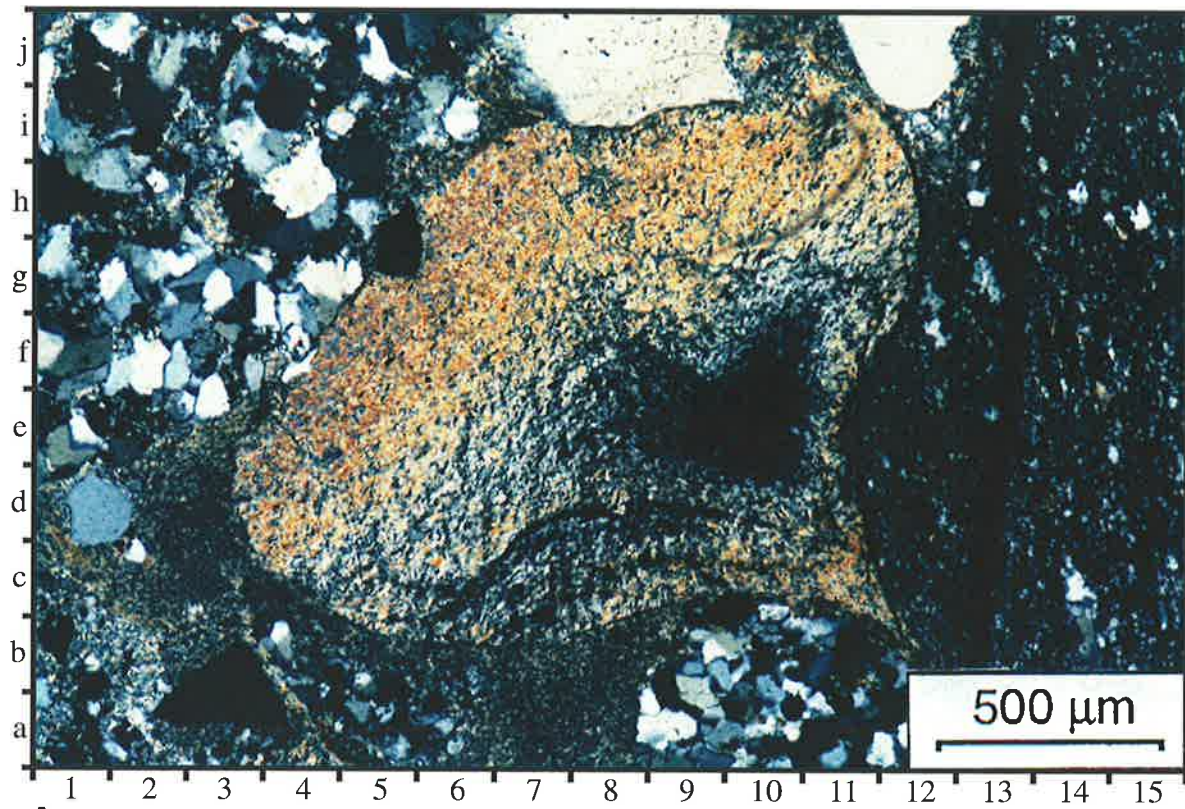
B) Frequency histogram. Shale rock fragments: Merrimelia Formation samples.

C) Frequency Histogram. Sedimentary rock fragments: Merrimelia Formation samples.

D) Photomicrograph - Merrimelia #1 (2943.6m) (Cross nicols x 2). Quartz arenite [3f], litharenite [10b], greywacke [14h] and shale [8f] rock fragments.

E) Photomicrograph - Merrimelia #1 (2942.41m) (Cross nicols x 10). Close up of a glauconitic rich litharenite rock fragment.

Plate II



Sub-litharenite rock fragments (Plate 11a[2i]), contain on average 80% quartz grains (the majority of which exhibit straight extinction with sutured and straight grain contacts), 0.8% unaltered feldspar grains, altered rock fragments, zircons and mildly compacted micas.

Green, rounded grains are present and are of glauconitic illite composition. At least two quartz cementation phases are present as numerous quartz grains exhibit two quartz cement rims. Illite also commonly lines pores within sub-litharenite clasts. Rarely quartz grains contain thin needles of rutile.

Litharenite clasts contain a great deal more illite, kaolin and glaucony than the sub-litharenite rock fragments (Plate 11e).

The glaucony fragments within litharenite and sub-litharenite rock fragments are the same mineral as that identified by Taylor *et al.* (1991) (“glauconitic illite”). These grains are described in more detail in the following chapter (Chapter Six).

Other sedimentary rock fragment types observed include siltstone, silty shales, arenites (Plate11a[10b]), and mudstones. Trace amounts of felsic, organic and conglomeratic sedimentary rock fragments were also observed.

5.2.1.3.2 Volcanic Rock Fragments: Petrography

Volcanic rock fragments account for 26.7% of all rock fragments observed in the Merrimella Formation (Table 5.2). However, a high proportion of samples (~63%) contained no such material (Fig. 5.8).

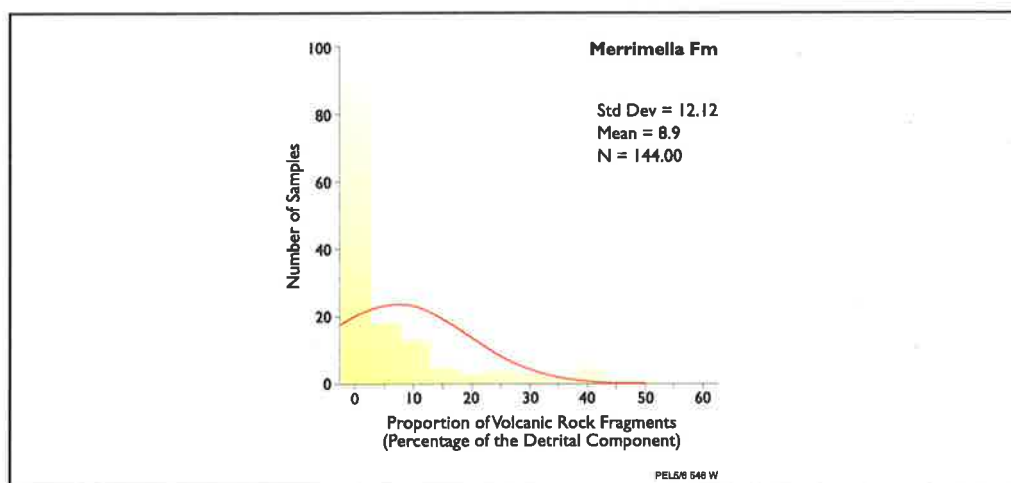


Figure 5.8 Frequency histogram of volcanic rock fragment in Merrimella sediments.

Locally in the Malgoona-Spencer region in the south and the Gidgealpa and Coongie regions in the north of the Cooper Basin (Fig. 1.2) are dominated by volcanic rock fragments (48%-24% and 18%-29% of the whole rock respectively). Regionally however, volcanic rock fragments account for much less of the whole rock with percentages varying between 0.1% to 6% (Table 5.2).

Plates 12a and 12b illustrate the similarities between volcanic rock fragments in the Cooper Basin (Merrimelia Formation) (Plate 12a) and the Warburton Basin (Mooracoochie Volcanics) (Plate 12b). This similarity suggests there is a link. It is likely, therefore, that the acid volcanic rock fragments in the Merrimelia Formation originally had rhyodacitic compositions similar to those described by Sun (1996) (Fig. 5.9) in the Warburton Basin. Accordingly, all volcanic and pyroclastic rock fragments observed in the Merrimelia Formation (and Tirrawarra Sandstone) in this study will be described within the guidelines outlined by Sun (1996) (Fig. 5.10). A more detailed discussion on the provenance of volcanic rock fragments is given in Appendix 4b.

A) Rhyodacite Rock Fragments

Porphyritic rhyodacite rock fragments typically exhibit illite altered feldspar and euhedral to sub-euhedral quartz phenocrysts within a foliated groundmass (Plate 12a). Sun (1996) interprets these rocks to be indicative of a coherent effusive lava. In rare cases, fresh feldspar phenocrysts were observed displaying simple and Albite twinning, along with euhedral quartz phenocrysts within a glassy groundmass (Plate 12e[11b]).

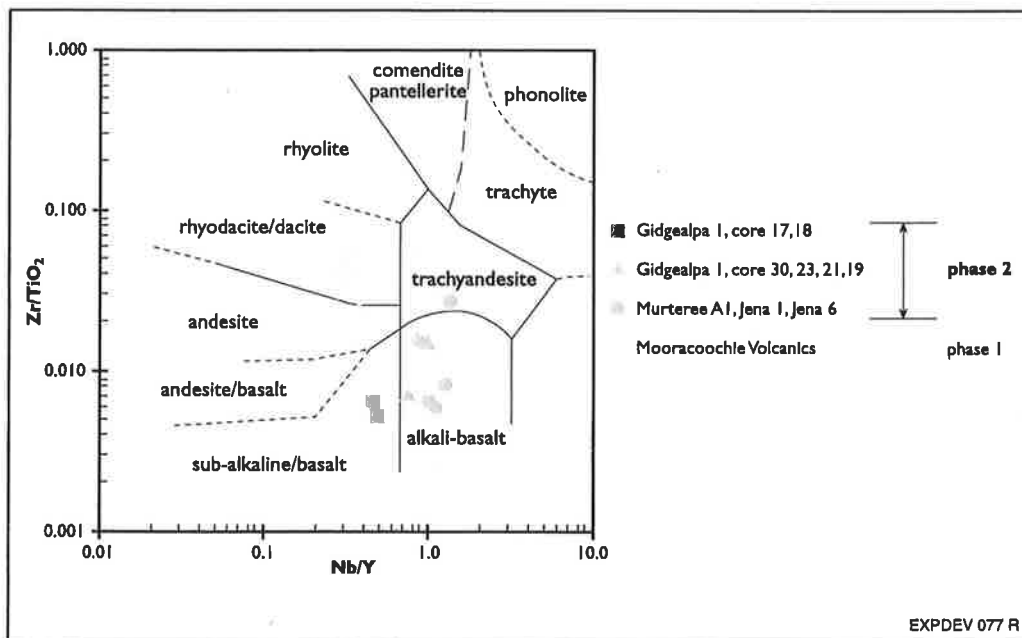


Figure 5.9 Composition of volcanics in the Warburton Basin (From Sun, 1996).

PLATE 12**Acid Volcanic Rock Fragments (Rhyodacite): 1**

A) Photomicrograph – Gidgealpa #3 (2319.4m) (Cross nicols x 5). Close up of rhyodacite rock fragment illustrating distinctive quartz phenocrysts with prominent resorption embayments and fracturing [11h]. Illitised feldspar phenocrysts are also common [4d]. This rhyodacite rock fragment is interpreted to be equivalent to Mooracoochie Volcanics facies association Phase 1, Facies type A (Sun, 1996).

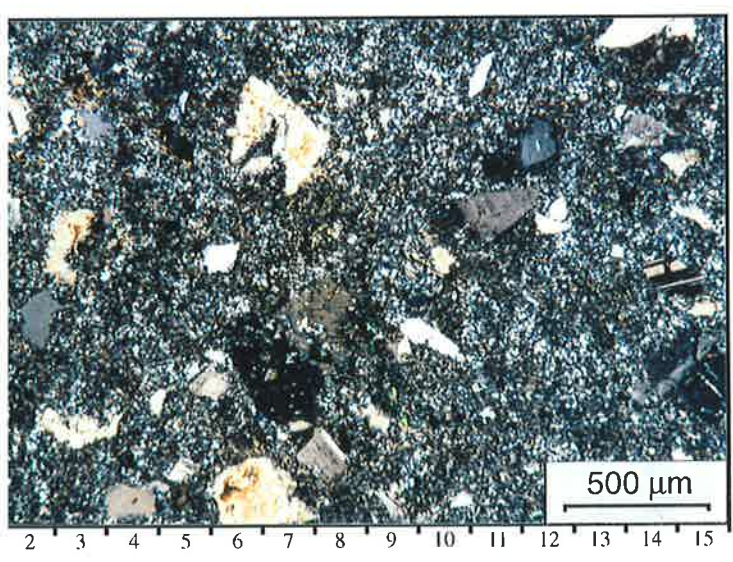
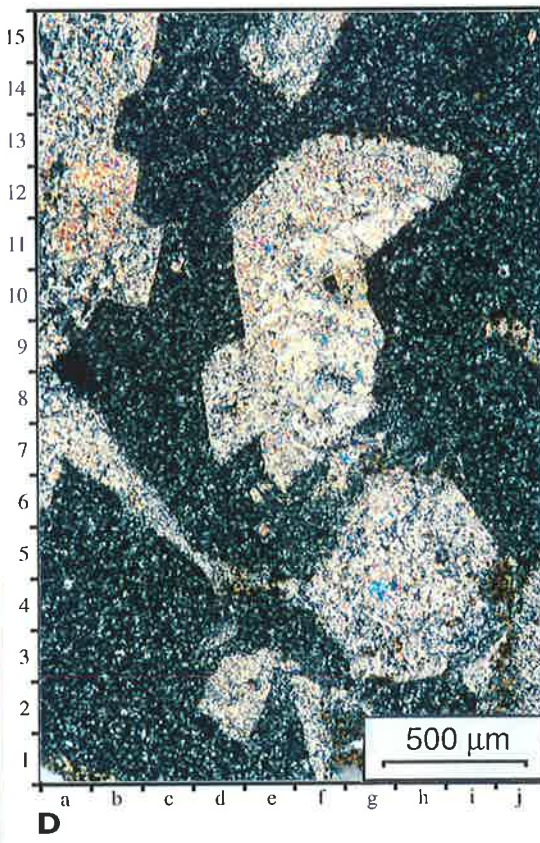
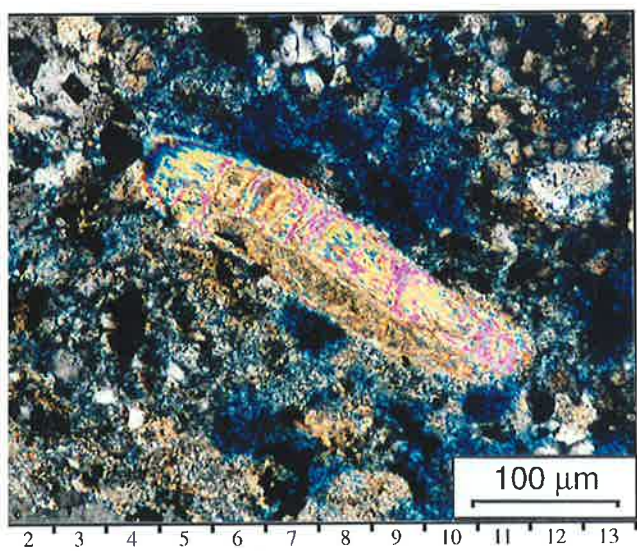
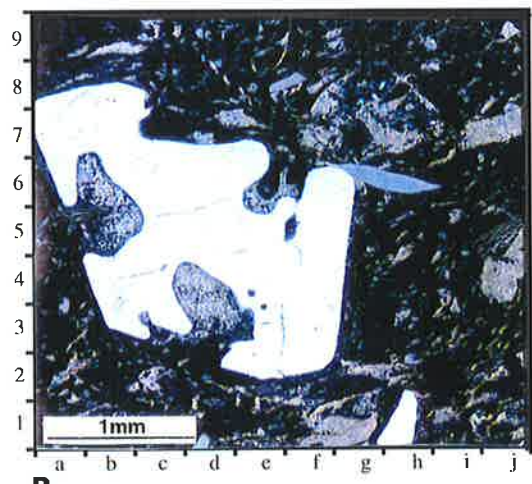
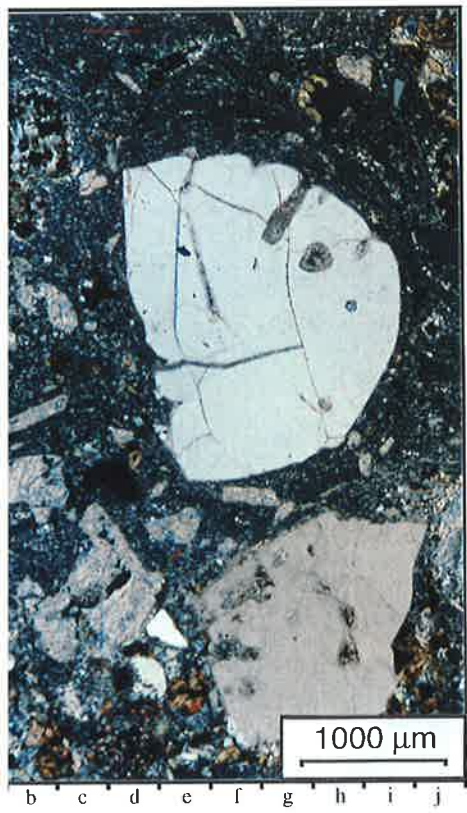
B) Photomicrograph – Taloola #1 (1921.76m) (Cross nicols x 2) Close up of rhyodacitic ignimbrite. The view is dominated by a quartz phenocryst that exhibits large resorption embayments. Compacted and illitised glass shards (fiamme) are also abundant. - Mooracoochie Volcanics (From Sun, 1996).

C) Photomicrograph – Malgoona #2 (2254.57m) (Plane polarised x 10). Close up of devitrified rhyodacite rock fragment with sericitised mica phenocryst prominent [8f].

D) Photomicrograph – Moorari #2 (3136.13m) (Cross nicols x 5). Close up view of Rhyodacite rock fragment illustrating large euhedral to sub-euhedral illitised feldspar phenocrysts [9f]. These rhyodacitic rock fragments display hyaloclastite or granoblastic textures, suggesting a sub-aqueous emplacement.

E) Photomicrograph – Tinga Tingana #1 (2094.35m) (Cross nicols x 5). Broad view of a rare rhyodacite rock fragment (Phase 1, Facies Type A – Mooracoochie Volcanics; Sun, 1996) illustrating fresh (non-illitised) feldspar phenocrysts with Albite twinning common [14f].

Plate 12



It is more common for the glassy groundmass of rhyodacitic rock fragments to have experienced differing degrees of illitisation (Plates 12a and 12c). These acidic rock fragments contain large embayed quartz phenocrysts of varying euhedral to sub-euhedral shape, displaying large resorption embayments within quartz phenocrysts along with occasional conchoidal fracturing and rare mica phenocrysts (Plate 12c). Any fractures and resorption embayments that were observed are generally filled by illite.

	Effusive	Explosive	Resedimented (syn-eruptive)	Epiclastic
Phase 1	Facies A: pheno-quartz-feldspar-porphyritic Facies B: pheno-feldspar porphyritic	Facies C: ignimbrite	Facies D: lava breccia / limestone	Facies E: conglomerate Facies F: tuffaceous sandstone
Phase 2	Facies G: porphyritic Facies H: amygdaloidal		Facies I: resedimented hyaloclastite	

EXPDEV 077 Q

Figure 5.10 Mooracoochie Volcanics facies associations (From Sun, 1996).

Porphyritic rhyodacite clasts were the most commonly observed volcanic rock fragment type observed in both the Merrimelia Formation and Tirrawarra Sandstone (Table 5.2).

i) Spherulite Rhyodacite Rock Fragments

Spherulite rhyodacite rock fragments (Plate 13a) were very rare, observed only in trace amounts (Table 5.2) within five wells throughout the basin. The spherulites were composed of radiating feldspar acicular crystals, and represent alteration during rapid cooling of the parent lava. Subsequent burial has illitised the spherulites and surrounding groundmass.

ii) Devitrified Acid Volcanic Rock Fragments

Devitrified acid volcanic rock fragments (Plates 13c and 13e), constitute 7.1% of all observed rock fragments. This clast type includes a variety of volcanic rock fragments of indistinguishable Warburton Basin facies association,

PLATE 13***Acid Volcanic Rock Fragments (Rhyodacite & Pyroclastic): 2***

A) Photomicrograph – Merrimelia #1 (2944.06m) (Cross nicols x 2). Broad view of spherulitic rhyodacite rock fragment illustrating distinctive feldspar spherulites [13c].

B) Photomicrograph – Malgoona #2 (2259.25m) (Cross nicols x 5). Layered lithic rich crystalline tuff (pyroclastic rock fragment). Cross cutting illite filled fractures [5g] and squeezed feldspar phenocrysts common [10e]. Equivalent to Phase 1, Facies C lithologies in the underlying Mooracoochie Volcanics (Sun, 1996).

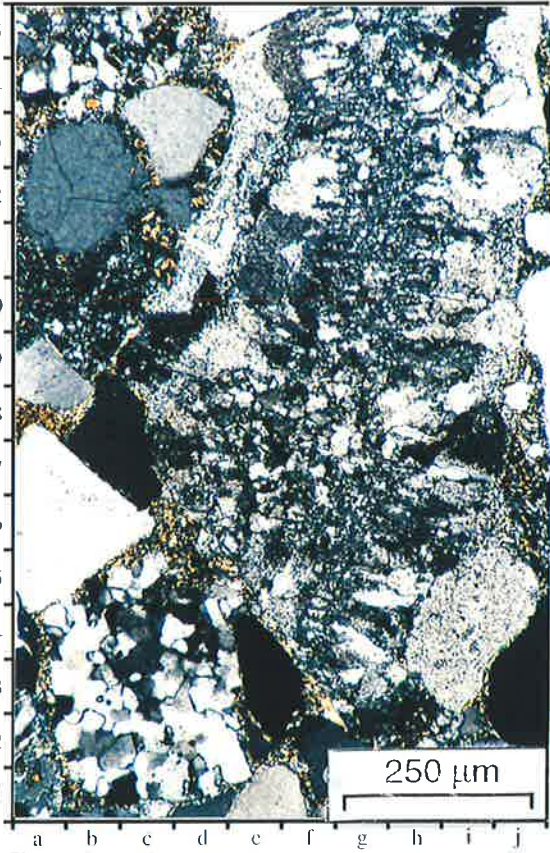
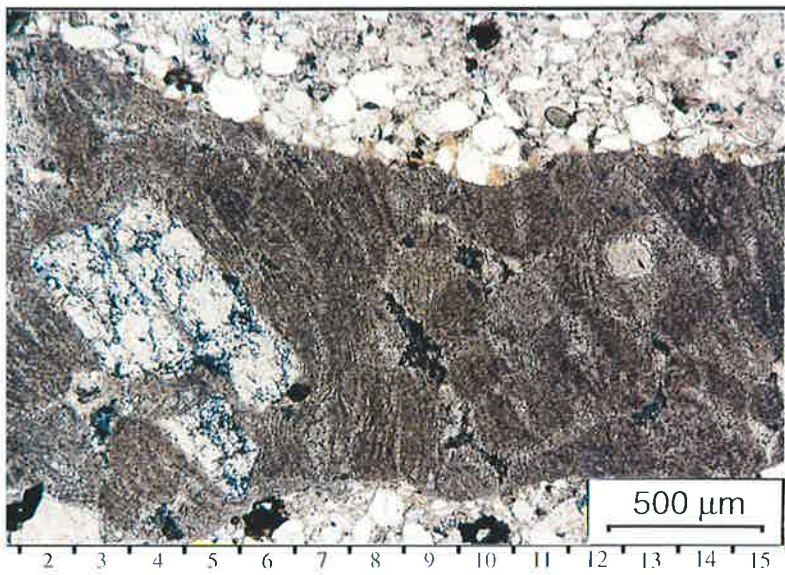
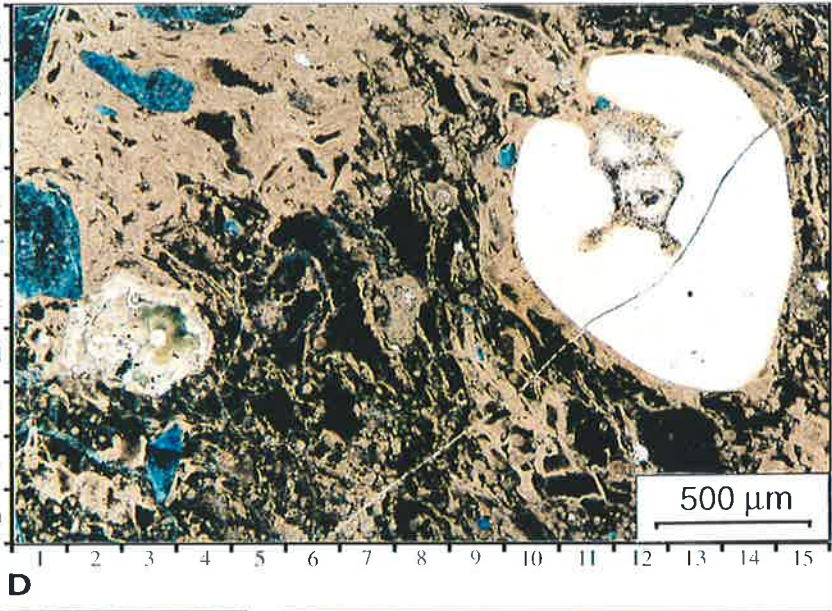
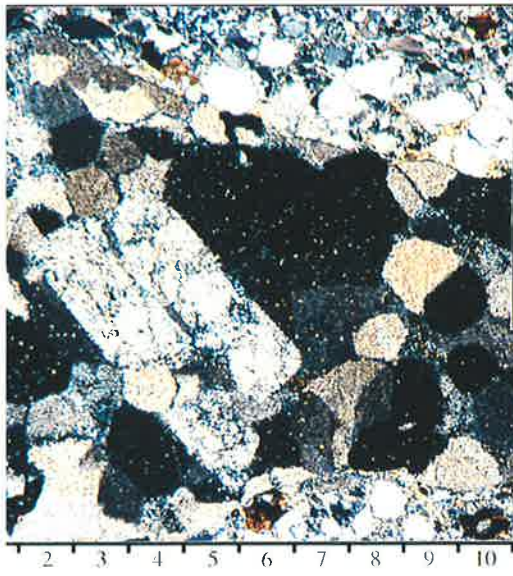
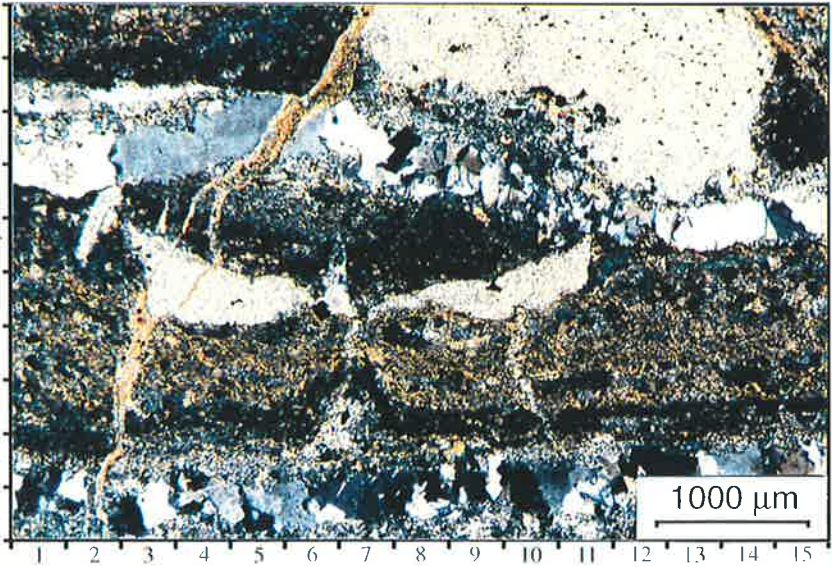
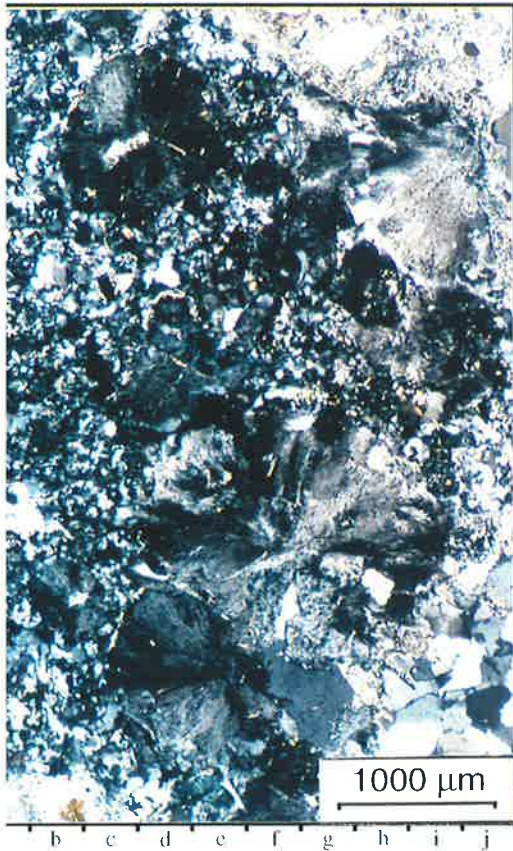
C) Photomicrograph – Spencer #1 (2012.59m) (Cross nicols x 5). Coarse grained devitrified acid volcanic rock fragment. (Note euhedral feldspar phenocryst [5e]). Equivalent to Phase 1, Facies B rhyodacite lithologies of the Mooracoochie Volcanics (Sun, 1996).

D) Photomicrograph – Malgoona #2 (2254.57m) (Cross nicols x 5). Welded ignimbrite rock fragment (pyroclastic rock fragment). Large quartz phenocrysts with extensive resorption embayments [13f]. Note: Ptigmatically distorted fiamme and psuedo-fiamme [10c] along with chlorite filled ammygdule exhibiting illitised coronas [3d]. Secondary pore space can be observed [1f], having formed via the dissolution of unstable glass shards. Equivalent to Phase 1, Facies C lithologies in the underlying Mooracoochie Volcanics (Sun, 1996).

E) Photomicrograph – Spencer #1 (2012.59m) (Plane polarised x 5). Same view as in Plate 13c. This Plate illustrates the flow banded nature of the devitrified acid volcanic rock fragment pictured in the afore mentioned Plate. Equivalent to Phase 1, Facies B rhyodacites of the Mooracoochie Volcanics (Sun, 1996).

F) Photomicrograph – Kudrieke #1 (3108.8m) (Cross nicols x 10). Broad view of acid volcanic rock fragment illustrating a recrystallised granoblastic texture of varying grain size.

Plate 13



F

displaying devitrified groundmass with no phenocrysts. The variable nature of these rock fragments is illustrated in Plates 13c and 13e. The large acid volcanic clast in the middle of Plate 13c under cross nicols exhibits a typical devitrified acid volcanic appearance, but when the same rock fragment is viewed in plane polarised light distinctive flow banding is observed (Plate 13e).

This particular rock fragment may in fact represent a feldspar-phenocryst dominated-porphyrific rhyodacite, typical of the Facies B rhyodacites described by Sun (1996), rather than a massive devitrified volcanic clast.

iii) Hyaloclastite And Granoblastic Rhyolite Rock Fragments

Hyaloclastite and granoblastic textured rock fragments were tentatively identified (Sheard pers. comm., 1995). The granoblastic rock fragments are coarse grained under cross nicols, with illitised micas and hornblende. The hyaloclastite rock fragments have a rhyodacitic appearance, dominated by a jig-saw of contorted euhedral to sub-euhedral illitised feldspar phenocrysts (Plate 12d). The numerous feldspar phenocrysts exhibit angular to cusped outlines. A very small number of these rock fragments were observed in Merrimelia sediments in the Merrimelia Field.

B) Pyroclastic Rock Fragments

Pyroclastic rock fragments constitute less than 4.9% of the total rock fragments observed in Merrimelia facies (Table 5.2). Pyroclastics are concentrated in three regions: Malgoona-Lake Hope-Spencer in the south west, Tinga Tingana #1 in the south and Gidgealpa #3 in the north. The majority of pyroclastic rock fragments observed in Merrimelia samples were from Tinga Tingana #1 (64% of total rock fragment component). Lesser amounts of pyroclastic rock fragments were observed in the Malgoona-Spencer (14% of total rock fragment component) and Gidgealpa (21% of total rock fragment component) regions.

Pyroclastic rock fragments in the Merrimelia Formation are of two types: a very coarse grained (up to 8cm) lithic-rich crystal tuff (Plate 13b) and a welded ignimbrite (Plate 13d). The crystal tuff rock fragments exhibit distorted laminae, poly-crystalline quartz veining, embayed euhedral to sub-euhedral feldspar (illitised) along with quartz phenocrysts, recrystallised poly-crystalline quartz grains, micas and acid volcanic country rock fragments (Plate 13b). Welded ignimbrites are the dominant rock fragment type in the Malgoona region where the majority of pyroclastic clasts exhibit ptigmatically distorted glass shards and fiamme (Plate 13d[10b]), chlorite-

filled amygdals, with illitised rims (Plate 13d[3d]), while brown coronas have commonly nucleated around country rock fragments (0.1mm in diameter).

C) Basic Volcanic Rock Fragments

Basalt, trachytic basalt and chalcedony rock fragments were all observed in trace amounts (0.8%) in Merrimelia sediments in localised areas. Plates 14a and 14b illustrate the two main styles of basic volcanic rock fragments observed in Merrimelia sediments. Plate 14b illustrates a basic volcanic clast, from Tindilpie #2, that is dominated by plagioclase feldspar laths forming a trachytic texture.

i) Trachytic Basalt Rock Fragments

Plagioclase laths in trachytic fragments are generally altered to illite. A number of altered clino-pyroxenes (hypersthene?) and possibly augite crystals have also been observed within these rock fragments as phenocrysts. Small biotite laths are rare and are generally almost completely replaced by siderite. It is common to observe basalt clasts where the majority of the groundmass has been replaced by chlorite. One basaltic rock fragment exhibited laths of plagioclase intergrown with sanidine and quartz.

ii) Amygdaloidal Basalt Rock Fragments

This basaltic rock type is vesicular, containing abundant amygdals and olivine phenocrysts within a fine grained trachytic groundmass. The vesicles (Plate 14a[12f]) and olivine phenocrysts (Plate 14a[5d]), within the amygdaloidal rock fragments, have been commonly replaced with illite.

iii) Ultrabasic Rock Fragments

In Gidgealpa #3, a small number of chloritised basic to ultrabasic clasts were observed. These clasts have been mainly altered to kaolin and exhibit a network of illite-filled fractures and possible olivine pseudomorphs (altered to illite). A corona was observed in one of the ultrabasic clasts, perhaps surrounding an olivine crystal that has now been replaced by illite. The corona too, has been altered to illite. The original composition may well have been finely (fibrous) intergrown clino-pyroxene and/or plagioclase.

5.2.1.3.3 Micro-Pegmatite And Granite Rock Fragments: Petrography

A) Micro-Pegmatite Rock Fragments

Rutilated quartz grains (Plate 14c) were observed in trace amounts in 61% of samples across the basin (Table 5.2).

PLATE 14

Basic Volcanic & Pegmatite Rock Fragments: 1

A) Photomicrograph – Gidgealpa #3 (2312.82m) (Cross nicols x 10). Close up view of an amygdaloidal basalt rock fragment, illustrating illite filled vesicles [12f], and illite filled olivine phenocrysts [5d]. Equivalent to Facies Type H (Mooracoochie Volcanics) (Sun 1996).

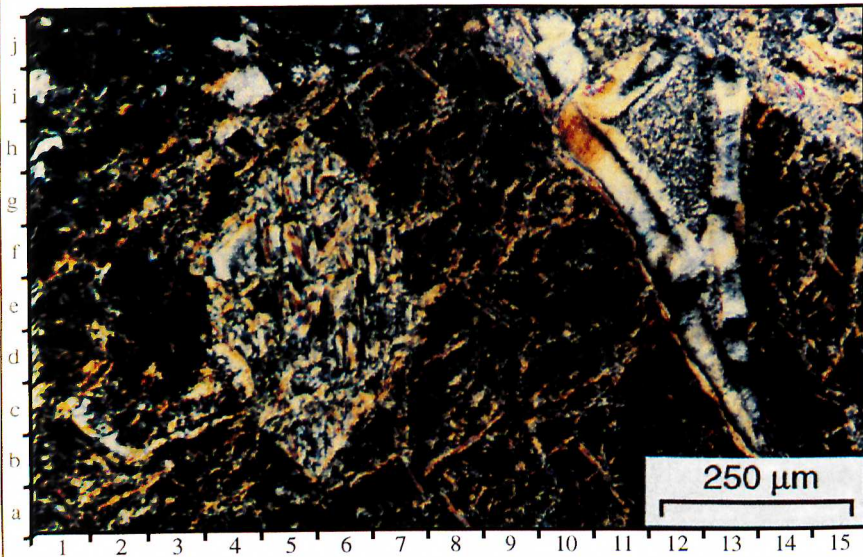
B) Photomicrograph – Tindilpie #2 (3364.43m) (Cross nicols x 10). Broad view of a trachytic basalt rock fragment, illustrating chlorite altered plagioclase feldspar laths [6h]. Equivalent to Facies Type G (Mooracoochie Volcanics) (Sun 1996).

C) Photomicrograph – Lake Hope #1 (2493.7m) (Cross nicols x 10). Broad view of a rutilated quartz grain in a pegmatite rock fragment.

D) Photomicrograph – Merrimelia #1 (2943.6m) (Plane polarised x 10). Broad view of a quartz grain with tourmaline inclusions [8h].

E) Frequency histogram. Granite rock fragments: Merrimelia Formation.

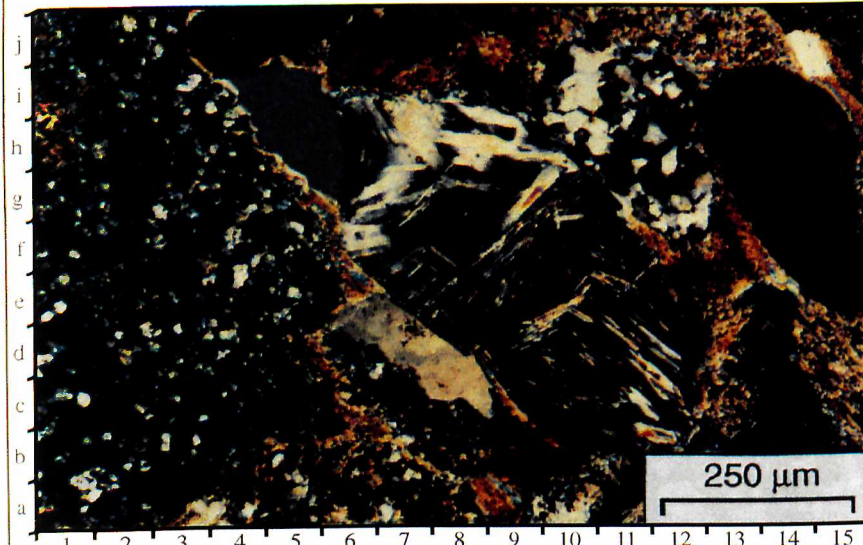
Plate 14



A



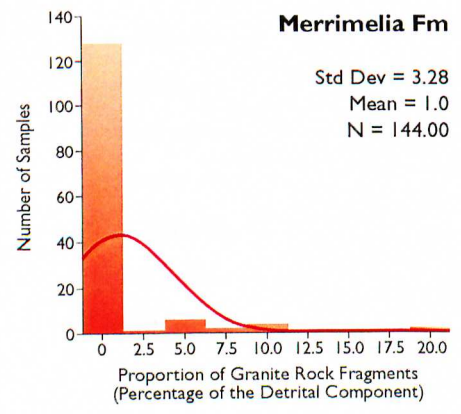
B



C



D



E

Tourmaline inclusions within quartz grains (Plate 14d) were also noted in trace proportions. These rutilated and tourmaline-impregnated quartz grains are possibly pegmatitic in origin.

B) Granitic Rock Fragments

Two different granitic rock fragment types are observed in Merrimelia sediments in less than 15 samples (out of 144) (Plate 14e).

i) Graphic Textured Granite Rock Fragments

The most distinctive granitic rock fragments exhibit graphic texture (Plate 15a), intergrown silica and feldspar. In most cases the feldspar, has been altered or replaced by illite leaving a distinctive 'hieroglyphic' texture. The intricately shaped quartz crystals of these rock fragments make up the whole clast. A trace amount of similarly intergrown granite clasts exhibiting myrmekitic (Plate 15b) and granophyric textures were also noted.

No graphic or myrmekitic textured granite has been observed in the locally derived Big Lake Suite (Boucher pers., comm., 1997 and Sun pers. comm., 1997) so it is likely then that these distinctive rock fragments have an extrabasinal provenance. A detailed discussion of graphic granite provenance is given in Appendix 4b.

Graphic textured granite is observed throughout the Merrimelia Formation (Fig. 5.11). This wide distribution combined with the distinctive appearance of this rock fragment has facilitated its use as a marker for clast movement into and within the Cooper Basin.

ii) Granular Granite Rock Fragments

Granular textured granite rock fragments are more commonly observed and typically exhibit illitised feldspars and micas. These rock fragments have a similar appearance to litharenite rock fragments with the exception that micas are observed terminating within quartz and feldspar crystals. The majority of granite clasts in the Cooper Basin were noted at Tallalia #1 in western Queensland. Plate 15c is typical of the granular granite rock fragments from these Queensland samples. Granular granite fragments in Tallalia #1 do not exhibit litharenite-like features, but fresh, intergrown, large microcline feldspars (Plate 15c[4b]), biotite (Plate 15c[7d]), and quartz. The freshness of these granitic rock fragments suggests they have undergone minimal transport.

PLATE 15

Granitic & Metamorphic Rock Fragments

A) Photomicrograph – Merrimelia #1 (2943.6m) (Cross nicols x 5). Close up of a graphic textured granite rock fragment illustrating the hieroglyphic style of the remnant quartz. The feldspar component, between the quartz [11d], has been altered to illite.

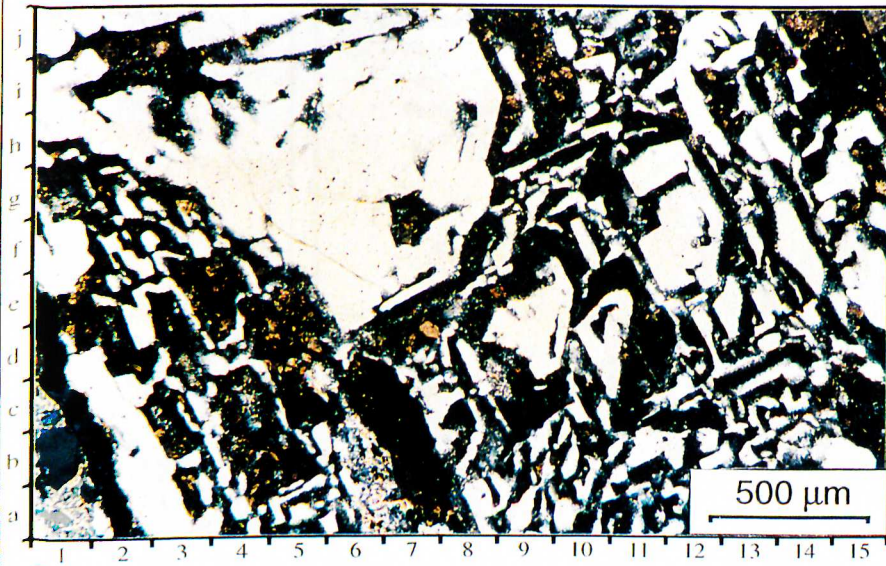
B) Photomicrograph – Tallalia #1 (3167.4m) (Cross nicols x 20). Broad view of a granitic rock fragment, equally dominated by a microcline feldspar [11d] and a quartz grain exhibiting myrmekitic feldspar and quartz [8h].

C) Photomicrograph - Tallalia #1 (3169.9m) (Cross nicols x 5). Broad view of a an unaltered granular granite rock fragment dominated by microcline feldspar crystals.

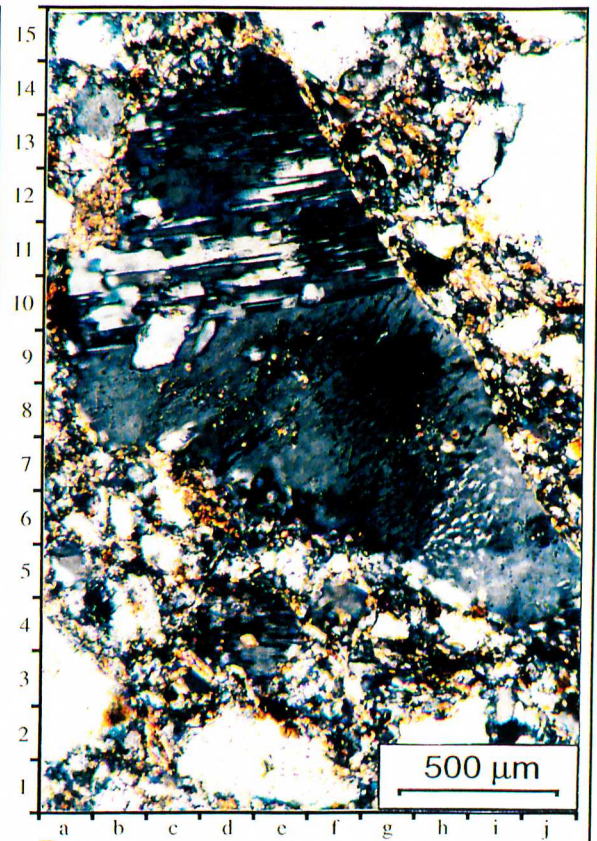
D) Photomicrograph – Tinga Tingana #1 (2094.35m) (Cross nicols x 5). Broad view of a biotite dominated schist, exhibiting a single undeformed foliation direction.

E) Photomicrograph – Welcome Lake #1 (2923.8m) (Cross nicols x 20). Broad view of a crenulated muscovite dominated schist. Note the muscovite has been altered to illite [7d].

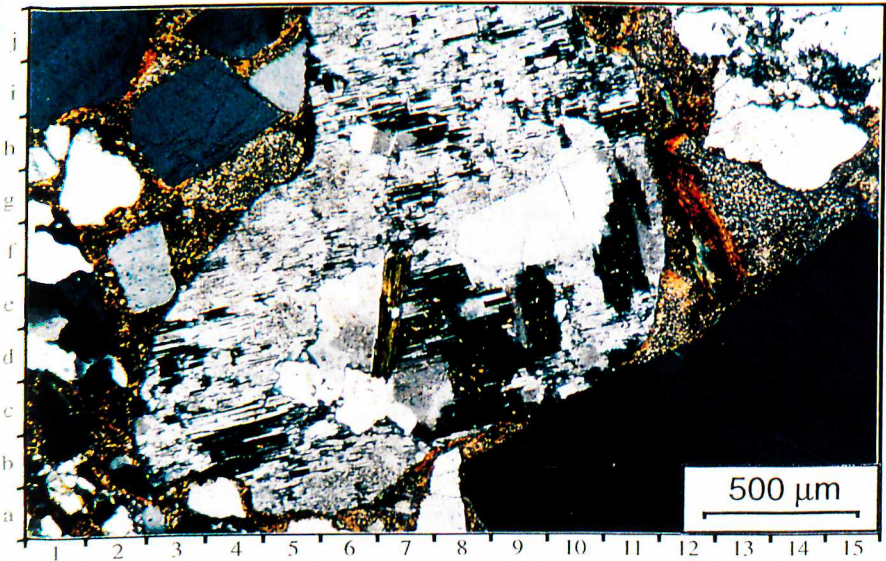
Plate 15



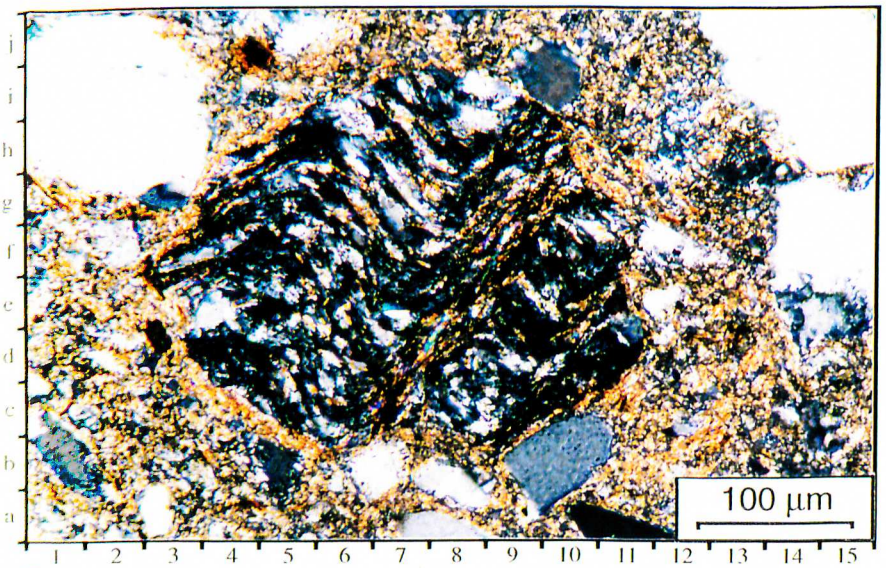
A



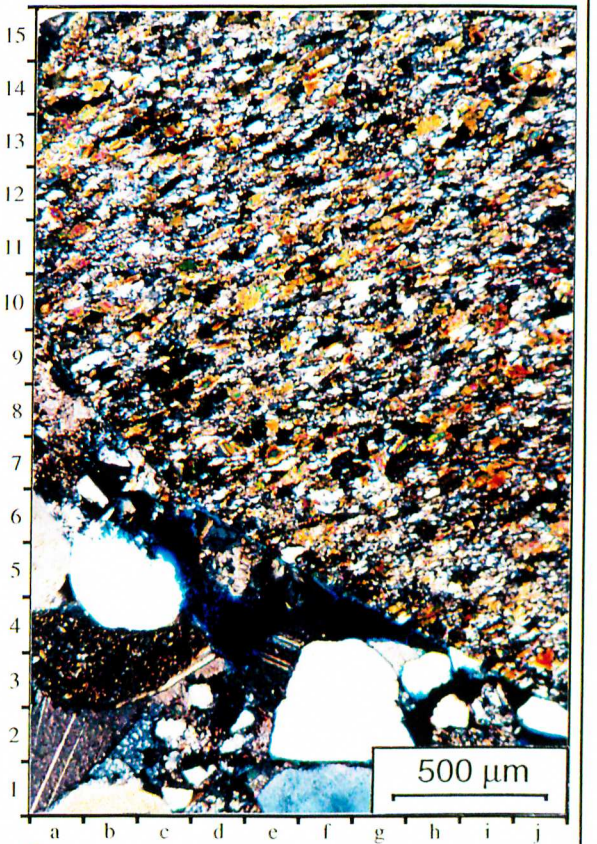
B



C



E



D

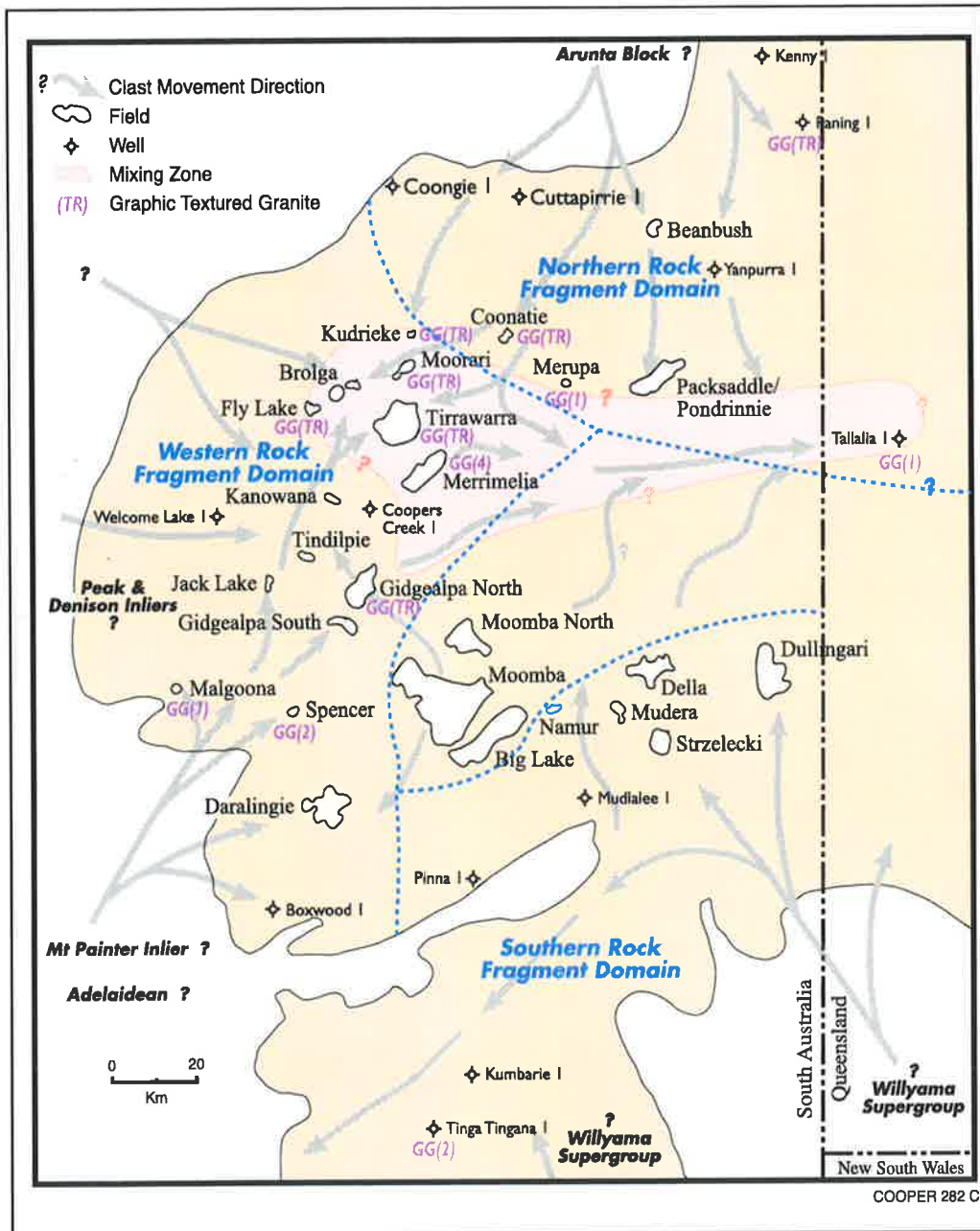


Figure 5.11 Rock fragment domains overlain by the distribution of graphic textured granite in the Merrimelia Formation and Tirrawarra Sandstone. (Modified from Cubitt et al., 1998).

5.2.1.3.4 Metamorphic Rock Fragments Petrography

Metamorphic rock fragments display twenty five lithologies accounting for 25.5% of the total rock fragments observed in the Merrimelia Formation (Table 5.2).

Only the most numerous metamorphic rock fragments are described here. A full list of metamorphic rock fragments is given in Appendix 4a. Metamorphic rock fragments are observed in just over half of the samples described (Fig. 5.12).

A) Low grade Metamorphic Rock Fragments

A positive identification of many low grade metamorphic rock fragments in Merrimelia sediments is not possible as they have been influence by alteration. These rock fragments do, however, commonly exhibit a recrystallised silica groundmass and porphyroblasts of quartz. In rare instances, they contain dark clinozoisite and epidote (?) as secondary porphyroblast minerals.

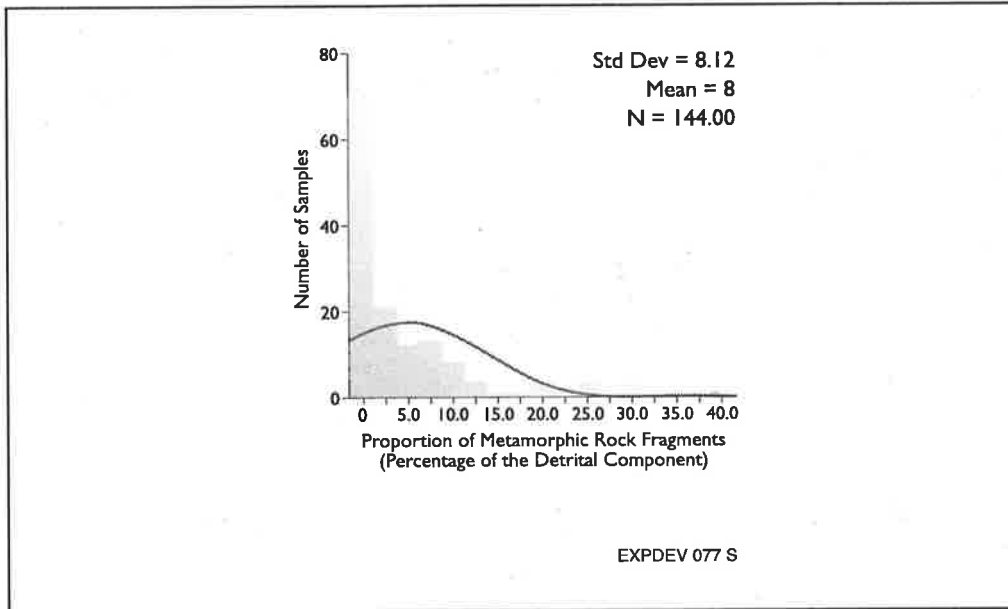


Figure 5.12 A histogram of metamorphic rock fragments in Merrimelia sediments (percentage of detrital component).

B) Phyllite Rock Fragments

Phyllites are rare rock fragments, but are observed throughout the entire Cooper Basin in trace amounts. These clasts exhibit micas and/or illite laths that are aligned along cleavage planes. Phyllites contain small proportions of quartz and are occasionally spotted.

C) Schist and Gneissic Rock Fragments

Plates 15d and 15e illustrate the two main types of schist clasts observed in Merrimelia sediments, the main difference being the dominant mica type within the schist fragments. Plate 15e illustrates a crenulated mica schist (now almost totally illitised) while Plate 15d shows a biotite-dominated schist. Gneissic clasts are dominated by schistose quartz crystals of varying size (quartz grains form the main porphyroblasts) with muscovite and subordinate biotite. Micas in the gneissic rock fragments form parallel bands between sutured mono-mineralic and poly-crystalline quartz crystals (Plate 16a).

PLATE 16

Metamorphic Rock Fragments

A) Photomicrograph – Dullingari #1 (2707.37m) (Cross nicols x 5). Close up view of a quartz dominated gneissic rock fragment, illustrating illitised mica between poly quartz grains [8d].

B) Photomicrograph – Spencer #1 (2004.26m) (Cross nicols x 20). Close up view of a sedimentary quartzite exhibiting a quartz arenite composition. Psammite rock fragments have litharenitic compositions, while pelite rock fragments are dominantly argillaceous in composition.

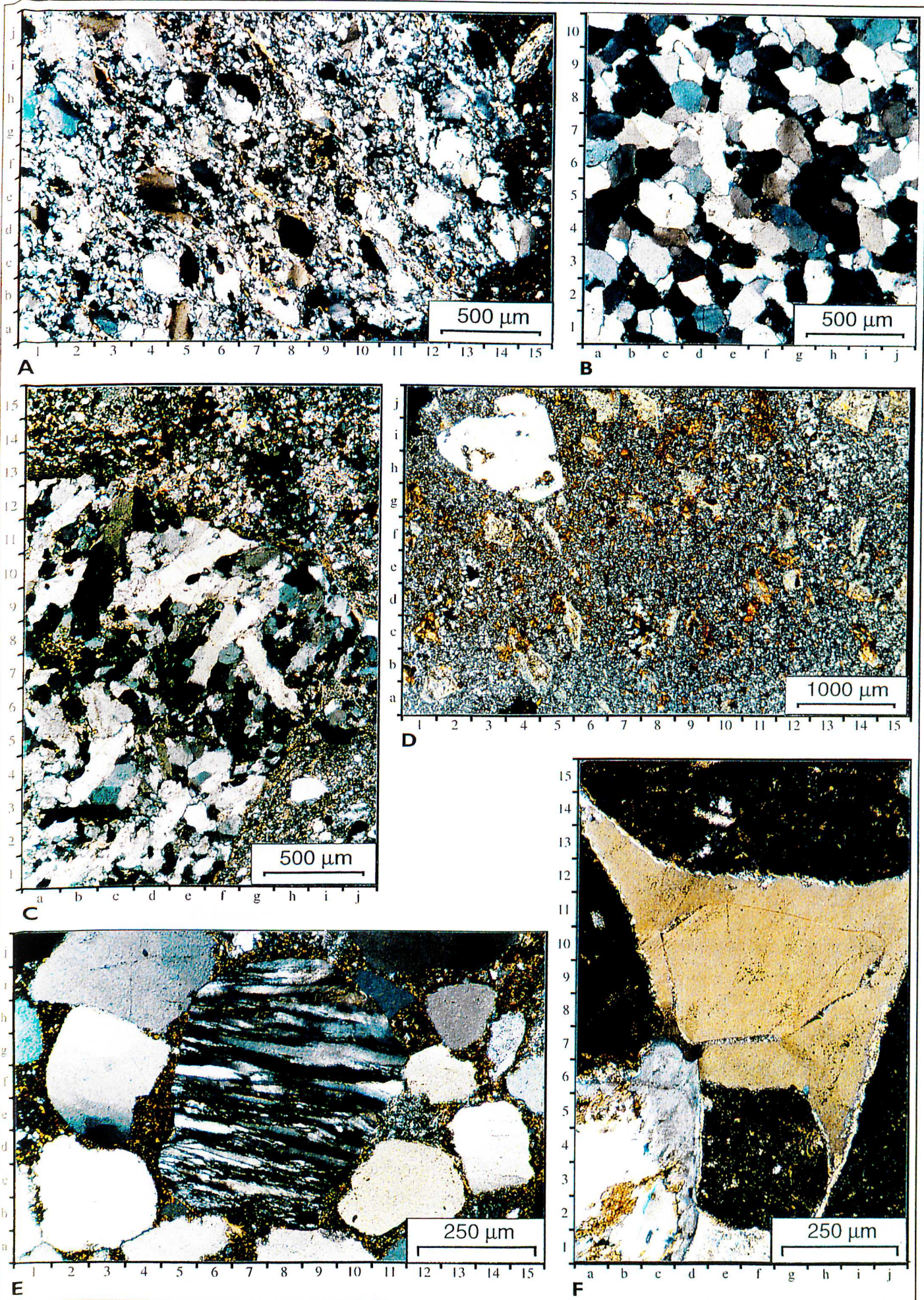
C) Photomicrograph – Merrimelia #1 (2943.6m) (Cross nicols x 5). Broad view of a rare, enigmatic quartzite rock fragment, which exhibit elongate, occasionally twinned hexagonal mono-mineralic quartz crystals [8f]. These clasts are tentatively interpreted to be recrystallised evaporitic minerals.

D) Photomicrograph – Gidgealpa #7 (2279.59m) (Cross nicols x 2). Close up view of a rhyodacite with a recrystallised, poly-crystalline quartz groundmass [7e] and feldspar phenocrysts which have also been replaced by poly-crystalline quartz [3e]. These rock fragments represent recrystallised pyroclastic fallout deposits

E) Photomicrograph – Kudrieke #1 (3108.8m) (Cross nicols x 10). An example of a meta-poly-crystalline quartz grain, illustrating foliation induced by extreme metamorphic conditions.

F) Photomicrograph – Spencer #1 (2052.82m) (Cross nicols x 10). Close up view of a recrystallised pore and quartz grain in the Mooracoochie Volcanics. Note that the fluid inclusions [11d] transect the quartz grain quartz cement boundary.

Plate 16



D) Psammite and Pelite Rock Fragments

Psammite rock fragments are defined here as recrystallised sandstones of litharenite composition and contain labile grains and remnant clays. A typical psammite rock fragment consists of large poly-crystalline quartz grains that are surrounded by a very fine grained, highly recrystallised quartz groundmass. The large poly-crystalline quartz grains exhibit sutured contacts with the groundmass and in some cases with adjacent quartz crystals. Remnant illite and unidentifiable rock fragments are also observed in these rock fragments. Illite partially surrounds quartz grains and replaces rare lithics. Other psammite rock fragments exhibit quartz (with rutile inclusions), trace feldspar grains (microcline), and rock fragments that have been altered to both illite and kaolin.

A very small number of pelitic rock fragments were observed which exhibit a schistose cleavage, strained quartz grains, and a high proportion of illite-altered labile rock fragments.

E) Quartzite Rock Fragments

Two varieties of quartzite rock fragments were identified in Merrimelia sediments. The most common type is sedimentary quartzite (Plate 16b) exhibiting a quartz arenite composition where quartz cement is visible surrounding all detrital quartz grains.

Within the quartzite rock fragments, grain-lining illite and illitised rock fragments are commonly noted along with rounded zircon grains. Sutured and concavo-convex contacts (Plate 16b[7f]) are common with orientation of quartz grains also evident (Plate 16b).

F) Meta-Acid Volcanic Rock Fragments

Recrystallised rhyodacite and pyroclastic rock fragments were observed in 16 wells throughout the basin but are most prevalent in wells that were underlain by the Mooracoochie Volcanics of the Warburton Basin (Malgoona #4, Coongie #1 and Paning #1). These rock fragments exhibit a totally recrystallised groundmass which consists of very fine grain intergrown poly-crystalline quartz crystals (Plate 16d[4b]). Nestled within this poly-crystalline quartz groundmass are remnant illitised feldspar phenocrysts (Plate 16d [4b]), and quartz phenocrysts many of which have also been recrystallised and have a poly-crystalline quartz appearance (Plate 16d[3e]). It is also common to observe poly-crystalline quartz veins transecting these clasts. Illite

stringers (laminae) are commonly observed transecting recrystallised rhyolite rock fragments.

Other features seen in meta-volcanic rocks include alternating coarse and fine horizontal laminae which have been recrystallised into coarse and fine quartz grains respectively. A number of grains appear to have caused sagging of the fine laminae due possibly to micro-ballistic impact. These clasts may represent pyroclastic surge and fallout deposits which have been subsequently recrystallized. A small number of meta-spherulite rhyodacite rock fragments were also observed.

G) Meta-Poly-Crystalline Quartz Grains

Metamorphic poly-crystalline quartz clasts have an intergrown appearance, with highly irregular sutured contacts between individual quartz crystals common (Plate 10[2g]). Other poly-crystalline-quartz grains exhibit aligned crystals forming a distinctive schistose texture (Plate 16e).

5.2.1.3.5 Feldspar And Accessory Component: Petrography

A) Feldspar

Feldspar grains constitute the smallest framework component in Merrimelia sediments (Fig. 5.1). The ternary diagram (Fig. 5.2) indicates that only a small number of samples contain appreciable amounts of feldspar. The majority of feldspars have been totally altered to kaolin and illite coalescing with the surrounding illite matrix (Plate 17d). A smaller proportion of feldspar grains, particularly those in the aeolian sandstones in the Merrimelia Field occur as partially altered feldspar grains where illite replaces the grains along cleavage planes (Chapter Six - Plates 27a & 27b). A small number of fresh feldspar grains were observed in Tallalia #1 (Queensland) and in Tindilpie #2 (South Australia).

These fresh feldspar grains displayed extinction patterns that were indicative of plagioclase (Albite twinning) (Plate 17a[6g]) and microcline.

Microperthite feldspar grains were also observed (Plate 17b[5j]). These grains exhibit a distinctive "intergrown" texture of potassium-rich and sodium-rich feldspar (MacKenzie and Guilford, 1980). These grains consist of parallel alternating white and dark banding, where the light areas are composed of sodium-feldspar and the darker regions potassium feldspar.

PLATE 17

Accessory Detrital Minerals: 1

A) *Photomicrograph – Tallalia #1 (3167.93m) (Cross nicols x 20). Broad view, illustrating a “fresh” plagioclase feldspar grain exhibiting albite twinning [5g].*

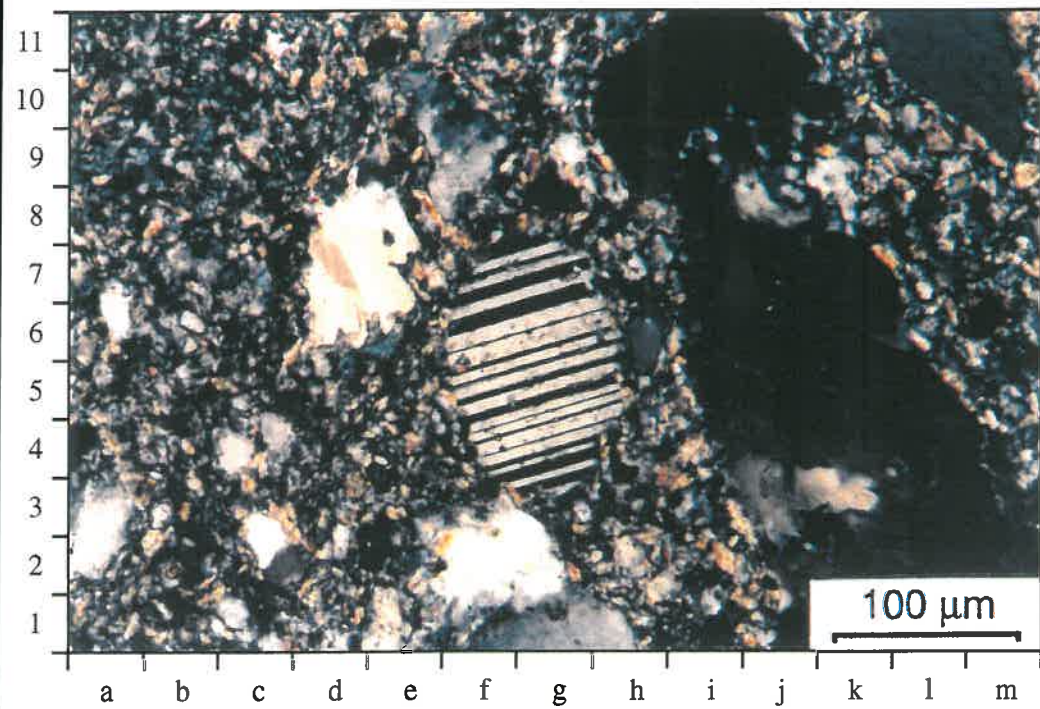
B) *Photomicrograph – Tallalia #1 (3167.93m) (Cross nicols x 10). Broad view of an unaltered perthite feldspar grain exhibiting distinctive twinning [4i].*

C) *Photomicrograph – Tirrawarra #7 (3056.66m) (Reflected x 50). Broad view of a framboidal aggregate of pyrite [8g], within an organic laminae.*

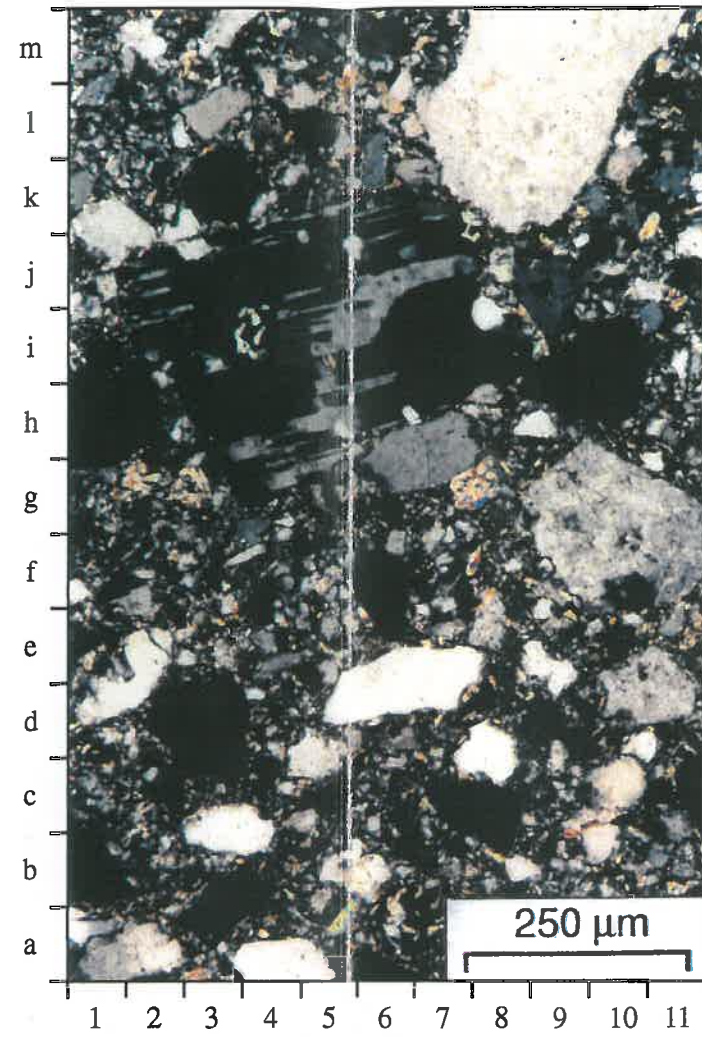
D) *Photomicrograph – Kenny #1 (2945.80m) (Fluoro x 20). Broad view of feldspar grains which have been totally altered to kaolin (black “dots” [6e]). Note: Illite infills remnant pore space and has also formed interwoven with kaolin booklets [6e].*

E) *Photomicrograph – Gidgealpa #3 (2319.4m) (Reflected x 20). Close up of detrital ilmenite grain (?) showing intricate crystal forms.*

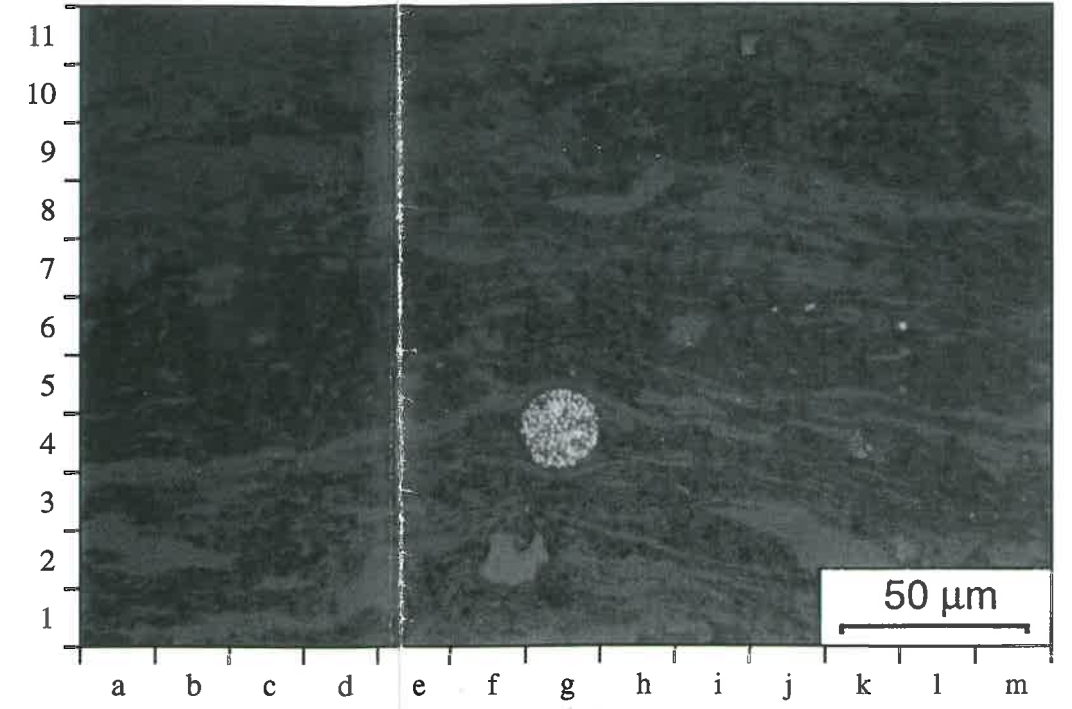
Plate 17



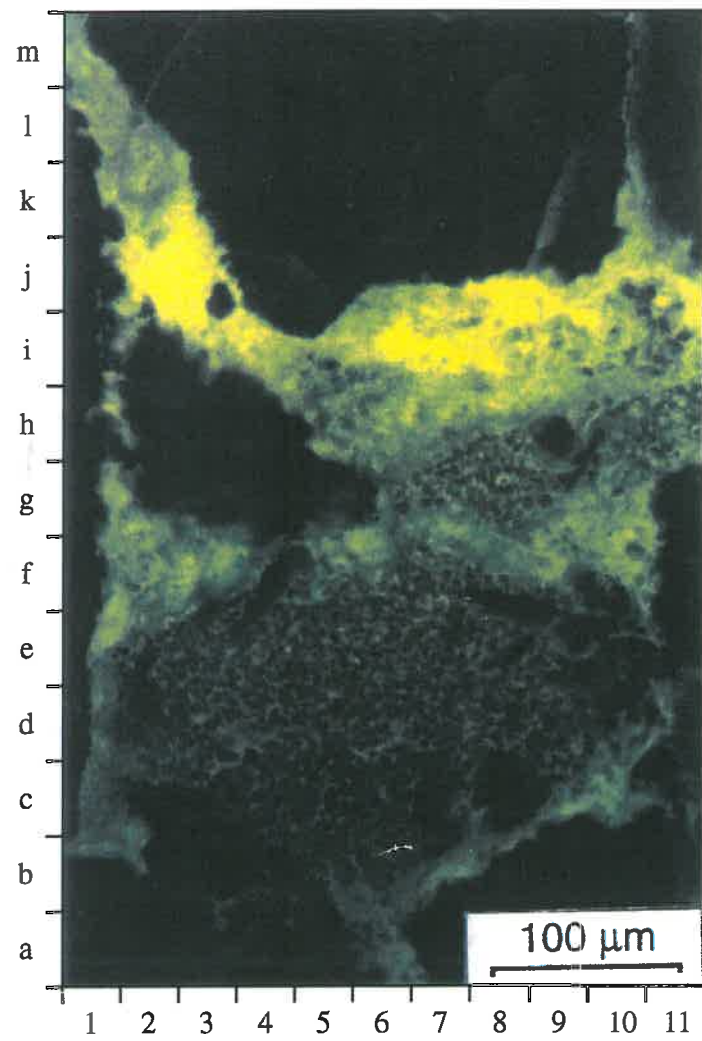
A



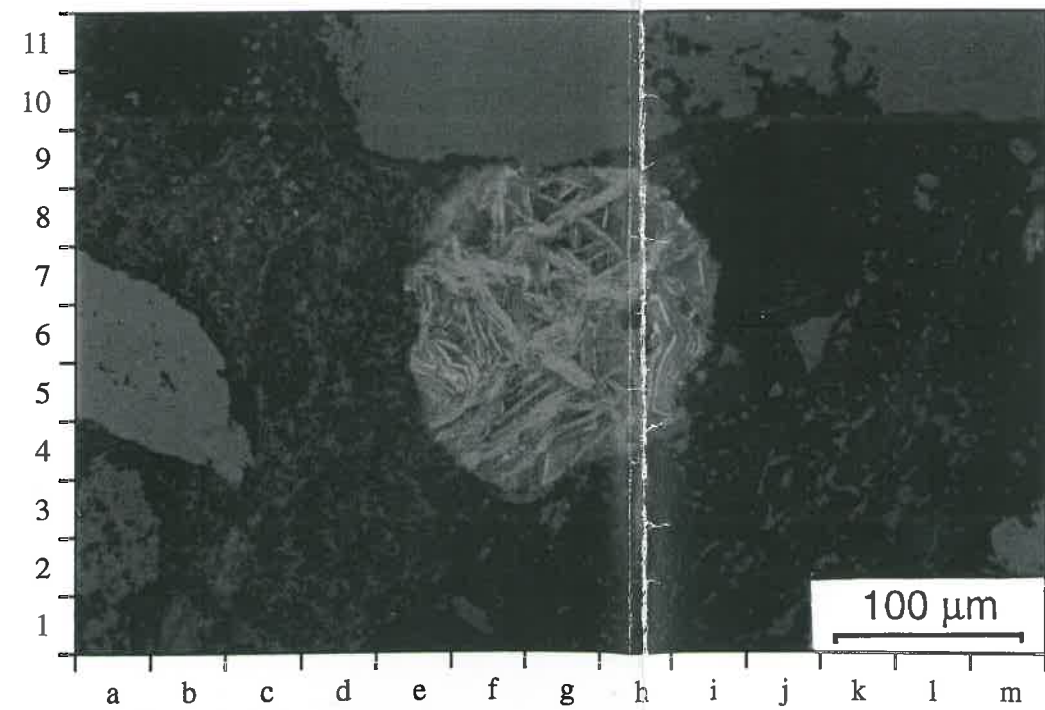
B



C



D



E

B) Micas

Micas were observed in trace amounts, approximately 1.7% of the total Merrimelia detritus (Table 5.2). The majority of micas are illitised muscovite and are generally deformed around more competent framework grains showing varying degrees of burial compaction distortion (Plate 18a). The detrital mica illustrated in Plate (18a) is a particularly fresh mica found in samples where fresh granite clasts predominate.

C) Accessory Minerals

Accessory minerals account for less than 1% of the total Merrimelia detritus (Table 5.2). The main accessory minerals observed were well rounded zircon (Page 163 - Fig. 5.14c[9j]) and tourmaline grains (Plate 18b[14d]). Rounded grains of rutile and ilmenite(?) (Plate 17e) were also noted in Merrimelia sediments. Compositional analyses confirms this petrographic identification (Table 5.5).

Magnetite was observed in a small number of highly contorted, foliated rhyodacite rock fragments. The magnetite, is seen as opaque inclusions, that permeate these rock fragments. This mineral is detrital in nature, and has not been observed forming *insitu*. Haematite was observed in Tirrawarra #2, but absent elsewhere.

SAMPLE	SiO ₂	TiO ₂	Al ₂ O ₃	Cr ₂ O ₃	MgO	CaO	MnO	FeO	ZnO	Na ₂ O	F	K ₂ O	Cl
MAL 2D	0.25	88.84	0.25	0.06	0	0.05	0	2.43	0	0	0.86	0.02	0.05
MAL 2D	0.63	84.73	0.54	0.04	0	0.11	0.01	1.67	0.06	0.04	0	0.12	0.05
MAL 4A	1.17	90.07	0.39	0	0.05	0.14	0.07	0.60	0.07	0	0.03	0.22	0.02
TIRA 8A	0.26	93.3	0.23	0.06	0	0.06	0	0.21	0.04	0.03	0	0.05	0.01

Table 5.5 Rutile microprobe composition (Wt.%).

Anatase was confirmed via TEM observations and EDAX compositional analysis (Chapter Six - Plate 24d) in both Merrimelia #18 and Malgoona #4. Grund (1966) described rounded anatase grains associated with zircons and tourmalines in Merrimelia #3, within a large angular to sub-angular pebble.

5.2.1.3.6 ORGANIC MATTER AND SOIL DEVELOPMENT(?)

Fluorescence microscopy was needed to identify the trace amounts (<1%) of organic matter in Merrimelia sediments. A green fluorescence colour (Plate 18d) distinguishes organic matter from illite (Plate 17d).

PLATE 18

Accessory Detrital Minerals: 2

A) SEM Photomicrograph – Durham Downs #1 (2686.5m). Detrital mica flakes [5e] with surrounding boxwork [2f] and filamentous illite [4b].

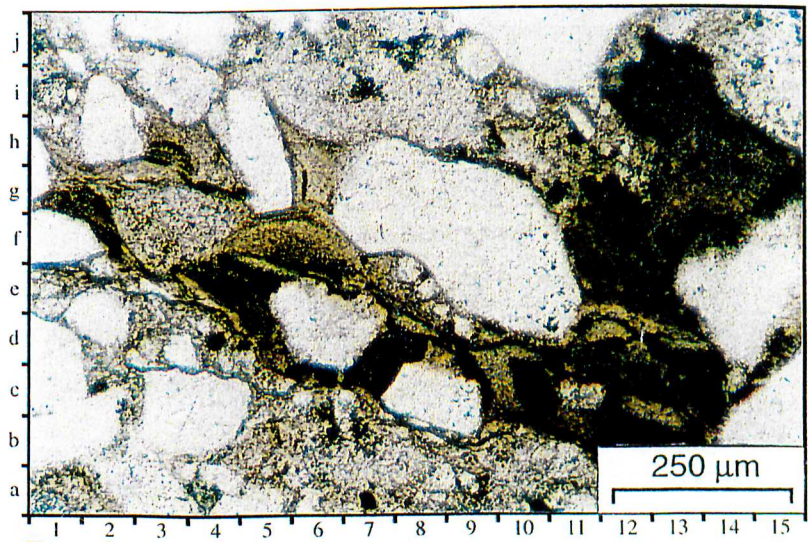
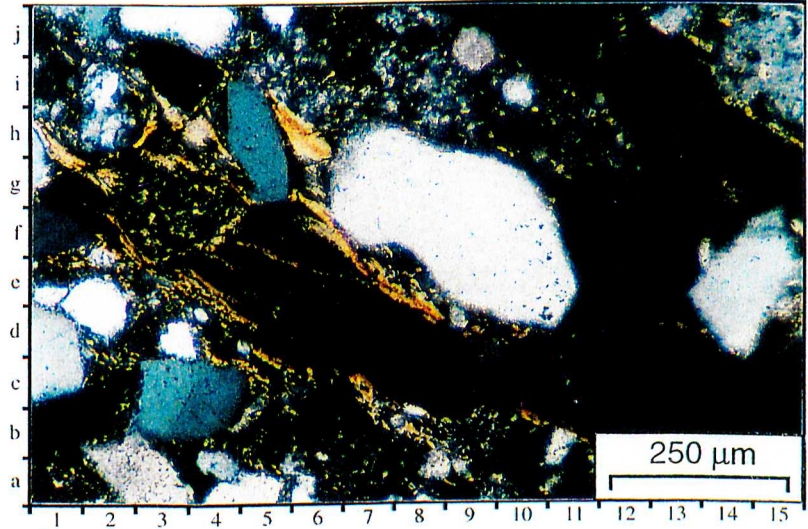
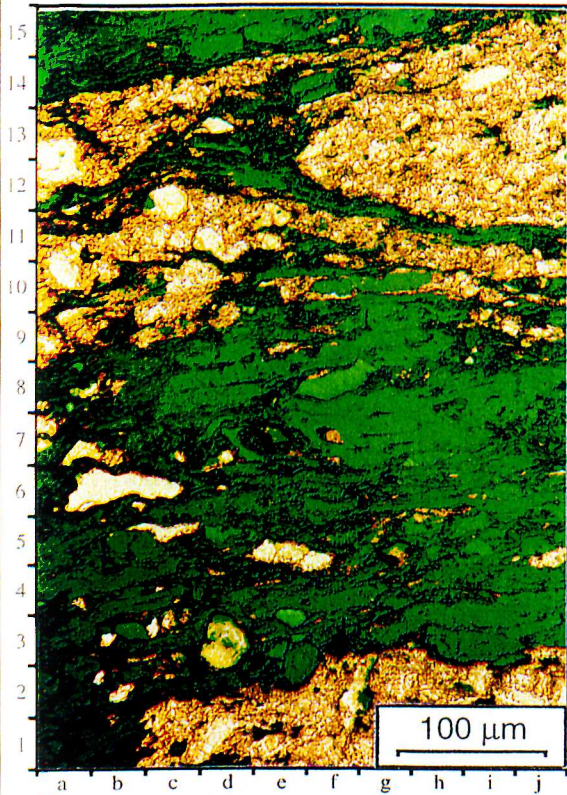
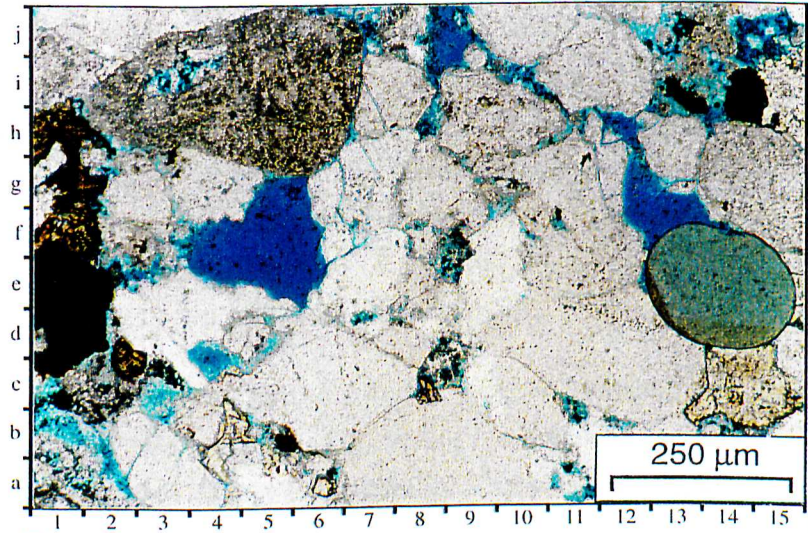
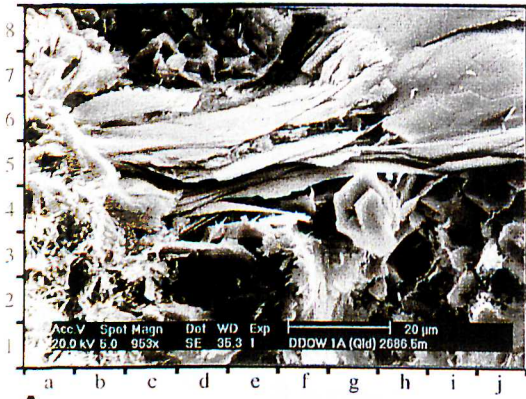
B) Photomicrograph – Lake Hope #1 (2499.49m) (Plane polarised x 10). Rounded tourmaline grain.

C) Photomicrograph – Merrimelia #1 (2644.67m) (Cross nicols x 10). The lack of internal structure indicates these rock fragments differ from other argillaceous rock fragments (shale). These clasts may represent a frozen, buried soil horizon, which thawed with depth and was subsequently deformed via overburden pressure. Alternatively they may represent partially chloritised and deformed mica flakes.

D) Photomicrograph – Tirrawarra #7 (3056.66m) (Fluoro & plane polarised x 20). Organic laminae (green) that formed insitu.

E) Photomicrograph – Merrimelia #1 (2644.67m) (Plane polarised x 10). Same view as Plate 18c, illustrating the nature of these enigmatic argillaceous rock fragments.

Plate 18



It appears that localised ponding of water in a delta top environment was the main method by which organic matter was preserved in the shale laminae.

More unusual shale like rock fragments were noted in Merrimelia sediments. These fragments, illustrated in Plates 18c & 18e, appear to flow between framework grains, as pseudomatrix. In cross nicols however these squeezed "shale rock fragments" do not exhibit the typical illite birefringence that is generally associated with pseudomatrix and shale rock fragments (Chapter six - Plate 24c[11g]).

It is possible that these rock fragments may just be partially chloritised biotite flakes. Alternatively, these shale clasts maybe a product of frozen soil formation. Shale clasts with similar cross-nicol characteristics have been described in Canada by King (pers. comm., 1998).

The development (and preservation) of frozen soil horizons in the Merrimelia glacial complex is likely. Such soil fragments would be preserved higher in the Merrimelia sequence (M1), when glacial activity waned and soil development in the lower fan was more likely.

5.2.2 FACIES CONTROL ON SEDIMENT COMPOSITION

The proportions of rock fragment framework grains and authigenic minerals is controlled by the mode of sedimentary deposition (Table 5.6). Poorly sorted lithologies are generally dominated by rock fragments (Table 5.6), whilst better sorted rocks tend to be quartz-dominated (Table 5.6). Facies thus controls the composition of sediments in the Merrimelia Formation. Rezaee and Lemon (1996a) in the Moorari-Fly Lake-Brolga region, observed a similar relationship in the Tirrawarra Sandstone (facies controls on diagenesis and reservoir quality are discussed in Chapters Six and Nine respectively).

5.2.3 COMPETENT AND INCOMPETENT ROCK FRAGMENTS

Competent and incompetent framework components are defined as follows:

- 1) Competent framework components withstand ice and water transport intact.
- 2) Incompetent, labile or ductile framework components are eventually destroyed by transport and reworking processes.

Mechanical compaction increases with burial, further weakening incompetent grains while competent grains remain intact providing a rigid rock framework. Table 5.7 lists the main competent and incompetent rock fragments observed in both

Merrimelia and Tirrawarra sediments. These lithic ductility categories broadly agree with the experimental results of Pittman and Larese, (1991).

A detailed discussion on the compactional properties displayed by the three groups of rock fragments on is given in Chapter Nine (Reservoir Quality).

FACIES TYPE	Rock Fragment Average	Rock Fragment Std Dev	Quartz Ave	Quartz Std Dev
LSZ - (Lacustrine Shore Zone)	5.8	13.5	45.5	20.5
ID - (Glacio-Aeolian Inter-Dune)	3.1	0.0	70.0	0.0
DU - (Glacio-Aeolian Dune)	3.5	5.0	61.4	10.3
FSZ - (Frozen Shore Zone)	3.0	4.2	45.0	7.1
DFS - (Delta Forsets)	3.8	4.5	51.5	10.9
FBT - (Fluvial Bar Top)	7.8	9.3	53.0	2.8
DGL - (Deep Glacio Lacustrine)	9.1	15.3	40.5	16.3
LSF - (Lacustrine Sand Flow)	8.9	10.1	45.9	13.2
DBS - (Delta Bottom Sets)	13.8	10.8	42.3	14.5
LIB - (Linguoidal Bar)	14.1	23.1	32.1	12.9
DTS - (Delta Top Sets)	19.3	27.3	40.0	21.9
DF - (Delta Flow)	27.8	20.4	33.1	18.5
RD - (Rain Out Diamictite)	31.0	16.7	26.3	11.5
SACG - (Sub-aqueous Channel Gravel)	48.0	37.0	16.7	20.8
TTMD - (Terminoglacial Tunnel Mouth Deposit)	38.3	23.6	36.0	28.5
FL - (Fluvial Sandstone)	41.9	27.4	28.3	23.6
LB - (Longitudinal Bar)	57.0	33.5	15.8	14.4
TOF - (Terminoglacial Outwash Fan)	53.2	20.5	10.7	10.1

Table 5.6. Facies vs rock fragment and quartz percentages (see Appendix 5b).

Sub-cropping carbonate lithologies of the Warburton Basin occur around the Gidgealpa Field and Coongie#1 well. Only two carbonate fragments have been observed in the Merrimelia Formation (Merrimelia Field). The lack of carbonate rock fragments observed is a function of the abrasive and destructive nature of glacial and fluvial environments and the incompetent nature of carbonate rock fragments. Similarly a very small proportion of Warburton Basin basalt has survived the rigours of glacial transport and deposition. Further to this, all rock fragments are then

agitated fluviially reducing the amount of rock fragments that are incorporated into the mineralogically mature Tirrawarra braid plain and deltaic facies sandstones.

ROCK FRAGMENT TYPES	ROCK FRAGMENT LITHOLOGY	FIGURES
Competent RF Type I	Acid Volcanic RF's	Plate 12e
	Silicic Metamorphic RF's	Plates 15a,15c, 16b & 16c
	Sub-litharenite to Litharenite RF's	Plates 11d[3f] & 11e
Competent RF Type II	Feldspathic Sandstone RF's	Plate 40a
	Pyroclastic RF's	Plate 13d
Incompetent RF	Shale RF's	Plate 11a[8f]
	Micaceous-Schist RF's	Plate 15d
	Illitised Volcanic RF's	Plate 13f

Table 5.7 *Competent and incompetent rock fragment (RF's) types.*

5.3 TIRRAWARRA SANDSTONE: PETROGRAPHY AND PROVENANCE

The formation of Tirrawarra facies required the reworking of glacial sediments and surrounding elevated basement via meltwater action (see Chapter Four). This concept is supported by the observation that all rock fragments in the Tirrawarra Sandstone have been described in the Merrimelia Formation.

Principle Component Analysis (PCA) of Tirrawarra rock fragment data reveals statistically significant rock fragment groupings. The methodology used to describe rock fragments in the Tirrawarra Sandstone were exactly the same as that used for the Merrimelia Formation rock fragment dataset³. The results are presented in Figure 5.13. Forty rock fragment types were observed and described in Tirrawarra sediments, markedly less than observed in Merrimelia sediments. The obliteration of incompetent (labile) rock fragment types (Table 5.7) by reworking accounts for this disparity.

³ See section 5.5.1.2 (this chapter) for an explanation of principle component analysis (PCA).

Only competent Merrimelia rock fragments survive reworking processes, and become part of the Tirrawarra sedimentary pile (Table 5.7). Notably, pyroclastic and volcanic rock fragments were destroyed.

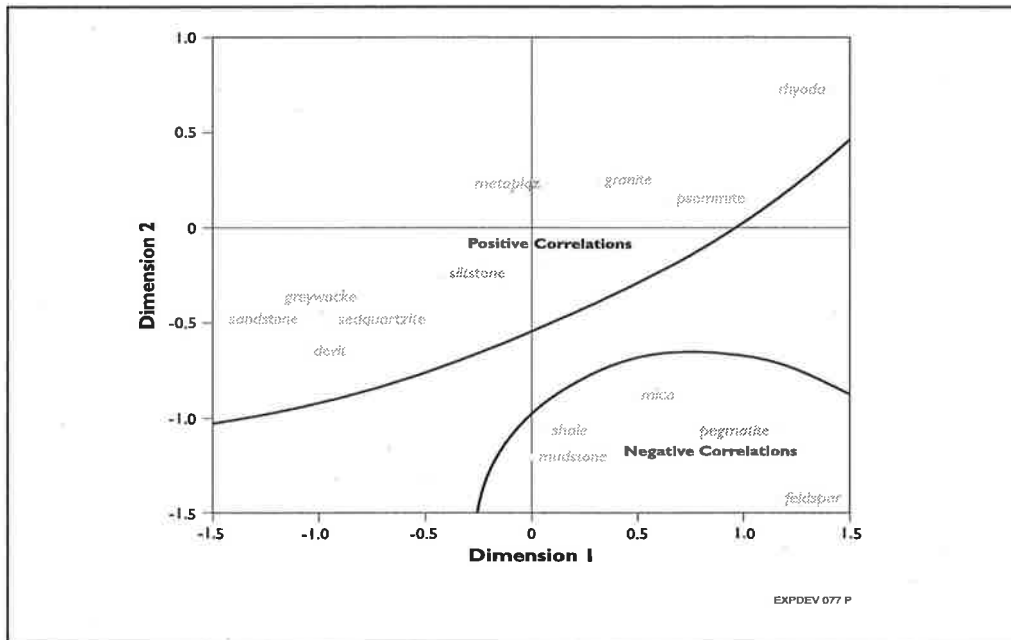
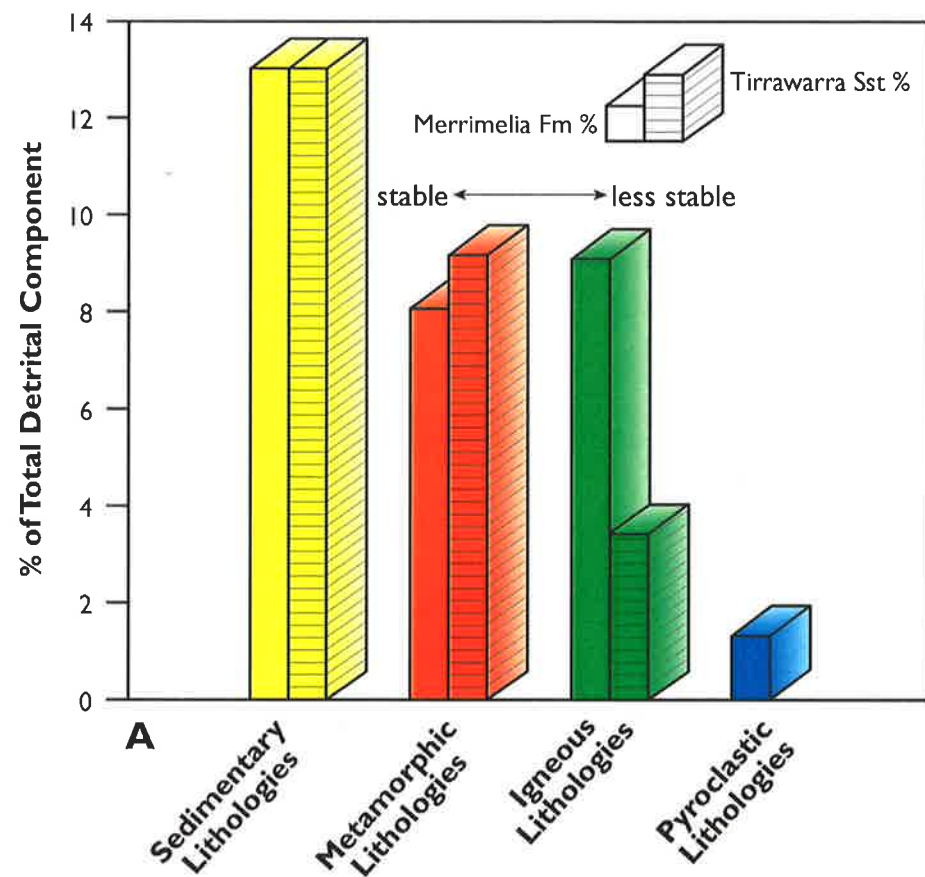


Figure 5.13 Principle Components Analysis (PCA) of rock fragments from the Tirrawarra Sandstone.

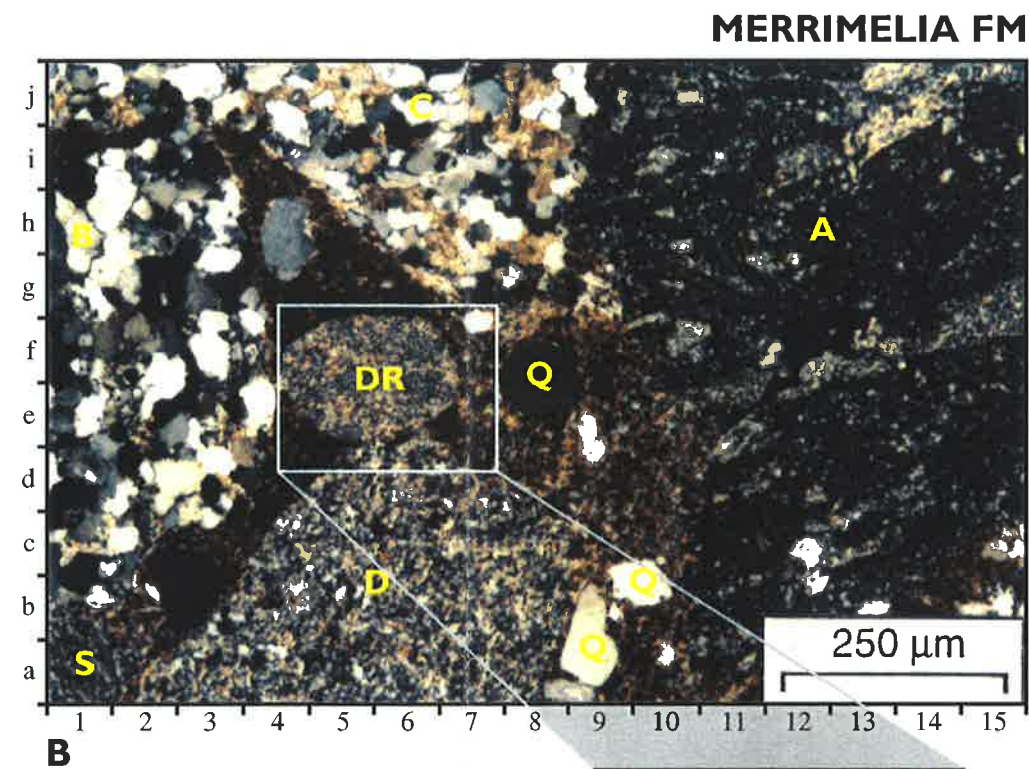
The proportions in the Tirrawarra Sandstone of both these rock fragment types were significantly lower than those observed in the Merrimelia Formation (Fig. 5.14a). Metamorphic clasts, which are generally silicic, were seen in similar to slightly greater proportions in Tirrawarra sediments compared with Merrimelia sediments (Fig. 5.14a). This small increase in metamorphic rock fragments is attributed to the liberation of schistose and stressed metamorphic poly-quartz grains from meta-sandstone and sandstone clasts in the Merrimelia Formation into the Tirrawarra Sandstone. Sedimentary rock fragments, such as shale, litharenite and siltstone, constitute approximately 33.6%, 9.5% and 4.3% respectively of the total amount of rock fragments observed in the Tirrawarra Sandstone (Table 5.2).

The proportion of clast lithology types in Tirrawarra sediments is shown in Figure 5.15. Sedimentary and metamorphic rock fragments are the most commonly observed while volcanic rock fragments are subordinate.

The majority of Tirrawarra Sandstone samples contain all three rock fragment types (sedimentary, volcanic and metamorphic), in proportions ranging from zero to 25% (Fig. 5.15).



- Igneous**
 DR - Devitrified Acid
 Volcanic
 A - Rhyodacite
Sedimentary
 B - Quartz Arenite
 C - Sub-Litharenite
 D - Greywacke
 Q - Quartz
 S - Shale



TIRRAWARRA SST

- Igneous**
 DR - Devitrified Acid
 Volcanic
Sedimentary
 S - Shale
Metamorphic
 SC - Schist

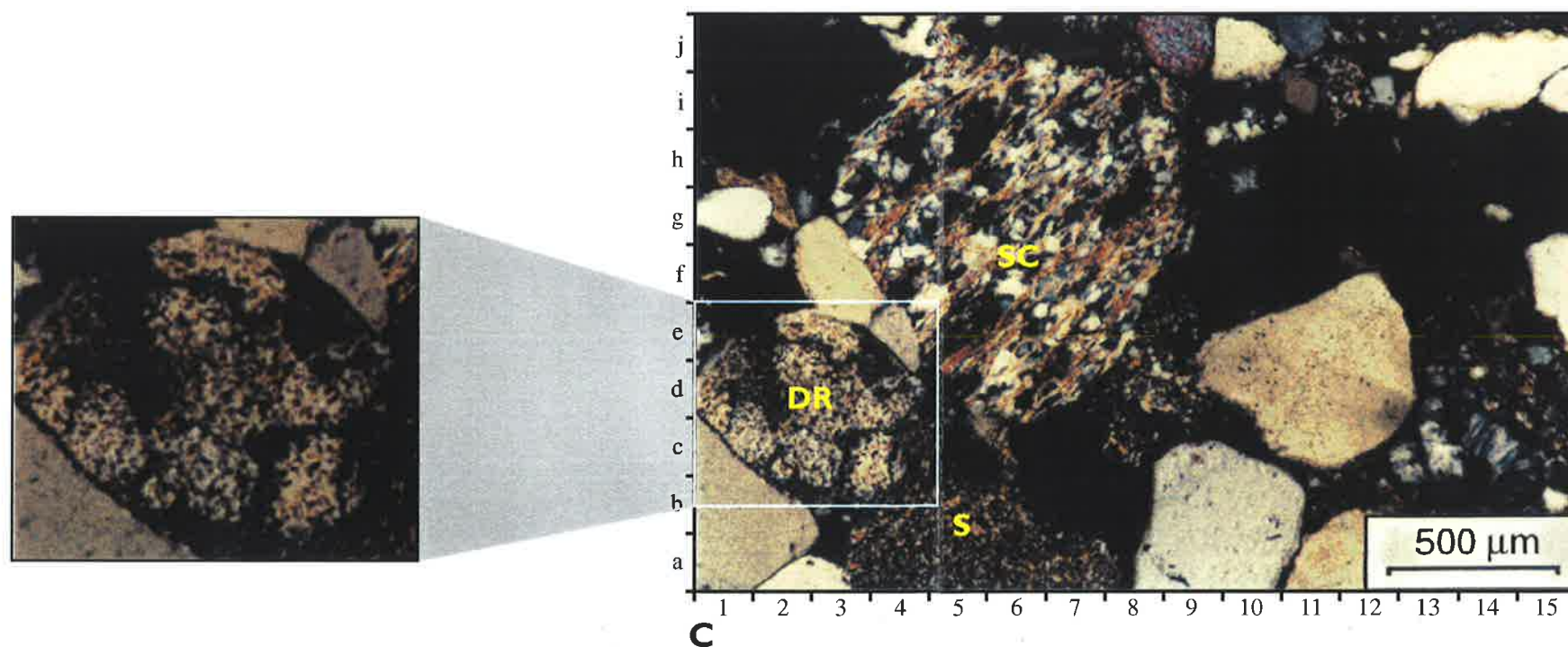


Figure 5.14 Merrimelia Formation and Tirrawarra Sandstone rock fragments (modified from Chaney et al., 1997). **A)** Rock fragment lithology histogram. **B)** Moorari #2 (3136.13m) litharenite [**Inset**] Devitrified acid volcanic rock fragment. **C)** Tirrawarra #21 (2967.9m) litharenite [**Inset**] Devitrified acid volcanic rock fragment.

A very small number of samples contain rock fragment proportions greater than 25% (Fig. 5.15) a direct result of meltwater reworking, with rinsing out of the labile rock fragments.

The framework component of the Tirrawarra Sandstone differs markedly from the Merrimelia Formation. Plates (2a through to 2e) illustrate that Tirrawarra sediments have a quartz-rich framework when compared to Merrimelia sediments. This supposition is confirmed statistically where the distribution of quartz grains in Tirrawarra sediments is skewed towards the high quartz end compared with Merrimelia sediments (Figs. 5.16a & 5.16b).

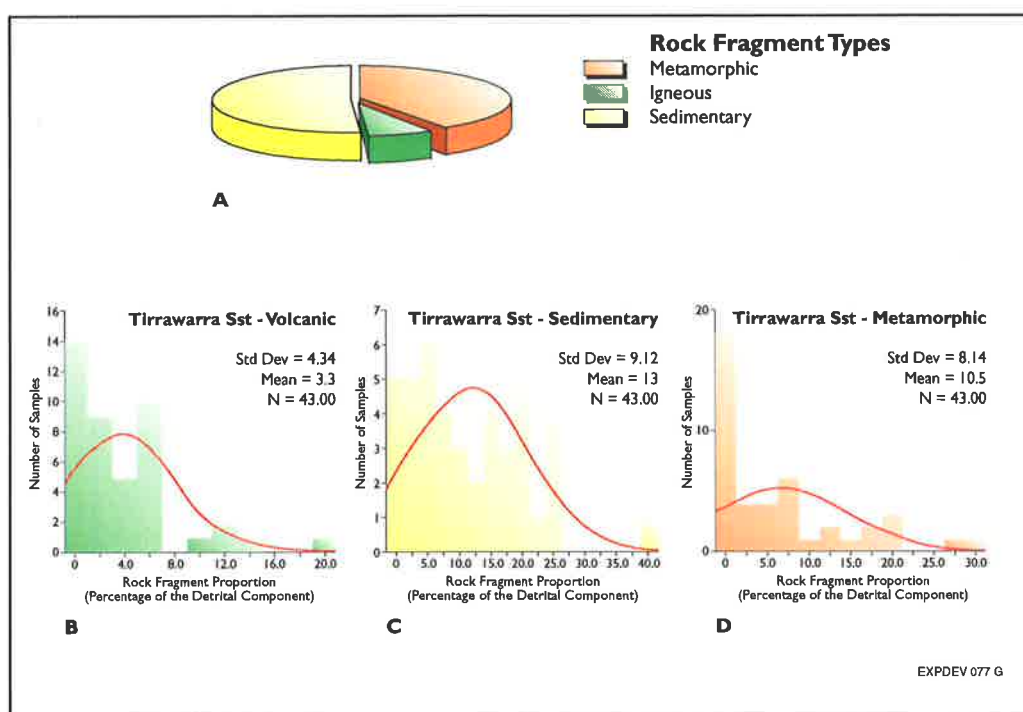


Figure 5.15 A) Rock fragment proportions in the Tirrawarra Sandstone. B) Frequency histograms of volcanic, C) sedimentary and D) metamorphic rock fragments in Tirrawarra sediments.

Regionally, Tirrawarra sediments with a high rock fragment component have a low quartz content. Equally, Tirrawarra samples that were dominated by a quartz framework, had low proportions of rock fragments. Rezaee and Lemon (1996a) observed the same inverse relationship between quartz and rock fragments in Tirrawarra sediments in the Moorari, Fly Lake-Brolga and Tirrawarra regions (Fig. 5.16c).

The most common rock fragments observed in Tirrawarra sediments are sedimentary, with shale and litharenite clasts the most prevalent (Table 5.2). Of the volcanic rock fragments observed, devitrified acid volcanic rock fragments (Plates 13c & 13e) were the most common type, constituting 8% of the rock fragment component (Table 5.2). All other volcanic rock fragments, rhyodacite (Plate 12a), granite (Plate 15c) and pegmatite (Plate 14c) were observed in proportions that were less than 2% of the total number of rock fragments described (Table 5.2).

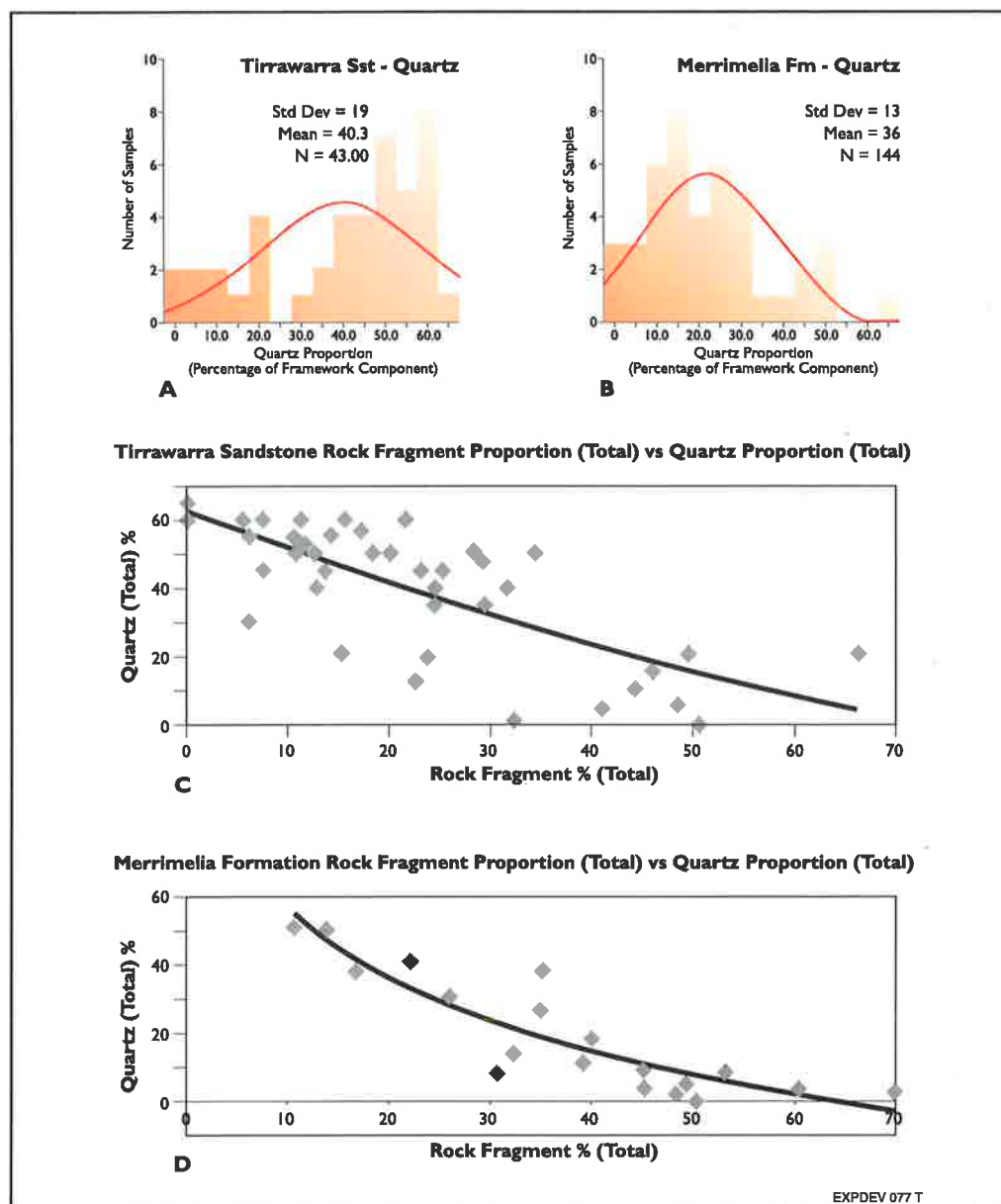


Figure 5.16 A) Frequency histograms of quartz proportions in the Tirrawarra Sandstone, and B) the Merrimelia Formation. Cross plot of quartz and rock fragment proportions in the C) Tirrawarra Sandstone and D) the Merrimelia Formation.

The most common metamorphic rock fragment types observed within the Tirrawarra Sandstone were competent (extrabasinal) schistose poly-crystalline quartz (Plate 16e), quartzite (Plate 16b) and psammitic rock fragments.

These four rock fragments account for 97% of metamorphic rock fragments in the Tirrawarra Sandstone while incompetent metamorphic rock fragment lithologies such as schist (Fig. 5.14c[6h]), gneiss (Plate 16a) and meta-rhyodacite (Plate 16d) constitute 3%. Less than 1% or trace amounts of zircon, tourmaline as well as glaucony were observed in the Tirrawarra Sandstone. Zircon and tourmaline were identified in proportions of <1% in 52% of Tirrawarra thin sections described.

5.4 RELATIONSHIP BETWEEN THE TIRRAWARRA SANDSTONE AND MERRIMELIA FORMATION

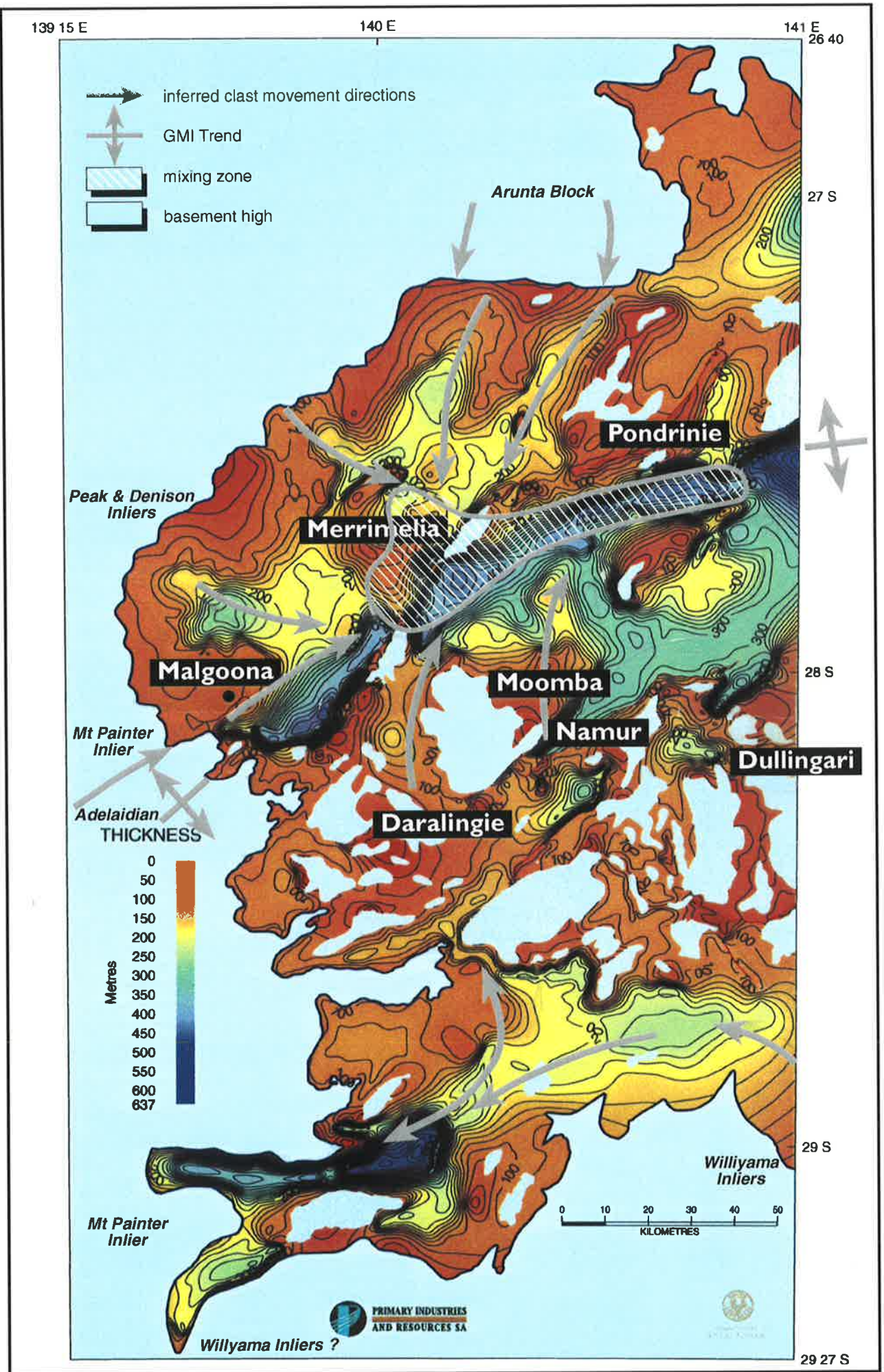
The Tirrawarra Sandstone mirrors the proportions of metamorphic and sedimentary rock fragments observed in the Merrimelia Formation (Fig. 5.14a).

Framework grains and rock fragments derived from the Merrimelia Formation have been further reworked by fluvial-deltaic processes into the mineralogically more mature Tirrawarra Sandstone.

Figure 5.14c (Tirrawarra Sandstone) and Figure 5.14b (Merrimelia Formation) both contain very similar rounded devitrified acid volcanic rock fragments in what appears to be medium grained, illite-dominated groundmass.

The strong similarity suggests that both of these rock fragments are derived from the same source. All rock fragment types observed in the Tirrawarra Sandstone are also observed in the Merrimelia Formation. Figure 5.14a shows that the stable rock fragments are observed in both formations in similar proportions whereas the less stable rock fragments are diminished or absent in the Tirrawarra Sandstone. This observation suggests that the Tirrawarra Sandstone has formed from the reworking of Merrimelia sediments.

The preservation of a high proportion of labile shale clasts in Tirrawarra sediments (shale rock fragments are the most commonly observed rock fragment in Tirrawarra sediments) indicates that these rock fragments have been transported only small distances from their Warburton Basin source.



PEL5/6 546 Z

Figure 5.17 Merrimelia-Tirrawarra combined isopach overlain with competent rock fragment movements in the Merrimelia Formation (Modified from Gravestock and Jensen-Schmidt, 1998).

The cannibalisation of Merrimelia sediments by Tirrawarra sedimentation processes indicates that direct sourcing of Tirrawarra detritus from Warburton lithologies is rare. The covering of the Warburton Basin by Merrimelia sediments would have prevented Warburton sediments being directly eroded by glacial meltwaters into the Tirrawarra Sandstone. Figure 5.17 indicates however, that there were emergent basement highs throughout the deposition of the MTGC. The amount of detritus sourced from these highs compared with the cannibalisation of Merrimelia sediments is small. In short, the provenance influence of the Warburton Basin diminished as the Merrimelia-Tirrawarra deposition evolved through time.

5.5 ROCK FRAGMENT PROVENANCE: RESULTS AND DISCUSSION

5.5.1 STATISTICS INTRODUCTION

Statistical analysis was used to determine if there was a link between rock fragment type, rock fragment percentage age and geographical location.

Firstly, Pearson correlation matrices and "t" statistic analysis were used to investigate significant statistical links between rock fragment types and to define statistically significant pairings. PCA was then performed on only the rock fragment data set pertaining to clasts identified as being statistically significant by Pearson correlation matrices. Cluster analysis was then performed to assess the spatial distribution of the main rock fragment types.

In addition, rock fragment distribution maps were constructed using rock fragment percentage data. These data were, krigged and contoured with semi-variograms produced for each map to assess the nugget effect in each case (Appendix 8c).

5.5.1.1 Pearson Correlation Coefficients

Pearson Correlation matrices assess the degree of interrelation between two variables and measures their influence on each other (Swan *et al.*, 1995). There are three types of correlations possible between two variables: positive, negative and zero correlation (Fig. 5.18).

The correlation coefficient (r) describes the strength of the correlations between variables. The correlation coefficient is the ratio of the covariance of the two variables to the product of their standard deviations (Equation 4).

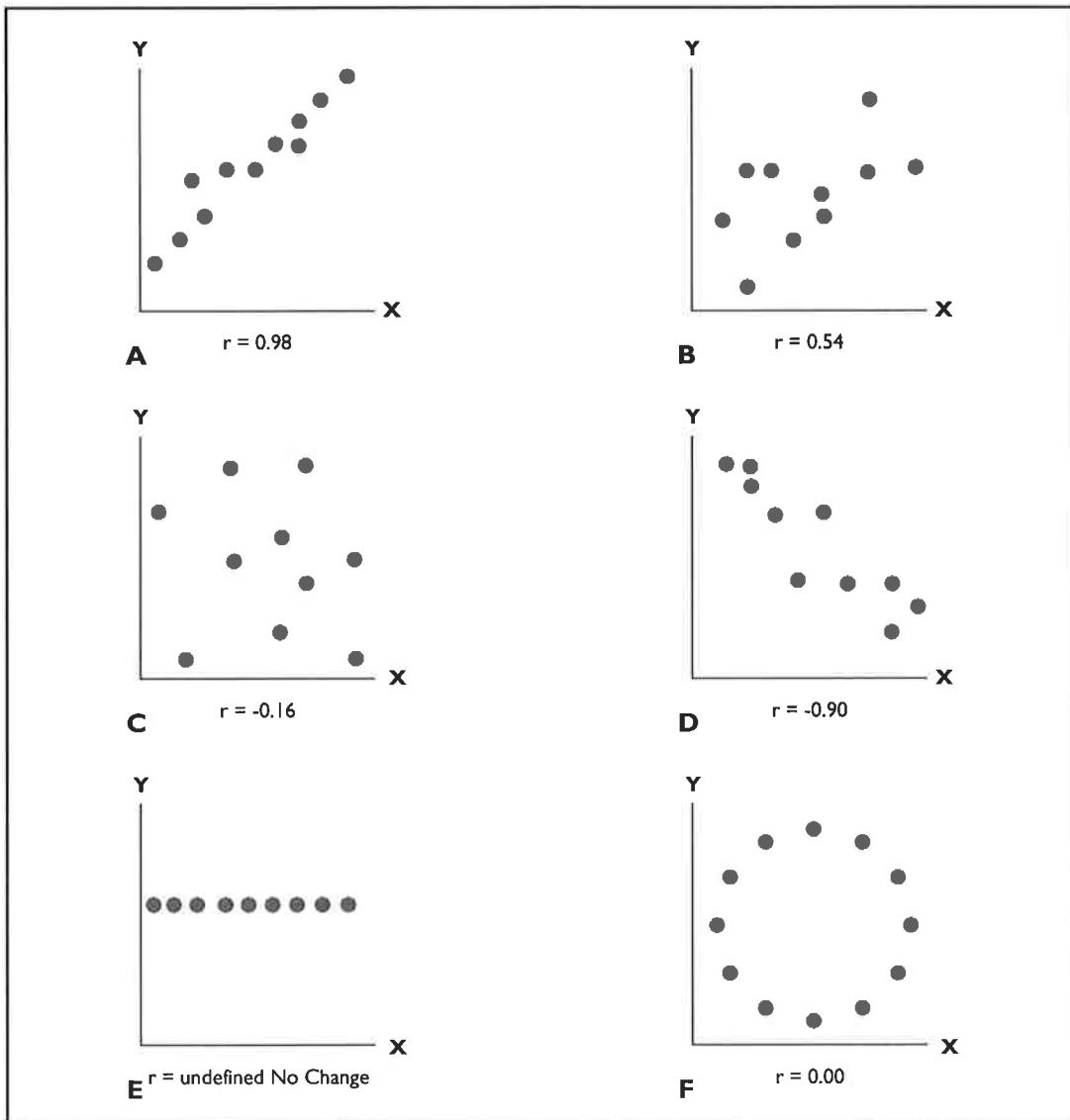


Figure 5.18 Positive, negative and zero Pearson Correlation plots illustrating the graphical representation of correlation coefficient values (r). (modified from Davis, 1986).

Correlation Matrix					
Merrimelia Formation			Tirrawarra Sandstone		
Variables	Correlation Coefficient (r)	't' statistic	Variables	Correlation Coefficient (r)	't' statistic
Quartz - Total Igneous RF's	-0.6 ^{-ve}	-8.8	Quartz - Sandstone	-0.75 ^{-ve}	-7.3
Quartz - Total Sed RF's	-0.53	-7.3	Quartz - Total Meta RF's	-0.7	-5.5
Quartz - Total Meta RF's	-0.5	-6.7	Feldspar - Greywacke	0.4	2.7
Quartz - Shale	-0.4	-5.2	Sandstone - Total Meta	0.44	3.1
Sandstone - Greywacke	0.4	5.2	Siltstone - Rhyodacite	0.534	4.0
Total SED RF's - Granite	0.4	5.2	Sedquartzite - Granite	0.56	4.3
Sedquartzite - Granite	0.44	5.9	Igneous RF's - Granite	0.58	4.5
Shale - Greywacke	0.52	7.2	Sedquartzite - Sandstone	0.63 ^{+ve}	5.2
Sedquartzite - Greywacke	0.63 ^{+ve}	5.9			

Table 5.8 Tirrawarra and Merrimelia rock fragments pairings that are statistically significant at a 95% confidence level (pairings that have the highest 't' statistics are shown). A complete listing of all significant pairings is given in Appendix 8.

$$R = \frac{\text{Covariance of the two variables}_{xy}}{(\text{Std dev}_x \times \text{Std Dev}_y)}$$

Equation 4

Thus if $r=0.98$ between two variables then there is a positive linear relationship between the two variables (Fig. 5.18a).

If the r value between two variables is calculated to be $-ve0.98$ then there is a negative correlation where one variable varies inversely with relation to the other (Fig. 5.18d). R -values that are mid-range imply correlations such as those shown in Figures 5.18b & 5.18c. An r -value that is close to zero implies that there is no linear relationship between the variables.

A significance test (at a 95% confidence level), the “ t ” statistic test, was employed in both Merrimelia and Tirrawarra datasets in order to rank Pearson correlations (Appendix 8a). The variable pairings with a “ t ” statistic greater than a critical value was deemed to be significant at a 95% confidence level (Appendix 8a). Table 5.8 lists variable pairings, which display end member “ t ” statistic values (both negative and positive). Overall, the same rock fragment pairs in both datasets exhibit consistent correlations (Table 5.8). Figure 5.18 indicates the main correlation styles observed in both rock fragment data sets.

Pearson correlation coefficients confirm that there is a negative correlation between quartz and rock fragments in both Tirrawarra and Merrimelia sediments, i.e., when quartz is present, rock fragments are minimal (Table 5.8). This statistical analysis confirms the findings of Rezaee (1996) who observed an inverse relationship between rock fragments and quartz in the Tirrawarra Sandstone. In addition petrological analyses of Tirrawarra and Merrimelia sediments in this study observed the same inverse relationship (Figs. 5.16c & 5.16d).

Results in Table 5.8 indicate that there are strong positive correlations between: greywacke, shale and sedimentary quartzite rock fragments. These results suggest an association where these particular Merrimelia framework components may share a similar provenance. In Tirrawarra sediments, there are strong positive correlations between siltstone-rhyodacite and feldspar-greywacke rock fragment pairs.

5.5.1.2 Principle Components Analysis (PCA)

Principle components analysis (PCA) is used in petrographic studies to determine the least number of variables needed to supply an adequate amount of information and

to find petrographic variables that are interrelated (Smith, 1969). PCA reduces the dataset to its essential components (Miller, 1994). Data reduction was deemed necessary in both the Tirrawarra and Merrimelia rock fragment data sets to reduce the large number of rock fragment types under investigation to a more manageable number. PCA was therefore performed on both data sets. This involved splitting the data from each formation into two subsets so that the amount of agreement between the split subsets was assessable. PCA was performed on normalised data so that the unit variances were zero using varimax rotation (Griffiths pers. comm., 1997). In PCA most of the variance is accounted for by two principle components (Figs. 5.6 and 5.13).

In essence, PCA divides data into that which is positively and negatively correlated. PCA performed on both the Merrimelia (Fig. 5.6) and Tirrawarra (Fig. 5.13) rock fragment datasets therefore grouped similarly correlated rock fragment types (Figs. 5.6 & 5.13). These negative and positively correlated framework components show good agreement with Pearson correlation coefficients listed in Appendix 8a, further corroborating statistically derived links between framework components in Merrimelia and Tirrawarra sediments.

5.5.1.3 Cluster Analysis

Average, single and centroid linkage cluster methods were employed to confirm provenance associations and clast movements derived from petrographic observations. Before cluster assessment, the distribution of rock fragment data was analysed using Kolmogorov-Smirnov and Shapiro-Wilk normality tests (Table 5.9).

MERRIMELIA Fm.	Kolmogorov-Smirnov ^a Statistic	Shapiro-Wilk Statistic
Accessory Minerals	0.223	0.98
Quartz Minerals	0.127	0.994
Metamorphic Minerals	0.407	0.625
Sedimentary Minerals	0.293	0.814
Volcanic Minerals	0.492	0.511

^a Lilliefors Significance Correction.

Table 5.9 Results of Kolmogorov-Smirnov and Shapiro-Wilks tests of normality (Merrimelia Formation).

The Kolmogorov statistic is low for accessory, quartz and sedimentary framework components, implying that these datasets are not normally distributed. Metamorphic

and volcanic rock fragment subsets, however, have KS statistics that are high (approaching 0.5) suggesting that a high proportion of data approaches a normal distribution. The Shapiro-Wilks statistic, a test that is designed to check for departures in normality, are low for the metamorphic and volcanic datasets, indicating that approximately half of the data deviate from a normal distribution. In contrast, the Shapiro-Wilks statistic for accessory, quartz and sedimentary rock fragments are all high, confirming that these datasets are not normally distributed.

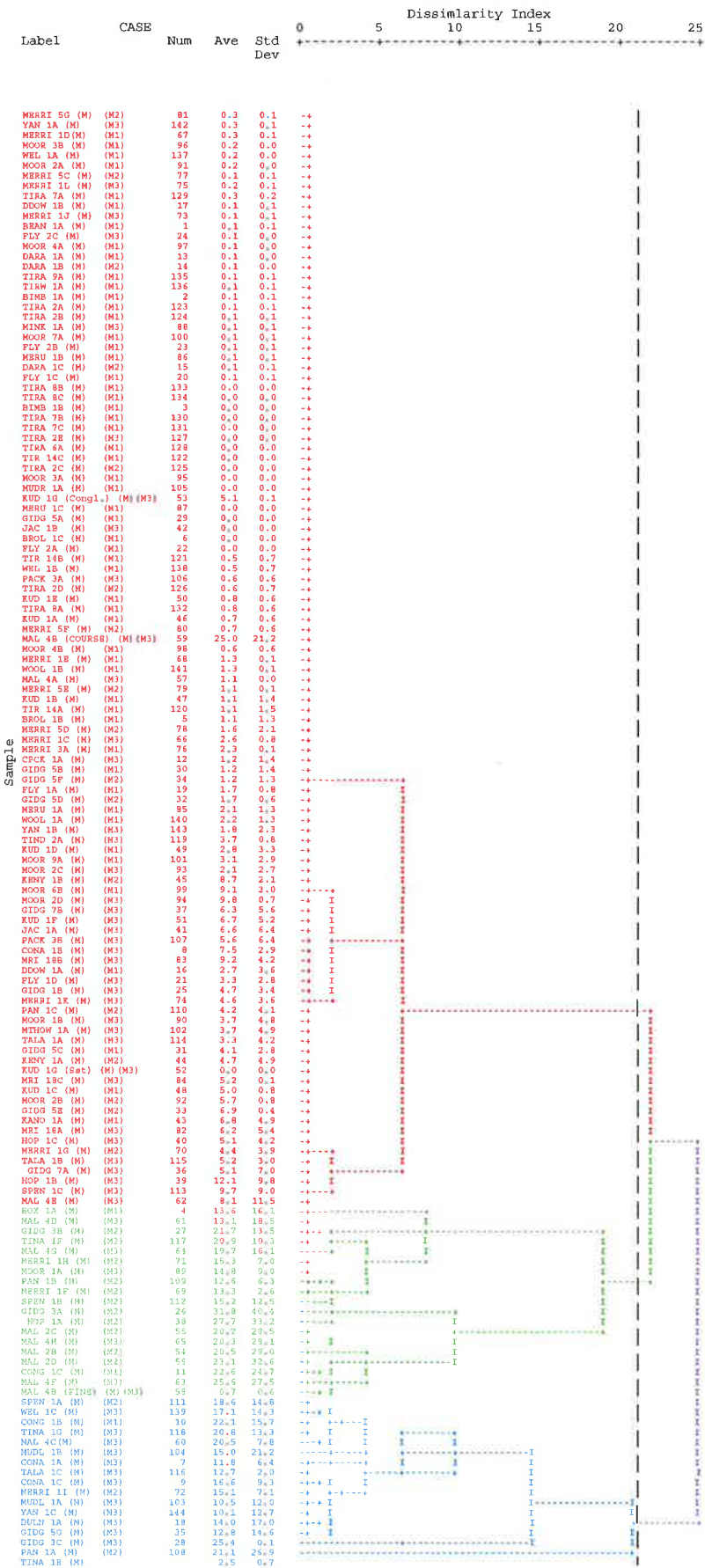
The rock fragment data set contains three subsets that are not normally distributed (accessory, quartz and sedimentary) and two datasets (metamorphic and volcanic) where approximately half of the data approaches a normal distribution. Accordingly the datasets that illustrated no normality were not standardized and the data that showed a normal distribution, were standardised (Griffiths pers. comm., 1997). The standardised and non standardised datasets were treated individually and clustered using the single, average and centroid linkage cluster techniques. Of the three cluster methods, centroid linkage cluster analysis was found to be the most stable and gave consistent results and was the least effected by outlier data.

Cluster stability was assessed by dividing the standardised and non-standardised datasets into two subsets, where the data was randomly sorted, and cluster analysis performed. The stability of each cluster analysis technique was assessed by clustering each subset of data and the data set as a whole. If there was agreement between the original data set and the subsets the cluster technique was deemed stable. All three cluster analyses illustrated good agreement, with the centroid linkage technique.

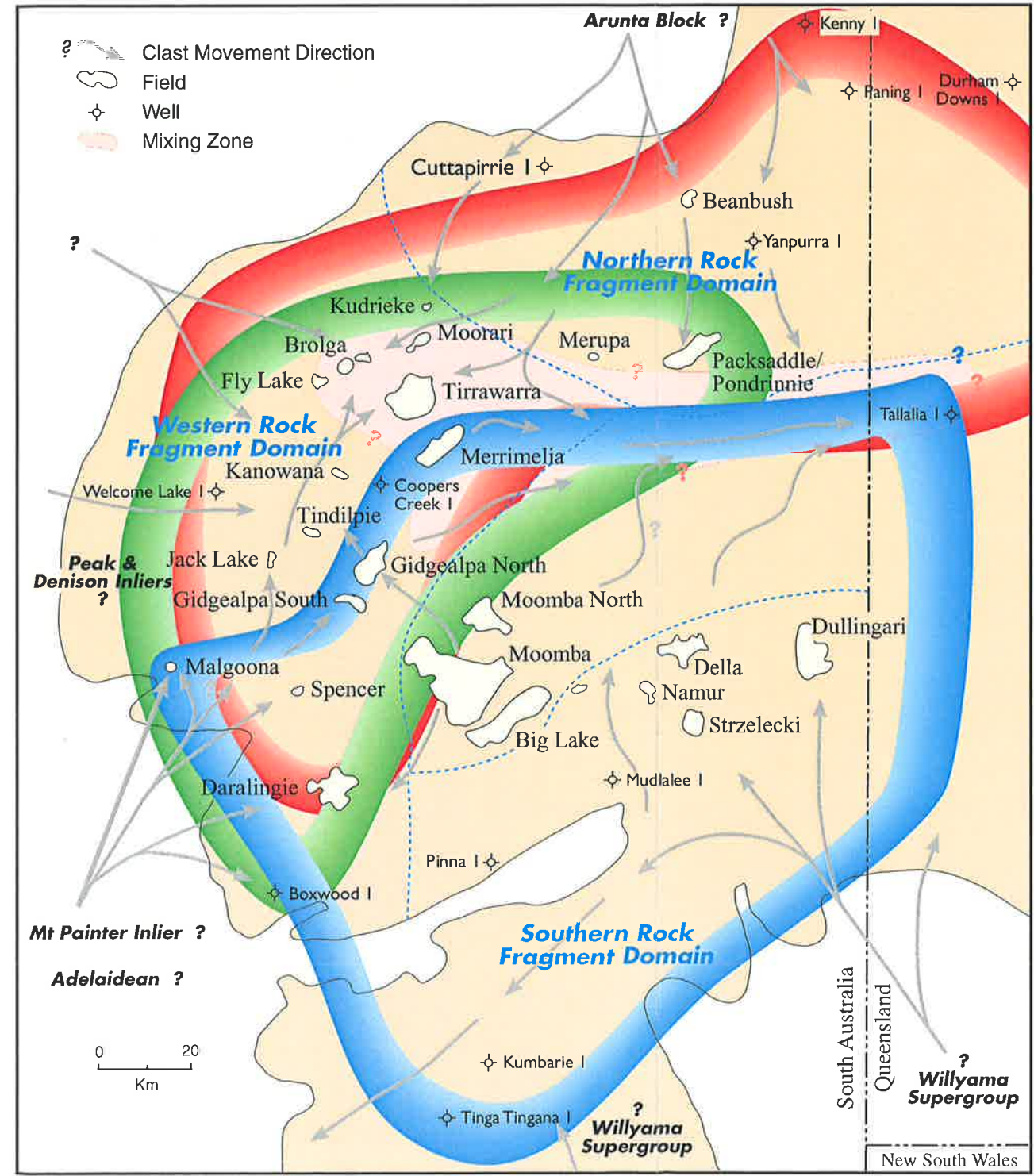
Cluster analysis of non-standardised (or raw data) datasets consistently produced four clusters at a squared euclidean distance of 21 units (Appendix 8b). Similarly, clustering the volcanic and metamorphic datasets using standardised Z scores revealed four clusters. The four clusters gained from all five data sets correspond with samples in the north, northwest central, central and southern parts of the Cooper Basin (Fig. 5.19).

Rock fragment data from Tirrawarra samples were subject to the same test of normality. The Kolmogorov-Smirnov and Shapiro-Wilks test of normality revealed that the data set was not normally distributed and was therefore not standardised before further analysis (Table 5.10). Cluster technique assessment was performed in the same way as for Merrimelia Formation data, and again, centroid linkage was found to be the most stable technique.

A



B



Merrimelia Fm Competent Rock Fragments

Figure 5.19 A) Cluster dendrogram of competent Merrimelia Formation rock fragments illustrating three clusters at a squared euclidean distance of 21. B) Distribution of clustered Merrimelia Formation data over the southern Cooper Basin. (modified from Cubitt et al., 1998). Note: high degree of overlap between southern and northern clusters.

Cluster analysis of Tirrawarra rock fragments from outside the basin (metamorphic rock fragments dataset) revealed four clusters (Fig. 5.20), where the clusters correspond to samples from the north, south, west and a zone of over lap. The similarity of cluster analysis results in both Merrimelia and Tirrawarra sediments provides further evidence that the provenance of the Merrimelia Formation and Tirrawarra Sandstone are similar and probably linked. These findings match the conclusions of Chaney *et al.* (1997).

TIRRAWARRA Sst.	Kolmogorov-Smirnov ^a Statistic	Shapiro-Wilk Statistic
Accessory Minerals	0.312	0.523
Metamorphic Minerals	0.209	0.794
Quartz Grains	0.177	0.875
Volcanic Minerals	0.204	0.779
Sedimentary Minerals	0.277	0.673

^a Lilliefors Significance Correction.

TABLE 5.10 *Results of Kolmogorov-Smirnov and Shapiro-Wilks tests of normality (Tirrawarra Sandstone).*

The degree of overlap is, however, not consistent for Merrimelia and Tirrawarra datasets (Figs. 5.19b & 5.20b). These figures reveal that the Merrimelia dataset (Fig. 5.19b) has a high degree of overlap, reflecting the chaotic nature of these sediments. Similarly the Tirrawarra dataset also has overlapping clusters. Unlike the Merrimelia dataset however, there appears to be minor overlap between northern and southern. This cluster arrangement suggests that the GMI Ridge was exerting influence on sedimentation during Tirrawarra time (T1), as there appears to be minor clast mixing⁴ between the Patchawarra and Nappamerri Troughs (Fig. 5.20b).

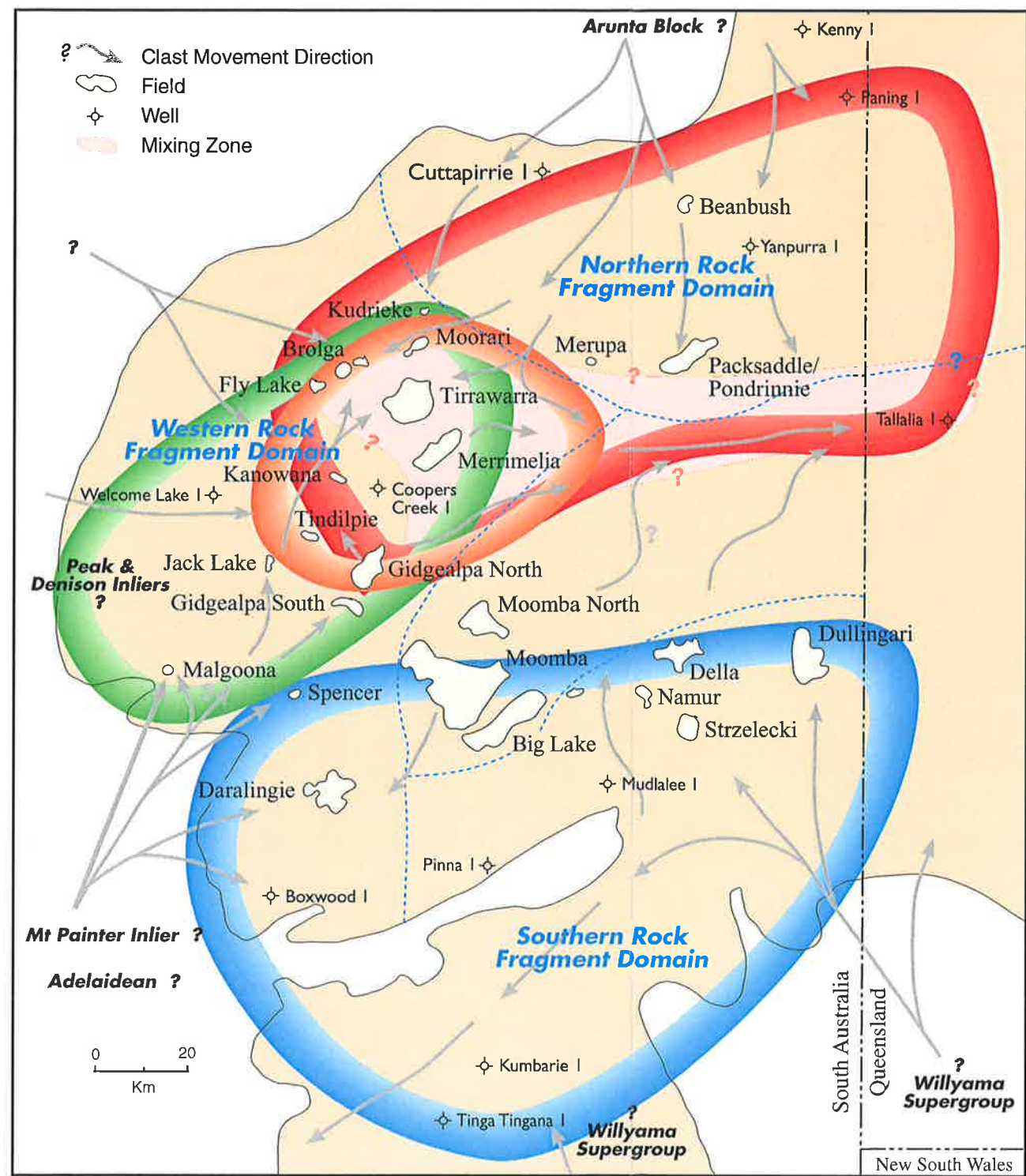
The localised presence of basaltic clasts to the north of Gidgealpa would suggest that at least this part of the GMI was emergent, providing sediment for incorporation into the Merrimelia sedimentary pile. It is possible then that by Tirrawarra time (T1) in the Gidgealpa region, and possibly the GMI trend as a whole, (Fig. 5.20b) had become positive, deflecting sediment supply into the Patchawarra and Nappamerri depocentres.

⁴ A small number of data points in Figure 5.20b do suggest that some sediment from around Coongie #1 area may have been transported south into the Nappamerri Trough.

A

Label	CASE	Ave	Std Dev	Num	Dissimilarity Index					
					0	5	10	15	20	25
KUDRIEKE #2		15.1	25.5	13	-	+				
LAKE HOPE #1		14.3	25.9	15	-	+	+	+		
TIRRAWARRA #14		15.1	25.9	39	-	+	I			
TIRRAWARRA #17		14.8	24.5	40	-	+	I			
MOORARI #6		8.1	17.9	28	-	+	I			
FLY LAKE #3		12.8	22.4	7	-	+	I			
MALGOONA #2		12.2	21.6	16	-	+	+	+		
FLY LAKE #5		13.7	21.2	9	-	+	+	+		
TIRRAWARRA #2		13.1	26.3	38	-	+	I	I		
WELCOME LAKE #1		12.0	26.8	43	-	+	I	I		
FLY LAKE #2		13.5	26.1	6	-	+	I	I		
MOORARI #4		13.1	23.5	25	-	+	+	+	+	
TINGA TINGANA #1		12.3	24.0	36	-	+	I	I		
MOORARI #5		16.3	24.6	26	-	+	I	I		
TIRRAWARRA #20		14.0	23.5	41	-	+	I	I		
MERRIMELIA #1		13.1	29.1	18	-	+	+	+	+	I
MERRIMELIA #6		15.7	20.7	20	-	+	I			
MOORARI #7		16.9	20.9	29	-	+	I			
GIDGEALPA #16		14.1	19.2	11	-	+	+	+	+	
MOORARI #3		15.3	20.7	24	-	+	I			
MERUPA #1		14.0	21.9	21	-	+	I			
FLY LAKE #1		10.5	19.4	5	-	+	+	+	+	I
MERRIMELIA #5		11.8	18.9	17	-	+	I			I
FLY LAKE #6		12.5	21.2	10	-	+	+	+	+	I
MOORARI #6		16.3	25.1	27	-	+	+	+	+	I
MOORARI #9		10.6	16.8	30	-	+	I	I		I
TIRRAWARRA #11		13.6	17.9	37	-	+	+	+	+	I
INNAMINCKA #2		12.9	16.2	12	-	+	+	+	+	I
MOORARI #1		12.9	13.6	22	-	+	+	+	+	I
KUMBARIE #1		11.9	13.7	14	-	+	I			I
MOORARI #2		7.3	12.8	23	-	+	+	+	+	I
CHALLUM #2		14.3	19.7	1	-	+	+	+	+	I
COONGIE #1		10.1	11.9	3	-	+	+	+	+	I
STRZELECKI #10		9.0	10.7	35	-	+	+	+	+	I
TIRRAWARRA #22		10.7	8.2	42	-	+	+	+	+	I
MERRIMELIA #13		6.6	10.6	19	-	+	+	+	+	I
FLY LAKE #4		13.9	8.6	8	-	+	+	+	+	I
SPENCER #1		12.3	7.0	34	-	+	+	+	+	I
COONATIE #1		17.3	10.2	2	-	+	+	+	+	I
MUDERA #1		8.6	10.4	31	-	+	+	+	+	I
PINNA #1		7.2	9.4	33	-	+	+	+	+	I
NAMUR #1		6.9	5.2	32	-	+	+	+	+	I
DELLA #2		10.8	16.3	4	-	+	+	+	+	I

B



Tirrawarra Sst Competent Rock Fragments

Figure 5.20 A) Cluster dendrogram of competent Tirrawarra Sandstone rock fragments illustrating four clusters at a squared euclidean distance of 16. B) Distribution of clustered Tirrawarra Sandstone data over the southern Cooper Basin. (modified from Cubitt et al., 1998). Note: the degree of overlap between northern and southern cluster groupings has diminished compared with the Merrimelia Fm dataset (Fig 5.19).

5.5.2 ROCK FRAGMENT MOVEMENTS IN THE COOPER BASIN: DISCUSSION

5.5.2.1 Metamorphic Rock Fragments

The competent nature of extrabasinal metamorphic rock fragments suggests that these clasts could have been transported vast distances by destructive glacial and/or fluvial depositional regimes without a high proportion being destroyed. These rock fragments can therefore be used as indicators in assessing the directional trends of clast movement throughout the basin.

Semivariogram analysis of the metamorphic rock fragment dataset indicates that realistic comparisons between metamorphic proportions can be made between samples with up to 60 kilometres of separation (Fig. 5.21b). Of all rock fragment data sets, the metamorphic rock fragment data exhibits the least (although still high) nugget effect of 40%. Almost all other rock fragment data exhibit flat sills (Appendix 8c) indicating that no spatial comparisons can be made with certainty. It would appear then that metamorphic rock fragments, from both a statistical and geological standpoint, are the best indicators of clast movement⁵ into and within the Cooper Basin at Merrimelia and Tirrawarra times.

5.5.2.1.1 Rock Fragment Domains: A Discussion

The percentage of metamorphic rock fragments in Merrimelia and Tirrawarra samples are not consistent over the basin (Fig. 5.21a). High percentages of metamorphic rock fragments (>20% of the rock total) were observed in the southern and northern parts of the basin, around Mudlalee, Dullingari in the south and in the Paning, Coonatie and Coongie regions in the north. Moderate proportions (between 10% and 20% of the rock fragment total) were observed in the Malgoona, Spencer, Gidgealpa regions and as far west as the Welcome Lake area. Trace and low proportions of metamorphic rock fragments (<1% and 0.1% to 10% of the rock fragment total respectively) were observed in the Merrimelia, Tirrawarra, Fly Lake, Broilga, Moorari, Minkie and Mudrangie regions (Fig. 5.21a). The highest concentrations of metamorphic rock fragments in the Merrimelia Formation (and Tirrawarra Sandstone accordingly) are concentrated in three distinct clast domains.

⁵ The clast movement arrows illustrated in Figure 5.21a are inferred by assessing the spatial distribution of metamorphic rock fragment proportions. Graphic textured granite, pyroclastic and basaltic rock fragment proportions were used to constrain localised clast movements.

The northern clast domain has sparse well coverage of 11 wells, the western clast domain has an even well coverage of 43 wells while the southern clast domain has 9 wells (Figs. 5.21a).

Examination of rock fragment distributions, clast provenance regions and isopach thicknesses (Figs. 5.21a and 5.17) imply that there are three dominant sediment input directions into the Cooper Basin during Merrimelia and Tirrawarra time.

A northerly input of sediment is inferred from both the metamorphic rock fragment map (Fig. 5.21) and isopach map (Fig. 5.17), with the most likely source of sediment being the Arunta Block to the north and northwest. Metamorphic rock fragment percentages decrease from the northern boundary of the clast domain towards the mixing zone in the south, indicating a gradual dilution of metamorphic clasts in this direction (Fig. 5.21a).

In the western rock fragment domain the highest metamorphic rock fragment percentages consistently occur in the south of the domain (Fig. 5.21a). This suggests a diminution of clasts in a northerly direction. High values in the west of this domain indicate that there was also a westerly input. These two directions of input coalesce with sediment from the north forming a mixing zone (Fig. 5.21a). Isopach thicknesses confirm these input directions and indicates that the dominant direction of input into the western rock fragment domain was from the south along what is now the GMI Ridge (Fig. 5.17).

A complex of basement highs restricts the movement of sediment in a north-south direction within the southerly rock fragment domain (Fig. 5.17). These restrictions have effectively concentrated metamorphic rock fragments along a zone from the Namur to the Dullingari region (Fig. 5.17). Geometries of basement highs indicated on the isopach map of the Merrimelia Formation may be considered analogous to modern day ice cap terrains. A comparison of maps in Figure 5.22 show patterns suggesting analogous development of glacial geomorphologies in the southern Cooper Basin similar to the present day Antarctic margin (Denton *et al.*, 1991).

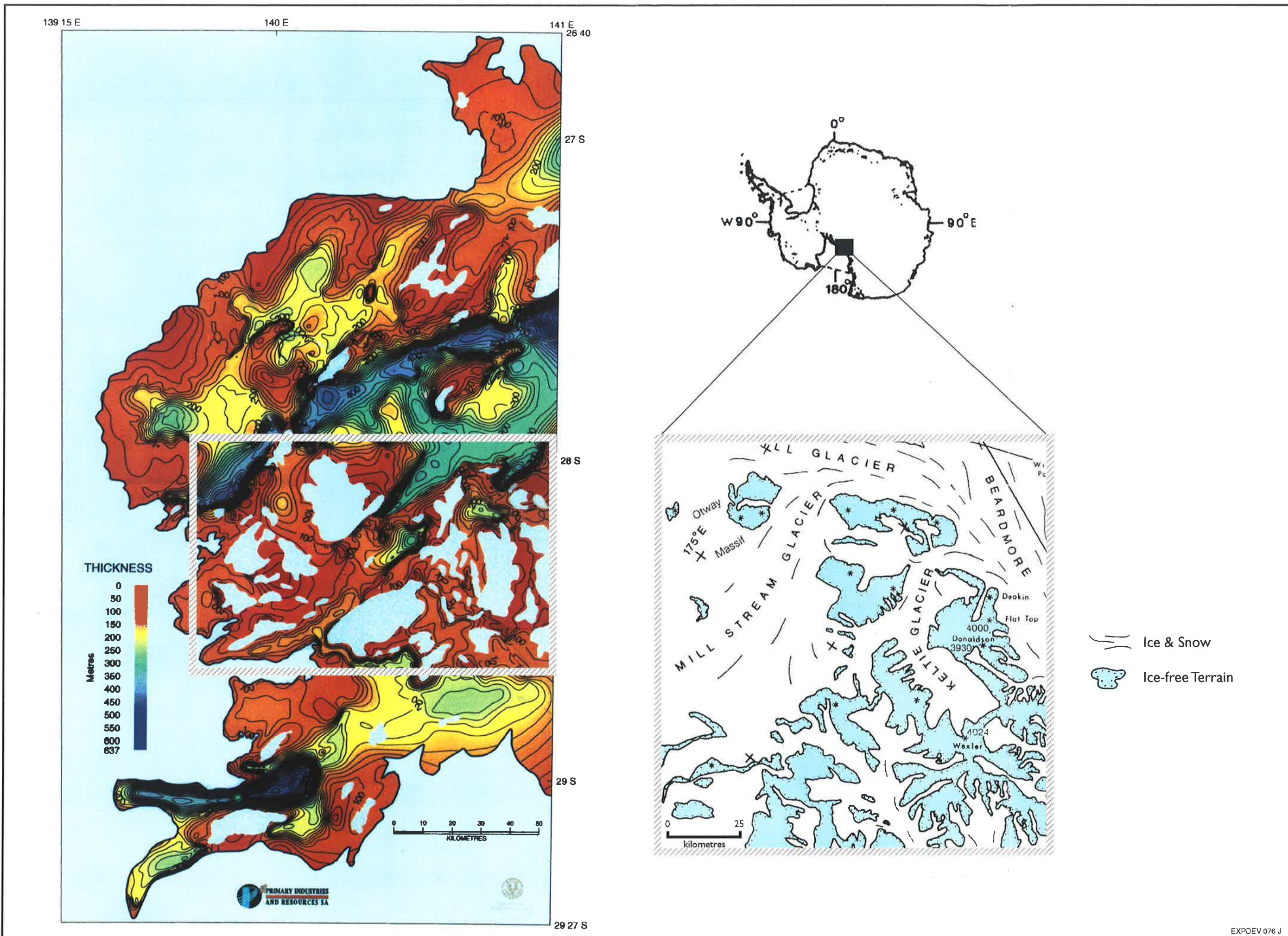


Figure 5.22 A comparison of the basement highs of the southern Cooper Basin (after Gravestock and Jensen-Schmidt, 1998) and the exposed basement of the Antarctic margin (modified from Denton et al., 1991).

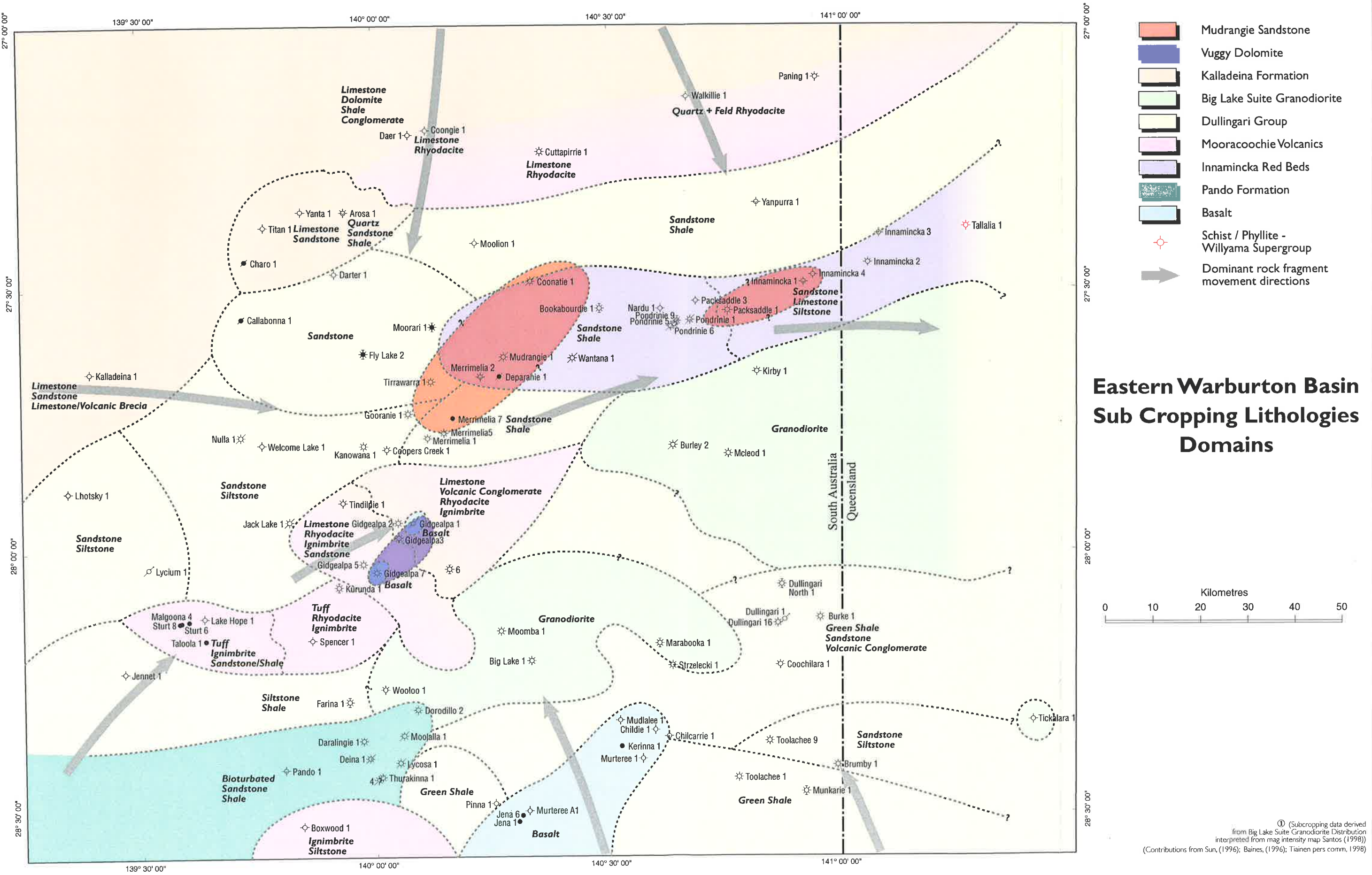
A) Rock Fragment Mixing Zone: A Discussion

Cluster analysis results of metamorphic rock fragments in the Merrimelia Formation, suggests that the northern and western domains overlap forming a mixing zone (Figs. 5.19b – green cluster and 5.20b – orange cluster). This mixing zone corresponds with the thickest section of Merrimelia-Tirrawarra sediments (Fig. 5.17), and, according to facies architecture analysis by Chaney (1998), correspond with glacial packages which merge from the north and south.

The movement of rock fragments, other than metamorphic rock fragments, (granular granite for instance) also supports the easterly movement of detritus along a “mixing zone” in what is now the GMI Ridge. The majority of granite clasts in Merrimelia sediments are granular in nature, and do not exhibit graphic or myrmekitic textures, suggesting they have been sourced from the Big Lake Suite Granodiorite. Such granitic rock fragments are observed in abundance in the Queensland-South Australia border region of the Cooper Basin at Tallalia #1. It is postulated that the fresh granite rock fragments in this well have been sourced from the Big Lake Granodiorite (Fig. 5.23) to the west of Tallalia and were subsequently moved eastward. This eastward movement is implied by the gradual deepening of the GMI Trough (GMI Ridge) towards Queensland where the deepest point along this trend is centred on the Tallalia region (Fig. 5.17). A comparison of Figures 5.21 and 5.17, shows that rock fragment movements mirror the depositional pathways indicated on the isopach map, suggesting that clast movement within the Merrimelia Formation and Tirrawarra Sandstone was towards this linear low, and then east towards Tallalia #1 in Queensland (Fig. 5.17).

5.5.2.2 Volcanic Rock Fragments

The proportion and appearance of acid volcanic rock fragments observed at Coongie #1 in the northern clast domain (Fig. 5.21), suggests that acid volcanic clasts have been derived locally, from around Paning #1 (Sun, 1996) and Cuttapirrie #1. A southerly movement of volcanic clasts from the Cuttapirrie region accounts for the high proportion of rhyolitic clasts observed in samples at Coongie #1, where basement lithologies are predominantly sedimentary and carbonate in nature. A moderate proportion (10% to 20%) of volcanic rock fragments was observed at Coonatie #1 to the south of Cuttapirrie#1 suggesting there was also a south to south westerly movement of acid volcanic clasts in the northern clast domain. The underlying Warburton Basin lithology at Coonatie is dominated by micaceous shale and quartzitic siltstones.



Eastern Warburton Basin Sub Cropping Lithologies Domains



- Mudrangie Sandstone
- Vuggy Dolomite
- Kalladeina Formation
- Big Lake Suite Granodiorite
- Dullingari Group
- Mooracoochie Volcanics
- Innamincka Red Beds
- Pando Formation
- Basalt
- Schist / Phyllite - Willyama Supergroup
- Dominant rock fragment movement directions

① (Subcropping data derived from Big Lake Suite Granodiorite Distribution interpreted from mag intensity map Santos (1998))
(Contributions from Sun, (1996); Baines, (1996); Tienen pers comn, 1998)

Figure 5.23 Eastern Warburton Basin Sub Cropping Lithology Domains ①

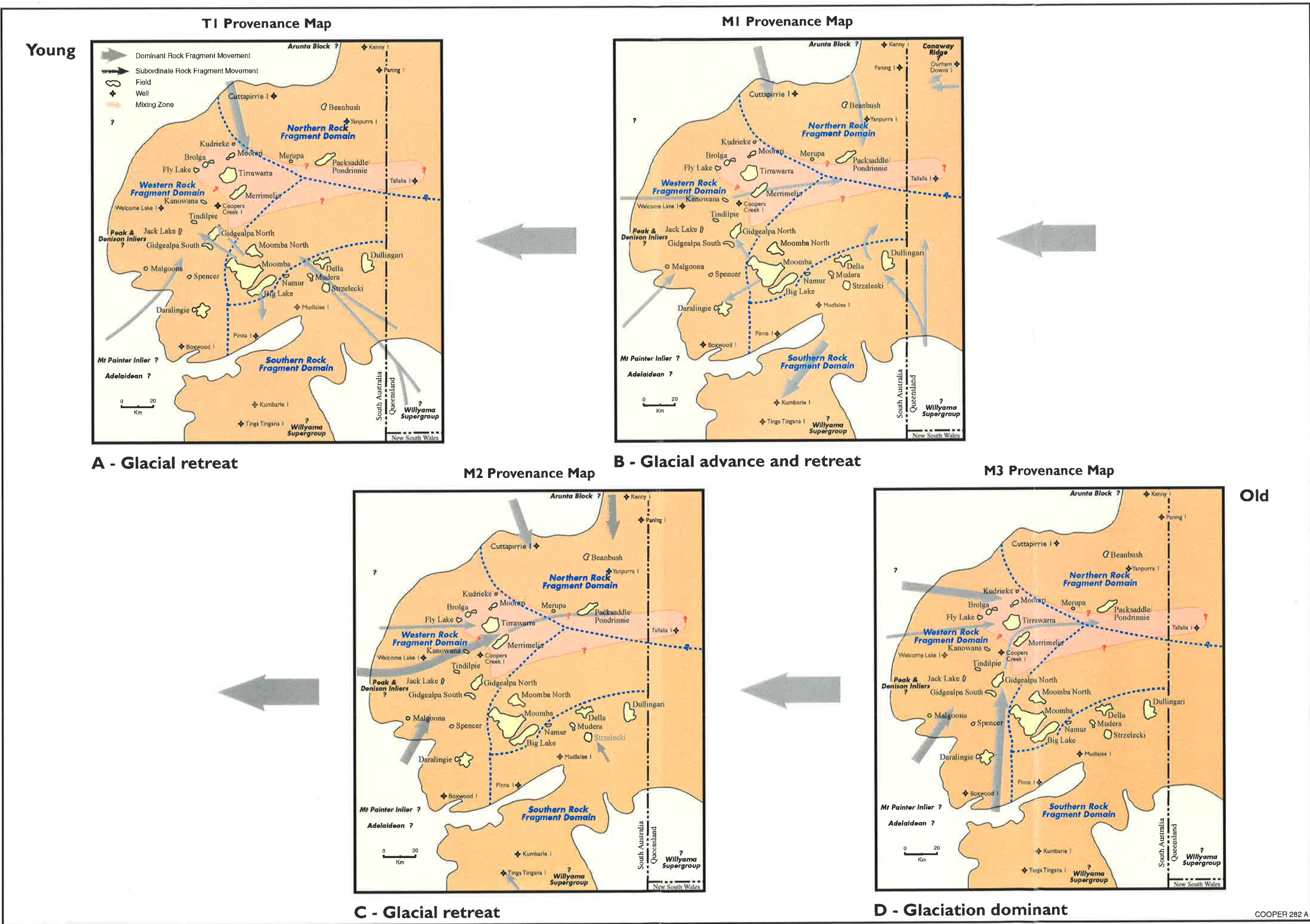
In the western rock fragment domain, trace amounts of distinctive trachytic basalt were observed in Tindilpie #2. A breccia of rhyodacite and trachyte was described at Gidgealpa #2 (Sun, 1996) to the south of the Tindilpie area. Other basaltic lithologies were also noted in the Gidgealpa Field (Sun, 1996). Basaltic rock fragments, including trachytic rock fragments, were only observed in wells to the north and north west of the Gidgealpa region. The movement of basic and acidic rock fragments within the Merrimelia Formation (and Tirrawarra Sandstone accordingly) in this region of the western rock fragment domain, coincides with the northerly movement trends of extrabasinal metamorphic rock fragments (see previous section).

5.5.3 CHANGES IN SEDIMENT INPUT DIRECTIONS THROUGH TIME

Sedimentological and petrographic data indicates that sediment input directions in the Cooper Basin during the deposition of Merrimelia and Tirrawarra sediments did not remain static. Figure 5.24, displays the fluctuations of sediment input into the basin from the earliest Merrimelia Formation deposition through to the deposition of the early Tirrawarra Sandstone.

Initially the dominant direction of sediment input into the Cooper Basin was from the south where the first glaciers of the encroaching Gondwanan glaciation scoured rock from the Broken Hill and Olary Block, and deposited them in the southern rock fragment zone (Fig. 5.24d). Deposition at this time also originated from the south west and west from possibly the Mt Painter/Mt Babbage inliers and, Adelaidean sediments from the Flinders Ranges and the Peak and Denison inliers. This suggests that glaciers to the west of the basin may have been more distal than southern glaciers and therefore deposited less detritus into the Cooper Basin at this time. No rock fragments were derived from the north of the Cooper Basin suggesting that glaciers hadn't developed to the north of the Cooper Basin during early Merrimelia (M3) deposition.

The southerly source of sediment into the Cooper Basin appeared to decline in the middle stage of Merrimelia deposition (M2). At this time, the dominant direction of sediment input were from regions in the north (Arunta Block) and the south west (Mt Painter/Mt Babbage Inliers, Adelaidean sediments of the Flinders Ranges and the Peak and Denison Inliers) (Fig. 5.24c).



COOPER 282 A

Figure 5.24 Variation in input directions into the Cooper Basin from surrounding geological provinces; from the inception of the Gondwanan glaciation (M3) to the waning of glacial influence (T1) (all maps modified from Cubitt et al., 1998). Note: M1 corresponds with the basal argillaceous third of the Merrimelia Formation. M2 corresponds with the middle portion of the Merrimelia Formation, where sandy facies may have developed. M3 coincides with the upper third of the Merrimelia Formation where sandy Tirrawarra Sandstone facies interfinger with Merrimelia Formation facies. T1 corresponds with the arenaceous Tirrawarra Sandstone.

It is likely that during M2 time, little meltwater was produced as a continental icecap locked up meltwaters and starved sediment dispersal northwards into the basin. Accordingly deposition from the north, southwest and west, was pronounced issuing from actively melting glaciers while deposition from the south was minimal.

The later stage of Merrimelia deposition is characterised by advancing and retreating glaciers (Chapter Four - Fig. 4.9), where "Tirrawarra type sandstones" interfinger with typical Merrimelia lithologies. The southerly input of sediments is again dominant, as retreating glaciers produced large volumes of meltwater. Sediment input from the west, at this time, all but ceased, while sediment originating from the north was still prominent (Fig. 5.24b). At this late stage, minor sediment input appears to have been sourced from the east. This observation is supported by the existence of schist and fresh granite rock fragments unknown in any other wells apart from Mount Howitt #1 and Durham Downs #1 in the eastern portion of the Cooper Basin in Queensland. It has been postulated that such sediments could have shed off the Canaway Fault scarp where phyllite, schist and granodiorite lithologies have been intersected (Pinchin and Anfiloff, 1986).

Input of sediment in late M1, early T1 time was mainly from the north (Fig. 5.24a) where melting glaciers on the northern rim of the basin disgorged sediment into the northern rock fragment domain. Melting glaciers in the south discharged sediment into the basin but to a lesser extent.

At the same time remnant ice caps on small basement highs (Moomba and emergent GMI blocks) dispersed detritus into adjacent lowlands (Fig. 5.24a).

5.6 CONCLUSIONS

- Merrimelia Formation sediments are texturally and mineralogically immature.
- The definition of the Tirrawarra Sandstone, in petrological terms, is a sediment that is mineralogically and texturally mature, quartz-rich with a low rock fragment component as the detrital component of Tirrawarra sediments is derived directly from the Merrimelia Formation.
- The overwhelming majority (80%) of Merrimelia Formation rock fragments can be traced from Warburton Basin units such as the Innamincka Red Beds, Dullingari Group and Mooracoochie Volcanics. The majority of Warburton Basin derived

rock fragments (intrabasinal) deform plastically due to compaction forces and are considered incompetent.

- Approximately one quarter of all Merrimelia Formation rock fragments are extrabasinal, having been mainly sourced from the Arunta Block (NT), Mount Painter/Mount Babbage (SA) Inliers, Willyama Supergroup-Broken Hill (NSW)/Olary (SA). Minor amounts of Merrimelia Formation sediment has been derived from the Peak and Denison Inliers, Flinders Ranges (Adelaidean), Eastern Gawler Craton (SA), Tibooburra Granites (NSW) and possibly the Canaway Ridge (QLD).
- The rock fragment content of Merrimelia sediments closely (but not exactly) mirrors the lithology of the underlying Warburton Basin. Discrepancies are attributable to extra-basinal rock fragments.
- Facies type was seen to be the major control on sediment composition with glacio-aeolian sandstone exhibiting the most mature composition and terminoglacial out wash fan deposits the least mature.
- All rock fragments observed in the Tirrawarra Sandstone were also found in the Merrimelia Formation. The appearance and provenance of rock fragments in Tirrawarra sediments was the same as those in Merrimelia sediments.
- Rock fragment movement into and within the Cooper Basin occurred over long distances. Locally sourced clasts, emanating from exposed terrain, moved shorter distances within clast domains.
- Petrological analysis of Merrimelia rock fragments, when limited to movements of competent rock fragments, revealed three distinct rock fragment domains (northern, southern and western). These rock fragment domains have received extrabasinal rock fragments from at least six different provenance regions.
- Petrological analysis of Tirrawarra rock fragments, when limited to movements of competent rock fragments, revealed four distinct rock fragment domains (northern, southern, western and a mixing zone).
- The degree of cluster overlap changes through time. The Tirrawarra data set shows less overlap between clusters than the Merrimelia dataset. There appears to be little north/south cluster overlap (with samples from Coongie #1 the exception)

in the Tirrawarra dataset. This may indicate that parts of the GMI Ridge were emergent and exerting influence forming a baffle to north south sedimentation during Tirrawarra time.

- The movement of rock fragments in the centre of the Cooper Basin was predominantly along a linear trend (now the GMI Ridge) towards Tallalia #1 in Queensland.
- Sediment input into the Cooper Basin was initially from the basin edges towards the centre of the basin where the dominant input direction was from the south and west. In mid-Merrimelia time sediment input began from the north of the Cooper Basin.

CHAPTER SIX

AUTHIGENIC COMPONENT & DIAGENESIS

6.0 INTRODUCTION

This chapter describes the differing authigenic minerals observed in Merrimelia sediments in terms of petrography, diagenetic mineral formation and paragenesis (diagenetic timing). The chapter is set out in two parts (outlined below). The first part of the chapter describes the petrography of authigenic minerals and the second the diagenesis of Merrimelia sediments

PART ONE

PETROGRAPHY

- Quartz Cement
- Authigenic Clays
- Carbonate Cement
- Trace Authigenic Cements

PART TWO

DIAGENESIS

- Quartz Cement
- Clay Authigenesis
- Carbonate Cement
- Trace Authigenic Cements
- Paragenesis

Diagenetic minerals lead to the enhancement or destruction of reservoir quality. Illite, the most prevalent diagenetic mineral in Merrimelia sediments, inhibits permeability and porosity substantially reducing reservoir quality. Understanding this diagenetic phase is the key to understanding and predicting reservoir quality in Merrimelia glacial sediments (Cubitt and Kaiko, 2000). Hence, authigenic illite is the main focus of this chapter. The issue of reservoir quality along with a discussion on porosity and permeability preservation in Merrimelia sediments is outlined in Chapter Nine.

The petrography and diagenetic formation of each authigenic phase is described and discussed in the first half of this chapter. The latter part of the chapter discusses diagenetic timing, on a local and regional basis.

6.1 STATISTICS

Kolmogorov-Smirnov normality tests indicates that the main diagenetic minerals (illite, carbonate, quartz and kaolin) in Merrimelia samples do not exhibit a normal distribution (Fig. 6.1a). This indicates a sporadic distribution most likely related to the highly variable distribution of lithologies in the Merrimelia Formation where particular authigenic minerals form preferentially in certain lithotypes (i.e. illite in argillaceous sediments).

More specifically:

- 1) Diagenetic phases comprise on average 48% of Merrimelia rocks (Fig. 6.1b).
- 2) The majority of samples contained between 25% and 60% authigenic minerals (Fig. 6.1b).
- 3) Illite is the most common diagenetic mineral with carbonate cements next most common (Fig. 6.1c).
- 4) Quartz and kaolin authigenic phases are observed in equal proportions (Fig. 6.1c).
- 5) Opaque cements such as pyrite and haematite occur in trace amounts.

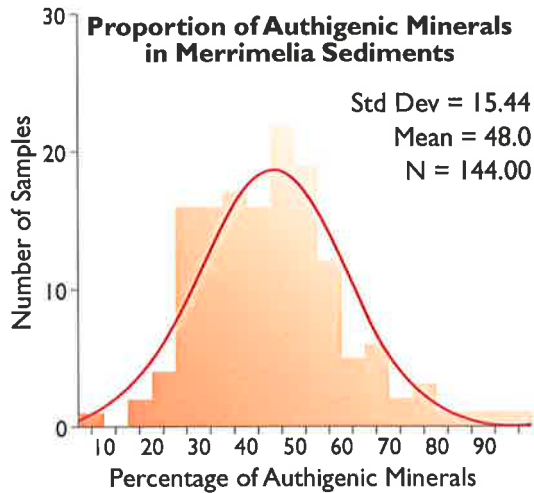
The authigenic minerals dataset was subjected to principle components analysis (PCA) utilising the same criteria as that used on the Tirrawarra and Merrimelia rock fragment data sets (Chapter Five). The analysis of the authigenic mineral dataset revealed three groupings of variables representing;

- 1) Clay (Fig. 6.1d),
- 2) Calcite/dolomite (Fig. 6.1d),
- 3) Quartz/chlorite/pyrophyllite/siderite (Fig. 6.1d).

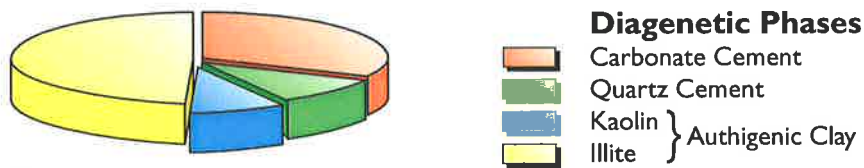
These statistical groupings may be suggestive of diagenetic links, where, groups of minerals are associated. For example, kaolin and illite are commonly observed together as are dolomite and calcite cements. In contrast, the PCA diagram in Figure 6.1 suggests that the occurrence of quartz cement and kaolin is unrelated. However, repeated observations indicate that these phases are cogenetic in arenaceous Merrimelia sediments. This lack of consistency (between diagenetic observation and statistics) diminishes the confidence level of statistical outcomes.

Kolmogorov-Smirnov Ratio				
	Carbonate	Illite	Quartz Cement	Kaolin
Z Value	0.159	0.178	0.234	0.24

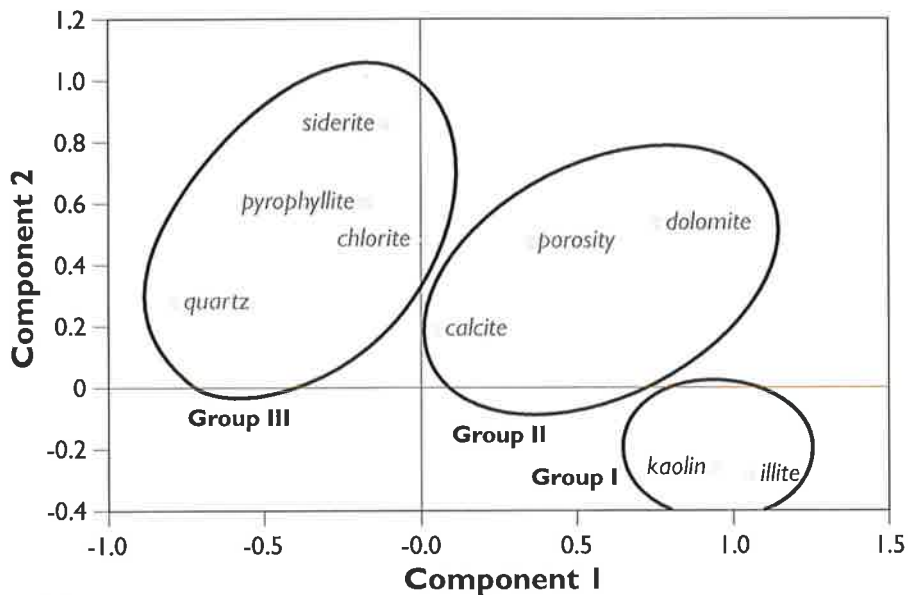
A



B



C



D

PEL5/6 546 N

Figure 6.1 A) Kolmogorov-Smirnov normality ratios for the main authigenic minerals observed in the Merrimelia Formation. B) Frequency histogram of authigenic minerals proportion in Merrimelia Formation samples. C) Pie chart showing proportions of diagenetic phases in the Merrimelia Formation. D) Principle Components Analysis (PCA) cross plot of authigenic minerals in Merrimelia Formation sediments.

The variability in this dataset is further borne out by the fact that no positive or negative correlation groupings were delineated by PCA (Fig. 6.1d). In contrast positive and negative correlation groupings were delineated in Merrimelia and Tirrawarra rock fragment datasets (Figs. 5.6 & 5.13). This lack of correlation again points to the variable distribution of authigenic mineral in Merrimelia sediments. Such variability is to be expected in a chaotic mix of at least twenty one anastomosing (laterally and vertically), glacially derived facies, which are generally dominated by a clast component that can contain up to 76 rock fragment types of contrasting chemical compositions.

6.2 PETROGRAPHY

6.2.1 QUARTZ CEMENT

Quartz overgrowths are by no means common in Merrimelia sediments. Plate 19a illustrates that most samples contain no quartz cement, and those that do generally contain between 5% to 10% overgrowth proportions. This is not surprising, as the majority of Merrimelia sediments are argillaceous in nature. In arenaceous Merrimelia lithologies however, quartz framework grains are commonly surrounded by syntaxial quartz overgrowths (Plate 19d), forming regions of quartz cementation (Plate 19d [5d]). The average composition of syntaxial quartz cement is given in Table (6.1). Druse quartz overgrowths also occur (Plate 19f), but are rare. However, locally, druse quartz overgrowths can dominate pore spaces (Plate 19e-Coonatie #1). Both syntaxial quartz and druse quartz cements are commonly observed in the same sample (Plate 19f).

Both quartz overgrowth phases will only form on quartz grains that are adjacent to other quartz grains and into pore spaces that are free of authigenic illite and/or squeezed ductile rock fragments (Plate 19b & 19d). Thus, sites for quartz overgrowths depend on the number of "clean" quartz to quartz contacts available (Plate 19b). An abundance of pore-filling clays or ductile rock fragments in the framework of a rock will inhibit quartz overgrowth development (Plate 19b & 19d).

These processes are illustrated in Plate 19. Plate 19b (a cartoon of Plate 19d) shows large syntaxial quartz overgrowths have developed adjacent to quartz grains. In contrast, limited quartz cement development has occurred where clays/ductile rock fragments dominate (Plate 19b[green region]). Quartz cement in these rock fragment-rich regions are subdued and seemingly intergrown with pore-filling clay in a fashion similar to that shown in Plate (19c).

PLATE 19

Authigenic Minerals: Quartz Cement

A) *Frequency histogram. Quartz cement: Merrimelia Formation*

B) *Cartoon of quartz cement relationships in an arenaceous Merrimelia-Tirrawarra sediment.*

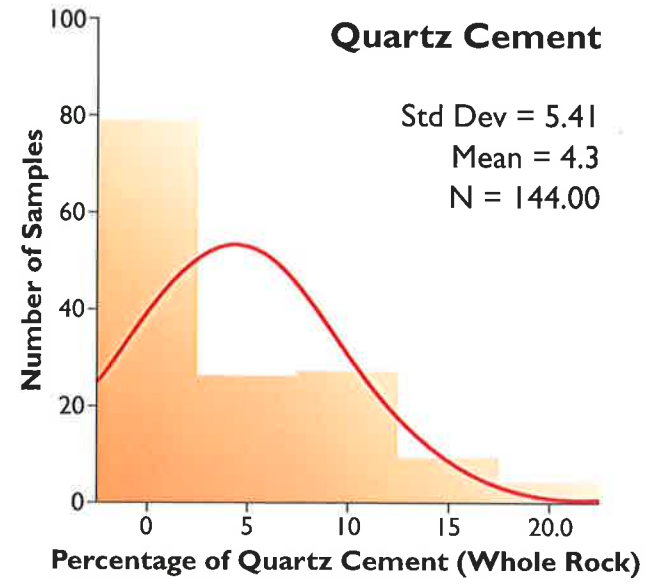
C) *SEM photomicrograph – Tirrawarra #14 (2960.52m). Close up of a region similar to that outlined (box) in Plate 19d. Quartz cement [4f] abutting a squeezed, argillaceous rock fragment.*

D) *Photomicrograph – Moorari #3 (2398.28m) (Plane polarised x 10). Broad field of view illustrating, a squeezed mica [3f], druse quartz cement [5c], syntaxial quartz overgrowths [5d] and a squeezed, chloritised labile grain occluding porosity [12e]. This plate corresponds with the cartoon in Plate 19b.*

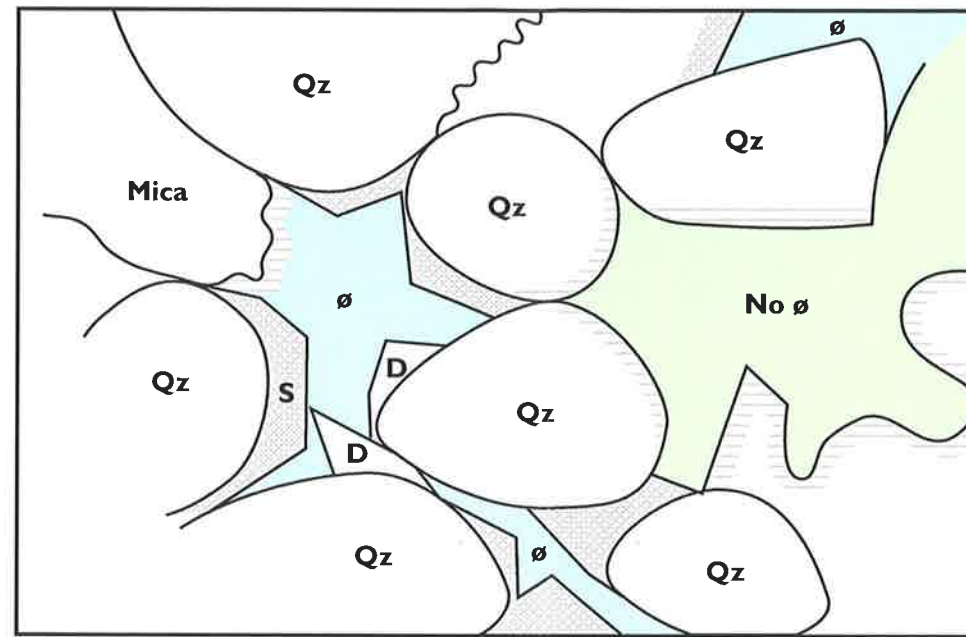
E) *SEM photomicrograph – Coonatie #1 (3149.19m). Close up of a region similar to that outlined (box) in Plate 19f. Druse quartz cement [3g] radiating into open pore space.*

F) *Photomicrograph – Coonatie #1 (3148.30m) (Plane polarised x 10). Broad field of view illustrating extensive druse quartz cementation.*

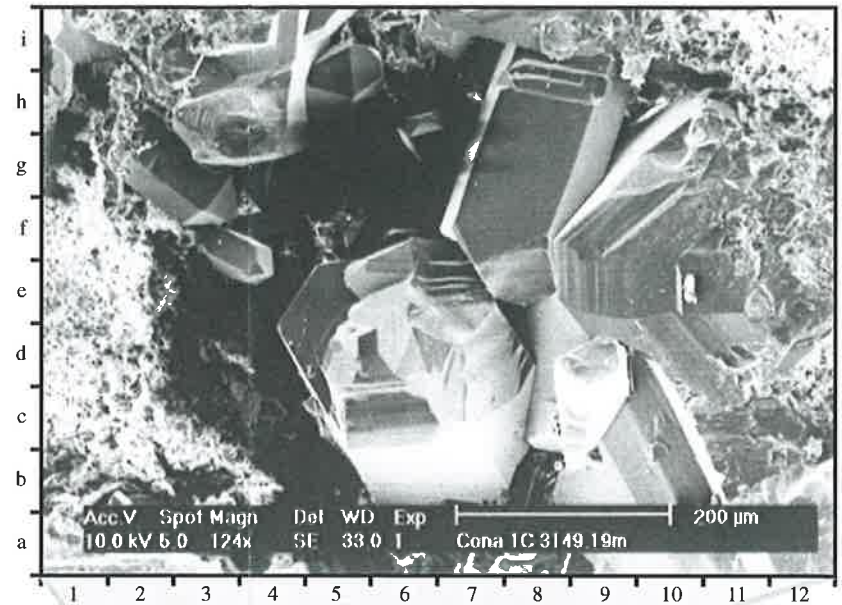
Plate 19



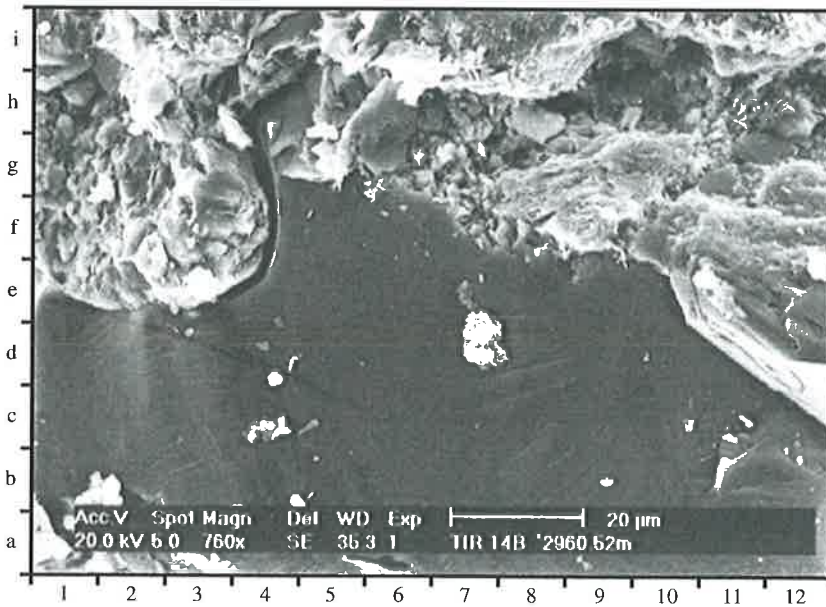
A



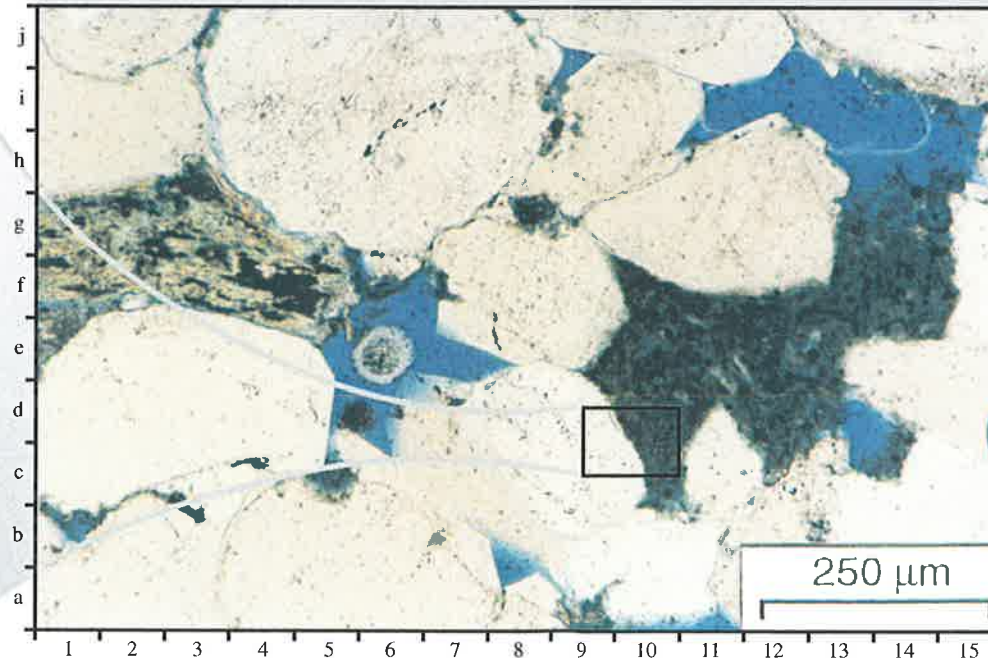
B S - Syntaxial quartz overgrowth, D - Drusy, Qz - Quartz overgrowth, Quartz cement growth site, Non quartz cement growth site, ø - pore space



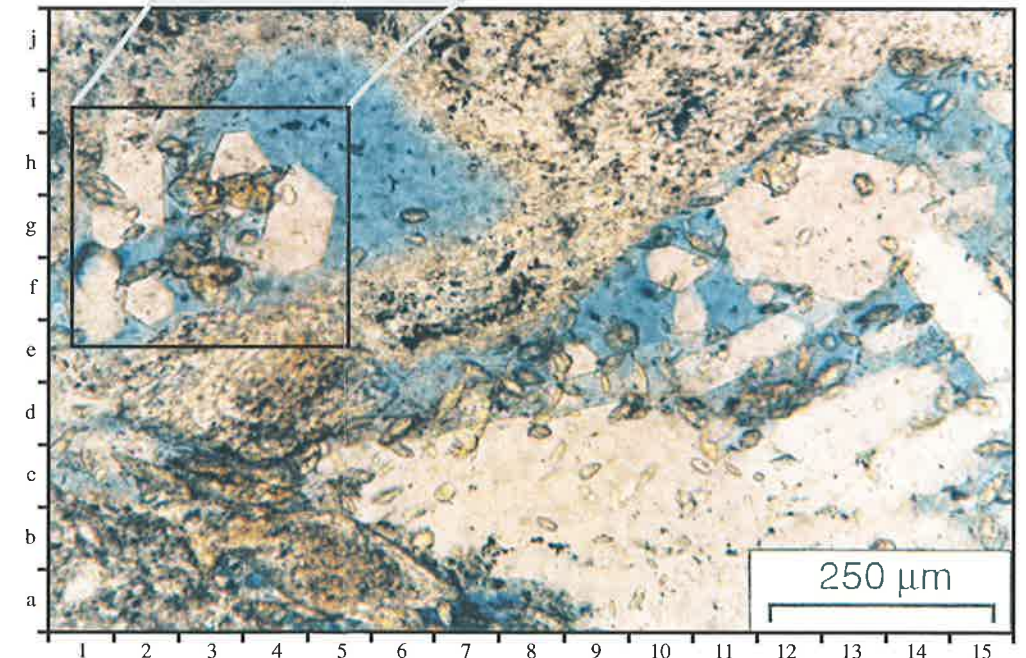
E



C



D



F

Sample	SiO ₂	Al ₂ O ₃	Cr ₂ O ₃	MgO	CaO	MnO	Fe ₂ O ₃	Ba ₂ O	K ₂ O
MOOR 2B	96.36	0.27	0.01	0.13	0.44	0	0.40	0.04	0.04
PAN 1C	98.04	0.36	0	0.06	0.05	0.08	1.008	0	0
MUDL 1B	99.05	0.06	0	0.02	0.001	0.04	1.10	0	0
MAL 4A	99.66	0	0	0	0	0.01	0.08	0	0
TIRA 8A	97.55	0.83	0	0.02	0.03	0	0.038	0	0

Table 6.1 Microprobe analysis of selected quartz overgrowths (Wt.%).

Therefore, if argillaceous rock fragments or matrix are the dominant component of a Merrimelia sediment, quartz cement will not form. Such a sediment is illustrated in Chapter Five (Fig. 5.2e). In contrast, if a Merrimelia sediment is dominated by an arenaceous framework (Chapter Five - Fig. 5.2b) then abundant sites are available for quartz overgrowths to form. Hence, facies type (argillaceous or arenaceous) and to a certain degree sediment provenance (rock fragment lithology), control the abundance of quartz cement in Merrimelia sediments.

6.2.2 AUTHIGENIC CLAYS

Authigenic clays are the most prevalent diagenetic phases in Merrimelia sediments (Fig. 6.1b), with illite dominating over kaolin (Fig. 6.2a). Less than five samples didn't contain authigenic clay (Fig. 6.2b). The other 139 samples described had clay fractions that constituted between 5% and 30% of the bulk sample (Fig. 6.2b). A small number of samples (argillaceous) were composed of up to 70% clay (Fig. 6.2b). Illite dominates the majority of samples, with most samples containing between 10% to 20% of this clay type (Fig. 6.2c). Kaolin was observed in less than half of the samples, in amounts varying from 5% to 10% (Fig. 6.2d). The presence of dickite was indicated by XRD analysis (Fig. 6.6c) in five samples.

Chlorite was seen in trace proportions, generally associated with chloritic, basic and biotite-dominated rock fragments. Glaucony and "Glauconitic illite" (as described by Taylor *et al.*, 1991) were also observed in trace proportions in the Merrimelia Formation (see section 6.2.2.2).

The average composition of all clay phases observed in Merrimelia sediments, along with the published composition of "glauconitic illite", are given in Table (6.2).

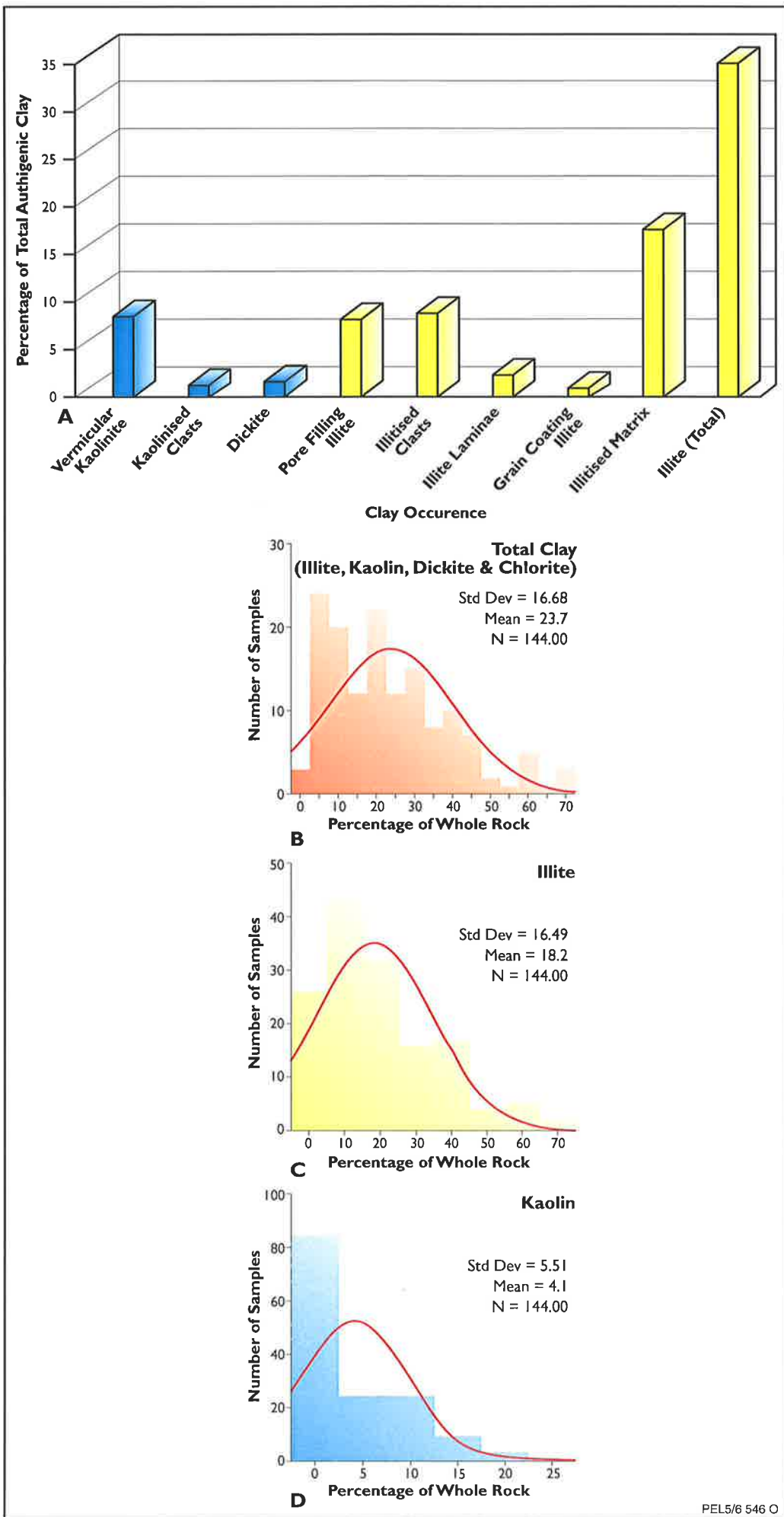


Figure 6.2 A) Histogram of clay proportions in the Merrimelia Formation. Sample frequency histograms of B) total clay, C) illite and D) kaolin in Merrimelia sediments.

Morphology	SiO ₂	TiO ₂	Al ₂ O ₃	MgO	CaO	MnO	Fe ₂ O ₃	Na ₂ O	K ₂ O
Kaolin	45.3	0.02	38.8	0.01	0.002	0.03	0.24	0.02	0.03
Bulk Illite	50.7	1.1	28.5	0.42	0.11	0.2	1.57	0.23	8.18
Glaucony	52.8	0.06	22.11	2.18	0.19	0	10.0	0.01	8.61
Glaucony	53.7	0.02	16.68	2.86	0.16	0	12.30	0.02	8.68
"Glauconic Illite"	53.9	0.05	15.91	3.34	0.11	-	13.78	0.13	8.96

Taylor *et al.*, (1991)

Table 6.2 Microprobe composition (Wt.%) of glaucony, "glauconic illite", kaolin and illite.

6.2.2.1 Illite

Illite profoundly effects reservoir quality in Merrimelia sediments (see Chapter Nine). Consequently illite diagenesis was a major focus of this study and therefore a large section of this chapter is devoted to illite. A summary of literature pertinent to "illite" is presented here to define commonly used illite terminologies and concepts.

6.2.2.1.1 Literature Review

Clay mica, sericite, hydrous mica and illite are terms that have been used in the literature to describe similar clay-sized phylloquartzite minerals (Nadeau and Bain, 1986). The term "illite" is used here to denote a non-expandable dioctahedral, aluminous, K-bearing micaceous clay phase. In contrast, the term "smectite" denotes a clay or component with expandable layers and a lower negative layer charge than illite (Sass *et al.*, 1987). Interstratified illite/smectite (I/S) clays are commonly referred to in the literature (and in this study) as mixed-layer (I/S) clays (Nadeau and Bain, 1986).

The swelling, and non-swelling nature of clay structures can be determined using ethylene glycol vapour/liquid which expands clay layers to a standard distance, changing the basal spacing of the clay (Velde, 1992). The basal spacing (the distance between sheet layers) varies between swelling and non-swelling clays.

Comparison of the basal spacings in glycolated and unglycolated (or air dried) clays distinguishes between swelling and non swelling clay types and discriminates between major swelling clays. Table 6.3 illustrates the major clay minerals and their respective basal spacings, glycolated and air dried (Velde, 1992).

All clays are sheet silicates with a similar arrangement of atoms. There are two basic building units, a silica-oxygen sheet of joined tetrahedral units and an aluminium-hydroxyl sheet of joined octahedral units.

Various clay types are built of differing sheet arrangements and different cations between the sheets (Fig. 6.3). Cation types are controlled by substitution of Al for Si in the tetrahedral sheets and Fe and Mg for Al in the octahedral sheets (Fig. 6.3). Inserting cations into holes between octahedral and tetrahedral sheets restores layer charge balance, induced by cation substitution. (Velde, 1992). There are two types of ion occupancy in octahedrally coordinated sites; trioctahedral (three ion site occupancy) and dioctahedral which has a two ion site occupancy.

	<i>Dominant elements</i>	<i>Basal spacing (Å) Glycol Dry</i>	
SWELLING TYPES			
Smectites			
Beidellite	Al	17	10
Montmorillonite	Al (Mg, Fe ²⁺ minor)	17	10
Nontronite	Fe ³⁺	17	10
Saponite	Mg, Al	17	10
Vermiculite	Mg, Fe ²⁺ , Al (Fe ³⁺ minor)	15.5	10-12
Mixed layer minerals*		10-17	<10
NON-SWELLING TYPES			
Illite	K, Al (Fe, Mg minor)	10	
Glaucanite	K, Fe ²⁺ , Fe ³⁺	10	
Celadonite	K, Fe ²⁺ , Mg, Fe ³⁺ , Al ³⁺	10	
Chlorite	Mg, Fe, Al	14	
Berthiérine	Fe ²⁺ , Al ³⁺ (minor Mg)	7	
Kaolinite	Al	7	
Halloysite	Al	10.2	
Sepiolite	Mg, Al	12.4	
Palygorskite	Mg, Al	10.5	
Talc	Mg, Fe ²⁺	9.6	

* Two or more types of basic layer interstratified in the same crystal

Table 6.3 XRD responses of major clay minerals (After Velde, 1992).

The firmly bonded layers and interlayer cations are stacked upon one another to form a three dimensional clay crystal (Velde, 1992). In each sheet there is an offset between the tetrahedral and octahedrally coordinated ions. This offset is monoclinic and places the different ions in more specific crystallographic sites. Thus as the sheets are stacked upon each other they will give differing XRD diffraction patterns due to the relative orientation of the stacked sheets. Hence different stacking arrangements (called polytypes) give different XRD patterns (Velde, 1992).

Illites are similar to muscovite in structure and composition. Charge imbalance lies in the substitution of Al for Si ions in the tetrahedral sheet while little substitution occurs in the octahedral sheet. However, a certain amount of Mg and Fe²⁺ is introduced into illite clay by octahedral site substitution. In summary, the major cations found in the tetrahedral coordinated layers are Si and Al, while the cations in the octahedrally coordinated layers are more varied with Al, Mg, Fe²⁺ being the principal species, while Fe³⁺, Ti, Ni, Zn, Cr, and Mn can also be present (Velde, 1992).

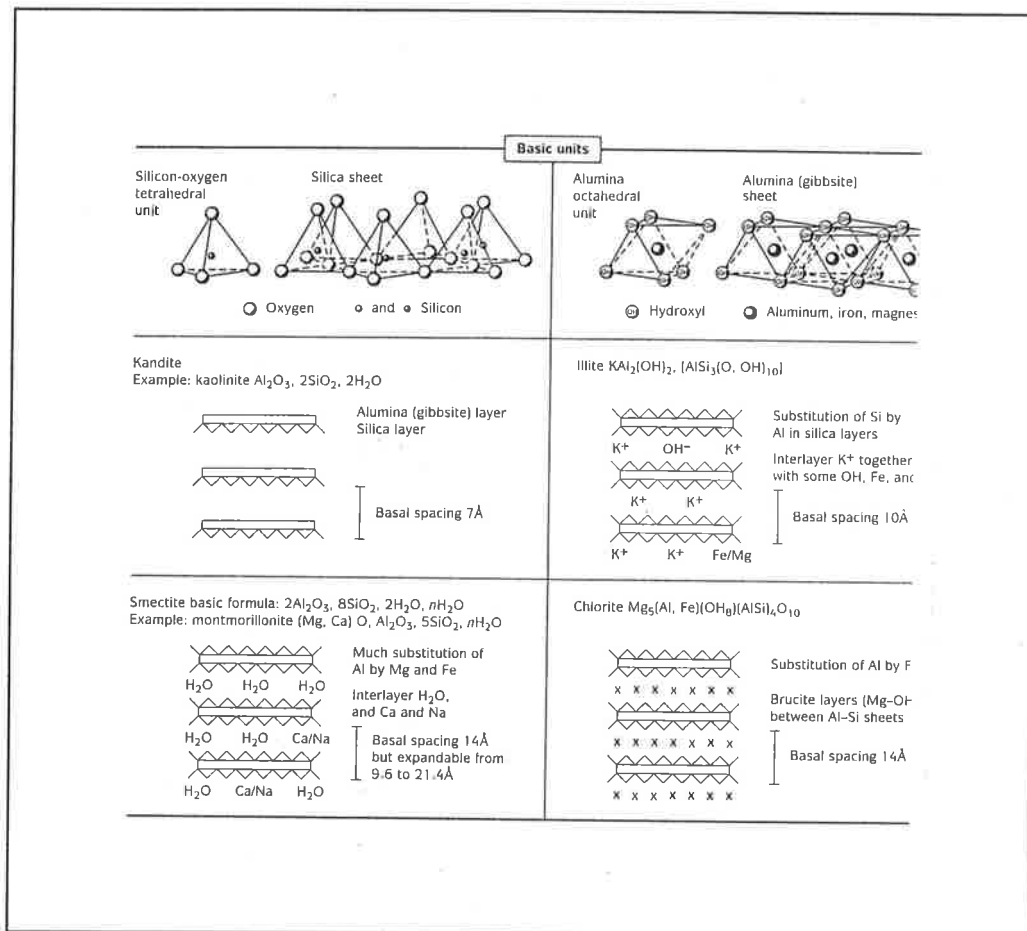


Figure 6.3 The basic structure of the most common clays observed in Merrimelia sediments (After Prothero and Schwab, 1996).

The interlayer cation species are varied but potassium cations are tightly fixed and therefore predominate. Table 6.4 illustrates typical illite compositions and unit cell dimensions (Å). Mixed layered clays usually indicate a change in physical or chemical variables.

Increasing temperature with depth brings about a change in the stability of one of the clay minerals in the mixed layered clay. In the case of illite-smectite mixed layered

clays, smectite clay become progressively more unstable as the depth of burial increases (Nadeau *et al.* 1984).

<i>Illite</i>				<i>Glauconite</i>				<i>Celadonite</i>			
<i>Typical</i>	<i>Range</i>			<i>Typical</i>	<i>Range</i>	<i>Typical</i>	<i>Range</i>				
Interlayer sites											
K	0.77	0.6	-0.80	K	0.8	0.75	-0.88	K	0.84	0.61	-0.92
Na	0.01	0	-0.07	Na	0	0.01	-0.07	Na	0	0	-0.13
C	0.02	0	-0.06	Ca	0	0	-0.07	Ca	0.03	0	-0.12
Octahedral sites											
Al	1.63	1.22	-1.77	Al	0.4	0.36	-0.50	Al	0.78	0.07	-1.22
Fe ³⁺	0.03	0.03	-0.45	Fe ³⁺	1.0	0.35	-1.55	Fe ³⁺	0.47	0.36	-1.14
Fe ²⁺	0.05	0	-0.22	Fe ²⁺	0.4	0.04	-0.51	Fe ²⁺	0.21	0.12	-0.26
Mg	0.30	0.15	-0.36	Mg	0.2	0.10	-0.51	Mg	0.68	0.48	-1.04
Ti	0.04	0	-0.06	Ti	0	0	-0.01	Ti	0	0	-0.02
Tetrahedral sites											
Si	3.40	3.18	-3.70	Si	3.90	3.54	-3.93	Si	3.88	3.50	-4.00
Al	0.60	0.30	-0.82	Al	0.10	0.07	-0.46	Al	0.12	0	-0.49
Cell dimensions											
(001)	10.1 Å				10.1 Å				10.1 Å		
(060)	1.50 Å				1.512-1.517 Å				1.507-1.509 Å		

Table 6.4 Composition of mica-like clays (Velde, 1992).

6.2.2.1.2 Distribution of Illite in the Merrimelia Formation

Extensive authigenic illite has been noted throughout the South Australian sector of the Cooper Basin in the Merrimelia Formation where there is a high concentration of ductile rock fragments (Fig. 6.4). Semi-variogram analysis of these maps (Figs. 6.4b & 6.4c) indicates that the nugget effect on maps in this figure is high. Accordingly the maps (Figs. 6.4a & 6.4c) represent trends within the datasets and not absolute areal distributions. The similarity between both ductile rock fragments and illite datasets suggests that there is an association. This relationship is most likely a result of the preferential replacement of argillaceous and devitrified volcanic rock fragments by illite.

Illite is also formed in arenaceous sediments which contain little or no argillaceous rock fragments. In general the proportions of illite¹ formed in arenaceous sediments (grain-coating and pore-filling illite) is subordinate to illite formed in argillaceous sediments (rock fragment and depositional matrix replacement).

¹ Illite proportions are estimated via image analysis of fluorescence illite images. A technique which will be expanded on in Chapter Seven.

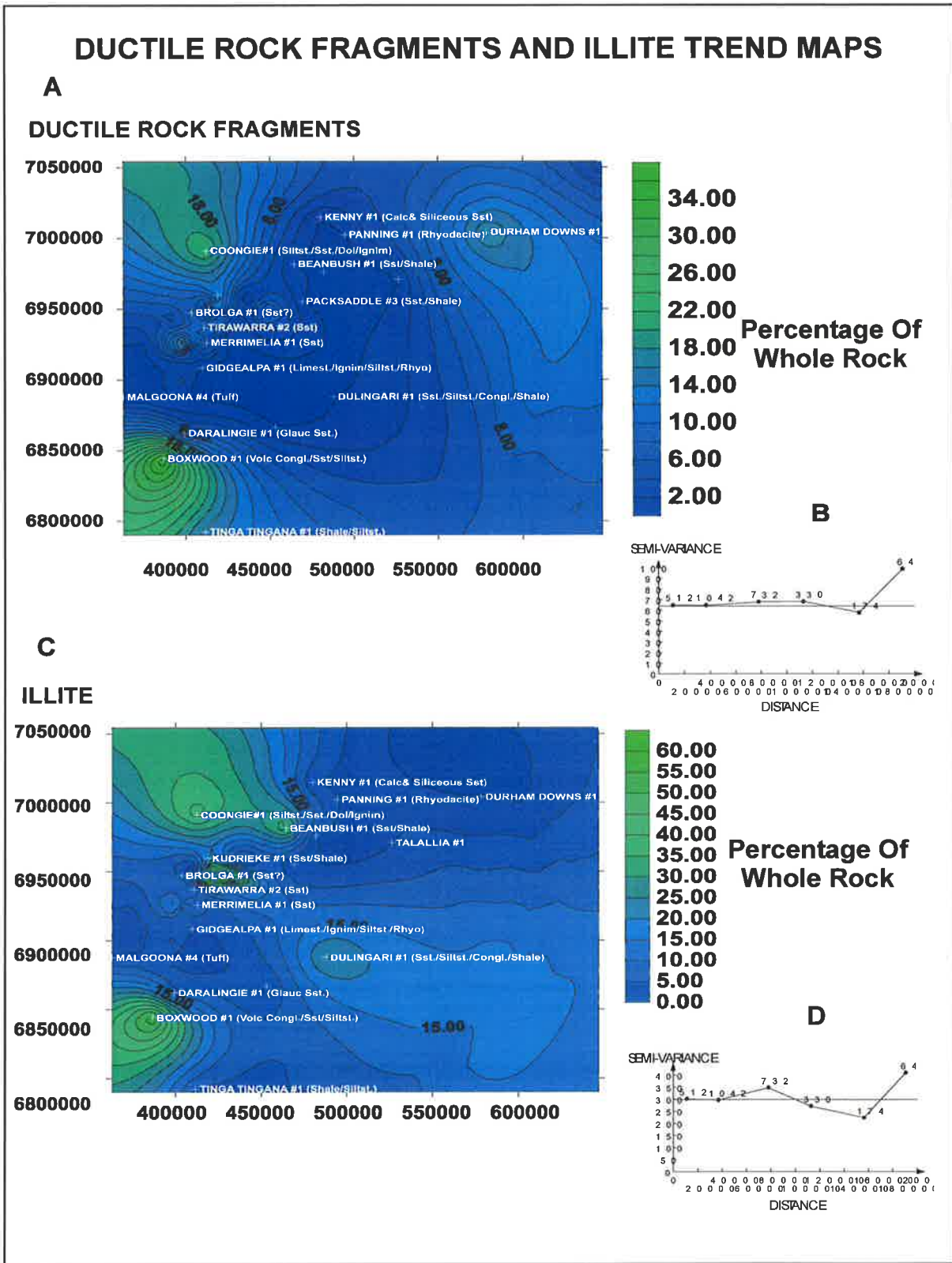


Figure 6.4 A) Ductile rock fragments trend map (Merrimelia Formation). B) Ductile rock fragments variogram (Merrimelia Formation). C) Illite trend map (Merrimelia Formation). D) Illite variogram (Merrimelia Formation).

6.2.2.1.3 Illite in the Merrimelia Formation: Nature and Composition

XRD analysis of the $<2\mu\text{m}$ fraction of a limited set of samples shows that the abundant illite observed in Merrimelia sediments is in fact an interstratified illite/smectite (I/S) with about 95% illite layers (Figs. 6.5a & 6.5b). Based on the XRD character of the oriented samples, the I/S has an ordered interstratification (Moore and Reynolds, 1989) with very little intermixed discrete illite (Fig. 6.5a & 6.5b). The broadness of XRD peaks, makes it difficult to be more precise, but, a range of illite contents is suggested by the changing shape of XRD peaks. Illite clays in Merrimelia sediments probably range from 85% to 95% illite within a mixed layered I/S clay.

Randomly oriented $<2\mu\text{m}$ illite samples were analysed using standard XRD techniques (Figs. 6.5a & 6.5b). The "noisy" spectra derived from these samples are hard to interpret but suggest turbostratic stacking of 2:1 layers. This interpretation is however at odds with selected area diffraction (SAD) images taken of the same two samples (Plates 20c & 20d). These images show electron diffraction patterns that tend to be distributed in an ordered arrangement of spots rather than rings, as would be expected for turbostratic stacking (Mathews pers. comm., 1996) (Plates 20c & 20d).

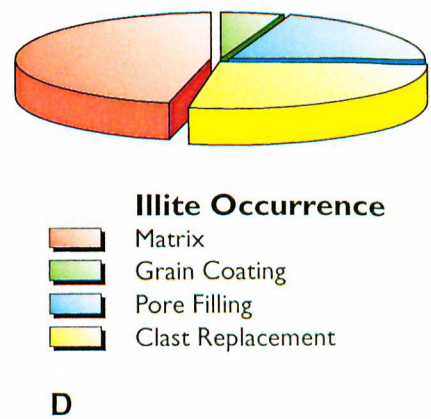
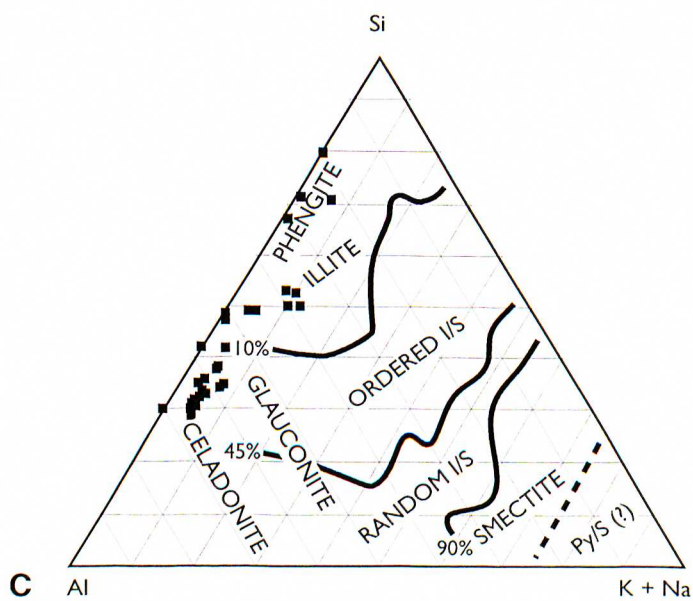
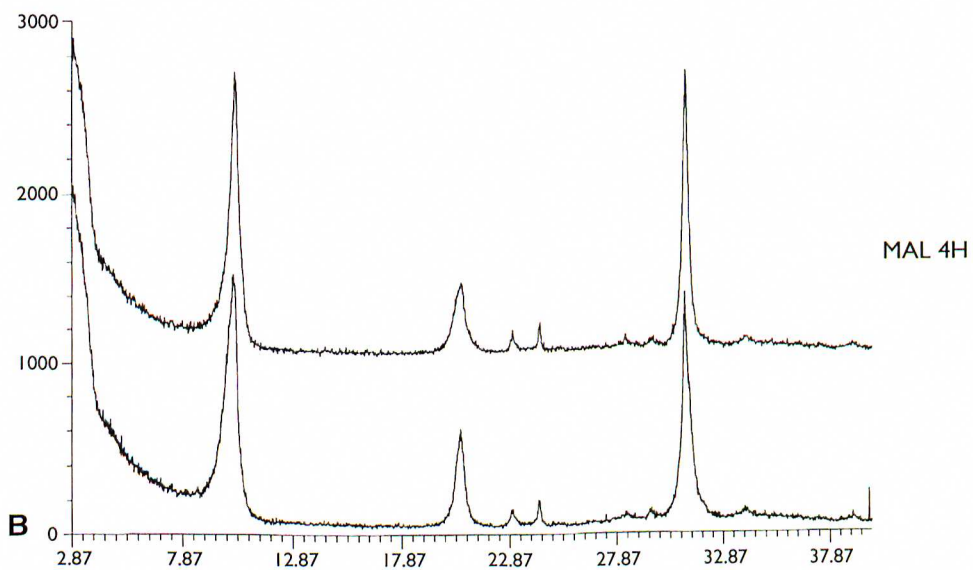
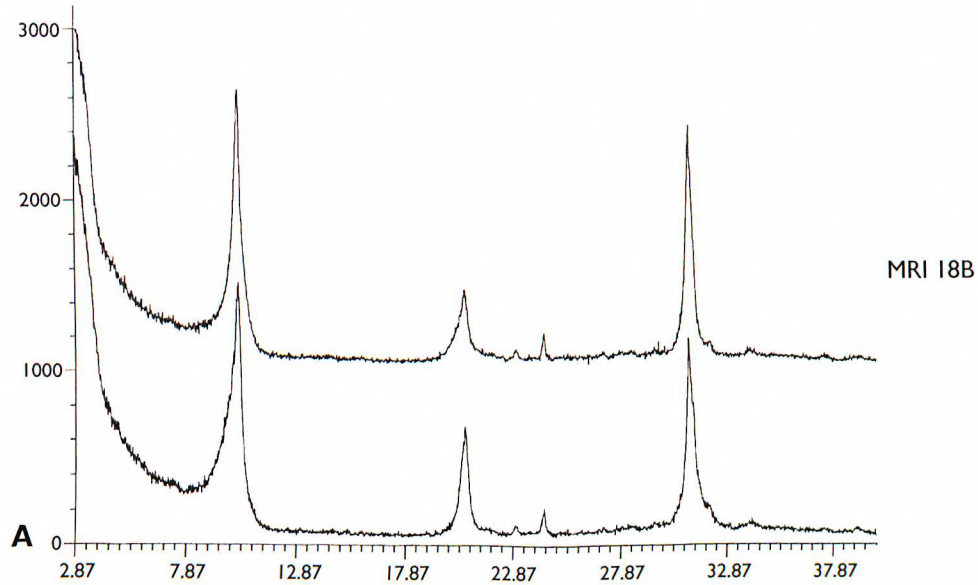
Compositional illite data are of two main types:

- 1) A detailed investigation of illite dated samples (2MAL4H and 2MRI 18B) using TEM and SEM analyses.
- 2) A cursory look at samples distributed over a larger area using SEM (fractured core surfaces) and microprobe (thin sections).

Data from microprobe and SEM analyses when plotted on a ternary diagram (Fig. 6.5c) indicates that the composition of illite in Merrimelia samples falls on the border of phengite illite and that of a mixed layered clay which is composed of 10% smectite.

TEM analysis confirms XRD analysis, indicating that the mixed layered I/S clay has been transformed to an ordered illite, with minor amounts of smectite remaining ($<10\%$ smectite). Illite/smectite proportions observed via TEM analysis are consistent with the I/S proportions seen in XRD, microprobe and SEM analyses.

TEM results indicate that the two samples, 2MRI 18B and 2MAL4H, are composed of laths ($2\mu\text{m}$ - $3\mu\text{m}$) and flakes ($2\mu\text{m}$) (Plates 20e & 20f).



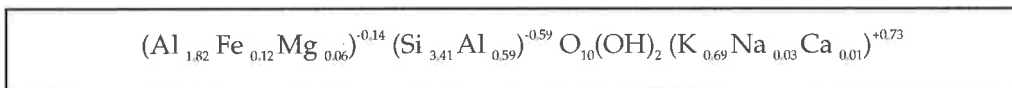
EXPDEV 076 O

Figure 6.5 A) Merrimelia #18 (2548.03m) XRD spectra of <2micron and <4micron illite fractions. B) Malgoona #4 (2179.01m) XRD spectra of <2micron and <4micron illite fractions. C) Ternary diagram illustrating illite and phengite compositions in Merrimelia Formation sediments. D) Illite occurrence in Merrimelia Formation sediments.

The flakes appear to be either coalesced laths which have been irregularly stacked by the collapse of laths during sample air drying (Mc Hardy *et al.*, 1982) or are laths which have thicker centres where laths grow away from the edges in certain limited orientations. The TEM analysis suggests that the majority of illite in these samples is lath-like in nature (Plates 20e & 20f). The dominance of laths in TEM and filamentous illite in SEM could possibly be related.

The composition of both laths and flakes are similar showing minor variance (Table 6.5). For example the data in Table 6.5 indicates that Al is lower in illite flakes than it is in laths. In contrast silica is elevated in flakes when compared with the silica content of laths. However, potassium contents in both lath and flake samples were similar (Table 6.5). In general, the similarity in both lath and flake compositions tends to suggest that they have formed in one illite phase.

The structural formulae of illite in Merrimelia sediments calculated from microprobe derived compositions using the method described in Srodon and Eberl (1987), is as follows:



This formulae is consistent with structural formulae published for illite by Srodon and Eberl, (1987).

SAMPLE	MgO	Al ₂ O ₃	SiO ₂	K ₂ O	Fe ₂ O ₃
Flake (2MAL 4H)	2.7	22.8	59.6	9.2	2.5
Flake (2MRI 18B)	4.2	20.5	58.2	7	10.1
Lath (2MAL 4H)	2.9	29.5	54.4	10.5	2.7
Lath (2MRI 18B)	2	29.7	55.1	6.4	6.8

Table 6.5 TEM/EDS lath and flake illite compositions (Wt.%).

6.2.2.1.4 Illite in the Merrimelia Formation: Optical Petrography

A) Air Drying Effects On Illite Clay

Caution has been exercised in interpreting illite morphologies and textures in this study. McHardy *et al.*, (1982) concluded that air drying TEM specimens tends to cause laths to form coalesced mats. Air dried TEM clay mounts used in this study do exhibit coalesced lath mats (Plate 20e[6g]) with misinterpretation as core and lath textures possible.

PLATE 20

Authigenic Minerals: Pyrophyllite & illite

A) Photomicrograph – Spencer #1 (2014.33m) (Cross nicols x 10). Authigenic pyrophyllite [5e] forming in pore spaces between rhyodacite rock fragments.

B) BSE Image – Malgoona #2 (2261m). Pyrophyllite forming between detrital grains.

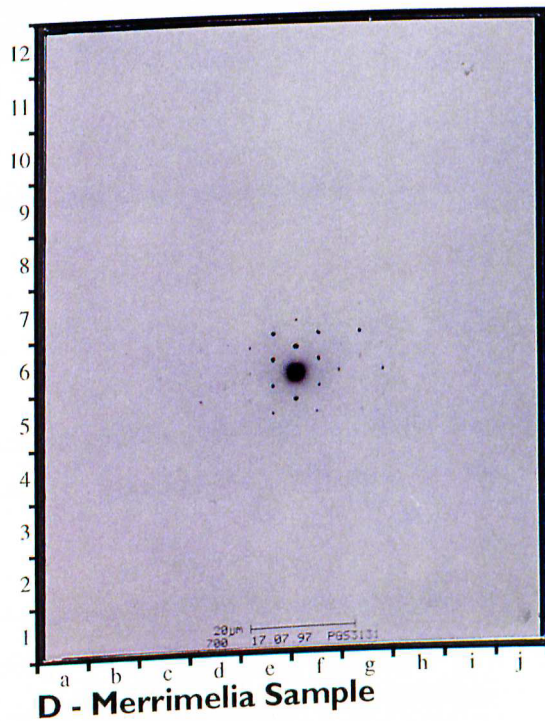
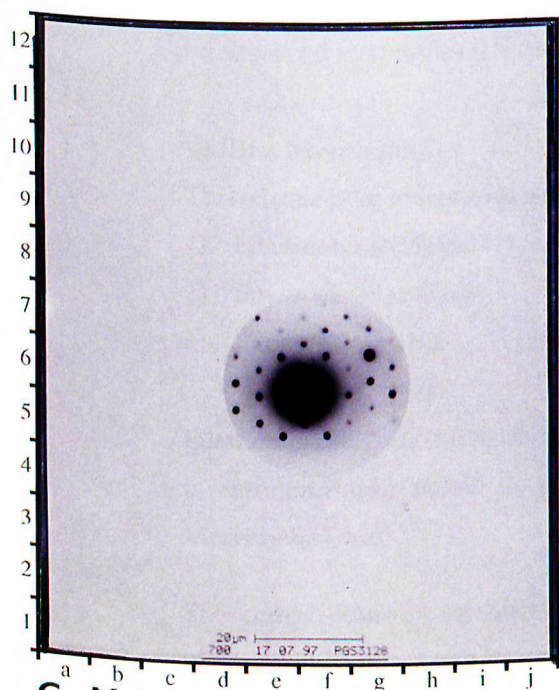
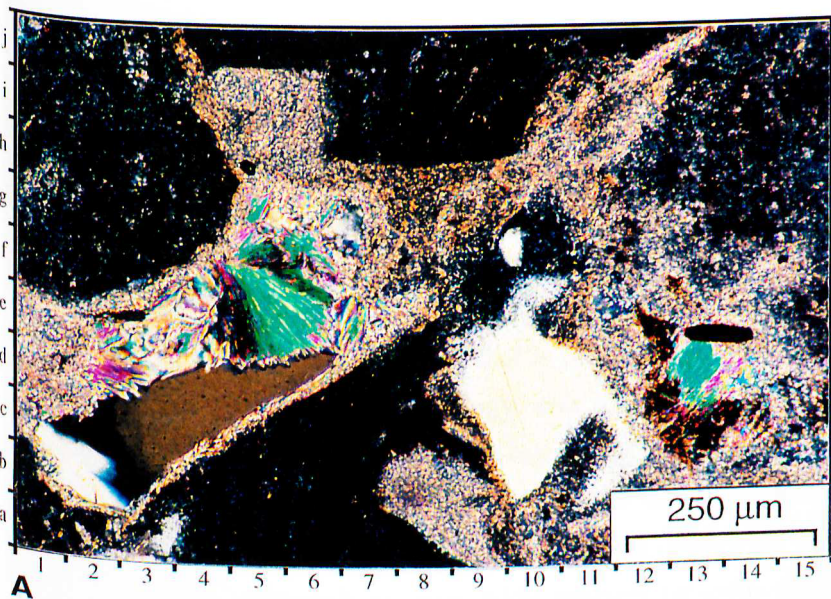
C) Selected Area Diffraction (SAD) photomicrograph – Malgoona #4 (2179.01m). Electron diffraction pattern of illite in the Merrimelia Formation at Malgoona Field.

D) Selected Area Diffraction (SAD) photomicrograph – Merrimelia #18 (2448.03m). Electron diffraction pattern of illite in the Merrimelia Formation at Merrimelia Field.

E) TEM photomicrograph - Malgoona #4 (2179.01m). Broad view of laths and flakes, indicating that sample purity is high. Note: Illite laths dominate.

F) TEM photomicrograph - Merrimelia #18 (2448.03m). Broad view of laths and flakes, indicating that sample purity is high. Note: Illite laths dominate.

Plate 20



BSE images also illustrate “collapsed illite” textures (Plate 21d[13e]). In this example, filamentous illite fibres have collapsed against pore walls. It is most likely that *in situ*, at reservoir temperatures and pressures, these illite fibres would have extensively intruded into the pore space, negatively impacting permeability. Likewise, SEM images also reveal illite collapse features (Plate 21e[6h]).

It is possible then, that in the SEM and BSE images outlined above, a biased account of illite morphology and distribution could be made, with any subsequent interpretation under-estimating the effect of illite on permeability. In this study however, SEM and BSE images were scrutinised for “collapsed illite” textures, with the majority of samples showing little or no “illite drying effects”. Subsequently, in illite-rich samples, SEM analysis typically reveals extensive boxwork and/or long filamentous pore-bridging illite textures (Plates 21b & 21a). Such textures would not be observed in samples adversely effected by air drying.

B) Illite Morphologies

Three basic illite morphologies are recognised in Merrimelia sediments,

- 1) Filamentous (Plate 21a)
- 2) Boxwork (Plate 21b)
- 3) Platey (Plate 21c).

Filamentous illite is the most common while boxwork illite is subordinate. Platey illite is rare and was noted in abundance only in glacio-aeolian sandstones of the Merrimelia Field.

The composition of the three basic illite morphologies in Merrimelia sediments is given in Table (6.6). Filamentous illite is observed filling pores, coating framework grains and as the main constituent of matrix (recrystallised detrital smectite) (Plate 21a). Filamentous illite also forms on the scalloped edges of illite boxwork textures (Plate 21b[Inset]).

Illite Morphology	MgO	Al ₂ O ₃	SiO ₂	K ₂ O	TiO ₂	FeO	Na ₂ O	CaO	MnO
Boxwork	2.2	26.83	56.23	8.58	0	6.15	0	0	0
Filamentous	0.12	32.93	55.43	8.55	1.1	1.78	0.04	0	0
Platey	1.07	33.86	52.54	9.83	0.06	1.49	0.13	0.31	0.02

TABLE 6.6 *Illite morphology compositions (Wt.%).*

PLATE 21**Authigenic Minerals: Illite Morphologies**

A) SEM photomicrograph – Lake Hope #1 (2499.49m). Filamentous illite surrounding a partially illitised feldspar. [Inset] Magnified view of filamentous illite.

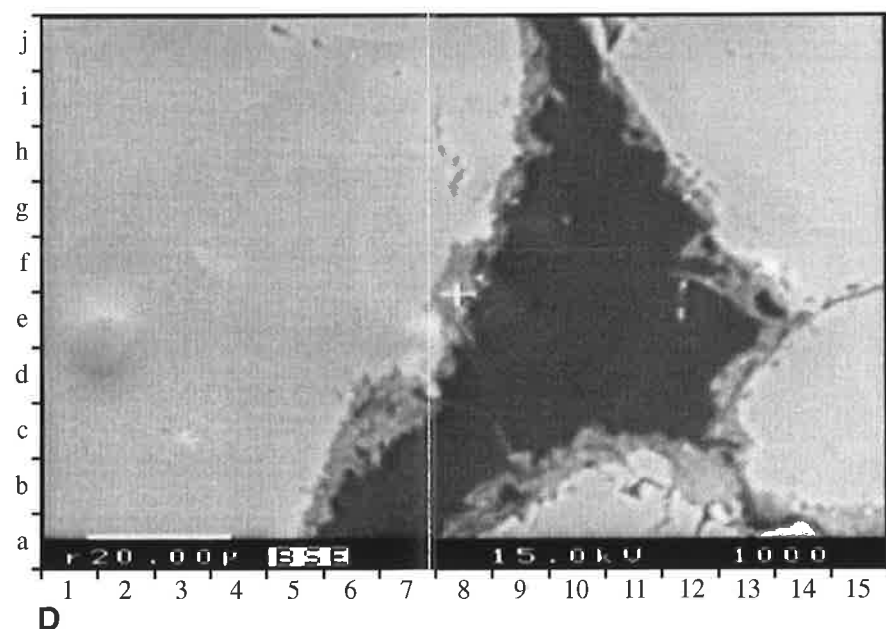
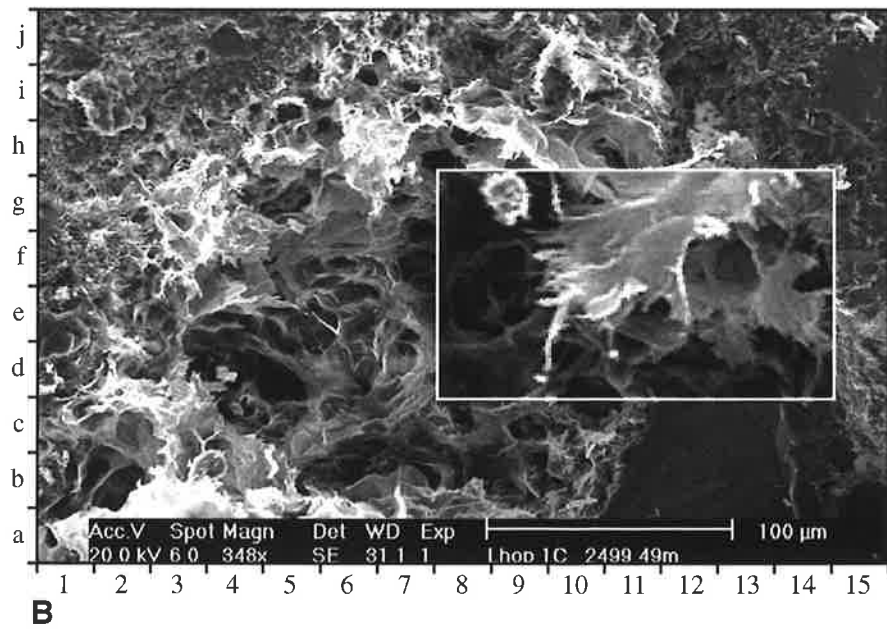
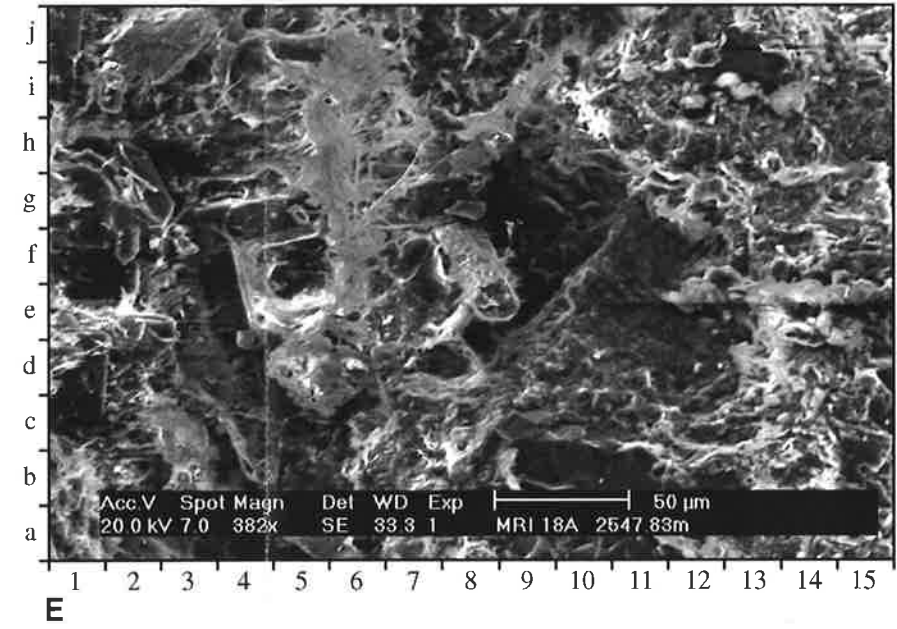
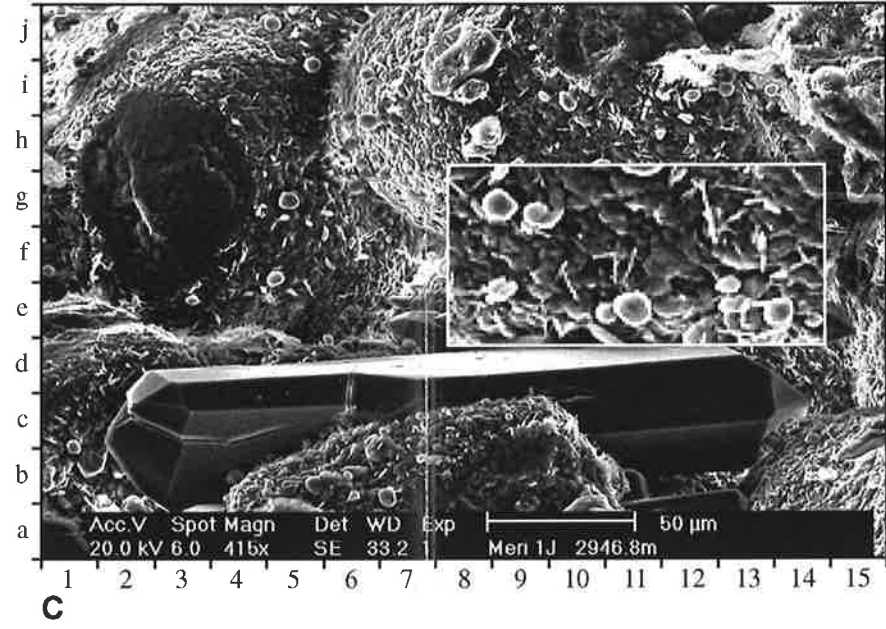
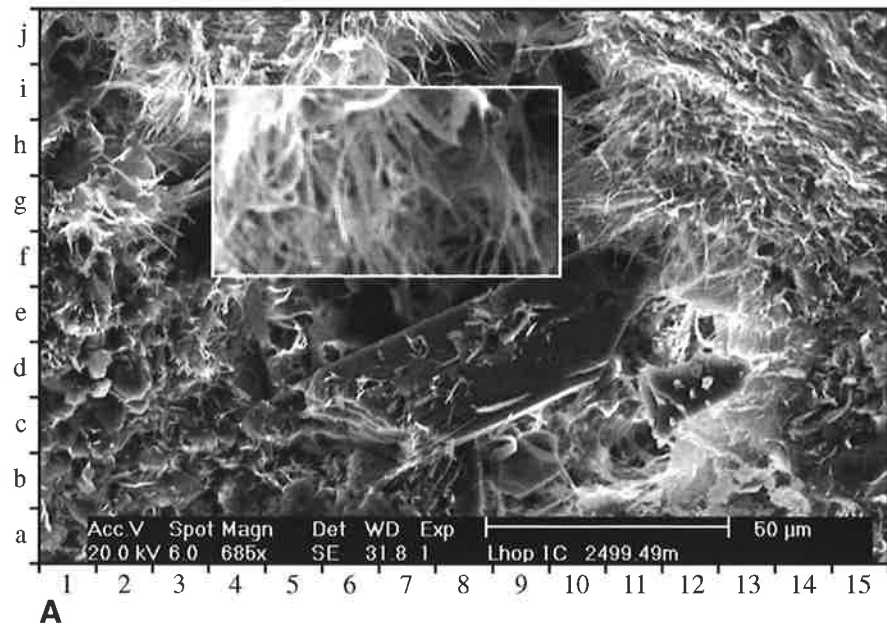
B) SEM photomicrograph – Lake Hope #1 (2499.49m). Boxwork illite after an argillaceous rock fragment. [Inset] Close up view of boxwork illite illustrating the boxwork substrate with protruding filamentous illite fibers.

C) SEM photomicrograph – Merrimelia #1 (2946.80m). Platey illite lining framework grains. A grain contact point [3g] illustrates the absence of illite clay at grain-grain boundaries. Note large double terminating druse quartz throughout the pore space.

D) BSE Image – Merrimelia #1 (2946.93m). Close up view of a pore with illite lining framework grains. Projecting filamentous illite [13f] suggests that at reservoir conditions filamentous illite would bridge across pore throats, severely reducing permeability. This image indicates that clay plucking during thin section manufacture has occurred along with the relaxation of filamentous illite against pore walls. Both of these induced features may lead to an underestimation of the detrimental effect of illite on permeability in glacio-aeolian sandstones.

E) SEM photomicrograph – Merrimelia #18 (2547.83m). General view of illite collapse textures [6h], induced by clay relaxation at ambient conditions.

Plate 21



Boxwork morphologies are generally observed associated with unstable framework components (Plate 21b) and are thus commonly observed in ductile-rock-fragment-rich lithologies.

Platey illite in the aeolian sequence in the Merrimelia Field forms very thin coatings on almost all framework grains (Plate 21c). This platey texture coats framework grains and in places, bridges pore throats (Plate 21d).

C) Illite Textures

The three basic illite morphologies outlined above form a myriad of textures (Table 6.7) which can be grouped into five textural categories. These illite textural styles are: isolated illite fibers (Plate 22a), ‘flame’ boxwork, (Plate 22b), honeycomb boxwork, (Plate 22c), platey grain coating illite (Plate 22c) and filamentous feldspar/unstable rock fragment replacement (Plate 22e).

Illite Textures	Illite Morphology
Isolated fibers	Filamentous
Honeycomb	Boxwork/Filamentous
Flame	Boxwork/Filamentous
Platey	Platey
Rock Fragment/Feldspar Dissolution	Boxwork/Filamentous

TABLE 6.7 *Illite textures and corresponding illite morphology type.*

6.2.2.2 Glauconitic Illite

Taylor *et al.* (1991) observed and analysed “glaucony grains” in Merrimelia sediments (Plate 22f) in the Daralingie region. The composition of these grains indicated that the proportion of Fe was too low and Al too high for these grains to be classified as glaucony. These authors concluded that the composition of these grains was somewhere between glaucony and illite, coining the term “glauconitic illite”.

Rock fragment grains with illite-glaucony components, whose compositions were similar to that described by Taylor *et al.* (1991) (Table 6.2), were observed commonly in this present study (the term “glauconitic illite” has been adopted in this study to describe glauconitic illite rock fragments observed in Merrimelia sediments).

Plate 22f illustrates typical glauconitic illite grains in the Merrimelia Formation. The arenite rock fragments in which most glauconitic illite grains are observed are most likely been derived from the underlying Warburton Basin.

PLATE 22

Authigenic Minerals: Illite Textures & Glauconitic Illite

A) SEM photomicrograph – Merrimelia #18 (2547.83m). Isolated filamentous illite texture.

B) SEM photomicrograph – Woolkina #1 (3038.80m). Flame boxwork illite texture, with protruding filamentous illite.

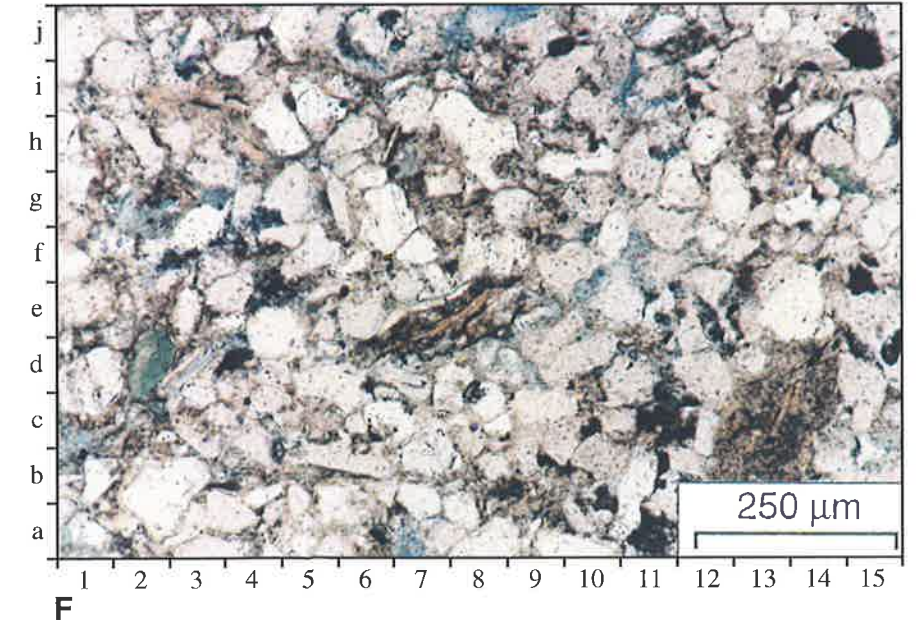
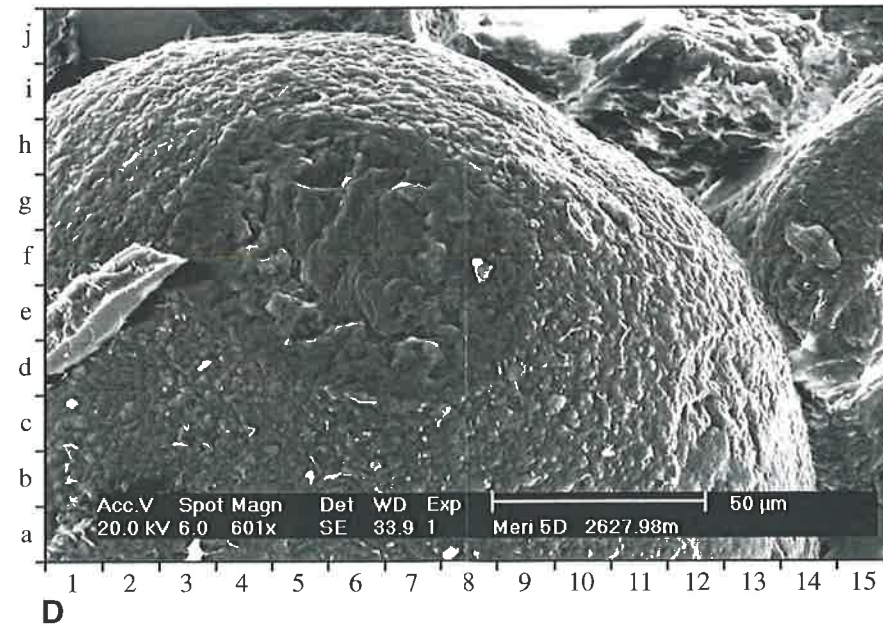
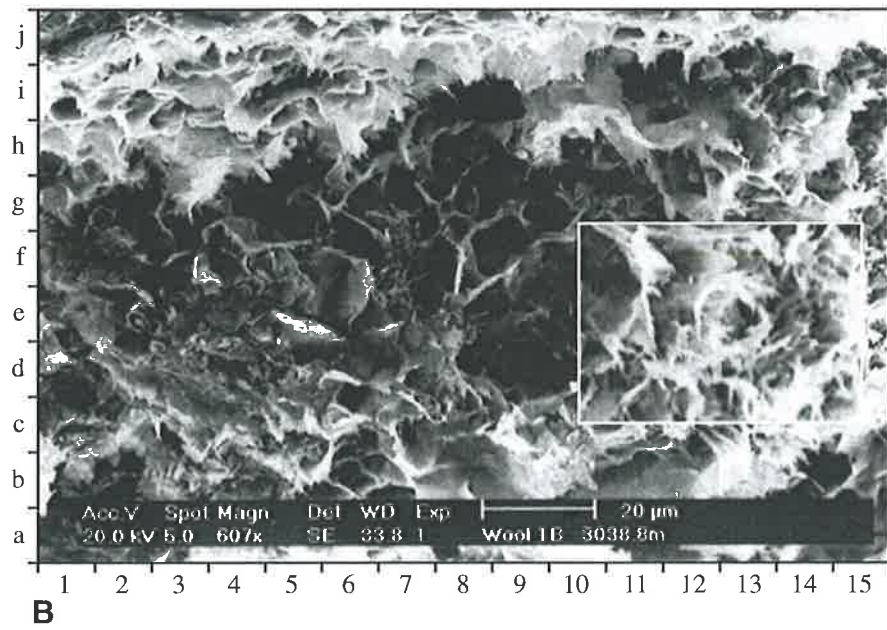
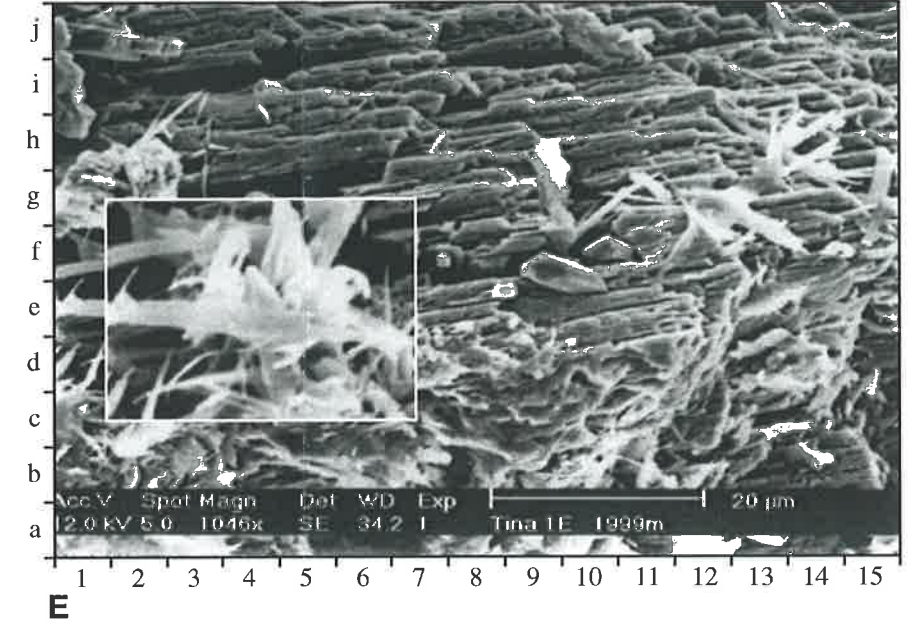
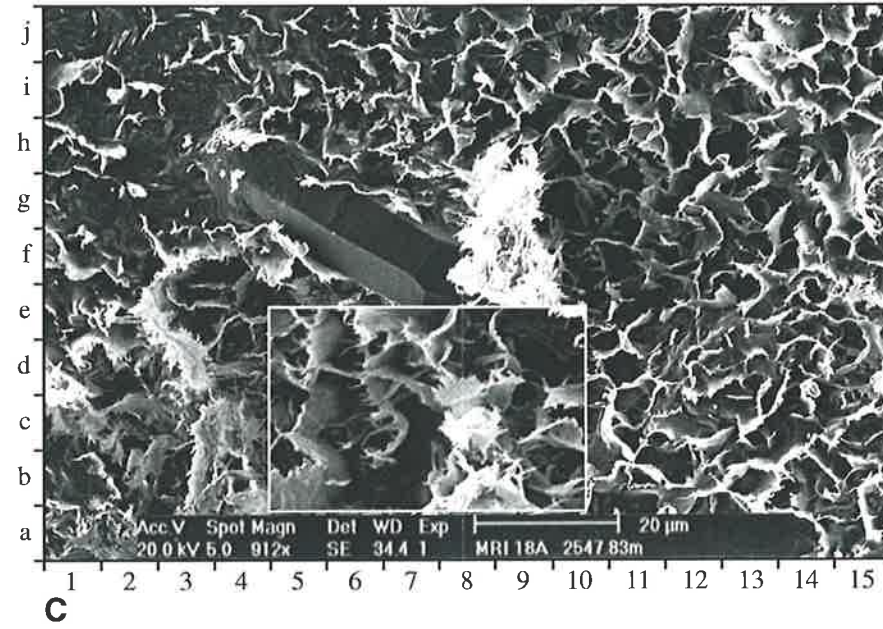
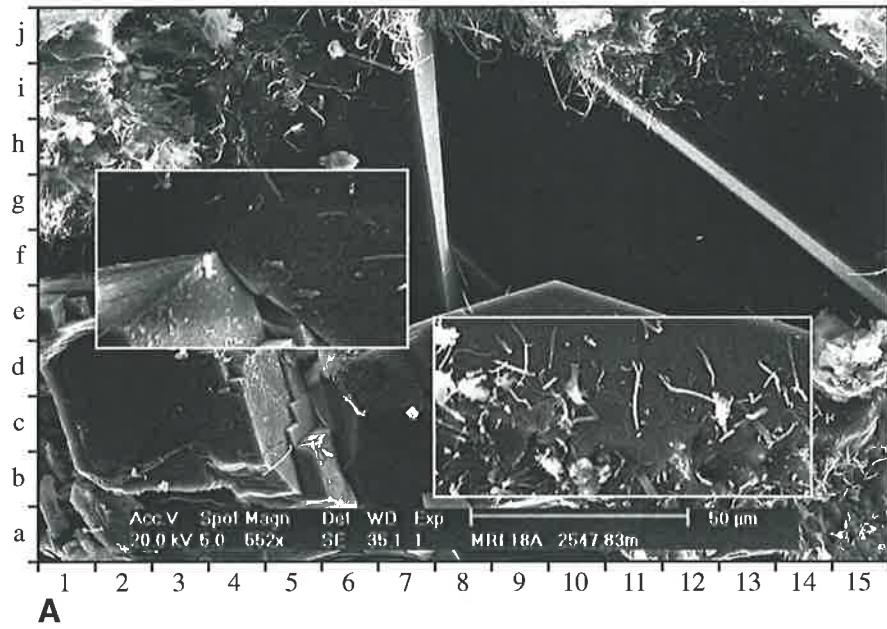
C) SEM photomicrograph – Merrimelia #18 (2547.83m). Honeycomb boxwork illite texture with filamentous illite forming in isolated patches as well as emanating from the boxwork substrate.

D) SEM photomicrograph – Merrimelia #5 (2627.98m). Platey illite texture. Rounded glacio-aeolian quartz framework grain coated by platey illite. The round clay free region in the centre of the grain [7e] represents a point contact with another rounded quartz grain. The frosted and pitted nature of the aeolian grains can be seen in this clay free grain contact [7e].

E) SEM photomicrograph – Tinga Tingana #1 (1999m). Feldspar/rock fragment alteration texture. Trace goethite and leucoxene cements were also observed [10e].

F) Photomicrograph – Daralingie #1 (2186.63m) (Plane polarised x 10). A general view of a glauconite bearing sandstone. Glauconitic illite pellet [2d].

Plate 22



The existence of “free” glauconitic illite grains higher up in the Cooper Basin sequence is more than likely a product of clast destruction via reworking, where glauconitic illite grains (and all other sandstone rock fragment components) are liberated and dispersed.

6.2.2.3 Kaolin

Kaolin forms pseudo-hexagonal booklets of up to 10-15 μ m across (Fig. 6.6a). Kaolin is generally observed either intergrown with quartz cement (Fig. 6.6a) or as a replacement of altered feldspars (Page 243- Plate 26b).

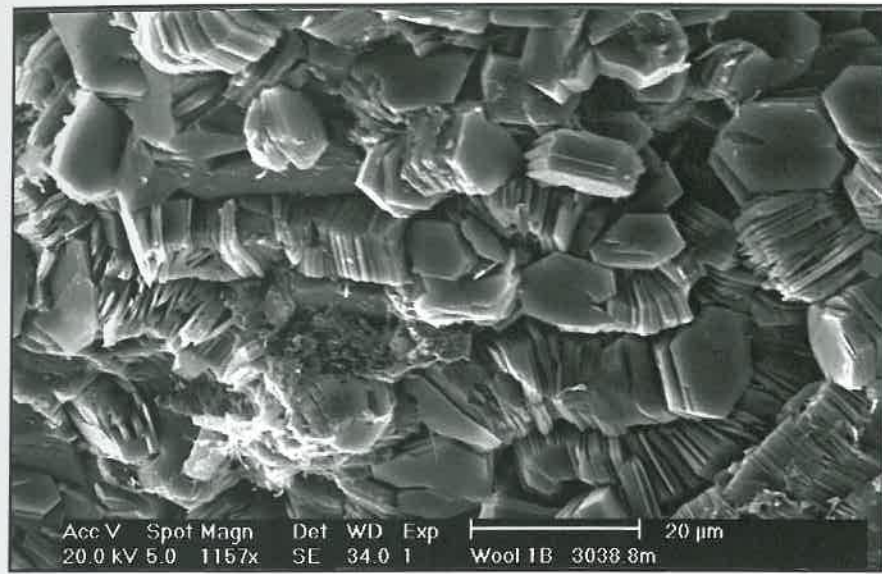
6.2.2.4 Dickite

Dickite was not reported by Rezaee, (1996) in the Tirrawarra Sandstone (Moorari, Fly Lake-Brolga and Tirrawarra fields), but was documented in great detail by Schulz-Rojahn (1991) within the Permian section of the Nappamerri Trough. This author describes dickite from XRD and SEM analysis to be coarser grained than kaolin while exhibiting the same crystal habit. XRD analysis, according to Schulz-Rojahn (1991) was the only method successful in identifying dickite from kaolin. He, utilised randomly orientated XRD samples to distinguish dickite from kaolin. Thick XRD smears can also be used to identify dickite from XRD analysis (Lemon pers. comm., 1996). Using this method, in combination with cuttings descriptions², dickite was identified in five samples. Figure 6.6c indicates the distinctive dickite XRD peaks (around 40 degrees 2 θ) compared with typical kaolin XRD peaks (Fig. 6.6c [around 12, 25 and 35 degrees 2 θ]). The main XRD peaks from both clays coincide and inspection of cuttings confirmed the identification of dickite in these samples based on grain size. XRD analysis indicates that samples from Gidgealpa #3 and Tirrawarra #7 are dominantly composed of dickite.

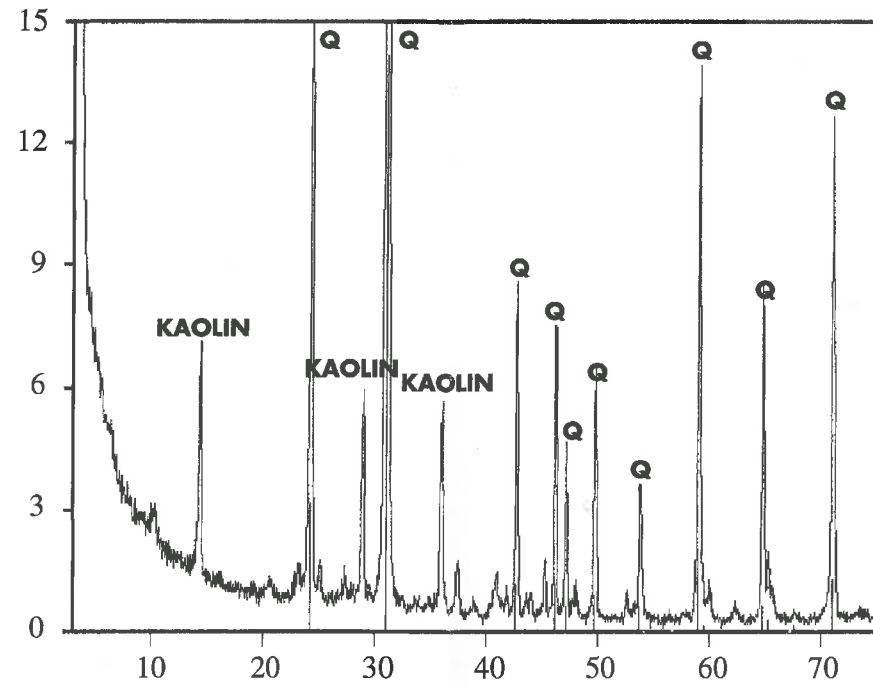
6.2.2.5 Chlorite

Authigenic chlorite in Merrimelia sediments is rare, exhibiting a mottled or a translucent green appearance (Fig. 6.6d[9f]). Detrital chlorite was commonly observed in association with basic volcanic, biotite dominated schist and biotite rock fragments (Fig. 6.6d[3f], 6.6e[9e] & Fig. 6.6f respectively).

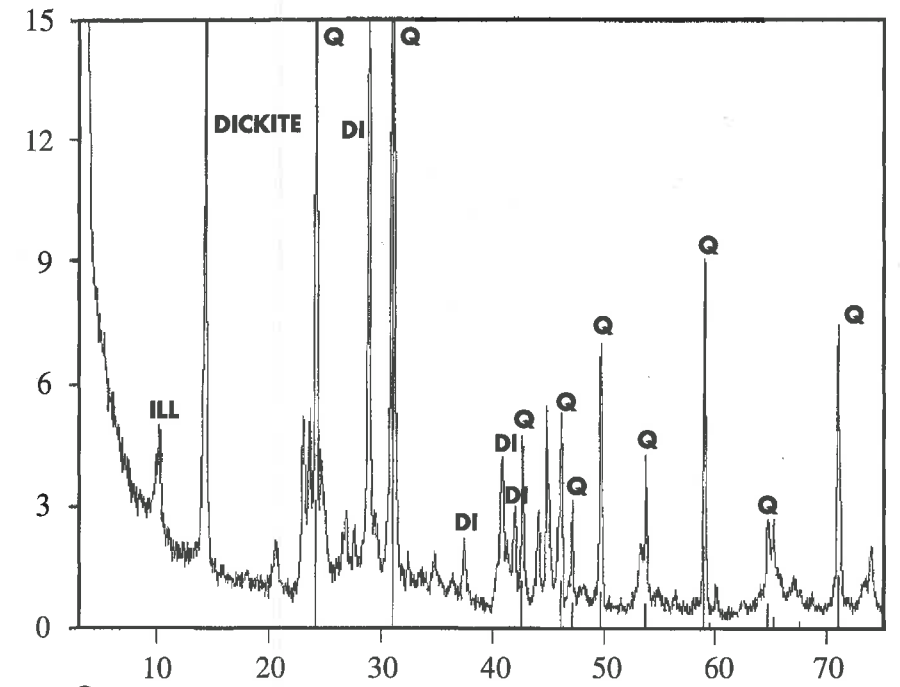
² In cuttings dickite has a distinct “coffee” colour (King pers. comm., 1998) while kaolin is white.



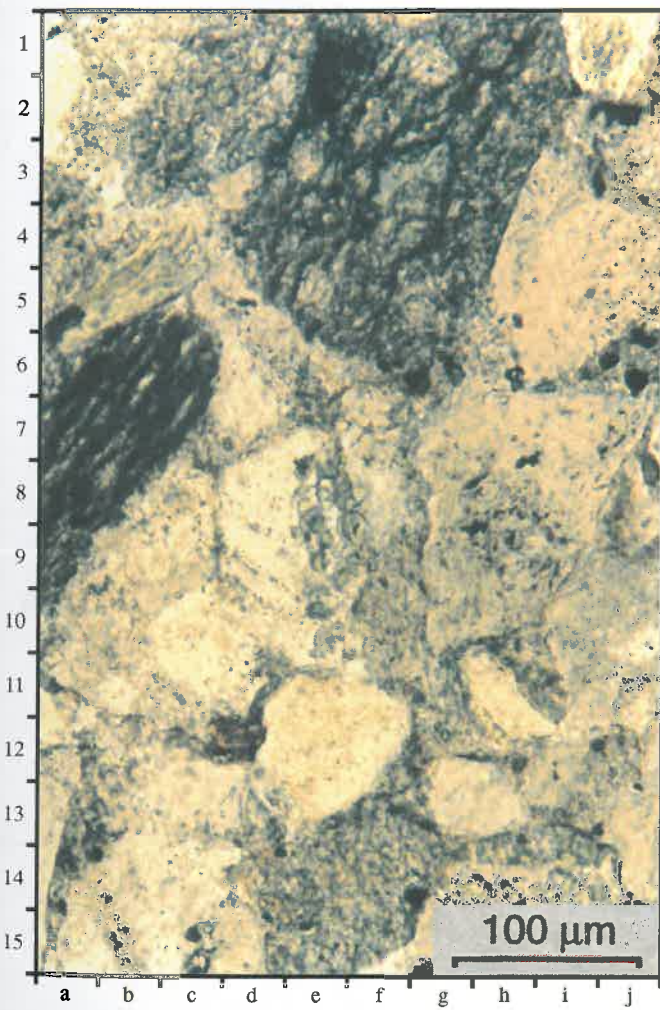
A



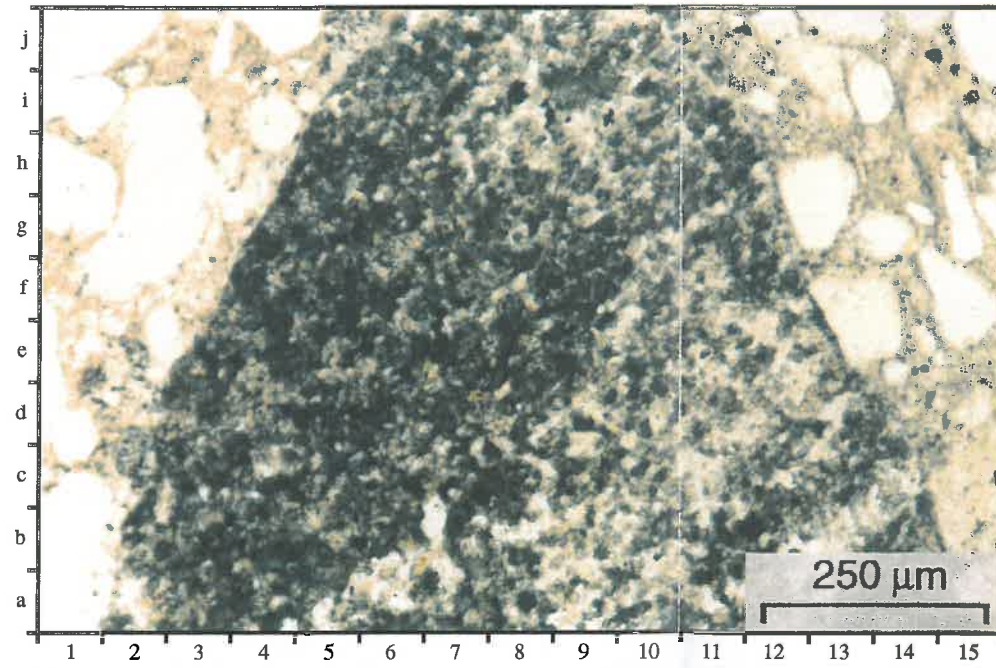
B



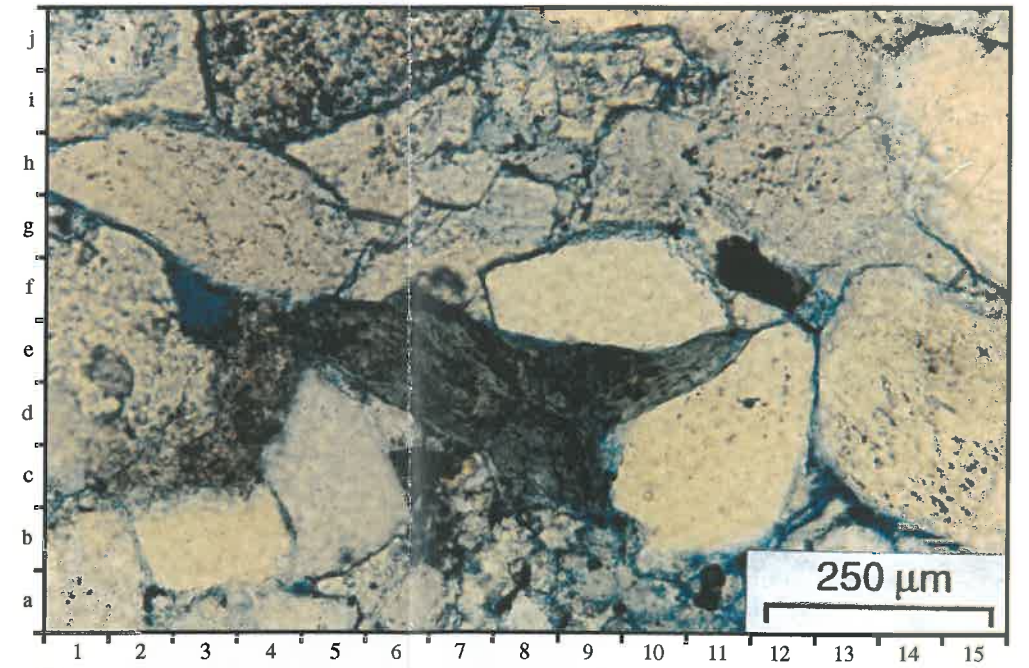
C



D



E



F

Figure 6.6 A) Woolkina #1 (3038.8m) SEM photomicrograph of vermicular kaolin booklets. B) Woolkina #1 (3038.8m) XRD spectra illustrating the position of kaolin peaks. C) Tirawarra #7 (3056.66m) XRD spectra showing dickite peaks. D) Talallia #1 (3167.93m) (Plane polarised x 20) Detrital chloritised basic rock fragments and authigenic chlorite cement. E) Merrimelia #1 (2644.67m) (Plane polarised x 10) Chloritised Biotite dominated rock fragment. F) Tinga Tingana #1 (1891.55m) (Plane polarised x 10) Authigenic chlorite replacing squeezed biotite mica.

6.2.2.6 Pyrophyllite

Pyrophyllite is mainly observed in a small number of samples within the confines of rock fragments derived from the Warburton Basin. Pyrophyllite in this context is detrital. However, authigenic pyrophyllite is observed (in three samples whose burial depths exceed 3350m), having formed in pore spaces replacing adjacent diagenetic phases and framework components. This authigenic phase is distinguishable under cross nicols from mica or illite by the display of very high order interference colours (Plate 20a). In BSE, images pyrophyllite has a micaceous habit (Plate 20b), forming a network of pore bridging crystals. Both EDAX and microprobe analysis confirms the composition of this mineral phase.

Schulz-Rojahn (1991) observed and described authigenic pyrophyllite in Patchawarra Formation sediments in the Nappamerri Trough.

6.2.3 CARBONATE CEMENT

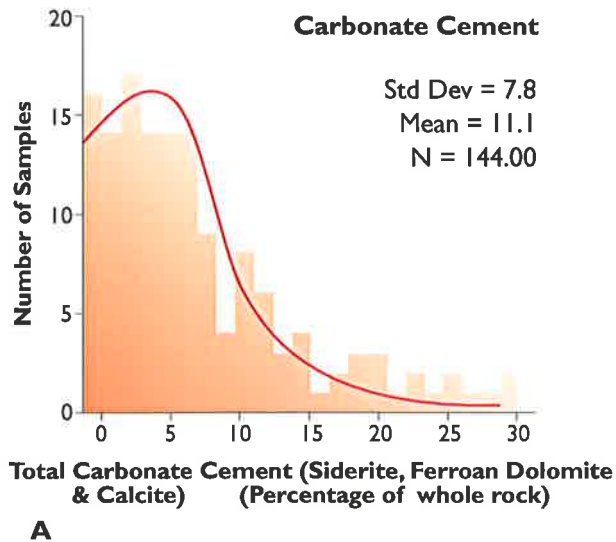
Siderite, calcite and dolomite carbonate minerals were observed in the majority of Merrimelia samples (Fig. 6.7a), with most samples having between 0% and 20% carbonate cement (Fig. 6.7a). Of the three carbonate phases observed, authigenic siderite was the most common; calcite and dolomite typically occur in trace proportions. Compositions gained via microprobe analysis of these three carbonate minerals are given in Table 6.8 (Fig. 6.7). The ternary diagram in the same figure, (6.7b), suggests that the composition of siderite varies considerably with a number samples showing magnesium and calcium rich compositions. Samples with more typical calcite, siderite and dolomite compositions plot in their respective corners (Fig. 6.7b).

Carbonate phases generally form in small, isolated patches and rarely form framework-engulfing poikilotopic crystals.

6.2.3.1 Siderite

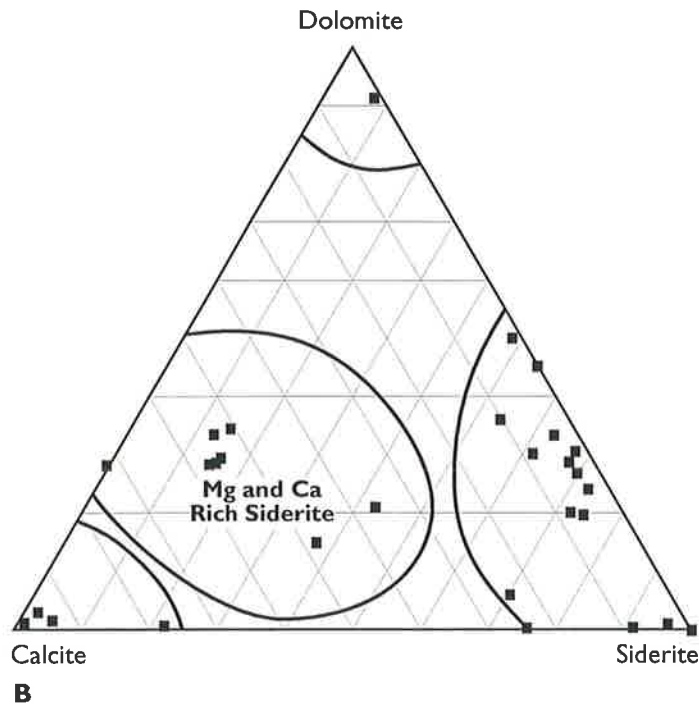
Siderite cement exhibits a diverse array of morphologies (Plate 23). These morphologies can be grouped into three categories:

- 1) Pore-filling cement (Fig. 6.8a),
- 2) Siderite rhombs or "Seeds" (Fig. 6.8b),
- 3) Patch cement (Fig. 6.8c).



Cement Type	MgCO ₃	CaCO ₃	MnCO ₃	FeCO ₃	Figure
Calcite	0.00	98.24	0.78	0.97	Fig 6.11
Fe Dolomite/Ankerite	27.15	51.84	1.60	19.41	Fig 6.10
Siderite	20.30	8.80	3.70	66.90	Fig 6.9

Table 6.8



EXPDEV 076 P

Figure 6.7 Carbonate cements A) Histogram illustrating the proportion of carbonate minerals in Merrimelia sediments. B) Ternary diagram showing the composition of carbonate cements in Merrimelia sediments. Note: the diversity of siderite composition which reflects the range of S1, S2 and S3 compositions.

Table 6.8 Microprobe analysis of ferroan dolomite (Wt%), calcite (Wt%) and siderite (Wt%) cements.

Rezaee (1996), in describing siderite cement within the Tirrawarra Sandstone at the Moorari and Tirrawarra Fields, observed three siderite cement phases (S1, S2 and S3) (Fig. 6.9b). These same three siderite phases were observed in siderite cement in the Merrimelia Formation (Fig. 6.9c) (the average composition of S1, S2 and S3 siderite cement phases in Merrimelia sediments is shown in Table 6.9). In Merrimelia sediments, S1 and S2 siderite phases were observed in all three siderite cement morphologies (Fig. 6.8). In contrast, S3 siderite was only observed in pore filling and "seed" siderite morphologies (Fig. 6.8).

In comparison with the Merrimelia Formation, siderite phases (S1, S2 and S3), in the Tirrawarra Sandstone, appears not to be as well developed (Fig. 6.9). In particular:

- 1) Siderite phases within Merrimelia sediments appear to be more pronounced.
- 2) Siderite phases within Merrimelia sediments are more consistent.

Siderite Phase	MgCO ₃	CaCO ₃	MnCO ₃	FeCO ₃
S1	12.0	3.4	7.6	76.8
S2	19.5	4.9	2.4	72.7
S3	29.5	18.1	1.1	51.3
Averages	20.3	8.8	3.7	66.9

Table 6.9 The average microprobe composition of S1, S2 and S3 siderite cement phases in the Merrimelia Formation (Wt.%).

The classification scheme used by Rezaee (1996) for the Tirrawarra Sandstone was modified to describe siderite cement in the Merrimelia Formation. This new classification scheme (Fig. 6.8) nests the three siderite cement phases (S1, S2 and S3) within the context of siderite cement morphologies (patch, pore-fill and "seed"). In this new scheme:

- 1) Pore-fill siderite has the greatest development of all three siderite phases (Fig. 6.8a & 6.8a').
- 2) Siderite "seeds" are generally composed of S1 and S2 phases, with encompassing S3 siderite.
- 3) Only S1 and S2 siderite phases develop in "patch" siderite (Fig. 6.8c).

The composition of siderite varies according to the cement phase (S1, S2 etc.). In general, S1 siderite is depleted with respect to Mg whereas S2 cement becomes progressively enriched. S3 siderite cement exhibits Mg proportions similar to those of S2 cement (Table 6.9). This compositional change is highlighted in Figure (6.9c), where differing grey tones reflect differing Mg proportions.

PLATE 23

Authigenic Minerals: Siderite Cement

A) Photomicrograph – Gidgealpa #3 (2312.82m) (Cross nicols x 10). Close up of a cluster of asymmetric siderite rhombs or “seeds”.

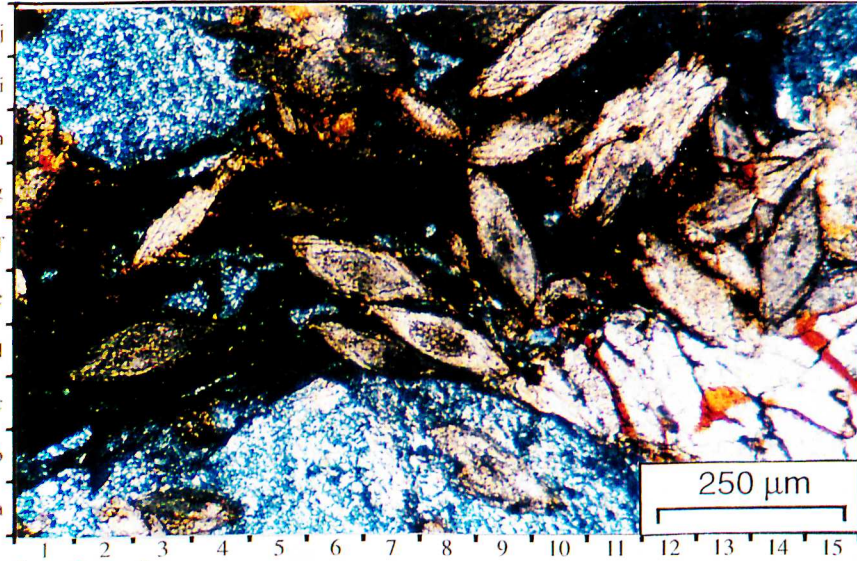
B) Photomicrograph – Kudrieke #1 (3116.27m) (Cross nicols x 5). Early formed poikilotopic siderite cement, engulfing framework grains preventing grain contacts and forming a floating framework.

C) Photomicrograph – Malgoona #2 (2254.57m) (Plane polarised x 10). Twinned siderite “seeds” occluding pore space. Note: secondary porosity formation development via the dissolution of siderite.

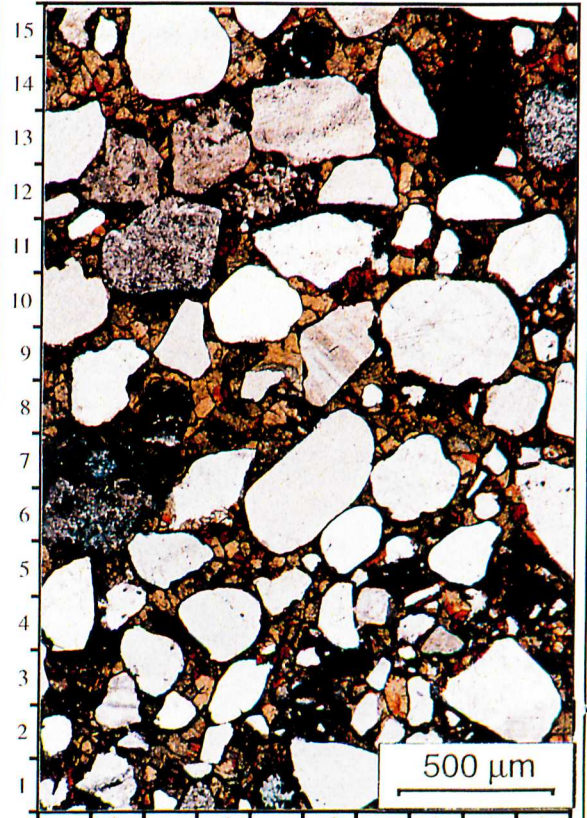
D) Photomicrograph – Mudlalee #1 (2022.95m) (Cross nicols x 10). Sparry, pore filling siderite cement, exhibiting rare dissolution pitting.

E) Photomicrograph – Kenny #1 (2945.80m) (Cross nicols x 10). Radial cluster of siderite “seeds”, exhibiting a distinctive radial extinction. Note: The earliest formed siderite is micritic, while the later, radiating siderite is sparry.

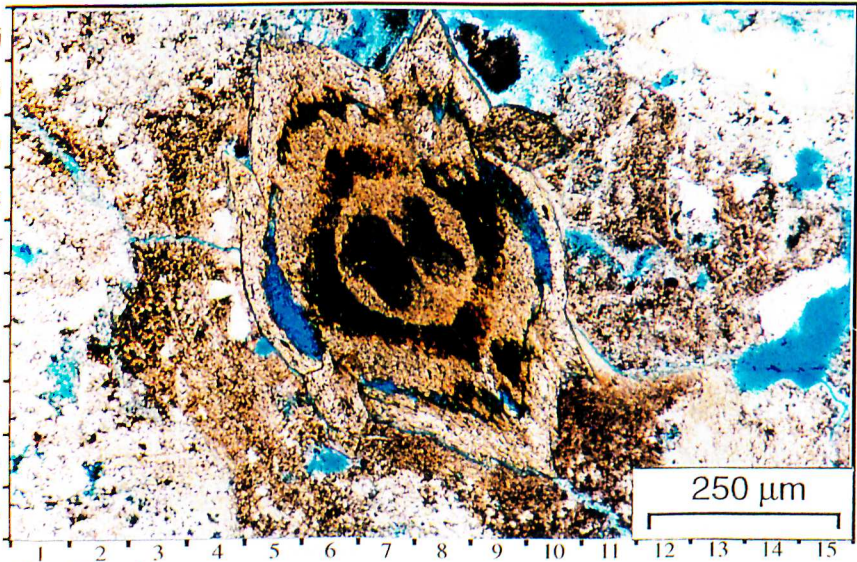
Plate 23



A - Seed



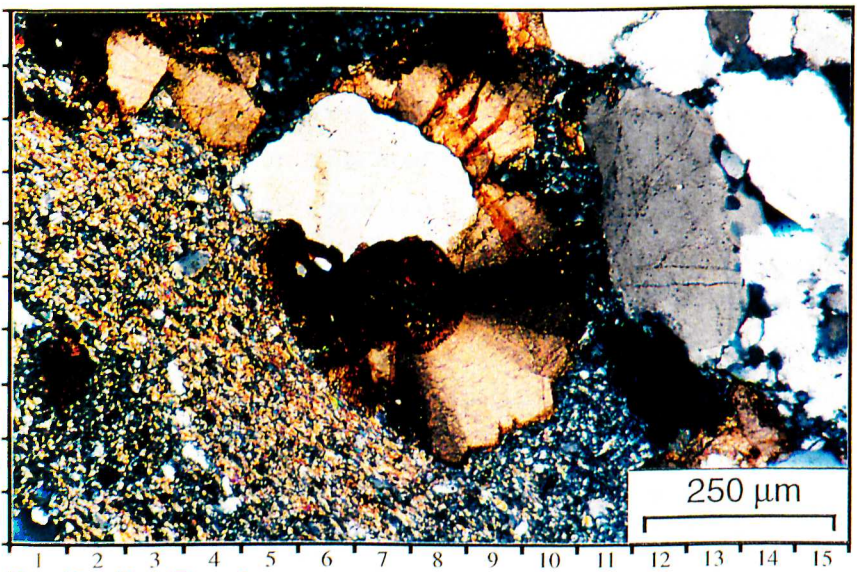
B - Poikolotopic Patch



C - Seed



E - Pore Fill



D - Radial Seed

It can be seen in Table 6.10 that the amount of Mg increases drastically from S1 to S2. Rezaee, (1996) observed similar Mg enrichment in S2 siderite, nominating that S2 siderite cement grades from a pistonsite-siderite cement to a homogeneous sideroplesite cement.

Table 6.10 gives an average composition of each siderite cement phase within the context of siderite cement morphology type (patch, "seed" and pore fill).

Sample	MgCO ₃	CaCO ₃	MnCO ₃	FeCO ₃
Pore Fill S1	7.4	3.9	1.4	87.4
Pore Fill S2	22.4	4.1	1.7	71.6
Pore Fill S3	25.3	23.6	1.1	50.0
"Seed" S1	15.1	2.5	0.7	81.3
"Seed" S2	20.6	8.0	2.6	68.1
"Seed" S3	33.6	12.6	1.2	52.6
Patch S1	14.6	4.0	20.7	61.7
Patch S2	15.5	2.6	3.0	78.4
Average	20.5	8.8	3.7	66.9

Table 6.10 *Microprobe composition (Wt.%) of patch, "seed" and pore-filling siderite cement.*

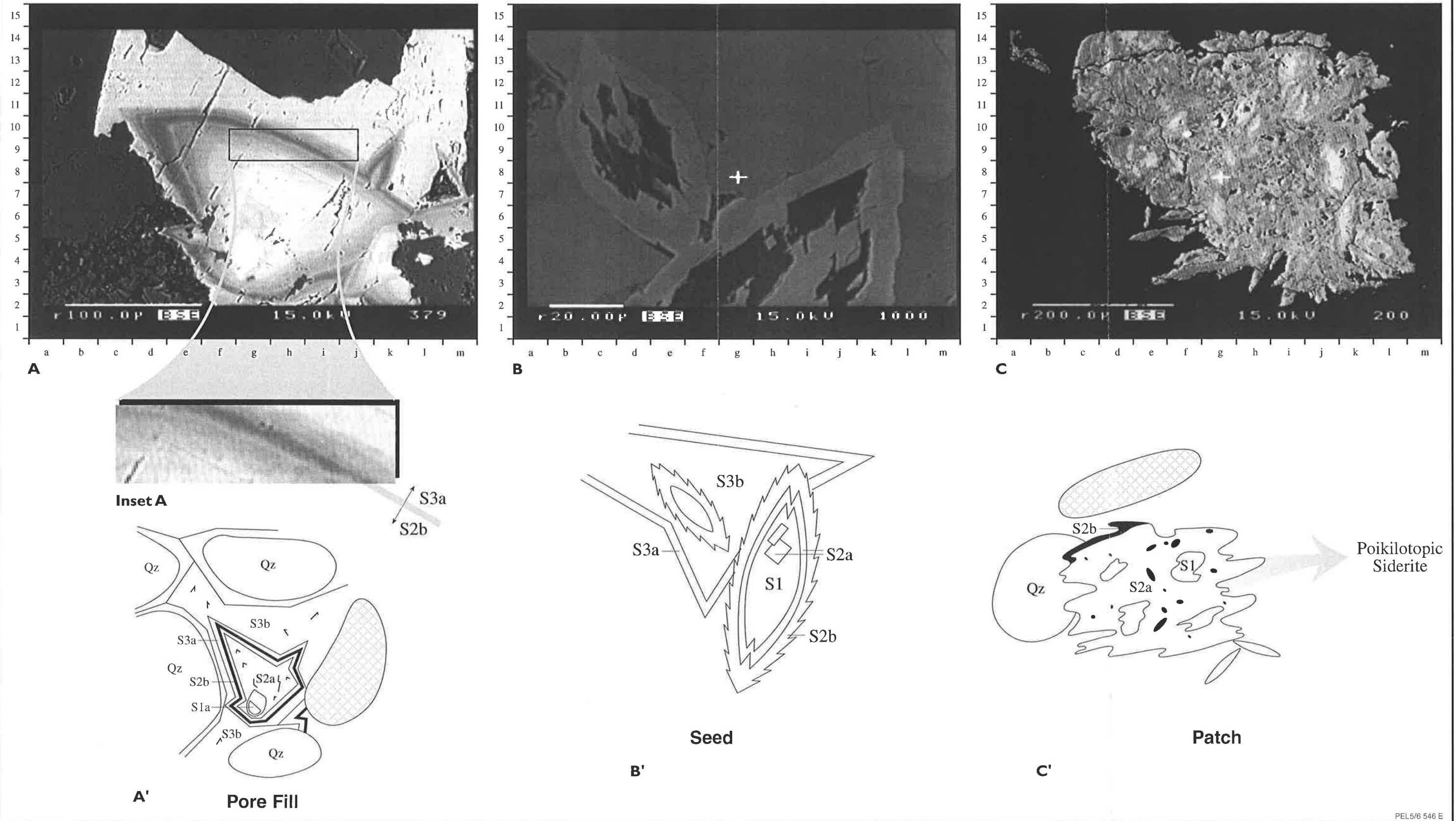
In thin section, differentiation between siderite phases is ineffective with only inner S1 and S2 phases discernible (Plates 23a, 23c & 23d). In thin section sparry pore filling carbonate cement appears homogeneous, but is equivalent to the zoned siderite illustrated in Figure 6.8a. The identification of S1, S2 and S3 siderite phases is most accurately achieved by microprobe.

The formation of siderite in Merrimelia sediments is influenced primarily by:

- 1) Pore fluid composition,
- 2) Pore fluid acidity,
- 3) Porosity and permeability.

The shape of siderite morphologies also indicates possible formation mechanisms. Siderite patches are irregular, with no defined or systematic crystal faces (Fig. 6.8c). Pore-fill siderite also exhibit irregular surfaces reflecting the shape of the infilled pore space (Fig. 6.8a). Both of these morphologies have infilled available pore space.

Siderite Morphologies : Merrimelia Formation



PEL5/6 546 E

Figure 6.8 A) Fly lake #1 (2948.22m) BSE image of pore fill siderite cement illustrating compositional banding. [Inset A] Boundary between S2 and S3 siderite cement stages. B) Merrimelia #18 (2548.03m) BSE image and cartoon of twinned siderite seeds. C) Woolkina #1 (3038.8m) BSE image and cartoon of sub-poikilotopic patch siderite.

In contrast, siderite “seeds” exhibit very well defined crystal faces (Fig. 6.8b) suggesting that siderite “seeds” have a formation mechanism different that of pore filling or patch siderite.

An examination of siderite “seed” distribution indicates that most “seeds” have formed in poorly permeable strata, suggesting that the “seeds” form in slow fluid flow conditions. The siderite “seeds” themselves are composed of rhombs (Fig. 6.8b), which, according to Dana (1955), coalesce forming a crystalline aggregate

Variations in mineral composition, which change the shape of the crystal produced, are observed in the majority of siderite “seeds”. For example, the inner S1 and S2 phases are asymmetrical when compared to the later formed S3 cement phase (Fig. 6.9e).

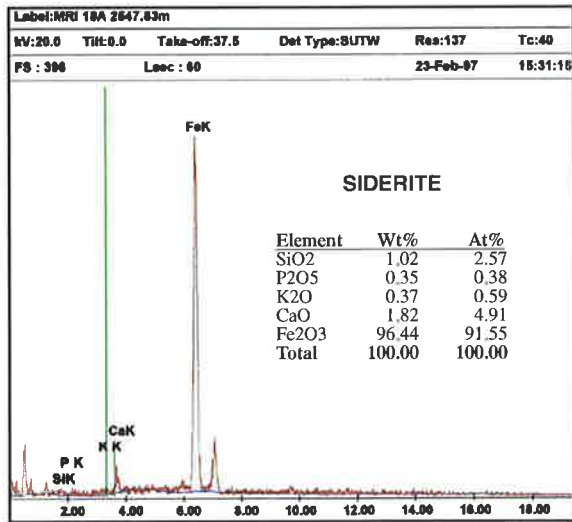
Siderite “seeds” are usually found in groups (Plate 23a) where twinning of smaller siderite “seeds” off larger siderite “seeds” is common (Plate 23c).

6.2.3.1.1 S1-Early Siderite Cement Phase

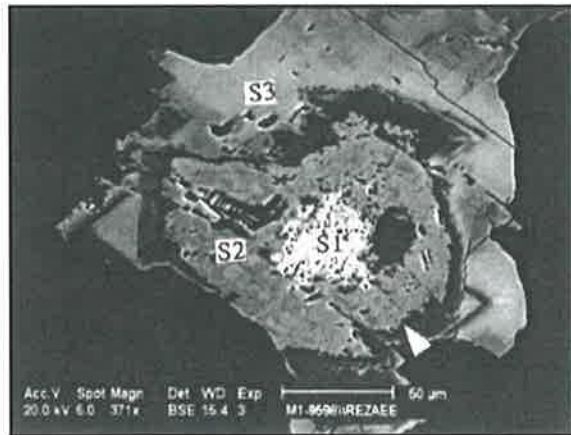
The earliest siderite cement phase occurs in the centre of porosity fill, “seed” or patch siderite, exhibiting a different appearance depending on siderite cement style. S1 siderite “patch” and “pore-fill” cement in BSE images has the lightest appearance of all siderite cement phases (Fig. 6.8a), exhibiting minor dissolution (Figs. 6.8a & 6.8c). In contrast, S1 cement in siderite “seeds” sometimes forms highly dissolved, nuclei. S1 cement dominates siderite cement patches and in some examples can form poikilotopic textures surrounding the whole rock framework (Plate 23b). S1 cement under the petrological microscope is dark brown and micritic, whereas S2 and S3 siderite cement phases appear light brown and typically sparry (Plate 23e).

The boundary between S1 and S2 cement in all cases is irregular suggesting there has been a period of dissolution prior to the precipitation of S2 cement. This same dissolution event was also noted by Rezaee, (1996). The same author also observed that S1 predominates in Tirrawarra sediments that are fine grained or organic-rich. The same was seen in Merrimelia sediments where S1 siderite cement phase dominates fine grained and argillaceous sediments. Siderite “seeds” for example are dominated by S1 siderite (Fig. 6.8b) and are almost exclusively observed in low porosity conglomeratic sediments whereas pore filling siderite cement (S2 and S3) are almost exclusively observed in porous Merrimelia sandstones (M1).

EDAX

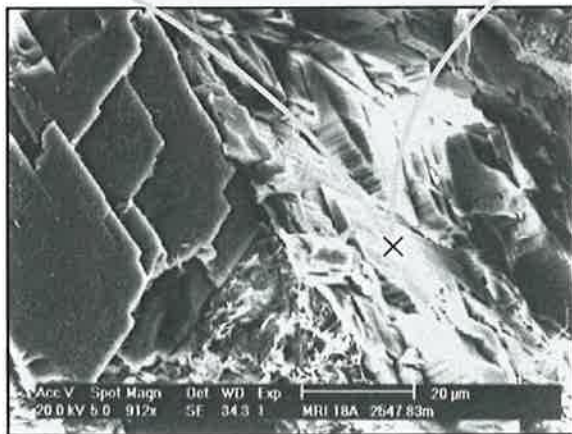


Tirrawarra Sst



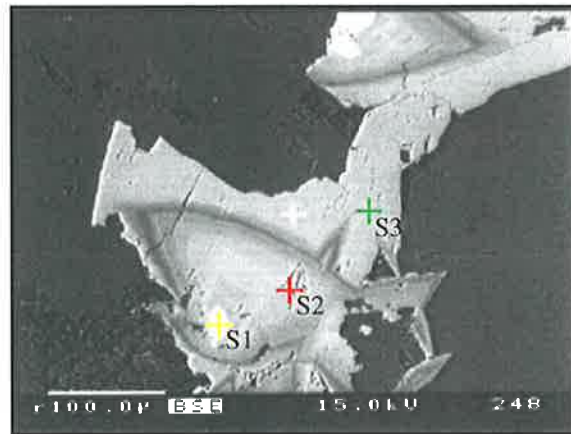
B BSE IMAGE
(From Rezaee 1996)

A



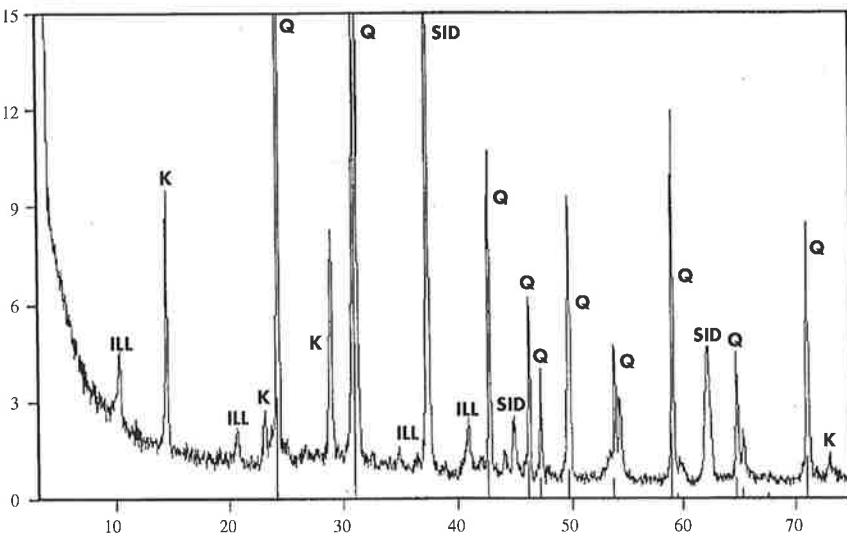
A' SEM IMAGE

Merrimelia Fm

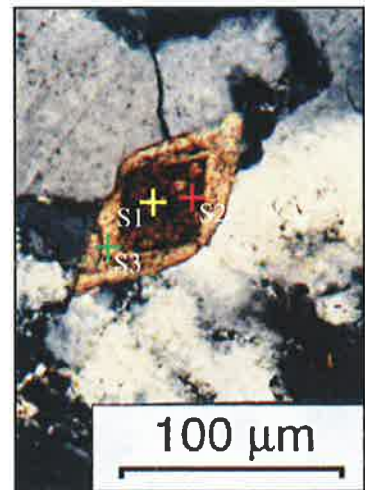


C BSE IMAGE

XRD



D



E

PEL5/6 546 D

Figure 6.9 A) EDAX composition spectra of siderite cement A') Merrimelia #18 (2547.83m) SEM photomicrograph of dolomite and siderite cement. B) BSE image illustrating pore filling siderite in the Tirrawarra Sandstone (From Rezaee, 1996). C) Fly Lake #1 (2948.22m) BSE image of pore filling siderite cement from the Merrimelia Formation, showing S1, S2 and S3 cement stages. D) Fly Lake #1 (2948.22m) XRD spectra with siderite peaks highlighted. E) Panning #1 (3129.9m) (Plane polarised x 20) Assymmetric S1 and S2 cement stages in a siderite seed.

Argillaceous (terminoglacial) sediments dominate the lower and middle Merrimelia Formation while porous lithologies (proglacial) form a veneer at the top of the unit. Thus siderite cement morphologies (pore fill, patch and “seeds”) and respective siderite cement phases (S1, S2 and S3) tend to be segregated, forming preferentially in either terminoglacial or proglacial Merrimelia sediments.

6.2.3.1.2 S2-Mid Siderite Cement Phase

Optically, S2 cement is difficult to distinguish from S1 and S3. S1 cement, however, commonly has a reddish appearance under plane light (Plate 23a[13b]) and is easily identifiable from sparry S2 and S3 phases (Plate 23e). S2 and S3 siderite cement are readily distinguishable in BSE images with S2 cement displaying complex compositional zonations (Fig. 6.8a & 6.8a’).

S2 cement is best developed as pore-filling siderite, where numerous compositional zones are observed (based on greyscale appearance) (Fig. 6.8a). These zones were found to be also present in siderite “seeds” (Fig. 6.8b) and to a lesser extent in siderite patches (Fig. 6.8c). The following descriptions relate to S2 siderite (as observed in BSE images) within “seeds” and pore-filling siderite cement. S2 cement development in siderite patches is generally compositionally consistent (Fig. 6.8c) or is not developed.

A) S2a-Siderite Cement Zone

Seen in the core of isolated “seeds” this phase can form small rhombs and may be highly dissolved (Fig. 6.8b & 6.8b’). The S2a phase also forms the inner zone of the outer “seed” wall and in some cases constitutes the majority of the “seed” (Fig. 6.8b’). In pore-filling siderite, this first S2 siderite zone is characterised by broad zonations (Fig. 6.8a) with dissolution pits common.

B) S2b-Siderite Cement Zone

In pore-filling siderite cement, this zone is characterised by progressively darker banding, where the darkest band marks the end of this phase (Fig. 6.8a[Inset A]). The relative amounts of Mg increase up to a maximum, corresponding to the darkest bands in this phase.

6.2.3.1.3 S3 Late Siderite Cement Phase

S3 cement is predominantly observed in pore-filling siderite and is composed of two main zones (Fig. 6.8a & 6.8a’). The zonation consists of dark grey, Mg-rich bands grading into homogeneous light grey cement (Fig. 6.8a). The contact between S2 and S3 cements in pore-filling cements is gradational, suggesting that siderite cement

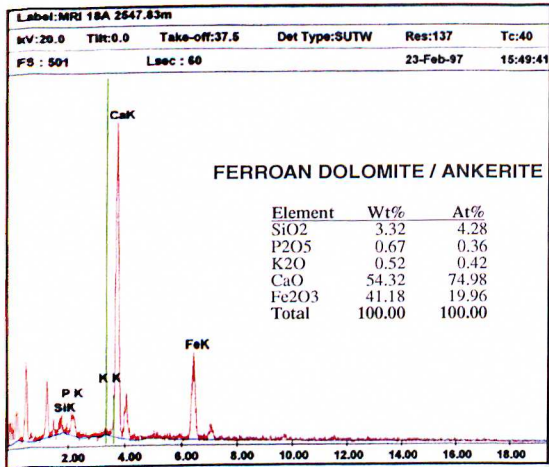
formation in pore spaces was continuous, reacting to changing pore water chemistry (Fig. 6.8a[Inset A]). This observation differs from Rezaee, (1996) who observed an irregular boundary between S2 and S3 cements in the Tirrawarra Sandstone (Fig. 6.9b). This irregular boundary was interpreted by this author to represent a dissolution event (D2 dissolution).

The pore-filling cement illustrated in Figure 6.8a[Inset A] shows no dissolution event between S2 and S3, but evidence of such a dissolution phase, in Merrimelia sediments is observed in other parts of the basin (Figs. 6.8b[L2] & 6.8b') (Table 6.11).

GEOGRAPHIC LOCATION	Dominant Lithology	Glacial Environment	Rezaee (1996) Dissolution Event: (Yes/No)	This Study Dissolution Event: (Yes/No)	Figure Plate Reference
	TIRRAWARRA SANDSTONE				
Fly Lake - Brolga Fields	Braid Plain Sandstones	Proglacial	Yes	Yes	Figure 6.9b
Moorari-Woolkina Fields	Braid Plain Sandstones	Proglacial	Yes	Yes	Figure 6.9b
Tirrawarra Field	Braid Plain Sandstones	Proglacial	Yes	Yes	Figure 6.9b
MERRIMELIA FORMATION: Arenaceous					
Merrimelia Field	Glacio-Aeolian Sandstones	Proglacial	Not Investigated	Yes	Figure 6.8b
	Longitudinal Bar Sandstones	Proglacial	Not Investigated	Yes	Figure 9.20b
Woolkina Field	Longitudinal Bar Sandstones	Proglacial	Not Investigated	Yes	Figure 6.8c
Malgoona Field	Longitudinal Bar Sandstones	Proglacial	Not Investigated	Yes	Plate 23c
Gidgealpa Field	Longitudinal Bar Sandstones	Proglacial	Not Investigated	Yes	Plate 33c
MERRIMELIA FORMATION: Argillaceous					
Fly Lake Field	Argillaceous Sandstone	Terminoglacial	Not Investigated	No	Figure 6.8a
Kenny #1	Diamictite	Terminoglacial	Not Investigated	No	Plate 23e
Mudlalee #1	Diamictite	Terminoglacial	Not Investigated	No	Plate 23d
Kudrieke #1	Diamictite	Terminoglacial	Not Investigated	No	No Illustration

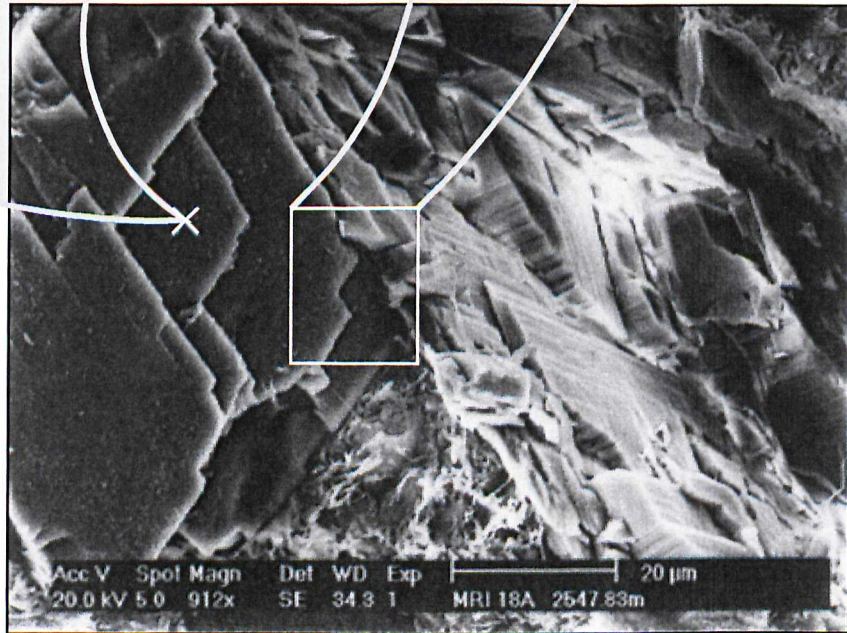
Table 6.11 D2 (S2/S3) siderite dissolution event: a comparison of results from Rezaee (1996) and this study.

EDAX



Inset A

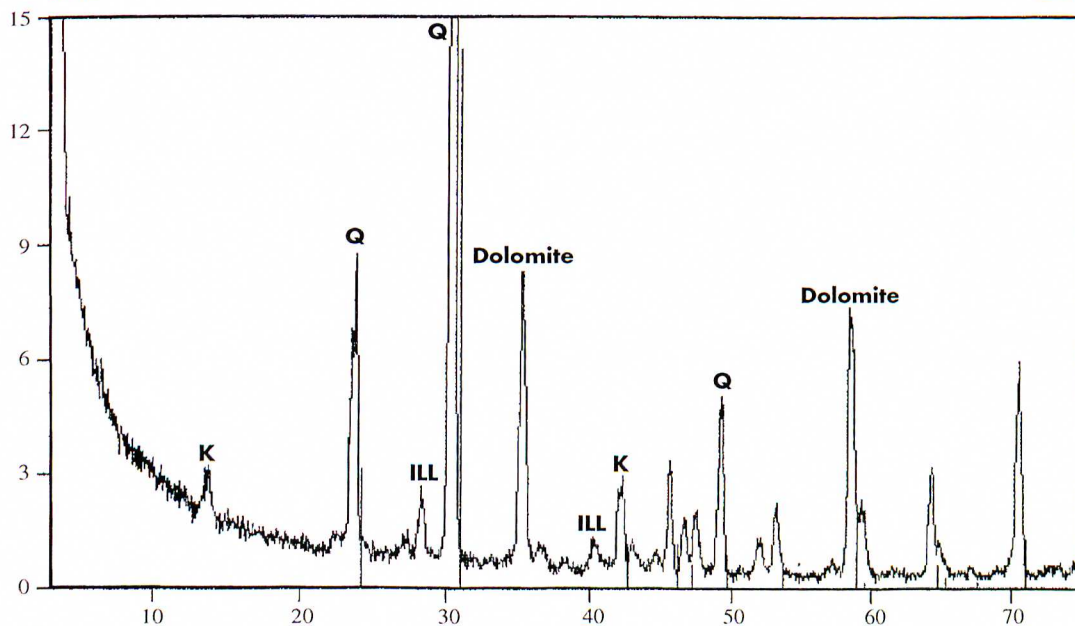
A



B

SEM IMAGE

XRD



C

Figure 6.10 A) EDAX composition spectra of ferroan dolomite cement. B) Merrimelia #18 (2547.83m) SEM photomicrograph of ferroan dolomite and siderite cement. C) Merrimelia #18 (2547.83m) XRD spectra illustrating dolomite peaks.

Regionally, the porous nature of the Tirrawarra Sandstone is relatively consistent if not buried too deep (quartz cement occludes pore space). It is more than likely then, that a dissolution phase between S2 and S3 in Tirrawarra sediments will be observed across the Cooper Basin.

In the Merrimelia Formation however, the D2 dissolution event exhibits regional variations depending on a sediment's permeability (facies type controls sediment permeability – see Chapter Nine).

A) S3a-Siderite Cement Zone

This cement phase is weakly banded, with an elevated Mg content (Fig. 6.8b'). Early S3 siderite cement grades into the homogeneous S3b siderite cement zone (Fig. 6.8a[Inset A]).

B) S3b-Siderite Cement Zone

S3b siderite cement zone has a light grey, homogeneous appearance in BSE images (Fig. 6.8a). Dissolution is minor in this cement phase. Commonly, S3b siderite fills adjacent pores, linking pores that exhibit similarly zoned S1, S2 and S3 siderite cement (Fig. 6.9c). S3b is the final siderite cement stage precipitated within Merrimelia pore spaces.

6.2.3.2 Ferroan Dolomite/Ankerite

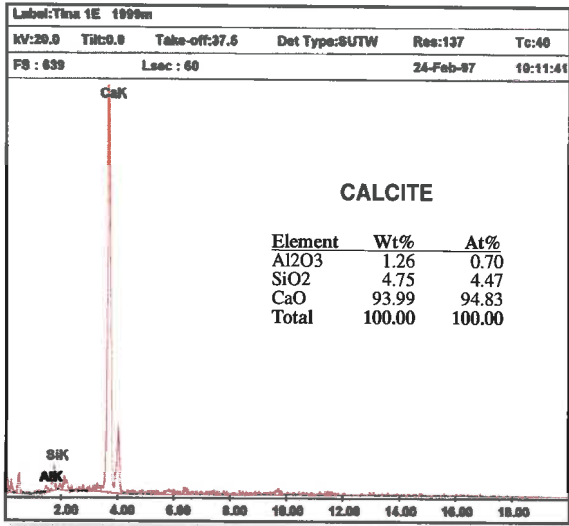
Ferroan dolomite/ankerite is a very rare carbonate phase observed in only eight samples. The existence of this cement was confirmed via bulk XRD and EDAX analyses (Fig. 6.10) in conjunction with SEM observations. Optically, Fe dolomite/ankerite cement is similar to the S2 and S3 sparry siderite phases.

On SEM images, dolomite appears as rhomboids comprising smaller intergrown rhombs (Fig. 6.10). Fe dolomite/ankerite postdates illite and late stage (S3) siderite (Fig. 6.10) such that the edges of Fe dolomite rhombs are smooth with little indication of dissolution embayments. These samples are, however, spread across the entire basin in dissimilar facies, suggesting that this carbonate cement has developed on a regional basis.

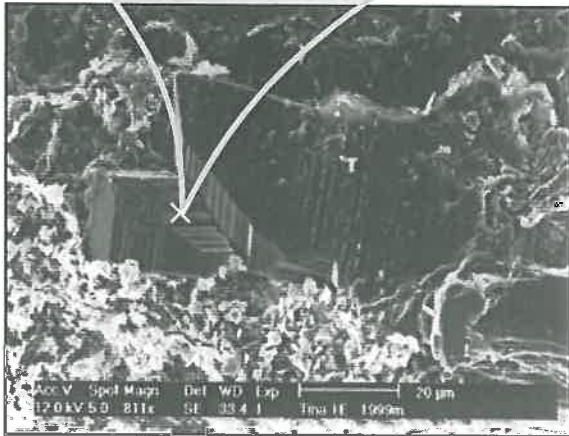
6.2.3.3 Calcite

Calcite is optically distinct from all other carbonate phases, exhibiting distinctive high interference coloured twinning under cross nicols (Fig. 6.11).

EDAX



A



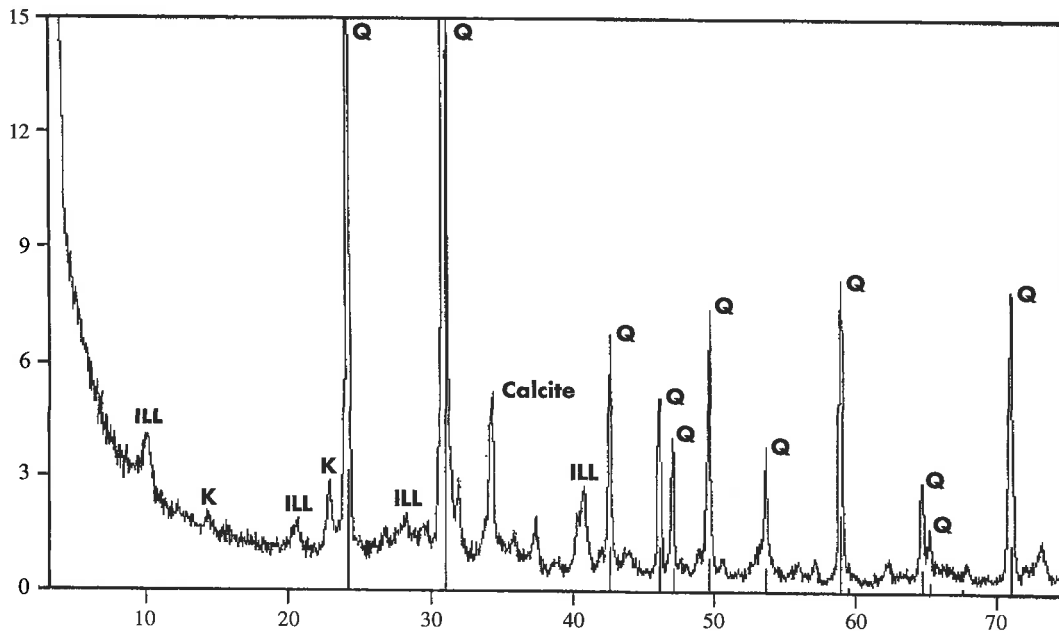
A'

SEM IMAGE



B

XRD



C

Figure 6.11 A) EDAX composition spectra of calcite cement, with corresponding SEM photomicrograph A') (Tina Tingana #1 (1999m). B) Lake Hope #1 (2493.7m) (Cross nicols x 10) Twinned poikilotopic calcite cement. C) Lake Hope #1 (2493.7m) XRD spectra of calcite cement.

Calcite forms crystals with a sub-poikilotopic to poikilotopic appearance, infilling pore spaces between framework grains. XRD and EDAX analyses (Fig. 6.11) further confirm this carbonate phase as calcite. Like dolomite, this phase is rare (seen in 10 samples), but is observed across the basin. Locally, around the Malgoona-Lake Hope and Merrimelia fields, calcite dominates longitudinal bar sandstones and conglomerates.

6.2.4 OPAQUE CEMENTS: PYRITE, GOETHITE AND LEUCOXENE

The most common opaque cement observed in Merrimelia sediments is pyrite (Plates 24a & 24b). Authigenic pyrite was observed in the majority of samples (average 2%). Pyrite occurs as small patches that overprint all other authigenic phases and surround framework grains to the extent that these grains appear to be floating (Plate 24b). Pyrite in the form of framboidal aggregates (Chapter Five - Plate 17c) were also noted.

In Kenny #1, the groundmass of the diamictite cored in that well appears to have been replaced by goethite cement. Whether this transformation occurred via sub-aerial exposure or through other diagenetic reactions is unknown. However, the latter scenario is favoured as goethite cement in all other Merrimelia sediments occurs in isolated patches.

Leucoxene was observed surrounding framework grains in ten samples. Leucoxene is light to translucent in colour and is only identifiable when using reflected light microscopy. In addition, euhedral anatase crystals (Plate 24d) were observed in trace proportions.

6.2.5 MATRIX COMPONENT

6.2.5.1 Argillaceous Matrix

The lower and middle levels (M2 and M3) of the Merrimelia Formation typically have high (>50% of the rock) argillaceous matrix contents (Average ~25% of the total rock). The matrix consists mainly of mixed layered smectite/illite clay with subordinate amounts of silt-sized quartz grains.

Subsequent transformation with burial of the mixed S/I clay to a more illitic composition occurred. The argillaceous matrix of Merrimelia sediments is thus dominated by illite with only 5%-10% mixed layered smectite\illite clay remaining (section 6.2.2.1.3 of this chapter).

PLATE 24

Matrix, Psuedo-Matrix, Pyrite & Accessory Minerals

A) *Photomicrograph – Gidgealpa #7 (2277.94m - Tirrawarra Sandstone) (Plane Polarised x 10) General view illustrating late stage pyrite cement overprinting framework components and earlier formed authigenic phases.*

B) *Photomicrograph – Malgoona #4 (2177.59m – Merrimelia Formation) (Cross nicols x 5). General view illustrating late stage pyrite cement overprinting framework components and earlier formed authigenic phases.*

C) *Photomicrograph – Malgoona #4 (2179.01m) (Cross nicols x 5). Pseudo-matrix, formed by the compression flow and coalescence of incompetent rock fragments.*

D) *TEM photomicrograph – Malgoona #4 (2179.01m). Detail of an anatase crystal amongst illite laths and flakes.*

E) *Photomicrograph – Kudrieke #1 (3116.27m) (Fluoro x 10). Pervasive illite matrix, formed via the transformation of detrital smectite to illite with increasing burial depth. Note: The brown fluorescing mineral is siderite.*

Plate 24

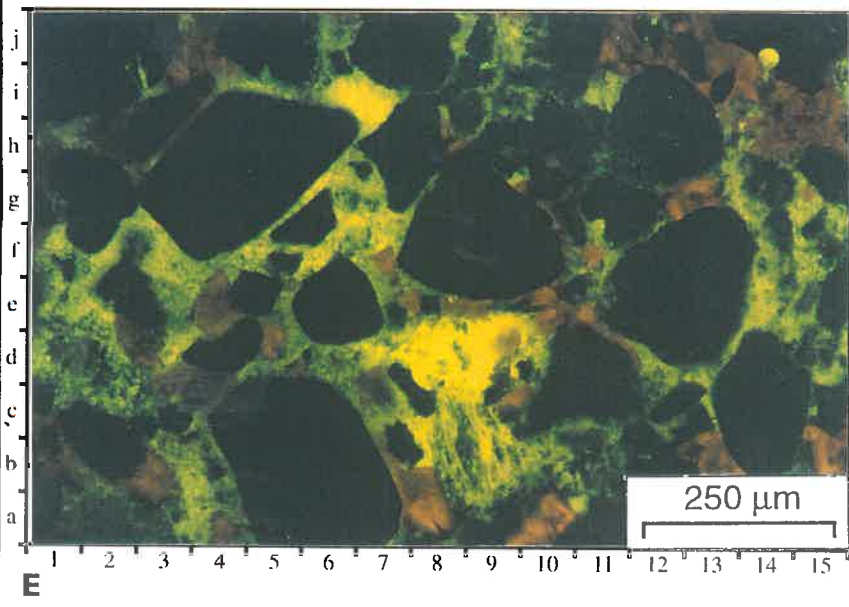
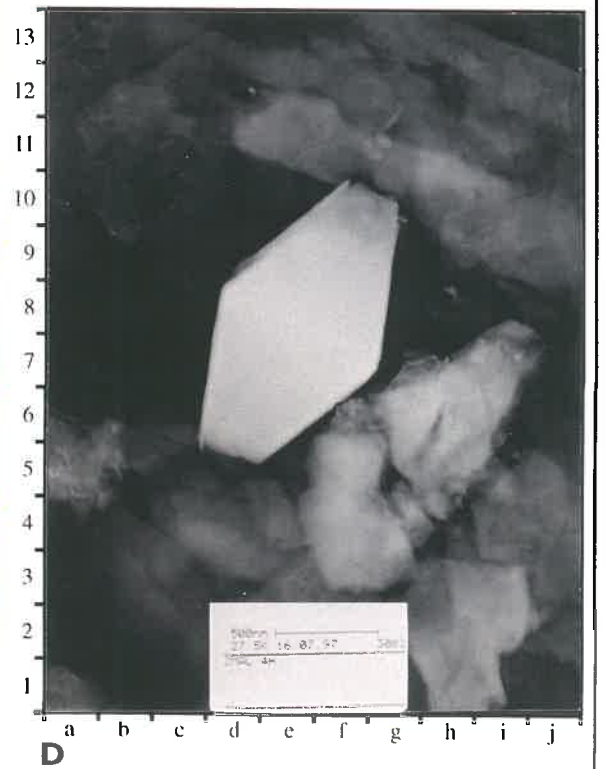
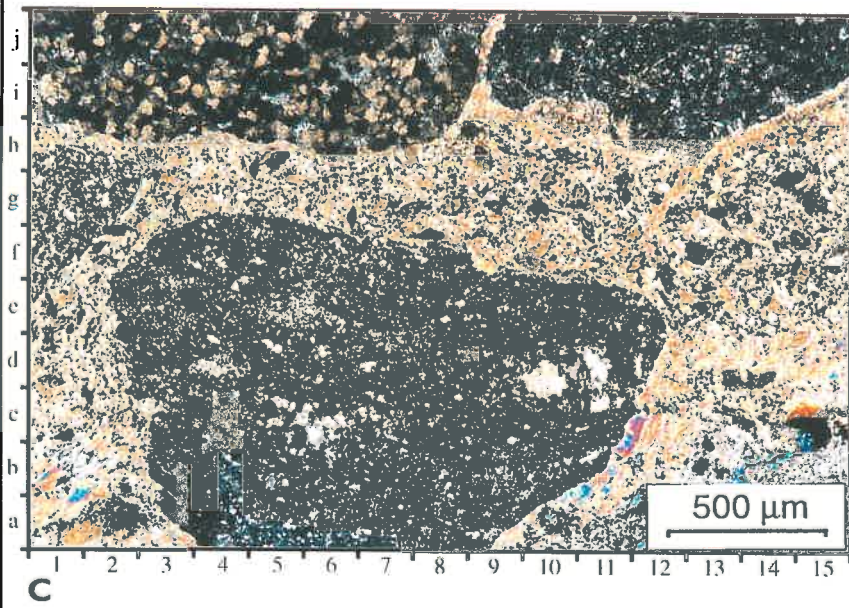
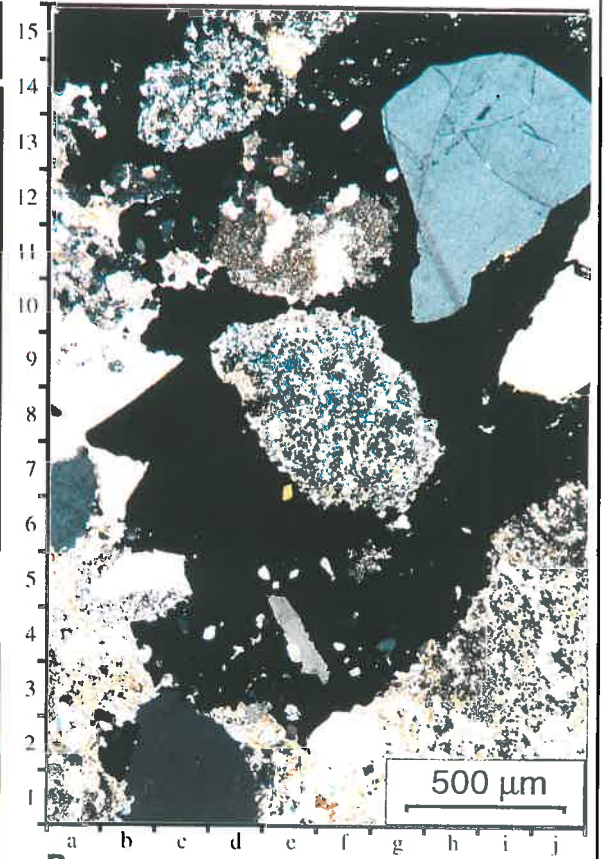
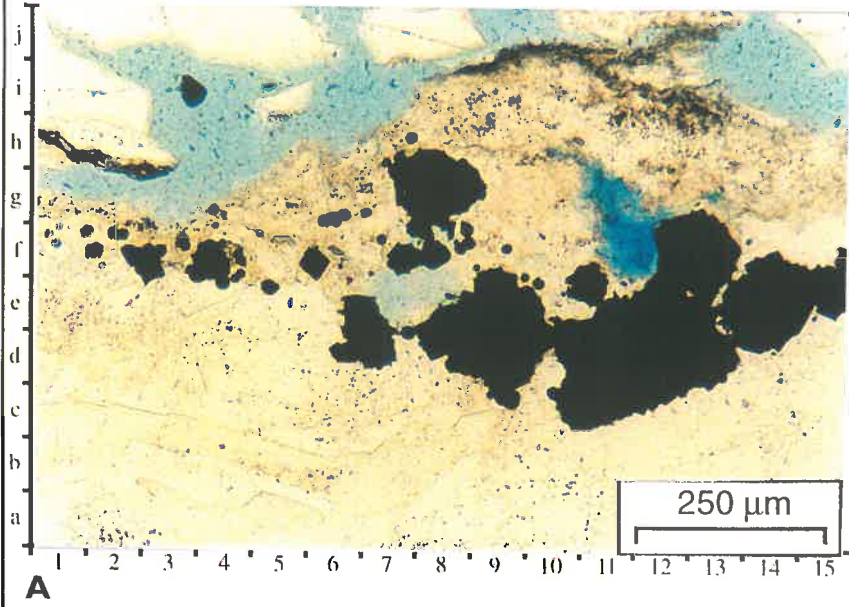


Plate 24e is typical of Merrimelia sediments that are dominated by argillaceous matrix. It can be seen that illite (green/yellow fluorescence) permeates the entire matrix surrounding sediment framework grains.

6.2.5.2 Pseudo-Matrix

Pseudo-matrix is commonly observed in lithologies with high proportions of argillaceous rock fragments. Like fine grained detrital matrix, pseudo-matrix is overwhelmingly illitic (Plate 24c). Pseudo-matrix forms where weak clay-rich rock fragments have squeezed between more competent rock fragments forming an enclosing diagenetic matrix (Plate 24c). Pseudo-matrix generally forms in particular regions where a number of highly squeezed ductile rock fragments occur as the dominant basement lithology (Fig. 5.23). Pseudo-matrix coalesces with detrital matrix making the identification of detrital and compaction-formed rock matrix difficult.

6.3 DIAGENESIS OF MERRIMELIA FORMATION SEDIMENTS

6.3.1 THE EFFECT OF ELEVATED BASIN TEMPERATURES ON DIAGENESIS

Diagenesis in sediments is dependent on the environment of deposition, pore water chemistry, overburden pressure, detrital mineralogy (which is linked to provenance region(s) and facies type) as well as temperature. This last variable, temperature, dictates the style and severity of some diagenetic reactions within a sedimentary pile. For example, Walderhaug (1994b) showed that in the North Sea, there is a positive correlation (Fig. 6.12) between increasing temperature and an increase in the rates of quartz cement precipitation

In the case of the Cooper Basin, temperatures are elevated (high geothermal gradients), with respect to other sedimentary basins in Australia and around the world (Schulz-Rojahn, 1991). Bottom hole temperatures of 410°F (210°C) have been reported in parts of the Big Lake Field (Big Lake #41~9,000'-10,000') while temperatures of 272°F (133°C) are common along the GMI Ridge and in the Patchawarra Trough (Beanbush #1). Galloway (1974) noted that cementation in the Queen Charlotte basin of western Canada is accelerated in areas of higher geothermal gradient, indicating that the rate of diagenetic precipitation of quartz cement is temperature dependent. The high geothermal gradients in the Cooper Basin of Australia will result in greater than normal diagenetic reaction rates and the appearance of minerals normally associated with the early stages of metamorphism

appearance of minerals normally associated with the early stages of metamorphism forming in the deeper parts of the basin. Schulz-Rohan (1991), observed pyrophyllite in the Patchawarra Formation in the Nappamerri Trough. The presence of this mineral suggests greenschist metamorphism conditions exist at depth in this region of the Cooper Basin. It follows then that the presence of pyrophyllite in the deepest Merrimelia sediments (Plate 20a), also suggests, that at depth, in the Patchawarra Trough greenschist metamorphism conditions exist. In such a basin as the Cooper; geothermal gradients have a major control on porosity/permeability formation and preservation.

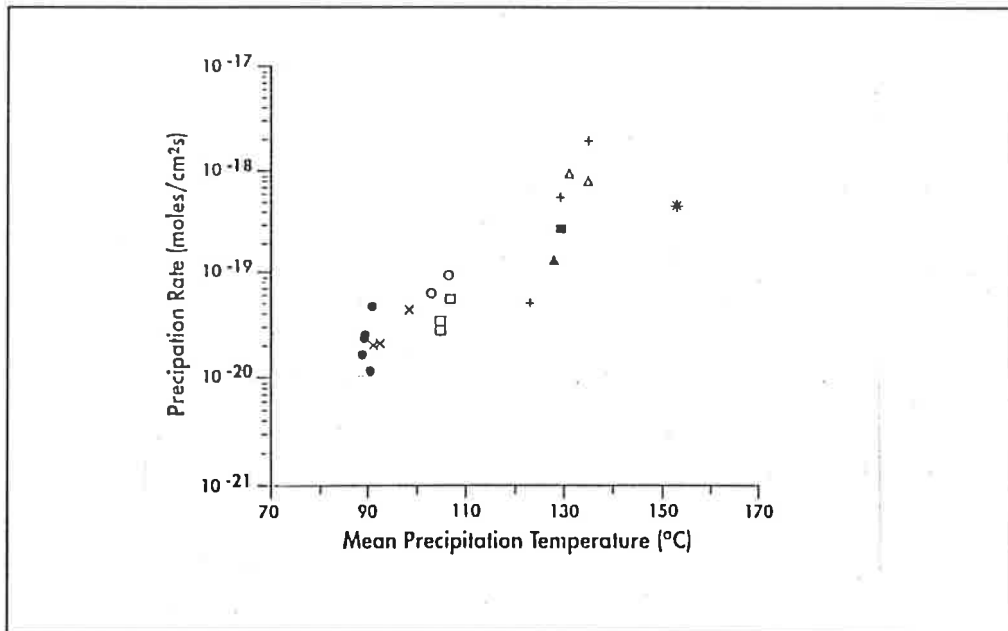


Figure 6.12 Rates of quartz cementation versus mean precipitation temperature (Modified from Walderhaug, 1994b).

6.3.2 SUMMARY OF PARAGENESIS

A paragenetic sequence was constructed using a combination of petrographic observations, SEM, XRD, TEM, fluorescence microscopy, CL and electron microprobe studies. Table 6.12 summarises the general paragenetic sequence established for Merrimelia sediments. This table represents diagenetic adjustments that are consistently observed in Merrimelia sediments across the Cooper Basin in South Australia and Queensland³.

³ The detrital and textural complexity of Merrimelia sediments in conjunction with changing diagenetic conditions has produced regional paragenetic variations. Regional paragenetic sequences are described in section 6.4.

- Calcite (twinned) formation.
- Secondary porosity formation-feldspar, glassy shards and pumice dissolution within sedimentary, volcanic and pyroclastic rock fragments.
- S2 siderite dissolution (D2).

LATE

- Neof ormation of illite/illitisation of kaolin.
- S3 siderite (sparry, poikilotopic).
- Late stage quartz cement/Chemical compaction.
- Ferroan dolomite authigenesis.
- Late pyrite formation.
- Feldspar, pyrite and pyrophyllite authigenesis.

In order to maintain a coherent chapter flow, diagenetic events observed in Merrimelia sediments are discussed in the following order (approximate paragenetic order):

- 1) Mechanical compaction.
- 2) Quartz authigenesis (early & late).
- 3) Clay /feldspar diagenesis (illite, kaolin, dickite chlorite & feldspar dissolution).
- 4) Carbonate diagenesis (siderite formation, siderite dissolution, dolomite & calcite).
- 5) Secondary porosity formation (micro & macro).
- 6) Opaque cements (feldspar, pyrite, pyrophyllite & zeolite).

Each diagenetic event outlined above is discussed in the following manner:

- 1) Key diagenetic observations.
- 2) Observations from the literature/discussion.
- 3) General and specific theories of formation.
- 4) The most likely formation mechanism in Merrimelia Formation sediments.

6.3.3 SUMMARY OF DIAGENESIS

Key observations and findings, as well as pertinent conclusions from the literature are summarised in Table 6.13. As a synopsis of the following diagenesis discussion, Table 6.13 is a listing of the most likely diagenetic mechanisms that have altered Merrimelia sediments since deposition. The following section therefore provides the details from which the findings in Table 6.13 have been drawn.

Table 6.13 A summary of diagenetic events in the Merrimelia Formation, South Australia and Queensland.

DIAGENETIC EVENT (In Paragenetic Order)	KEY OBSERVATIONS	REFERENCE PLATE(S)/FIGURE(S)	OBSERVATIONS FROM THE LITERATURE	AUTHOR(S)	AGREE/DISSAGREE WITH LITERATURE	MOST LIKELY DIAGENETIC FORMATION MECHANISM IN MERRIMELIA SEDIMENTS
COMPACTION	Squeezed shale rock fragments Contorted mica Concavo-convex grain contacts	Plate 25a Plate 25b Plate 29a	Grain size does not influence the compaction of lithic-rich sediments The relative size of ductile and non-ductile grains influences the severity of compaction	Pitman and Larrese (1991) Rittenhouse (1971)	Dissagree Agree	Sediment sorting (Faces Controlled) Rock fragment composition (Provenance controlled) Quartz cement development (Faces and provenance controlled)
SMECTITE-ILLITE TRANSFORMATION	Honeycomb and flame boxwork illite morphologies	Plate 22c & Plate 22b	Interlayer Model: Smectite to illite transformation occurs by cation exchange at layer edge dislocations Interparticle Model: Smectite to illite transformation occurs by the dissolution of smectite and the reprecipitation of illite particles	Freed and Peacor (1989) Ahn and Peacor (1986) Boles and Franks (1979) Nadeau and Bain (1986) Nadeau <i>et al.</i> (1984b)	Agree Agree Agree Dissagree Dissagree	The transformation of smectite to illite by the interlayer model is the most likely mechanism for converting detrital smectite to illite in the Merrimelia Formation across the Cooper Basin
ALTERATION OF ROCK FRAGMENTS	Illitisation of argillaceous rock fragments Illitisation of volcanic rock fragments Illitisation of granitic rock fragments Illitisation of feldspars	Plate 30d Plate 30a Plate 30c Plate 30c	Illite reduces the rigidity of volcanic, granitic and argillaceous rock fragments	Pitman and Larrese (1991)	Agree	The smectite-illite transformation is the most common rock fragment alteration mechanism in Merrimelia Formation sediments across the Cooper Basin
BOXWORK/FILAMENTOUS ILLITE FORMATION	Filamentous fibers protruding from a boxwork (flame or honeycomb) substrate	Plate 21b	Neoformed illite grows from from an early formed (smectite/illite transformation) substrate	Lee <i>et al.</i> (1989) Burley and Fisch (1989)	Agree	Boxwork/filamentous illite in Merrimelia Formation sediments across the Cooper Basin form in two stages: 1. Detrital smectite is transformed to illite with increasing burial. The resulting illite retains a smectite morphology (boxwork morphologies - flame or honeycomb) 2. Using the boxwork illite as a substrate filamentous illite forms from solution (neoformed), on the leading edges of the boxwork illite
S1 SIDERITE CEMENT FORMATION	Micritic, highly dissolved siderite cement Forms the nucleus of pore filling siderite cement and siderite seeds	Figure 6.8 Figure 6.8	Early formed, highly dissolved carbonate phase was described in the Tirrawarra Sandstone at the Tirrawarra, Fly Lake-Broga Fields	Rezaee (1996)	Observed across the Cooper Basin in the Merrimelia Formation	The formation of S1 siderite in Merrimelia Formation sediments across the Cooper Basin occurred at 30C in near surface reducing conditions
SYNTAXIAL QUARTZ CEMENT FORMATION	Quartz cement overgrowths surround detrital quartz grains	Plate 19b & Plate 19d	Early formed syntaxial quartz overgrowths were described in the Tirrawarra Sandstone at the Tirrawarra, Fly Lake-Broga Fields	Rezaee (1996)	Observed across the Cooper Basin in the Merrimelia Formation	The sources of early silica cement in Merrimelia Formation sediments across the Cooper Basin are: 1. The transformation of detrital smectite to illite 2. The alteration of detrital feldspars
COGENETIC QUARTZ CEMENT FORMATION	Quartz cement formed with kaolin clay Quartz cement formed with illite clay	Plate 26b Plate 26a	Cogenetic kaolin and quartz cement were described in the Tirrawarra Sandstone at the Tirrawarra, Fly Lake-Broga Fields The smectite-illite transformation is a major source of quartz cement	Rezaee (1996) Boles and Franks (1979) McBrde (1989)	Observed across the Cooper Basin in the Merrimelia Formation Agree Agree	Cogenetic quartz/illite forms as a byproduct of feldspar dissolution in Merrimelia Formation sediments across the Cooper Basin Cogenetic quartz/illite forms as a byproduct of the transformation of detrital smectite to illite in Merrimelia Formation sediments across the Cooper Basin
FELDSPAR DISSOLUTION	Replacement of detrital framework feldspar grains	Plate 32c	Feldspar dissolution was observed in the Tirrawarra Sandstone at the Tirrawarra, Fly Lake-Broga Fields Feldspar dissolution occurs by the influx of acidic pore waters	Rezaee (1996) Rezaee (1996)	Observed across the Cooper Basin in the Merrimelia Formation Observed across the Cooper Basin in the Merrimelia Formation	Feldspar dissolution in upper (M1) Merrimelia sediments across the Cooper Basin occurs by contact with acidic meteoric waters Feldspar dissolution in lower (M3) Merrimelia sediments across the Cooper Basin by acidic meteoric waters is restricted by the impermeable nature of middle (M2) and lower (M3) Merrimelia sediments
KAOLIN FORMATION	Pore spaces in arenaceous lithologies filled with crystalline kaolin booklets	Figure 6.6a	Feldspar dissolution by acidic meteoric waters forms crystalline kaolin in the Tirrawarra Sandstone at the Tirrawarra, Fly Lake-Broga Fields Meteoric flush is a widespread kaolin formation mechanism	Rezaee (1996) Duffa (1992) Bjorkyke and Brendsal (1986)	Observed across the Cooper Basin in upper (M1) Merrimelia Formation sediments Agree Agree	Kaolin formation in upper (M1) Merrimelia sediments across the Cooper Basin occurs as a byproduct of feldspar alteration by acidic meteoric waters Kaolin formation in lower (M3) Merrimelia sediments across the Cooper Basin by limited as feldspar is alteration is restricted by the impermeable nature of middle (M2) and lower (M3) Merrimelia sediments
DICKITE FORMATION	Brown kaolinitic clay (transmitted light microscopy) Bulk XRD confirmed presence of dickite	Figure 6.5c	Dickite was described in Toolachee Formation sediments of the Nappamer Trough Dickite in the Nappamer trough formed from circulating groundwaters	Schulz-Rohan (1991) Schulz-Rohan (1991)	Observed across the Cooper Basin in the Merrimelia Formation Observed across the Cooper Basin in the Merrimelia Formation	Dickite in the Merrimelia Formation across the Cooper Basin formed via precipitation from migrating ground waters
D1 SIDERITE DISSOLUTION	S1 siderite cement shows extensive dissolution pitting	Figure 6.8b	S1 siderite in the Tirrawarra Sandstone at the Tirrawarra and Fly Lake-Broga Fields exhibits dissolution pitting (Fig 6.4b)	Rezaee (1996)	Observed across the Cooper Basin in the Merrimelia Formation	S1 siderite in the Merrimelia Formation across the Cooper Basin was dissolved by acidic meteoric waters
S2 SIDERITE FORMATION	Zoned sparry siderite cement	Figure 6.8	Zoned, sparry siderite cement was described in the Tirrawarra Sandstone at the Tirrawarra and Fly Lake-Broga Fields The formation of S2 siderite is linked to organic maturation, with formation occurring between 68C-102C	Rezaee <i>et al.</i> (1997) Rezaee and Schulz-Rohan (1996)	Agree Dissagree	The main source for S2 siderite reactants in M2 and M3 sediments across the Cooper Basin is the smectite-illite transformation Organic decarboxylation is the main source of S2 siderite reactants in M1 and Tirrawarra sediments across the Cooper Basin It is also possible that S2 siderite reactants may have been sourced from ground waters that had been in contact with Warburton Basin carbonate lithologies and cements
CHLORITE FORMATION	Green translucent minerals which commonly overprint basic volcanic rock fragments	Figure 6.5d(e)	Chlorite formation associated with the transformation of smectite to illite Chlorite formation occurs by the breakdown in kaolin in Mg-rich pore fluids	Hower <i>et al.</i> (1976) Jahren and Aagaard (1989)	Agree Minor reaction in Merrimelia Formation sediments across the Cooper Basin	Chlorite formation in Merrimelia Formation sediments across the Cooper Basin is a byproduct of reactants released by the alteration of basic rock fragments
SECONDARY POROSITY FORMATION	Micro porosity between vermicular kaolin booklets	Figure 9.9	Kaolin micro-porosity is a major component of the Tirrawarra Sandstone at the Tirrawarra and Fly Lake-Broga Fields	Rezaee (1996)	Observed across the Cooper Basin in upper (M1) Merrimelia Formation sediments	Effective secondary porosity in Merrimelia sediments forms via two mechanisms: 1. Feldspar destruction by acidic meteoric waters forming crystalline kaolin booklets 2. The alteration of "weak" components within competent rock fragments i.e. feldspar grains in an arkose rock fragment
D2 SIDERITE DISSOLUTION	In arenaceous Merrimelia sediments a D2 carbonate dissolution phase is marked by a irregular boundary between S2 and S3 siderite	Figure 6.8	A siderite dissolution phase (D2) was observed in the Tirrawarra Sandstone at the Tirrawarra and Fly Lake-Broga Fields	Rezaee (1996)	Observed across the Cooper Basin in upper (M1) Merrimelia Formation sediments Inconsistently observed in lower (M3) Merrimelia sediments across the Cooper Basin	Organic acids derived from the maturation of organic matter increases the acidity of pore fluids dissolving S2 siderite The impermeable nature of middle and lower Merrimelia Formation sediments across the Cooper Basin restricts the influence of acidic pore fluids and limits S2 dissolution
NEOFORMED ILLITE FORMATION	Filamentous illite, within porous quartzose lithologies	Figure 6.23	Illite formation directly from solution without a smectitic precursor	Nadeau and Bain (1986)	Agree	The sources of neoformed illite in Merrimelia Formation sediments across the Cooper Basin are: 1. Dewatering of argillaceous lithologies adjacent to porous lithologies 2. Feldspar destruction
ILLITISATION OF KAOLIN	Vermicular kaolin booklet disintegration with filamentous illite protruding from kaolin booklet	Plate 28c	Kaolin becomes unstable at elevated temperatures transforming to illite	Bjorkyke (1983) Smaet <i>et al.</i> (1992) Srodon and Eberl (1987)	Agree	Kaolin in Merrimelia Formation sediments across the Cooper Basin transforms to illite in regions of elevated temperatures and potassium-rich pore fluids
S3 SIDERITE FORMATION	Sparry homogenous carbonate cement which encloses early formed Mg-carbonate cement	Figure 6.8	A high temperature (>100C) siderite phase was described in the Tirrawarra Sandstone at the Tirrawarra and Fly Lake-Broga Fields	Rezaee (1996)	Observed across the Cooper Basin in (M1) Merrimelia Formation sediments	The formation of S3 siderite in Merrimelia Formation sediments across the Cooper Basin is a byproduct of the later stages of the smectite-illite transformation where the later neoformation of illite acts as a pH buffer
CALCITE (Twinned) FORMATION	Sparry, poikilotopic carbonate cement	Fig 6.11b	Possible sources of calcite cement include: feldspar dissolution and heavy mineral/mica destruction	Waldterhaug and Bjorkum (1992)	Minor reaction in Merrimelia Formation sediments across the Cooper Basin	Calcite in Merrimelia Formation sediments across the Cooper Basin have formed as byproducts of the transformation of detrital smectite to illite Minor sources of calcite in Merrimelia sediments across the Cooper Basin include: 1. Feldspar dissolution 2. A byproduct of siderite dissolution
CALCITE (Cow Pat) FORMATION	Concentrically zoned carbonate/illite cement	Plate 34	Calcite formation is linked to the formation of chlorite	Hutcheon <i>et al.</i> (1980)	Not observed in this study	"Cowpat" calcite/illite in Merrimelia Formation sediments across the Cooper Basin formed as detrital feldspar grains were altered by acidic/alkaline pore fluids and replaced by calcite and illite
LATE QUARTZ CEMENT FORMATION (Chemical Compaction)	Sutured grain contacts (illite tends to fill suture) between quartz framework grains Localised redistribution of quartz cement	Plate 27b & Plate 27e	Overburden pressure at grain contacts releases silica which reprecipitated locally Temperature and illite drives the release of silica at grain contacts, precipitating in inter-stylole regions	Hutcheon <i>et al.</i> (1980) Waldterhaug (1994a) Foscolos (1990) Bjorkum <i>et al.</i> (1998)	Not observed in this study Observed across the Cooper Basin in (M1) Merrimelia Formation sediments Observed across the Cooper Basin in (M1) Merrimelia Formation sediments Observed across the Cooper Basin in (M1) Merrimelia Formation sediments	Late quartz cement in Merrimelia sediments across the Cooper Basin is derived from silica released via chemical compaction The inter-stylole model is the most likely chemical compaction mechanism operating in Merrimelia sediments across the Cooper Basin A minor source of late quartz cement maybe the dissolution of siliceous rock fragments
FELDSPAR OVERGROWTH FORMATION	Feldspar projections into pore cavity	Figure 6.30a	Feldspar overgrowths form from the breakdown of glassy and acidic volcanic rock fragments	Mc Brde (1989) Schluger (1979)	Insufficient evidence	No link between siliceous rock fragments and feldspar overgrowths was observed. Feldspar overgrowth formation mechanism in Merrimelia sediments across the Cooper Basin is unknown
FERROAN DOLOMITE FORMATION	Sparry carbonate with distinctive rhombic crystal structure	Figure 6.10	The formation of dolomite maybe a byproduct of the smectite-illite transformation	Stewart (1986) Boles and Franks (1979)	Dissagree	The most likely source of dolomite cement reactants in Merrimelia sediments across the Cooper Basin are S2 siderite ions liberated by the D2 siderite dissolution event
POIKILOTOPIC PYRITE FORMATION	Opaque mineral overprinting all authigenic and framework components	Plate 24b	At elevated temperatures the reactants needed for pyrite formation are released by complexing organic acids	Dixon <i>et al.</i> (1989)	Agree	Decarboxylation of organic matter releases ionic agents which form poikilolitic pyrite (Tirrawarra & M1 sediments) Breakdown of acid volcanic rock fragments (M2 and M3 sediments)
PYROPHYLLITE FORMATION	High interference coloured mineral at depths greater than 11000ft	Figure 6.30c	Pyrophyllite forms from the dehydration of kaolin	Schulz-Rohan (1991)	Insufficient evidence	No link between kaolin and pyrophyllite was observed. The mechanism for pyrophyllite formation in Merrimelia sediments across the Cooper Basin is unknown

6.3.4 DIAGENETIC EVENTS IN THE MERRIMELIA FORMATION

6.3.4.1. Mechanical Compaction

6.3.4.1.1 Key Observations

The mechanical compaction of Merrimelia sediments started soon after deposition. Primarily this involved mechanically unstable rock fragments and micas (Chapter Five - Table 5.7), being compressed and crushed between more rigid framework grains (Plate 25a & 25b). In matrix-rich Merrimelia sediments, muddy matrix is commonly deformed by compaction to a stage where all depositional features have been obliterated (Plate 25c). The crushing of the labile components in more arenaceous Merrimelia sediments proceeded until quartz cementation produces a rigid self supporting framework (Plate 25d).

The mineralogy of Merrimelia sediments controls the severity of mechanical compaction (Fig. 6.13a & 6.13b). As the proportion of ductile rock fragments⁴ increases, the amount of primary pore loss from mechanical compaction (Compaction Index (CI)) also increases (Fig. 6.13c). The calculation of CI in Merrimelia sediments was achieved using the relationship outlined by Rezaee (1996) (Equation 5).

The CI of each facies was estimated using the IGVo data generated by Beard and Weyl (1973) (see Chapter Nine - Fig. 9.17e). The results indicate that facies rich in rock fragments (terminoglacial) have had the most primary pore space reduction, while facies with low proportions of rock fragments (proglacial) have had the least reduction of depositional pore space (Fig. 6.13c).

$$\text{Compaction Index (CI)} = \left[\frac{(IGVo - IGV)}{IGVo} \right] \times 100$$

IGVo = Original intergranular volume

IGV = Present intergranular volume

Equation 5

⁴ Ductile rock fragments: incompetent rock fragments listed in Table 5.7.

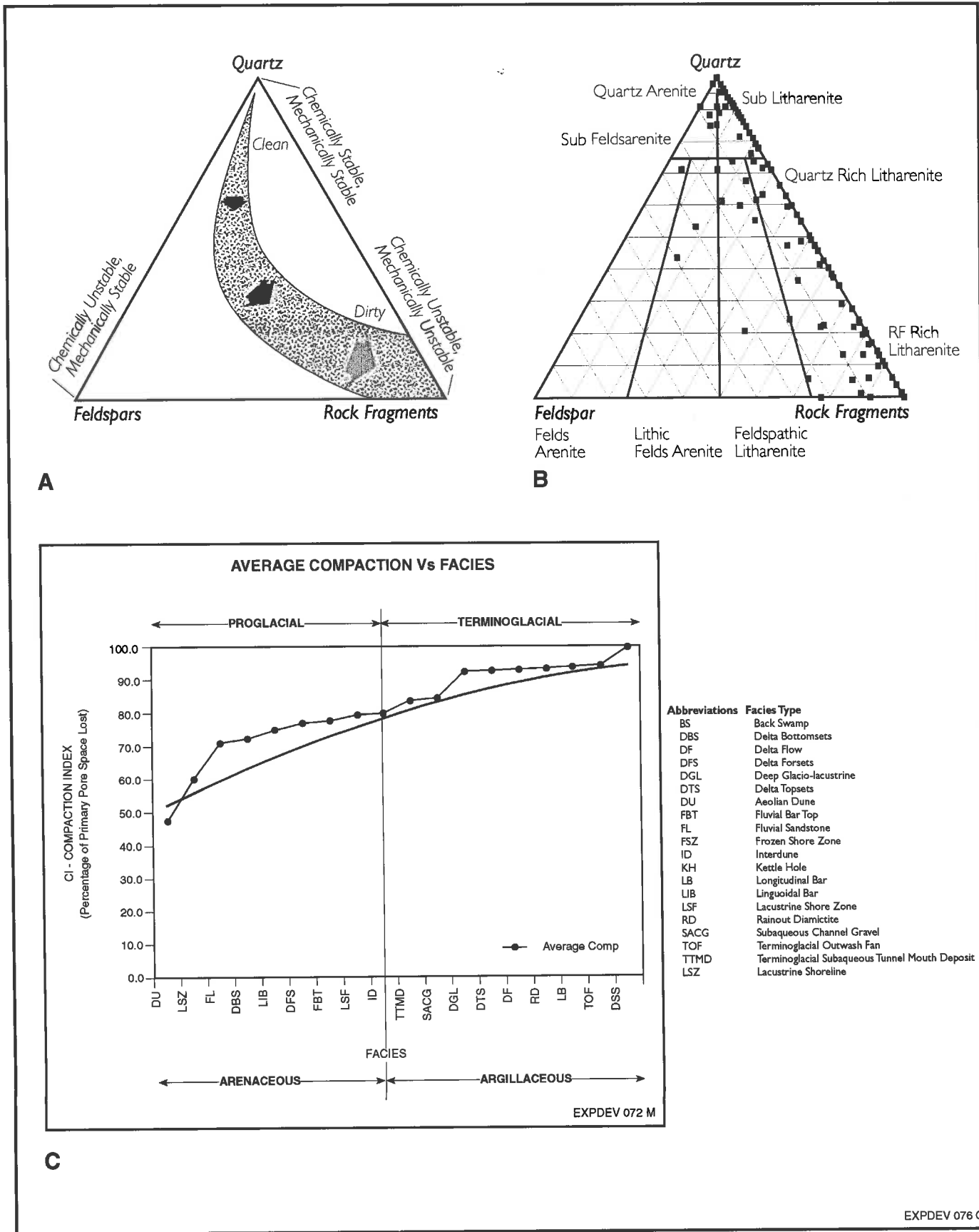


Figure 6.13 Mechanical compaction. **A)** A comparison of the ternary diagram cartoon of Schuliga, (1979) and the **B)** sediment composition of Merrimelia sediments with respect to mechanical compaction. **C)** A cumulative histogram where all facies types are ranked according to CI loss. Note: the destruction of primary pore space (CI) becomes more evident as the argillaceous nature of a facies begins to dominate.

In addition to the amount of ductile material in a sediment, the following criteria also induce pore space reduction in the Merrimelia Formation:

- 1) The compressibility and brittleness of rock fragments (discussed in Chapter Nine)
- 2) The distribution of labile and competent grains throughout the sediment
- 3) The size of labile rock fragments with respect to adjacent competent framework grains.

6.3.4.1.2 Discussion

Pittman and Larese (1991) showed that if competent lithics were clustered together the grains form a "shelter zone" of porosity preservation, whereas clustered labile grains lead to localised porosity loss. These authors also stated that grain size does not have any effects on lithic-rich sediment compaction. In contrast Rittenhouse (1971) stated that for poorly sorted sands (i.e. the bulk of porous Merrimelia sediments), the relative size of ductile grains (lithic rock fragments) and non ductile grains (quartz and silicic rock fragments), influences the severity of sandstone compaction. For instance, if ductile grains are smaller than the surrounding framework, they may be protected from compaction (Plate 19d[3f]). Conversely, if ductile grains are larger than the surrounding framework, compaction of these grains is inevitable (Plate 25d[8g]).

The brittle fracturing of quartz grains is rarely observed in Merrimelia sediments. Pittman and Larese (1991) in this regard, conclude that the amount of fractured quartz grains varies inversely with the amount of ductile material present. The lack of brittle grain failure and dominance of labile material observed in Merrimelia sediments supports this conclusion.

6.3.4.1.3 Key Findings

The principle controls on mechanical compaction in Merrimelia sediments are:

- 1) Sediment sorting
- 2) Rock fragment composition
- 3) Quartz cement development

The controls on compaction in Merrimelia sediments are directly related to:

- 1) Sediment provenance,
- 2) The environment of deposition.

PLATE 25

Compactional Effects

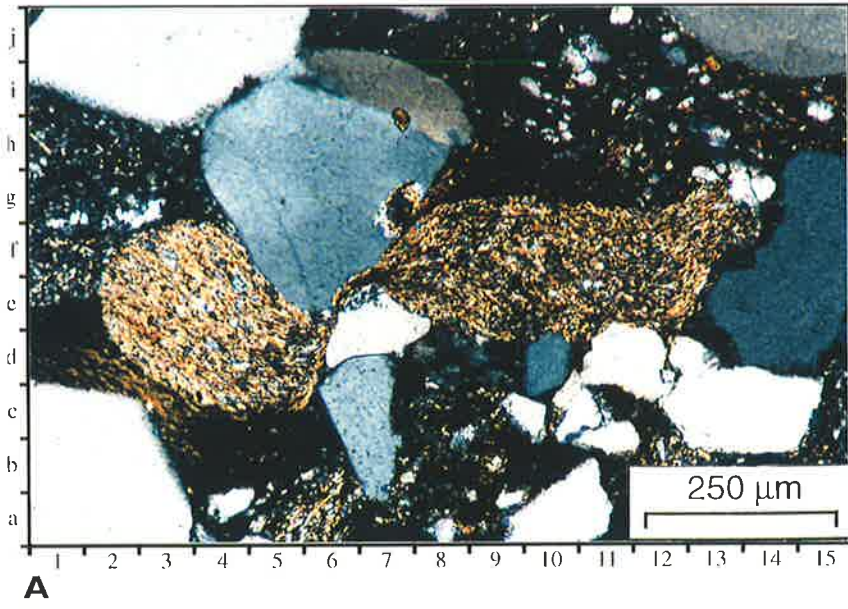
A) Photomicrograph - Brolga #1 (2947.7m) (Cross nicols x 10). Incompetent shale rock fragment squeezed between competent quartz grains.

B) Photomicrograph - Tinga Tingana #1 (1732.99m) (Cross nicols x 20). Bow tie mica lath, formed by competent framework component compressing the middle section of the mica with the end spraying out and filling adjacent pore spaces.

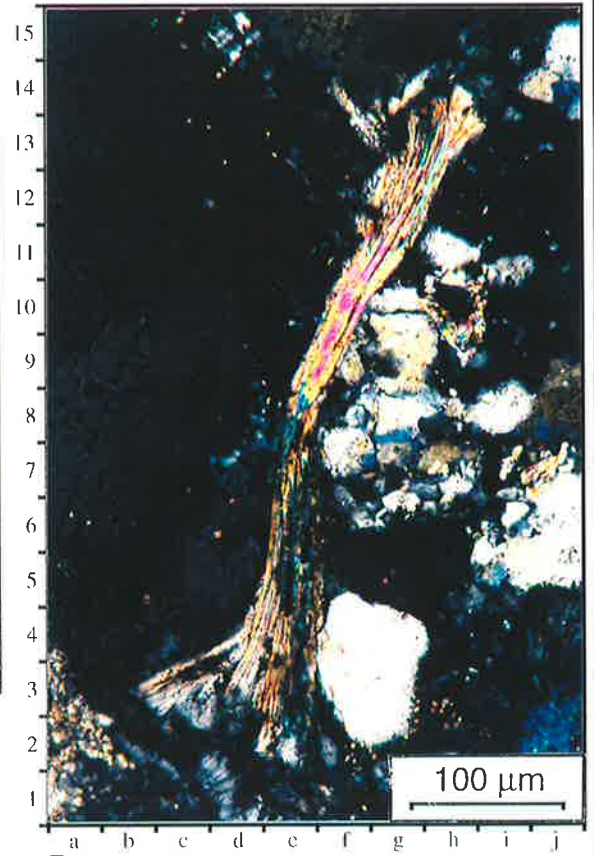
C) Photomicrograph - Merrimelia #1 (2943.6m) (Cross nicols x 5). Compaction of argillaceous matrix, which has subsequently obliterated all depositional features, filling all available pore space.

D) Photomicrograph - Tinga Tingana #1 (1891.55m) (Plane polarised x 10). Argillaceous rock fragments in arenaceous Merrimelia sediments will distort and fill all adjacent pore space until quartz cementation produces a rigid framework, whereby the squeezing of the ductile material is held in check.

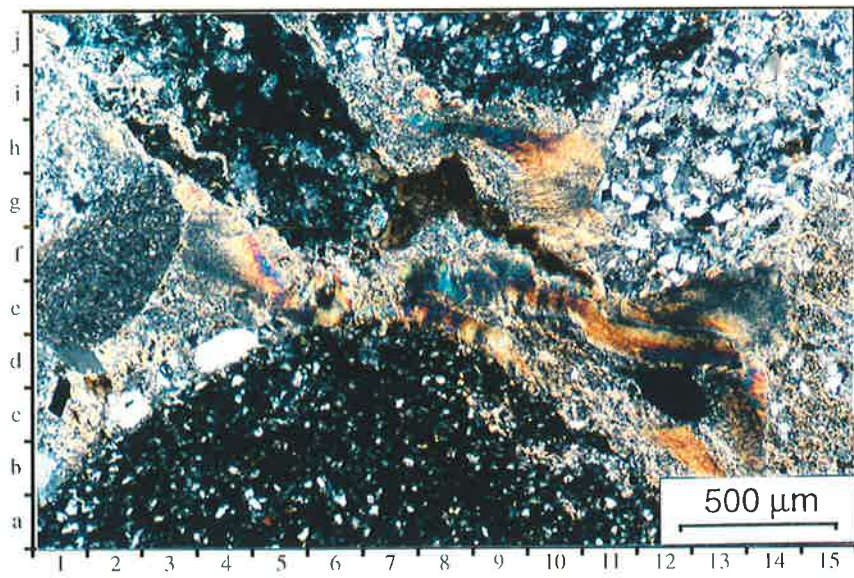
Plate 25



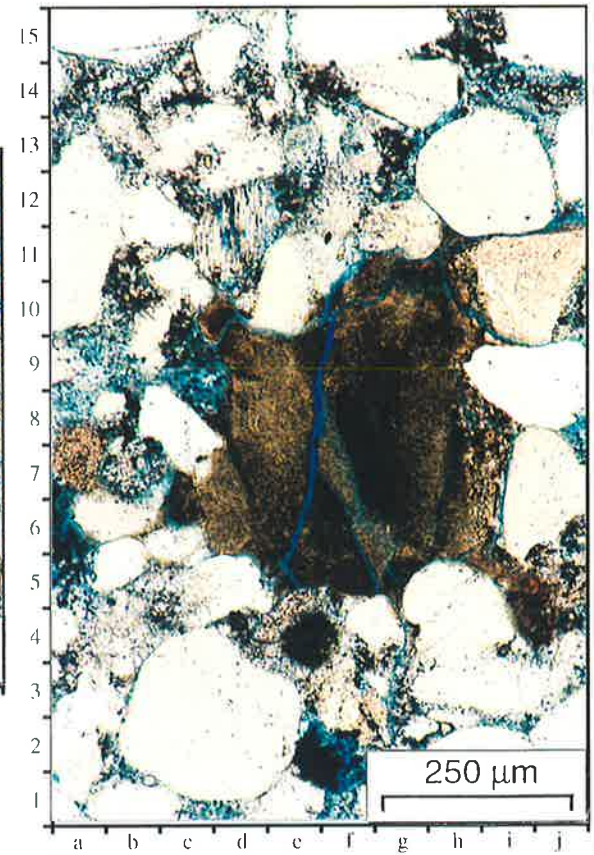
A



B



C



D

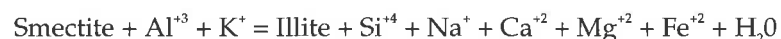
6.3.4.2 Quartz Authigenesis

6.3.4.2.1 Early Quartz Cementation and Co-genetic Illite and Kaolin

A) Key Observations

Quartz overgrowths in Merrimelia sediments are confined to arenaceous intervals where quartz-quartz contacts commonly occur. These arenaceous intervals mainly form in the upper Merrimelia section where removal of the rock fragment component has been at a maximum, a consequence of when thawing conditions prevailed over freezing conditions (Chaney *et al.*, 1997). It is within the more quartzose upper Merrimelia sediments (M1) that quartz overgrowths can dominate diagenesis.

Juxtaposed in the upper reaches of the Merrimelia formation are argillaceous sediments deposited via direct glacial action (terminoglacial sediments). These sediments contain extensive illite, formed via the transformation of detrital smectite to illite. In this transformation process silica (as well as water) is also produced (Equation 6). It is possible then that silica from the transformation of smectite to illite in argillaceous sediments may precipitate as quartz cement in adjacent arenaceous Merrimelia rocks.



Equation 6

B) Discussion

The smectite-illite transformation has been cited by numerous authors as a major source of quartz cement (Blatt, 1979; Milliken *et al.*, 1981; McBride, 1989; Boles and Franks, 1979; Hower *et al.*, 1976; Ehrenberg and Nadeau, 1989). In reviewing the main sources of quartz overgrowths, McBride (1989), concluded that large volumes of silica are generated by the transformation of smectite to illite. Less certainty however surrounds the expulsion of smectite/illite-sourced silica out of shales and into adjacent sandstone layers (Blatt, 1976; McBride, 1989). Hugget (1996) concluded that silica can be exported from adjacent mudrocks, with expulsion efficiencies of generally less than 50%. Even at these low expulsion efficiencies, and assuming that 60% of the mudrocks when deposited at the surface were smectite (McBride, 1989), then the amount of silica produced by this reaction is more than enough to account for the small volumes of quartz cement observed in arenaceous Merrimelia sediments. For example, illite constitutes, on average, 34% (matrix plus neoformed illite) of the total authigenic component of Merrimelia sediments while quartz cement accounts for (on average) 8% (of the total authigenic component). Assuming pessimistic expulsion efficiencies and an original smectite percentage of 60% all

quartz cement in Merrimelia sediments can be accounted for by the transformation of smectite to illite (Equation 7).

$$0.4 (\text{Expulsion Efficiency}) \times 0.34 (\text{Illite } \%) \times 0.6 (\text{Smectite } \%) = 8\% (\text{Qz Cement } \%)$$

Equation 7

SEM images from samples around the Coonatie region, illustrate the cogenetic nature of illite and early quartz cement (Plate 26a). Cogenetic quartz\illite (Plate 26a) is normally observed in the vicinity of dissolved feldsic rock fragments and/or K-feldspar framework grains.

These observations suggest that the dissolution of feldspathic grains within these pores spaces liberated ionic species (Si, Al and K) forming localised quartz cement and co-genetic illite. The samples in which isolated filamentous illite are observed (Plate 22a), are conglomeratic in nature with small amounts of isolated porosity indicating a more localised or closed system of formation.

The other main source of early quartz cement in Merrimelia sediments is the alteration of feldspars to kaolin (Equation 8 – See Pg. 244) and illite (Equation 6 – See Pg.240). The dissolution of feldspar is reported by Moncure *et al.*, (1984), McBride, (1989) and Macchi *et al.*, (1990) to be a major source of quartz overgrowth development in sandstones worldwide. Bjørlykke (1983) concluded that each volume of feldspar dissolved is likely to precipitate 60% kaolin and 40% quartz cement.

Locally other sources of quartz cement in Merrimelia sediments may include:

- 1) Micro-sized particles of quartz, produced by glacial ablation (rock flour),
- 2) Devitrification of glassy shards and siliceous volcanic groundmasses in acid volcanic rock fragments.

This later quartz cement source maybe important in sediments at Malgoona Field where pyroclastic rock fragments dominate. Both of these silica sources will supply quartz cement locally but be insignificant on a regional basis.

The solubility of silica, according to Bjørlykke (1983) is low, thus very little of this cement can be held in solution, and must be eventually precipitated (Equation 8).

PLATE 26

Paragenetic Relationships: Quartz, Siderite, Kaolin & Illite

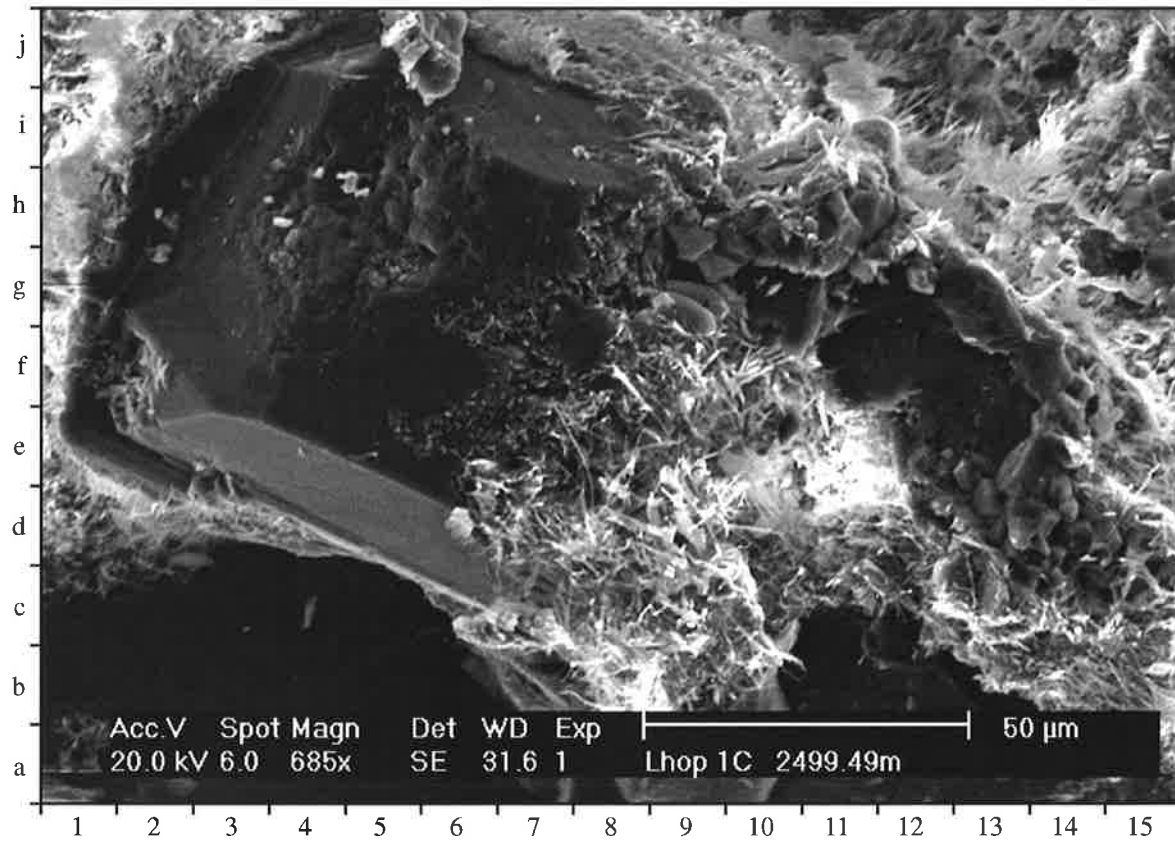
A) SEM photomicrograph – Lake Hope #1 (2499.49m). General view which illustrates the cogenetic nature of syntaxial quartz cement and filamentous illite [9e].

B) SEM photomicrograph – Moorari #3 (2893.28m). Close up view of the cogenetic relationship between kaolin and syntaxial quartz cement [4d]. This is the most commonly observed cogenetic relationship between authigenic minerals in both Merrimelia and Tirrawarra sediments.

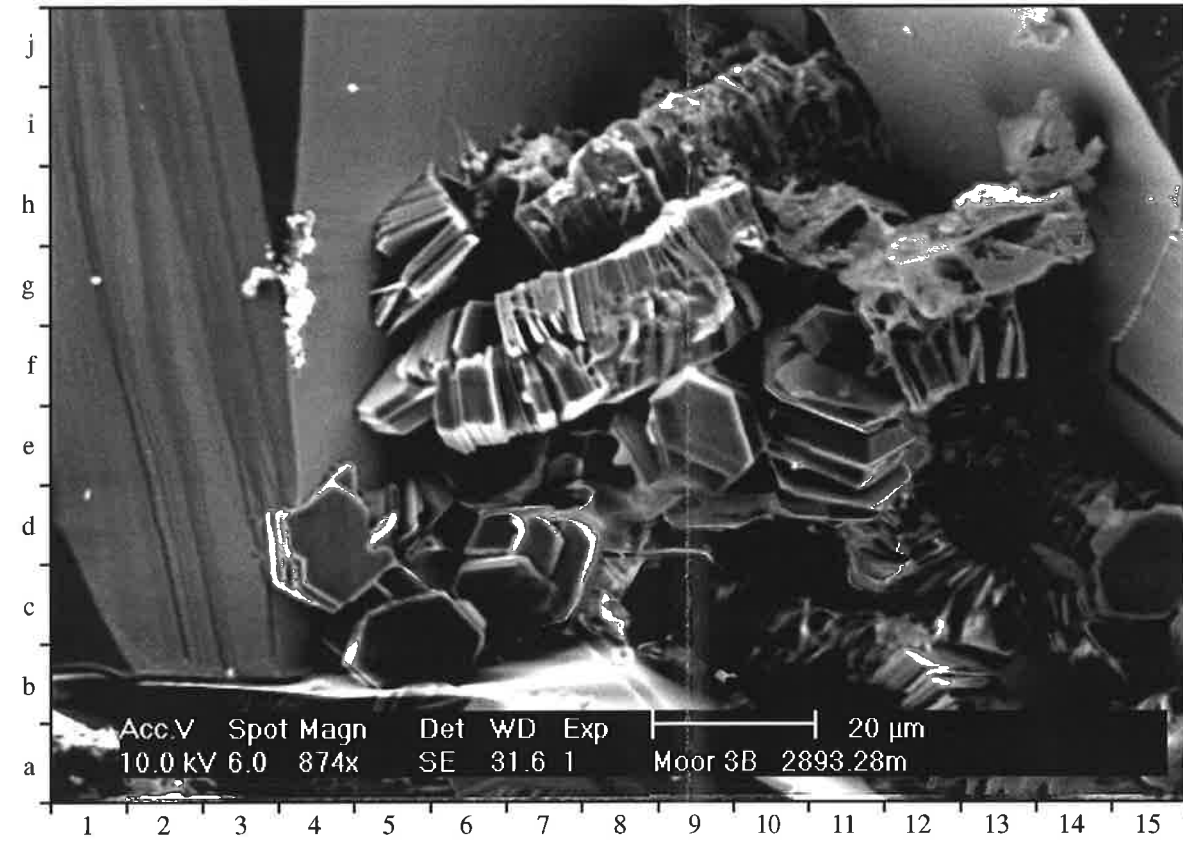
C) SEM photomicrograph – Moorari #3 (2893.28m). An example of illite [14i] and kaolin [6e] simultaneously forming with druse quartz cement [13i]. Note: The illite forms cogenetically with kaolin [13i].

D) SEM photomicrograph – Gidgealpa #5 (2302.45m). Broad view illustrating the cogenetic nature of siderite and quartz cement [4e] along with kaolin [9d].

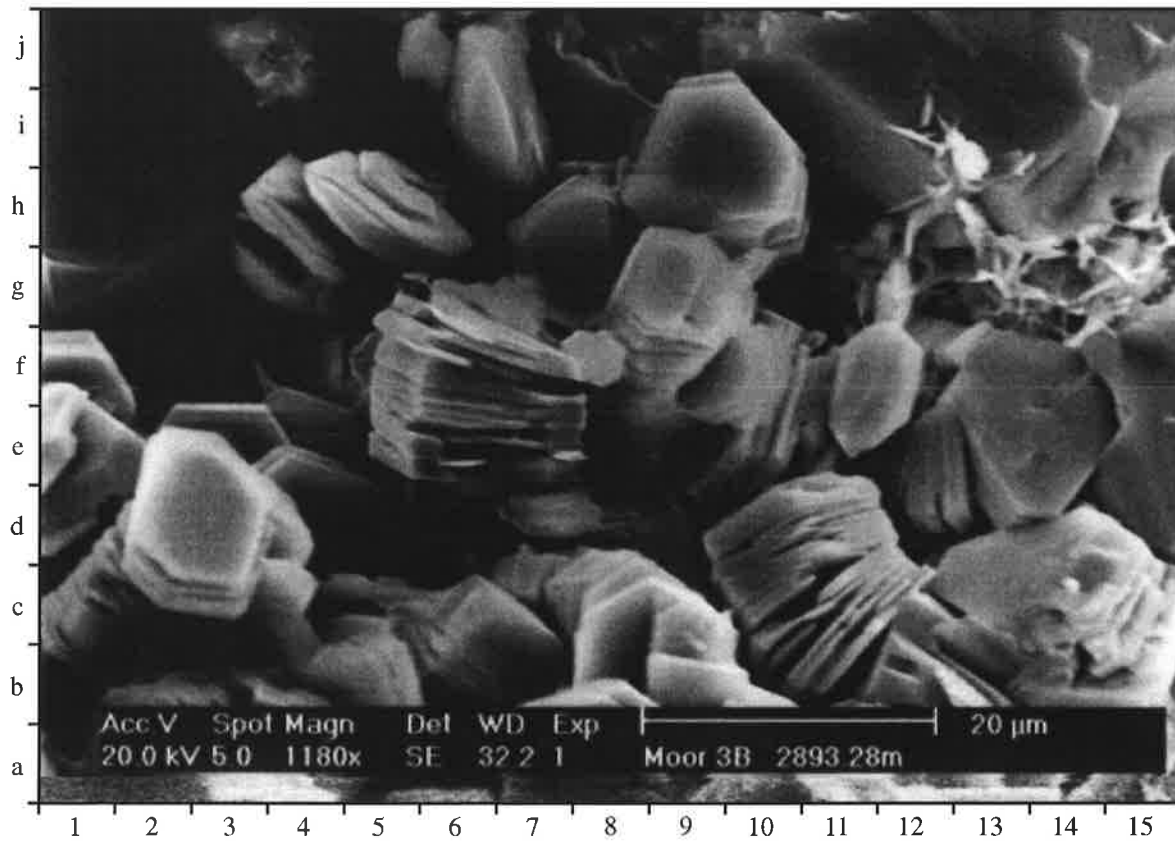
Plate 26



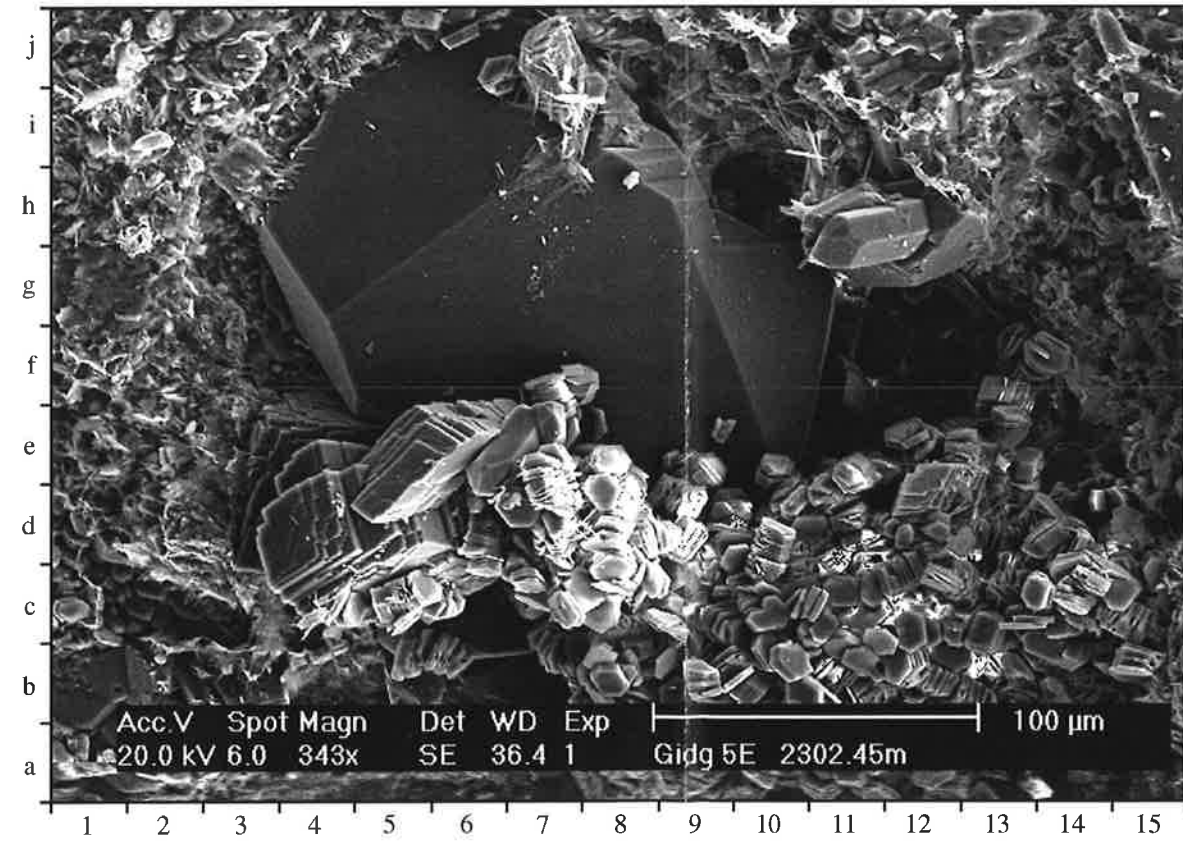
A - Illite and Quartz Cement



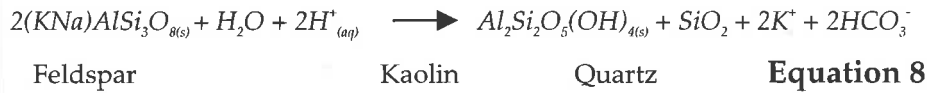
B - Kaolin and Quartz Cement



C - Illite / Kaolin and Quartz Cement



D - Siderite and Quartz Cement



The cogenetic nature of kaolin and quartz is ubiquitous in Merrimelia samples (Plate 26b[4c]). This implies that the reaction represented by Equation 8 is an important source of both diagenetic phases. However, the amount of feldspar grains observed in Merrimelia sediments is low (Appendix 5b – 0.8% as a proportion of the whole rock) whereas the amount of quartz cement and kaolin as a percentage of the whole rock is much greater (Appendix 5c – 4.5% and 4.3% respectively).

These figures would suggest that Equation 8 is unlikely to occur in Merrimelia sediments. However, the texture within most kaolin filled pores indicates that these are actually not infilled pore spaces but the kaolinised remnants of detrital feldspar grains (Plate 30c). Petrographic results show that kaolinised feldspars account for up to 1.2% of the total rock volume. Therefore at the time of deposition approximately 2% of Merrimelia detritus was feldspar (that is currently observed feldspar 0.8% and kaolinised feldspar 1.2%). Thus, if the original proportion of feldspar grains was approximately 2%, and the present proportion observed is 0.8%, then 60% of feldspars have been destroyed. The likely products are, according to Equation 8, kaolin and quartz. According to Hugget, (1996) the dissolution of a rock volume containing 1.2% feldspar (kaolinised feldspars only) will yield, at a conversion efficiency of 40% (Bjorlykke 1983), 0.5% quartz cement as a percentage of the whole rock volume (or 1.6% of the authigenic component). This cement volume accounts for all of the quartz cement observed (1.3% of the authigenic component) in Merrimelia sediments.

C) Key Findings

The predominance of co-genetic kaolin and quartz (as opposed to cogenetic-illite and quartz or illitised feldspar grains) suggests that the reaction described in Equation 8 is the most important source of quartz cement in Merrimelia sediments. There are, however, examples where all three phases (kaolin, illite and quartz) coexist intergrown together (Plate 26d) implying that Equation 9 does indeed produce silica but in volumes subordinate to that produced by Equation 8.

6.3.4.2.2 Chemical Compaction/Late Stage Quartz Cement

A) Chemical Compaction

Houseknecht (1987) defines chemical compaction as “bulk volume loss caused by the dissolution of framework grains in contact, due to overburden pressure”.

i) Key Observations

Evidence of chemical compaction in Merrimelia sediments is widely observed (Plate 27). Chemical compaction features such as stylolitis along organic laminae (Plate 27a), localised redistribution of detrital quartz as quartz overgrowths (Plates 27b & 27c) and sutured contacts are generally observed in conglomeratic, fine grained and argillaceous Merrimelia sediments (Plates 27d, 27e & 27f).

ii) Discussion

Blatt (1979) stated that detrital quartz grains serve as both a source of dissolved quartz as well as a substrate for precipitated quartz. This is true for quartz grains in arenaceous Merrimelia sediments. Quartz grains, where overburden pressures are unequal across a grain contact, show the diffusion of silica from the grain contact to the pore space (Plate 27b & 27c) (Hutcheon, 1982). This redistribution of detrital quartz at grain contacts is described by numerous authors (Hayes, 1979; Schmidt and McDonald, 1979; McBride, 1989; Bjorlykke, 1983). The later author concluded that the solubility of mineral species increases with increasing stress at the grain contact. Plate (27e) is typical of a grain suture contact in sediments where compaction has been severe. Most samples however, exhibit mainly concavo-convex grain contacts (Plate 27b[2g]). A very small number of samples, usually those matrix or organic rich, indicate that they have experienced extreme compaction exhibiting highly sutured contacts (Plate 27d & 27f).

Most suture contacts are lined by illite (Plates 27e & 27f). This illite was most likely emplaced as clay rims which were subsequently squeezed between adjoining framework grains. The resulting texture is stylolitic in appearance with the illite appearing to accentuate the shape of the suture (Plate 27e[8g]).

Contrary to popular wisdom, work done by Oelkers *et al.* (1992), Walderhaug (1994a) and Walderhaug (1996) suggested that there is no relationship between overburden stress and quartz cement formation. Foscolos (1990) and Bjørkum and Nadeau (1998) also concluded the same, suggesting that illite between grain contacts facilitates local quartz formation by diffusion into an interstylolite region (Fig. 6.14) where, according to Walderhaug (1996) and Bjørkum *et al.* (1998), it is then precipitated as quartz cement by kinetically controlled surface reactions.

Bjørkum and Nadeau (1998) and Walderhaug (1996) claim that this process is independent of effective vertical stress and dependent on increasing temperature.

PLATE 27**Paragenetic Relationships: Chemical Compaction**

A) Photomicrograph – Merrimelia #4 (2589.27m) (Plane polarised x 5). Stylolised organic laminae, illustrating framework etching by associated organic acids [5d].

B) Photomicrograph – Tirrawarra #3 (2988.86m) (Cross Nicols x 20). Chemical compaction of adjacent quartz grains liberating and re-precipitating quartz cement. Note extensive quartz cement development at quartz-quartz contacts [2c], whereas at quartz-labile grain contacts [8f], no quartz cement is developed.

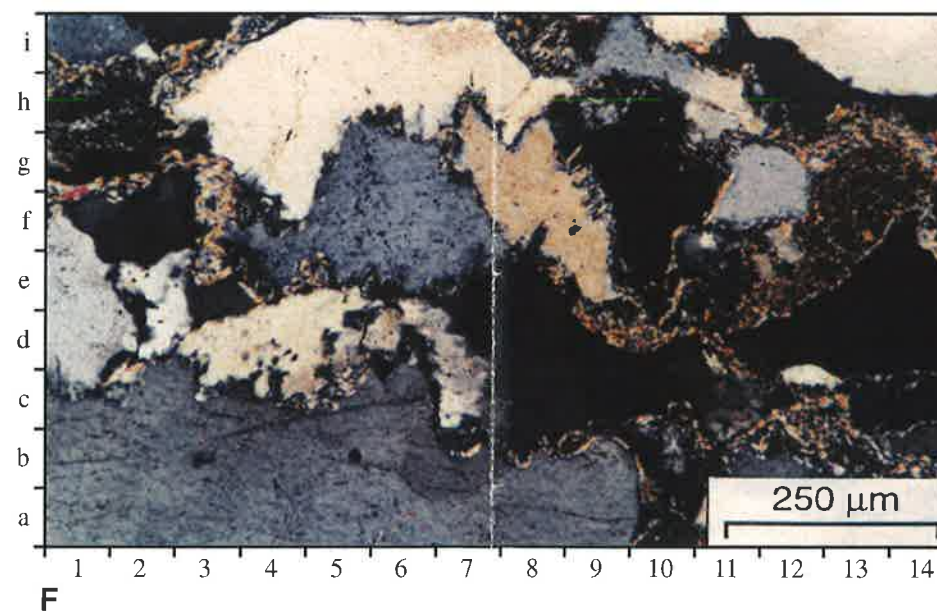
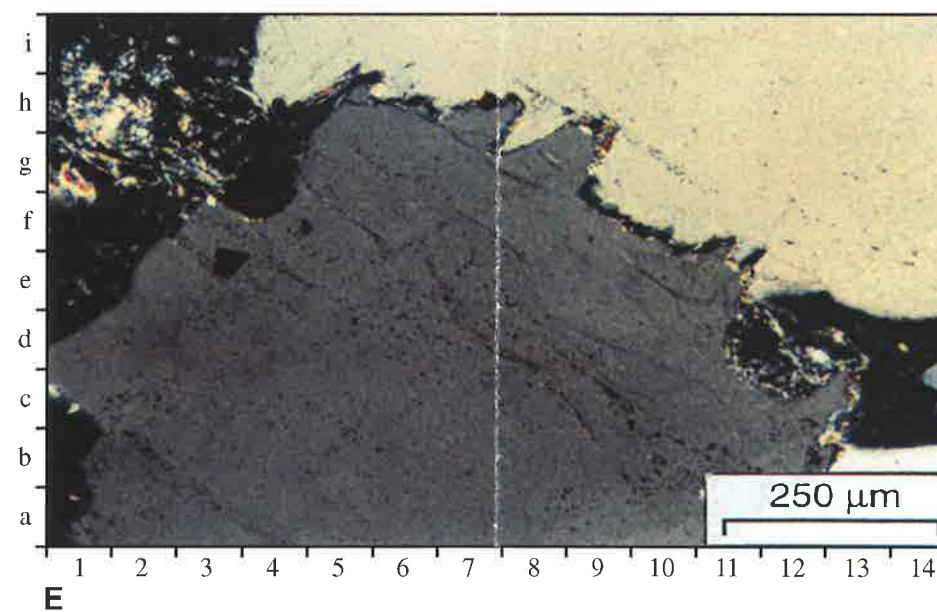
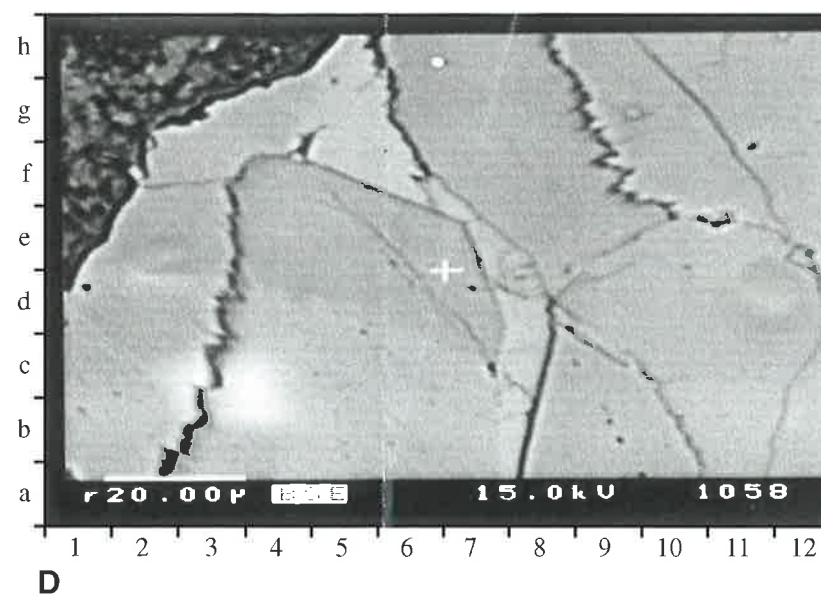
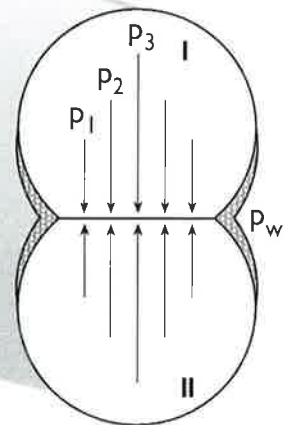
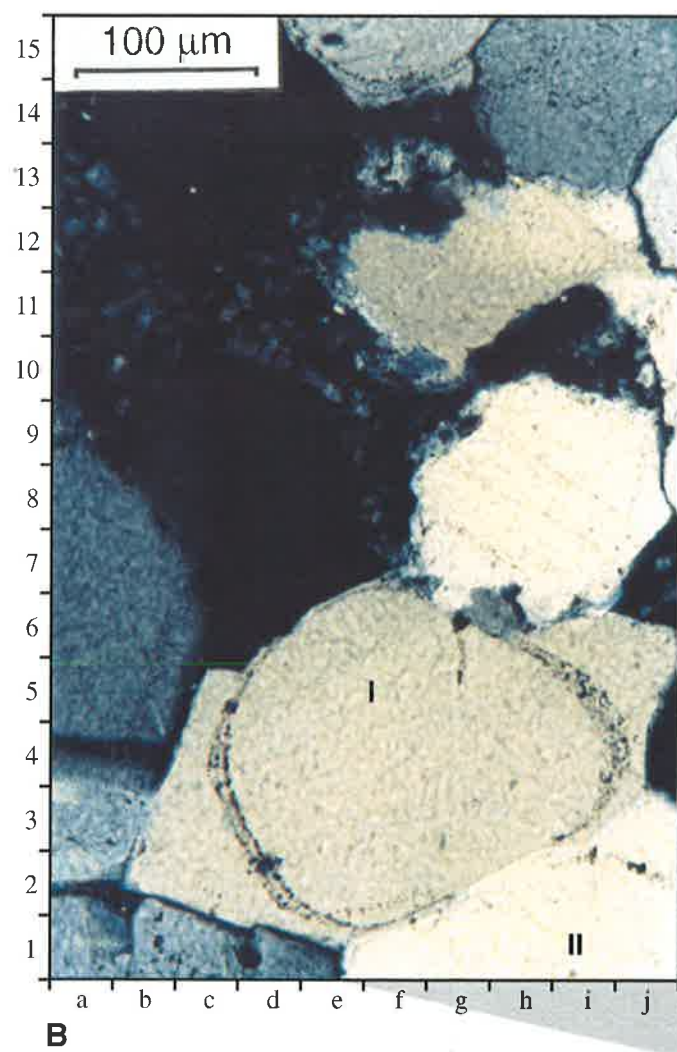
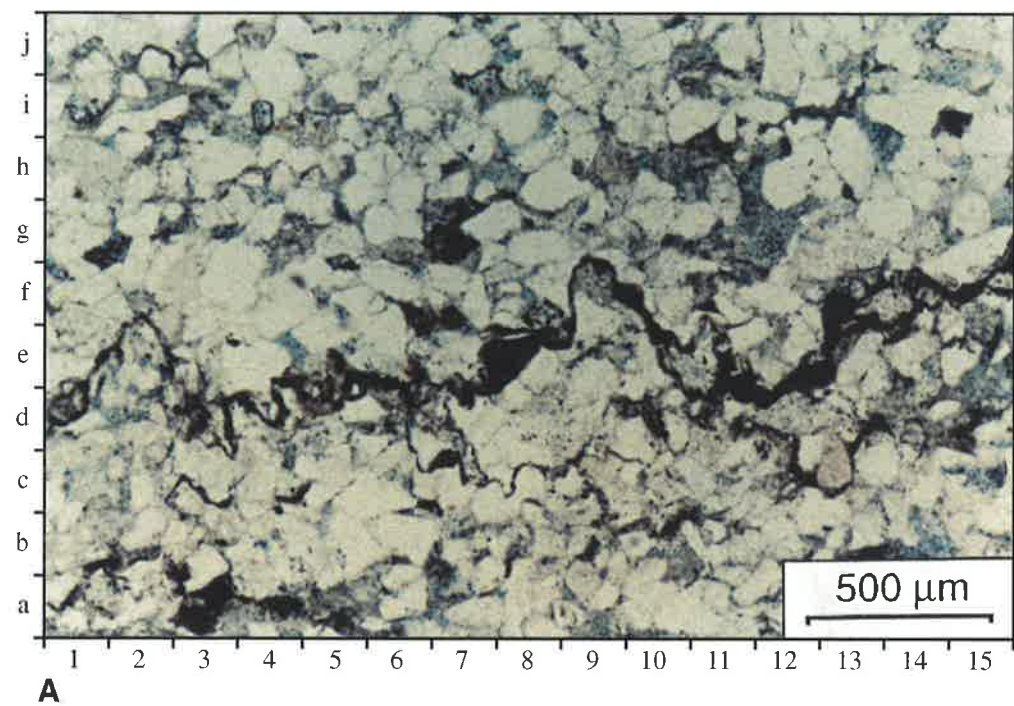
C) Cartoon of the idealised redistribution of quartz cement, by chemical compaction forces (After Hutcheon, 1982).

D) BSE Image – Tinga Tingana #1 (2094.35m). Micro-stylolites and fractures in a quartzose sediment.

E) Photomicrograph – Gidgealpa #7 (2277.94m) (Cross nicols x 10). Illite filled suture boundary between two compressed quartz framework grains. The illite is a remnant “clay rim”, which serves as a catalyst in redistributing quartz cement while at the same time also accentuates the sutured grain contact.

F) Photomicrograph – Kanowana #1 (3092.44m) (Cross nicols x 10). Highly sutured zone, suggestive of intense shearing. Quartz framework grain shapes obliterated by suturing. Illite in sutures acts as a catalyst for the liberation and redistribution of silica.

Plate 27



Walderhaug (1996) explains that quartz cementation rates depend exponentially on temperature and not pressure. Bjørkum *et al.* (1998), in studying the effects of pressure and quartz precipitation, disagreed with the stylolitisation model, concluding that overburden pressure had a minor influence on quartz cement growth in sandstones.

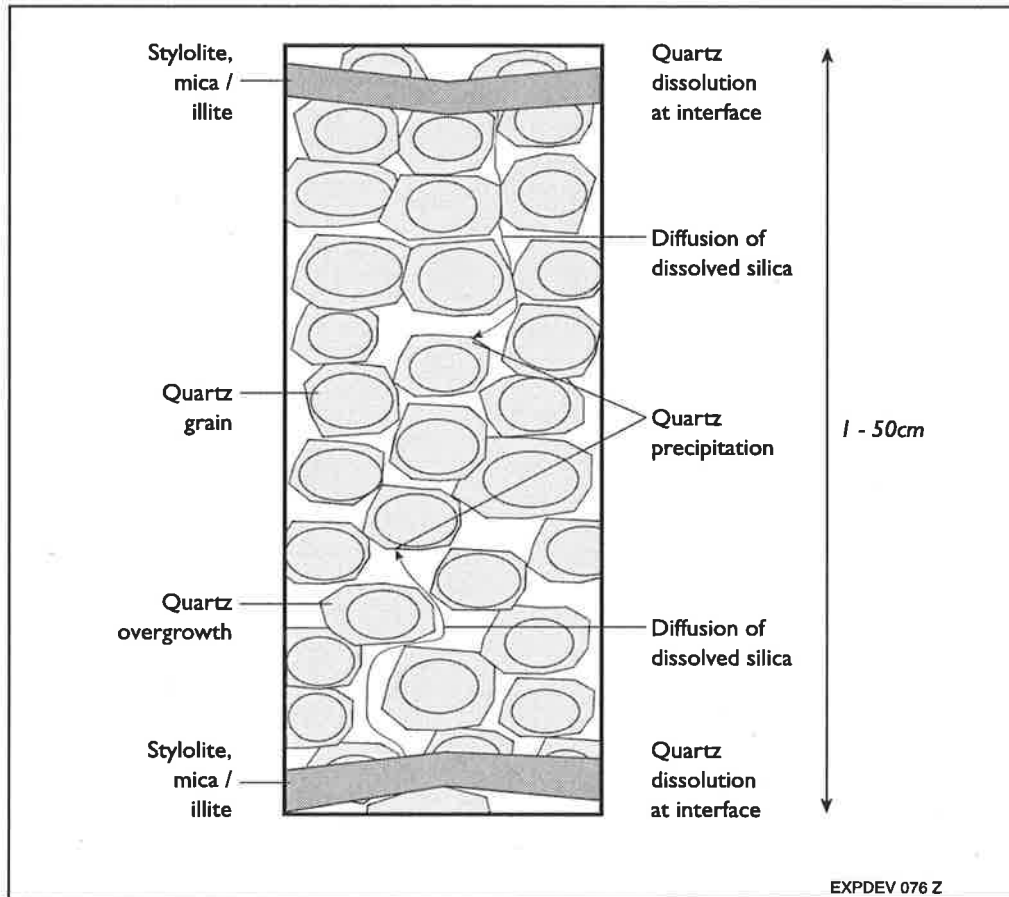


Figure 6.14 Stylolite quartz cementation model, where quartz dissolution occurs at the quartz grain stylolite interface and is precipitated in an inter-stylolite zone. (After Bjørkum *et al.*, 1998).

The bulk of recent opinion, however, favours silica mobilisation via stylolitisation rather than grain contact. Silica redistribution in this process is precipitated as burial increases, into regions between stylolites (Fig. 6.14). This has the effect of increasing the strength of the sandstone, as the effects of mechanical compaction are arrested and chemical compaction begins to dominate (Ehrenberg, 1990 and Bjørkum *et al.*, 1998). Bjørkum and Nadeau (1998) claim that this change over from mechanical compaction to thermally controlled stylolitic processes occurs above 60°C.

iii) Key Findings

In arenaceous Merrimelia sediments quartz cementation appears to be greatest near stylolised laminae (Plate 27a). The reprecipitation of quartz cement at quartz-quartz grain boundaries (Plate 27b) was rarely observed. It is likely then that the dominant chemical compaction mechanism operating in arenaceous Merrimelia sediments is the inter-stylolitisation model as proposed by Walderhaug (1996).

B) Late Quartz Cementation

i) Key Observations

Figure 6.15 indicates that there are two phases of quartz precipitation in Merrimelia sediments; at shallow and deep burial depths.

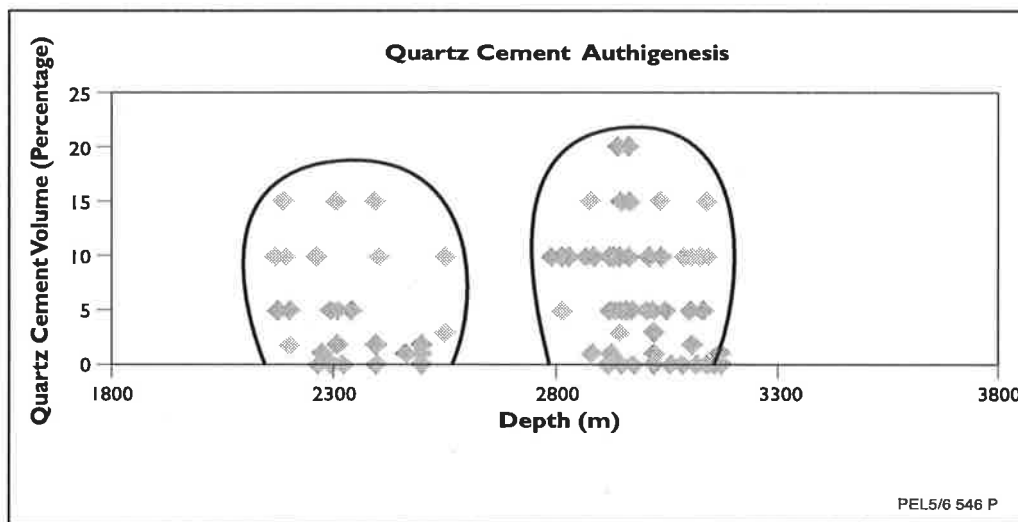


Figure 6.15 Quartz cement volume percentages versus depth (m).

Rezaee (1996) describes three quartz cementation phases (Z1, Z2 & Z3) in the Tirrawarra Sandstone in the Moorari-Tirrawarra, Fly Lake-Brolga region. These three quartz phases were delineated using microprobe analysis coupled with fluid inclusion homogenisation temperatures. The results of these analyses indicated that Z1 quartz cement phase precipitated at temperatures of between 65°C and 80°C, while Z2 precipitation occurred between 80°C-100°C and Z3 quartz cement formation was initiated at temperatures in excess of 130°C (Rezaee 1996).

It is likely that very few Merrimelia sediments have been subject to three consecutive quartz cementation phases as only arenaceous sediments would have been permeable enough to allow quartz precipitation and maintain open pores large enough to receive Z3 quartz cement. Rezaee (1996) concurred saying that Z3 quartz is observed in only a few Tirrawarra samples. Microprobe and CL analysis of quartz cement,

sourced from arenaceous Merrimelia samples basin wide, was unable to discriminate three separate quartz phases.

However, petrographic observations indicated consistently that there are two quartz phases in Merrimelia sediments. These two phases occur early and late, forming syntaxial quartz overgrowths (early) and druse quartz crystals (late). Plate 28a[4f] illustrates the early quartz cement phase (off white) and Plate 28b[10e] the later quartz cement phase (pure white).

ii) Discussion

The formation of early quartz has already been discussed, and is related to feldspar dissolution. SEM and petrographic observations suggest that the formation of late quartz cement is linked to the formation of illite. Plates 28c, 28d, and 28e illustrate the common association of illite and druse quartz.

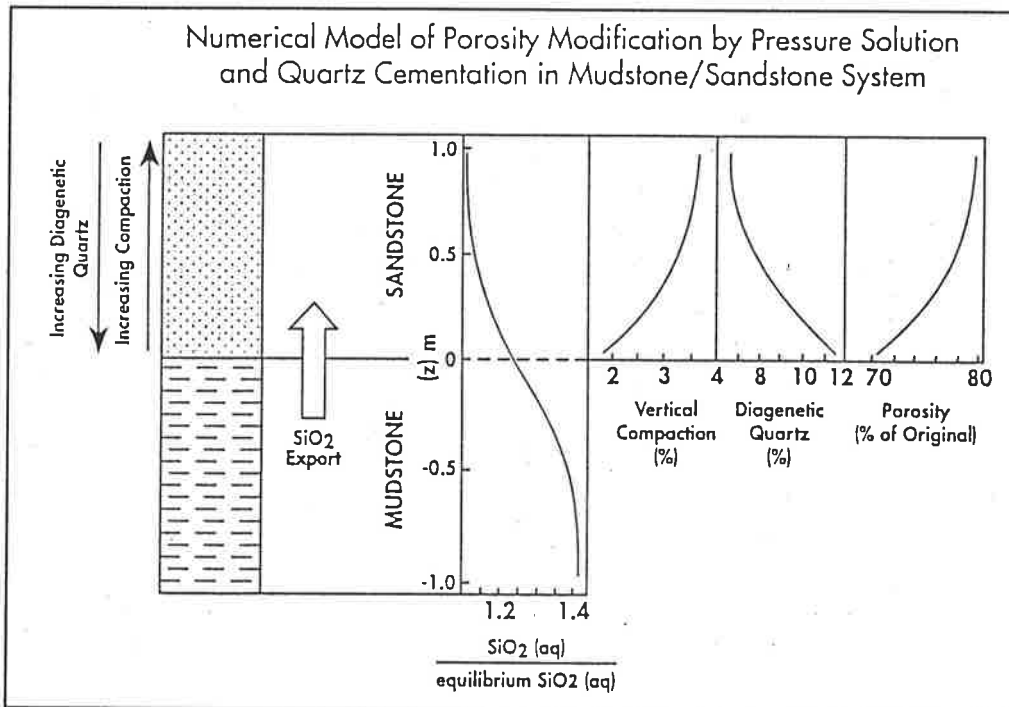


Figure 6.16 Quartz cementation in a arenaceous/argillaceous system (After Wilson and Stanton, 1994).

The association of druse quartz and illite in argillaceous lithologies tends to suggest that, in these sediments at least (Plates 28d), late quartz cement is being sourced from silica associated with the smectite-illite reaction. In contrast, late quartz formation in arenaceous Merrimelia sediments tends to form where concavo-convex and illite lined sutured contacts dominate.

PLATE 28

Authigenic Minerals: Druse Quartz Cement

A) Photomicrograph - Woolkina #1 (3038.80m) (Plane polarised x 20). Broad view illustrating a cluster of druse quartz overgrowths [4e].

B) Photomicrograph - Coonatie #1 (3148.30m) (Plane polarised x 10). Broad view of a pore that exhibits both syntaxial [15d] and druse quartz cement [10e].

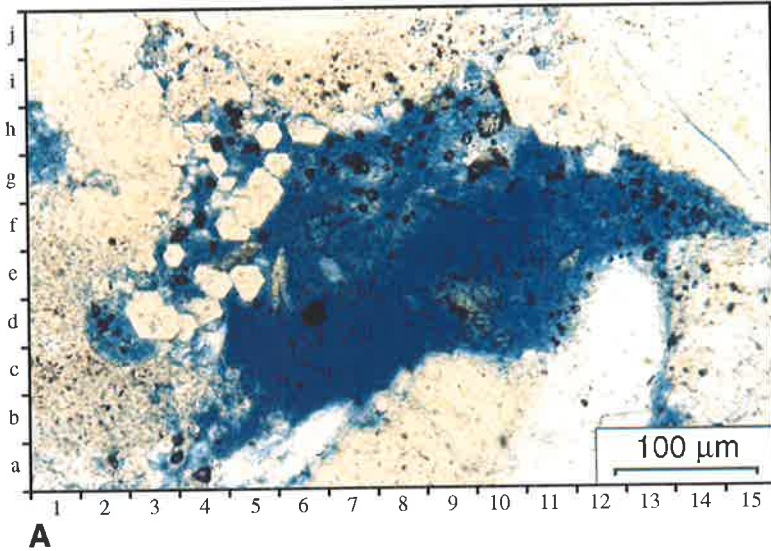
C) Photomicrograph - Woolkina #1 (3038.80m) (Cross nicols x 20). C-axis orientated druse quartz cement coated with thin films of illite [5b].

D) SEM Photomicrograph - Woolkina #1 (3038.80m). Close up of druse quartz forming out of quartz substrate, surrounded by boxwork illite clay.

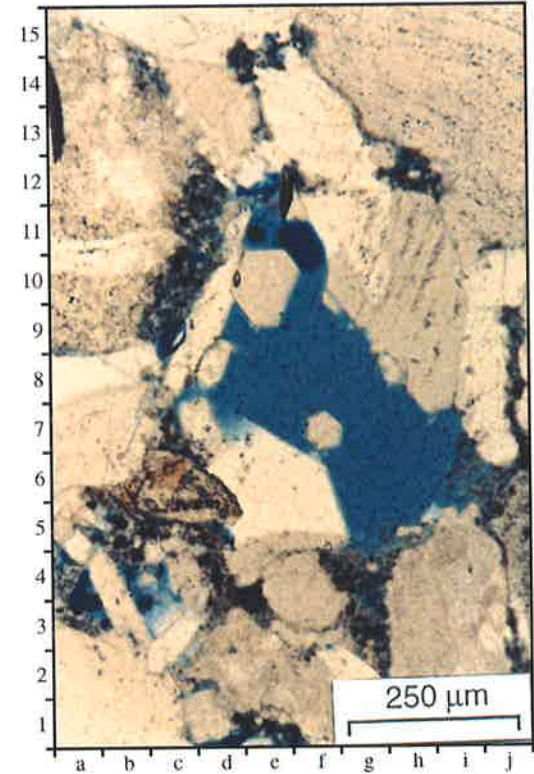
E) SEM photomicrograph - Malgoona #2 (2255.51m). Broad view of druse quartz intergrown with boxwork and filamentous matrix illite.

F) SEM photomicrograph - Tirrawarra #3 (2988.86m). Large cluster of druse quartz suggestive of an open, clay free, high flow pore pathway.

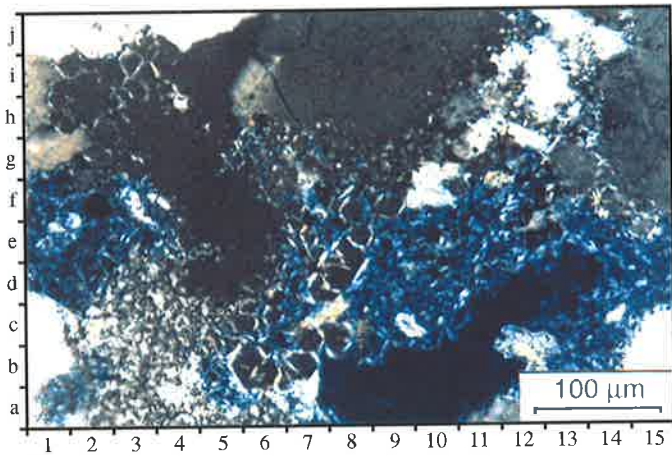
Plate 28



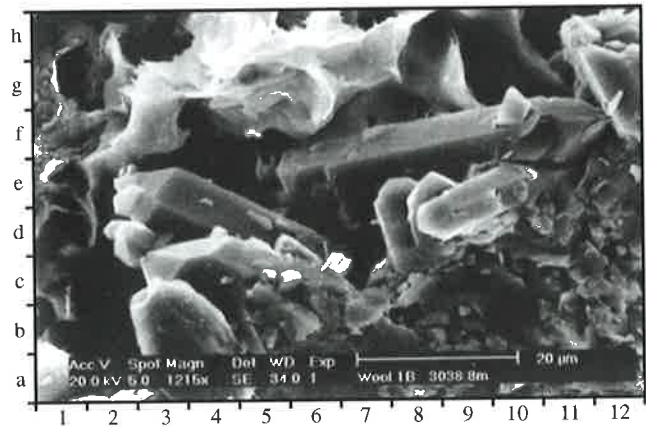
A



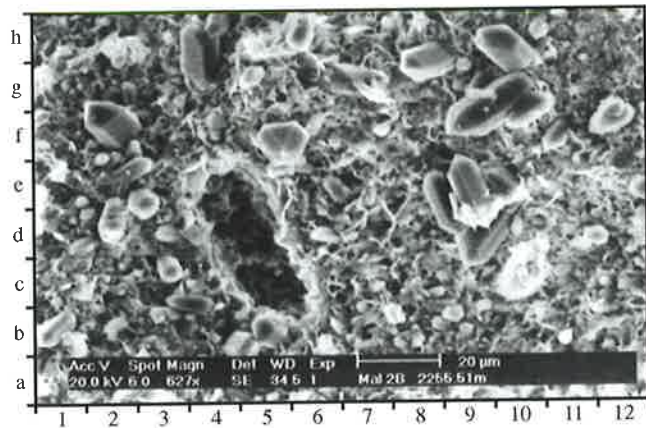
B



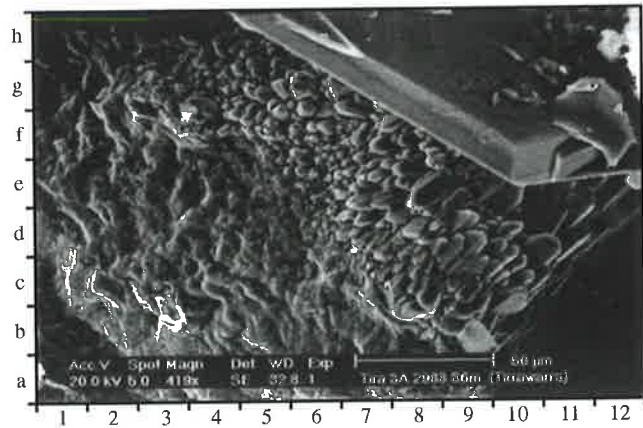
C



D



E



F

This observation suggests that late quartz precipitation in arenaceous Merrimelia sediments proceeds according to the process illustrated in Figure (6.14).

In interfingering arenaceous and argillaceous Merrimelia and Tirrawarra sediments (M1 & T1), it is likely that quartz cementation is related to silica export from compacting shales. Mullis (1992) found a positive link between silica generation in mudstones (smectite-illite transformation) and quartz precipitation in adjacent sandstones where the diffusion of Si and subsequent precipitation is concentrated adjacent to the shale/sandstone interface (Fig. 6.16).

iii) Key Findings

It is probable that silica released from either the illitisation of smectite or by chemical compaction has re-precipitated in the form of quartz cement late in the diagenesis of Merrimelia sediments.

Several sources for early and late quartz cement are likely. The following lists the most volumetrically important source of quartz cement to the least:

- 1) Smectite/Illite transformation (Equation 6) (Early).
- 2) Feldspar Alteration (Early).
- 3) Chemical compaction (Late).
- 4) Dissolution of siliceous rock fragments (Late).

6.3.4.3 Clay Diagenesis

6.3.4.3.1 Illite Authigenesis

A) Key Observations

Plate (29a [5e]) is typical of matrix illite observed throughout the Merrimelia Formation. The more yellowish or higher intensity areas in this image (Plate 29a [4j]) are completely illitised argillaceous rock fragments. It appears that the illitised rock fragments and the matrix illite merge (pseudo-matrix) with the only difference being that the rock fragment areas are entirely dominated by boxwork/filamentous illite (Plate 29b) as opposed to filamentous illite in the matrix (Plate 29d). These observations are noted in lithologies with predominantly argillaceous matrix and in lithologies that have predominantly argillaceous rock fragments. Illite-rich lithologies are therefore, typically rock-fragment-rich, having formed near glaciers (low chemical maturity) and are dominated by a clay sized matrix.

Distal proglacial sediments, such as varvite mudstones, are also almost entirely dominated by clay-sized matrix.

PLATE 29

Authigenic Mineral: Illite

A) *Photomicrograph - Gidgealpa #5 (2298.57m) (Fluoro x 10). Matrix illite [4d] and pseudo-matrix [4k] formed by the destruction of labile grains.*

B) *SEM photomicrograph - Malgoona #2 (2255.51m). Boxwork filamentous illite, surrounding druse quartz cement.*

C) *Photomicrograph - Merrimelia #1 (2946.80m) (Cross nicol x 10). Litharenite rock fragment that exhibits, grain lining illite "clay rims" [4h], illite lining sutured contacts [5c] and the illitisation of unstable rock fragments [4f].*

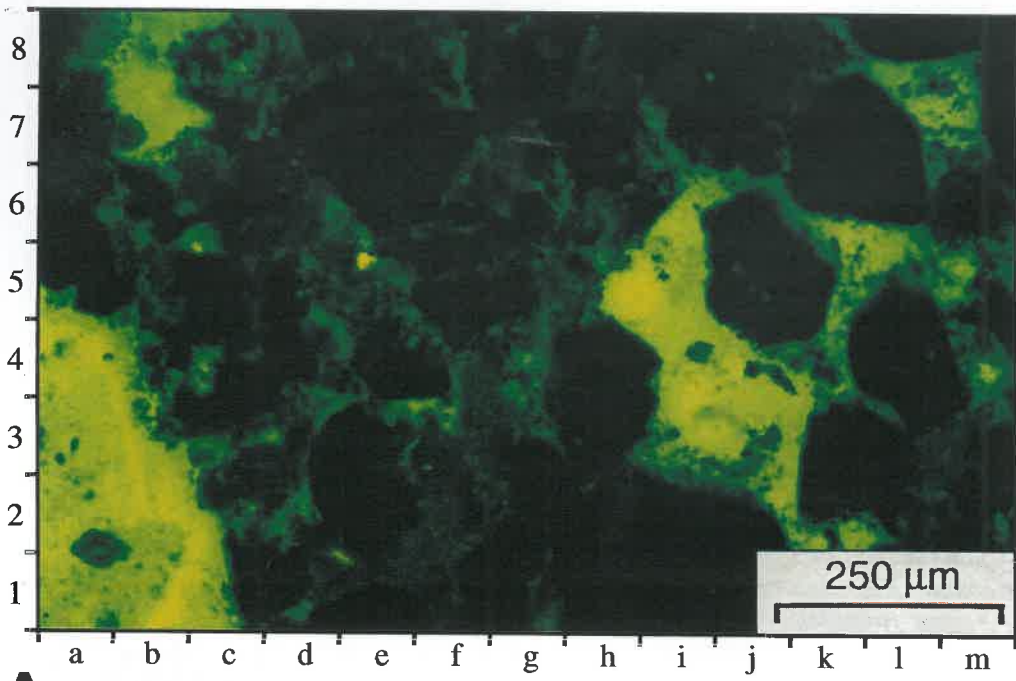
D) *SEM photomicrograph - Malgoona #2 (2255.51m). Close up view of filamentous illite.*

E) *Photomicrograph - Merrimelia #5 (2622.19m) (Cross nicol x 20). Close up view of illite lining framework grains in the economically significant glacio-aeolian sandstones of the Merrimelia Field.*

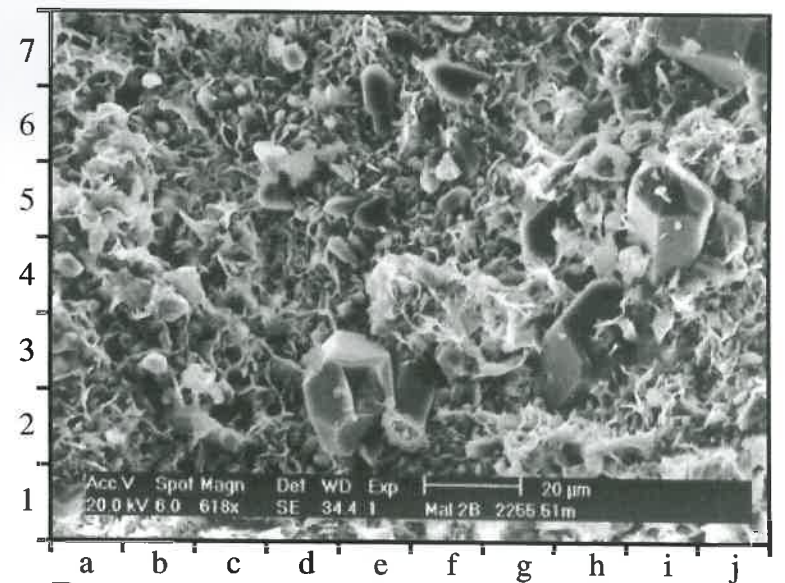
F) *SEM photomicrograph - Merrimelia #1 (2946.80m). Grain contact illustrating the surrounding illite "clay rim" [3c], platy illite coating of framework grains [Inset A] and the illitisation of unstable rock fragments [5c].*

G) *Photomicrograph - Merrimelia #1 (2627.98m) (Fluoro x 20). Close up view illustrating the pervasive nature of grain lining illite in glacio-aeolian sandstones. Note: The intense yellow regions [6i] are labile grains that have been completely illitised and subsequently squeezed into adjoining pore space.*

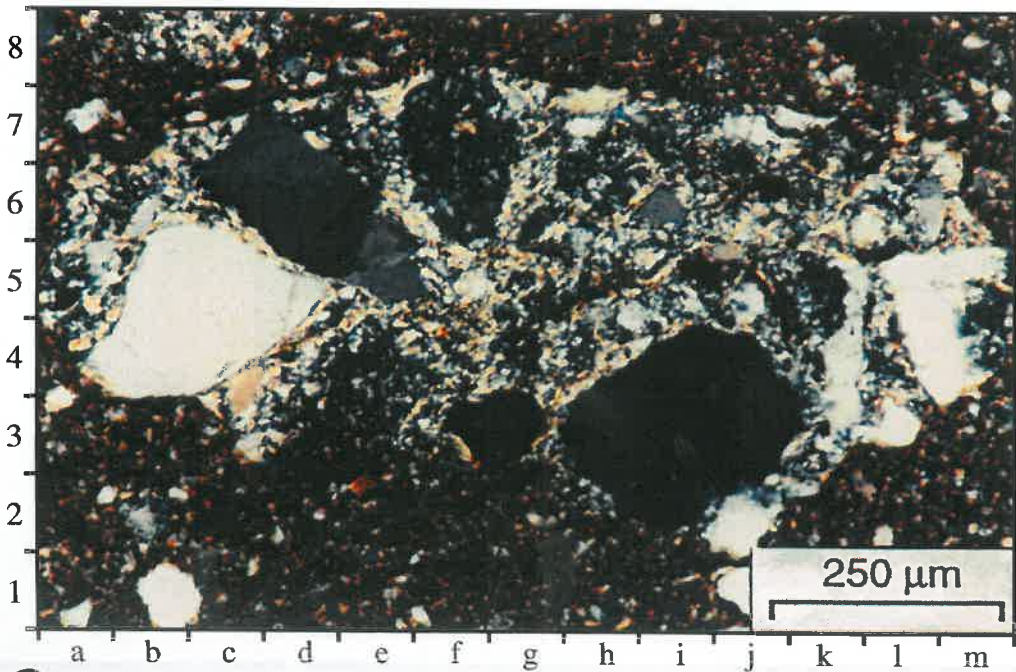
Plate 29



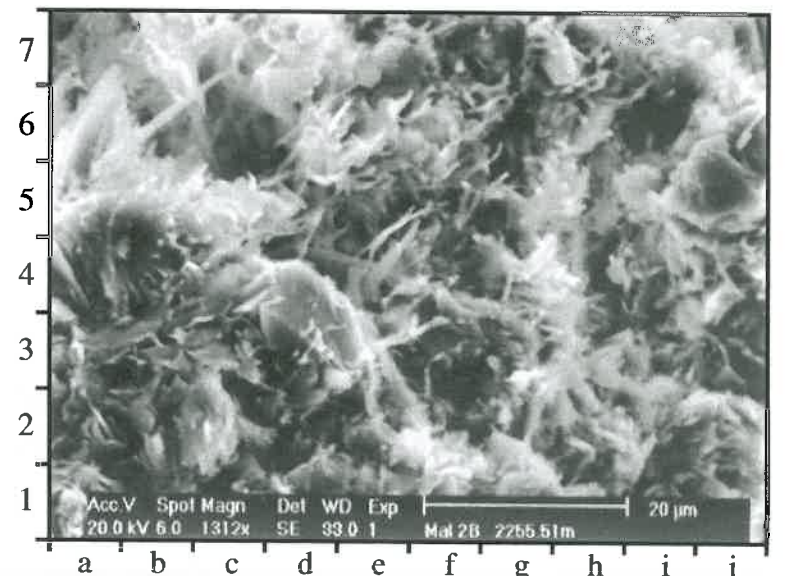
A



B



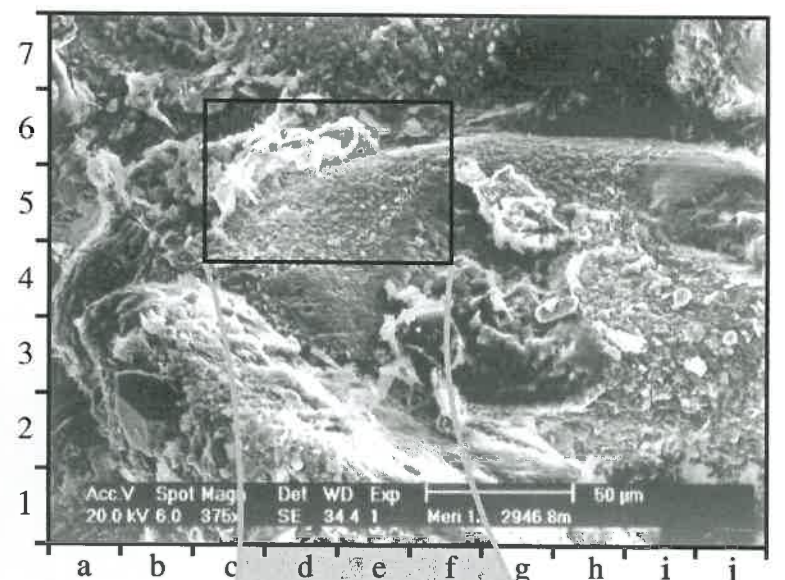
C



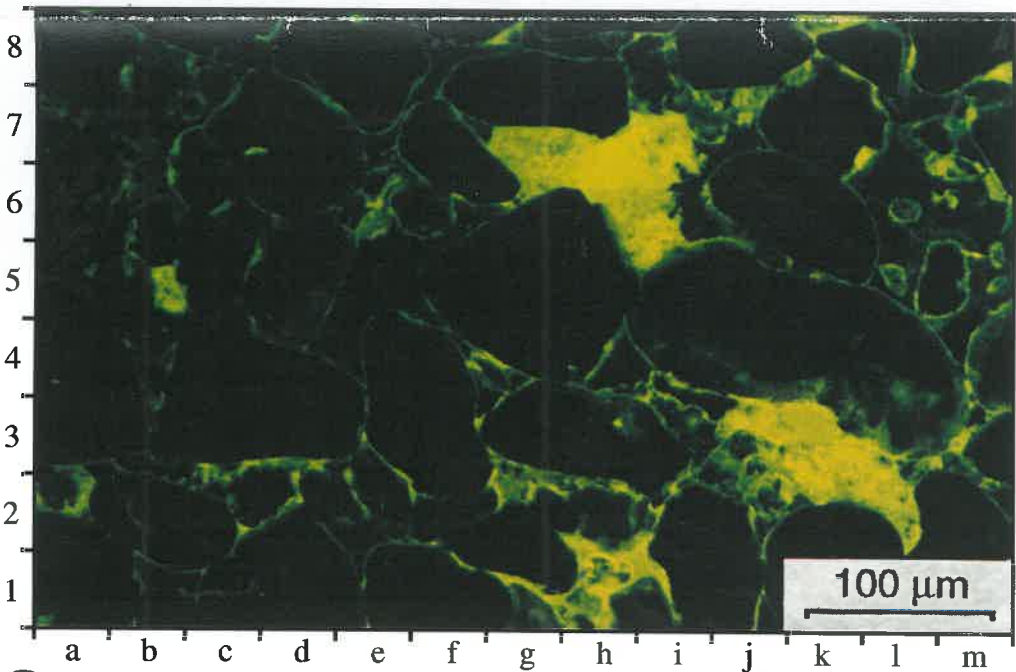
D



E



F



G



Inset A

Conversely distal proglacial sandstones tend to be dominated by filamentous illite porous where illite fibers grow into pores spaces, bridging pore throats (Plate 29d). Petrological observations indicate that illite forms differently in different Merrimelia facies. In general however, the two main mechanisms by which illite forms in Merrimelia sediments are:

- 1) The transformation of detrital smectite to illite.
- 2) The neoformation of illite from circulating pore waters.

The transformation mechanism is the dominant illite formation process and the neoformation of illite subordinate. The transformation mechanism occurs in Merrimelia rocks dominated by argillaceous components (matrix and rock fragments). The neoformation of illite occurs in arenaceous Merrimelia sediments.

Argillaceous Merrimelia facies tend to be illite-rich, while arenaceous facies tend to be illite-poor (kaolin is generally the dominant clay type in arenaceous Merrimelia facies). Figure 6.17 illustrates the facies with the highest illite proportions are fluvial or lacustrine in nature. Lacustrine sediments would be expected to contain high proportions of illite however it seems unusual for fluvially derived sediments to be illite rich. A closer examination reveals that the fluvial sediments are terminoglacial in nature (LB, FL and RD) and contain relatively high proportions of fine grained (argillaceous) matrix. In the better sorted sandstones facies such as dune (DU) and shorezone (LSZ) we see that illite concentrations are less. This clearly shows that there is a relationship between sediment sorting and illite development.

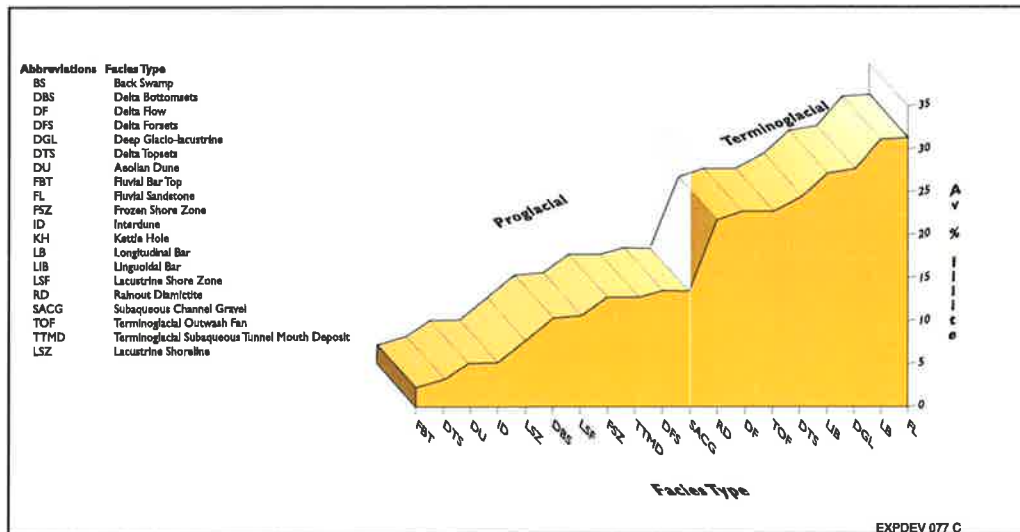


Figure 6.17 Ranked cumulative histogram of illite proportion versus facies type.

Illite growth is accelerated by the presence of fine grained detrital clay and argillaceous rock fragments. The less reworked facies have a greater percentage of matrix and rock fragments and contain more illite. Other factors which help form illite include:

- 1) Rock fragment type,
- 2) Basin temperatures,
- 3) Fluid/rock ratios,
- 4) And access to illite forming reactants.

These processes to a degree overprint the relationship between facies type and illite percentage. For example one would expect to see more illite in terminoglacial tunnel mouth deposits (TTMD) than that is shown in Figure 6.17

The lack of illite in these sediments is likely to be a function of the subaqueous nature of these sediments where contact with clay-rich infiltrating meltwaters was not possible. In contrast longitudinal bar (LB) sediments (another clast dominated facies type) has relatively high illite percentages. These sediments unlike tunnel mouth deposits, were more susceptible to clay development as they were periodically exposed to clay-laden meltwaters.

B) Discussion: Illite Diagenesis, A Review

i) Controls on Illite Formation

Hamilton *et al.* (1992) suggested that the main controls on authigenic illite formation are;

- 1) Temperature,
- 2) Concentration of reactants,
- 3) Rate of supply of reactants,
- 4) Time,
- 5) Presence of an aqueous pore fluid.

In contrast, Chamely (1989) concluded that the major control on illite formation is sediment permeability which determines the fluid/rock ratio and whether illite forms in an open or closed system (or a combination of both). However, Small *et al.* (1992) stated that filamentous illite formation in sandstone reservoirs maybe linked with pore fluids enriched in carboxylates. According to Hower *et al.* (1976), temperature is the most important factor in the illitisation of Gulf Coast sediments. Conversely, Chamely (1989) reviewed numerous published data and concluded that the residence time of a sediment, at a given temperature, is more important for illite formation than

the absolute instantaneous temperature reached. Argostegui *et al.* (1991) agreed stating that apart from temperature, residence time is an important factor in the transformation of smectite to illite. In contrast, experimental observations conducted by Aja *et al.* (1991) disagreed with Hower *et al.*, (1976) showing that illitisation reactions are strongly dependent on both absolute temperature and pore solution chemistry. Aja *et al.* (1991) observed that illitisation of smectite (and kaolin) will not occur at low pH but will convert directly to the illite end member in silica saturated solutions with a pH >8 (Sass *et al.*, 1987).

There is little agreement in the literature as to what are the main controls on illite formation. However, what can be gleaned from the literature is that the controls on illite formation are not consistent between basins, and that differing geological circumstance influences the controls on illite authigenesis. Ahn and Peacor (1986) agree saying that caution must be exercised when using the smectite to illite reaction to determine burial depth or temperature, as a host of factors control these reactions making absolute comparisons between basins unreliable. Argostegui *et al.* (1991) go further suggesting that it is difficult to make comparisons between illite formation mechanisms between different sectors of the same basin. However, consistent illite morphology observations (i.e. boxwork illite forms from rock fragment alteration) in Merrimelia sediments from across the Cooper Basin tend to suggest that illite has formed in different areas of the basin by similar mechanisms.

The factors which are most frequently referred to in the literature as playing an important role in illite diagenesis are:

- 1) Original composition of smectite,
- 2) Chemical activity of the diagenetic medium,
- 3) Temperature,
- 4) Formation water residence time,
- 5) Sediment permeability (Ahn and Peacor, 1986; Inoue *et al.*, 1988, 1989; Srodon and Eberl, 1987).

A review of the literature pertaining to illite diagenesis indicates that illite forms by two processes:

- 1) The transformation of detrital smectite to illite in argillaceous sediments.
- 2) The precipitation of illite from solution in porous sediments.

ii) Smectite to Illite Transformation

Smectite to illite transformation in argillaceous sediments has been the focus of innumerable studies in the past two decades. Interest in this clay transformation, within the petroleum industry, has been intense as the transformation of smectite to illite releases a large volume of water (Equation 6), providing the flux and transportation for other diagenetic phases while also aiding the movement of hydrocarbon phases (Freed and Peacor, 1989). The reaction has also been used as an indicator of burial temperatures.

The two main closed system models that attempt to explain the transformation of smectite to illite, with increasing burial depth, in mixed layer clays are:

- 1) The interlayer model (Ahn and Peacor, 1986; Boles and Frank, 1979; Srodon and Eberl, 1987; Sass *et al.*, 1987; Hower *et al.*, 1976; Bethke & Altaner, 1986; Bethke *et al.*, 1986).
- 2) The interparticle model (Nadeau and Bain, 1986; Nadeau *et al.*, 1984).

a) *The Interlayer Model*

The interlayer model states that smectite layers are transformed to illite layers by cation pathways associated with layer edge dislocations.

Initially, smectite dominates the smectite/illite mixed layer clay assemblage and is composed of sub-parallel layers of variable thickness (Freed & Peacor, 1989). Smectite layers are wavy whereas illite layers are straight in appearance. With increasing depth, the proportion of wavy layers compared to straight layers decreases, i.e., the mixed-layer clay becomes more ordered (Ahn and Peacor, 1986).

b) *Interparticle Model*

The interparticle transformation model, argues that when smectite transforms to illite, the smectite particles dissolve with illite particles precipitating as a result. In this process the illite composition increases with the illite particle size. The interparticle model views the layer arrangements within mixed-layered clays as a random sequence of illite and smectite particles which, when diagenesis proceeds, the smectite particle population becomes unstable and dissolves (Nadeau and Bain, 1986).

c) *Interparticle and Interlayer Model Discussion*

Aronson and Douthitt, (1986) compared both illitisation models. These authors found that as the illitisation of smectite proceeds, Al and K fixing begins in a particular

interlayer. Succeeding insertions of Al and K were more likely within this same interlayer. The conclusions of Aronson and Douthitt, (1986) are contradictory to that of the Nadeau *et al.* (1984 & 1985) interparticle model. The interlayer substitution model of Ahn and Peacor (1986), based on TEM observations shows that smectite and illite packets co-exist at depth supporting the observations of Aronson and Douthitt, (1986).

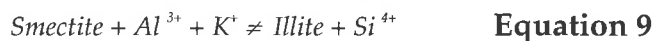
More recently, in a detailed review of illite transformation models in argillaceous sediments Chamley (1989) stated that there is little agreement on formation models. In assessing both models, Chamley (1989) concluded that the TEM-based observations of Ahn and Peacor (1986) should be regarded with more certainty than the XRD based observations of Nadeau *et al.* (1984).

d) Cation Sources for Both Smectite/Illite Transformation Models

The source of illitising reactants that fuel the above illite transformation models are accounted for by two 'closed system' mechanisms.

Mechanism 1

Hower *et al.* (1976) and others have proposed that the smectite to illite transformation can be approximated by the following reaction (Equation 9):



This reaction implies that smectite transforms to illite directly by fixation of K in interlayer sites, resulting in the collapse of smectite layers to form illite layers (Nadeau and Bain, 1986) and accompanying substitution of Al for Si in tetrahedral sites (Ahn and Peacor, 1986). This illitisation process forms in an essentially closed system (Hower *et al.*, 1976), where K and Al are supplied locally by the dissolution of K-feldspar and/or micas. The local dissolution of K-feldspars and micas in a closed system has been examined by Sass *et al.* (1987). These authors conducted experiments which supports Equation 8 as a geologically viable reaction stating that illite and smectite are, in most circumstances, incompatible in the presence of K-feldspar and micas below a critical temperature.

Mechanism 2

A different illite formation mechanism was proposed by Boles and Franks (1979). They surmised that the Al required for formation of illite layers was derived from the smectite itself and not from detrital sources such as K-feldspars. In this model, three

smectite layers transform to form 2 illite layers, destroying some of the original smectite layers. The model proposed by Hower *et al.* (1976) is in conflict with this layer destruction model as all of the basic 2:1 structural units are retained.

iii) The Neoformation Of Illite

The neoformation of illite proceeds in porous and permeable rock which favour the migration of fluids. In this circumstance, illite can form without requiring precursor smectite or as the end product of smectite /illite transformation reactions (Nadeau and Bain, 1986). In this case, illite forms directly by precipitation from pore fluids (neoformation). This 'open system' illite formation model involves illite crystallising from cations that have been transported into sandstones from nearby argillaceous sources.

C) Illite Formation Mechanisms in the Merrimelia Formation

Illite diagenesis in argillaceous and arenaceous Merrimelia sediments proceeds as follows:

- 1) Illitisation of argillaceous depositional matrix.
- 2) Illitisation of grain coating detrital clay.
- 3) Illitisation of rock fragments forming flame boxwork texture.
- 4) Formation of honeycomb box work illite textures (after kaolin).
- 5) Neoformation of illite (filamentous illite protruding from boxwork and clay coating illite).
- 6) Illitisation of kaolin

The following section discusses each illite authigenesis scenario in approximate order of formation.

i) Illite Growth in the Merrimelia Formation

The rate of illite growth throughout the Cooper Basin may not have always been constant. This is particularly true around the Merrimelia Field where up to eight phases of calcite and illite cement fill scattered pores in a "cowpat" like fashion (see section 6.3.4.9.6).

Petrographic and SEM observations suggest that illite formation in argillaceous Merrimelia sediments across the Cooper Basin has followed a path similar to that illustrated in Figure 6.18a. This figure shows that initially illite formation proceeded slowly gaining momentum as temperatures of burial increased. The formation of illite then slowed as the amount of smectite available for illite transformation lessened.

In porous rock Huang *et. al.* (1986) stated that, illite platelets initially grow rapidly in small pore spaces (neof ormation of illite). After initial, exponential illite growth, the rate slows considerably and becomes more constant. This indicates that the majority of illite is formed in the initial stages with the amount of newer illite formation decreasing (until more favourable conditions occur)⁵. In the specific case of the Merrimelia Field, such a spasmodic illite formation regime may have persisted (Fig. 6.18b) responding to localised changes in pore water chemistry (see section 6.3.4.9.6 for details).

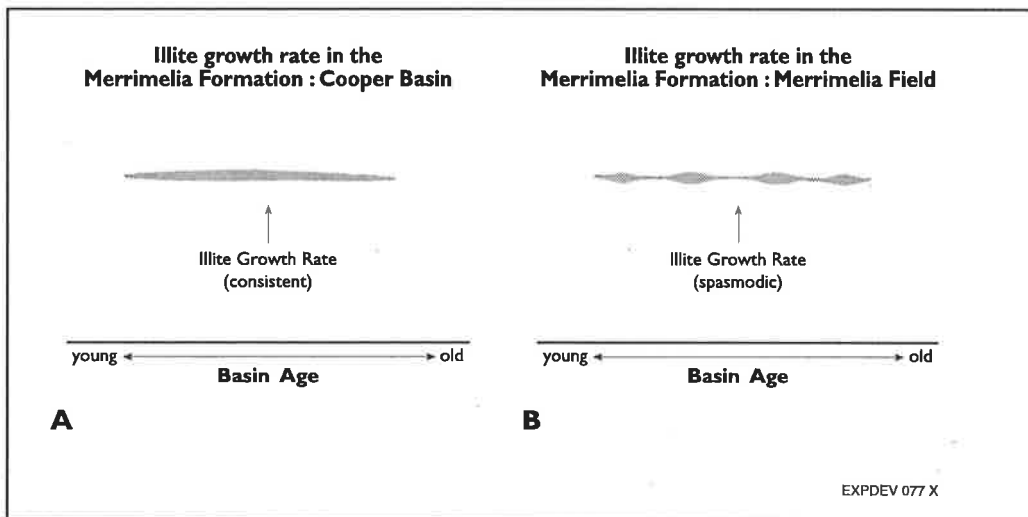


Figure 6.18 Illite growth rates (Modified from Lee *et al.*, 1989).

ii) Smectite-Illite Transformation in Merrimelia Sediments

Compaction of argillaceous lithologies (which form the bulk of Merrimelia sediments) is a complex combination of mechanical compression and water expulsion generated from the transformation of smectite to illite within the argillaceous matrix. This transformation results in a 24% weight loss as 80% of the original smectite layers (within the original mixed illite/smectite clay) is reduced to 20% smectite (Freed and Peacor, 1989). This mass reduction occurs as water loss and is produced by a process that is most likely a multi-stage phenomena which responds to the differing stages of sediment burial (Fig. 6.19). The clay transformation process can produce abnormal fluid pressures by the relocation of water from collapsing clay layers into adjacent pore spaces.

⁵ This has implication for illite age dating in porous Merrimelia sediments, a topic that will be discussed at length in Chapter Eight.

Diagenetic reactions are thus by no means uniform throughout a sediment but reflect the heterogeneity of the sediment. In the case of Merrimelia sediments, this results in a diagenetic mosaic where only the presence of illite is consistent throughout. This observation suggests that illite initially formed in closed conditions (i.e. the impermeable nature of most Merrimelia sediments prevented the precipitation of illite from solution) having been transformed via local reactants from precursor smectite clay. The transformation of detrital smectite to illite in Merrimelia sediments occurs from the earliest burial of sediments throughout the burial history until open diagenetic conditions prevailed curtailing this process but accelerating the production of neoformed illite (Table 6.12).

Detailed XRD examination contends that illite in Merrimelia sediments contains approximately 5% expandable smectite clay. It follows then that the precursor to illite in Merrimelia sediments was detrital smectite. It is also likely that some detrital illite (Warburton Basin) was incorporated into argillaceous Merrimelia sediments. However, SEM observations indicate, that the replacement of detrital smectite by illite is common in the Merrimelia Formation. It is concluded therefore that, in general smectite formed a detrital precursor to illite in argillaceous Merrimelia sediments, with detrital illite subordinate.

The addition of K^+ ions required for the transformation of smectite to illite are, according to Hower *et al.* (1976), supplied by detrital feldspars or micas (see section 6.3.4.3.1Bd - mechanism 1). However, this source of K^+ ions appears unlikely in Merrimelia sediments as detrital feldspars and micas accounted for only 6% of the total detritus at deposition (illite accounts for 25% of the majority of Merrimelia sediments).

This has three ramifications:

- 1) Most of the illite observed in the Merrimelia Formation formed via pore fluids and are not a product of smectite transformation.
- 2) That K^+ -rich brines were necessary for the widespread illitisation of smectite (Macchi *et al.*, 1990).
- 3) The detrital smectites that later formed illite were enriched with K^+ ions (Boles and Franks, 1979; Ahn and Peacor, 1986).
- 4) Illite (as opposed to smectite) was inherited into Merrimelia Formation sediments from the Warburton Basin.

The first two scenarios can be discounted as K^+ rich brines would not be able to penetrate impermeable Merrimelia sediments and therefore not enable the ubiquitous illitisation of argillaceous Merrimelia sediments. The third scenario (K^+ -rich detrital smectite) is a likely source of K^+ ions for illite formation in argillaceous Merrimelia sediments. In addition, the predominance of smectitic clay morphologies (now boxwork illite) also suggests that illite has on a consistent basis pseudomorphed detrital smectite (Plate 29b).

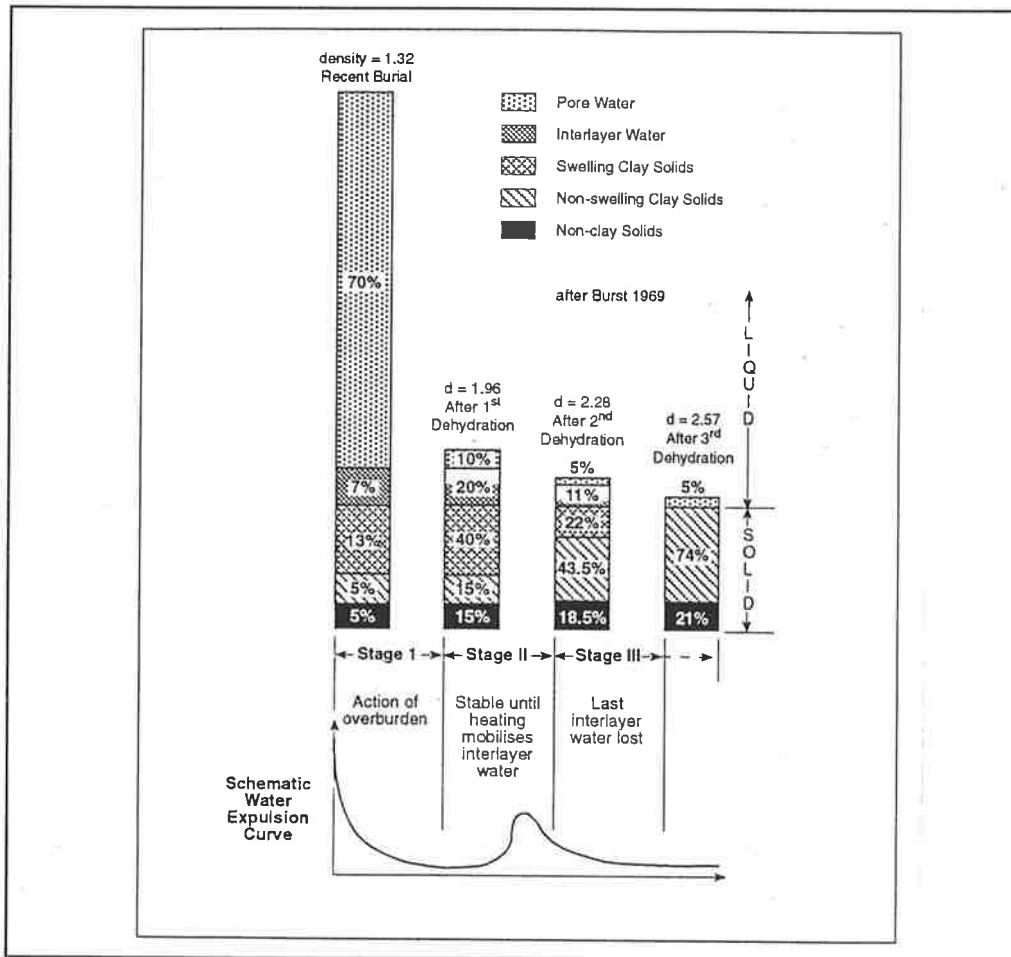


Figure 6.19 Water expulsion volumes arising from the transformation of smectite to illite (After Aggett et al., 1995).

The last scenario may also be a source of K^+ ions for the transformation of smectite to illite in Merrimelia sediments. Prior to the formation of the Cooper Basin, Warburton Basin sediments were subject to illitisation of detrital smectite. Subsequently, Warburton Basin detritus was incorporated into the MTGC sedimentary pile rich in illite and as well as smectite. As mentioned previously however, the abundance of boxwork illite morphologies suggests that the majority of detrital clay incorporated in to Merrimelia sediments was in fact smectitic (it is noted here that boxwork illite may

not be the only indicator of a smectitic precursor). Detrital illite volumes are interpreted to be less than detrital smectite.

Neoformation is the subordinate illite formation mechanism but is the dominant illite formation mechanism in the later stages of diagenesis.

In summary, the pervasive illitisation of fine grained Merrimelia sediments occurs in a closed system. Smectite to illite transformation in Merrimelia sediments has been via the mobilisation of ions at layer dislocations within a K^+ rich smectite precursor.

iii) Sources of Detrital Clay in Merrimelia Sediments

The dominance of the smectite-illite transformation in Merrimelia sediments necessitates large volumes of detrital clay (smectite) being incorporated into the sedimentary pile. Smectite is likely to have been incorporated in to Merrimelia sediments at the surface either as:

- 1) A component of rock fragments, inherited from a previous lithification. (Unstable rock fragments [Chapter Five - Table 5.6] break down quicker and will contain clays developed from surface weathering).
- 2) As fine grained matrix. (Sedimentological evidence suggests that the majority of detrital clay in Merrimelia sediments is matrix, formed either in lacustrine dominated regions or from glacial pulverisation of detritus).

The majority of rock fragments exhibit varying degrees of illitisation dependent on rock fragment lithology. Litharenite and greywacke clasts commonly exhibit grain and suture lining illite and pore-filling fine grained matrix (Plate 29c). These textures suggest that illite in these rock fragments was formed in a previous sedimentary cycle. However these rock fragments, account for only 1% and 2% respectively of the total rock fragment component, so the amount of inherited illite incorporated into Merrimelia sediments is minimal. In dominantly argillaceous rock fragments such as shales, inherited clays form the majority of the rock.

Shale rock fragments are the most numerous (Chapter Five - Table 5.2) contributing a large proportion of the detrital clay component in Merrimelia sediments. In contrast, silicic metamorphic rock fragments rarely have any associated detrital clays (gneiss and schist only) and contribute little to inherited clay volumes. The proportion of detrital clay in the Merrimelia glacial complex therefore varies according to rock fragment type and proportion. These factors in turn are controlled by:

- 1) Sedimentation style (proglacial or terminoglacial),

- 2) Sediment provenance,
- 3) Destruction of rock fragments (competent or incompetent).

Of all rock fragment types, sedimentary rock fragments provide the majority of detrital clay in Merrimelia sediments. However, Dutta (1992) suggests that in a glacial setting, a large amount of clays form from the break-down of volcanic rock fragments. Locally therefore (i.e. Gidgealpa Field) it is probable that volcanic rock fragments may also contribute significantly to detrital clay volumes. This contribution maybe small however, as low chemical activities operate in glacial settings (Velde, 1992) (i.e. Gondwanan Glaciation) subduing the development of surface clays.

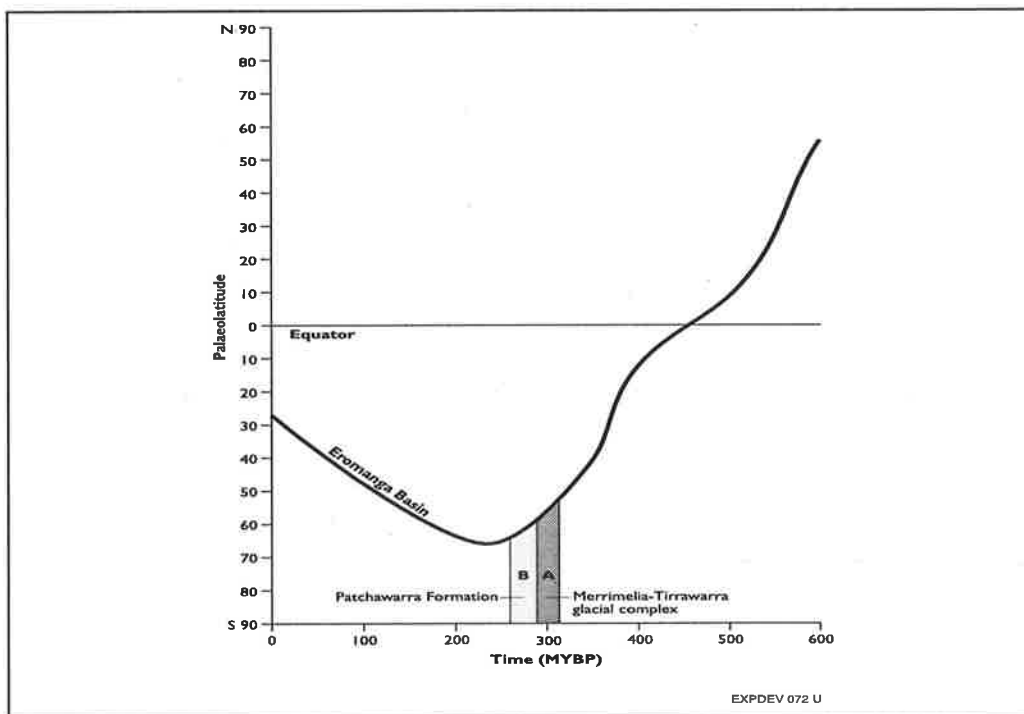


Figure 6.20 Palaeo-latitude positions of the Cooper Basin during Patchawarra Formation, Merrimelia Formation and Tirrawarra Sandstone deposition (After Carne, 1984).

Mechanical weathering in such a setting dominates over chemical weathering. Accordingly the amount of clay development in both Tirrawarra and Merrimelia sediments having been deposited at polar latitudes (Fig. 6.20) would have been minimal compared to sediments deposited in more temperate climates.

It is reasonable then to conclude that detrital clay development in MTGC sediments was minimal and that most detrital clay incorporated into Merrimelia sediments was inherited from a previous lithification (i.e. Warburton Basin lithification).

iv) Formation Of Illite Textures Observed In The Merrimelia Formation

a) Illitisation Of Labile Components

Illite, derived from the alteration of labile grains, is the second most important source of this clay type in Merrimelia sediments (Fig. 6.4d).

Commonly illite forms along cleavage planes and in the internal fractures within chemically unstable rock fragments (Plate 30a). Plate 30b illustrates that illite not only replaces (or partially replaces) unstable detrital grains but also fills quartz embayments (Plate 30b[10b]) within competent quartz framework grains. It is also common to observe illite intergrown with kaolin after the dissolution of feldspars (Plate 30c).

Plate (30e) illustrates a graphic textured granite that has had the intergrown feldspar component totally altered to illite. Plate (30f) is representative of most volcanic rock fragments in that a high proportion of the original glassy groundmass of these rock fragments has been illitised (Plate 30f[4h]) along with feldspar phenocrysts (Plate 30f[11e]) and spherulites. Illitised clasts/feldspar grains account for approximately 9% of the total amount of clay observed in the Merrimelia Formation (Fig. 6.2a).

The illitisation of labile components is primarily a result of the smectite/illite transformation. The dominant illite morphology observed associated with altered labile components are boxwork in nature. Plate (21b) is a typical example of boxwork illite after rock fragment replacement.

b) Grain Coating Clay

Thin grain coating illite (Plate 31b) is a rare feature of proglacial sediments (Figs. 6.2a & 6.4d). Clay coatings are either detrital or have formed at the near surface via the infiltration of clays into newly buried sediments via glacial meltwater. However, in Merrimelia sediments textural evidence is somewhat ambiguous suggesting that the emplacement of grain coating illite may occur by both detrital and authigenic processes.

An examination of grain contact zones in this sandstone (Plate 29g) suggests that the clay rims observed in glacio-aeolian sandstones are not entirely a depositional feature, but may have also formed during burial diagenesis. Plate 29g[5i] illustrates a grain contact area that has no grain-coating illite which suggests that the clay coating around these two framework grains formed after deposition as clay had not encompassed the quartz grains prior to burial.

PLATE 30

Authigenic Minerals: Illitisation of Rock Fragments

A) Photomicrograph – Merrimelia #1 (2946.93m) (Fluoro x 20). Feldspar grain exhibiting illitisation along cleavage planes.

B) Photomicrograph – Merrimelia #1 (2946.93m) (Reflected Light x 20). Same scene as above detailing the illite filled grain fractures in reflected light.

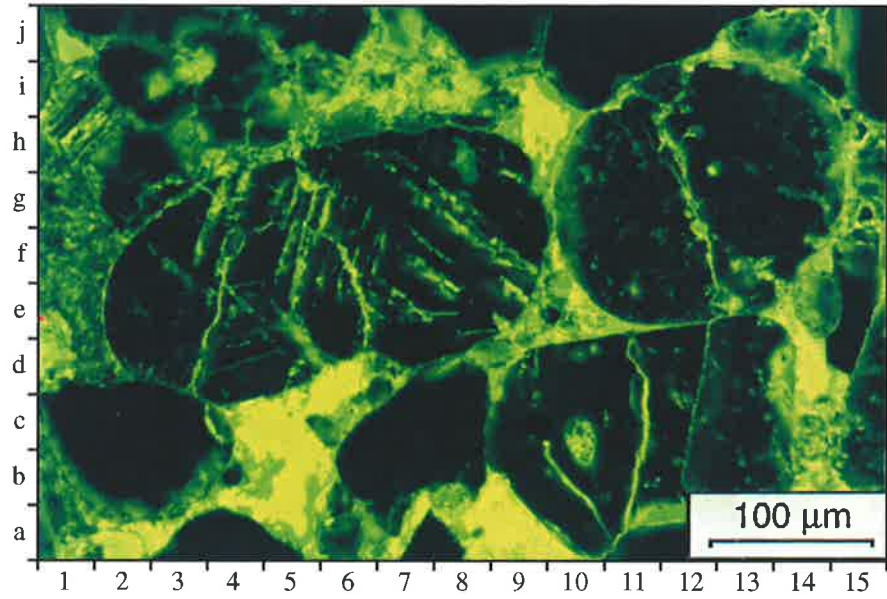
C) Photomicrograph – Durham Downs #1 (2186.63m) (Fluoro x 20). Close up view of two completely altered feldspar grains. The dark regions [6e] are kaolin booklets, the yellow/green regions represent illite.

D) Photomicrograph – Gidgealpa #1 (2759.40m) (Fluoro x 10). Completely illitised rock fragments [11c] which have been almost coalesced with the surrounding illite matrix [10e].

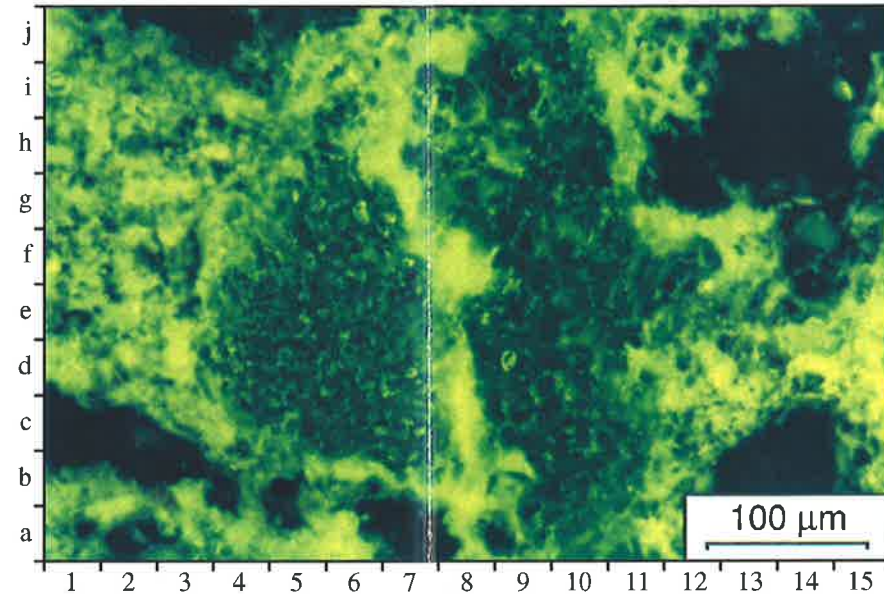
E) Photomicrograph – Tirrawarra #8 (2941.37m) (Fluoro x 10). Close up of a graphic textured granite rock fragment illustrating the presence of illite (after feldspar) in between quartz growths.

F) Photomicrograph – Tinga Tingana #1 (2094.39m) (Fluoro x 10). Close up view of a rhyodacite, illustrating the partial illitisation of the groundmass [3h] and feldspar phenocrysts [11e].

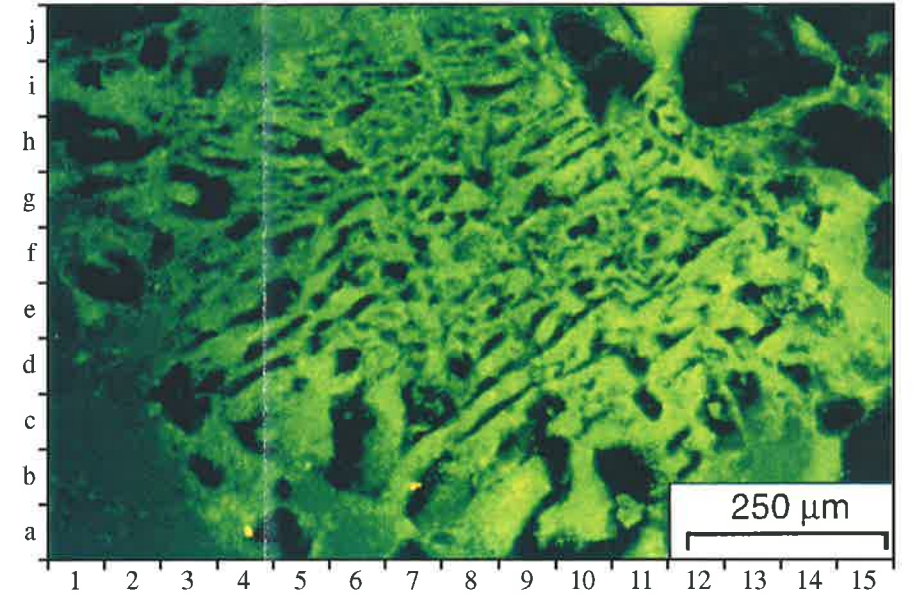
Plate 30



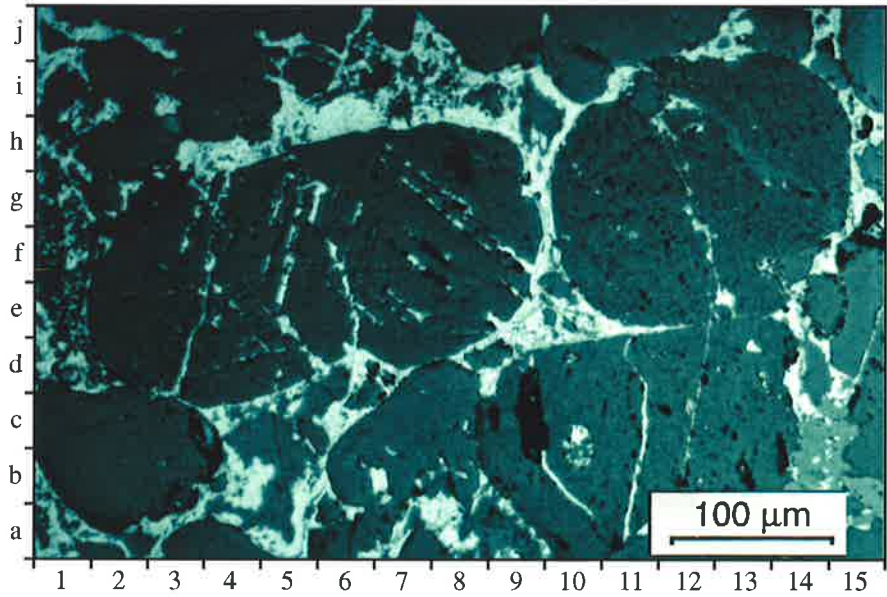
A



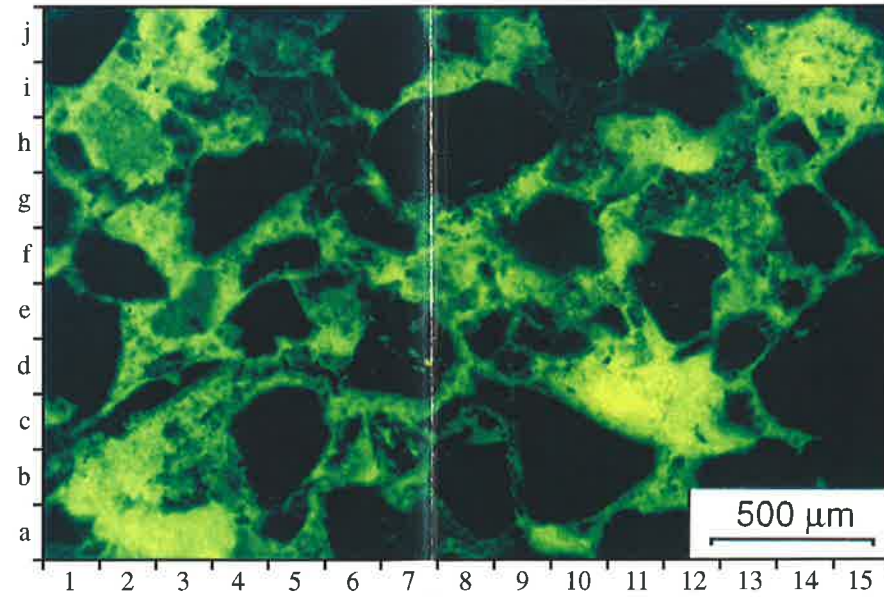
C



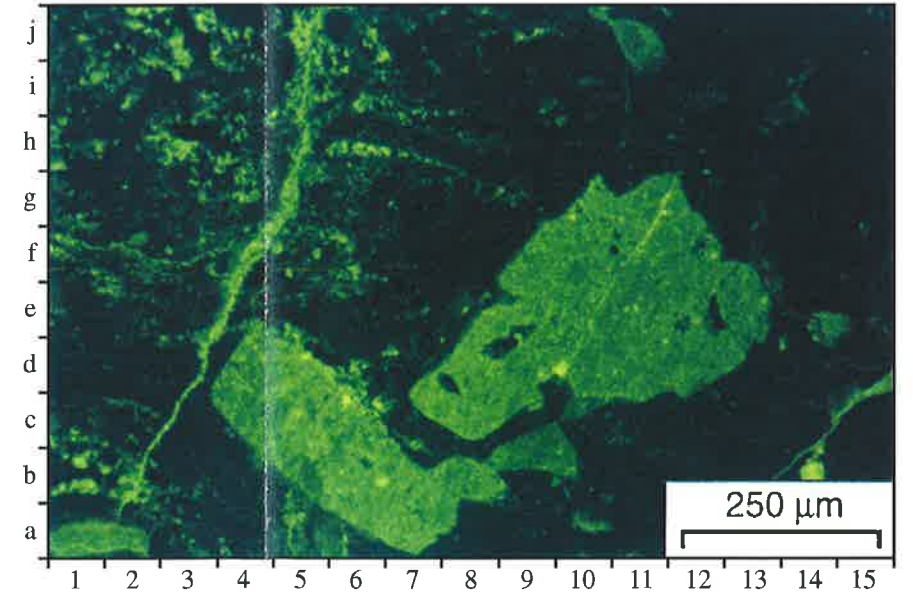
E



B



D



F

If the quartz grains were coated by clay prior to burial illite would be expected between the contacting quartz grains. Wilson (1992) agreed stating that inherited grain-rimming clays enclose framework grains, leaving no clay free regions even when in contact with other framework grains (Fig. 6.21). It would appear then that many of the illite-coated framework grains have been subject to authigenic emplacement (Plate 29g[7e]).

In contrast, Plate (29g[7i]) indicates that a high proportion of grain contacts are lined by illite, suggesting that clay in these contacts was incorporated prior to burial.

Wilson and Pittman, (1977) explain that detrital sand grains during compaction may rotate (especially rounded aeolian grains) which causes pore lining clays formed during earlier stages of diagenesis to be shifted to points of grain to grain contact. This process is also likely to have occurred within glacio-aeolian sandstones at the Merrimelia Field.

It is clear that evidence for both detrital and diagenetic formation of grain-coating clay can be observed in these sediments. Some clay may be deposited by infiltration through porous sands. In this case clay will form on all surfaces but will be absent from grain contact zones. Alternatively illite may form from solution during burial.

Thus, as the glacio-aeolian sandstones are buried and the sand grains settle a mosaic of clay-filled and clay-free contact zones is observed throughout the sandstone (Plate 29g).

Although different in emplacement, both detrital and authigenic clay rims share the same illite texture (flame boxwork) (Plate 31a[7c]). This morphology gives an indication of the original grain coating type.

As mentioned previously, the "flame boxwork" illite texture (illustrated in Plate 31a), is characteristic of smectite clay (Keller *et al.*, 1986). During burial, these smectitic grain coats were almost entirely transformed to illite, however the original smectitic textures of the grain coating clay was retained (illite pseudomorphed smectite) (Plate 31a).

In thin section, (Plate 31b), grain coating illite (Plate 31a[7i]) occurs commonly in quartz-quartz contacts (Plate 31a[8h]).

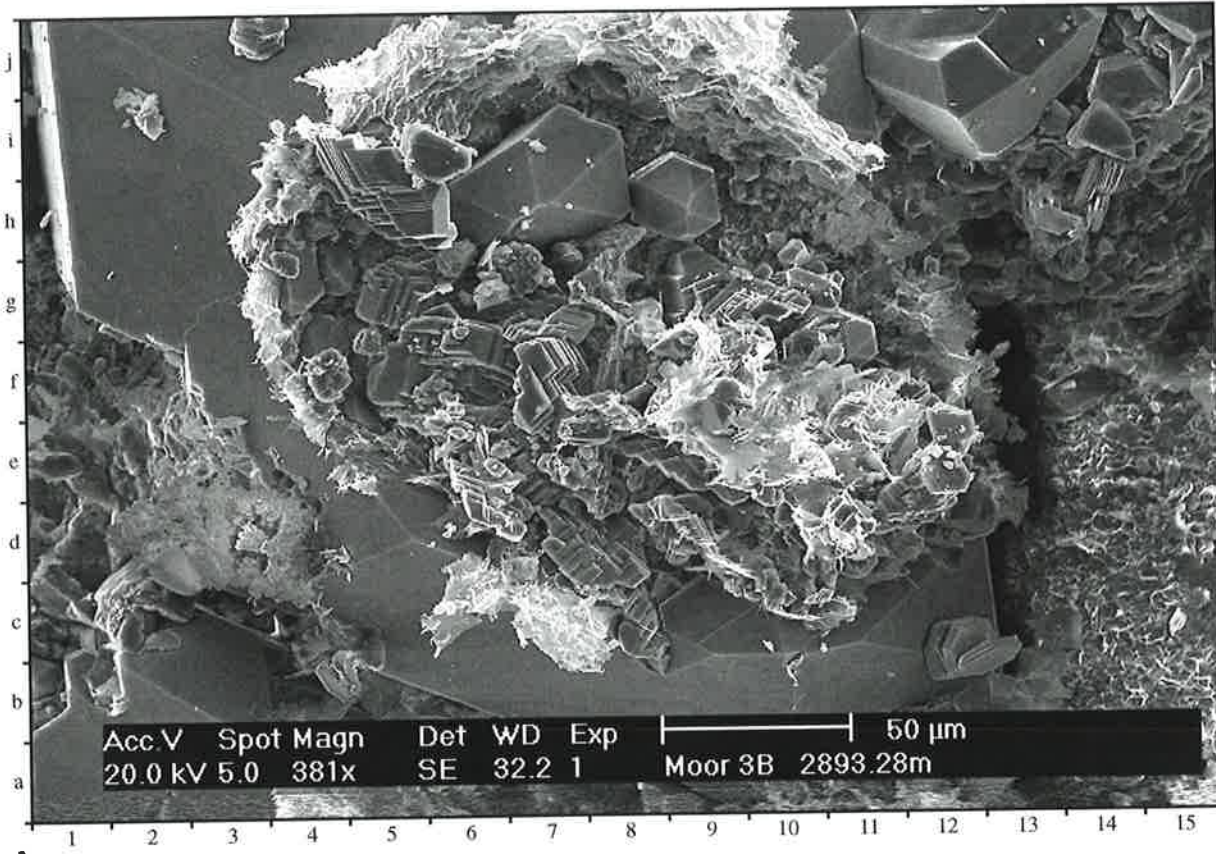
PLATE 31

Authigenic Minerals: Relationship Between Illite Clay Rims and Syntaxial Quartz Cement

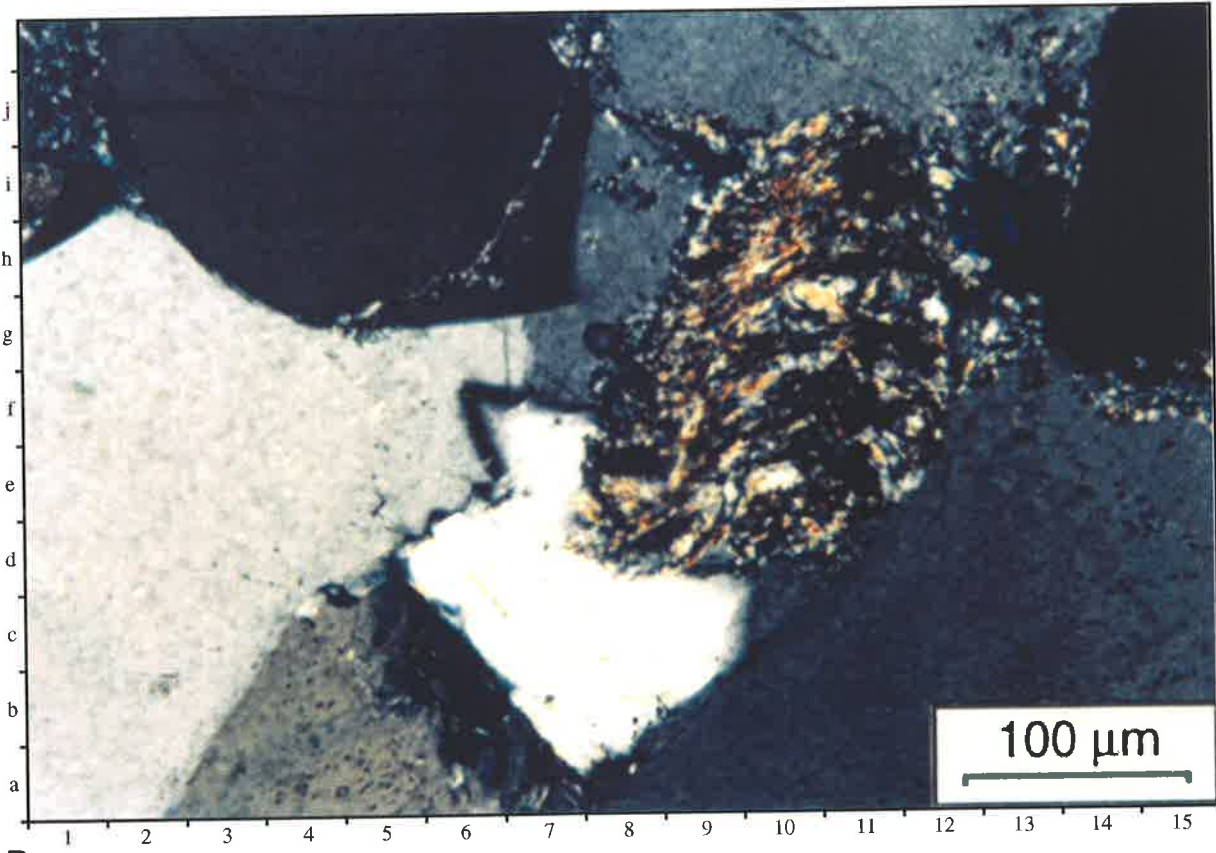
A) SEM photomicrograph – Moorari #3 (2893.28m). Syntaxial quartz cement surrounding quartz grain. The quartz grain has been removed revealing an illite clay rim [3h] of boxwork illite morphology and a pore space that is filled with siderite [8c], druse quartz [7h], boxwork [11e] and filamentous illite [11e]. Note the cogenetic formation of kaolin booklets and quartz cement [12b].

B) Photomicrograph – Yanpurra #1 (2177.59m) (Cross nicols x 5). Close up view of illite clay rims marking the detrital edge of framework quartz grains [6g]. Quartz cement surrounds a small shale rock fragment in the middle of the field of view.

Plate 3 I



A



B

As mentioned previously, the “flame boxwork” illite texture (illustrated in Plate 31a), is characteristic of smectite clay (Keller *et al.*, 1986). During burial, these smectitic grain coats were almost entirely transformed to illite, however the original smectitic textures of the grain coating clay was retained (illite pseudomorphed smectite) (Plate 31a).

In thin section, (Plate 31b), grain coating illite (Plate 31a[7i]) occurs commonly in quartz-quartz contacts (Plate 31a[8h]). In these instances, quartz overgrowths prevent pore fluid contact with grain coating clay, preventing the neoformation of illite as a grain coating clay (Plate 31a). This indicates that illite observed around framework grains, where syntaxial quartz overgrowths engulf the illite rim (Plate 31a), have formed without the contact of pore fluids in a closed system via the transformation of smectite to illite.

Clay morphology and cement stratigraphy both indicate that grain coating illite in Merrimelia sediments formed via the transformation of smectite to illite.

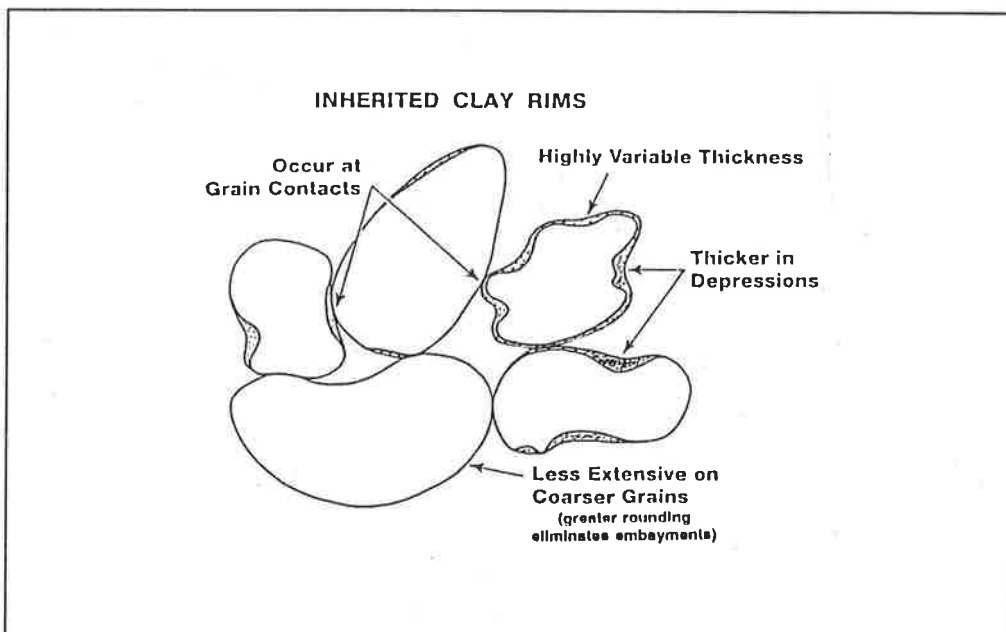


Figure 6.21 Identification of inherited clay rims (After Wilson, 1992).

c) Formation of Illite Coatings in Glacio-Aeolian Sandstones

Grain coating illite (Plate 29g & Fig 6.20[8c]) is common in the economically significant glacio-aeolian sandstones of the Merrimelia Field. These clay rims have great effect on the reservoir quality of these sediments and as such the authigenesis is described here in detail.

dominate. The silt and clay is entrained by the wind and deposited where wind intensity diminishes (Tucker, 1991). Thus, for clay rims to form around framework grains, depositional conditions have to be low in energy. Seemann (1982), suggested that air born dust was introduced into the Rotliegend aeolian sandstone (Southern Permian Basin, North Sea) shortly after or during the initial deposition of the sandstone accounting for the thin clay films observed. These conditions are likely to have existed during the deposition of Merrimelia glacio-aeolian sandstones.

During burial diagenesis, the local development of clay rims may have acted as crystallisation sites for new clay minerals or the transformation of existing ones (Seemann, 1982). In the Merrimelia glacio-aeolian realm, however, other depositional processes may have contributed to the formation of grain-coating clay. Dissipation structures, for example, as described by Fryberger (1993), closely resemble the wavy laminations found in Merrimelia glacio-aeolian sandstones (Chaney, 1998). These features form from the infiltration of meltwater from snow and ice into the aeolian sediments, locally concentrating clay and thus coating aeolian framework grains. This implies that these sediments have undergone a small degree of fluvial reworking, which is likely as the sediments that exhibit dissipation structures are interdunal in nature. It seems probable then that interdunal or dune sediments that have been fluvially reworked (as opposed to aerially reworked) will have detrital clay rims surrounding framework grains.

Walker and Crone (1974) concluded that desert alluvium which is essentially clay-free when deposited becomes clay-rich due to the mechanical infiltration from ephemeral stream flows. Dutton, (1993) agreed, stating that tangentially orientated illite flakes (such as those observed in glacio-aeolian sandstones – Plate 21c) are authigenic, having entered the sandstones by mechanical infiltration and were subsequently recrystallised during burial diagenesis.

Compositional and textural observations (see above discussion on grain contacts) suggest that both infiltration (authigenic) and saltation (detrital) process have emplaced clay rims in glacio-aeolian sediments where the clay rims have then been illitised during later burial, forming nucleation sites for sparse neoformed filamentous illite growth.

Dune sediments, like interdune and fluvially reworked aeolian sediments, show thin illite rims. The formation of illite rims in dune sandstones differ from the “wetter”, muddier interdune and fluvially reworked dune sediments. The constant collisions of

quartz grains as a result of traction and saltation processes produces micro-pitting (Plate 22d[7f]), grain frosting and rock flour (clay and crushed quartz). The regions of micro-pitting provide the most favourable nucleation sites for illite growth (Small *et al.*, 1992). This fact, coupled with a local supply of cations (alteration of feldspars and rock flour), have provided favourable conditions for the areally extensive and pervasive growth of grain-coating illite in glacio-aeolian dune sandstones.

d) Formation of Flame /Filamentous Illite Textures

The formation of flame/filamentous illite textures appears to form by the progressive illitisation and pseudomorphing of the original smectitic/illite clay structures. The resulting illite clay retains the distinctive smectitic boxwork morphology (Ahn and Peacor, 1986) (Fig. 6.22a). The smectitic textured illite clay structure then becomes the nucleation site for subsequent filamentous illite growth (Fig. 6.22b) in doing so forms a host of textures, depending on the original smectite clay and its host grain morphology.

e) Formation of Honeycomb/Filamentous Textures

Honeycomb/filamentous illite textures were rarely observed. It is likely that this illite texture formed as local reactants were liberated from the destruction of kaolin and associated unstable feldspar grains (Bjørlykke, 1983), where the resulting illite exhibits a distinctive honeycomb texture (Plate 22c). This illite formation mechanism accounts for firstly the dissolution of feldspar and kaolin and secondly the preservation of illite. Similar honeycomb textures and modes of formation have been described in the Rotliegend aeolian sandstones of the southern Permian Basin (North Sea) by Rossel (1982).

Like the flame boxwork illite texture, the honeycomb illite substrate acts as nucleation sites for later filamentous illite growth. It can be seen in plate 22c [Inset] that regions of filamentous illite not only emanate from the scalloped edges of the honeycomb substrate but also form regions of purely fibrous growth (Plate 22c[Inset]). These spatial relationships suggest that both honeycomb and flame boxwork illite morphologies predates the extensive filamentous illite morphology.

v) Neoformation of Illite in Merrimelia Sediments

Neoformed illite is pervasive throughout porous sandstone lithologies in the Merrimelia Formation. Throughout the South Australian and Queensland sectors of the Cooper Basin, filamentous illite morphologies dominate (Plate 21a).

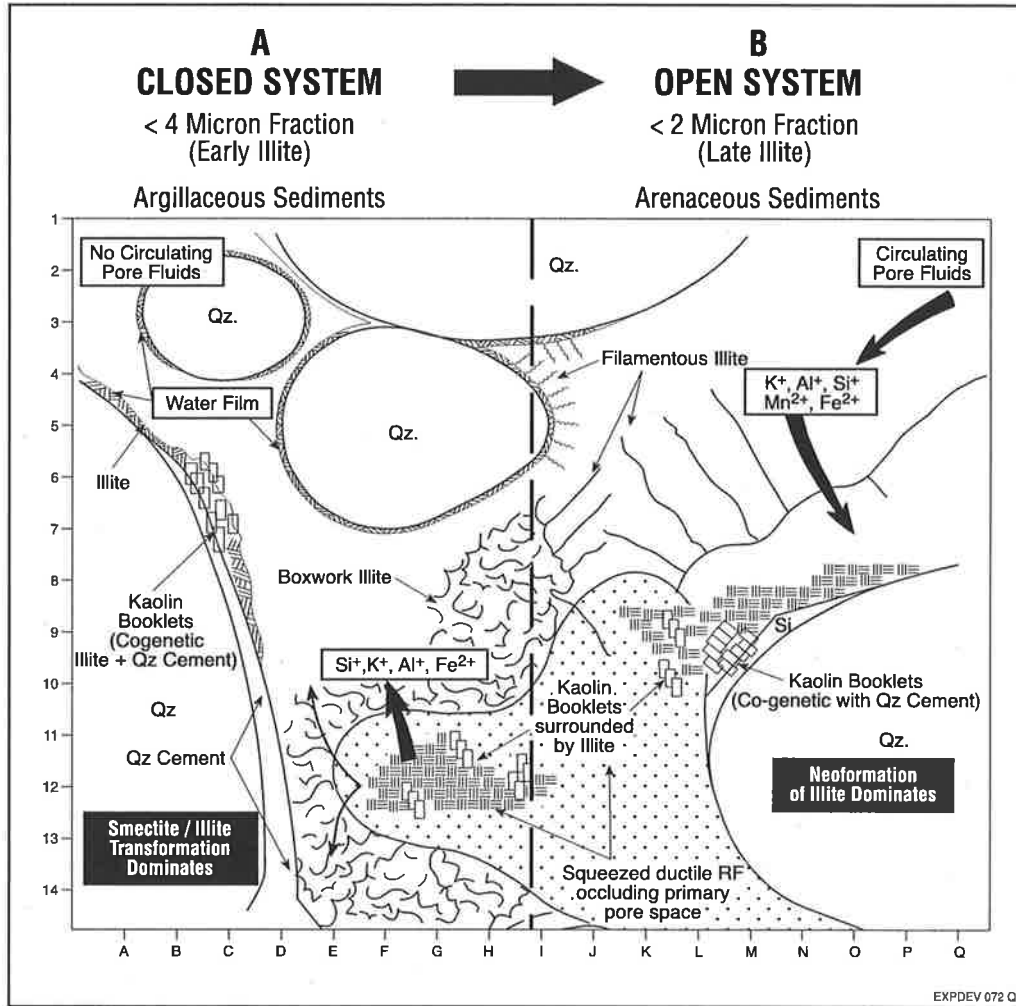


Figure 6.22 A) Cartoon of “closed system” diagenesis in Merrimelia sediments where the transformation of smectite to illite is the dominant diagenetic reaction. B) Cartoon of an “open system” where the neoformation of illite is the dominant diagenetic reaction.

Locally however, boxwork and filamentous/boxwork textures can dominate where associated unstable rock fragments and feldspar proportions are high (Plate 21b).

The amount of neoformed illite, on average, in porous Merrimelia lithologies ranges between 4%-22%. Present day proportions of micas and feldspar grains, on average, account for approximately 3% of the total detrital component but relict feldspar/mica grains as a proportion of the total rock volume account for <1.5%. However, the original volume of feldspars in Merrimelia sediments was much greater than can now be observed (kaolin + kaolinised clasts) (Fig. 6.2a). It is likely that the alteration of these feldspar grains not only formed kaolin but, provided cations for illite formation. The volume of kaolin and kaolinised clasts in Figure 6.2a however, suggests that there is not enough cations released from the alteration of original feldspars to

account for the volume of neoformed illite currently observed. In general, the amounts of authigenic pore-filling illite, relict feldspar/micas grains (1% of total framework) and kaolin do not match.

Another possible source of fluids capable of precipitating the large volumes of neoformed illite is the expulsion of water from adjacent fine grained argillaceous lithologies. The volume of argillaceous rock in the Merrimelia Formation is approximately double that of porous rock. The amount of water and cations being expelled from argillaceous would therefore be more than enough to account for the illite observed in adjacent interbedded porous lithologies. Circumstantial evidence would suggest that this is the most plausible source of illite cations for neoformation. This infers that cations for illite diagenesis in porous lithologies are being sourced distally (allochthonous fluids), implying that within porous lithologies, illite is forming in an open system. Locally however, pore-filling illite may also form adjacent to dissolving feldspar and mica grains.

Neoformation of illite in porous Merrimelia sediments is similar to the mechanism proposed by Lee *et al.* (1989) where newer illite replaces coarser grained, pre-existing illite in a continuous process. The illite substrate is flame-like in shape (Fig. 6.23a) with the younger later-formed illite becoming more filamentous. It is postulated in porous Merrimelia lithologies that neoformed illite forms on an illite substrate that pseudomorphs smectite related to the transformation process occurring in argillaceous sediments. The later filamentous illite is interpreted to have been precipitated from circulating pore waters (neoformation) following the almost complete transformation of smectite to illite (Burley and Flisch, 1989) (Fig. 6.23b & 6.23c).

The sequential development of pore-filling clay in arenaceous Merrimelia sediments is a strong argument in favour of an open diagenetic system. Almon and Davies, (1979) describe similar pore-filling clays in the Muddy Sandstone of the Powder River Basin (Wyoming and Montana) and concluded that the ions necessary for the development of late stage clay would not have arisen from local detrital grains as this material would have been incorporated into earlier diagenetic phases. It is proposed that the same is true for the diagenetic processes in Merrimelia sediments, where late stage diagenetic alterations have formed in an open system, in response to changing thermal conditions and pore water chemistry.

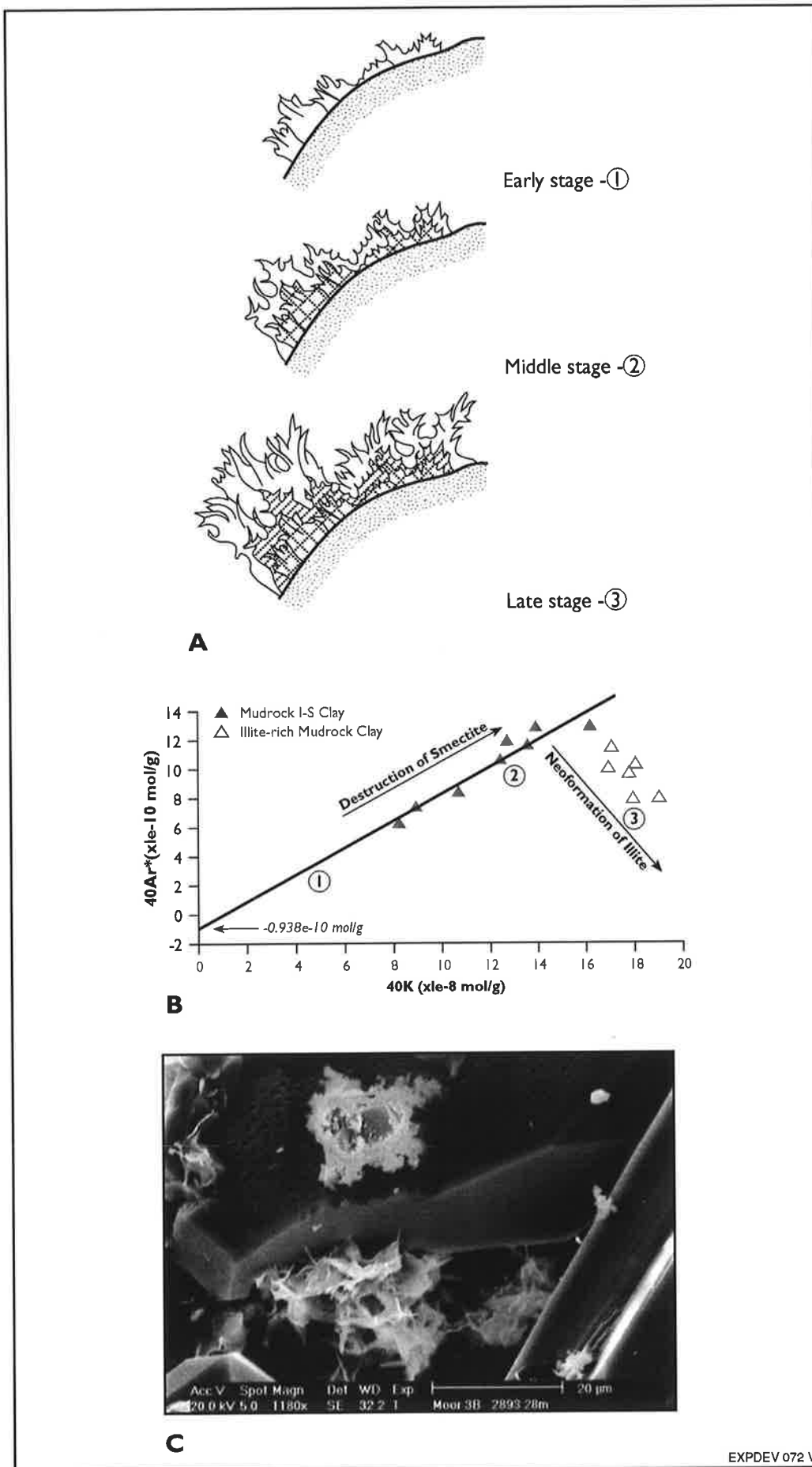


Figure 6.23 A) Cartoon of illite growth stages (From Lee et al., 1989). B) Smectite to illite transformation and subsequent neoformation of illite (From Burley and Flisch, 1989). C) Moorari #3 (2893.28m) SEM photomicrograph of boxwork morphology substrate (S/I transformation) with protruding, neoformed, filamentous illite.

In summary, filamentous pore-filling illite forms in open pores from circulating pore fluids sourced from relatively proximal argillaceous lithologies.

vi) Illitisation of Kaolin

The illitisation of kaolin (Plate 32a[7c]) (Bjørlykke, 1983; Srodon and Erberl, 1987; Small *et al.*, 1992) is another, albeit minor, diagenetic process leading to the formation of illite in Merrimelia sediments. This adjustment occurs at a late diagenetic stage, where kaolin becomes unstable with respect to illite and burial temperatures exceed 100°C (Aja *et al.*, 1991; Sass *et al.*, 1987; Prothero and Schwab, 1996) and proceeds according to equation 10 (Bjørlykke, 1983).



Huang *et al.* (1986) suggested that the illitisation of kaolinite may be triggered by a decreased rate of acidic fluid influx during burial diagenesis. Small *et al.* (1992) experimentally produced pseudomorphed illite after kaolin in very acidic solutions at 400°C. Foscolos (1990), on the other hand, stated that in conditions where potassium concentrations are elevated, illitisation of kaolin will proceed at 100°C. This author also stated that if the concentration of potassium is halved the temperature of illitisation is raised to 200°C.

Illitisation of kaolin in Merrimelia sediments is not commonly observed even though basin temperatures are considered to be abnormally high (BHT +200°C) (Schulz-Rojahn, 1991). The lack of illitised kaolin may suggest that higher temperatures may be needed for kaolin to illitise in Merrimelia sediments.

PLATE 32

**Diagenetic Reactions: Illitisation of Kaolin/Feldspar
Dissolution/Cogenetic Siderite/Kaolin**

A) SEM Photomicrograph – Daralingie #1 (2187.85m). Kaolin filled pore with subordinate filamentous neoformed illite [7c] in an arenaceous Merrimelia sediment. Note: this lithology is similar to Tirrawarra sandstones.

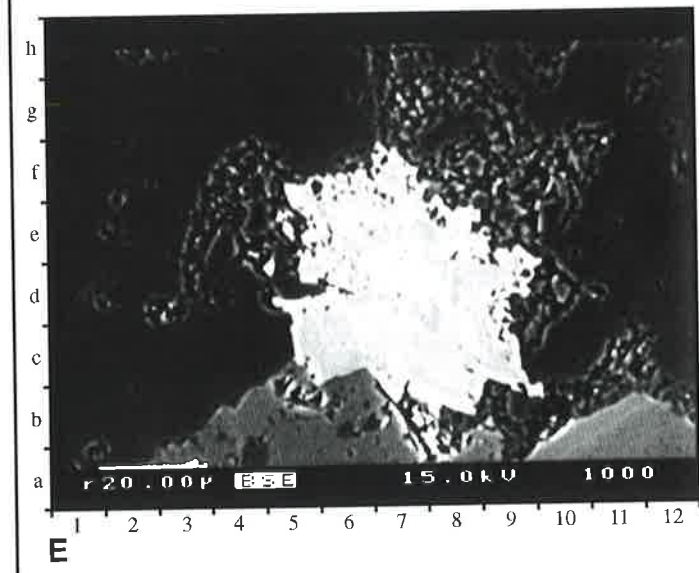
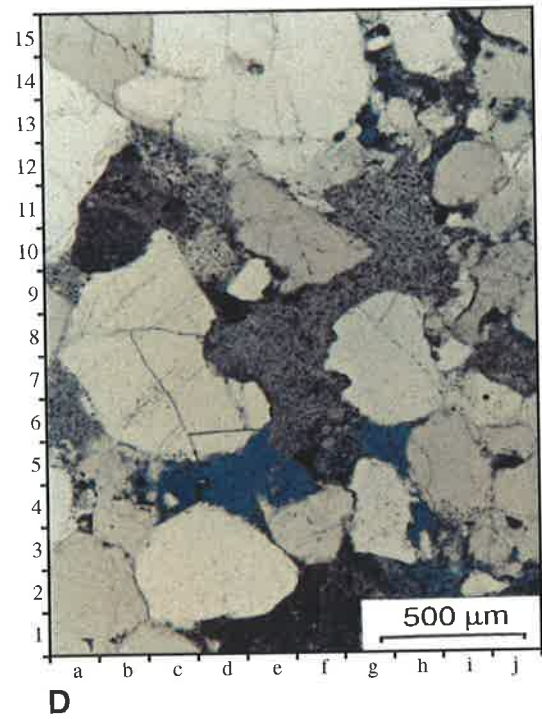
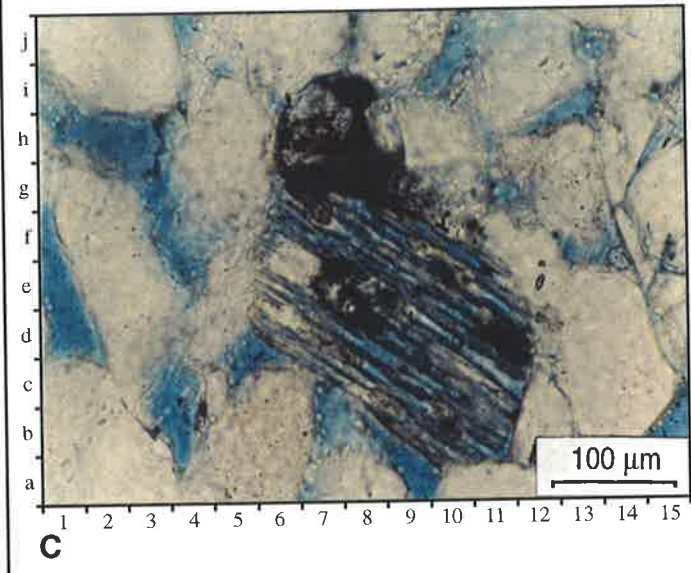
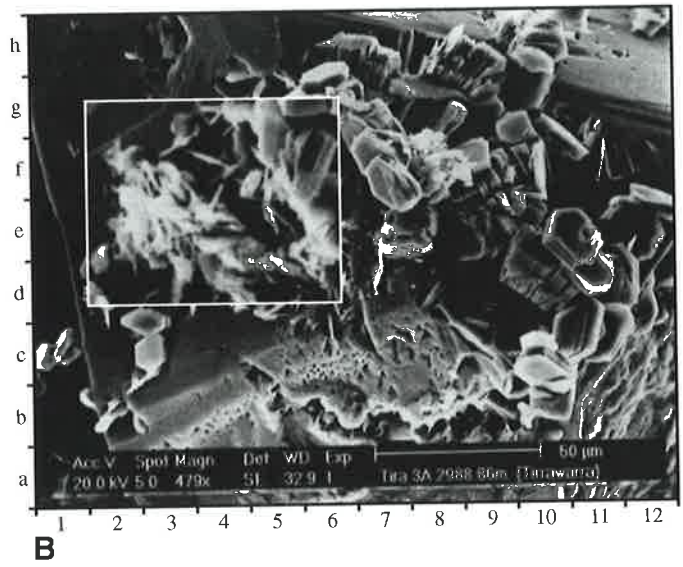
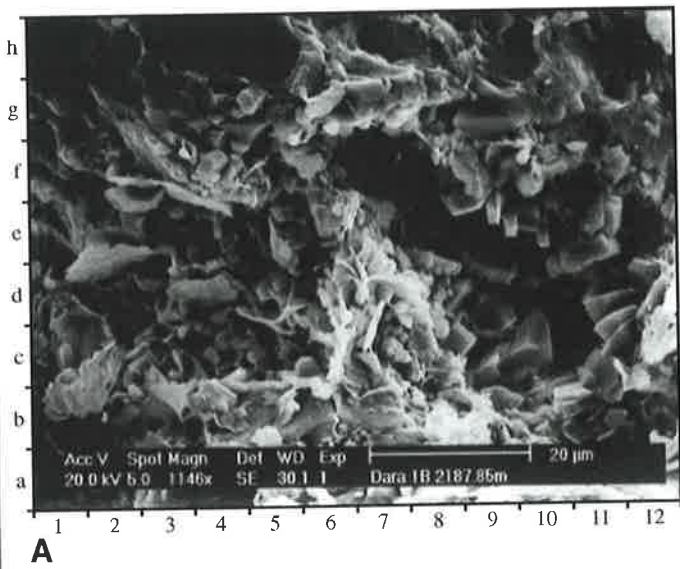
B) SEM Photomicrograph – Tirrawarra #3 (2988.86m). Sucrosic, stacked kaolin booklets. [Inset] Localised Illitisation of kaolin booklets.

C) Photomicrograph – Merrimelia #1 (2946.80m) (Plane polarised x 5). Dissolution of a feldspar grain within the glacio-aeolian sedimentary pile. The destruction of such unstable framework components forms secondary pore space.

D) Photomicrograph – Tirrawarra #11 (3081.55m) (Plane polarised x 5). Alteration of feldspar grain to kaolin and subsequent compaction squeezing.

E) BSE Image – Kenny #1 (2945.80m). S2 siderite (outer edge of siderite patch) exhibits a serrated edge indicative of dissolution. The acidic waters that have etched the S2 siderite have, in this case, induced locally the formation of kaolin booklets.

Plate 32



This may indicate that Merrimelia pore solutions are not acidic enough and need increasingly higher temperatures for the kaolin/illite reaction to proceed. Alternatively the lack of illitised kaolin maybe related to a lack of K^+ ions and not pore water acidity. In this scenario the majority of K^+ ions are consumed by the formation of illite, where increasing illite crystallinity consumes more K^+ ions. There is thus little K^+ left to supply the conversion of kaolin to illite. Hence the lower concentrations of K^+ necessitate higher temperatures to transform kaolin to illite. Such high temperatures may only be reached in a limited number of areas in the Patchawarra Trough. This latter scenario is more consistent with petrographic observations.

Srodon and Eberl (1987) cite numerous studies concerning the illitisation of kaolin concluding, "that kaolinite is illitised completely before smectite is completely illitised". The data in this study do not support this hypothesis. It has been established that mixed layered clays in Merrimelia sediments have been transformed almost to completion and only the partial illitisation of kaolin is observed in SEM images (Plate 32b[Inset]). Hence, when observed, the illitisation of kaolin reflects a zone that has K^+ -rich pore waters coupled with anomalously high basin temperatures ($>130^{\circ}\text{C}$).

vii) Illite Authigenesis in Merrimelia Sediments: Open or Closed Diagenesis?

Considering the Merrimelia Formation as a whole, the unit is dominantly argillaceous with an upper section that is more porous and interfingers with the 'clean' Tirrawarra Sandstone. Hugget (1996) considered a similar sequence of rocks and observed illite formation mechanisms that mirror illite formation processes in the MTGC. For example, Hugget (1996) observed that lath shaped (filamentous) authigenic illite not only precipitated from solution (neof ormation) in sandstones (upper Merrimelia Formation and Tirrawarra Sandstone) but also formed simultaneously in adjacent, low permeability, low porosity mudrocks (M2 and M3 strata).

Chamely (1989) and Pye and Krinsley (1986) suggested, however that intermediate situations may exist where there is synchronous growth of illite from the transformation of smectite (closed system) and of neoformed illite (open system) within adjacent pore spaces. These observations indicate that illite formation processes specific to argillaceous and arenaceous sediments may theoretically proceed with increasing depth simultaneously in adjacent sandy and shaley rocks. Chamely (1989) stated further that transitional illite formation stages or combinations of argillaceous and arenaceous illite diagenesis mechanisms occur between shale-

dominated and sand-dominated rocks, locally depending on the dominant rock lithology. Accordingly, a sequence of strata with closely stacked inter-fingering shales and sandstones would be expected to exhibit a complex interplay of simultaneous illite formation processes.

The contemporaneous formation of illite from open and closed systems in adjacent argillaceous and arenaceous sediments, is applicable to observed illite formation scenarios within upper (M1) Merrimelia lithologies. At depth (M2 and M3), however, smectite to illite transformation reactions dominate.

D) Key Findings

Illite in Merrimelia sediments forms via three differing mechanisms:

- | | |
|---------------------------------------|----------------------------|
| 1) Smectite to illite transformation, | 2) Neoformation of illite, |
| | 3) Illitisation of kaolin. |

Illite in the Merrimelia Formation forms in the following circumstances:

- 1) As a grain coating clay via the transformation of smectite to illite.
- 2) From the partial or total replacement of unstable feldspars and/or rock fragments via the transformation of smectite to illite.
- 3) From the transformation of detrital smectite matrix to illite.
- 4) From solution in arenaceous sediments (neoformation).
- 5) From the illitisation of kaolin.

6.3.4.3.2 Segregation of Illite and Kaolin

A) Key Observation

Illite and kaolinite clays are segregated within the MTGC where illite dominates terminoglacial Merrimelia facies and kaolin Tirrawarra.

B) Discussion

Organic maturation (organic acids) and kaolin development have been linked by many workers (Dixon *et al.*, 1992; Reed and Hajash, 1992 and Surdam *et al.*, 1989). Huang *et al.* (1986), through experimental analysis, modelled the formation of both illite and kaolin waters containing organic acids. The results suggested that kaolin formed preferentially in pore spaces where kaolin was already present and where there was constant pore water influx. Conversely, these authors suggested that the most favourable conditions for the neoformation of illite is a rapid release of Al and Si into an acidic solution within a low permeability sediment. Interestingly these authors go on to state that as pore water influx slowed, significant authigenic illite

formed. Thus they concluded that illitisation during deep burial could be caused by the reduced influx of acid fluids in a poorly permeable sediment.

Acidic fluid influx in Tirrawarra sediments is constantly replenished by organic acids percolating through the open pore system, forming kaolin preferentially, as kaolin is stable at this temperature range ($>100^{\circ}\text{C}$) (Foscolos, 1990; Reed and Hajash, 1992). The Merrimelia Formation, conversely, is relatively impermeable and hotter (see Chapter Eight). The same acidic fluids will inconsistently penetrate Merrimelia sediments and at a much slower rate; a product of poorer permeability. The resulting clay precipitation in Merrimelia sediments, according to the mechanisms described by Huang *et al.* (1986), is more likely to be illitic than kaolinitic. These processes may partially explain the enrichment of kaolin in Tirrawarra sediments and illite in Merrimelia strata.

In addition to these controls, it is likely also that the lack of illitic matrix in Tirrawarra sediments promotes the formation of kaolin rather than illite. Conversely the dominance of matrix in Merrimelia sediments will promote illite and not kaolin formation.

Small amounts of illite are observed in Tirrawarra sediments. In this scenario, Tirrawarra pore spaces become filled with kaolin booklets decreasing the water/rock ratio. Once the water/rock ratio decreases enough, the amount of kaolin will cease precipitating in the pores and, if reactant supply remains constant, illite will begin to precipitate preferentially (Plate 32a). This follows the model of Hutcheon (1982) who suggested that the rate of fluid flow is critical to clay formation within arenaceous sediments. In addition, Small *et al.* (1992) stated that illite generally nucleates from detrital grain surfaces and not syntaxial quartz cement. Therefore little illite will be observed in quartz-cemented pores in the Tirrawarra Sandstone.

C) Key Findings

The segregation of illite and kaolin within the MTGC is controlled by:

- 1) Lack of illitic matrix in Tirrawarra sediments.
- 2) Illite tends to form on detrital surfaces and not on authigenic quartz.
- 3) Illite in the Cooper Basin forms in sediments where temperatures are elevated and muddy matrices and low fluid flow characteristics (low permeability) predominate. Terminoglacial Merrimelia facies (the majority of the Merrimelia Formation) display these characteristics; Tirrawarra sediments do not.

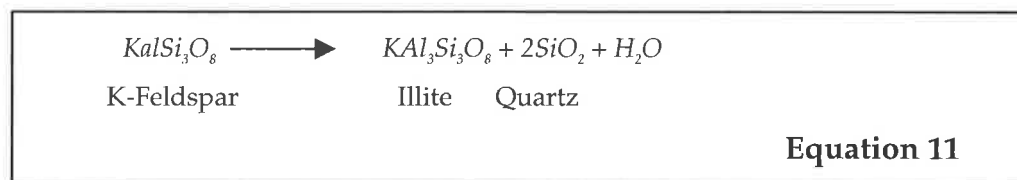
6.3.4.3.3 Feldspar Dissolution

A) Key Observations

The dissolution of feldspar is an important diagenetic process in Merrimelia sediments, particularly so in the aeolian sandstones of the Merrimelia Field (Plate 32c). As discussed earlier, this process provides silica for quartz overgrowths and at the same time produces kaolin and illite (Equations 8 & 11).

B) Discussion

Potential controls on this reaction are numerous. Chamely (1989) stated that the dissolution of feldspars within sandstones is favoured by acidic conditions and the presence of relict organic matter. Surdam *et al.* (1984) demonstrated that the mobility of aluminium ions in solution is increased when transported by organic complexes within organic acids. That is to say the dissolution of feldspars is controlled by the mobility of Al⁺ ions, a mobility that is normally low, but in the presence of carboxylic acids, increases to such a level that extensive replacement of feldspar framework grains and carbonate cements will occur. Plate 22e illustrates the dissolution of feldspar grains under SEM. The most obvious product in this image is the development of fibrous illite (Plate 22e[Inset]). This process proceeds according to the following equation:



Variation of the fluid/rock ratio and flow rate has a significant effect on the mechanics of feldspar dissolution and subsequent illite formation (Huang *et al.*, 1986).

The concentration of dissolved CO₂ dictates whether feldspar grains are dissolved or preserved in circulating pore waters. Elevated CO₂ in pore waters encourages feldspar dissolution. CO₂ in pore waters can increase when organically-derived maturation acids increase or with the percolation of acidic meteoric waters. In Merrimelia sediments both processes potentially operated but at different times and on differing sediments.

Surdam *et al.* (1984) stated that even relatively low concentrations of carboxylic acids will increase the rate of feldspar dissolution. The Merrimelia Formation in general and terminoglacial sediments in particular, are devoid of organic material (Boreham and Hill, 1998), having been deposited in conditions where little organic matter would

have survived. Conversely the lower braid plain on which proglacial Merrimelia and Tirrawarra sediments were deposited (Fig. 4.5) shows evidence of marsh development (Plate 7e). Organic matter was therefore exclusively developed in upper Merrimelia (proglacial) and Tirrawarra sediments (Fig. 4.5). Surdam *et al.* (1989) stated that for organic acid dissolution and porosity preservation to be influential in inorganic diagenesis, close proximity to organic-rich rocks is necessary. The Tirrawarra Sandstone is proximal to organic matter, whereas Merrimelia sediments are not. This suggests that the development of organic acids may have been confined to upper Merrimelia (M1) and Tirrawarra (T1) sediments with little percolation of early diagenetic acidic pore water down through the entire Merrimelia section.

For feldspar grains to be dissolved by organic acids, organic acids have to be produced by maturation. Surdam *et al.* (1989) concluded that this process occurs between 80°C and 120°C, well above the temperature of burial of upper Merrimelia sediments. Thus organic acid production in upper Merrimelia and Tirrawarra sediments would have been a late diagenetic event as the temperature of burial during early diagenesis was not sufficient to produce organic acids.

Figure 6.24 suggests that in the basal parts of the Merrimelia Formation (M2 & M3 [3000m-3500m]), feldspar proportions are elevated when compared with M1 and Tirrawarra (T1) sediments. This indicates that either 1) feldspar proportions have varied through time or that 2) feldspars have been preferentially destroyed in T1 and M1 sediments when compared to M2 and M3 sediments.

Provenance data suggests that feldspar grains have been mainly sourced from greywackes of the Warburton Basin and Big Lake Suite granodiorites. External sources provided minimal feldspar detritus. It is therefore reasonable to assume that the input of feldspar detritus into the MTGC has been relatively constant with no wide ranging fluctuations between feldspar input into basal M2/M3 and M1/T1 sediments.

Cannibalisation of earlier formed sediments would have been the most likely source of feldspars in later formed Cooper Basin sediments.

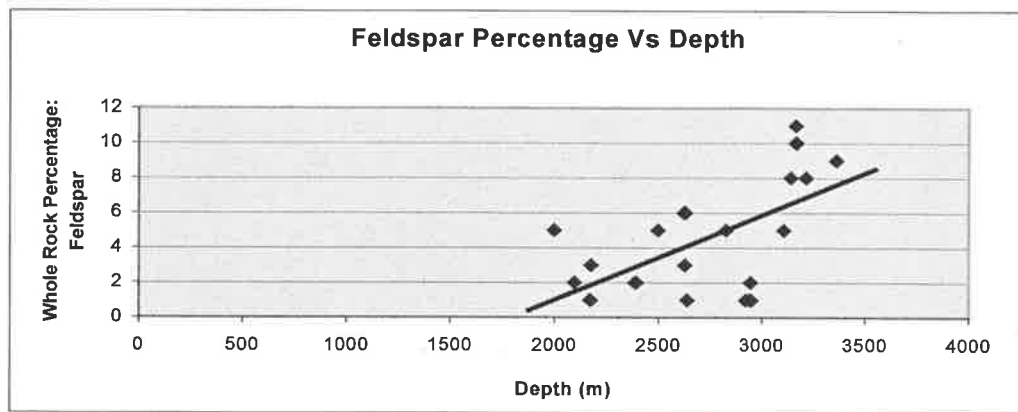


Figure 6.24 *Feldspar proportions in Merrimelia Formation sediments.*

With feldspar proportions relatively consistent throughout the MTGC, a mechanism is therefore needed to preferentially preserve feldspars in basal Merrimelia sediments and destroy feldspar in M1 and T1 sediments. The most likely mechanism involves the restriction of acidic groundwaters into poorly permeable M2/M3 sediments. In this scenario, feldspar grains in M1 and T1 sediments are exposed to acidic meteoric waters and dissolve. Simultaneously, in M2/M3 sediments meteoric waters have less influence (the low permeability of M2/M3 rocks restricts meteoric flushing) preserving feldspar grains.

C) Key Findings

Acidic pore water flushing via meteoric percolation is the most likely cause of feldspar dissolution in M1 (proglacial) and T1 sediments. Feldspar grains have been preferentially preserved in M2 and M3 Merrimelia sediments. This suggests that diagenesis in Merrimelia sediments is of two types:

- 1) An upper zone dominated by acidic pore waters where kaolin/quartz and neoformed illite development dominates.
- 2) A lower zone where the transformation of smectite to illite is the dominant diagenetic reaction.

6.3.4.3.4 Kaolin Authigenesis

A) Key Observations

Plate 30c is dominated by two kaolin regions (dark areas). These regions are consistent with the shape of compacted feldspar grains. The kaolin in these regions is regarded as having formed as a by product of the dissolution of detrital feldspars.

Hence feldspar dissolution and kaolinite formation in Merrimelia sediments are connected.

B) Discussion

The acidification of pore waters, whether it is by organic maturation or meteoric flush is generally regarded as the key to the formation of kaolin (Bjørlykke and Brendsal, 1986; Dutta, 1992). Rezaee (1996) agreed establishing that meteoric flushing is the most likely cause of early feldspar dissolution (as opposed to organic acids) in Tirrawarra (T1) sediments.

Figure 6.25 illustrates that there is a decrease in kaolin proportions with depth where kaolin is found predominantly in proglacial sediments (Fig. 6.26).

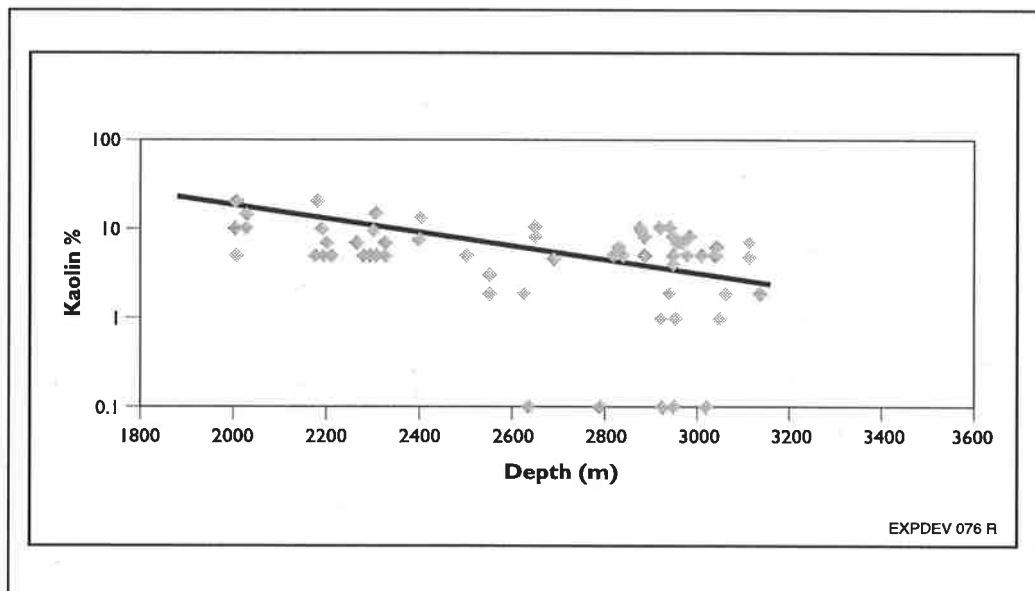


Figure 6.25 Scattergram of kaolin proportion versus depth.

These data support the hypothesis that kaolin forms preferentially in upper Merrimelia/Tirrawarra sediments coinciding with an absence of feldspars. Hence, like feldspar dissolution, kaolin development appears to preferentially occur in M1 (proglacial sediments) (Figure 6.26) as the necessary meteoric water for kaolin formation in M2 and M3 sediments is restricted by low permeabilities (terminoglacial sediments). Rezaee (1996) also concluded that the absence of feldspars and abundance of kaolin in Tirrawarra sediments is an indication that kaolin has been derived from feldspar alteration.

In addition, the co-genetic nature of kaolin and quartz (Plate 26b) indicates that the reaction described by Equation 8, is the dominant kaolin forming process in Merrimelia sediments.

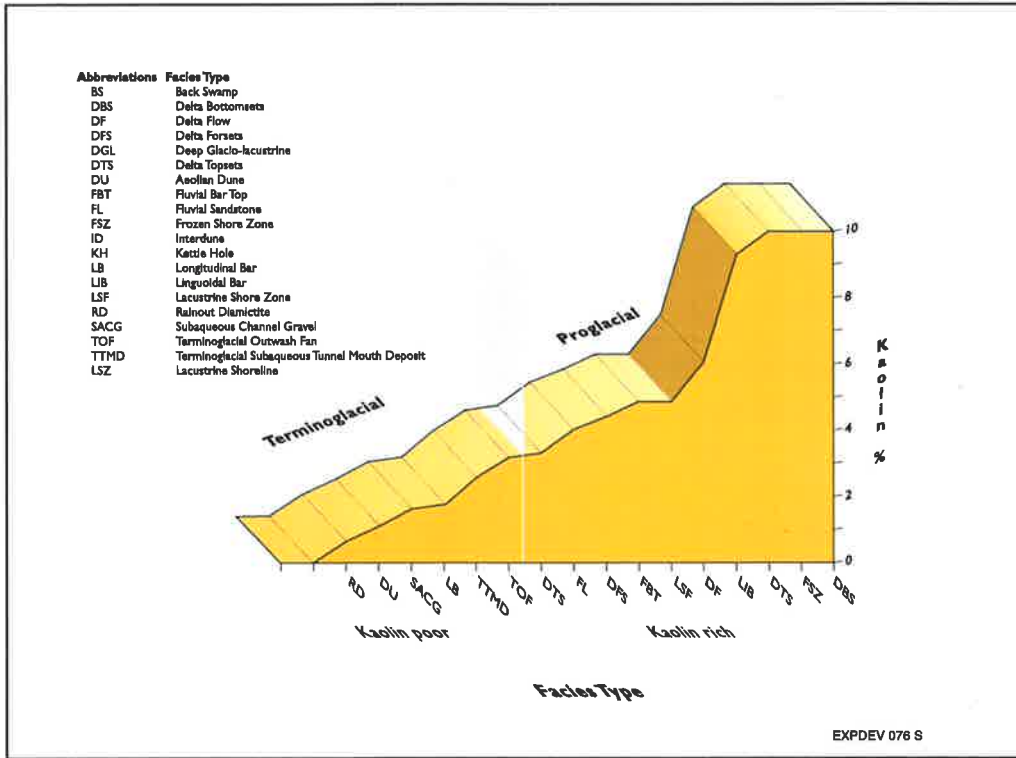


Figure 6.26 Ranked cumulative histogram of kaolin proportions in Merrimelia facies. Note: terminoglacial are kaolin poor with respect to proglacial facies. The exception being glacio-aeolian dunal sandstones (DU) which form in the proglacial setting but are illite not kaolin-rich.

C) Key Finding

Kaolin formation is associated with altered feldspars (Plate 30c [6e]), syntaxial quartz cement (Plate 26b[5g]) and ultimately the availability of acidic pore fluids.

6.3.4.3.5 Kaolin Formation and S2 Siderite Dissolution

A) Key Observation

Textural relationships between kaolin and S2 siderite gained via back scattered electron images (Plate 32e) suggest that there is a connection between S2 dissolution and kaolin formation.

B) Discussion

Plate (32e) illustrates a siderite patch where S1 (brightest middle phase) and S2 are visible (zoned darker phase). The outer edges of S2 are serrated and appear to be

intergrown with kaolin booklets. This suggests a relationship between S2 siderite and kaolin, where kaolin formation is promoted locally by acidic pore waters (Huang *et al.* 1986), pore waters which also etched the S2 siderite.

C) Key Finding

It is likely that pore waters containing organic acids (as opposed to acidic meteoric waters) have been the catalyst for kaolin formation and siderite dissolution.

6.3.4.3.6 Dickite Authigenesis

A) Key Observations

- 1) Dickite in the Merrimelia Formation was present in only five XRD traces (Fig. 6.6c).
- 2) No dickite was reported by Rezaee (1996) in the Tirrawarra Sandstone in the Tirrawarra-Fly Lake-Brolga-Moorari region.

B) Discussion

Schulz-Rojahn (1991), describes dickite within the Patchawarra section of the Nappamerri Trough. This author envisages dickite formation occurring within the pore space via the action of migrating ground waters. Chamely (1989) discusses the formation of dickite in the Sydney Basin, stating that dickite precipitated very slowly from circulating pore fluids as a late stage diagenetic phase. Schulz-Rojahn (1991), concluded similarly in Cooper Basin sediments, stating that dickite formation was a late stage process.

The formation of dickite in the basal most Merrimelia sediments of the Patchawarra Trough is envisaged to occur by the same processes and in the same thermal conditions as that described by Schulz-Rojahn (1991), for dickite formation in the Nappamerri Trough. Accordingly dickite should be observed associated with kaolin. This does not, in general, appear to be the case. Despite this it appears reasonable to assume, that this clay phase, like that described by Schulz-Rojahn (1991), is a late formed diagenetic mineral after early kaolin development.

C) Key Finding

There is insufficient data to accurately describe the formation of dickite in Merrimelia sediments. It is assumed however, that dickite formation is similar to that described by Schulz-Rojahn (1991).

6.3.4.3.7 Chlorite Formation

A) Key Observations

"Translucent" chloritoid minerals (Fig. 6.6[9e]) are observed in Merrimelia sediments almost exclusively associated with basic clasts (Fig. 6.6d), biotite dominated schist rock fragments (Fig. 6.6e) and biotite micas (Fig. 6.6f). "Translucent" chloritoid minerals appear to overprint later formed quartz cement and/or siderite mineral phases.

B) Discussion

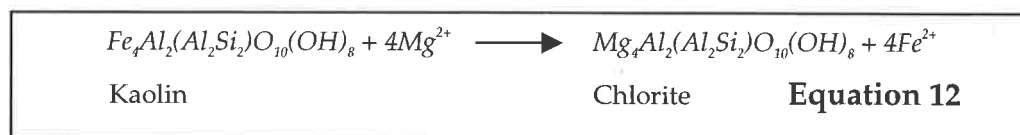
It is most likely that the majority of chloritoid minerals associated with basic rock fragments have been inherited from the Warburton Basin and incorporated into the Merrimelia sedimentary pile. However, it is also possible that some chloritoid minerals in Merrimelia sediments may form from a precursor clay, by the transformation of basic rock fragments to chlorite with increasing burial depth.

"Translucent" chloritoid minerals, unlike chloritoid minerals within mafic clasts, appear to have been formed *insitu*. There are three possible mechanisms by which "translucent" chlorite can form in Merrimelia sediments:

- 1) By products (Fe^{2+} and Mg^{2+}) from the smectite/illite transformation formed "translucent" chlorite locally (near basic rock fragments).
- 2) "Translucent" chlorite authigenesis occurred as the end product of the reaction kaolin + Mg^{2+} .
- 3) Formation of "translucent" chlorite occurred via the breakdown products of mafic rock fragments containing chloritoid minerals.

Hower *et al.* (1976) suggested that, in deep burial potential sources of Fe^{2+} and Mg^{2+} for chloritoid development maybe released during the conversion of smectite to illite. Ahn and Peacor (1986) confirmed this relationship by TEM utilising the Hower *et al.* (1976) samples. In this model, the high Fe^{2+} content of chlorite relative to Mg^{2+} is a product of the preferential loss of Fe^{2+} with respect to Mg^{2+} in the S/I conversion. The ions necessary for siderite development are Mg^{2+} and Fe^{2+} (the same as chlorite.) The rarity of translucent chloritoid cement with respect to siderite cement suggests that siderite cementation uses up most of the Mg^{2+} and Fe^{2+} released by the S/I transformation process. This would suggest that the S/I transformation is a minor source of reactants for the formation of "translucent" chlorite.

Jahren and Aagaard, (1989) discuss the formation of chlorite from kaolin in conjunction with Mg^{2+} (Equation 12). No association however, was observed between kaolin and chlorite in Merrimelia sediments.



The localised development of “translucent” chloritoid minerals near detrital chloritised clasts suggests a link where “translucent” chlorite incorporated ions from the disintegration of detrital chlorite. Jahren and Aagaard, (1989) stated that chlorite minerals try to incorporate all available Fe^{2+} from localised pore waters. This mechanism of chlorite formation sees the majority of Mg^{2+} and Fe^{2+} in regions surrounding chloritised rock fragments preferentially forming chloritoid minerals and not siderite. The cannibalisation of detrital chlorite to form authigenic chlorite appears to be the most likely formation mechanism for “translucent” chlorite in Merrimelia sediments.

C) Key Findings

- 1) Chloritisation of basic clasts, biotite-rich clasts and micas most likely occurred prior to inclusion into the Merrimelia sedimentary pile.
- 2) It is unlikely that the smectite-illite transformation plays a major role in supplying the ionic species necessary for “translucent” chlorite formation.
- 3) The breakdown of chlorite-rich (detrital) mafic rock fragments is the more likely main source of Mg^{2+} and Fe^{2+} reactants necessary for the formation of “translucent” chlorite.

6.3.4.4 Carbonate Authigenesis

6.3.4.4.1 S1 Siderite Formation

A) Key Observations

Backscattered images reveal that S1 siderite is the first formed siderite phase (Fig. 6.27d - annotated), precipitating prior to early quartz cementation.

SEM images commonly reveal euhedral siderite crystals (Plate 26d[5d] and Plate 22a[3d]) which most likely represent the later formed S2 or S3 siderite phases as the amount of dissolution pitting, indicative of S1 cement, is absent. S1 cement is most likely encapsulated within these siderite crystals by later formed S2 and S3 cement phases and is thus not often visible via SEM analysis.

B) Discussion

According to Rezaee *et al.* (1997) S1 siderite precipitation took place at about 30°C. This temperature of S1 siderite formation is consistent with (Bjørlykke, 1983) who stated that low temperatures are generally needed for iron cations to be incorporated into the siderite crystal lattice. The low temperature of S1 siderite formation also suggests that this carbonate cement was probably formed in near surface reducing conditions. In this reaction, which is bacterially modified (Curtis, 1978), Fe^{2+} and CO_3^{2-} form an early siderite precipitate.

C) Key Finding

Observations indicate that S1 siderite in Merrimelia sediments is the earliest carbonate precipitant, forming in conditions the same as that described by Rezaee (1996) in the Tirrawarra Sandstone in the Tirrawarra-Fly Lake-Brolga-Moorari region. Accordingly S1 siderite formed at burial temperatures of around 30°C.

6.3.4.4.2 D1 Early Siderite Dissolution**A) Key Observations**

S1 siderite cement in Merrimelia sediments across the Cooper Basin reveals extensive etching (Plate 33c[8d]) indicative of a significant period of siderite dissolution (D1) prior to the precipitation of S2 siderite (Plate 33a). In this image (Plate 33c) S1 siderite appears almost totally dissolved sharing an irregular boundary with the darker, zoned S2 siderite.

B) Discussion

Rezaee, (1996) observed the same siderite dissolution phase (naming it D1) between S1 and S2 siderite cement phases in Tirrawarra sediments in the Fly Lake-Brolga-Tirrawarra-Moorari region. This author concluded, from fluid inclusion data, that the D1 dissolution event took place at burial temperatures between <30°C and 68°C, indicating that dissolution occurred at relatively shallow burial depths. The dissolution of S1 siderite before the precipitation of S2 marks a temporary increase in pore water acidity. Surdam *et al.* (1989) describes carbonate stability in terms of P_{CO_2} , where siderite will dissolve in acidic (high P_{CO_2}) and form in low P_{CO_2} conditions. The acidification of the pore waters in these shallow buried sediments, has been argued by Rezaee (1996) in Tirrawarra sediments to be a product of the infiltration of low-pH meteoric waters into the pore space.

C) Key Findings

It is likely that the same acidic pore fluids which dissolved feldspars and formed early kaolin in Merrimelia sediments also partially dissolved S1 siderite. This relationship is observed in Plates (33b & 33d) where S1 siderite has almost been completely dissolved and been replaced by kaolin booklets (Plate 33d).

D1 siderite dissolution in Merrimelia sediments is the same as that described by Rezaee (1996) in the Tirrawarra Sandstone in the Tirrawarra-Moorari region.

6.3.4.4.3 S2 Siderite Formation (Zoned)

A) Key Observations

The highly zoned nature of S2 siderite (Plates 33c) suggests that pore water chemistry has fluctuated markedly. These pore water fluctuations are manifested in the variation of magnesium (Table 6.14 [in Plate 33]) from the earliest formed S2 band until the last (Plate 33c). In contrast, S3 siderite illustrates little compositional banding (Figure 6.8a[13e]), indicating that pore water chemistry was more stable. Rezaee (1996) and Rezaee *et al.* (1997) observed the same features in Tirrawarra sediments in the Tirrawarra-Fly Lake-Brolga-Moorari region. These authors concluded that the zonations in S2 are indicative of siderite that has precipitated from solution and has not undergone neomorphic recrystallisation. The present study extends this concept basinwide, with no recrystallisation of S2 siderite cement observed. The fluid inclusion temperature range of S2 cement of 68°C-102°C (Rezaee *et al.*, 1997) are thus regarded as being indicative of S2 precipitation across the Cooper Basin in Merrimelia sediments.

B) Discussion

In Tirrawarra and Merrimelia sediments alkaline pore fluids again prevailed where external buffering by acetate species (Surdam *et al.*, 1989) allowed the precipitation of S2 siderite. At temperatures over 100°C, buffering of acid waters ceases and conditions suitable for carbonate dissolution occur (Surdam *et al.*, 1989). This dissolution phase continues, according to Surdam *et al.*, (1989), continues to around 120°C where the carbonate system will regain internal buffering and carbonate species will again precipitate (S3 siderite, dolomite and calcite). This scenario of carbonate evolution/dissolution appears to have operated in Merrimelia sediments, where burial history modifications are superimposed. The highly zoned nature of S2 siderite is indicative of such modifications (Fig. 6.8a).

PLATE 33

**Diagenetic Reactions: Siderite Precipitation, D1 Dissolution and
Siderite Dissolution/Kaolin Formation**

A) BSE Image – Gidgealpa #3 (2314.7m). Siderite “seed” exhibiting compositional banding. D1 dissolution edge is annotated.

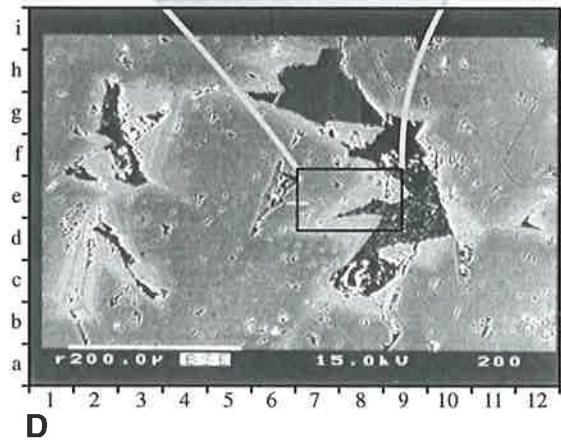
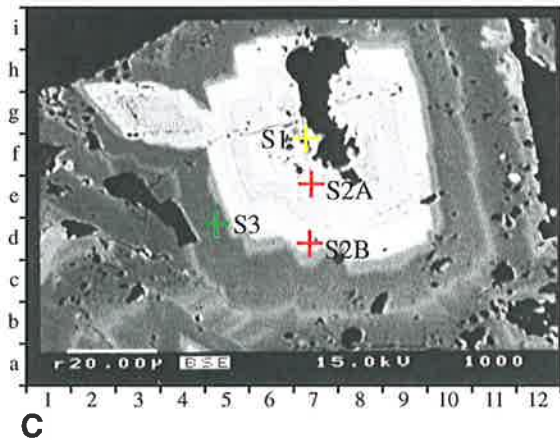
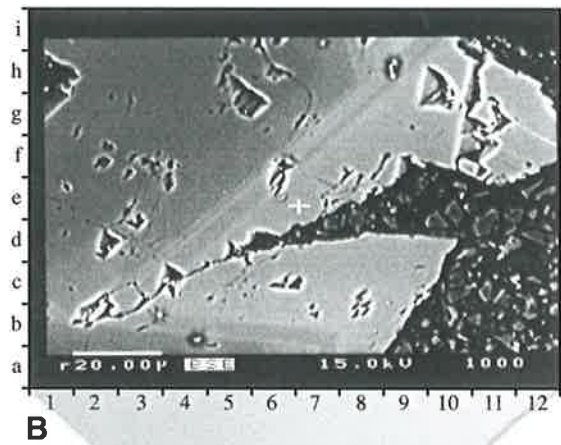
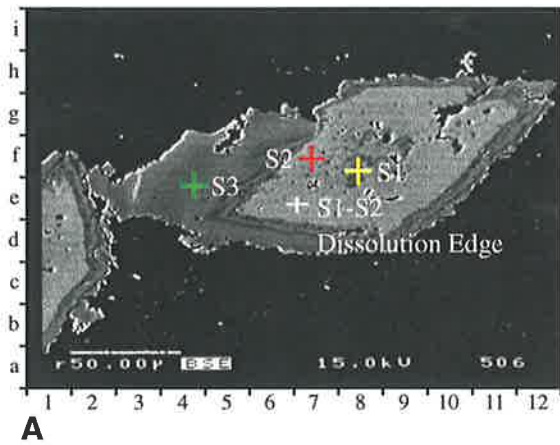
B) BSE Image – Kenny #1 (2945.8m). Close up view of kaolin booklets replacing siderite

C) BSE Image – Gidgealpa #5 (2298.57m). Close up view of pore filling siderite illustrating the intricate compositional banding which correspond with S1, S2, and S3 siderite phases. Spot compositions detailed in Table 6.8 correspond with “A” and “B” in this plate.

D) BSE Image – Kenny #1 (2945.8m) Broad view of Plate 33b illustrating the replacement of S1 siderite by kaolin booklets [9e].

Table 6.14 – S2 siderite compositions.

Plate 33



	MgCO ₃	CaCO ₃	MnCO ₃	FeCO ₃
S2 Siderite				
S2 Siderite A	8.01	10.35	1.11	80.52
S2 Siderite B	28.5	8.5	1.8	61.1
<i>Average</i>	<i>18.26</i>	<i>9.43</i>	<i>1.46</i>	<i>70.81</i>
<i>Std Dev</i>	<i>14.49</i>	<i>1.31</i>	<i>0.49</i>	<i>13.73</i>
S3 Siderite				
MRI 18C#5	28.7	54.5	0.9	15.8
MRI 18A#11	33.1	53.7	0.4	12.8
MOOR 2B#19	31.3	3.5	2.0	63.2
FLY 1D#7	21.6	1.8	1.1	75.5
MRI 18C#3	27.9	55.5	1.4	15.2
MOOR 2B#25	33.8	51.1	0.4	14.7
MOOR 2B#26	39.4	6.1	1.3	53.3
MRI 18C#1	27.7	54.5	1.7	16.1
FLY 1D#18	21.1	2.0	1.1	75.8
WOOL 1B#3	20.5	0.2	1.1	78.2
WOOL 1B#3	18.3	0.5	1.1	80.0
<i>Average</i>	<i>27.6</i>	<i>25.8</i>	<i>1.1</i>	<i>45.5</i>
<i>Std Dev</i>	<i>6.60</i>	<i>26.96</i>	<i>0.48</i>	<i>30.21</i>

Table 6.14 S2 and S3 Siderite Compositions (Wt%)

Plotting S1, S2 and S3 siderite formation temperatures on geohistory plots, constructed at Malgoona (basin rim) and Merrimelia (GMI Ridge),⁶ fields gives an indication of siderite formation with respect to sediment burial and uplift (Fig. 6.27). This figure illustrates the effect of burial history with respect to S2 zonation compositions where the changing Mg proportions in this cement phase record fluctuations in pore water chemistry and temperature gradients. Fluctuations appear to be mainly controlled by temperature and therefore depth of burial. Sediment permeability is the other main control on siderite development.

The supply of Mg^{2+} fluctuates with temperature. Rezaee and Schulz-Rojahn (1996) indicate that the isotopic signature of Mg in S2 siderite within Tirrawarra sediments (Moorari-Tirrawarra region) is indicative of Mg produced at temperatures that are equivalent to the decarboxylation of organic matter. The same authors also contend that Mg^{2+} ions for the later formed S3 siderite was produced during kerogen maturation above 100°C.

In Tirrawarra sediments of the Moorari-Tirrawarra region, the thermal breakdown of organic matter is the most likely source of Mg for S2 siderite cement. However, the impermeable and organically barren nature of Merrimelia sediments limited the infiltration of organic acids, lessening the effect of acidic pore waters at depth. In contrast, acidic water more easily penetrated Tirrawarra sediments with highly dissolved siderite cement phases a consequence. This effect is not absolute, as the abundance of illite (or kaolin) in Merrimelia sediments suggests that pore waters were at some stage acidic, indicating that a certain stages during burial, acid organic waters may have influenced the composition of Merrimelia pore fluids.

S2 siderite in Merrimelia sediments appears to be better defined than S2 siderite in Tirrawarra sediments (Figs. 6.9b & 6.9c). This may suggest that the Mg source for S2 siderite was operating more efficiently in Merrimelia rather than Tirrawarra sediments. This conclusion however, seems to contradict the notion that the influence of acidic waters (either meteoric or organic) diminished with depth (see sections on feldspar dissolution – 6.3.4.4 and kaolin development – 6.3.4.5) in the MTGC. It follows then that if the influence of acidic waters is less in Merrimelia than in Tirrawarra sediments then some other mechanism must provide at least some Mg for S2 siderite precipitation in Merrimelia sediments.

⁶ A full explanation of geohistory model construction is given in Chapter Eight.

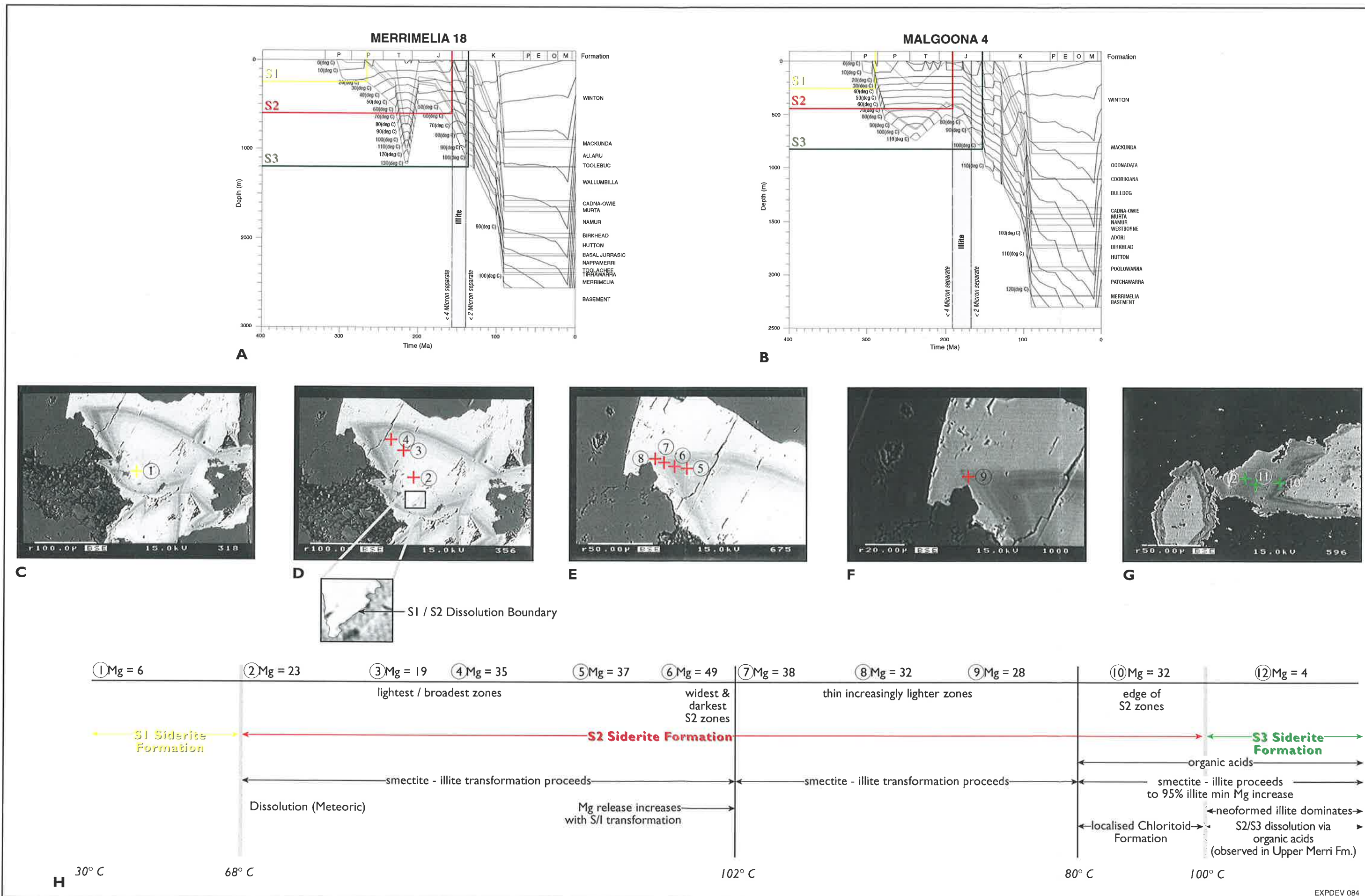


Figure 6.27 A) Geohistory plot of Merrimelia #18 with S1, S2 and S3 Siderite formation temperatures. B) Geohistory plot of Malgoona #4 with S1, S2, and S3 Siderite formation temperatures. C-F) Fly Lake #1 (2948.22m) BSE photomicrograph showing the location of S1 and S2 spot analyses. G) Gidgealpa #3 (2314.7m) BSE photomicrograph illustrating the location of S3 spot analyses. H) Schematic of Mg proportions relative to S1, S2 and S3 siderite, smectite to illite transformation, organic maturation and the neoformation of illite.

Such a mechanism maybe the transformation of smectite to illite within dewatering shales. This reaction, unlike the infiltration of organic acids, is more prevalent at depth in Merrimelia sediments. Nadeau and Bain (1986) and Hower *et al.* (1976) propose that Mg^{2+} , Fe^{2+} and Ca^+ ions are released in this reaction (Equation 6); ions which are necessary for siderite formation

Another possible source of siderite cement may involve circulating brines contacting marine shales of the Warburton Basin and precipitating siderite up section. However, the proportions of Mg^{2+} across the Cooper Basin in Merrimelia Formation S2 siderite varies consistently, unlike the occurrence of marine shales (Kalladeina Formation & Dullingari Group) of the Warburton Basin (Fig. 5.23). In contrast, the conversion of detrital smectite to illite in Merrimelia sediments is consistently observed across the Cooper Basin, and is the more likely source of Mg^{2+} for siderite cement development in M2 and M3 sediments than either marine shales or maturing organic matter.

The smectite-illite transformation is dominantly temperature controlled, peaking in the middle stages of diagenesis (Fig. 6.28). Thus, increasing burial temperatures accelerate the S/I reaction and subsequently the Mg^{2+} output. The products from this reaction (Mg^{2+} included) are incorporated into pore waters which become progressively enriched in Mg^{2+} ions, ions which are then incorporated into S2 siderite, forming bands where Mg^{2+} progressively increases (Fig. 6.27).

Thus increasing Mg^{2+} in S2 siderite corresponds with an increasing burial temperature. It follows then that the first formed S2 siderite has the least Mg^{2+} (lowest formation temperature) and the last formed the most (highest temperature). Microprobe data confirm these findings (Fig. 6.27h). Lower Mg^{2+} proportions in S3 siderite is linked to illite neof ormation (see section 6.3.4.3.1Cv).

C) Key Findings

Dewatering of argillaceous Merrimelia sediments, and not organic maturation or Warburton Basin carbonates, appear to be the main source of Mg^{2+} (and Fe^{2+}) ions for S2 siderite cement development in M2 and M3 sediments.

In M1 and T1 sediments organically derived acids appear to play the dominant role in providing Mg^{2+} and Fe^{2+} reactants for S2 siderite formation.

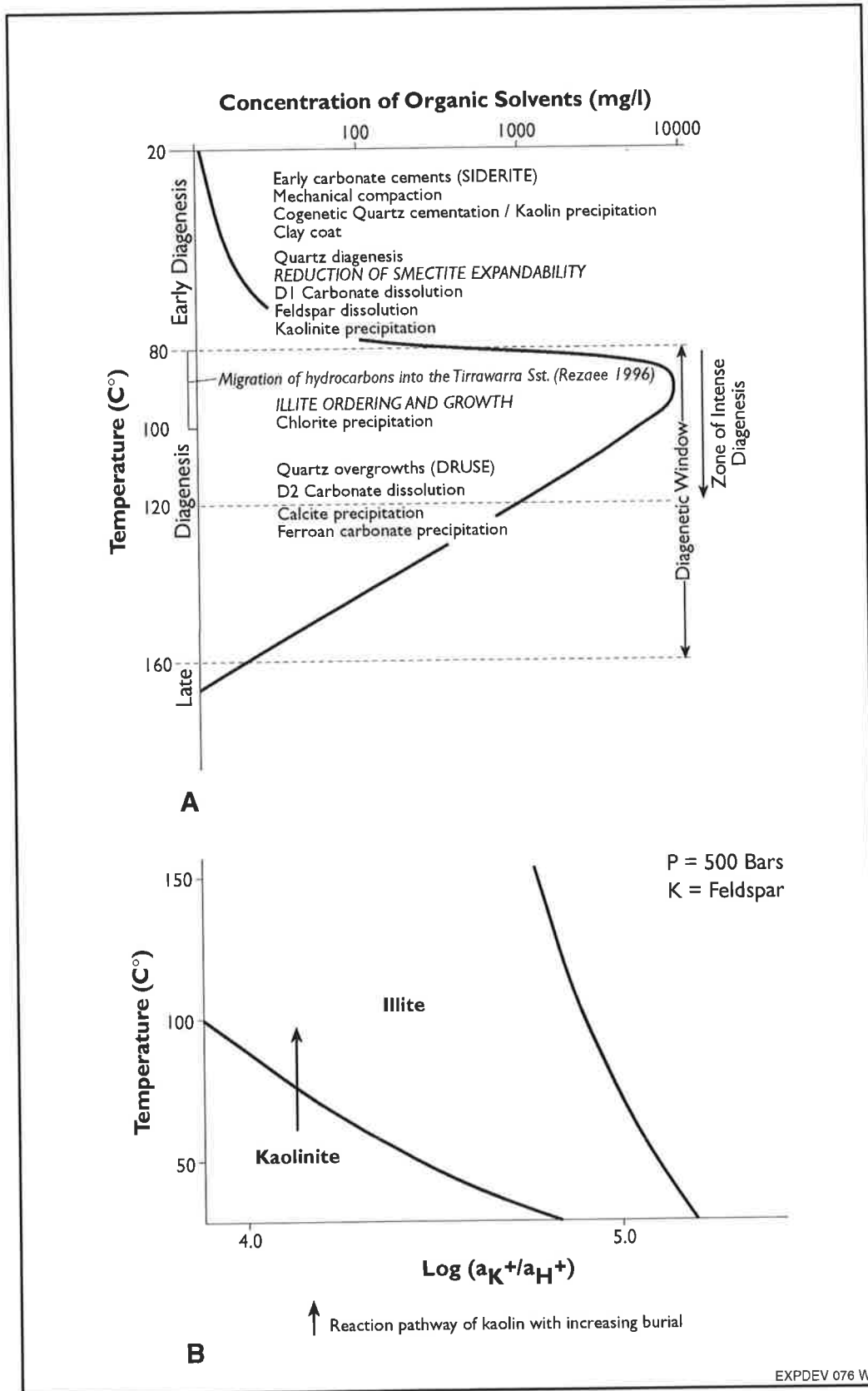


Figure 6.28 A) Organic maturation and the main diagenetic adjustments observed in the Merrimelia Formation (Modified from Surdam et al., 1989). B) Illite/kaolin stability diagram (From Cowan and Shaw, 1991).

6.3.4.4.4 D2 - Late Siderite Dissolution

A) Key Observations

In porous (M1) Merrimelia sediments the contact between S2 and S3 siderite is irregular (Fig. 6.8b'). In addition S2 cement is commonly etched (Fig. 6.8a) whereas S3 siderite is virtually devoid of pitting (Fig. 6.8a). Both observations point to a siderite dissolution event (D2) between the precipitation of S2 and S3 siderite.

In argillaceous Merrimelia sediments there is little evidence of a D2 dissolution phase between S2 and S3 siderite phases.

B) Discussion

Rezaee *et al.* (1997) and Rezaee (1996) describe a dissolution period (D2) between the precipitation of S2 and S3 siderite phases. This is based on the identification of dissolution edges on S2 siderite from samples in the Tirrawarra Sandstone at Tirrawarra, Fly Lake-Brolga and Moorari fields. These authors postulate that this dissolution phase broadly corresponds with the temperature of organic maturation (100°C) (Tissot and Welte, 1978), surmising that organic acids produced in this process have dissolved S2 carbonate (Surdam *et al.*, 1984; Schmidt and McDonald 1979). Petrological evidence (Rezaee, 1996) backs up the connection between organic maturation and D2 dissolution. That author recognised dead oil within inclusions between S2 and S3 cements concluding that oil generation was synchronous with the D2 dissolution event, and prior to S3 precipitation. This link suggests that organic acids formed during hydrocarbon generation and expulsion have dissolved S2 siderite prior to S3 formation (Fig. 6.28a).

Chamely (1989) relates water expulsion from the smectite illite transformation with hydrocarbon generation. This author concluded that the main expulsion of water from smectitic sediments during illitisation occurs around 90°C-100°C. Thus the peak of illitisation and water expulsion coincides with D2 dissolution and hydrocarbon charge. It follows then that water expelled from the smectite to illite reaction may have provided the media for transportation of organic maturation products (acids and hydrocarbons) and in the processes has indirectly helped dissolve S2 siderite cement.

The supply of organic acids from maturing Patchawarra and Tirrawarra organic matter most likely increased pore water acidity in Tirrawarra sediments forming a uniform D2 dissolution event (Fig. 6.9b). In Merrimelia sediments the upper more porous facies (proglacial) register an D2 dissolution phase (Fig. 6.8b[4e]), whereas,

non-permeable Merrimelia sediments (terminoglacial) may, or may not, register a D2 dissolution event depending on the infiltration of acidic fluids through the muddy sediment pile (Fig. 6.8a[Inset A]). The local supply of organic acids in terminoglacial sediments is minimal.

C) Key Findings

In porous Merrimelia sediments, organic acids formed during hydrocarbon generation and expulsion have most likely dissolved S2 siderite prior to S3 precipitation.

Variable organic content may also contribute to the sporadic nature of D2 siderite dissolution in Merrimelia sediments.

6.3.4.4.5 S3 Siderite Formation

A) Key Observations

S3 siderite in the Merrimelia Formation appears as a blocky and homogenous carbonate cement (Fig. 6.8a) indicative of little fluctuation in pore water chemistry, in contrast to the highly variable S2 siderite.

B) Discussion

The Mg^{2+} content of S3 siderite varies little, indicating that the supply of ions was relatively constant (Fig. 6.27h). The initiation of illite formation from pore waters (neof ormation) coincided with the growth of S3 siderite (Fig. 6.27a & 6.27b). This suggests there may be a link. The secession of illite production from smectite transformation reduced the amount of Mg^{2+} available for siderite. This reaction does proceed past 100°C but at a much reduced, rate as almost all of the mixed layered clay has been transformed to illite. It is postulated here that the remaining Mg^{2+} from this ongoing reaction is incorporated into S3 siderite at a low but constant rate (Table 6.14 illustrates typical S3 $MgCO_3$ compositions).

The smectite-illite reaction is supplanted by the formation of illite from pore waters. The authigenesis of neof ormed illite according to Huang *et al.* (1986) Small *et al.* (1992) and Reed and Hajash (1992) relies on mildly acidic conditions. The abundance of neof ormed illite is testament to the acidity of pore waters during later diagenesis. In this acidic environment sideritic cements would be expected to dissolve. The appearance of S3 siderite contradicts this, indicating minor dissolution only (Fig. 6.8a). This suggests that here must be a carbonate buffer that enables late siderite (S3), calcite and ferroan dolomite to form. The most likely acid-consuming reaction in the

later stages of diagenesis is the neoformation of illite. The pervasive nature of this reaction in Merrimelia sediments has most likely had the effect of lowering pore water acidity making it possible for S3 siderite and other late diagenetic phases to form and be preserved.

C) Key Findings

S3 siderite formation in Merrimelia sediments has a consistent composition (unlike S2 siderite) coinciding with the cessation of the smectite to illite transformation. Mg^{2+} from this ongoing, but diminished reaction, is incorporated into S3 siderite at a constant rate.

The neoformation of illite is an acidity buffer, allowing S3 siderite to form and be preserved with minimal etching.

6.3.4.4.6 Calcite (Twinned, "Cowpat") Formation

A) Key Observations

Calcite in Merrimelia sediments is observed in two forms:

- 1) Poikilotopic cement filling porosity and overprinting earlier formed carbonate, quartz overgrowths and clay minerals (Plate 34a).
- 2) Concentric siderite-calcite-illite cement ("cow pat") (Plates 34c & 34e).

B) Discussion

The existence of calcite in Merrimelia sediments as twinned poikilotopic to sub-poikilotopic crystals and concentrically zoned cement ("cow pat" cement) is dependent on calcite stability. Wood and Hewitt (1984) and Blatt (1979) describe calcite solubility as being retrograde, as calcite solubility decreases as burial temperatures increases. Thus calcite precipitation occurs more readily with depth. Surdam *et al.* (1989) stated that the solubility of calcite depends on more parameters than just temperature alone. The solution pH also exerts a strong influence, and can reverse the retrograde solubility of calcite. Calcite solubility is therefore controlled by pH and temperature where calcite precipitation above 100°C is internally buffered and calcite solubility suppressed (precipitation accentuated) (Surdam *et al.*, 1989).

Petrographic observations indicate that calcite is indeed a late precipitate (Fig. 6.31b) in Merrimelia sediments, replacing remnant feldspar grains and siderite phases (Plate 34b). The ions necessary for calcite formation are thus unlikely to be organically derived.

PLATE 34**Authigenic Mineral: Calcite**

A) Photomicrograph – Tinga Tingana #1 (2094.35m) (Cross nicols x10). Twinned poikilotopic to sub-poikilotopic pore filling calcite cement.

B) Photomicrograph – Lake Hope #1 (2493.70m) (Cross nicols x20). Calcite replacement of sparry and micritic siderite cement.

C) Photomicrograph – Merrimelia #5 (2627.89m) (Cross nicols x10). Concentric calcite/illite cementation (“cowpat calcite”) [8e], surrounded by poikilotopic calcite cement [13c].

D) Photomicrograph – Merrimelia #5 (2627.98m) (CL x 5). Broad view of poikilotopic calcite cement, with concentric calcite/illite cement patches within oversized pore space. Dissolving feldspar grains are thought to provide the nucleation sights for these concentric cement patches as well as a localised supply of calcite and illite cations.

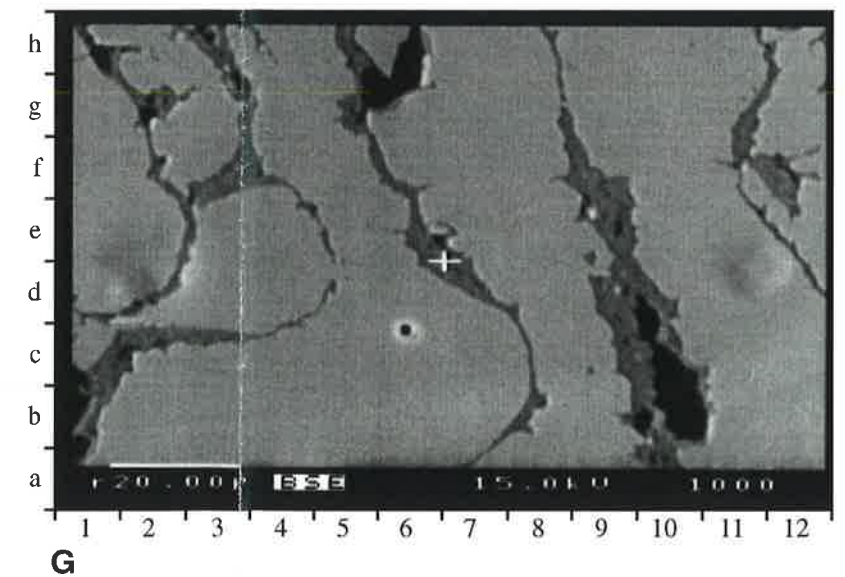
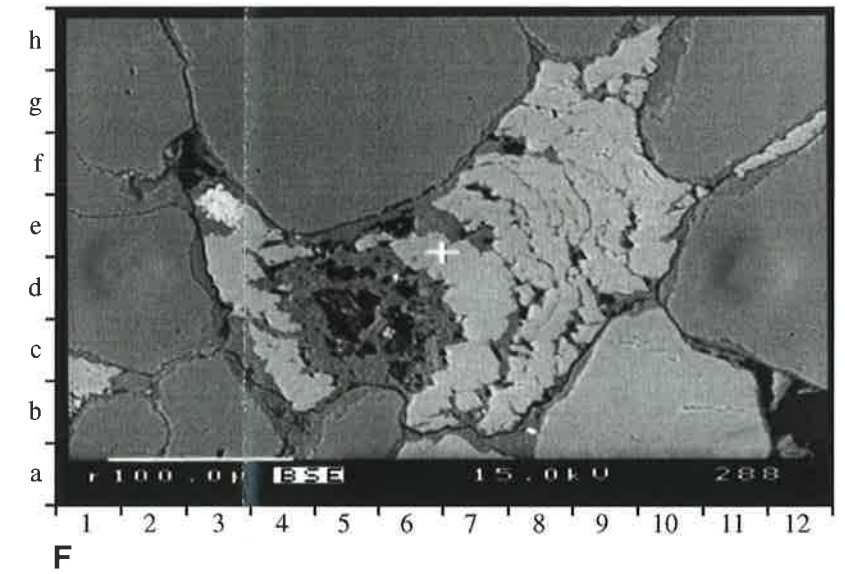
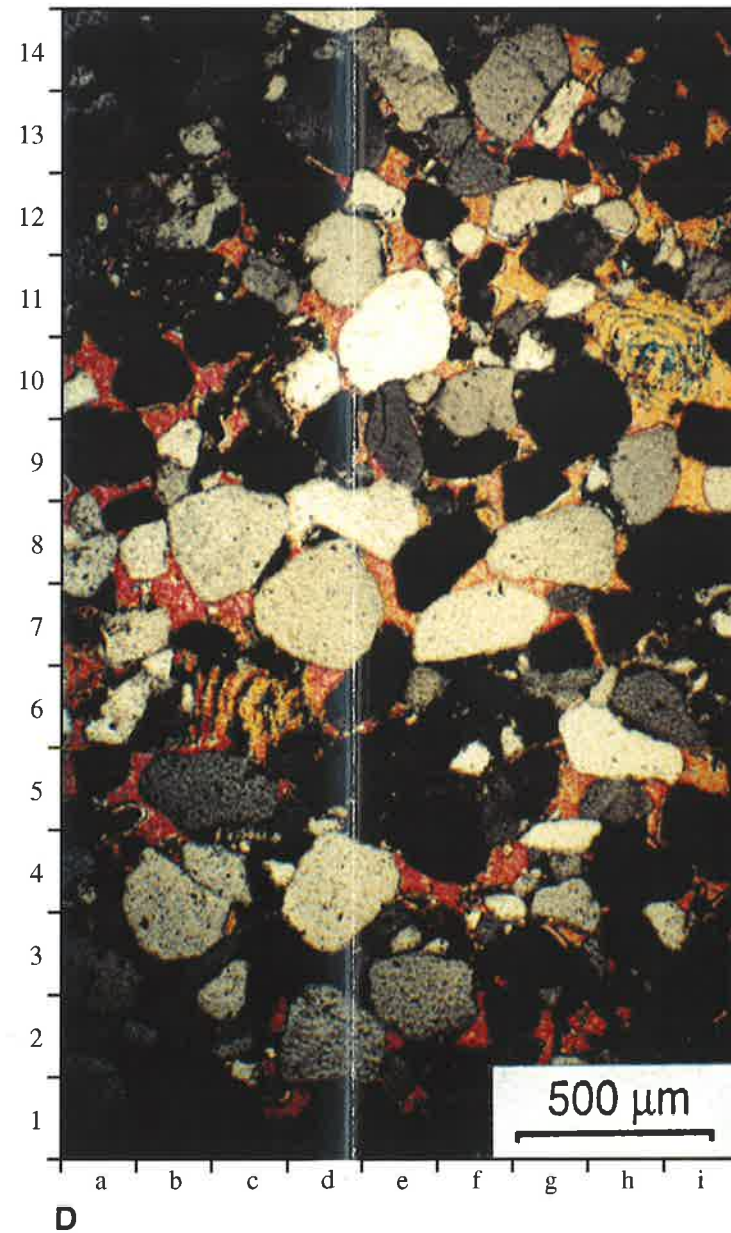
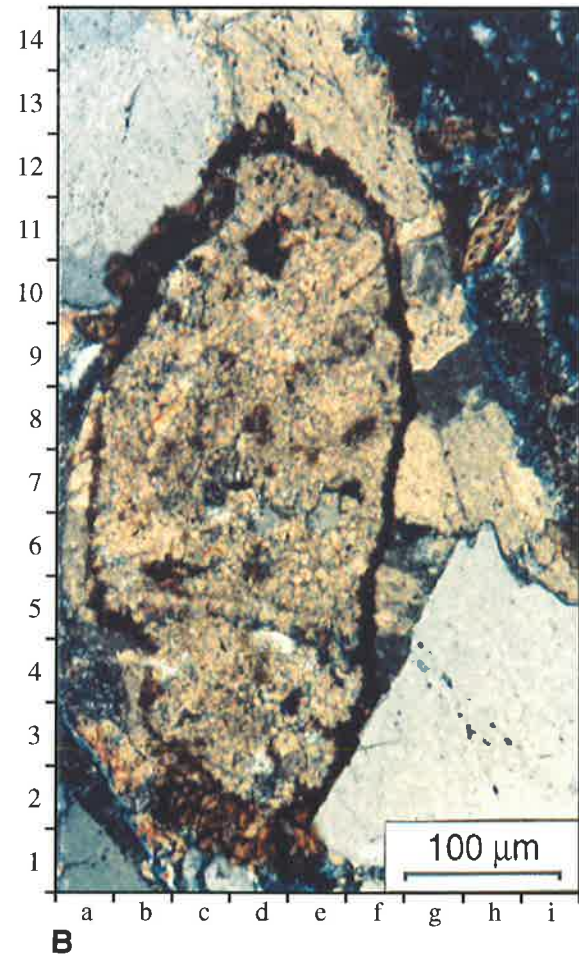
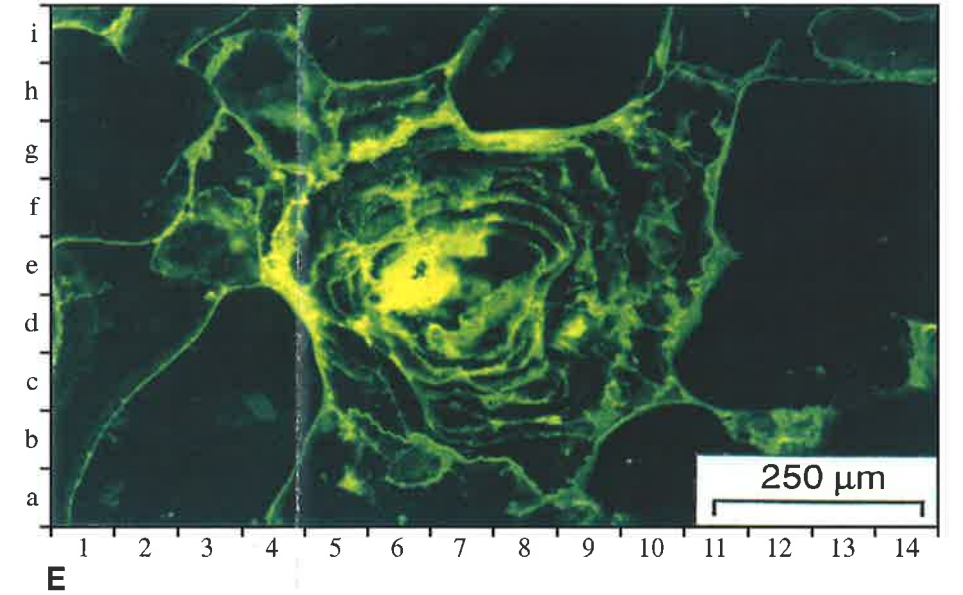
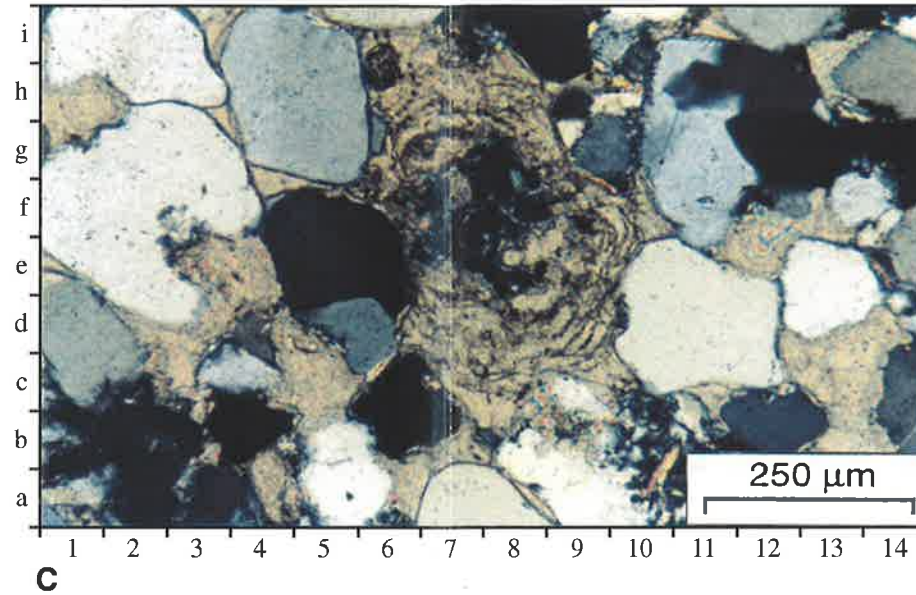
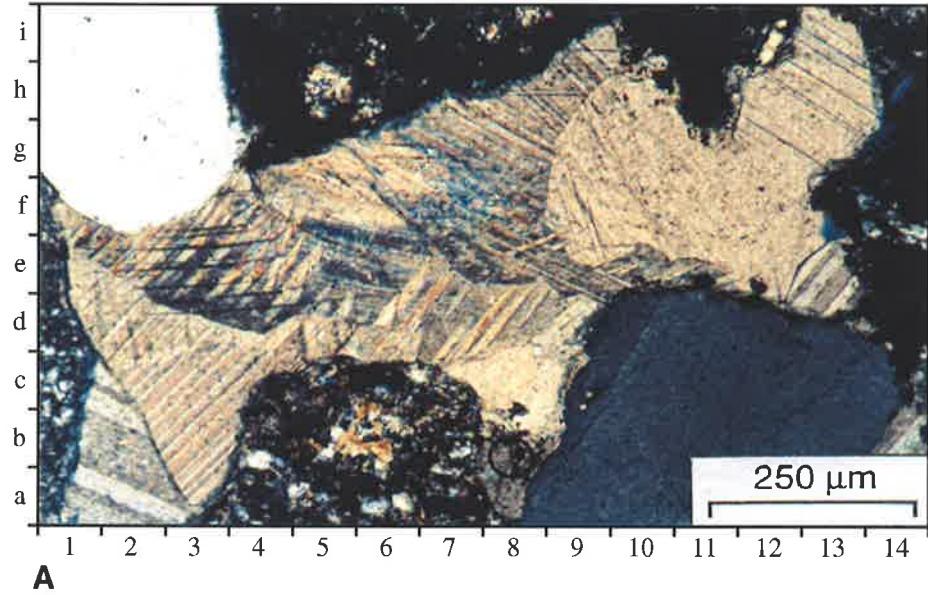
E) Photomicrograph – Merrimelia #5 (2627.98m) (Fluoro x 10). Close up view of concentric “cowpat calcite” illustrating the entwined formation of illite (green) and calcite (black).

F) BSE Image – Merrimelia #5 (2627.89m). Broad view of a “cowpat calcite” indicating where an EDAX spot composition was taken (cross). The composition at the point marked corresponds with the “cowpat calcite” composition in Table 6.15.

G) BSE Image – Merrimelia #5 (2627.89m). Broad view of a “cowpat calcite” indicating where an EDAX spot composition was taken (cross). The composition at the point marked corresponds with the “cowpat illite” composition in Table 6.15.

Table 6.15 – Composition of “cowpat calcite” and “cowpat illite”.

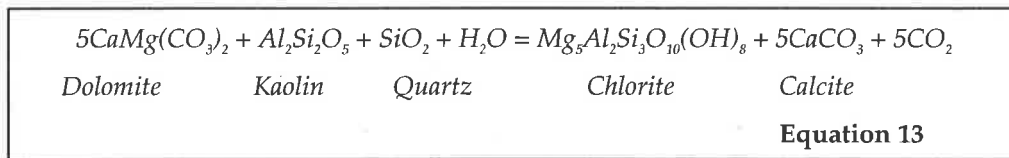
Plate 34



	MgCO ₃	CaCO ₃	MnCO ₃	FeCO ₃	SrCO ₃						
'Cow Pat' Calcite	0.00	97.36	0.43	2.21	0.00						
'Cow Pat' Calcite	0	97.76	0.30	1.93	0						
	SiO ₂	TiO ₂	Al ₂ O ₃	MgO	CaO	MnO	FeO	Na ₂ O	K ₂ O	H ₂ O	
'Cow Pat' Illite	38.92	0.00	24.99	1.19	4.03	0.01	1.22	0.27	7.53	0.00	
'Cow Pat' Illite	39.01	0.06	25.11	1.18	4.03	0.01	1.18	0.24	7.21	0.19	

Table 6.15 Composition of 'Cowpat' Illite and Calcite (Wt%)

Walderhaug and Bjørkum (1992) discuss at length possible sources of Ca²⁺ ions for calcite formation. Likely sources discussed by these authors include, feldspar dissolution, heavy mineral and mica destruction. In Merrimelia sediments these minerals represent a very small proportion of the detritus (Fig. 5.1), a proportion that is however comparable to the amount of authigenic calcite observed. The consistent association with previous carbonate phases (Plate 34b) and illite (Plate 34e) suggests that Ca²⁺ derivation may be linked and that Ca²⁺ from the destruction of accessory minerals is unlikely. Hutcheon *et al.* (1980) link the formation of dolomite and late stage chlorite with calcite formation (Equation 13).



This reaction maybe a possible source of both calcite and chlorite, but dolomite exists only in small proportions, limiting the products of this reaction (Chlorite and calcite are rare authigenic minerals). The association of chlorite and calcite, which would be expected if this reaction were to proceed, is not well established but, poikilotopic calcite has been observed filling pore space between basic, chloritised rock fragments suggesting a link (Plate 34a).

More commonly, calcite is associated with siderite and not basic or chlorite altered rock fragments indicating that the aforementioned carbonate phase is cannibalising the earlier formed siderite. The source of Ca²⁺ ions in this scenario may be related to the transformation of smectite to illite (Equation 6) or sourced externally from solution.

Surdam *et al.* (1989) indicates that calcite dissolution will occur at a late stage (120°C-160°C) as Pco₂ increases. The presence of calcite in Merrimelia sediments may indicate that Pco₂ levels have remained subdued or that the limited calcite observed in Merrimelia sediments exists at depth because of the impermeable nature of these sediments.

i) "Cowpat" Calcite

For the most part calcite formation can be explained in terms of associations with siderite, chlorite and feldspar. In the glacio-aeolian sandstones of the Merrimelia Field a unique pore filling calcite/illite cement ("cowpat") was observed (Plate 34d).

"Cowpat" cement authigenesis is unlike all other cements encountered in the Merrimelia Formation as calcite and illite cement phases form around a nucleating particle in the centre of pores in a roughly concentric pattern (Plate 34e), similar to that illustrated in (Fig. 6.8a), where further cement growth infills pore spaces. The distribution and shape of "cowpat" cements (Plate 34d) is suggestive of feldspars that have been destroyed. Dissolved feldspars are commonly observed in the aeolian sandstone (Plate 32c). The ionic products from this dissolution (Equation 8) may have provided the local products needed for "cowpat" formation. Walderhaug and Bjørkum (1992) recognise dissolving K-feldspars as a possible source of Ca^{2+} for calcite formation, albeit a minor one. It is possible that the dissolution of feldspars in these aeolian sandstones may have provided the Ca^{2+} needed for concentric calcite formation. The illite between calcite rings (Plate 34e), is most likely formed from products released via illite transformation of the original grain coating smectite which surrounds all framework grains (Plate 21c).

The initial stage (nucleus) of carbonate cement in "cowpat" cement is sideritic in composition (S1) and has, in most cases, been almost entirely dissolved (Plate 34c[8f]). Subsequent concentric cement phases are composed of alternating illite and calcite cements that entirely fill in the pore space, with the last calcite cement phase forming part of an extensive poikilotopic calcite cement (Plate 34d). The sequence of "cowpat" illite/calcite cement formation is as follows:

- 1) Smectite to illite precipitation releases Fe^{2+} , Ca^{2+} and Mg^{2+} ions (Equation 6) in a slightly acidic low fluid flow environment (Huang *et al.*, 1986). The illite forms around a nucleus, which is normally S1 siderite. The acidic pore waters partially dissolve the siderite cement.
- 2) As illite reactants are used up and S1 siderite is dissolved, the pH of the pore water becomes more alkaline and enriched in Ca^{2+} , Mg^{2+} and Fe^{2+}
- 3) The change to alkaline pore waters stops illite precipitation and siderite dissolution. The reactants mobilised by illite formation/siderite dissolution, combine to form calcite.
- 4) Calcite forms until the local supply of reactants are used up. The pore water becoming more acidic until calcite starts dissolving in the increasingly more acidic pore waters. This dissolution is indicated by the irregular edges of the concentric calcite rings (Plate 34f).
- 5) As the acidity of the pore water increases, Si, Al and K reactants are introduced into the system. These ions are possibly sourced from the dissolution of adjacent K-feldspars and/or the illitisation of grain rimming smectite. Illite then forms on the surface of the last partially dissolved calcite cement phase.

- 6) This process is repeated as many as ten times to form the distinctive pore-filling "cowpat" illite/calcite cements.

The process outlined above maybe explained by the experimental observations of Huang *et al.* (1986). These authors stated that the most favourable conditions for the neof ormation of illite is the rapid release of Al and other clay reactants into the system (step 5) followed by the rapid withdrawal of these components to form an essentially alkaline solution (steps 1 & 2).

Oscillating acidic/alkaline pore water chemistry is controlled by the periodic input of illite forming cations into an essentially carbonate forming system. The controls on the oscillation of water chemistry in these sandstones is conjecture, but is possibly controlled locally, with water chemistry changing as localised ionic sources are exhausted and replenished. An external control is equally valid, where the production of organic acids in surrounding sediments changes pore water pH (Fig. 6.27a). It is most likely that a combination of external and internal controls dictate the oscillation of pore water chemistry in aeolian sandstones.

C) Key Findings

Ca⁺ ions for twinned calcite cement precipitation are most likely derived from:

- 1) Earlier formed siderite,
- 2) The smectite/illite transformation,
- 3) Breakdown products from organic maturation.

Concentric cement patches observed in Merrimelia sediments at Fly Lake and Merrimelia Fields are composed of a siderite nucleus which is engulfed alternating calcite cement and illite. The alternating mineral assemblage of "cow pat" cement reflects oscillating water chemistry which is most likely related to local variations in pore water pH.

6.3.4.4.7 Ferroan Dolomite Authigenesis

A) Key Observation

Ferroan dolomite is generally observed forming after S3 siderite (Fig. 6.10).

B) Discussion

Figure 6.10 illustrates dolomite growing around the etched edges of S3 siderite cement (Fig. 6.10[Inset]). There is however, a suggestion that S3 siderite in fact overlies what would be an earlier formed dolomite crystal (Fig. 6.10[Inset]). However,

the S3 boundary, in the same image, appears to represent a dissolution edge with dolomite having formed after S3 siderite on this dissolution surface. This apparent ambiguity has made the exact relationship between ferroan dolomite and siderite hard to confirm. The majority of textural observations suggest however, that the earliest precipitated ferroan dolomite formed penecontemporaneously with or just after the latest formed S3 siderite.

Microprobe and SEM/EDAX analyses indicate that dolomite cements in Merrimelia sediments are high in iron (Fig. 6.10). The origin of high amounts of Fe^{2+} maybe related to a number of sources. The production of Mg^{2+} from smectite-illite reaction has been postulated by Stewart, (1986) as the possible source of dolomite cement in the Fulmar Formation of the North Sea. Boles and Franks, (1979) also suggested that the smectite to illite reaction may provide ions necessary for dolomite (and siderite) formation. The formation of dolomite after S3 siderite indicates that dolomite formation has occurred after the main phase of smectite-illite transformation. This would limit the supply of Mg^{2+} and Fe^{2+} from this source. Stewart (1986), suggested that Mg^{2+} , Ca and Fe^{2+} for dolomite authigenesis can be supplied via organic matter maturation. The absence of organic matter in Merrimelia sediments indicates that this ionic source would be negligible. Rezaee, (1997) in a study of fracture fill cements in Warburton Basin sediments observed ankerite cement in McKinlay #1 well. It is possible that iron from dissolving high Mg/Fe carbonates of the Warburton succession, maybe a source of Mg^{2+} and Fe^{2+} for ferroan dolomite in Merrimelia sediments. The distribution of high Fe^{2+} carbonates in Warburton sediments is unknown thus attributing Warburton Basin carbonates with supply of ions for Merrimelia carbonates is speculation.

C) Key Findings

The almost exclusive association of ferroan dolomite and siderite indicates that there is a link. The most likely source of ions for ferroan dolomite is probably the dissolution of earlier formed S2 siderite (D2 dissolution) which is dissolved locally and precipitated nearby enriched in Fe^{2+} and Mg^{2+} .

Ferroan dolomite formed coincident with or just after the latest formed S3 siderite.

6.3.4.5 Secondary Porosity Formation

6.3.4.5.1 Key Observation

Porosity is generally low in Merrimelia sediments (Table 6.16) accounting for just over 10% of the total rock volume. Secondary porosity is twice as voluminous as

primary pore space; a product of primary pore space destruction via mechanical compaction and authigenic mineral formation.

Authigenic mineral formation in Merrimelia sediments is dominated by clay, the most prevalent of which is illite, with subordinate kaolin. Micro-pore space associated with illite is not effective in hydrocarbon terms (see Chapter Nine) and is not included in calculating the proportion of secondary micro-porosity. Micro-pores between kaolin booklets represent effective pore space (see Chapter Nine) and are included in secondary pore space calculations.

6.3.4.5.2 Discussion

The amount of micro-pore space in kaolin masses of the Tirrawarra Sandstone was estimated at 20% of the total effective pore space (Rezaee, 1996). Using this approximation, the effective secondary porosity component in Merrimelia sediments is dominated by kaolin micro-pore space (Table 6.16). Dissolution secondary pore space (macro) is subordinate (Table 6.16).

POROSITY TYPES IN MERRIMELIA SEDIMENTS	
Primary	Average Percentage (Whole Rock)
Interstitial	1.9
Intraclast	0.1
Primary Sub-Total	2.0
Secondary	
Macro	4.5
Micro (Kaolin)	1.5
Moldic	0.3
Intraclast	0.1
Secondary Sub-Total	6.4
Total Porosity	8.4

Table 6.16 *Proportion of porosity types in the Merrimelia Formation.*

Bloch (1994) stated that the maximum amount of moldic porosity, is a function of the abundance of mechanically rigid grains (Figure 6.29). Merrimelia sediments are, in the main, dominated by ductile grains or matrix thus the preservation of moldic pore space is rare (Table 6.16).

Pore fluids derived from acidic meteoric waters promote the alteration of feldspars and form kaolin at an early diagenetic stage. Hence kaolin micro-porosity represents early-formed secondary porosity. Dissolution of carbonate cement, rock fragments and rock fragment components occurs at a middle to late diagenetic stage when

maturation of organic matter releases organic acids. The scarcity of organic matter in terminoglacial Merrimelia sediments however reduces dissolution and subsequently reduces secondary porosity generation.

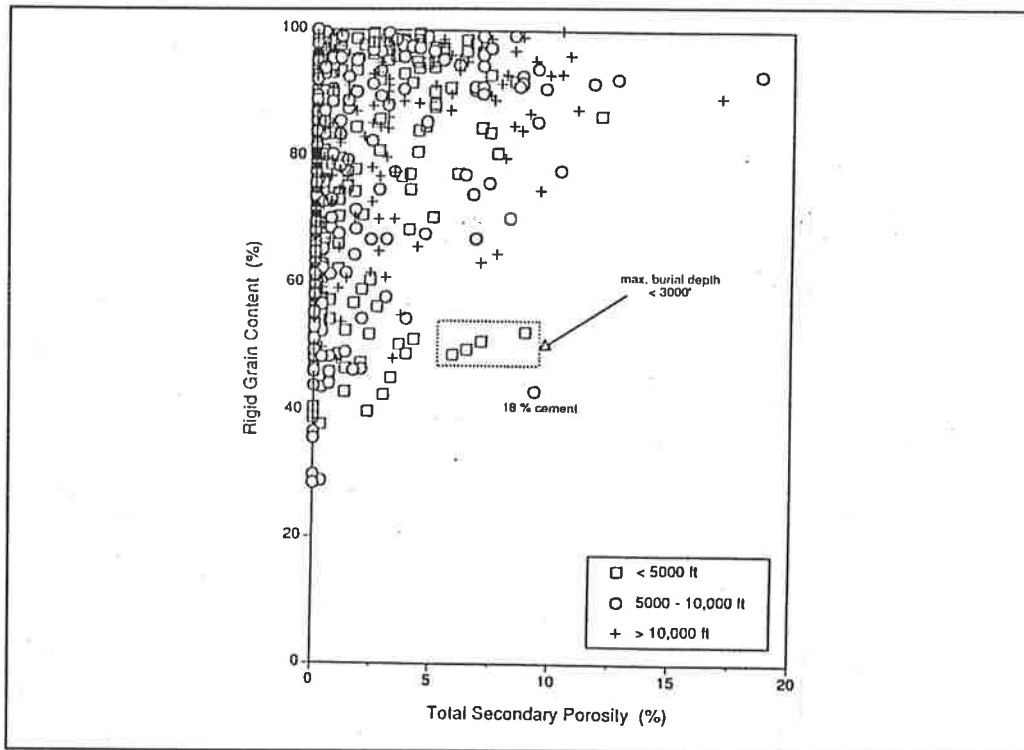


Figure 6.29 Scattergram of rigid grain content versus the maximum amount of secondary porosity (After Bloch, 1994).

The controls on porosity preservation and formation (primary and secondary) in Merrimelia sediments are discussed in detail in Chapter Nine.

6.3.4.5.3 Key Findings

Effective secondary porosity is dominated by kaolin (macro dissolution porosity is rare) and therefore mainly occurs in porous (proglacial) M1 sediments. Illite micro-porosity dominates M2 and M3 but is regarded as ineffective.

6.3.4.6 Feldspar Overgrowths

6.3.4.6.1 Key Observations

SEM analysis suggests that feldspar overgrowths may occur in Merrimelia sediments (Fig. 6.30a). They appear to only develop in sediments that are rich in volcanic rock fragments.

6.3.4.6.2 Discussion

McBride (1989) and Schluger (1979) suggested that the breakdown of glassy shards and acidic volcanic rock fragments promote the liberation of alkali earth cations which are then free to be incorporated into authigenic clays, zeolites and authigenic feldspars.

6.3.4.6.3 Key Finding

There maybe a link, but only a few feldspar overgrowths were observed and any diagenetic link with disintegrating acidic volcanic rock fragments was unable to be confirmed.

6.3.4.7 Pyrite Authigenesis

6.3.4.7.1 Key Observations

Pyrite occurs in two forms, framboidal aggregates (Plate 17c) and poikilotopic cement of varying extent (Plates 24a & 24b). Framboidal pyrite aggregates are an early formed phase, whereas poikilotopic pyrite is a late stage authigenic precipitant, which overprints all other authigenic phases and detrital grains (Plate 24b)

6.3.4.7.2 Discussion

The iron needed for poikilotopic pyrite formation may have been released from limited late stage siderite dissolution (seen as small pits in S3 cement Fig. 6.8a[12i]) and conserved by late stage pyrite cement (Plate 24b) (Boles, 1984). Dixon *et al.* (1989) concluded that, at higher temperatures, the reactants necessary for pyrite formation are released by complexing with organic acids. If sulfur is present, pyrite will form, especially in the reducing conditions existing at depth. The controls pertaining to the origin of sulfur has not been addressed with any certainty. There does however appear to be an association between acid volcanic rock fragments and pyrite (see Appendix 9a-Malgoona #4 lithological log). The presence of late pyrite in the majority of samples does (Fig. 6.30b) suggest that the source of sulfur for pyrite formation is consistent (unlike the distribution of acid volcanic rock fragments) across the entire basin.

6.3.4.7.3 Key Finding

Late stage pyrite formation in Merrimelia sediments is possibly linked to:

- 1) The break down of acid volcanic rock fragments (M2 and M3 sediments).
- 2) The maturation of organic matter (Tirrawarra and M1 sediments).

6.3.4.8 Pyrophyllite Authigenesis

6.3.4.8.1 Key Observation

The formation of pyrophyllite is very rare, having been mostly observed in the vesicles of volcanic rock fragments (Fig. 6.30c).

6.3.4.8.2 Discussion

When not associated with volcanic fragments, pyrophyllite forms by the transformation of illite to pyrophyllite. This transformation process occurs at temperatures of greater than 300°C (Bjørlykke, 1984). Only the deepest buried Merrimelia sediments in the Patchawarra Trough have achieved temperatures high enough for this reaction to occur, thus the occurrence of this authigenic phase is restricted.

At these high burial temperatures, according to Bjørlykke (1984), not only will illite form pyrophyllite but kaolin can dehydrate and also form pyrophyllite. So at high temperatures both illite and kaolin may form pyrophyllite.

6.3.4.8.3 Key Finding

As pyrophyllite is commonly observed in the hotter Nappamerri Trough a better understanding of formation is possible (Schulz-Rojahn, 1991). This author concluded that pyrophyllite formed from kaolin and not illite, where the habit of the pyrophyllite did not reflect the precursor mineral.

6.3.4.9.1 Zeolite (?)

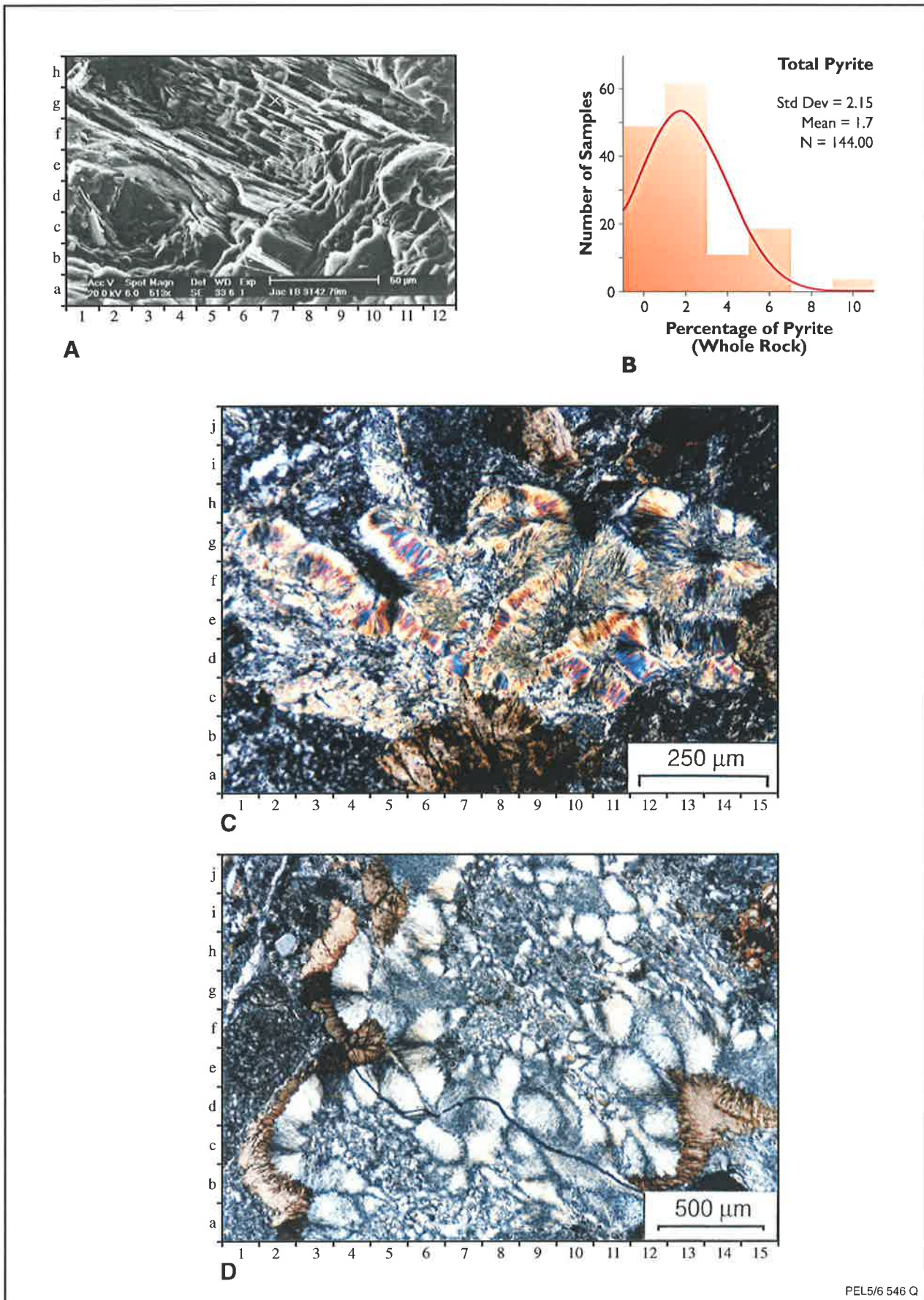
6.3.4.9.2 Key Observation

Figure 6.30[6d] illustrates a mineral that was exclusively observed with basic, vesicular rock fragments.

6.3.4.9.3 Discussion

Textural evidence suggests that this mineral phase is not authigenic but inherited, displaying neither illite nor pyrophyllite interference colours. The association of this mineral with basic volcanic rock fragments along with its crystal habit tends to suggest that this mineral maybe zeolitic in nature.

After inclusion into Merrimelia sediments, the zeolite(?) minerals have been partially replaced by siderite cement (Fig. 6.30[14d]) where the carbonate cement has assumed a similar crystal habit.



PEL5/6 546 Q

Figure 6.30 A) SEM photomicrograph - Jack Lake #1 (3142.79m). Close up of feldspar overgrowths, forming on the partially dissolved remnants of a feldspar grain. B) Frequency histogram. Pyrite mineral proportion in Merrimelia sediments. C) Photomicrograph - Gidgealpa #3 (2312.82m) (Cross nicols x 10). Pyrophyllite replacement of an illite filled vesicle within a basic volcanic rock fragment. The pyrophyllite in this case is detrital having formed prior to burial within the Merrimelia-Tirrawarra sedimentary pile. D) Photomicrograph - Gidgealpa #3 (2319.44m) (Cross nicols x 4). Detrital zeolite within a basic volcanic rock fragment. Note: The later crystallisation of siderite mimics the morphology of the zeolite [2b].

6.3.4.9.3 Key Finding

Zeolite minerals are inherited associated with basic volcanic rock fragments. Later formed siderite pseudomorphs this mineral phase.

6.4 PARAGENETIC SEQUENCE: REGIONAL VARIATIONS

Diagenetic reactions in arenaceous Merrimelia sediments are different from those in argillaceous sediments. The most obvious example of this is quartz precipitation, which is common in arenaceous units but rare in muddy intervals. Figure 6.31 illustrates the different paragenetic sequences for arenaceous and argillaceous rocks of the Merrimelia Formation.

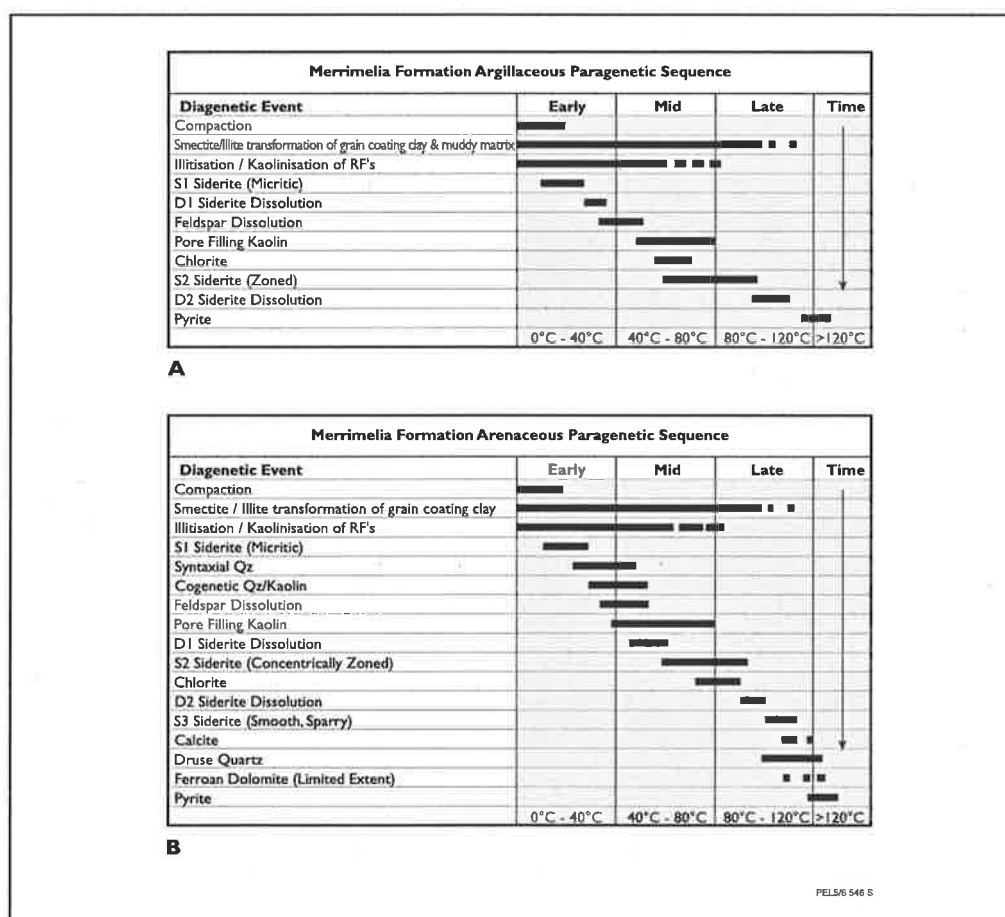


Figure 6.31 Paragenetic sequences in A) argillaceous and B) arenaceous Merrimelia Formation sediments.

The Merrimelia Formation is predominantly argillaceous in nature. The paragenetic sequence illustrated in, Figure (6.31a) is therefore applicable to most sediments in this study. Conversely, the paragenetic sequence illustrated in Figure (6.31b), is applicable

to upper, arenaceous Merrimelia sediments (M1) where interfingering with Tirrawarra sandstones dominates.

Chaney *et al.* (1997) describe the Merrimelia Formation as complex of laterally and vertically interfingering proglacial and terminoglacial facies. Regional variation in Merrimelia sediments is accordingly extreme. Areas such as the Merrimelia Field are dominantly arenaceous, whereas Merrimelia sediments in the Malgoona Field are dominated by muddy or clay-rich volcanoclastic conglomerates. The paragenetic sequence in Merrimelia sediments varies accordingly. Facies type, sediment composition (provenance) and thermal overprint all combine to produce local variations in the paragenetic sequence of Merrimelia sediments. These three parameters are thus the main controls on diagenesis in Merrimelia sediments. Figure 6.32 illustrates the variation in the Merrimelia paragenetic sequence across the basin where there is the greatest sample control, and in fields whose reservoir quality is investigated in detail (Chapter Nine).

6.5 FACIES CONTROLS ON DIAGENESIS

Sediment composition is controlled by facies type (Chapter Four), which in turn determines the kinds of diagenetic reactions that operate in a particular sediment, when buried. The composition of a sediment is widely reported in the literature to be one of the main controls on diagenesis (Blatt, 1979; Bodard *et al.*, 1984; Stonecipher *et al.*, 1984). In particular, the composition of sandstones is critical to which diagenetic mineral assemblage forms during sediment burial (Stonecipher *et al.*, 1984).

Chaney *et al.* (1997) concluded that rock-fragment-rich Merrimelia sediments have less quartz cement development as cementation sites are limited. The opposite is true for arenaceous Merrimelia sediments. These authors stated that sediment composition is controlled by thawing and freezing conditions relative to the position of advancing and retreating glaciers (Chapter Four). Burial diagenesis assemblages in the Merrimelia-Tirrawarra complex are, therefore, dictated by the position of glaciers.

The formation of kaolin or illite in the MTGC is an example of this; kaolin predominantly forms in the arenaceous Tirrawarra Sandstone and illite in the poorly permeable Merrimelia Formation.

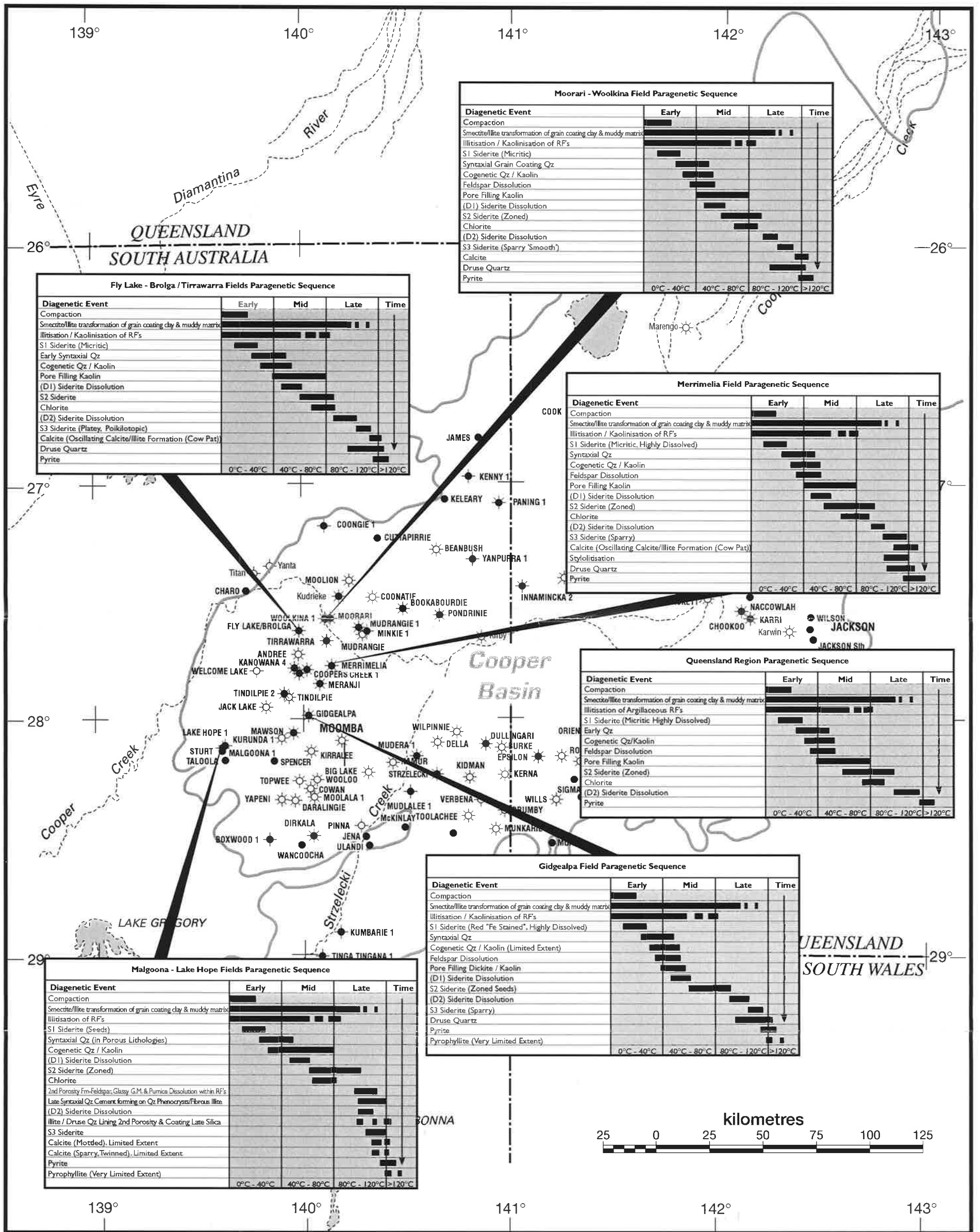


Figure 6.32 Regional paragenetic sequences of the Merrimelia Formation.

Observations by Rezaee and Lemon (1996a), confirm the facies control on burial diagenesis in Tirrawarra sediments, stating that the nature of the environments in which these sediments were deposited is the principle factor controlling the composition of framework grains and hence diagenesis.

In the Merrimelia Formation, like the Tirrawarra Sandstone, quartz and authigenic clay proportions are dictated by sediment composition and thus facies type (Figs. 6.33a & 6.33b). Ductile rock fragment proportions are predominantly controlled by facies type with the better sorted sediments containing the least amount of ductile clasts (Fig. 6.32c). The presence of ductile clasts promotes clay formation (Fig. 6.32d) (particularly illite), hastens mechanical destruction of primary pore space (Fig. 6.13a) and reduces rock rigidity.

6.6 DISTRIBUTION OF AUTHIGENIC MINERALS

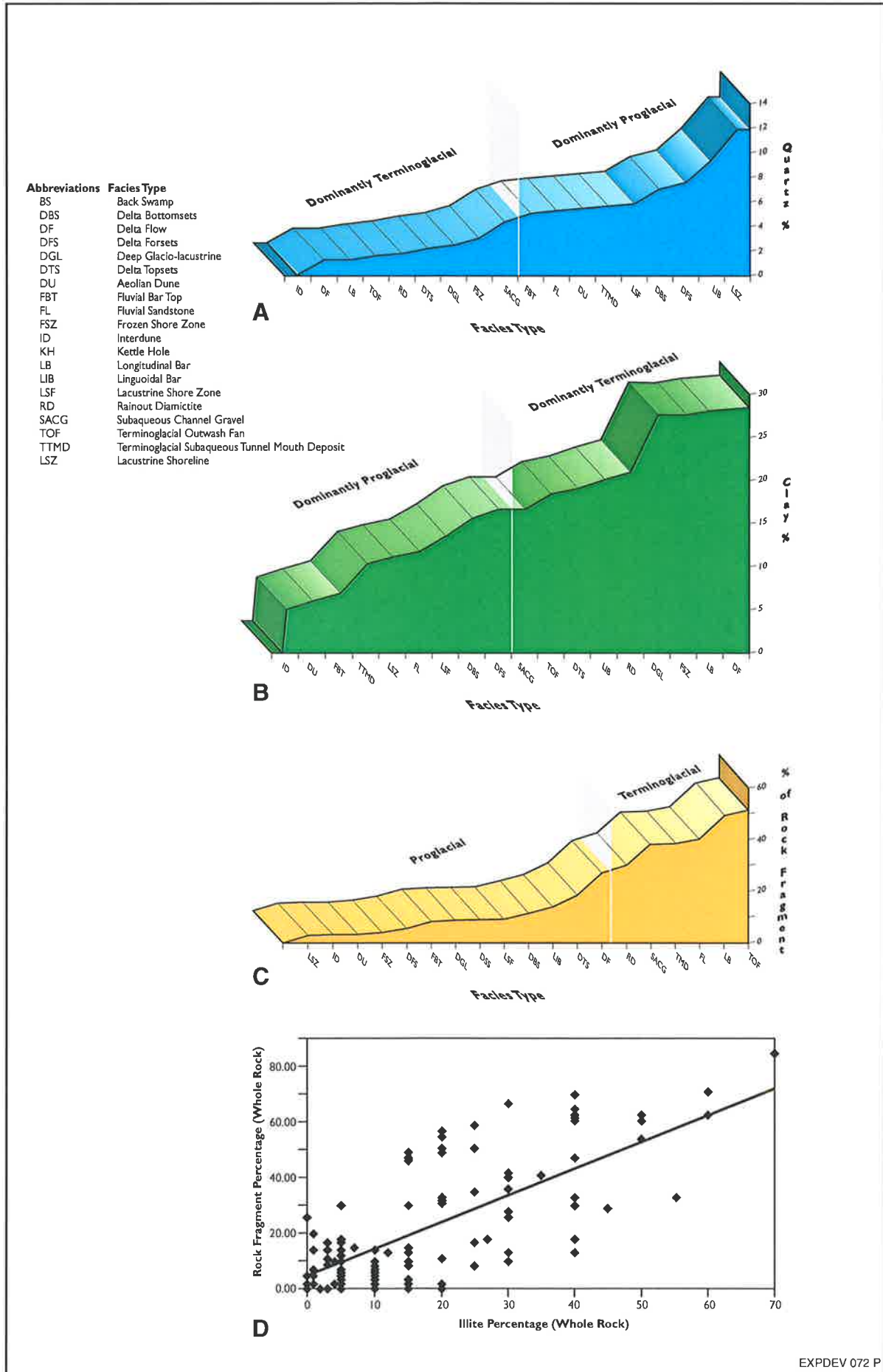
Petrological, SEM, XRD, TEM and microprobe data imply a connection between rock fragments and authigenic mineral production in Merrimelia sediments. Statistical analyses were also employed to test the results gained by analytical techniques.

The Pearson correlation coefficients of most mineral combinations are less than ± 0.2 (Appendix 8a). The exceptions are a negative correlation between quartz cement and illite (-0.443) and positive correlation between quartz cement and kaolin (0.252). These correlations are statistically significant at a 95% confidence level and match observed relationships (Figs. 6.34a & 6.34b).

The lack of correlations (negative or positive) reveals that there is considerable noise inherent in the authigenic Merrimelia mineral dataset. This noise is indicative of sampling an inconsistent (patchy) distribution of authigenic minerals within Merrimelia sediments. This inconsistency is a product of highly variable sediment compositions which in turn reflects the kaleidoscopic nature of facies architecture present in the Merrimelia Formation. The lack of meaningful correlations indicates that the sampled dataset is highly variable confirming petrographic and core logging observations.

Cluster analysis was performed on unstandardised⁷ quartz cement and clay data using the same method described in Chapter Two.

⁷ Unstandardised data were used in a Kolomogorov-Smirnov test, which indicated the data was not normally distributed (Fig. 6.1a).



EXPDEV 072 P

Figure 6.33 A) Cumulative histogram of quartz cement vs facies type (terminoglacal and proglacial). B) Cumulative histogram of total clay content vs facies type (terminoglacal and proglacial) C) Cumulative histogram of rock fragment proportion vs facies type (terminoglacal and proglacial). D) Cross plot of rock fragment proportion vs illite proportion.

This analysis reveals two clusters at an euclidean distance of 12 units (Fig. 6.35). The geographical spread of samples within each of the authigenic mineral clusters is however diverse, negating any reliable geographical interpretation of the data.

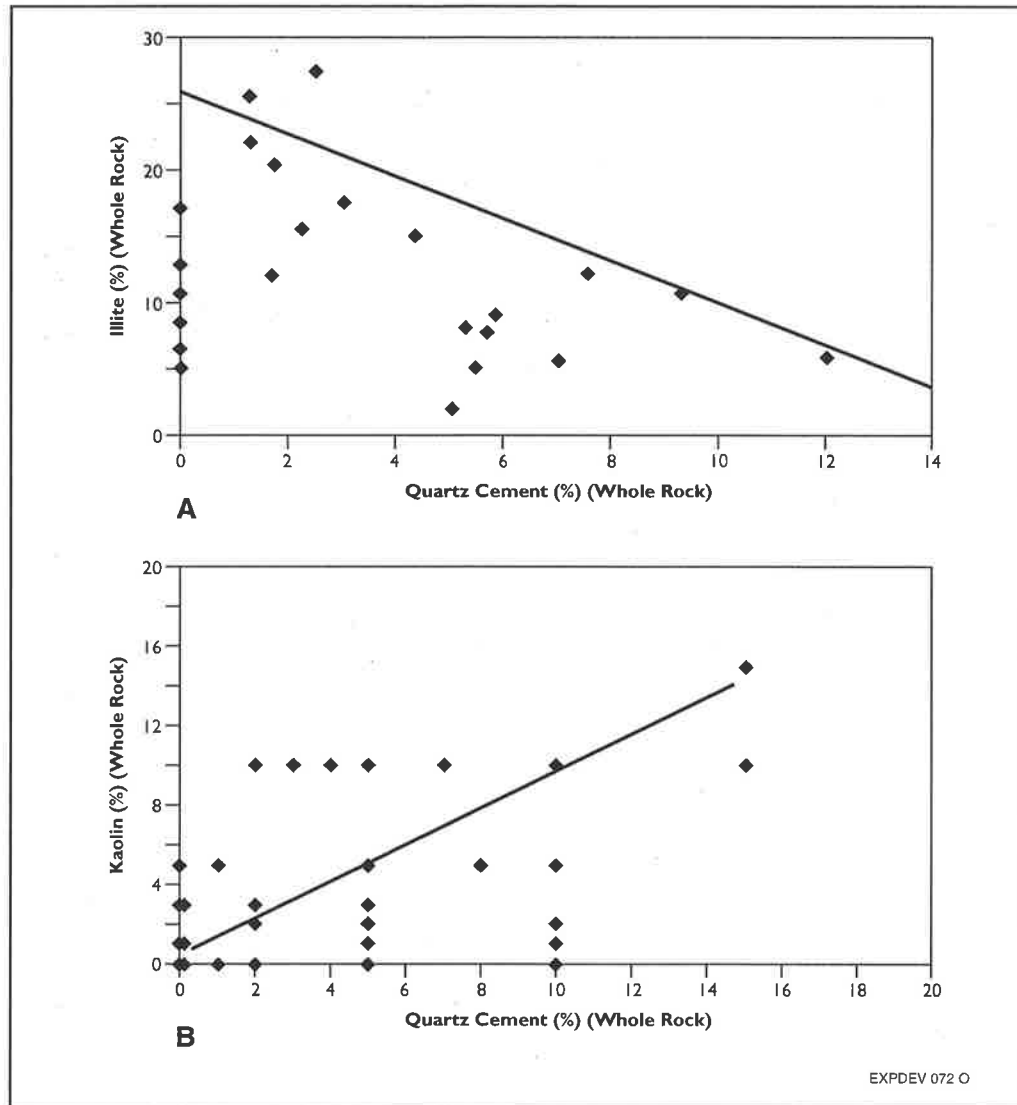


Figure 6.34 Scattergrams of A) illite versus quartz cement proportions and B) Quartz cement versus kaolin proportions in Merrimelia sediments.

It is unlikely in such sediments to observe strong correlations between authigenic minerals and geographical location. Despite this conclusion, the authigenic dataset was krigged and subsequently plotted in an attempt to better delineate trends within the authigenic dataset.

However, the “patchwork quilt” facies distribution of the Merrimelia Formation, combined with well spacing in the Cooper Basin, made mapping the areal distribution of authigenic minerals highly inaccurate.

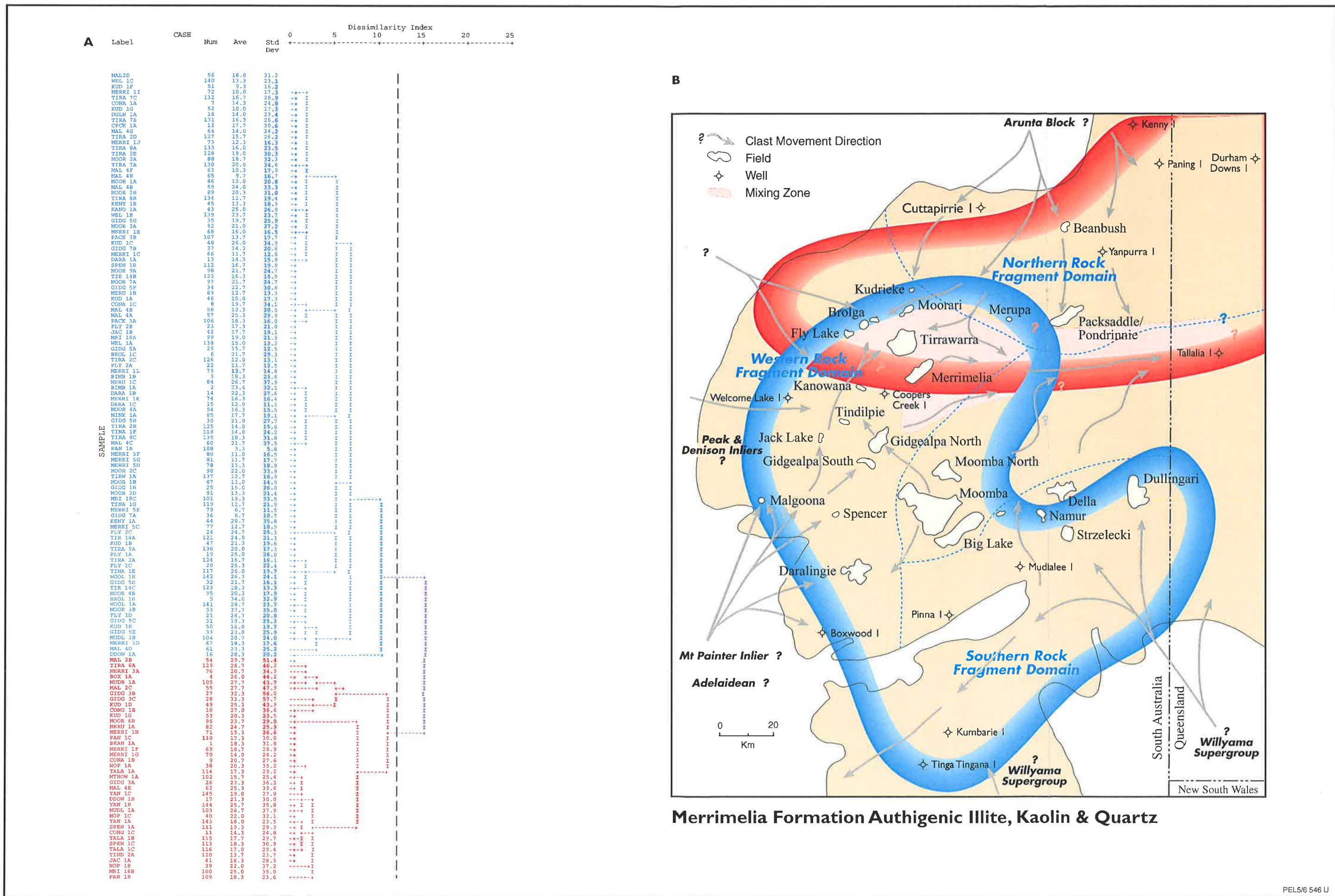


Figure 6.35 A) Cluster dendrogram of illite, kaolin and quartz authigenic phases. B) Rock fragment provenance map illustrating two overlapping clusters at a squared euclidean distance of 12 units (modified from Chaney et al., 1997).

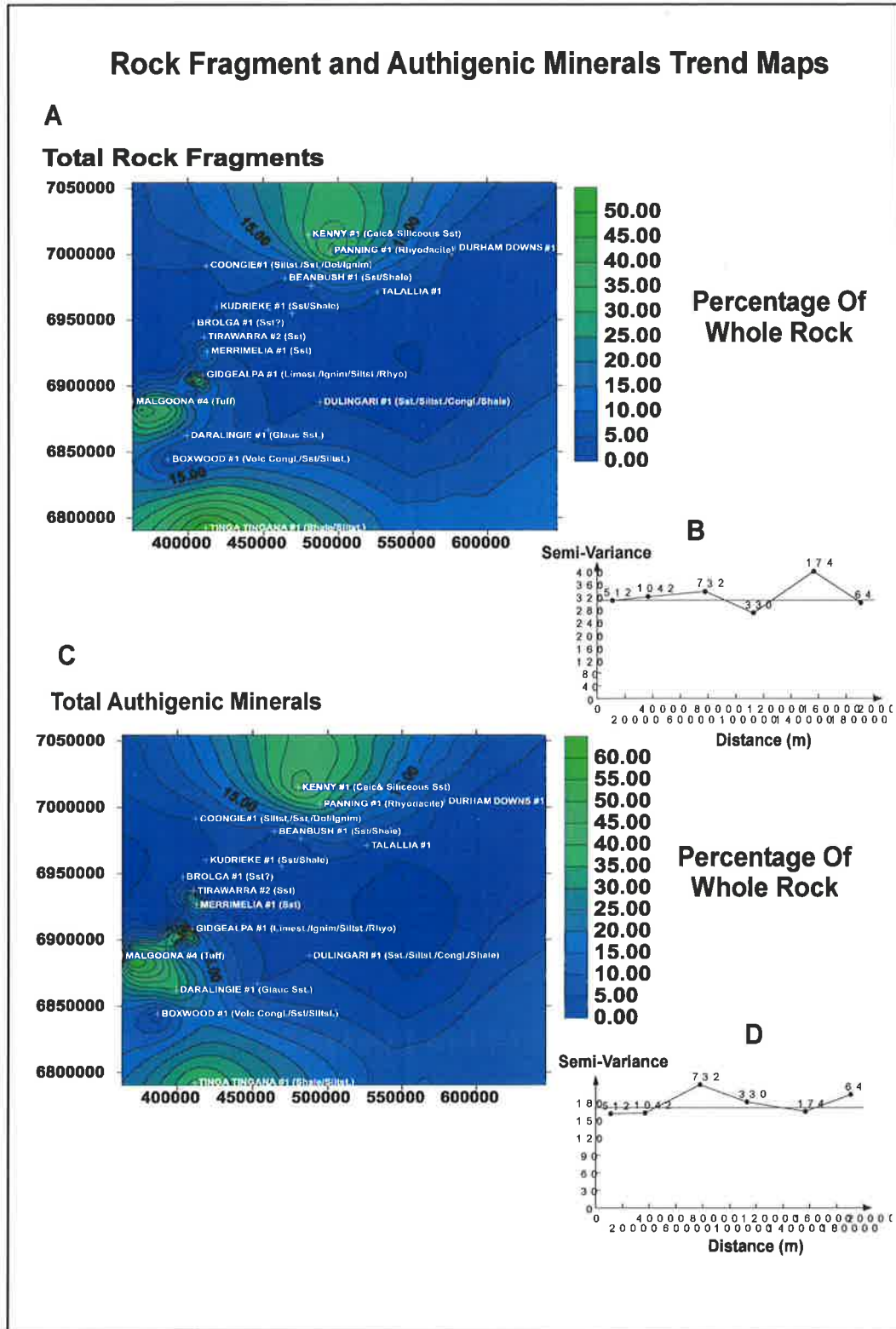


Figure 6.36 A) Total rock fragments (Merrimelia Formation) trend map. B) Total rock fragments (Merrimelia Formation) variogram. C) Total authigenic minerals (Merrimelia Formation) trend map. D) Total authigenic minerals (Merrimelia Formation) variogram.

Semi-variogram analysis of all three major diagenetic mineral groups (quartz, clay and carbonates) attest to this revealing nugget effects which approached 100% (Appendix 8c).

Therefore no attempt was made to map data of individual minerals. Krigging and plotting all authigenic mineral data (Figs. 6.36b) did however marginally improve the nugget effect (Fig. 6.36d) to 60%. The same krigging was performed on a combined rock fragment dataset (Fig. 6.36a) with semi-variogram analysis suggesting a 67% nugget effect on the data (Fig. 6.36c). The nugget effect on all maps in Figure (6.36) indicates that a detailed interpretation of the areal distributions will be highly inaccurate. The maps do however indicate trends in the dataset but not absolute values.

A comparison of data trends in the maps illustrated in Figure 6.36 show a very similar distribution. This similarity suggests that there is a relationship where elevated rock fragment content promotes the generation of authigenic minerals.

6.7 CONCLUSIONS

- Sediment composition, which is related to the position of glaciers, dictates diagenetic adjustments in Merrimelia sediments.
- Mechanical compaction is manifested in numerous forms within Merrimelia sediments. Pseudo-matrix formation and squeezing of ductile grain are the two most observed mechanical compaction effects. Grain squeezing drastically reduces pore space in sediments with a high rock fragment proportion (terminoglacial). Proglacial sediments, where meltwater rinsing dominates, have less pore space reduction by labile grain squeezing.
- Quartz overgrowths are rare in Merrimelia sediments, as sites for quartz cement growth are limited by the dominance of detrital argillaceous material and high proportion of labile rock fragments. Matrix mud and alteration clay effectively occlude pores during compaction.
- Silica for early quartz cementation was derived from;
 - 1) The dissolution of feldspars and,
 - 2) The conversion of smectite to illite.The latter process is the dominant source of silica for quartz cement in Merrimelia Formation sediments.

- Chemical compaction is the main source of later syntaxial and druse quartz cement. The reprecipitation of silica derived from quartz framework grains is envisaged to be temperature independent and linked to overburden pressures.
- Authigenic clays were the most pervasive authigenic phases observed in Merrimelia sediments. Illite was the most prevalent with kaolin the next most voluminous. Chlorite, glauconitic illite and dickite were seen in trace proportions.
- XRD and TEM analyses confirmed that illite in Merrimelia sediments is composed of 95% illite and 5% smectite, having a structural formulae that is consistent with that published in the literature.
- Illite exhibits an enormous range of forms. These differing illite forms were classified into three basic morphologies: filamentous, boxwork and platey. These three morphologies combine to form five basic illite textures; isolated fibers, flame/boxwork, honeycomb/boxwork, platey grain-coating and feldspar/rock fragment dissolution texture.
- The distribution of illite tends to mirror that of ductile rock fragments in the Merrimelia Formation indicating that there is a link between illite formation, rock fragment provenance, sediment maturity and reservoir quality.
- The transformation of smectite to illite during sediment burial is the dominant illite producing mechanism in argillaceous Merrimelia sediments and is indicative of illite formation in a closed system.
- The S/I transformation also operates locally in porous sediments, where the detrital components of argillaceous rock fragments and grain-coating clays convert from smectite to illite. This forms a substrate which commonly exhibits smectitic textures (flame boxwork), from which, neoformed filamentous illite grows. The neoformation of illite dominates porous Merrimelia pore spaces and is indicative of illite formation in an open system.
- Platey/filamentous illite is only observed in glacio-aeolian sandstones in the Merrimelia Field. It is postulated that the grain-lining clay was formed by percolation of glacial meltwaters which, was subsequently illitised with depth.

Later neoformed illite emanates from earlier formed illite plates into the open aeolian pore spaces blocking pore throats.

- The formation of illite in Merrimelia sediments is interpreted to have occurred simultaneously in open and closed systems, with the reactants necessary for neoformation of illite in porous lithologies coming from nearby argillaceous sediments.
- The source of detrital clay in Merrimelia sediments is primarily from the grinding action of glaciers and sediment settling in lacustrine-dominated regions. Detrital clays in rock fragments are most likely inherited from a previous lithification as chemical activities when the majority of Merrimelia sediments were deposited was minimal.
- Temperature and the supply of necessary illite cations are important factors controlling illite formation in Merrimelia (and Tirrawarra) sediments. In addition, the water/rock ratio or the relative size of pore space is also an important control. Thus illite formation maybe triggered by a combination of hydrological controls, temperature and reactant supply.
- Glauconitic illite was observed, confirming the findings of Taylor *et al.* (1991). No petrological evidence was found, however, to confirm marine influence in Merrimelia sediments. This is in disagreement with the above authors, who suggest that the formation of "glauconitic illite" has occurred in relation to a marine incursion. All petrological evidence points to the original glauconitic illite grains having been derived from Warburton Basin litharenites and subsequently illitised with increasing burial.
- Kaolin was observed forming co-genetically with quartz cement and as pseudomorphic replacements of detrital feldspars. The formation of kaolin in upper Merrimelia sediments is related to acid meteoric pore waters and organic acids that have progressively dissolved detrital feldspars. In lower, impermeable and organically-barren Merrimelia sediments, the dissolution of feldspars has been retarded.
- The higher permeability of Tirrawarra sediments, allows kaolin to form preferentially, whereas illite has formed almost exclusively in the low

permeability Merrimelia sediments. The segregation of these clays, in two units that share the same hydrological continuum, is a product of:

- 1) Facies type (low detrital matrix – kaolin-dominated; high detrital matrix - illite-dominated).
- 2) Permeability.

- Chlorite is observed associated within basic rock fragments and more rarely as discrete chloritoid minerals. The chlorite minerals within basic clasts are an inherited alteration product. The small “translucent” authigenic chloritoid minerals associated with basic clasts are thought to be the products of the breakdown of these fragments. The trace proportions of chloritised basic rock fragments is reflected in the small volume of authigenic chlorite observed.
- Three carbonate species were identified in Merrimelia sediments: siderite, calcite and ferroan dolomite: The later two carbonate cements were only observed in trace proportions.
- Siderite occurs in three distinct stages (S1, S2, and S3) and are similar to the phases outlined by Rezaee *et al.* (1997) in the Tirrawarra Sandstone. The development of these stages is more pronounced in Merrimelia sediments. The development of these siderite stages was observed basin-wide, extending the findings of Rezaee (1996) which were confined to the Fly Lake-Brolga and Moorari-Tirrawarra fields.
- Siderite occurs in a very wide range of habits which can be grouped into three categories: porosity fill, patch and “seed”.
- The formation of S1, S2 and S3 siderite stages in Merrimelia sediments is most likely linked to organic maturation initially and later, the transformation of smectite to illite sediments. The compositional zonations of S2 siderite are indicative of Mg proportions in circulating pore waters and may reflect the progressive Mg output of smectite-illite reactions.
- Two siderite dissolution phases were observed (D1 and D2). The initial S1/S2 dissolution (D1) was observed consistently throughout Merrimelia sediments. This phase of carbonate dissolution was initiated by the same acidic pore waters that dissolved detrital feldspars and formed co-genetic kaolin and quartz in M1 sediments. The later S2/S3 siderite dissolution phase (D2) is not consistently

observed in Merrimelia sediments across the basin. This event is consistently observed in arenaceous Merrimelia sediments and the Tirrawarra Sandstone where organic acids penetrated. In the lower poorly permeable Merrimelia sediments, the influence of organic acids was reduced and therefore the later dissolution of siderite in these lower sediments is inconsistently observed.

- The preservation of calcite is also linked to carbonate buffering above 100°C. This mineral shows retrograde solubility with respect to the other two carbonate phases, forming in close association with siderite cement.
- Calcite exists in two forms; poikilotopic twinned cement and as a radial cement that has intergrown with illite. This later cement style, named "cowpat" calcite is restricted to two regions and reflects oscillating pore water acidities.
- Ferroan dolomite formation is also linked to siderite, but maybe associated with the dissolution of ankerite in the underlying Warburton Basin basement.
- Secondary porosity formation after feldspar, is limited in Merrimelia sediments.
- The formation of micro-porosity in kaolin masses is the most consistent pore space created in Merrimelia sediments. Feldspar and rock fragment component dissolution are important forms of secondary porosity formation locally in the Merrimelia and Malgoona fields respectively.
- Pyrophyllite was observed in the deepest Merrimelia samples (Beanbush #1) indicating a very hot diagenetic environment. In such an environment, diagenetic modifications are extensive and proceed at a much higher rate.
- Variations in the paragenetic sequence was observed locally, largely controlled by arenaceous and argillaceous sediments, which in turn reflect the variations in sediment composition. The ultimate control on the paragenesis of Merrimelia sediments was provenance and facies type.
- Facies type and provenance are the main controls on diagenesis in the MTGC. Statistical analysis indicates that the kaleidoscopic nature of Merrimelia facies and inconsistent well control negates the possibility of accurately mapping the areal distribution of authigenic mineral phases. Trends in the data do indicate

that there is a positive link between the presence of authigenic minerals and rock fragments in Merrimelia sediments.